Book of peer-reviewed papers

10th Congress of the Alps Adria Acoustics Association

International Scientific Congress

20. – 21. September 2023, Izola, Slovenia

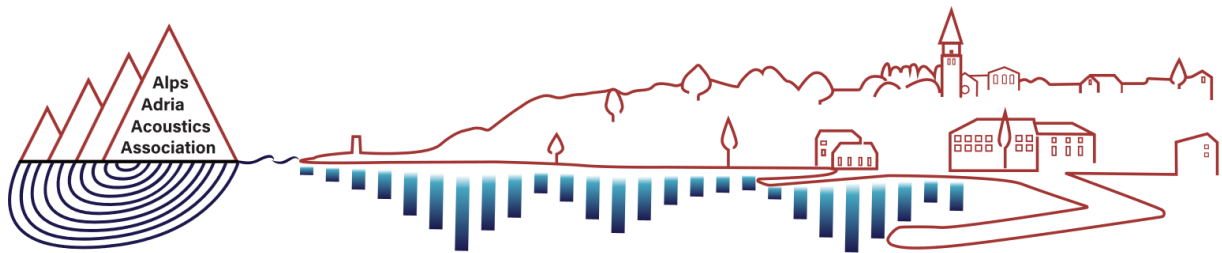Hrvatsko akustičko društvo
Acoustical society of Croatia

AAAA 2023 IZOLA 20. - 21. September
10th CONGRESS OF THE ALPS ADRIA ACOUSTICS ASSOCIATION

Book of peer-reviewed papers.
10th Congress of the Alps Adria Acoustics Association, 20. – 21. September 2023, Izola, Slovenia.
International Scientific Congress

AAAA 2023 IZOLA 20. - 21. September
10th CONGRESS OF THE ALPS ADRIA ACOUSTICS ASSOCIATION

Prof. Dr. Mirko Čudina, founder of SDA and one of the founders of the AAAA and EUROREGIO, University of Ljubljana, Faculty of Mechanical Engineering, Slovenia
Dr. Ferdinand Deželak, retired researcher
Prof. Dr. Daniel Svenšek, University of Ljubljana, Faculty of Mathematics and Physics, Slovenia
Dr. Jernej Polajnar, National Institute of Biology, Slovenia
Assoc. Prof. Dr. Jurij Prezelj, University of Ljubljana, Faculty of Mechanical Engineering, Slovenia
Assoc. Prof. Dr. Nikola Holeček, University of Ljubljana, Faculty of Chemistry and Chemical Technology, Faculty of Environmental Protection, Slovenia
Prof. Dr. Tino Bucak, HAD, University of Zagreb, Faculty of Transport and Traffic Sciences, Croatia
Prof. Dr. Kristian Jambrošić, University of Zagreb Faculty of Electrical Engineering and Computing, Croatia
Beáta Mesterházy, M.Sc., President of the Department of Acoustics of OPAKFI, BME (Budapest University of Tecnology and Economics), Department of Building Constructions, Laboratory of Building Acoustics
András Muntag, M.Sc., President of the Department of Noise and vibration control of OPAKFI, Enviroplus Kft. (Ltd), Hungary
Prof. Dr. Marko Horvat, President of the HAD, Faculty of Electrical Engineering and Computing, University of Zagreb
Prof. Dr. Antonio Petošić, University of Zagreb, Faculty of Electrical Engineering and Computing, University of Zagreb
Assist. Prof. Dr. Jurica Ivošević, University of Zagreb, Faculty of Transport and Traffic Sciences, Croatia
Attila Balázs Nagy, M.Sc., BME (Budapest University of Technology and Economics), Laboratory of Building Acoustics, Hungary
Viktor Jemec, M.Phil., Društvo vzdrževalcev Slovenije (DVS), SDA

The Book of peer-reviewed abstracts was made as part of the 1th Congress of the Alps Adria Acoustics Association, 2. – 21. September 223, Izola, Slovenia.
Papers are peer-reviewed.

AAAA 2023 IZOLA 20. - 21. September
10th CONGRESS OF THE ALPS ADRIA ACOUSTICS ASSOCIATION

AAAA 2023 IZOLA 20. - 21. September
10th CONGRESS OF THE ALPS ADRIA ACOUSTICS ASSOCIATION

Organizing Institution
Slovensko društvo za akustiko,
Slovenian Acoustical Society (SDA)
Jamova cesta 2, 1000 Ljubljana, Slovenia

Contact
Congress Secretariat
E-mail: info@alpsadriaacoustics.eu
Postal address: Slovensko društvo za akustiko, Slovenian Acoustical Society (SDA)
Jamova cesta 2, 1000 Ljubljana, Slovenia

Organizers
Slovensko društvo za akustiko, Slovenian Acoustical Society (SDA)
InnoRenew CoE
University of Ljubljana, Faculty of Civil and Geodetic Engineering (UL FGG)

Co-organisers
Alps Adria Acoustics Association (AAAA)
Hrvatsko akutsičko društvo, Acoustical Society of Croatia (HAD)
Hungarian Scientific Society for Optics, Acoustics, Motion Picture and Theatre Technology (OPAKFI)
European Acoustics Association (EAA)

Gold sponsors
IMS Merilni sistemi d.o.o.
Rothoblaas
DEWESoft
Knaufinsulation

Silver sponsors
HEAD acoustics
Getzner

Bronze sponsors
Fragmat
Domel
Ursa

Contents

AAAA 2023 IZOLA 20. - 21. September
10th CONGRESS OF THE ALPS ADRIA ACOUSTICS ASSOCIATION

Preface

Welcome to the 10th Congress of the Alps Adria Acoustics Association! The 10th Congress of the Alps Adria Acoustics Association will be held in Slovenia, at InnoRenew CoE in Izola, from 20th to 21st September 2023.

The Alps Adria Acoustics Association (AAAA) was founded by the acoustics societies of Slovenia, Croatia and Austria in 2002 as a new regional association. In 2019 the Hungarian Scientific Society for Optics, Acoustics, Motion Picture and Theatre Technology (OPAKFI) joined instead of Austria. The original goal of AAAA was to promote all aspects of research in the field of acoustics in the region. In addition, the Association's aim was to improve the overall cooperation among the countries and their respective national societies.

Every two years, one of the three member societies of the AAAA organizes a scientific congress on acoustics. The main goal of these congresses is to bring together acousticians from Croatia, Hungary and Slovenia, as well as from the other European countries, in order to exchange knowledge, share research outcomes and strengthen mutual cooperation among these societies for the benefit of the whole region. The last event took place in Budapest in 2021. During the congress days, national and international experts present a number of scientific and applied papers on their research and professional activities in all fields of acoustics. In particular, the congress topics cover architectural and building acoustics, auditory and speech acoustic, environmental and transportation noise, machinery noise and vibration control, computational acoustics, electroacoustics, legislation in acoustics, musical acoustics, measurement techniques, non-linear acoustics, psychoacoustics and perception of sound, signal processing, sound generation and radiation, ultrasonics, hydroacoustics, etc.

The scientific programme includes keynote lectures given by eminent international experts. The AAAA 2023 Congress deals with topics that are the focus of interest in the scientific community and among researchers working in the industry. The 2023 Congress is organized by the Slovenian Acoustical Society (SDA) acting on behalf of the Alps Adria Acoustics Association.

The conference is planned to be a live conference. Looking forward to meeting you in Izola in September 2023!

Assoc. Prof. Dr. Mateja Dovjak, Congress Chair, President of the Slovenian Acoustical Society (SDA), Faculty of Civil and Geodetic Engineering of the University of Ljubljana, Slovenia
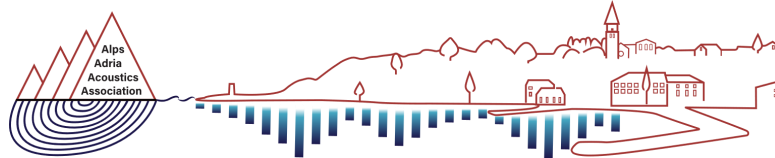
AAAA 2023 IZOLA 20. - 21. September
10th CONGRESS OF THE ALPS ADRIA ACOUSTICS ASSOCIATION

Program overview

WEDNESDAY, SEPTEMBER 20	TIME	LOCATION
REGISTRATION	8:00 - 9:00	SEQUOIA LECTURE ROOM
OPENING CEREMONY	9:00 - 9:30	SEQUOIA LECTURE ROOM
KEYNOTE Invited speech: Prof. Dr. Janko Slavič	9:30 - 10:30	SEQUOIA LECTURE ROOM
COFFEE BREAK	10:30 - 10:50	MAIN HALL
MORNING SESSIONS	10:50 - 12:50	SEQUOIA AND QUERCUS LECTURE ROOM
LUNCH BUFFET	12:50 - 13:50	MAIN HALL
ACOUSTIC LABORATORY VISIT - GROUP 1	13:50 - 14:10	ACOUSTIC LABORATORY INNORENEW COE
GOLDEN SPONSOR PRESENTATION - SPONSOR ROTHOBLAAS	14:10 - 14:20	SEQUOIA LECTURE ROOM
GOLDEN SPONSOR PRESENTATION - SPONSOR KNAUF INSULATION	14:20 - 14:30	SEQUOIA LECTURE ROOM
KEYNOTE Invited speech: Prof. Dr.-Ing. Roland Sottek	14:30 - 15:30	SEQUOIA LECTURE ROOM
COFFEE BREAK	15:30 - 15:50	MAIN HALL
AFTERNOON SESSIONS	15:50 - 17:30	SEQUOIA AND QUERCUS LECTURE ROOM
FREE TIME		
TRANSPORTATION TO DINNER	18:45	IN FRONT OF INNORENEW COE BUILDING
GALA DINNER	19:00-22:00	RESTAURANT KAMIN

AAAA 2023 IZOLA 20. - 21. September
10th CONGRESS OF THE ALPS ADRIA ACOUSTICS ASSOCIATION

THURSDAY, SEPTEMBER 21	TIME	LOCATION
KEYNOTE Invited speech: Prof. Dr. Jonas Brunskog	8:30 - 9:30	SEQUOIA LECTURE ROOM
TECHNICAL KEYNOTE Invited speech: Assist Prof. Dr. Rok Prislan	9:30 - 10:30	SEQUOIA LECTURE ROOM
COFFEE BREAK	10:30 - 10:50	MAIN HALL
MORNING SESSIONS	10:50 - 12:50	SEQUOIA AND QUERCUS LECTURE ROOM
LUNCH BUFFET	12:50 - 13:50	MAIN HALL
ACOUSTIC LABORATORY VISIT - GROUP 2	13:50 - 14:10	ACOUSTIC LABORATORY INNORENEW COE
GOLDEN SPONSOR PRESENTATION - SPONSOR DEWESOFT	14:10 - 14:20	SEQUOIA LECTURE ROOM
GOLDEN SPONSOR PRESENTATION - SPONSOR IMS MERILNI SISTEMI D.O.O.	14:20 - 14:30	SEQUOIA LECTURE ROOM
KEYNOTE Invited speech: Prof. Dr. Goran Pavić	14:30 - 15:30	SEQUOIA LECTURE ROOM
COFFEE BREAK	15:30 - 15:50	MAIN HALL
AFTERNOON SESSIONS	15:50 - 17:30	SEQUOIA AND QUERCUS LECTURE ROOM
CLOSING CEREMONY	17:30 - 18:00	SEQUOIA LECTURE ROOM
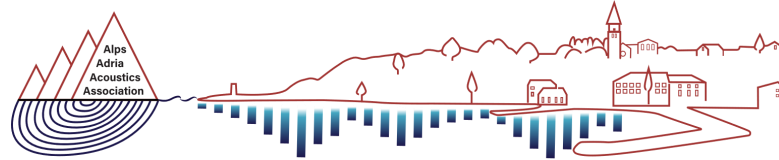
AAAA 2023 IZOLA 20. - 21. September
10th CONGRESS OF THE ALPS ADRIA ACOUSTICS ASSOCIATION

Program

Registration   **WEDNESDAY, SEPTEMBER 20   8:00 - 9:00**

Opening ceremony   **WEDNESDAY, SEPTEMBER 20   9:00 - 9:30**

Assoc. Prof. Dr. Mateja Dovjak, Congress Chair, President of the Slovenian Acoustical Society (SDA), Faculty of Civil and Geodetic Engineering of the University of Ljubljana, Slovenia

Welcome speech

On behalf of Slovenian Acoustical Society and Faculty of Civil and Geodetic Engineering of the University of Ljubljana, Assoc. Prof. Dr. Mateja Dovjak, Congress Chair, President of the SDA, Slovenia

On behalf of InnoRenew CoE, Prof. Dr. Andreja Kutnar, director of the InnoRenew CoE, Slovenia

On behalf of Hungarian Scientific Society for Optics, Acoustics, Motion Picture and Theatre Technology (OPAKFI), Beáta Mesterházy, M.Sc., President of the Department of Acoustics of OPAKFI, BME (Budapest University of Tecnology and Economics), Department of Building Constructions, Laboratory of Building Acoustics

On behalf of Hrvatsko akutsičko društvo, Acoustical Society of Croatia (HAD), Prof. Dr. Marko Horvat, President of the HAD, Faculty of Electrical Engineering and Computing, University of Zagreb, Croatia

AAAA 2023 IZOLA 20. - 21. September
10th CONGRESS OF THE ALPS ADRIA ACOUSTICS ASSOCIATION

WEDNESDAY, SEPTEMBER 20 - morning session

SEQUOIA LECTURE ROOM
SS04 - ROOM ACOUSTICS
Session chair: Prof. Dr. Kristian Jambrošić, University of Zagreb Faculty of Electrical Engineering and Computing

TIME	TITLE	PRESENTER
10:50	Acoustic Design of a New Concert Venue for Classical Music in Split, Croatia	Kristian Jambrosic (University of Zagreb Faculty of Electrical Engineering and Computing)
11:10	Real or Synthetic? A Machine Learning Approach to Classifying Room Impulse Responses	Marko Pap (School of Electrical Engineering, University of Belgrade)
11:30	LCA study of different recycled sound absorbers from melamine foam waste	Urban Kavka (InnoRenew CoE)
11:50	Multichannel Reverberation Time Measurements of Miura-Ori Origami in Alpha Chamber	Andrej Hvastja (University of Ljubljana, Faculty of Mechanical Engineering)
12:10	Reverberation time estimation from emotional speech signals	Andrea Andrijasevic (Polytechnic of Rijeka, Croatia)
12:30	Determination of the position of equipment noise sources in educational institutions according to subjectively evaluated speech intelligibility	Mateja Dovjak (University of Ljubljana, Faculty of Civil and Geodetic Engineering)

QUERCUS LECTURE ROOM
SS01 - NOISE AND VIBRATIONS
Session chair: Prof. Dr. Antonio Petošić, University of Zagreb, Faculty of electrical Engineering and Computing

TIME	TITLE	PRESENTER
10:50	Integration of Psychoacoustic Perception for Enhanced Design of Axial Fans	Nejc Cerkovnik (University of Ljubljana, Faculty of Mechanical Engineering)
11:10	Noise generating mechanisms analysis and its optimization on electronical commutated wet-dry vacuum cleaner suction unit	Andrej Biček (Nela d.o.o)
11:30	Modeling and assessment wind turbine noise at different meteorological conditions	Antonio Petošić (University of Zagreb, Faculty of Electrical Engineering and Computing)
11:50	Evaluation of model based noise protection study based on in-situ vibro-acoustic railway track analysis	Krešimir Burnać (Faculty of Civil Engineering, University of Zagreb)
12:10	Steel reilway bridge noise, lack of reduction effect on airborne noise due to vibration dampers possibly acting a s noise sources	Rok Rudolf (ZAG)
12:30	Psychoaoustics of Pseudosound in Turbulent flow of Centrifugal Fan used in Household Appliance	Jurij Prezelj (University of Ljubljana, Faculty of Mechanical Engineering)

AAAA 2023 IZOLA 20. - 21. September
10th CONGRESS OF THE ALPS ADRIA ACOUSTICS ASSOCIATION

WEDNESDAY, SEPTEMBER 20 - afternoon session

SEQUOIA LECTURE ROOM
SS02 - ADVANCED MEASUREMENT TECHNIQUES IN ACOUSTICS
Session chair: Assist. Prof. Dr. Rok Prislan, InnoRenew CoE

TIME	TITLE	PRESENTER
15:50	Challenges in the introduction of timbre coordinates for violoncelli	Daniel Svenšek (University of Ljubljana, Faculty of Mathematics and Physics)
16:10	Soundscape monitoring system for earthquake-affected urban spaces – Zagreb case study	Karlo Filipan (Catholic University of Croatia)
16:30	Immission Directivity as a tool for generation of Noise Maps	Jurij Prezelj (University of Ljubljana, Faculty of Mechanical Engineering)
16:50	Data Selection for Reduced Training Effort in Vandalism Sound Event Detection	Stefan Grebien (Joanneum Research)
17:10	Experimental sound field characterization with automated high-resolution impulse response measurements	Rok Prislan (InnoRenew CoE)

QUERCUS LECTURE ROOM
SS06 - ACOUSTIC SOFTWARE AND TRAINING
Session chair: Assoc. Prof. Dr. Mateja Dovjak, University of Ljubljana, Faculty of Civil and Geodetic Engineering

TIME	TITLE	PRESENTER
15:50	Audio exercises: quality, pitch statistics and long-term spectra of the sound files	Andrea Andrijasevic (Polytechnic of Rijeka, Croatia)
16:10	Acoustics Knowledge Alliance project: the development of open-access interactive online educational materials in acoustics - strategy and results	Marko Horvat (University of Zagreb, Faculty of Electrical Engineering and Computing)

THURSDAY, SEPTEMBER 21 - morning session

SEQUOIA LECTURE ROOM
SS05 - BUILDING ACOUSTICS
Session chair: Beáta Mesterházy, M.Sc., President of
the Department of Acoustics of OPAKFI, BME

TIME	TITLE	PRESENTER
10:50	Design and construction of a temporary test facility for sound insulation measurements of doors	Nika Šubic (MK3 d.o.o.)
11:10	Acoustic performance of buildings, components and materials as a parameter for ecological and social sustainability assessments	Franz Dolezal (IBO - Austrian Institute for Building and Ecology)
11:30	Possible applications of high-performance floating floors and consequent relevant dimensions of performance and design criteria	Zoltán Horváth (CDM Stravitec Kft.)
11:50	Improvement of impact sound insulation with tile underlay materials – impact sound insulation without floating floors	Beáta Mesterházy, (Department of Acoustics of OPAKFI, BME)

QUERCUS LECTURE ROOM
SS01 - NOISE AND VIBRATIONS
Session chair: Prof. Tino Bucak, HAD, University of Zagreb,
Faculty of Transport and Traffic Sciences, Croatia

TIME	TITLE	PRESENTER
10:50	ILEGAL USE OF FIRECRACKERS AND ITS CONSEQUENCES - CASE STUDY OF HUMAN RIGHTS VIOLATION AT SLOVENIAN COURTS – PART I: LEGISLATION AND COURT PROCEEDINGS	Ferdinand Deželak (Retired researcher)
11:10	ILEGAL USE OF FIRECRACKERS AND ITS CONSEQUENCES - CASE STUDY OF HUMAN RIGHTS VIOLATION AT SLOVENIAN COURTS – PART II: PHYSICAL BACKGROUND	Ferdinand Deželak (Retired researcher)
11:30	Low frequency noise measurement in the passenger cabin	Samo Beguš (University of Ljubljana, Faculty of Electrical Engineering)
11:50	Measurement and Characterization of Control Valves Noise	Egon Susič (Danfoss Trata d.o.o.)

SEQUOIA LECTURE ROOM
SS03 - SOUNDSAPE AND SOUND REPRODUCTION TECHIQUES
Session chair: Prof. Dr. Marko Horvat, President of the HAD,
Faculty of Electrical Engineering and Computing, University of
Zagreb

TIME	TITLE	PRESENTER
12:10	The soundscape of university campuses: sound essays on the Polytechnic University of València	Alberto Quintana-Gallardo (Centre for Physics Technologies (CTFAMA), Universitat Politècnica de València)
12:30	Accuracy of Dynamic Sound Source Localization in Binaural Audio Systems with Head-Tracking Utilizing Generic and Individual HRTFs	Vedran Planinec (Faculty of Electrical Engineering and Computing, University of Zagreb)

THURSDAY, SEPTEMBER 21 - afternoon session

SEQUOIA LECTURE ROOM
SS03 - SOUNDSCAPE AND SOUND REPRODUCTION TECHIQUES
Session chair: Prof. Dr. Marko Horvat, President of the HAD, Faculty of Electrical Engineering and Computing, University of Zagreb

TIME	TITLE	PRESENTER
15:50	Application of Ambisonics to Building Acoustics – Challenges and Opportunities	Armin WILFLING (IBO)
16:10	A Comparison between Real and Reproduced Sound Fields for Impact Noise Annoyance Ratings	Martina Vrhovnik (InnoRenew CoE)

QUERCUS LECTURE ROOM
SS01 - NOISE AND VIBRATIONS
Session chair: Dr. Egon Susič, Danfoss Trata d.o.o., Slovenia

TIME	TITLE	PRESENTER
15:50	Proposing noise barriers along existing national roads through settlements - the case of Novo mesto and its surroundings	Mihael Žiger (Nacionalni laboratorij za zdravje, okolje in hrano)
16:10	Measurement and modelling uncertainty in accredited acoustic procedures	Antonio Petošić (University of Zagreb, Faculty of electrical Engineering and Computing)
16:30	Development of a special standard for outdoor music events in Slovenia based on measurements and calculations	Luka Čurović (University of Ljubljana, Faculty of Mechanical Engineering)

SEQUOIA LECTURE ROOM
SS02 - ADVANCED MEASUREMENT TECHNIQUES IN ACOUSTICS
Session chair: Assist. Prof. Dr. Samo Beguš, University of Ljubljana, Faculty of Electrical Engineering

TIME	TITLE	PRESENTER
16:30	Estimating Speed of Sound in Granular Materials: Impulse Response Extraction and Wave Decomposition in an Extended Impedance Tube	Anže Železnik (University of Ljubljana, Faculty of Mechanical Engineering)
16:50	A smart method to calibrate universal testing machines by incorporating acoustic methods	Sharath Peethambaran Subadra (Hochschule für Angewandte Wissenschaften Hamburg)
17:10	Unsupervised Classification of Welding processes based on Psychoacoustic Sound Features	Jurij Prezelj (University of Ljubljana, Faculty of Mechanical Engineering)

AAAA 2023 IZOLA 20. - 21. September
10th CONGRESS OF THE ALPS ADRIA ACOUSTICS ASSOCIATION

Closing ceremony **THURSDAY, SEPTEMBER 21 17:30 - 18:00**

Assoc. Prof. Dr. Mateja Dovjak, Congress Chair, President of the Slovenian Acoustical Society (SDA), Faculty of Civil and Geodetic Engineering of the University of Ljubljana, Slovenia

An invitation to the 11th AAAA in Zagreb 2025: Prof. Dr. Marko Horvat, President of the HAD, Faculty of Electrical Engineering and Computing, University of Zagreb, Croatia
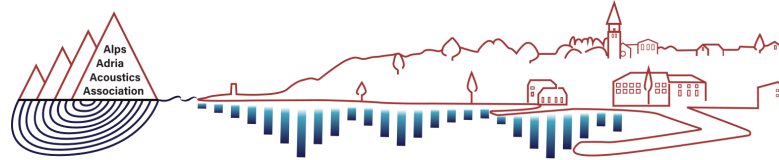
AAAA 2023 IZOLA 20. - 21. September
10th CONGRESS OF THE ALPS ADRIA ACOUSTICS ASSOCIATION

Keynote
Invited speech

High-speed camera based identification of sound and vibrations

Prof. Dr. Janko Slavič

Ladisk, Faculty of Mechanical Engineering, University of Ljubljana

E-mail: janko.slavic@fs.uni-lj.si

Professor Dr. Janko Slavič is a full professor at the Faculty of Mechanical Engineering at the University of Ljubljana. Prof. Slavič is a recipient of the Fulbright scholarship (University of Texas at Austin 2005-2006) and is a co-author of 82 scientific articles, 56 of which are in category Q1. His works have been cited over ten thousand times. As a mentor or co-mentor, he has supervised 16 completed doctoral theses. In the last 10 years, his research has made significant contributions to the development of science in four scientific areas: vibration fatigue, experimental modal analysis based on high-speed camera recordings, 3D printing of sensors, and research based on open-source code.

Image-based measurement techniques have recently gained popularity and are increasingly used in various applications as a viable alternative to traditional measurement methods. Image-based techniques offer high spatial density of information, and with advancements in hardware, they can also provide a high frequency of image acquisition, such as 20k frames per second at megapixel resolution.

In his lecture, dr. Slavič will review the origins of image-based methods and explain the well-established classical method of digital image correlation (DIC). Advanced signal processing methods will be presented, as well as the challenges associated with noise and overdetermination in image data. It will be shown that amplitude identification is successful for harmonic motion up to the resolution of 1/100,000th of a pixel. Finally, selected methods will be explored that have great potential for future research, such as 3D vibration reconstruction based on frequency domain triangulation and the spectral optical flow imaging experimental technique.

AAAA 2023 IZOLA 20. - 21. September
10th CONGRESS OF THE ALPS ADRIA ACOUSTICS ASSOCIATION

Contributed papers
Room acoustics

1. Acoustic Design of a New Concert Venue for Classical Music in Split, Croatia
   Kristian Jambrosic (University of Zagreb Faculty of Electrical Engineering and Computing)
2. Real or Synthetic? A Machine Learning Approach to Classifying Room Impulse Responses Marko Pap
   (School of Electrical Engineering, University of Belgrade
3. LCA study of different recycled sound absorbers from melamine foam waste
   Urban Kavka (InnoRenew CoE)
4. Multichannel Reverberation Time Measurements of Miura-Ori Origami in Alpha Chamber
   Andrej Hvastja (University of Ljubljana, Faculty of Mechanical Engineering)
5. Reverberation time estimation from emotional speech signals
   Andrea Andrijasevic (Polytechnic of Rijeka, Croatia)
6. Determination of the position of equipment noise sources in educational institutions according to subjectively evaluated speech intelligibility
   Mateja Dovjak (University of Ljubljana, Faculty of Civil and Geodetic Engineering)
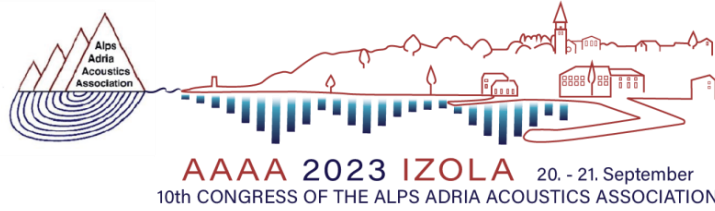
ACOUSTIC DESIGN OF A NEW CONCERT VENUE FOR CLASSICAL MUSIC IN SPLIT, CROATIA

Kristian Jambrošić [1], Marko Horvat [2]

University of Zagreb, Faculty of Electrical Engineering and Computing, Unska 3, Zagreb, Croatia
[1] kristian.jambrosic@fer.hr, [2] marko.horvat@fer.hr

Abstract: *This paper presents the key points of acoustic design of a new concert venue in Split, based on the revitalization of an old building. This venue is dedicated to showcasing classical music performances by soloists and small orchestras. It is built as a classical shoebox-shaped main hall with a small balcony and a seating capacity of 250 that is used for small ensemble performances, accompanied by a smaller hall accommodating up to 60 attendees that is used for mostly solo performances. Throughout the design and construction phases, careful consideration was given to preservation of the historical and architectural value of the building. The acoustic design process aimed to create an exemplary venue lauded for its superior sound quality by both the audience and performers. The paper outlines the decision-making process behind the selection of appropriate interior materials and the placement of acoustic elements, to achieve optimal acoustics in the halls. Furthermore, the paper presents the results of comprehensive acoustic measurements conducted during the construction period, highlighting the effectiveness of the implemented design. By evaluating the acoustical performance of the halls before and after their refurbishment, this study provides valuable insights into the successful integration of architectural design and acoustic considerations.*

Keywords: concert hall acoustics, stage design, room acoustics simulation, acoustic measurements

1. INTRODUCTION

The representative building of the Croatian Home ("Hrvatski dom" in Croatian) in Split was constructed in 1908 as the headquarters of Croatian nationalist societies, according to the design by engineer Kamilo Tončić. The project was created in accordance with the contemporary tendencies of the Viennese Wagner School. Art Nouveau influences can be seen in the design of the main facade, enriched with geometric and stylized floral decorations, as well as in the interior of the Ceremonial Hall on the upper floor. But, the hall was completely neglected from the early years after World War II.

Preparations for the renovation of the building began in 2005 with a clear idea of its future purpose, which would include a puppet theatre on the ground floor and a multipurpose concert hall on the upper floor, with all other spaces serving the purpose of concert activities. The comprehensive restoration of the physically destroyed original appearance of Tončić's work, characterized by a strong Art Nouveau expression, became an imposed approach to the renovation, Fig. 1.

With the establishment of the company "Public Institution in Culture, Croatian Home Split", the town of Split gained a professional concert hall for the first time in its history.

Fig. 1. Renovated facade of the Croatian Home building.

The Ceremonial Hall, reconstructed in detail as it looked like before the World Was II, has a seating capacity of 250 visitors, 216 of which are seated on the ground floor and 34 on the balcony in the back of the hall, Fig. 2 and 3.

Fig. 2. The interior of the Ceremonial Hall, view from the beginning of the stage towards its back.

Fig. 3. The interior of the Ceremonial Hall, view from the balcony towards its stage.

The smaller hall, the Jakov Gotovac Music Salon, did not exist as a public event space before. A large room in the topmost floor has been adapted as a multipurpose space because of high demands for such smaller venues. It can accommodate between 50 and 70 visitors, Fig. 4 and 5.
Both spaces are equipped with top-quality audio-visual equipment, allowing for a high production level of musical and other events. In addition to musical and cultural purposes, the spaces are suitable for various events such as congresses, lectures, presentations, anniversary celebrations, and more.

Fig. 4. The interior of the Jakov Gotovac Music Salon, view towards its back.

Fig. 5. The interior of the Jakov Gotovac Music Salon, view towards its stage.

2. ACOUSTIC DESIGN OF THE CONCERT VENUES

The task of the authors of this paper was to provide to the venue owners an acoustic design project for both concert halls prior to the reconstruction work. It had to predict the acoustic quality of both halls and to prove that they will be appropriate for their intended purposes. The Ceremonial Hall is primarily built for concerts of classical music by small orchestras and soloists, and for occasional use as a venue for speech, choirs, jazz music, and other events that will fit the owner's need. The Music Salon, given its size, primarily aims to host speech events (conferences, drama plays), but also soloist concerts.

To simulate the acoustics of both halls, 3D wireframe models were prepared, and detailed simulation have been done in the Odeon Auditorium room acoustic simulation software [1]. Wireframe models for both halls can be seen in Fig. 6 and Fig. 7.
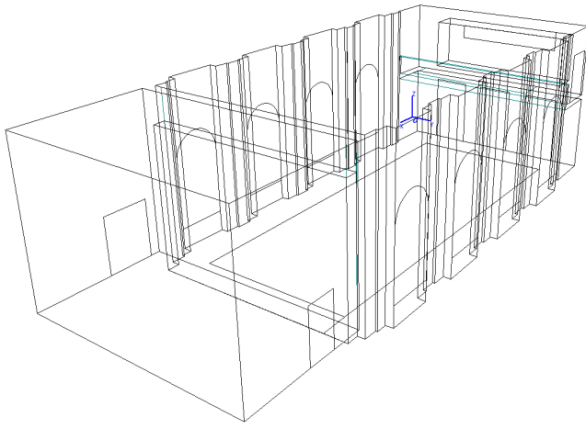
Fig. 6. 3D wireframe model of the Ceremonial Hall.
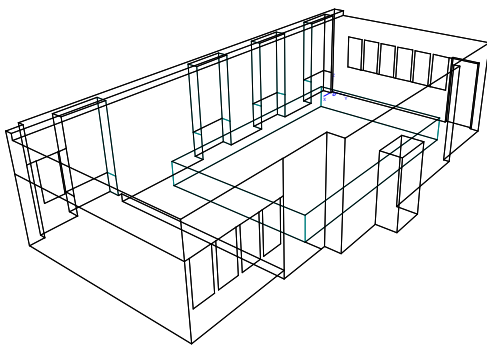
Fig. 7. 3D wireframe model of the Jakov Gotovac Music Salon.

Measurements of the room acoustic parameters were planned as part of the acoustic design project after the reconstruction works to prove the quality of the acoustic design.

The criteria for the acoustic design and the optimal values of acoustic parameters depend on several important features of the halls. The first is certainly the purpose of the halls, where one should distinguish between halls intended for musical performances (concert halls of all sizes), halls intended for speech (theatres, cinemas, multifunctional halls), as well as halls intended for both music and speech (opera, theatres). Furthermore, the acoustic parameters of halls intended for music depend

on the type of music performed (organ music, symphony orchestra, chamber music, solo performances and recitals, dance music, amplified modern music). The next important feature of the hall that determines the optimal range of acoustic parameters is its size, that is, the volume of the hall. All of this should be taken into account when assessing and evaluating the acoustic quality of halls, as stated in the reference standards and publications that describe and determine the acoustic properties of the space.

The requirements from the EN ISO 3382-1:2009 standard cover the widest range of uses, which is why they are the least strict ones [2]. A finer distinction is given by the criteria according to Beranek [3] and Rossing [4], with the fact that Beranek covers more parameters and purposes, and Rossing deals with halls whose volume is outside Beranek's criteria. The rating according to Long [5] is used to determine the specific volume (m^3/seat) and acoustic conditions for speech purposes. A good reference is also the book by Barron [6].

2.1. The Ceremonial Hall

The volume of the hall is about 1,650 m^3, which places it the category of smaller halls intended primarily for chamber music performances. From the volume of the hall and the number of seats, the specific volume is obtained, that is, the volume per seat, which in this case is **6.6 m^3/seat**.

The shape of the hall is particularly interesting since it is built as a shoe-box type hall with the dimensions almost ideally half the length, width, and height of the world most famous hall for classical orchestra music, the Musikverein Hall in Vienna. Only the height of the Ceremonial Hall is around one meter smaller than half the height of the Vienna Hall. Thus, the shape of the hall is already a good indication that that, at least from the perspective of its geometry, it should function acoustically very well!

It must be noted that there was little space for adding any acoustic elements that would diverge the occurrence of the Ceremonial Hall from its original looks as this was the prerequisite of the conservators. The only possibility was to carefully chose the materials of the surfaces and especially audience seats, with a little more freedom in the stage ceiling since it was not visible form the audience due to an existing portal (Fig. 3). Therefore, the reverberation time of the hall was tuned with a proper amount of the porous acoustic absorbers mounted on the

ceiling above the stage where stage technique equipment is mounted, but not necessarily in enough extent to prevent flutter echo for the musicians.

Based on the above considerations, the value ranges of the basic acoustic parameters, i.e. reverberation time RT_{60} and clarity of music C_{80}, were chosen for primarily music performances, according to [2] and [7].

In particular, the value of the reverberation time at medium frequencies that needs to be achieved in a full hall should be in the range **of 1.5 to 1.7 seconds**. In an empty hall, an increase in the reverberation time of up to 10%, to a maximum of 1.85 seconds, is permissible. The specified range represents the optimal values for the Ceremonial Hall, considering its size and intended purpose.

The average value of the clarity of music at medium frequencies for the entire auditorium should ideally range **from -2 to +3 dB**.

The range of possible values of the early sound decay time is not defined because the initial decay of the sound level in the room is defined primarily by the layout of the acoustically treated surfaces. In this case, it is fixed and cannot be changed, which is why the amount of early decay time cannot be influenced.

2.2. The Jakov Gotovac Music Salon

There were no constrains by the conservators regarding the acoustic design of the Music Salon, in terms of the amount and placement of acoustic elements in the room. The proposed solution for the acoustic treatment of the salon must solve the problems of the parallel side walls on the stage and the front and back walls of the hall, which are also parallel.

The solution consists of placement of medium-upholstered concert chairs in the auditorium, the sound absorption of which largely determines the overall reverberation in the room and enables the relative uniformity of the hall's reverberation, regardless of the number of listeners present, and installation of sound diffusers on the side walls of the stage, and additionally diffusers on the wall opposite the stage, at the entrance to the salon.

Typical value ranges of individual acoustic parameters defined in [2] for concert and multi-purpose halls show that the early decay time EDT is typically in the range **of 1 to 3 seconds**, while the clarity of music C_{80} is typically in the range **of -5 to 5 dB**. Given that in a room of such a

small volume, the concert chairs significantly affect the acoustics of the room, it was necessary to predict very precisely the sound-absorbing characteristics of the concert seats. Therefore, in consultation with the owners, subsequent measurements of the acoustic parameters in the salon were carried out to measure the impact of the finally selected concert chairs.

According to [7], the specific volume per seat for a room for speech and music events should be in the range between 6 and 8 m^3/seat, and for exclusively musical events it should be greater than 7 m^3/seat. Considering the volume of the hall of 233 m^3, to meet the above conditions, the hall should have a maximum of 39 seats for the audience for mixed speech-music performances, that is, no more than 33 seats for exclusively musical performances. The planned 50 - 60 seats for the audience exceed the stated figures, so it is necessary to keep in mind that an excessive number of visitors leads to excessive acoustic damping of the space, which directly affects the quality and experience of the musical performance.

For primary musical performances, according to [7] the recommended reverberation time RT60 is **1.1 seconds**, given as an average value in tertiary bands with central frequencies from 200 to 2500 Hz.

3. ACOUSTIC MEASUREMENTS OF THE CONCERT VENUES

The measurements of acoustic parameters were carried out to determine the acoustic situation in the hall after restoration with installed acoustic treatment.

The measurement of the acoustic parameters of the stage of the Ceremonial Hall was also carried out in a later stage of the projects in order to evaluate the acoustic situation in the area of the stage.

All measurements were carried out by the impulse response integration method using a sinusoidal signal of continuously variable frequency as an excitation signal. Impulse responses of the spaces were obtained from which it is possible to calculate the values of all relevant acoustic parameters depending on the frequency with the corresponding values of the relevant single parameters.

At the time of measurement, the halls were empty, i.e. without an audience, but fully equipped and completed according to the renovation projects and in accordance with the acoustics project.

3.1. Ceremonial Hall

Fig. 8. shows the averaged reverberation time over all measured locations in the whole frequency range of interest (from 50 Hz to 10,000 Hz in 1/3 octave bands), and Fig. 9 the averaged clarity C_{80} in the same frequency range.
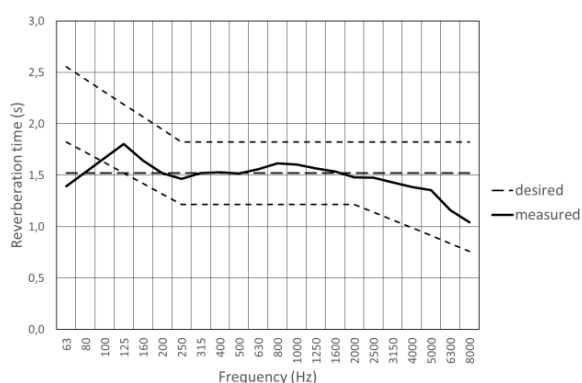
Fig. 8. Average reverberation time vs frequency in the Ceremonial Hall.
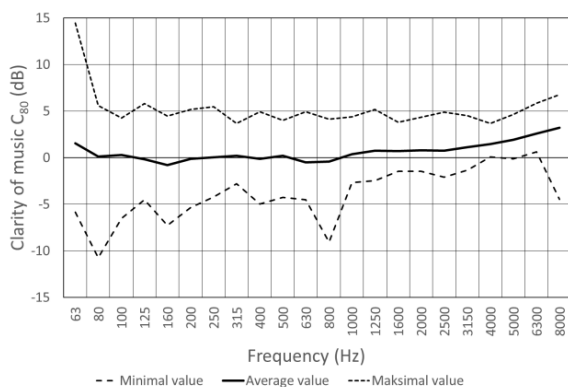
Fig. 9. Average clarity of music vs frequency in the Ceremonial Hall.

The single-number values for both parameters are:

$$\text{Reverberation time } RT_{60,\ 400\text{-}1250\ Hz} = 1.57 \text{ s}$$
$$\text{Clarity } C_{80,\ 400\text{-}1250\ Hz} = 0.05 \text{ dB}$$

Bot values fit perfectly the expected optimum values for this hall, thus proving that, at least from the acoustic parameters standpoint of view, the hall might be considered to be successful.

3.2. Jakov Gotovac Music Salon

Fig. 10. shows the averaged reverberation time over all measured locations in the whole frequency range of interest (from 50 Hz to 10,000 Hz in 1/3 octave bands).
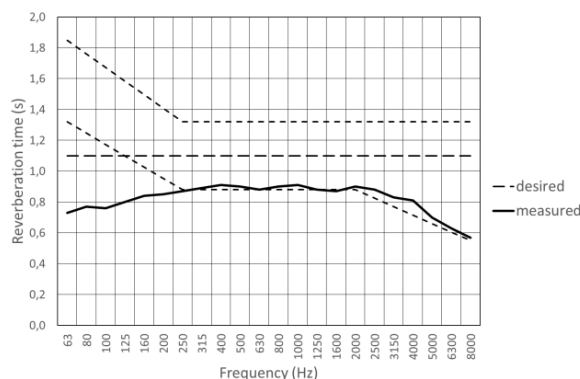
Fig. 10. Average reverberation time vs frequency in the Jakov Gotovac Music Salon.

It is evident that the reverberation time in Jakov Gotovac's salon is at the lower limit of tolerance, even when it is empty. This is the result of sound absorption due to the large number of upholstered concert chairs. The short reverberation time at low frequencies is more suitable for speech than for music and is a direct consequence of the presence of a large amount of plasterboard in the suspended ceiling.

Whenever the program allows it, it is recommended to reduce the number of chairs for visitors to or below the maximum recommended number, which will achieve greater liveliness of the space in terms of acoustics. This will have a favourable effect on the experience of the performed music, both for the visitors and the performers.

4. STAGE ACOUSTICS OF THE CEREMONIAL HALL

During the initial acoustic project of the Ceremonial Hall in 2015, an important limitation in terms of possible intervention in the interior of the hall as part of the acoustic treatment project was the conservator's request that the hall be completely renovated in accordance with the original plans from the first half of the 20th century. Accordingly, the acoustic treatment of the hall had to be designed to fully respect its original form. For this reason,

it was not possible to change the shape of the stage or add any additional acoustic elements to the walls of the hall or stage.

The concert hall has a built-in portal opening between the stage and the rest of hall. The upper part of the portal opening (overhang), unfortunately, prevents the use of ceiling surfaces as natural reflectors of sound towards the auditorium, both those above the stage itself and those directly in front of the portal.

4.1. Proposed solutions

Based on the conversation with the owners and through past experiences of musical performances in the concert hall since its opening, the following problems with the acoustics of the stage were recognized:

1. The parallel smooth side walls of the stage cause a fluttering echo when any transient sounds occur, which bothers the performers on the stage.
2. The space of the stage, which is bounded by the side parallel walls, the back smooth wall, and the opening of the portal, is subjectively too loud for the performers, especially when there is an ensemble on the stage with many performers who then try to reduce the volume of their performance.
3. The stage, as well as the hall, is too small for large ensembles, although there is a need to hold musical events that precisely include such ensembles.

The optimal solution to these problems is the use of an orchestra shell (fixed or movable). It eliminates parallel surfaces and the fluttering echo associated with them, and in lowers the problem of excessive volume by scattering the sound energy in all directions.

The basic sketch of this solution is shown in Fig. 11. The owners have confirmed on several occasions that this solution is not acceptable due to the lack of space for storing elements of the orchestra shell, i.e. the lack of a service room in the immediate vicinity of the stage.

Another solution is to bevel the parallel side walls of the stage at an angle greater than 7°, as shown in Fig. 12. This solution prevents the occurrence of a fluttering echo but does not provide an additional reflective surface that would target sound energy from the stage to the auditorium area, as is the case with the orchestra shell. The owners did not accept this solution either, because it would reduce the area of the stage, which is too small for some performances as it is. Moreover, soon the owners intend to replace the existing stage with a new, sector-variable stage with a system of height-adjustable modules.

Fig. 12. Second version of the stage acoustics solution.

Finally, the only possible solution to the stage acoustic problems is to install diffuser elements on the existing walls. The basic sketch of the solution is shown in Fig. 13., and the appearance of the stage is shown in Fig. 14.

Fig. 13. Third version of the stage acoustics solution.

Fig. 11. Fist version of the stage acoustics solution.

Fig. 14. The stage after installation of diffuser elements.

4.2. Influence of the diffusing elements

The acoustic parameters of the stage are defined to evaluate its acoustic properties from the perspective of musicians, or performers in general. At the same time, it is important that the acoustic conditions in the hall enable the performers on stage to hear each other well and to hear well the response of the hall itself.

According to [2], the ST_{Early} parameter shows how well the musicians on the stage can hear each other, while the ST_{Late} parameter quantifies the response of the hall itself from the performer's position, i.e. its perceived resonance. Both parameters are obtained in a similar way as the acoustic parameters of the hall, i.e. from measured impulse responses at certain points on the stage.

The single value of the ST_{Early} and ST_{Late} parameter in the middle frequency range for all measurement points, i.e. the average value for the entire stage, before the installation of the diffusers, are:

$$ST_{Early,\ 250-2000\ Hz} = -8.5\ dB$$
$$ST_{Late,\ 250-2000\ Hz} = -11.9\ dB$$

The values of the same parameters after the installation of the diffusers are:

$$ST_{Early,\ 250-2000\ Hz} = -8.9\ dB$$
$$ST_{Late,\ 250-2000\ Hz} = -12.9\ dB$$

The installation of diffusers lowered the ST_{Early} and ST_{Late} values. Moreover, this had also some influence on lowering the reverberation time of the hall and raising the clarity of music, as can be seen in Fig. 15. and Fig. 16.
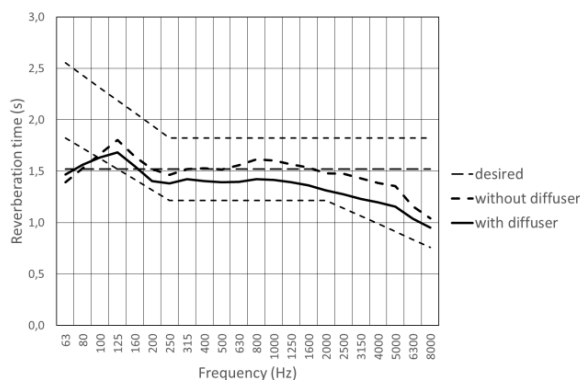
Fig. 15. Average reverberation time vs frequency in the Ceremonial Hall after the installation of diffusers.
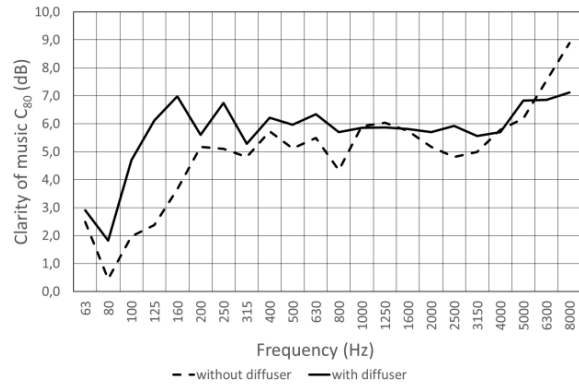
Fig. 16. Average clarity of music on the stage vs frequency after the installation of diffusers.

The shortening of the EDT early decay time and the increase in the C_{80} music clarity values indicate an increase in the energy of direct sound compared to the energy of reverberant sound in the stage space. In other words, the performers of musical (and spoken) performances will hear their own performance and the performance of other members of the ensemble more clearly after the intervention and, consequently, will more easily perform phrases with a faster tempo and greater dynamics, compared to the situation before adding the diffuser.

The global change in the acoustic conditions on the stage is also reflected in the difference in the single-digit average values of the ST_{Early} and ST_{Late} parameters measured before and after the mentioned intervention.

In particular, the values of the ST_{Early} parameter obtained by measuring on the stage of the hall in question before the intervention amount to -8.5 dB for all measurement points. After the intervention, the values of the specified parameter measured and calculated in the same way drop to -8.9 dB for both methods of calculation. Since this parameter basically expresses the ratio of the total energy of early reflections arriving from the stage space itself and the energy of direct sound, the obtained values indicate that the sound volume on the stage itself will be somewhat lower after the acoustic intervention, but not significantly. A significant reduction of the sound volume on the stage is possible only a) by adding a large amount of extremely sound-absorbing material, which would significantly impair the acoustic properties of the hall, and/or b) by limiting the number of performers on the

stage, which would set limits on the variety of the musical program performed in the hall.

The values of the ST_{Late} parameter obtained by the measurement before the intervention amount to -11.9 dB for all measurement points. After the intervention, these values drop to -12.9 dB. This result indicates that the response of the hall from the listening point of the musicians themselves will be slightly weaker than before the intervention, but still very strong.

The values of both parameters measured both before and after the intervention are at the upper limit of the typical range of values and indicate that the musicians on stage can hear each other very well both with and without installed diffusers.

The influence of the installed diffusers can be seen very clearly in the impulse responses measured on the stage of the hall. Fig. 17. shows an example of two impulse responses measured at the same point on the stage before and after the installation of the diffuser. It is clear that the sound energy contained in strong individual reflections from smooth wall surfaces is truly dispersed and divided into much weaker components, which was the goal of installing the diffuser.
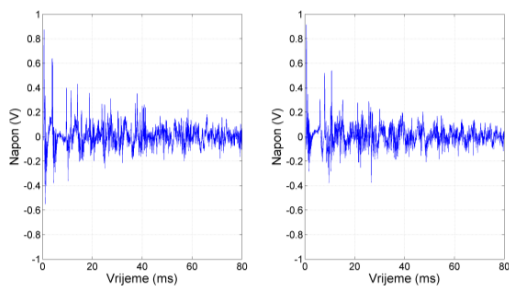
Fig. 17. Impulse response measured in the same location of the stage, before (left) and after (right) adding diffusers.

5. CONCLUSION

The process of the acoustical design of the two halls of the Croatian House in Split, the Ceremonial Hall, and the Jakov Gotovac Salon, proved to be very successful. The correct modelling of both halls and the subsequent acoustic measurements are very well in agreement. Moreover, the measured acoustical parameters are in their optimal ranges. The only deviation can be seen in the Jakov Gotovac Salon when the number of audience chairs

exceeds their optimal number and thus add to much absorption to the room.

However, to receive a final confirmation of the acoustical quality of both venues, it was necessary to wait for the verification of real audience visiting actual music performances. In general, the audience reported that the acoustic comfort in the halls is very good, and that the overall clarity of music performances is high, even on the balcony of the Ceremonial Hall. Some of the performers in some orchestras had objections to the sound on stage, especially the high volume. By subsequently installing the diffusers on the stage walls, this problem was also successfully solved. The sound of the performance did not change significantly in the audience, and it was confirmed that the volume on the stage was lower, with a reduced probability of flutter echo occurrence.

6. REFERENCES

[1.] **Odeon Auditorium 17 Room Acoustic Software**. Available at: https://odeon.dk/ (Accessed 28 August 2023).

[2.] ISO 3382-1:2009. **Acoustics — Measurement of room acoustic parameters — Part 1: Performance spaces**.

[3.] Beranek, L. **Concert halls and opera houses: music, acoustics and architecture**. Springer-Verlag, 2004.

[4.] Rossing, D. **Springer Handbook of Acoustics**. Springer Verlag, 2007.

[5.] Long, M. **Architectural Acoustics**. Academic Press, 2006.

[6.] Barron, M. **Auditorium Acoustics and Architectural Design**, Sp on Press, 2009.

[7.] DIN 18041:2012. **Audibility of rooms**.

REAL OR SYNTHETIC? A MACHINE LEARNING APPROACH TO CLASSIFYING ROOM IMPULSE RESPONSES

Marko Pap[1]**, Miloš Bjelić**[2]

[1] **School of Electrical Engineering, University of Belgrade, Belgrade, Serbia**
[2] **School of Electrical Engineering, University of Belgrade, Belgrade, Serbia**

Abstract:

This paper presents an innovative dual-branch neural network classifier designed to discern between real and synthetic room impulse responses. Responding to the critical need for verifying the authenticity of room impulse responses used in applications such as audio forensics, acoustic environment modeling, and virtual reality, our classifier uniquely combines a Convolutional Neural Network (CNN) and a Fully Connected Network (FCN) to analyze both spectrogram data and a set of acoustical features. The CNN branch processes spectrogram representations, capturing time-frequency characteristics, while the FCN branch attends to a set of predefined acoustical features, enabling comprehensive analysis. This dual-branch approach allows the classifier to leverage the strengths of both networks, contributing to an exceptional performance of 99% accuracy on the test set. We provide a detailed description of the classifier's architecture, underlining the features and design choices that enable its high accuracy. Our results imply the classifier's potential as a tool in maintaining the integrity and authenticity of room impulse responses. We discuss the potential applications and directions for future work, adding a valuable contribution to the field of audio and acoustic research.

Keywords: *Dual-branch neural network, Room impulse responses, Authenticity verification, Audio forensics, Acoustic environment modeling, Convolutional Neural Network (CNN), Fully Connected Network (FCN), Spectrogram data, Acoustical features, Classifier performance, Classifier architecture*

1. INTRODUCTION

Room impulse responses (RIRs) are crucial in various applications such as audio forensics, acoustic environment modeling, and virtual reality, due to the intricate acoustical properties they capture [1,2]. Determining whether these responses are authentic or synthetically generated is vital for maintaining the integrity of data utilized within these domains [1].

Identifying the genuineness of RIRs is a complex task that has seen advancements through digital signal processing and machine learning. Nonetheless, there remains a need for a classifier that is more efficient, accurate, and comprehensive, especially when handling diverse data types.

To address this challenge, we have designed an innovative dual-branch neural network classifier. Our approach integrates the strengths of two potent neural network models - a Convolutional Neural Network (CNN) and a Fully Connected Network (FCN). The CNN branch concentrates on processing spectrogram representations, thereby capturing time-frequency characteristics, while the FCN branch focuses on a set of specific acoustical features [3]. Recent advancements in neural-network-based RIR generation and analysis, such as the FAST-RIR [4] and deep prior approaches [5], highlight the potential of such methods in the field.

The acoustical features extracted for the FCN include:

- Spectral centroid
- Spectral bandwidth
- Spectral flatness
- Spectral contrast
- Zero-crossing rate
- Root mean square (RMS) value
- Mel-frequency cepstral coefficients (MFCCs)
- Energy split between early and late reflections of the sound [6]

These features are fundamental in providing a holistic understanding of RIRs, as demonstrated by recent works on room acoustical parameter estimation using deep neural networks [7] and virtually supervised learning for mean absorption estimation [8].

Our dual-branch approach is designed to harness the strengths of both the CNN and the FCN, thereby enhancing the classifier's overall performance. With an accuracy rate of 99% on the test set, our classifier demonstrates high effectiveness.

This paper provides a detailed exploration of our dual-branch neural network classifier's architecture, emphasizing the

design choices and the extracted acoustical features that contribute to its high accuracy. We believe our classifier has the potential to serve as a reliable tool in verifying the authenticity of room impulse responses. Additionally, we also discuss potential applications and explore avenues for future research, aiming to provide a significant contribution to the audio and acoustic research field.

2. METHODS

2.1 Neural Network Model Architecture and Training

Our dual-branch neural network classifier is built using the TensorFlow framework, a popular choice for implementing neural networks in various applications, including medical imaging [9]. The classifier architecture combines a fully connected network (FCN) for acoustic feature analysis and a convolutional neural network (CNN) for spectrogram analysis, similar to the approach used in distributed acoustic sensors [10].

The FCN is particularly suited for the analysis of a variety of acoustic features. The reasons for its design are as follows:

1. **Acoustic Feature Input:** Using acoustic features of the room impulse response (RIR) as the input provides a compact representation of the RIR's characteristics. By focusing on these features, the network can efficiently learn patterns that are most relevant for the classification task.

2. **Sequential Dense Layers:** Two Dense layers sequentially process and transform the input features into higher-level representations. The choice of 256 nodes in the first layer allows for the extraction of a broad set of features, while the subsequent reduction to 64 nodes ensures a focus on the most critical features.

3. **ReLU Activation:** The ReLU activation function introduces non-linearity, allowing the network to capture complex relationships in the data. Additionally, it offers computational efficiency and mitigates the vanishing gradient problem.

4. **Dropout for Regularization:** After each Dense layer, Dropout is introduced to prevent overfitting. By randomly deactivating certain neurons during training, it enhances the model's generalizability.

For spectrogram representations, the CNN is specifically designed:

1. **Spectrogram Input:** Given that spectrograms provide a two-dimensional representation of a signal's frequency and time attributes, the CNN, with its ability to recognize local spatial patterns, becomes apt for such inputs.

2. **Hierarchical Convolutional Layers:** Three convolutional layers ensure the extraction of hierarchical features. Basic patterns are captured in initial layers, while deeper layers understand complex ones. The increasing number of nodes across layers (32, 64, and 128) aids this extraction process, a design inspired by architectures like VGGNet [11].

3. **3x3 Filters:** Empirical research, such as the work by the Visual Geometry Group [11], supports the efficiency of 3x3 filters, which are adept at recognizing local patterns.

4. **MaxPooling2D for Dimensionality Reduction:** Following each convolutional layer, MaxPooling2D reduces the spatial size of the feature maps, accelerating computations and inducing translational invariance.

5. **Flattening for FCN Integration:** Prior to merging with the FCN, the CNN's two-dimensional output is flattened, facilitating its integration with fully connected layers.

The outputs of both FCN and CNN branches are concatenated, followed by a Dropout layer for additional regularization. The final output layer has nodes corresponding to the number of classes (real and synthetic in this case), with a softmax activation for probability distribution.

Training the model entails the use of the Adam optimizer, a learning rate of 0.01, and the categorical cross-entropy loss function. We've adopted early stopping (with 5 epochs patience) and restore the best weights when training ends. If the validation loss doesn't improve for 2 consecutive epochs, we employ a learning rate reduction strategy, decreasing it by a factor of 0.5 until reaching a minimum delta of 0.01.

2.2 Data Extraction and Suitability for RIR Classification

Data plays an indispensable role in training any machine learning model. For our RIR classification task, we focus on using audio data files, from which we extract a range of spectral and temporal features using the Librosa library.

We start by loading the audio file with a sample rate of 16,000 Hz, ensuring it is in mono and truncated or padded to a duration of 2.5 seconds. The decision to limit the audio to 2.5 seconds stems from the nature of room impulse responses. In many environments, especially those of interest in our study, the majority of critical acoustic information is contained within the initial 2.5 seconds of the RIR. This includes the direct sound, early reflections, and the start of the reverberation tail. By truncating or padding the signals to this duration, we focus on this rich, informative segment, ensuring that the model is exposed to the most characteristic parts of the RIR while eliminating potential noise or less informative parts that might occur in longer recordings.

This uniformity in data presentation further allows the model to focus on salient feature patterns, promoting a consistent training process and avoiding biases or inconsistencies that might arise from variable data sizes or formats.

2.2.1 Spectral Features

The spectral features extracted include the spectral centroid, spectral bandwidth, spectral flatness, and spectral contrast.

These features provide insight into the tonal characteristics of the sound.

The spectral centroid is a measure that indicates where the center of mass of the spectrum is located. Mathematically, it is defined as:

$$C = \frac{\sum_{n=0}^{N-1} f(n) \cdot X(n)}{\sum_{n=0}^{N-1} X(n)} \qquad (1)$$

where $f(n)$ is the frequency at bin n, $X(n)$ is the magnitude of the frequency bin n, and N is the total number of frequency bins.

The spectral bandwidth is a descriptor that provides the width of the spectral band. It shows how wide the range of frequencies in which most of the spectral content is located. Mathematically, it is defined as:

$$B = \sqrt{\frac{\sum_{n=0}^{N-1} (f(n) - C)^2 \cdot X(n)}{\sum_{n=0}^{N-1} X(n)}} \qquad (2)$$

where C is the spectral centroid calculated using Equation (1).

Spectral flatness measures how noise-like a signal is, as opposed to being tonal. A higher spectral flatness indicates a more noise-like signal. It is defined as the ratio of the geometric mean to the arithmetic mean of the magnitude spectrum:

$$F = \frac{\left(\prod_{n=0}^{N-1} X(n)\right)^{1/N}}{\frac{1}{N} \sum_{n=0}^{N-1} X(n)} \qquad (3)$$

Spectral contrast is defined for each spectral band as the difference between its peak and valley. For each band k:

$$C_k = \max_{f \in B_k} X(f) - \min_{f \in B_k} X(f) \qquad (4)$$

where B_k is the set of frequency bins in band k and $X(f)$ is the magnitude of the frequency bin corresponding to frequency f.

2.2.2 Temporal Characteristics

We also calculate the zero-crossing rate and root mean square (RMS) value, which capture the signal's temporal characteristics. The Zero Crossing Rate is a measure that indicates the rate at which the signal changes from positive to negative or vice versa. Mathematically, it is defined as:

$$Z = \frac{1}{N-1} \sum_{n=1}^{N-1} |\text{sgn}(x(n)) - \text{sgn}(x(n-1))| \qquad (5)$$

where $\text{sgn}(x)$ is the sign function, defined as:

$$\text{sgn}(x) = \begin{cases} 1 & \text{if } x > 0 \\ 0 & \text{if } x = 0 \\ -1 & \text{if } x < 0 \end{cases}$$

and N is the total number of samples in the signal.

The Root Mean Square (RMS) is a measure that provides the square root of the average of the squares of the values in the signal. Mathematically, it is defined as:

$$R = \sqrt{\frac{1}{N} \sum_{n=0}^{N-1} x(n)^2} \qquad (6)$$

where $x(n)$ is the nth sample in the signal, and N is the total number of samples in the signal.

2.2.3 Mel Frequency Cepstral Coefficients (MFCC)

Mel Frequency Cepstral Coefficients (MFCCs) are widely used for speech and audio analysis. The procedure to compute MFCCs involves multiple steps:

The first step often involves pre-emphasizing the signal to increase the amplitude of high-frequency bands. The pre-emphasized signal $y(n)$ is computed from the original signal $x(n)$ as:

$$y(n) = x(n) - \alpha x(n-1) \qquad (7)$$

where α is the pre-emphasis coefficient, typically around 0.97.

The pre-emphasized signal is divided into overlapping frames and each frame is windowed. A commonly used window is the Hamming window:

$$w(n) = 0.54 - 0.46 \cos\left(\frac{2\pi n}{N-1}\right) \qquad (8)$$

The Fourier Transform is computed for each windowed frame to obtain its frequency spectrum.

A Mel filterbank, consisting of overlapping triangular filters, is applied to the power spectrum to extract frequency bands. The Mel scale aims to mimic the non-linear human ear perception of pitch.

Finally, the Discrete Cosine Transform (DCT) is applied to the log energies of the Mel frequencies to obtain the MFCCs:

$$\text{MFCC}_k = \sum_{n=0}^{N-1} \log(E_n) \cos\left(\frac{\pi k(2n+1)}{2N}\right) \qquad (9)$$

where E_n is the energy in the nth Mel filter, and N is the total number of Mel filters.

This results in a set of coefficients that serve as the feature vector for the frame. The procedure is repeated for each frame to obtain a feature matrix for the entire signal.

2.2.4 Energy Distribution of Early and Late Reflections

For Room Impulse Response (RIR) classification, the energy distribution between the early reflections (first 5% of the audio file) and the late reflections (remaining 95%) can provide crucial information.

To compute these features, the signal $x(n)$ is divided into two parts: $x_{\text{early}}(n)$ and $x_{\text{late}}(n)$. The energies E_{early} and E_{late} for these segments are calculated as:

$$E_{\text{early}} = \sum_{n=0}^{N_{\text{early}}-1} x_{\text{early}}(n)^2 \tag{10}$$

$$E_{\text{late}} = \sum_{n=0}^{N_{\text{late}}-1} x_{\text{late}}(n)^2 \tag{11}$$

where N_{early} and N_{late} are the number of samples in the early and late segments, respectively.

2.2.5 Mel Spectrogram

In addition to the features already discussed, a Mel spectrogram of the audio data is also computed for use in Convolutional Neural Networks (CNNs). The power spectrogram is converted into decibels (dB) and its dimensions are expanded to fit the input requirements of the CNN.

$$\text{Spectrogram}_{\text{dB}} = 10 \cdot \log_{10}(\text{Spectrogram}_{\text{Power}}) \tag{12}$$

The expanded dimensions ensure compatibility with the CNN's architectural requirements, providing an enhanced feature set for more robust classification or regression tasks.

It is worth noting how a Mel spectrogram differs from a regular spectrogram in several key aspects:

- **Linear vs Non-linear Frequency Scaling:** A regular spectrogram employs linear frequency scaling, where all frequency bins are equally spaced. On the other hand, a Mel spectrogram utilizes the Mel scale, which is a non-linear scale that mimics the human ear's response to different frequencies.

- **Uniform vs Variable Resolution:** A regular spectrogram offers uniform frequency resolution across the spectrum. In contrast, a Mel spectrogram has higher resolution at lower frequencies and lower resolution at higher frequencies, better aligning with human auditory perception.

- **FFT-Based vs Filter Banks:** A regular spectrogram is often derived directly from the Fast Fourier Transform (FFT) of the signal. In contrast, a Mel spectrogram is usually obtained by applying a set of Mel filters to the power spectrum of the signal.

- **Psychoacoustic Properties:** Due to its design, the Mel scale in a Mel spectrogram captures psychoacoustic properties that are more in line with human perception, making it more useful for tasks like speech and audio recognition.

These diverse and rich features ensure our dataset's aptness for RIR classification. The amalgamation of spectral, temporal, and cepstral features encapsulates both local and global characteristics of the room impulse responses, permitting an exhaustive analysis and thus promising high-accuracy classification.

2.3 Dataset Description

Our dataset was categorized into two primary divisions: Real Room Impulse Responses (RIRs) and Synthesized Impulse Responses.

Real RIRs were captured in various environments, including:

- Faculty classrooms
- Offices
- Residential premises
- Concert halls
- Theaters
- Music studios
- Musical direction areas

The first 2.5s of a real RIR are shown in Fig. 1.
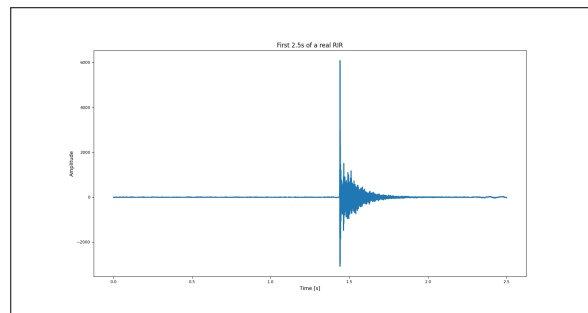
Fig. 1. *First 2.5s of a real RIR.*

Synthesized Impulse Responses were generated using the ODEON software. This software models a variety of spaces, including:

- Parallelepiped rooms
- Churches
- Concert halls
- Rooms with irregular shapes

The first 2.5s of a synthetic RIR are shown in Fig. 2.

About ODEON Software: ODEON is a renowned tool in spatial acoustics, used for both simulations and measurements. It is applied in analyzing sound fields in enclosed environments, such as theaters, concert halls, and music studios, as well as more expansive spaces like stadiums. The software employs a combination of ray tracing models and image-source methods for its simulations.
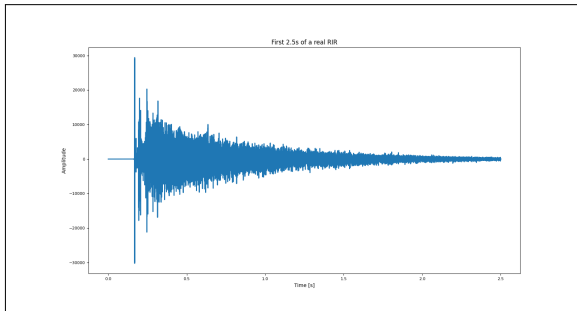
Fig. 2. *First 2.5s of a synthetic RIR.*

With ODEON, users can design rooms of any shape and size, and subsequently inspect the key sound field characteristics at desired points within the room. Its versatility makes it a go-to choice for predicting acoustic profiles in large areas such as concert halls, airport terminals, and metro stations. Furthermore, ODEON introduces a specialized ray tracing algorithm tailored for noise prediction.

Generating an acoustic profile within a room using ODEON requires a geometric model of that room. Users can either create this directly within ODEON or import it from 3D drawing applications like AutoCAD. Once the model is created, ODEON offers tools for visual model validation to ensure its completeness. Any discrepancies detected can be quickly addressed. Every model is comprised of surfaces, each associated with a specific material. These materials, characterized by frequency-dependent absorption coefficients, are well-represented in ODEON's extensive database. This database encompasses almost all conceivable materials found in real-world scenarios. Additionally, users have the flexibility to expand the database by adding new materials and defining their unique absorption coefficients.

Our dataset, diverse in nature, encompasses a broad spectrum of both real and synthesized spaces. With 127 synthetic samples and 267 real samples, it serves as the foundation for our research, aiming for robust and generalized results.

3. RESULTS

This heatmap shown in Fig. 3 illustrates the classifier's performance on the test set. The X-axis represents the predicted labels and the Y-axis represents the true labels. The values in the matrix indicate the number of instances for each combination of predicted and true labels. The high values on the diagonal indicate that the classifier correctly identified a large majority of both real and synthetic room impulse responses, with 88 true positives and 75 true negatives. The off-diagonal values indicate misclassifications, with only one instance of a real response incorrectly classified as synthetic (false positive), demonstrating
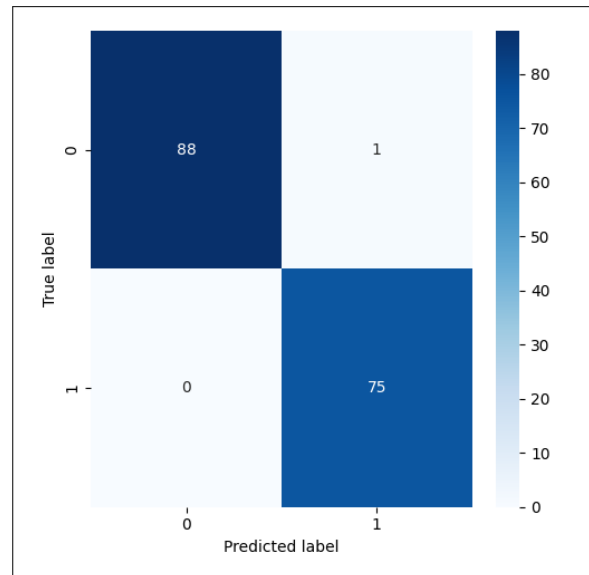
Fig. 3. *Confusion Matrix of the Dual-branch Neural Network Classifier.*

the model's high accuracy.

Metric	Value
Accuracy	0.9939
Balanced Accuracy	0.9944
Recall	0.9944
Selectivity	0.0056
F1 score	0.9939

Table 1. Performance metrics of the dual-branch neural network classifier.

Table 1 represents the performance metrics of the dual-branch neural network classifier. The accuracy, which is the proportion of instances that the model correctly predicted out of all instances, stands at 0.9939, suggesting that our model was able to correctly classify about 99.39% of the instances in the test data. Balanced accuracy, the average of recall obtained on each class, stands at 0.9944. This high score indicates the model's reliability and effectiveness in identifying both real and synthetic room impulse responses. Recall, also known as sensitivity or true positive rate, is a measure of how well the model identified real room impulse responses. With a score of 0.9944, the model correctly identified 99.44% of the real room impulse responses. Selectivity, or the true negative rate, is at a minimal 0.0056, meaning the model misclassified only 0.56% of synthetic room

impulse responses. Finally, the F1 score, which provides a balance between precision and recall, is at a near-perfect 0.9939, indicating that the model achieved an exceptional balance between these two crucial metrics.

4. CONCLUSION

The dual-branch neural network classifier we presented in this paper has shown exceptional performance in distinguishing between real and synthetic room impulse responses, as demonstrated by our results. This performance not only adds credibility to the technique but also opens new avenues for acoustic and audio research, where such distinction plays a pivotal role.

Our model achieved an impressive accuracy rate of 99.39%, demonstrating its robustness in classifying room impulse responses. This high accuracy indicates that the dual-branch architecture, utilizing both a Convolutional Neural Network (CNN) and a Fully Connected Network (FCN), allows for comprehensive analysis of data. The combination of time-frequency characteristics derived from spectrograms processed by the CNN branch, along with a set of acoustical features processed by the FCN branch, was clearly effective.

Moreover, the model achieved a balanced accuracy score of 99.44%, demonstrating its ability to avoid bias and maintain a high level of performance across different classes. This is particularly important in applications where the distribution of real and synthetic room impulse responses can vary widely.

Despite the high performance achieved by our model, it is essential to consider these results within the scope of the current study. The dual-branch classifier's efficacy and efficiency have been proven with our specific dataset and chosen acoustical features. The results may differ if we use other types of data or feature sets. Future studies may further validate and generalize the utility of our model by testing it on other datasets and using other acoustic features.

The implications of our model extend to several domains. In audio forensics, verifying the authenticity of room impulse responses can aid in the detection and prosecution of audio forgery. In acoustic environment modeling and virtual reality, ensuring the accurate representation of room acoustics is crucial for user experience and system performance. We believe our model offers a novel, accurate tool to maintain the integrity and authenticity of room impulse responses in these applications.

5. FUTURE WORK

While the results of our study are promising, there are several areas for further research and improvement:

1. **Dataset Validation:** Further validation of our model on a variety of datasets will contribute to generalizing the model's utility. Different types of room impulse responses and acoustic environments could be used to challenge and refine our model's classification capabilities.

2. **Model Refinement:** The model's performance in specific applications, such as audio forensics or virtual reality, could be investigated and optimized. This would involve tailoring the model to the unique requirements and constraints of these applications, which could lead to improvements in model performance and practical utility.

3. **Feature Set Expansion:** Exploring ways to incorporate other types of data and feature sets into our model can offer new perspectives and enhance the model's performance. Future research could consider the inclusion of additional or alternative acoustic features, or even consider other forms of input such as spatial or temporal data.

4. **Model Interpretability:** As our model becomes more complex, understanding why it makes certain predictions can be as important as the predictions themselves. Future work could include developing methods to better interpret the model's predictions and understand its decision-making process.

In taking these future steps, we will continue to refine and expand the applications of our dual-branch neural network classifier, contributing to the growth and development of the field of audio and acoustic research.

6. REFERENCES

[1] Pätynen, J. and Lokki, T. **Evaluation of Concert Hall Auralization with Virtual Symphony Orchestra,** The Journal of the Acoustical Society of America, 101(6), pp.3517-3524, 2011.

[2] Deppisch, T. and Garí, S. V. A. and Calamia, P. and Ahrens, J. **Direct and Residual Subspace Decomposition of Spatial Room Impulse Responses,** IEEE/ACM Transactions on Audio, Speech, and Language Processing, 31, pp. 927-942, 2023.

[3] Mi, Huan and Kearney, G. and Daffern, H. **Impact Thresholds of Parameters of Binaural Room Impulse Responses (BRIRs) on Perceptual Reverberation,** Applied Acoustics, 134, pp. 1-7, 2022.

[4] Ratnarajah, Anton et al. **Fast-Rir: Fast Neural Diffuse Room Impulse Response Generator,** IEEE International Conference on Acoustics, Speech and Signal Processing (ICASSP), pp. 571-575, 2022.

[5] Pezzoli, Mirco et al. **Deep Prior Approach for Room Impulse Response Reconstruction,** Sensors, 22(7), p.2710, 2022.

[6] Dilungana, Stéphane and Deleforge, Antoine and Foy, C. and Faisan, S. **Geometry-Informed Estimation of Surface Absorption Profiles from Room Impulse Responses,** 30th European Signal Processing Conference (EUSIPCO), pp. 867-871, 2022.

AAAA 2023 IZOLA 20. - 21. September
10th CONGRESS OF THE ALPS ADRIA ACOUSTICS ASSOCIATION

[7] Yu, Wangyang and Kleijn, W. **Room Acoustical Parameter Estimation From Room Impulse Responses Using Deep Neural Networks,** IEEE/ACM Transactions on Audio, Speech, and Language Processing, 29, pp. 436-447, 2020.

[8] Foy, C. et al. **Mean absorption estimation from room impulse responses using virtually supervised learning,** The Journal of the Acoustical Society of America, 150(2), pp.1286-1299, 2021.

[9] Meng, Xiaojing et al. **Diagnostic model optimization method for ADHD based on brain network analysis of resting-state fMRI images and transfer learning neural network,** Frontiers in Human Neuroscience, 2022.

[10] Kayan, Ceyhun Efe et al. **Intensity and phase stacked analysis of a Φ-OTDR system using deep transfer learning and recurrent neural networks,** Applied Optics, 2022.

[11] Simonyan, Karen and Zisserman, Andrew. **Very deep convolutional networks for large-scale image recognition,** arXiv preprint arXiv:1409.1556, 2014.

LCA STUDY OF DIFFERENT RECYCLED SOUND ABSORBERS FROM MELAMINE FOAM WASTE

Urban Kavka[1], Alberto Quintana-Gallardo[2], Martina Marija Vrhovnik[1], Rok Prislan[1]

[1] **InnoRenew CoE, Livade 6a, Izola, Slovenia (urban.kavka@innorenew.eu)**
[2] **Center for Physics Technologies, Universitat Politècnica de València, València, Spain**

Abstract:
The main focus of this study was to investigate the use of melamine foam waste in the production of sound absorption panels, with emphasis on performing a life cycle assessment analysis (LCA) for two different types of sound absorbers. LCA Impacts were studied for panels made from rigid monolithic melamine foam and from randomly cut fragments. Most importantly, the different shape requirements can greatly affect the recycling potential of the material as well as the acoustic and environmental performance. Environmental impacts were calculated for different units. It has been shown that per surface area of sound absorbing panel, which is 0.675 m2, the difference between the two types can be misleading. Therefore, evaluating the environmental impact per sound absorption area in each octave band provides greater potential for a holistic comparison of performance. Along with the acoustic performance studies, the overall performance and impact of each type was determined, with the monolithic type having better overall performance up to 250 Hz and the fragment absorber above. The study provides important insight into the evaluation process by offering a novel comparison of overall performance, P_{AE}.

Keywords: *LCA Study, reusing waste foam, sound absorbers, P_{AE}*

1. INTRODUCTION

The building sector generally needs more sustainable solutions, as the use of buildings accounts for between 30 and 40 percent of total global energy consumption and consequently between 40 and 50 percent of all greenhouse gases [1]. However, not all building components and design areas are pressured into a change equall; among the less affected is building acoustics. Even though its material contribution to the overall building is relatively modest, the drive to reduce the environmental footprint should be as strong in this particular sub-sector as in others.

Two equally important steps can be taken to obtain acoustic elements with lower environmental impacts: either manufacturing elements from renewable materials or recycling and reusing waste materials to extend the life of already embodied energy in the materials. The latter is conventionally overlooked because it is very time consuming, but could be a good option if higher quality waste materials are recycled. One such example is explored in this paper, where melamine foam waste from the production of anechoic chamber at InnoRenew CoE was recycled into sound-absorbing panels meant for lecture halls and offices. The melamine foam waste is of higher quality due to its sound absorbing properties, and it makes sense to reuse it in this case. This was done in two ways; producing sound panels from monolithic foam blocks and using melamine foam fragments obtained by grinding smaller leftovers. The aim of this study is to upgrade comparison of an acoustic performance of two different types of sound insulation panels by assessing and comparing their environmental performance using a life cycle assessment (LCA).

A comparison of sound-absorbing performance was made in a previous study [2], but a calculation error was later discovered and the corrected values are presented here. The calculation error occurred in the calculation of the ratio of melamine foam to voids in the case of the sound absorber type with loose fragments. This ratio was calculated as 2:1, while in reality it is 1:2, which means that there are about 33 % of melamine foam and 67 % of air cavities. This error does not necessarily affect the performance of the panels, but the analysis of the results and the discussion is renewed in this paper.

2. METHODOLOGY

2.1 Subject of study

In this study, two types of sound-absorbing panels with difference in shape of absorption material were analysed; the figure 1 shows the monolithic type with blocks of melamine foam, and the figure 2 shows the absorber with loose melamine foam fragments.

For LCA purposes, a list of materials used in the production

Fig. 1. *Monolithic type of a sound absorber*

Fig. 2. *Fill-in fragment's type of a sound absorber*

of both types of sound-absorbing panels was prepared and is presented in the table 2.1. The main difference between the two types of panels is the amount of melamine foam used and the amount of front textile.

2.2 LCA

A comparative LCA has been performed to assess the differences in environmental impacts of a 0.675 m^2 acoustic panel made with monolithic blocks of waste melamine foam and a similar panel made using fragments of waste melamine foam with fragment sizes up to $\phi 3.0 cm$.

The LCAs were performed according to the guidelines described in ISO 14040:2006 [3] and EN 15804:2020 [4]. The modules considered are A1 to A3, which takes into account all processes from the extraction of raw materials to the manufacture

Material	Monolithic type	Fragment type
Wooden frame (fiberboard)	4,05 dm^3	4,05 dm^3
Fabric (front, 100 % PET)	180 g (Single-layered)	360 g (Double-layered)
Fabric (back, 100 % PP)	150 g	150 g
Melamine foam	255 g	90 g
Screws	8 pieces	8 pieces
Staples	80 pieces	80 pieces

Table 1. List of materials used for the production of <u>one</u> sound absorbing panel for each type.

of the product. This can be considered as "cradle to gate" LCA. One reason for limiting the scope of this study is that cradle-to-gate LCA is considered appropriate for this study, as the possible end-of-life scenarios of both panels can be considered similar, as both use the same raw materials.

2.2.1 Functional unit

The functional unit in a study of LCA refers to the element used as a comparative reference. In this case, the functional unit is the production of a 0.675 m^2 acoustic panel for both types.

2.2.2 Allocation principle

The allocation principle used in this study is end-of-life (EoL) allocation according to EN 15804:2020 [4]. The methodology was adapted from Baldassarri et al. [5] and Lavagna et al. [6] implemented.

2.2.3 Life Cycle Inventory

The software used to create the LCI was Simapro v9.5. Simapro incorporates Ecoinvent V3.9.1, the most comprehensive database for LCA calculations [7]. The data extracted from Ecoinvent represent the average European production of the studied processes.

3. RESULTS

The Environmental Footprint characterization results, given in the table 3, show that the fill-in fragments panel reduces the environmental impact of each studied category. For some impact categories, the impacts are only slightly lower, such as climate change potential, which is reduced by 20 %, and acidification, which is reduced by about 27 %. In the case of water consumption, the water consumption required to manufacture a panel is reduced by 70 %.
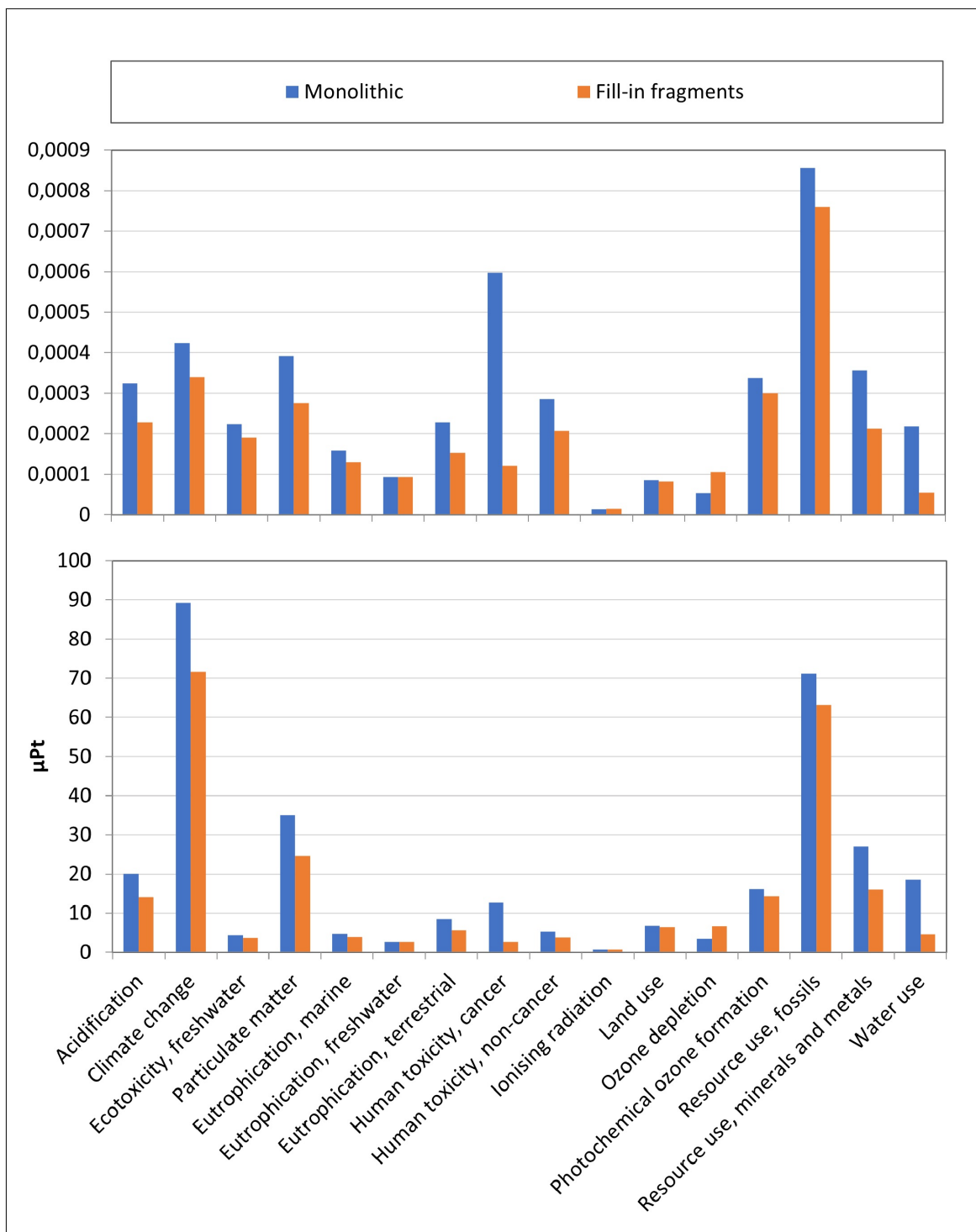
Fig. 3. *Environmental footprint results, firstly normalized (upper graph) and then weighted (bottom graph)*

Damage category	Unit	Monolithic type	Fragment type
Acidification	mol H+ eq	0.0180	0.0127
Climate change	kg CO2 eq	3.20	2.57
Ecotoxicity, freshwater	CTUe	0.0079	0.0083
Particulate matter	disease inc.	3.1905	2.5585
Eutrophication, marine	kg N eq	0.0028	0.0028
Eutrophication, freshwater	kg P eq	7.9059	6.7599
Eutrophication, terrestrial	mol N eq	4.7943	4.0539
Human toxicity, cancer	CTUh	11.3550	9.4744
Human toxicity, non-cancer	CTUh	0.3900	0.4077
Ionising radiation	kBq U-235 eq	0.9552	0.9316
Land use	Pt	2.33E-07	1.64E-07
Ozone depletion	kg CFC11 eq	3.09E-03	2.54E-03
Photochemical ozone formation	kg NMVOC eq	1.50E-04	1.50E-04
Resource use, fossils	MJ	4.04E-02	2.71E-02
Resource use, minerals, and metals	kg sb eq	1.03E-08	2.08E-09
Water use	m3 depriv.	1.32E-09	1.10E-09

Table 2. Environmental footprint characterization results for the monolithic and fragment type of sound absorbing panel.

In the upper graph of Figure 3, the normalized results reveal a high impact on Resource Use in both panels. There is a significant difference between the human toxicity category in the two panels. The main reason for this result is the toxins associated with the urea production, which is necessary to manufacture melamine foam. According to the weighting (see lower diagram in Figure 3), the categories Climate Change and Resource Use are those with the higher relative importance. Considering that the results are normalized and weighted, the environmental footprint offers the possibility of obtaining a single impact score result by adding up each category. The single score result for the monolithic panel is 326.22 µPt, while that for the fill-in fragments is 244.70 µPt.

4. DISCUSSION

Selection of the most suitable sound absorbers focuses on the acoustic performance of the panels, which is later influenced by the LCA study or the comparison of other aspects. Therefore,

the sound absorption coefficients are the key to decision making and are shown in the figure 4.
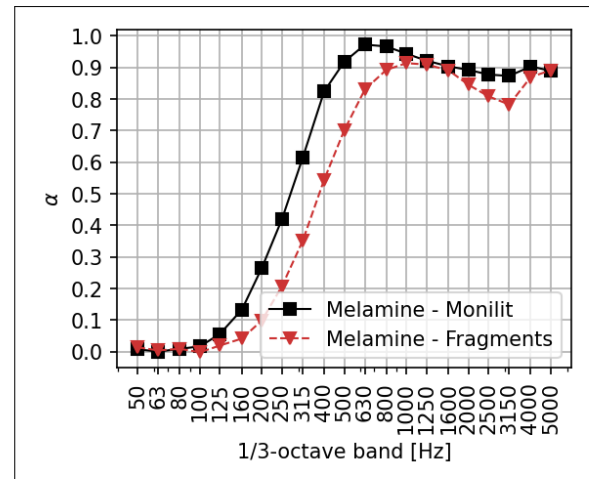
Fig. 4. *Sound absorption coefficients for monolithic melamine foam panels and panels with fill-in melamine foam fragments in 1/3-octave bands*

As can be seen in the figure, the fragment absorber curve shifts to the higher frequencies for about two 1/3-octave bands. Considering the final use of the panels in lecture halls and offices, the focus of the study was narrowed down to octave bands between 125 Hz and 4000 Hz, covering the octave bands of the human voice and the highest sensitivity of human hearing.

The objective of the study was to determine a single value representing both sound absorption and environmental performance, although frequency dependence could not be avoided. Since an increasing value of α improves the performance of the panel, and a decrease in the single score result of LCA also improves the performance, the following equation for calculating a single value performance, denoted by P_{AE}, was proposed to merge the two characteristics:

$$P_{AE} = \frac{\alpha}{LCA_{single\ score}}$$ (1)

,

where $LCAsingle_score$ is the single score result calculated as the sum of the weighted and normalized significant parameters of the LCA study, and α is the sound absorption coefficient in each octave band of the respective product. The calculated values of P_{AE} for the monolithic and fragmented types are shown in the table 4, where a higher value represents a panel with better overall performance.

As can be seen in the table 4, the monolithic panel type generally has better overall performance up to the 250 Hz octave band and the fragment type of a panel has better overall performance above 250 Hz.

Frequency [Hz]	P_{AE}	
	Monolithic	**Fragment**
63	0.00	4.09×10^{-5}
125	1.84×10^{-4}	8.17×10^{-5}
250	1.23×10^{-3}	8.17×10^{-4}
500	2.54×10^{-3}	2.82×10^{-3}
1000	2.64×10^{-3}	3.68×10^{-3}
2000	2.48×10^{-3}	3.47×10^{-3}
4000	2.48×10^{-3}	3.47×10^{-3}

Table 3. P_{AE} values for both types of panels in each dependency of the frequency.

There are also two ways to ease this comparison. First, the thickness of the fill-in fragment type could be increased so that the curve of the absorption coefficient in the figure 4 would shift to lower frequencies to the point where the curves of both elements would coincide. In this way, it could be assumed that the acoustic performance of both types is the same. Based on the modified dimensions of the acoustic panels, a new LCA study would then be carried out, the results of which would already be suitable as individual values for comparing the overall performance.

Second, a fill-in fragment type could be modified so that the consumption of melamine foam would be the same for both elements. Assuming that the consumption of other materials does not change significantly, or that a change in their quantity does not significantly affect the LCA study, an assumption of equal environmental footprint results could be made. Thus, acoustic performance would be the main subject of performance comparison. However here it is important to check for the effect of each material used and determine if melamine foam has the greatest impact on the environmental footprint.

5. CONCLUSION

The fill-in fragment panel reduces the carbon footprint by 20 %, which is similar to reduction in the absorption coefficient in the frequency range 125 and 500 Hz, where the difference between the two absorbers is largest. According to the individual results obtained by the Environmental Footprint methodology, the total environmental impact is reduced by 25 % in the case of the fragmented absorber type compared to the monolithic type.

Finding ways to reuse materials is crucial for a more sustainable construction industry. In terms of environmental performance, these materials have two main advantages: first, the amount of waste is reduced due to a higher recycling rate, and second, the use of new raw materials and the impacts associated with the production process of the new product are avoided. In the case of the sound absorbers studied, the melamine foam and the PP fabric were used as waste materials from the pro-

duction of other products, hence their influence on the overall environmental footprint could be disregarded. Such a principle could be applied in our study, but it would significantly change the results of the LCA study. Consequently, the influence of processes would be higher, so it would be important to consider the exact differences in the processes required and their resources for the production of each absorber type.

For a holistic assessment of the overall performance of absorbers, the production processes and their environmental footprint should be included, along with an extension of the LCA study to cradle-to-cradle scope. Most importantly, different shape-related requirements can largely influence the recycling potential of the material. Therefore, it would be important to ask how the reusability and recyclability, especially of the fill-in fragment panel type, can be assessed or even quantified.

The proposed single-value characterization of overall acoustic and environmental performance, P_{AE}, is a novel step towards a holistic evaluation of acoustic elements to not only obtain desired acoustic result, but also to contribute to the reduction of environmental impact in the building sector. Nevertheless, the proposed single-valued performance quantifier needs further development and research as it is still frequency dependent. Another obstacle to be overcome is that the acoustic performance is normalized and quantified between 0 and 1. On the other hand, the single score result of the LCA study depends on the selection of significant parameters and has no upper limit. Hence dividing α by the LCA single-score result yields small numbers, and the difference between the scores of the different subjects in the comparison does not necessarily tell us about the actual difference in overall performance. It could also be modified to consider only a single category of environmental footprint category, such as water use. Another way to overcome this obstacle, instead of using P_{AE}, is to change the dimensions of the panels to match either the acoustic performance or the LCA results, and then compare the other. Nevertheless, the novel integration of LCA and acoustic performance is recognised as a potential area for future research.

6. REFERENCES

[1] T. Ramesh, R. Prakash, and K. Shukla, "Life cycle energy analysis of buildings: An overview," *Energy and Buildings*, vol. 42, pp. 1592–1600, 10 2010.

[2] U. Kavka, M. M. Vrhovnik, and R. Prislan, "The potential of melamine foam waste: Performance comparison of monolithic foam block and loose foam fragments used as a filler for sound absorbing panels," 2023.

[3] Standard, "Iso 14040:2006 environmental management — life cycle assessment — principles and framework," 2006.

[4] C. E. N. EN, "15804: 2012+ a2: 2019—sustainability of construction works—environmental product declarations—core rules for the product category of construction

products," *European Committee for Standardization (CEN): Brussels, Belgium*, 2019.

[5] C. Baldassarri, K. Allacker, F. Reale, V. Castellani, and S. Sala, *Consumer Footprint. Basket of Products indicator on Household goods*. 2017.

[6] M. Lavagna, C. Baldassarri, A. Campioli, S. Giorgi, A. D. Valle, V. Castellani, and S. Sala, "Benchmarks for environmental impact of housing in europe: Definition of archetypes and lca of the residential building stock," *Building and Environment*, vol. 145, 2018.

[7] G. Wernet, C. Bauer, B. Steubing, J. Reinhard, E. Moreno-Ruiz, and B. Weidema, "The ecoinvent database version 3 (part i): overview and methodology," *International Journal of Life Cycle Assessment*, vol. 21, 2016.
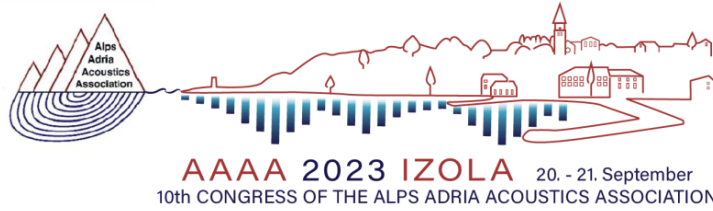
MULTICHANNEL REVERBERATION TIME MEASUREMENTS OF MIURA-ORI ORIGAMI IN ALPHA CHAMBER

Jurij Prezelj, Andrej Hvastja, Ema Letnar, Miha Brojan

Faculty of mechanical engineering, University of Ljubljana

Abstract: *In this research, we introduce and validate a novel LabVIEW program tailored to evaluate sound absorption characteristics of materials in custom made alpha chamber, specifically for Miura-Ori origami structures crafted from thick paper. Initial validation involved simulating sound dissipation signals, using harmonic signal with an exponential function representing sound energy decay. Software validation was performed by matching synthesized theoretical signal with the program's outputs. Practical validation was demonstrated using a stone wool sample, with known sound absorption from interlaboratory comparison. During validation a hypothesis that progressively increasing the number of reverberation time evaluations in the alpha chamber, averaged result drifts closer to its inherent reverberation time. The purpose of new LabView program for multichannel measurements of reverberation time and sound absorption is to observe a relationship between material/structure acoustic attributes and experimental setups, and to confirm the hypothesis that a significant correlation exists between the sound absorption frequency and the spatial frequency of the Origami surface. This hypothesis was placed after a reactive behavior in the sound absorption mechanism of Miura-Ori Origami structure was identified while observing a correlation between the sound absorption spectrum and the spatial Fourier transformation spectrum of the origami structure surface.*

Keywords: Reverberation Time, Sound Absorption Coefficient, Spatial frequency, Two-dimensional Fourier transformation, Alpha Chamber, Diffuse Sound Field, Resonant Absorption, Multichannel Software

1. INTRODUCTION

Noise control is vital in numerous engineering applications, from designing quiet vehicle interiors to developing noise-dampening building materials, advanced communication technologies, and medical devices. A successful noise control strategy hinges on a profound understanding of the sound absorption and resonance characteristics of the involved materials and structures.

Traditionally, sound management has relied on materials with static geometric properties. Once manufactured and installed, their acoustic properties remain fixed. This rigidity has prompted researchers to seek adaptive, flexible structures capable of dynamic sound absorption and directionality control, entering the world of origami-inspired structures.

Origami, the Japanese art of paper folding, is renowned for its distinctive mechanical attributes and adaptability. Beyond art, its principles can inspire the creation of versatile, reconfigurable structures apt for various engineering feats. In acoustics, such structures hint at groundbreaking sound-absorbing materials and devices. These devices can dynamically alter their form and functionality, enabling real-time modulation of acoustic properties. Our research therefore bifurcates into two interconnected segments:

1. Development and Validation of Measurement Procedure: We introduce an innovative multichannel procedure to determine the reverberation time (T) within a compact reverberation chamber. Our methodology circumvents the hurdles tied to capturing precise T measurements in imperfectly diffusive acoustic environments. We achieve this by amplifying the

measurement volume and enhancing their spatial distribution.

2. Exploration of Origami Mechanics in Acoustics: Delving deep into the mechanics of origami structures, we probe their sound absorption capabilities. Our objective is twofold: to recognize potential acoustic resonances and to assess the adaptability of origami for acoustic applications. We harbor a keen interest in understanding the relationship between the two-dimensional Fourier transformation of the origami surface and its sound absorption coefficient.

2. ORIGAMI IN ACOUSTICS

Origami, inspired by the ancient art of paper folding, has stimulated innovation across numerous engineering domains, from robotics and biomechanics to architecture and aerospace [1]. Fonseca et al. emphasized this trend, noting that its full potential, especially in acoustics, is still untapped [1].

Benefits of Origami Designs: Origami structures bring about transformative capabilities like structural reconfigurability, acoustic tunability, and design flexibility. Such features address current shortcomings in sound attenuation devices, especially the limited adaptability of silencers to multiple operational scenarios [2].

Broadband Acoustic Absorption: The pursuit for effective absorption across a wide frequency range is paramount. Yet, many contemporary methods face challenges, such as bulky designs or narrow absorption bandwidths. Origami structures, however, shine by widening the sound absorption spectrum and bolstering low-frequency sound absorption — a promising avenue for controlling low-frequency noise [2, 3].

Innovative Origami Applications:
o J. Xiaomeng et al. developed origami windows whose opening area can be adjusted by a single-degree-of-freedom folding mechanism, achieving significant transmission loss while maintaining ventilation [44].
o Harne et al. highlighted the utility of a Miura-Ori-based acoustic array for focused acoustic energy, while Pratapa et al. engineered origami-inspired metamaterials with notable acoustic switching potential [5, 6].
o Yu et al. and Xiang et al. explored reconfigurable 3D sound barriers using the Miura-Ori pattern, emphasizing their advantages over traditional barriers in terms of adaptability, portability, and cost [7].

o Diamant et al. innovated an acoustic tank with Miura-Ori patterned absorption plates [8], while Zou et al. investigated arrays rooted in origami tessellations [9,10].
o Modular origami as adaptable silencers were studied by Fang et al. and Zhu et al., with a focus on tunable sound attenuation [2, 11].
o Jiang et al. unveiled an origami-based sound absorber displaying adjustable resonance frequencies, with a noticeable average sound absorption coefficient [3].
o Cambonie et al. employed origami spirals in compact quarter-wavelength resonators, simulating the absorption properties of longer designs [12].

Origami and Wave Energy: The periodic nature of origami structures, with inbuilt bandgap features, can effectively guide wave energy [13]. The potential to adjust waveguide frequency, especially during transitions between lattice types, underscores the adaptability of origami in acoustic applications [13].

Considering the promising directions identified in existing literature, our research sought to bridge a gap, by placing a hypothesis:

Hypothesis 1: A significant correlation exists between the sound absorption frequency and the spatial frequency of the Origami surface.

We conceptualized a multichannel measurement system (Alpha chamber with the fitted LabVIEW program) for speeding up the assessments of sound absorption. With most of the research emphasizing impedance tube measurements, a void remains concerning origami structures' sound absorption evaluations in real-world settings, particularly in diffuse sound fields. This experimental pursuit is made to understand the origami structures' sound absorption abilities.

3. MEASUREMENTS OF SOUND ABSORPTION

Sound absorption materials are critical in diverse noise control scenarios, spanning room acoustics to automotive interiors. Standard practice often measures their attributes using impedance tubes and small samples, working under the presumption of a one-dimensional sound field. Yet, these conditions seldom mimic real-world scenarios, where materials of varying sizes and shapes are used in multidimensional sound fields.

In response to this discrepancy, the reverberation chamber, in line with the international standard ISO 354,

2003 [14], has emerged as an alternative. However, crafting these expansive chambers for absorption coefficient evaluations is both costly and labor-intensive. A more recent solution has been the introduction of alpha chambers, compactly sized at roughly 6.4 m³.

Still, alpha chambers are not without limitations. Their performance tends to falter, particularly at lower frequency ranges, where a distinct shift from the standing sound field to the diffuse sound field becomes apparent. In such scenarios, factors like the chamber's geometry, positioning of samples, location of the sound source, and microphone placement can greatly skew absorption coefficient readings.

A diffuse sound field has uniformly distributed sound energy where propagation directions are random at any point. Perfect diffusion is theoretical and used for reverberation time calculations. Randall et al. [15], highlighted that poor absorption distribution reduces diffusion in specific frequencies. Adjusting room geometry can improve diffusivity but might negatively impact other frequencies. Better surface absorption distribution or introducing artificial diffusers can enhance room diffusivity.

In the work of Cops et al. [16], they raised the question, "Does the room's diffusivity improve with the increase in the number of diffusers or by decreasing the axial and tangential modal locations at the reverberation corners?" Figure 1 shows a test with one wall covered in absorbent material (condition A8), leading to uneven absorption. In condition A9, 12 diffusers were added, and in A10, they were replaced with absorbent material. The overall room absorption in the frequency range remained largely consistent. Diffusers significantly influence the room's absorption.
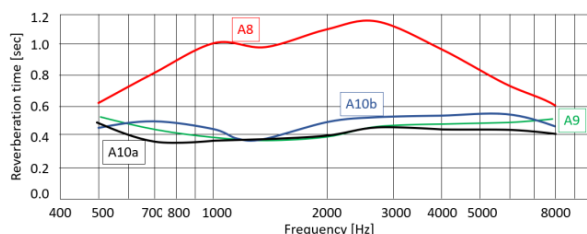

Figure 1: Reverberation time of the space under conditions A8, A9, and A10, [15].

When examining a room where absorption was unevenly distributed, placing diffusers and improving the distribution of absorption throughout the room enhanced the level of diffusion. They observed that measurements taken in a slightly larger room with non-parallel walls showed that the difference between untreated and treated walls was not so pronounced. This indicates that non-parallel walls improved the diffusion level, regardless of wall treatment.

Despite large amount of literature, there is no study available in which necessary number of measurements would be proposed as function of the Relative Standard Deviation (RSD), and to dive into the possibility to overcame problems of non ideal diffuse field by significantly increasing the number of measurements. Driven by this insight, our research postulates the second hypothesis:

Hypothesis 2: By progressively increasing the number of reverberation time evaluations in the alpha chamber, we inch closer to the chamber's true, inherent reverberation time.

Based on the outlined problem, we developed software for sound absorption measurements in small reverberation chambers. This software offers multi-channel reverberation time measurements. Such multi-channel measurement capability allows for simultaneous signal capture from microphones at various positions, considerably shortening the measurement procedure duration. Furthermore, the streamlined nature of the process enables the execution of a larger number of measurements. As the number of measurement points increases, the measurements become less influenced by the chamber's inherent characteristics, such as the challenge presented by an imperfect diffuse sound field, which is a significant concern in the utilization of such systems.

3.1 Theoretical background

The evaluation of acoustic properties within enclosed environments necessitates the understanding and accurate calculation of reverberation time (T). Reverberation time is a pivotal parameter, defined as the duration for the sound pressure level in a space to decrease by 60 dB after the cessation of a sound source. Its precise calculation offers insights into the acoustic quality of spaces, from intimate living quarters to grand concert halls. For the calculation of reverberation times, we can use several methods presented in the work of Kinsler et al. [20]. Historically, researchers have employed

various methods to compute reverberation times. One of the influential works in this field is that of Kinsler et al. [20], which presents a more methodologies. Among these, Sabine's and Eyring's methods are frequently employed due to their efficacy and historical significance. As presented in the work of Beranek [17], Sabine's equation is derived under the assumption that sound waves reflect sequentially from wall to wall. Another commonly used method, the Eyring method, assumes that the initial waves reflect off all the walls of the room at once, with subsequent reflections reducing the sound energy by the average absorption coefficient of the room. However, in our study the standardized EN SIO 354-2003 method was used.

In the EN ISO 354-2003 standard, two methods for performing T reverberation time measurements are presented: the interrupted sound source method and the integrated impulse method. When using the signal interruption method, the standard provides the following recommendations:

- Microphones used for reverberation time measurements should be omnidirectional.
- Multiple measurements should be made with microphones spaced at least 1.5 m apart. They should be at least 2 m away from the sound source and at least 1 m away from the walls.
- The number of independent sound energy dissipation measurements should be at least 12. At least three microphone setups and two different sound source locations should be used for measurements.
- The noise playback time should be sufficient to fill the space with sound and achieve a balanced sound pressure level across the entire frequency range. Only then can the source be turned off.
- The sound pressure level before turning off the source should be high enough that the measurement ends at least 10 dB above the ambient sound pressure level.

To reduce measurement uncertainty, the standard recommends averaging at least three measurements on each microphone. In calculations, it is important to consider that the starting point of the considered range is 5 dB below the initial sound level. The range should be within 20 dB. The lower limit of the range should be 10 dB above the background noise level.

As mentioned at the beginning of the chapter, to determine the absorption coefficient, the equivalent surface of the sample must first be calculated. The calculation of the equivalent surface of the sample is approached as follows. First, we calculate the equivalent absorption surface of the empty reverberation chamber A_1 using the following equation:

$$A_1 = \frac{55{,}3\,V}{cT_1} - 4Vm_1 \tag{1}$$

where V is the volume of the empty reverberation chamber in cubic meters, c is the speed of sound, T_1 is the reverberation time of the empty reverberation chamber in seconds, and m_1 represents the coefficient for recording the climatic effects on sound absorption in the air. This changes with changes in temperature, humidity, and air pressure in the reverberation chamber. The coefficient m1m1 is calculated using the following equation:

$$m_1 = \frac{\alpha}{10 \log e} \tag{2}$$

The sound damping coefficient α is due to atmospheric influences. As presented in the ISO 9613-1:1993 standard [14], this is calculated as follows:

$$\alpha = 8{,}8686 f^2 \left(\left[1{,}84 \cdot 10^{-11} \left(\frac{p_a}{p_r}\right)^{-1} \left(\frac{T}{T_0}\right)^{1/2} + \left(\frac{T}{T_0}\right)^{-5/2} \right. \right. \tag{3}$$
$$\cdot \left\{ 0{,}01275 \left[e^{\frac{-2239{,}1}{T}} \right] \left[f_{rO} + \left(\frac{f^2}{f_{rO}}\right) \right]^{-1} \right.$$
$$\left. \left. + 0{,}1068 \left[e^{\frac{-3352{,}0}{T}} \right] \left[f_{rN} + \left(\frac{f^2}{f_{rN}}\right)^{-1} \right]^{-1} \right\} \right)$$

The coefficients f_{rO} and f_{rN} represent the relaxation frequencies of oxygen and nitrogen. Their values are given by the following equations:

$$f_{rO} = \frac{p_a}{p_r} \left(24 + 4{,}04 \cdot 10^4 h \frac{0{,}02 + h}{0{,}391 + h} \right) \tag{4}$$

$$f_{rN} = \frac{p_a}{p_r} \left(\frac{T}{T_0}\right)^{-1/2} \left(9 + 280h \cdot e^{-4{,}170 \left[\left(\frac{T}{T_0}\right)^{-1/3} - 1 \right]} \right) \tag{5}$$

Similarly, we calculate the values when using a sample. The equivalent absorption surface of the reverberation chamber with the inserted sample A_2 is calculated using the equation (1) where the values V, c and m have the same values, but T1 is replaced by T2 representing the reverberation time of the reverberation chamber with the inserted sample. The equivalent surface of the absorption material A_T is then calculated using the equation:

$$A_T = A_2 - A_1 = 55{,}3V \left(\frac{1}{c_2 T_2} - \frac{1}{c_1 T_1}\right) - 4V(m_2 - m_1) \tag{6}$$

With the calculated equivalent surface of the absorption material, the sound absorption coefficient α_s is calculated using the equation (9), where S represents the floor or wall surface covered by the sample.

$$\alpha_s = \frac{A_T}{S} \qquad (7)$$

3.2 Experimental setup

The acoustic measurements for our study were conducted in a reverberation chamber, with a sound field volume of V=6.44 m³. As described by Vrtovec [18], the chamber has a dimensional ratio of 1.4:1.2:1. The primary support structure, depicted in Figures 1 and 2, integrates wooden and wood-steel composite beams. Both the interior and exterior surfaces of the chamber are lined with 2 layers of plasterboard, and recycled compressed polyurethane foam offers the necessary sound insulation.
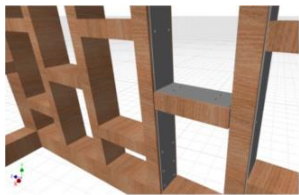
Figure 2: Wood-steel composite beams detail [18]

Figure 3: Load-bearing structure overview [18]

Standing sound fields, observable across all frequencies as shown in Figure 3, are marked by positional variances in their minima (represented as lines) and amplitude fluctuations (deduced from the color scale). The interplay between the sample's positioning and the standing sound field's orientation is critical. The variation in standing wave patterns necessitates a higher measurement frequency, ensuring results are more accurate and indicative of the actual sound behavior within the chamber.
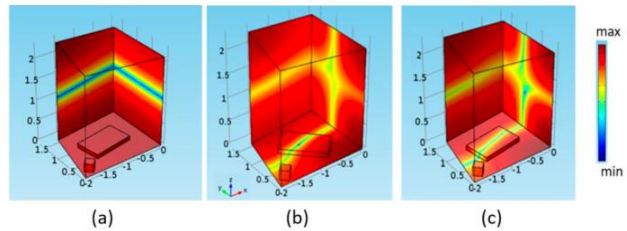

Figure 3: Reverberant modal sites as influenced by audio signal frequency.

Considering the influence of various standing wave patterns on results, executing a higher number of measurements is imperative. This approach ensures minimizing any discrepancies introduced by the natural interactions of sound waves within the chamber, rendering results more accurate and representative.

Our signal generation combines a cosine function (simulating harmonic sound wave propagation) and an exponential function (emulating sound energy decay over time). The reverberation time, T, represents the period required for a sound level to drop by 60 dB. For this study, a synthesized signal with a T set to 1s at 1000 Hz frequency was chosen. Figure 5 depicts the decline in sound pressure level during the validation process.
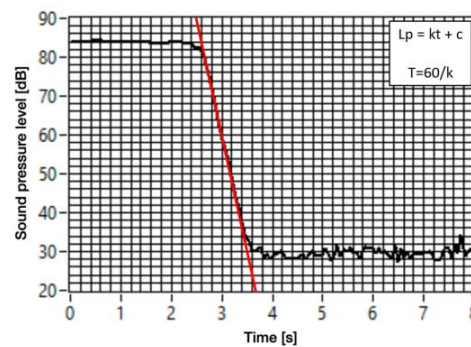
Figure 4: Sound pressure level drop during validation

Table 1: Reverberation Times obtained during the Validation, performed on synthesized signal.

Central frequency [Hz]	500	630	793,7	1000	1259,9	1587,4
Measured reverberation time T [s]	NaN	NaN	1.0405	1.0112	1.0393	NaN

Table 1 shows the measured values of *T* for selected narrow range of central frequencies. A NaN (Not a

Number) value is noted where the level calculation was unsuccessful, due to either the absence of the signal in that frequency range or a too low signal-to-noise ratio.

4. MEASUREMENTS RESULTS

4.1 Reference Measurement

Selected reference sample for validation of the method is stone wool, a non-flammable fibrous material widely recognized for its thermal insulation capabilities, largely attributed to its sound isolation qualities. With dimensions of 0.6 m x 1 m x 0.06 m, the sample has a width-to-length ratio of 0.6. When we account for side surfaces, its total surface area is 0.984 m^2. This results in a ratio E=5.3 between the perimeter and surface area of the sample. This sample was particularly appealing for our study as it had undergone previous reverberation time measurements, has therefore known values of sound absorption, obtained from interlaboratory comparisons, using traditional methods, making it an ideal reference point for our research.

The reference measurement was conducted in the same alpha chamber as the subsequent measurements. The reference method is considered the commercial method provided by the instrument Norsonic Nor-140. As shown in Figure 5, 39 reverberation time measurements were taken in the empty alpha chamber, while 19 were recorded with the stone wool sample present. The sample, comprising two stone wool pieces described earlier, was positioned at the chamber's center floor. These pieces were stacked, resulting in dimensions of 0.6 m x 1 m and a thickness of 0.12 m. The sample was angled at 45° relative to the entrance plane. Throughout the measurements, only the microphone positions varied; the sound source and sample remained constant, with the source located at the bottom-left corner of the alpha chamber. Graphical representations are provided, illustrating the stabilization of the reverberation time value T with increasing number of measurements, and hence drifting the results to its true value, Figures 5 to 8.

These stabilization graphs were constructed in such a way that the n-th measurement of the reverberation time represents the average of all previous measurements. At lower frequencies, there's visible "creep," potentially indicating a too-small number of measurements. With an increased number of measurements, the creep is changed

to drift and finally stabilizes to constant value. Transition depends on frequency. Value of T for Frequencies above 300 Hz is stabilized much sooner, while below 300 Hz a noticeable drift is observed even after 35 measurements.
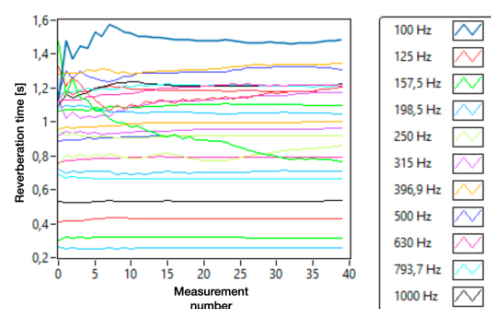
Figure 5: Drifting of the averaged reverberation time value to its inherent value with increasing number of measurements, for the reference measurement of the empty alpha chamber.
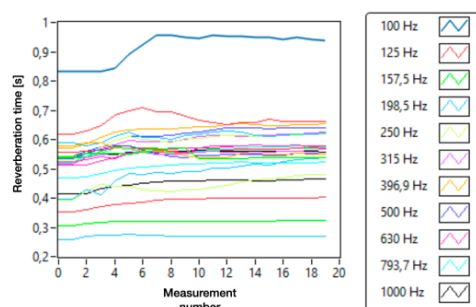
Figure 6: Drifting of the averaged reverberation time value to its inherent value with increasing number of measurements, for the reference measurement of in the presence of a sample.

We closely examined the length of the signal playback, impacting the data points captured for determining the sound level decay curve. We conducted 80 reverberation time measurements in the alpha chamber: both when empty and with a sample shown in Figures 7 and 8, which was a 0.6 m x 1 m stone wool layered configuration angled at 45° to the entrance plane. While we adjusted microphone and sound source positions throughout the experiment, the sample remained stationary. Playback durations varied between a shorter 4-second span and a longer 9-second span, with noise filtered between 80 Hz and 10,000 Hz.

Figure 7: Stabilization of the reverberation time values for the shorter (A) and longer (B) playback time measurement in the case of an empty alpha chamber.

Figure 8: Stabilization of the reverberation time values for the shorter (A) and longer (B) playback timer measurement in the presence of a sample.

Crucially, the outcomes from the 80 measurements using our methodology and software were consistent, displaying results within ±5% of sound absorption for frequencies above 300 Hz, in line with the reference method. Our system displayed superior precision in measuring reverberati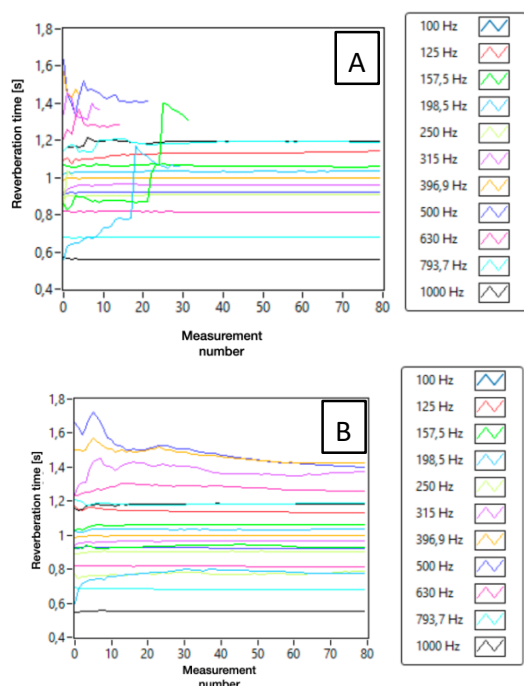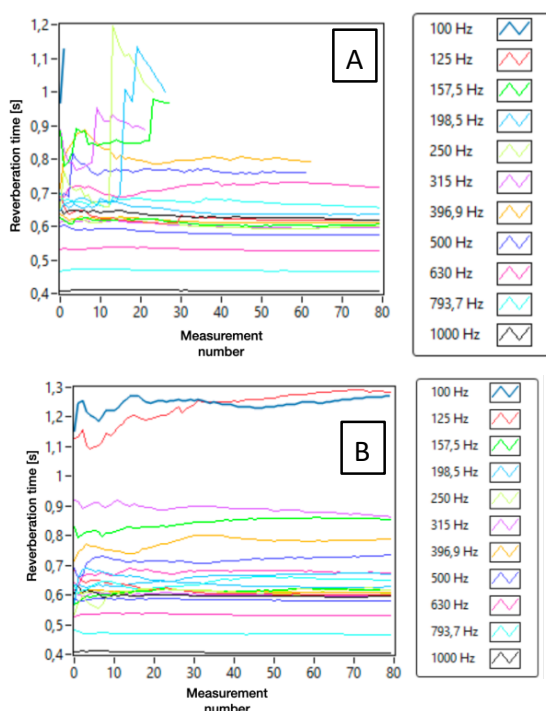on time T below 300 Hz compared to the reference method. Furthermore, the use of our advanced software ensured that the time required for the 80 measurements (consisting of 10 repetitions with 8 microphones) was equivalent to that of 20 repetitions using the reference system with a single microphone. This highlights the enhanced efficiency and precision of our approach.

As the number of measurements increased, clear variations appeared, indicative of the stabilization of reverberation times. This pattern supports the primary hypothesis: increasing data points for reverberation time measurements progressively approximates the true reverberation time inherent to the alpha chamber.

4.2 Precision assessment - Probing with a plain Paper

A plain paper, sized 0.60 m x 0.60 m, was placed centrally on the alpha chamber's floor to evaluate measurement accuracy. In an unobstructed environment, 79 reverberation time readings were collected, compared to 55 when the paper was present. Notable variations in the Relative Standard Deviation of Reverberation Time Measurement (RSD) were observed within the 100 Hz to 500 Hz frequency range. This suggests the possible presence of resonant absorption elements. The inconsistencies in the measurements might stem from the paper's uneven placement and its direct contact with the floor. The presence of an air gap could have made the paper act as a reflective surface. This emphasizes the importance of maintaining an air gap for resonant absorption materials, allowing for energy dissipation through sample oscillations. However, Figure 9 demonstrates that the paper, when placed on the floor, primarily absorbs in a restricted higher frequency range, while deviations from zero in frequency range below 300 Hz can be attributed to the non diffuse field. We can say again that method and measuring system provide acceptable results in frequency range above 300 Hz and very good results in frequency range above 1000 Hz and up to 5 kHz.
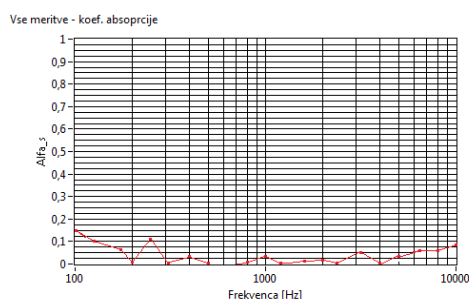
Figure 9: Coefficient of absorption of paper sheet

4.3 Measurement results of the origami structure

Figure 10 displays samples of the Miura-Ori origami crafted from paper. Their corresponding absorption coefficient spectra are depicted in Figure 11. An analysis of these results reveals that different samples exhibit peak absorption coefficients at varying frequencies. Specifically, samples ORIG_1_1,2,3 achieve their highest absorption at 3125 Hz (as seen in Figure 11A), while samples ORIG_2_4,5,6, indicate their peaks absorption at 1600 Hz (Figure 11B).

results below 300 Hz possess a deviation exceeding 0.1 s, thereby affecting the precision of the absorption calculations. Conversely, for frequencies above 500 Hz, the deviation is less than 0.05 s, which assures accurate results. Remarkably, a consistent frequency of the absorption peak is observed for the same type of folding.
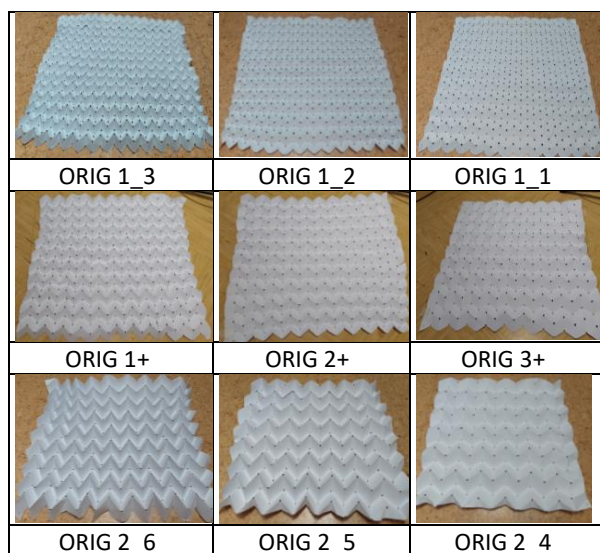
Figure 10: Samples of the Miura-Ori origami, made from paper are shown.

Notably, the sound absorption measurements suggest that some samples may have limited absorption in the frequency range below 300 Hz. This observed behavior could potentially stem from the higher RSD in this frequency range. The relative standard deviation of these measurements is presented in Figure 11D. It's evident that

Figure 11: Sound absorption measurement for samples:
A (ORIG 1_1, ORIG 1_2 and ORIG 1_3)
B (ORIGAMI 2_4, ORIGAMI 2_5 and ORIG 2_6)
C (ORIG 1+, ORIG 2+ and ORIG 3+)
and relative standard deviation RSD of reverberation time measurement, averaged for all measurements in D

To interpret the measured results, we considered the impact of sound refraction. Consequently, the surface of the origami structure was analyzed in detail, based on the analytical description of its surface, followed by a Fourier transformation analysis. Following hypothesis can be proposed: There is significant correlation between Sound absorption frequency and spatial frequency of Origami surface.

5. CORRELATION BETWEEN THE SPATIAL FREQUENCY AND SOUND ABSORPTION FREQUENCY

The specimens studied in this research were flexural specimens and the Miura-Ori model was used to make them. The geometric relationships required to achieve the Miura pattern were extracted from the reference [19]. The Miura-Ori pattern is specified on an unfolded plane by parameters a, b, and φ. The angles between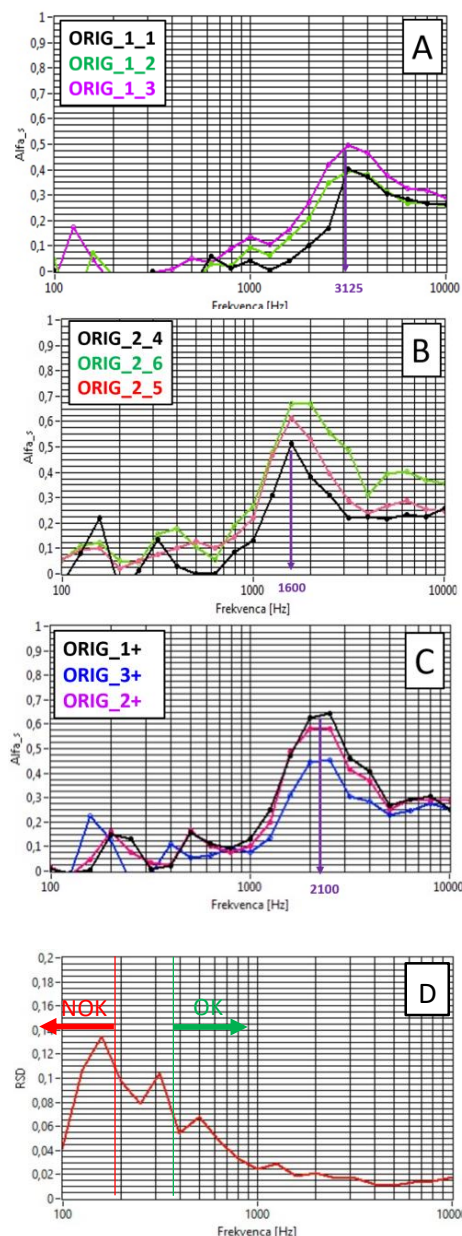 the planes are denoted as θ_A and θ_Z and the angles between the edges as η_A and η_Z and were used to determine the geometry of the folded shape, as shown in figure below.

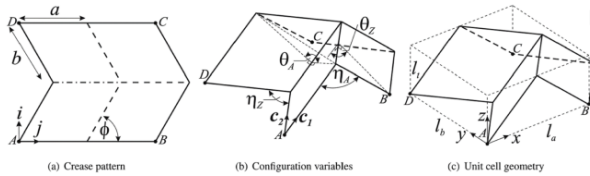(a) Crease pattern   (b) Configuration variables   (c) Unit cell geometry

Figure 12: Miura-Ori geometry

In this model, the following six relationships are established between the parameters:

$(1 + \cos\eta_Z)(1 - \cos\eta_A) = 4\cos2\phi$ (10)

$\cos\eta_A = \sin2\phi\cos\theta_Z - \cos2\phi$ (11)

$\cos\eta_Z = \sin2\phi\cos\theta_A + \cos2\phi$ (12)

$l_a = 2a\sin(\eta_A/2)$ (13)

$l_b = 2b\sin(\eta_Z/2)$ (14)

$l_t = a\cos(\eta_A/2)$ (15)

The locations of all vertices can be obtained in any folded state using these parameters. For the pattern shown in Fig. 12(a), all straight-crease lines (m) have been numbered beginning from the bottom, and zigzag crease lines (n) beginning from the left. The vertex at the intersection of the i-th straight crease line and the j-th zigzag crease line is denoted as $V_{i,j}$, where i = 1, 2,…m, and

j = 1, 2,…n. The 3D Cartesian coordinate system, along with its origin and orientation, is shown in Fig. 12(c). The coordinate vector (x, y, z) of $V_{i,j}$ can be given as:

$$x = \begin{cases} (j-1)\,a\sin\left(\frac{\eta_A}{2}\right) & \text{odd } i \\ (j-1)\,a\sin\left(\frac{\eta_A}{2}\right) + b\cos\left(\frac{\eta_Z}{2}\right) & \text{even } i \end{cases} \quad (16)$$

$$y = (i-1)b\sin\left(\frac{\eta_Z}{2}\right) \quad (17)$$

$$z = \begin{cases} 0 & \text{for odd } j \\ a\cos\left(\frac{\eta_A}{2}\right) & \text{for even } j \end{cases} \quad (18)$$

Twelve parameters a, b, φ, m, n, θ_A, θ_Z, η_A, η_Z, l_a, l_b, l_t have been defined to specify the Miura-Ori pattern. The first five parameters are the pattern constants because they remain fixed regardless of the folded shape. The last seven parameters are the pattern variables because they depend upon the shape of the fold. Among these, the six independent geometric relations have been defined in Eqs. (10) through (15). This means that six independent parameters are required to determine all the parameters of a unique Miura pattern. In a specific Miura pattern, these six parameters can be determined using five pattern constants and one pattern variable. Based on this equation the surface of the origami was constructed in MATLAB, as shown in Fig. 13.

Table 4 Geometric characteristics of Miura-Ori specimens.

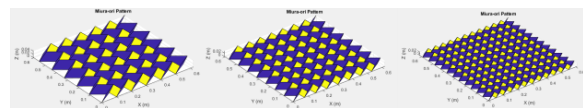|	S_{ttoris} [m^2]	$S_{površina}$ [m^2]	H [cm]	a [cm]	b [cm]	φ [°]	θ_A [°]	θ_Z [°]	m [/]	n [/]
ORIG_1_3	0,36	0,56	2,2	2,9	2,8	62	45	89	32	28
ORIG_1_2	0,36	0,47	1,6	2,9	2,8	62	67	102	29	26
ORIG_1_1	0,36	0,39	1,2	2,9	2,8	62	78	112	27	24
1+	0,36	0,68	2,1	4,3	4,0	62	47	86	23	22
2+	0,36	0,50	1,8	4,3	4,0	62	80	96	22	21
3+	0,36	0,4	1,3	4,3	4,0	62	106	115	20	18
ORIG_2_6	0,36	0,79	3,8	5,5	5,3	62	45	84	20	19
ORIG_2_5	0,36	0,54	2,6	5,5	5,3	62	58	93	17	16
ORIG_2_4	0,36	0,40	1,4	5,5	5,3	62	131	116	14	13

Figure 13: Mathematical model of Miura-Ori samples of the same dimensions and with different density of the ridges.

The Miura-Ori origami structure's mathematical framework facilitated its digital representation, enabling

us to execute a two-dimensional Fourier transformation. The two-dimensional Fourier transform (2D FT) is instrumental in analyzing two-dimensional signals or functions within frequency space. While the primary use of 2D FT is in photo analysis, its applicability extends to assessing surface geometries, such as surface topography investigations. The operating principal echoes that of the one-dimensional Fourier transform, albeit in two dimensions. For a function, f(x,y), which delineates a surface, the 2D FT is expressed as:

$$F = (u,v) = \iint\limits_{-\infty}^{\infty} f(x,y)e^{-i(ux+vy)}dxdy \qquad (19)$$

Here, u and v stand for the spatial frequencies in the x and y directions respectively, and F(u,v) takes the amplitude and phase of the structure at these frequencies. Via spatial frequency space analysis, we can discern various patterns or spatial frequencies on the surface. A surface with a consistent wave-like pattern, for instance, manifests in spatial frequency space as a pronounced peak at a specific frequency.

The efficacy of the 2D FT lies in contrasting surfaces based on their frequency attributes. It's crucial to understand that in the context of surface geometry analysis, "spatial frequencies" are distinct from temporal frequencies, referencing the rate of surface feature variations across space. Yet, incorporating the speed of sound and sample dimensions, the lowest spatial frequency can be aligned with the sample length's sound wavelength. This alignment allows us to correlate spatial with temporal frequency.

The outcome of the 2D FT for surface topography remains two-dimensional, illustrated in Fig. 14. Given the diffuse nature of sound within the reverberation chamber, it's uniformly dispersed around the sample. To transpose the two-dimensional Fourier transformation into a one-dimensional surface spectrum harmonized to a diffuse sound field, the subsequent algorithm was employed:

$$A(r) = \frac{1}{N}\sum_{j=1}^{N} A(r,j) \qquad (20)$$

Here, A(r) signifies the mean of all values from the 2D FT at an identical radius r, as showcased in Fig.14. The number of averages increases with spatial frequency, culminating at the spatial frequency's peak for the 1D Fourier. This

number then decreases to one at the diagonal's apex, signifying the lowest spatial frequency. The spatial frequency's averaged outcomes at an individual radius, scaled to 1/4 wavelength for the 600 x 600 mm sample, across the 2D FT, are conclusively illustrated in Fig. 15.
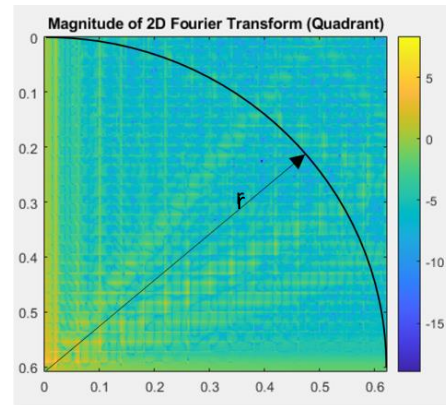
Figure 14: 2D FT of origami surface magnitude, and radius r as descriptor for spatial frequency of diffuse sound reflection
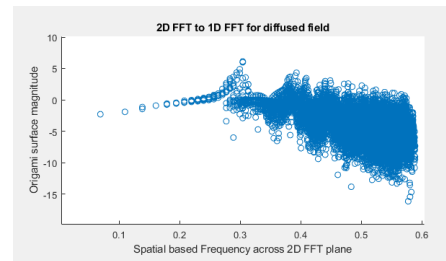
Figure 15: Correlation between Fourier transformation of origami surface magnitude and spatial frequency on the radius r for all elements on the two-dimensional Fourier transformation surface

Figure 16 displays the results of the spatial Fourier transformation for three distinct Miura-Ori Origami samples. While all samples maintain identical dimensions, their geometries differ. The visual representation of these samples is provided in Figure 10, with their corresponding mathematical models illustrated in Figure 13. The defining parameters of these models are detailed in Table 4.

The 2D FT distinctly yields spectra characterized by prominent peaks. These peaks are representative of the density of physical elevations and depressions within the origami samples. A higher count of these physical features

in the sample corresponds to a more elevated spatial frequency peak in the spectrum.
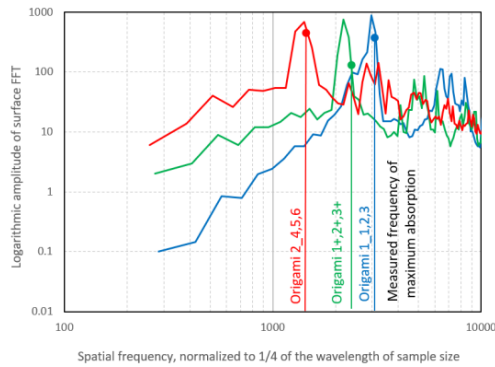
Figure 16: Averaged values of two-dimensional Fourier transformation on the same radius, normalized to 1/4 wavelength for the sample size of 600 x 600 mm.

Table 5: Comparison of frequencies, for measured sound absorption and for maxima of 2D Fourier transformation

	Max. in the 2D FT [Hz]	Max. in measured absorption [Hz]
ORIGAMI 2_4, 5, 6	1490	1600
ORIGAMI 1+, 2+, 3+	1927	1900
ORIGAMI 1_1, 2, 3	2974	3150

Extracting the maximal sound absorption frequency from measurements and comparing it with the peak spatial frequency derived from the sample's mathematical model reveals a visible correlation. This linkage substantiates the prediction that 1/4 of the sound wavelength can be employed to standardize spatial frequency. Moreover, the radial and planar averaging of the two-dimensional Fourier transformation provides insights into the behavior of the diffuse sound field above the sample plane. With this the second hypothesis, that a a significant correlation exists between the sound absorption frequency and the spatial frequency of the Origami surface, is confirmed.

4. DISCUSSION

Our study has revealed that a minimum of approximately 50 measurements is essential to obtain valid reverberation times, despite non ideal diffuse field. We also identified challenges when computing

reverberation times with exceedingly short signal playback durations and the existing criteria for source and background noise level calculations. Leveraging multichannel measurements and new software we enhanced both speed and accuracy of sound absorption measurement.

Our investigations validated both hypotheses. Their affirmation ensures the precision of reverberation time measurements within the alpha chamber, setting the stage to effectively evaluate the sound absorption properties of origami.

The implemented measuring system demonstrated a high degree of precision, aptly differentiating the acoustic variances across diverse Origami configurations. Its reliability not only identifies the unique acoustic characteristics of each Origami geometry but also serves as a foundation for constructing physical models that describe the acoustic dynamics of Origami structures.

Incorporating both measurement outcomes and numerical analyses of the origami surface, there seems to be potential to establish a correlation between the frequencies of sound absorption and the spatial frequencies intrinsic to the origami design, but further research is needed.

5. CONCLUSIONS

In this study, we performed a validation of the alpha chamber and multichannel system for measurements of reverberation times and consequently for assessment of sound absorption, a pivotal metric when evaluating the absorption coefficient of new acoustic materials specifically the Miura-Ori Origami paper structure. Central to this investigation was the development and deployment of a multichannel software solution tailored for increased number of measurements reducing the influence of non ideal diffuse field. Our findings underscore several relevant points:

Software Efficacy: The newly developed software not only streamlined the process of reverberation time measurements but also enhanced its accuracy. This suggests a promising avenue for its broader adoption in acoustic research and applications.

Influence of Parameters: The study elucidated the paramount importance of specific parameters in the measurement process. Specifically, the signal playback duration and the total number of measurements markedly influence the accuracy of reverberation times.

AAAA – 2023 – IZOLA - Conference Proceedings

System Resolution: An illustrative test involving plain thick paper affirmed the system's capability to discern even minute differences, underscoring its high resolution and sensitivity.

Convergence to True Value: Our empirical data bolstered the postulate that with an incremental increase in measurement points for the alpha chamber's reverberation time, we gravitate towards its intrinsic global value. This convergence phenomenon underscores the importance of extensive sampling in achieving accurate measurements.

Interplay of Sound Wavelength and Room Dimensions: A noteworthy revelation from this research was the evident correlation between the desired error in global reverberation time for the alpha chamber and the ratio of sound wavelength to the chamber's dimensions. This provides an analytical framework for optimizing measurements in similar acoustic setups.

Correlation between Sound absorption frequency and spatial frequency of Origami surface: Presented analysis delineated the potential of correlating sound absorption frequencies with the spatial frequencies intrinsic to the Miura-Ori origami structure, bridging the gap between physical geometry and acoustic behavior.

In summary, this research not only underscores the pivotal role of optimized measurement strategies in acoustic research but also paves the way for novel methodologies that interlink structural geometry with sound behavior, by confirming both hypotheses.

6. REFERENCES

[1] Larissa M. Fonseca , Guilherme V. Rodrigues , Marcelo A. Savi, **An overview of the mechanical description of origami-inspired systems and structures**, International Journal of Mechanical Sciences 223 (2022) 107316

[2] Hongbin Fang , Xiang Yu and Li Cheng, **Reconfigurable origami silencers for tunable and programmable sound attenuation**, Smart Mater. Struct. Vol. 27, (2018), pp. 095007, https://doi.org/10.1088/1361-665X/aad0b6

[3] Pingting Jiang, Tianxi Jiang, and Qingbo He, **"Origami-based adjustable sound-absorbing metamaterial"** Smart Mater. Struct. Vol.30, (2021), pp.057002, https://doi.org/10.1088/1361-665X/abf420

[4] Xiaomeng Jin, Hongbin Fang, Xiang Yu, Jian Xu, Li Cheng, **Reconfigurable origami-inspired window for tunable noise reduction and air ventilationm**, Building and Environment 227 (2023) 109802

[5] Ryan L Harne and Danielle T Lynd, **Origami acoustics: using principles of folding structural acoustics for simple and large focusing of sound energy**, 2016 Smart Mater. Struct. Vol. 25 pp. 085031

[6] Pratapa PP, Suryanarayana P, Paulino GH. **Bloch wave framework for structures with nonlocal interactions: application to the design of origami acoustic metamaterials**. J Mech Phys Solids 2018;118:115–32.

[7] Xiang Yu, Hongbin Fang, Fangsen Cui, Li Cheng, Zhenbo Lu, **Origami-inspired foldable sound barrier designs**, Journal of Sound and Vibration 442 (2019) 514e526

[8] Diamant R, Shahar I, Rosenberg T, Weiss A. **Origami-Inspired Adaptive Acoustic Tank for Optimal Reflection Mitigation**. IEEE Sens J 2020;20(24):15193–203.

[9] Zou C, Lynd DT, Harne RL. **Acoustic wave guiding by reconfigurable tessellated arrays**. Phys Rev Appl 2018;9(1):014009.

[10] Zou C, Harne RL. **Tailoring reflected and diffracted wave fields from tessellated acoustic arrays by origami folding**. Wave Motion 2019;89:193–206.

[11] Zhu Y, Fei F, Fan S, Cao L, Donda K, Assouar B. Reconfigurable **origami-inspired metamaterials for controllable sound manipulation**. Phys Rev Appl 2019;12(3): 034029

[12] Tristan Cambonie, Emmanuel Gourdon, **Innovative origami-based solutions for enhanced quarter-wavelength resonators**, Journal of Sound and Vibration 434 (2018) 379–403

[13] M. Thota, K.W. Wang, **Tunable waveguiding in origami phononic structures**, Journal of Sound and Vibration 430 (2018) pp.93-100,

[14] ISO 354, *Acoustics-Measurement of sound absorption in a reverberation room*. 2003.

[15] K. E. Randall and F. L. Ward, "**Diffusion of sound in small rooms**."

[16] A. Cops, J. Vanhaecht, and K. Leppens, "**Sound Absorption in a Reverberation Room: Causes of Discrepancies on Measurement Results**," 1995.

[17] L. L. Beranek, "Analysis of Sabine and Eyring equations and their application to concert hall audience and chair absorption," J Acoust Soc Am, vol. 120, no. 3, pp. 1399–1410, Sep. 2006, doi: 10.1121/1.2221392.

[18] T. Vrtovec, "**Načrtovanje odmevne komore**" Univerza v Ljubljani, Fakulteta za strojništvo, Ljubljana, 2017.

[19] Ali Mohammadsalehi, Davood Mostofinejad, **Behavior of high-performance concrete canvas Miura-origami structures under flexural loading**, Structures, Vol. 54, (2023) 928–945
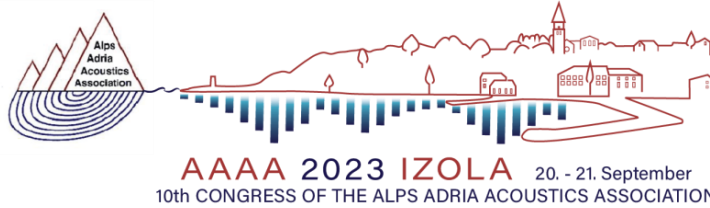
REVERBERATION TIME ESTIMATION FROM EMOTIONAL SPEECH SIGNALS

Andrea Andrijašević

Polytechnic of Rijeka, Vukovarska 58, 51 000 Rijeka, Croatia

Abstract:

Many of today's speech signal processing systems, from the low-power ones embedded in the hearing aids to the large and complex deep learning based systems for automatic speaker identification, and speech or speech emotion recognition, rely on their speech enhancement pre-processing module to reduce the signal degradation introduced by the room reverberation and background noise. Even though in the former type of systems this type of pre-processing is performed in order to improve the intelligibility of the input speech, whereas in the latter so as to provide feature robustness, in each case the room parameters need to be estimated from the received signal, most commonly the full-band reverberation time (T_{60}). In this study, we examined the robustness of two reverberation time estimation algorithms to changes in speaker's emotions encoded with the acoustic features such as tempo, voice intensity and pitch height. The results obtained on a set of room impulse responses measured in 11 rooms with T_{60} in the 0.2 to 1.2 s range, indicate that a spectral decay distributions-based estimator is less sensitive to such type of changes than an estimator based on the modified ISO 3382-2:2008 method. The performance of the latter was successfully enhanced with the introduction of a dynamic range criterion, however it did not surpass the performance of the former algorithm.

Keywords: reverberation time, emotion, speech signal, pitch, speech rate, subglottal pressure

1. INTRODUCTION

Speech enhancement is a signal processing procedure commonly performed in a wide array of electronic consumer devices with integrated microphones, e.g. mobile phones, tablets, and hearing aids, with the aim of reducing the damaging effects of background noise and reverberation either on the performance of systems for automatic speech, speaker or emotion recognition or on the intelligibility of received speech [1-5]. For this task, an estimate of room reverberation time (T_{60}) is often required, and thus usually obtained from the received reverberant speech signal itself.

Even though both the influence of background noise and speech phonetic content on the performance of algorithms for T_{60} estimation have been well researched [6-8], the influence of speaker's emotional state remains unexplored since the speech material used in [6-8] was uttered in only one speaking style.

Throughout our lives, we continually experience sometimes quicker, sometimes slower changes in our conscious mental reactions, subjectively experienced as strong feelings and typically accompanied by physiological and behavioural changes, which we commonly refer to as emotions [9]. In speech communication, many acoustic features, such as pitch, sound intensity, and tempo carry important emotional information [10]. As the changes in emotional state can be sudden, it is even more important to evaluate the robustness of algorithms to them. It is well known that the ratio of the duration of vowels to the duration of consonants changes with speech rate [11], that the subglottal pressure affects the tilt of the spectral envelope and the overall sound pressure level (SPL), and that speaker's intonation is reflected in the fundamental frequency (F0) of voiced speech sounds [12].

Therefore, in this study we assess the robustness of T_{60} estimation algorithms to emotions conveyed through changes in speaker's fundamental frequency, speech rate and subglottal pressure. To this end, we use phonetically

balanced speech material uttered in six different speaking styles convolved with room impulse responses measured in 11 rooms at up to 5 different source-receiver distances, from which T_{60} is estimated using two of the best performing algorithms from [7].

The remainder of the paper is organised as follows. In Section 2, we present the algorithms used for T_{60} estimation, whereas in Sections 3 and 4 we provide the analyses of emotional speech recordings and room impulse responses, respectively. We continue by presenting the results in Section 5 and proposing two algorithm modifications in Section 6. Finally, with Section 7, we conclude our work.

2. T_{60} ESTIMATION ALGORITHMS

The first algorithm for T_{60} estimation used in this study is Prego's algorithm [13, 14], in which estimation is carried out in the short-time Fourier transform (STFT) domain. The so-called free-decay regions of speech signal are detected independently in each of the frequency bands in the 0 - 4 kHz range. Estimation of T_{60} is performed on the energy decay curves (EDCs) calculated from these free-decays using a procedure that closely resembles Schroeder's method [15, 16]. The final estimate is obtained as the output of a linear mapping function whose input is the median of frequency bands T_{60} medians.

The second algorithm, Eaton's, operates in the mel-frequency STFT domain [17]. In this algorithm, the sound decay rates are estimated for each mel-frequency band independently as the slope of a linear least-squares fit. The negative-side variance (NSV), defined as the variance of negative slopes in the distribution of decay rates, is used as the input to a polynomial mapping function whose output is the estimate of T_{60}.

The performance of these two algorithms under different background noise conditions and with different phonetic content has been well researched and documented in [7, 8, 18], enabling us to focus on the evaluation of their robustness to emotional speech signals. Accordingly, since high signal-to-noise ratio (SNR) recordings were used in this study, no signal de-noising was performed and the linear mapping function parameters were set as in [13] for Prego's algorithm, whereas in Eaton's algorithm the NSV was calculated from the distribution of all obtained negative decay rates.

3. SPEECH RECORDINGS

The OLdenburg LOgatome (OLLO) corpus, a speech database designed for the comparison of recognition performance of automatic speech recognizers and human listeners, ver. 2.0 [19] was used in this study. Namely, we used the recordings of 50 phonetically balanced sentences in French language, uttered in six speaking styles by nine speakers whose identification numbers are as follows:

- o female speakers: 41, 45, 47, and 49,
- o male speakers: 42, 43, 44, 46, and 48.

This set was chosen as it consists of recordings of the same speech material uttered using different tempi (speech rates), different intonations (pitch curves), and in which different SNRs arise due to changes in the subglottal pressure the speaker uses, which cannot be imitated by adding different levels of pre-recorded or synthetic noise to the normal style speech recordings. In the following subsections, we present and analyse the aforementioned aspects of the recordings.

3.1. Signal-to-noise ratio

Noise power was estimated from the first 100 ms of the recordings, which contained no speech activity. Interestingly, it was observed that the noise power spectral density (PSD) differed between speakers. This was due to breathing noise – the recording microphone had been placed about 25 cm from the speaker's mouth, hence the inspiration and expiration noise was quite noticeable for a few speakers whereas others succeeded in directing minimal noise towards it. With most of its power in the 60 - 600 Hz range [20, 21], breathing noise became superimposed onto recording equipment noise. Speech signal power was calculated as the active speech level of the recording, estimated using the ITU-T P.56 Method B [22, 23], from which the previously estimated noise power was subtracted. For the normal style speech recordings, the median SNR across the speakers was in the 39 - 55 dB range.

As the initial tests had shown that a single sentence recording was not sufficiently long to produce a T_{60} estimate, the 50 recordings uttered by a single speaker in one speaking style needed to be concatenated into one speech file. To this end, since the OLLO corpus recordings come normalized, in order to make the background noise of the concatenated recordings constant, the individual

recordings were first de-normalized using the normalization factors provided with the corpus.

3.2. Speech rate

Since the same phonetically balanced speech material was uttered in six speaking styles, the ratio of the fast, slow, loud, soft, and questioning speaking styles speech duration to the duration of the normal style speech informs of the change in the rate of speech introduced by the speaker. Therefore, for each of the 54 speech files, a speech duration estimate was calculated by multiplying the speech file nominal duration in seconds by its activity factor, defined as the ratio of the voice active to the total number of speech samples in a file, obtained with [23].

Figure 1 shows the calculated speech duration ratios. They agree quite well between the sexes. Interestingly to notice, the speech rate for the questioning style is somewhat higher than for the normal style. An outlier, a data point with the value of 2.05, present for the slow style, belongs to the female speaker number 49.
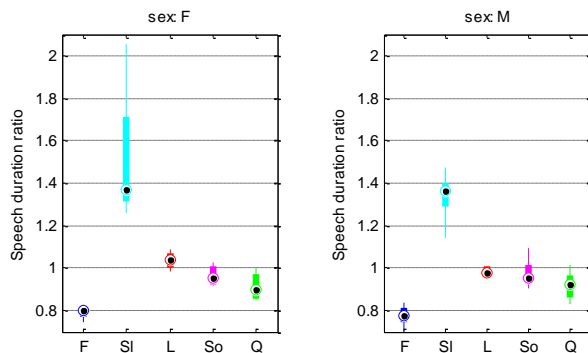

Fig. 1. Speech duration ratios, with normal speaking style as reference. x-axis labels: 'F' – fast, 'Sl' – slow, 'L' – loud, 'So' – soft, and 'Q' – questioning speaking style

3.3. Subglottal pressure

In controlled settings, subglottal pressure (SGP) can be tracked by analysing the flow glottogram, whose peak flow and the negative peak amplitude of its derivative, referred to as the maximum flow declination rate, increase with SGP [12]. In case a glottogram is not available, the changes in the subglottal pressure, perceived as changes in loudness, can be (under the assumption of a fixed speaker-microphone distance) estimated either from the changes in the active speech level (ASL) of the recording or from the slope of the

envelope of voiced speech sounds spectra, where the steeper the slope, the lower the SGP.

Figure 2 presents the long-term average spectra of the 54 root-mean-square (RMS) normalized speech files, averaged across the same sex speakers files. Changes in the underlying subglottal pressure are visible in the 1 - 5 kHz range – LTAS, and therefore the SGP as well, has considerably higher values for the loud style and somewhat lower values for the soft style than for the remaining four speaking styles.
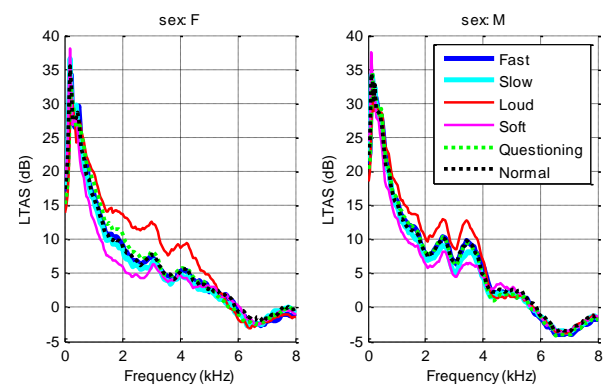

Fig. 2. LTAS of the RMS-normalized speech files

3.4. Fundamental frequency

Figures 3 and 4 show the ratios of the estimates of fundamental frequency mean and standard deviation obtained in Praat [24] for single sentence speech recordings, with normal style as reference.

The mean F0 ratios change across the five speaking styles similarly for female and male speakers, with mean F0 being about 1.3 times higher for the loud and questioning styles than for the normal style. Although F0 is controlled primarily by laryngeal muscle activity, the subglottal pressure also has an influence on its value – as the SGP increases, the F0 increases as well [12], which explains the increase observed for the loud style.

Figure 4 shows that the changes in the ratio of the standard deviation of F0 across the five speaking styles are also quite similar between the sexes. Since, among its many functions, F0 is used to signal syntactic information such as the difference between statements (normal style) and questions (questioning style), where the latter are recognized by a sharp rise in its value as the speaker approaches the end of the final word in a sentence [25],

an increase in its variation is present for the questioning style recordings (Figure 4) in addition to the previously observed increase in its mean value (Figure 3).
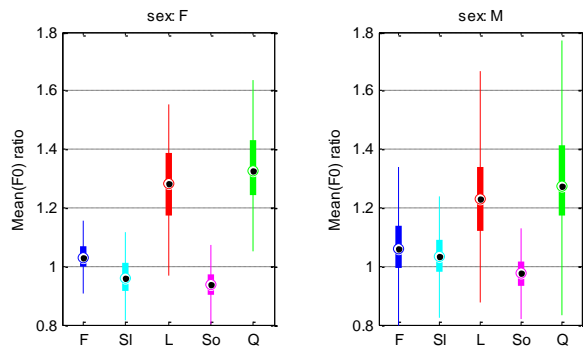

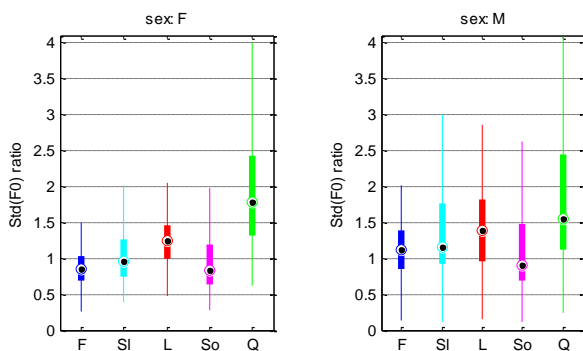**Fig. 3.** Ratios of mean F0, with normal speaking style as reference

Fig. 4. Ratios of standard deviation of F0, with normal speaking style as reference

4. ROOM IMPULSE RESPONSES

Two sets of measured room impulse responses (RIRs) were utilized in this study. The first set consists of 28 impulse responses from the ACE Corpus [7], whereas the second set comprises 32 impulse responses from the Aachen Impulse Response (AIR) database v1.4 [26].

4.1. Ground truth T_{60}

The ACE room impulse responses were obtained with a linear eight-channel microphone array, namely its channels 1 and 8, at two different source-receiver distances within seven different rooms. The estimates of

their mean ground truth full-band T_{60} (from here onwards denoted as T_{GT}) [7], are presented in Table 1.

The AIR set comprises impulse responses measured in four rooms. In each room, RIRs were measured using two microphones and, depending on the room size, either three or five different source-receiver distances were utilized. For each room impulse response of this set, the associated T_{GT} was calculated in accordance with [15], as the T_{20} obtained from its full-band energy decay curve. The mean T_{GT}s are presented in Table 2. The variance of T_{GT} was less than $4.4 \cdot 10^{-3}$ s^2 in the rooms, thus validating the assumption of position-invariant reverberation time. As can be seen from Tables 1 and 2, the ACE and AIR sets jointly cover a large T_{GT} range, which coincides with the ranges reported in [27] and [28] for private, public, and work spaces.

Room name	T_{GT} (s)	DRR$_{min}$ (dB)	DRR$_{max}$ (dB)	SF$_{min}$	SF$_{max}$
Office 1	0.332	-0.61	8.85	0.82	0.87
Meeting room 2	0.371	3.94	7.96	0.83	0.87
Office 2	0.390	1.80	9.74	0.81	0.87
Meeting room 1	0.437	3.21	7.89	0.83	0.88
Lecture room 1	0.638	1.03	8.04	0.83	0.91
Building lobby	0.646	1.46	8.52	0.83	0.86
Lecture room 2	1.220	-0.33	6.00	0.84	0.90

Table 1. The ACE set

Room name	T_{GT} (s)	DRR$_{min}$ (dB)	DRR$_{max}$ (dB)	SF$_{min}$	SF$_{max}$
Booth	0.178	1.55	10.01	0.83	0.92
Meeting room	0.277	2.10	3.93	0.81	0.84
Office	0.546	-3.19	5.07	0.80	0.90
Lecture room	0.819	-7.52	3.01	0.80	0.84

Table 2. The AIR set

4.2. Direct-to-reverberant ratio

As the room impulse responses were measured at up to five different source-receiver distances, their direct-to-reverberant ratio (DRR) was calculated using the method presented in [7]. The minimal and maximal DRRs shown in Tables 1 and 2 indicate that the majority of RIRs were measured at distances smaller than the critical distance [1], at which the energy of the direct path component is higher than the total energy of reflections.

4.3. Spectral flatness

In case the magnitude spectrum of a room impulse response is flat, the SNR of a clean speech recording can be used as a proxy for the SNR of its reverberant version. To check whether this applies to the ACE and AIR RIRs, spectral flatness (SF) [29], the ratio of the geometric to the arithmetic mean of the magnitude spectrum coefficients, was calculated in the 0 - 8 kHz range. The minimal and maximal SFs given in Tables 1 and 2 indicate that the magnitude spectra are indeed flat, thus enabling the use of clean speech SNRs in the analyses presented in the following sections.

5. RESULTS
5.1. Overall results

The performance of the algorithms was first assessed with the mean squared error and estimation bias, i.e., the mean error, for the T_{60} estimates obtained from the normal style speech files as they are later used as baseline in the analyses of inter-style differences. The first algorithm, Prego's, achieved a mean squared error of 0.095 s^2 and a bias of 0.269 s, whereas Eaton's performed better with a mean squared error of 0.017 s^2 and a bias of 0.058 s.

Figures 5 and 6 present the inter-style differences (ISDs), defined as the difference between the T_{60} estimates obtained from the fast, slow, loud, soft and questioning style speech files and the corresponding T_{60} estimate obtained from the normal style speech file. It should be noted that since the Pearson correlation coefficient revealed that for both algorithms the T_{60} estimates relationship with T_{GT} is linear (PCC higher than 0.9), the bias observed for Prego's algorithm was not corrected as it had no influence on the ISD curve shape. In both Figures,

for each T_{GT}, the source-receiver distance increases from left to right, by which neither algorithm is substantially affected. Figures also indicate that the largest ISDs occur for the loud and soft speaking styles, as well as that, as the T_{GT} increases, the absolute value of ISD decreases. For Prego's algorithm, a similar, but less pronounced, trend as for the loud style can be observed for the questioning style.

Based on the results presented in Figures 5 and 6, it can be concluded that even though Prego's algorithm performed somewhat better than Eaton's in [7], the latter is, at high SNRs, robust to a number of changes that speakers introduce, with more than 95 % of ISDs within the [-50, 50] ms range. Since Eaton's algorithm only switches the decay rate sub-selection rule based on the estimated SNR, it is not unreasonable to assume that the with the introduction of a de-noising step its performance under low SNR conditions could be further improved.

5.2. Prego's algorithm – detailed results

In order to find the cause for the large ISDs observed for Prego's algorithm, we explore their relationship with speech signal characteristics. Since the largest ISDs are present for the loud and soft styles, we focus on the relationship of ISD with SGP. In the following analysis, the changes in the ASL of clean speech files are used as a proxy for the changes in the utilized SGP under the previously verified assumptions of spectral flatness and noise power invariability across the clean speech files of different speaking styles.

Given this, the relationship between the ASL ratio and ISD is presented in Figure 7, with the former defined as the ratio of the ASL of the first five styles to the ASL of the normal style. As can be seen from Figure 7, there is a considerable variation in how much the speakers changed the SGP across the speaking styles. Moreover, it can be also observed that some of the speakers increased the loudness of their voice for the questioning style as well, which had in turn made their questioning style ISDs more similar to those present for the loud style.

Finally, it can be summarized:
o as the SGP increases above (decreases below) its normal level, the ISD becomes negative (positive),
o the larger the change in SGP, the higher the absolute value of ISD,
o for longer T_{GT} (> 0.6 s), the influence of SGP on ISD becomes considerably reduced.
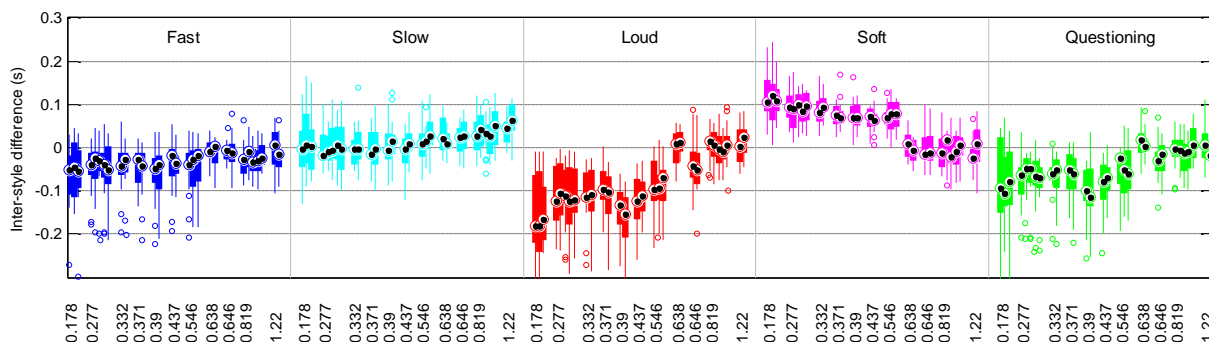
Fig. 5. Inter-style differences for Prego's algorithm. T_{GT} is shown on the x-axis
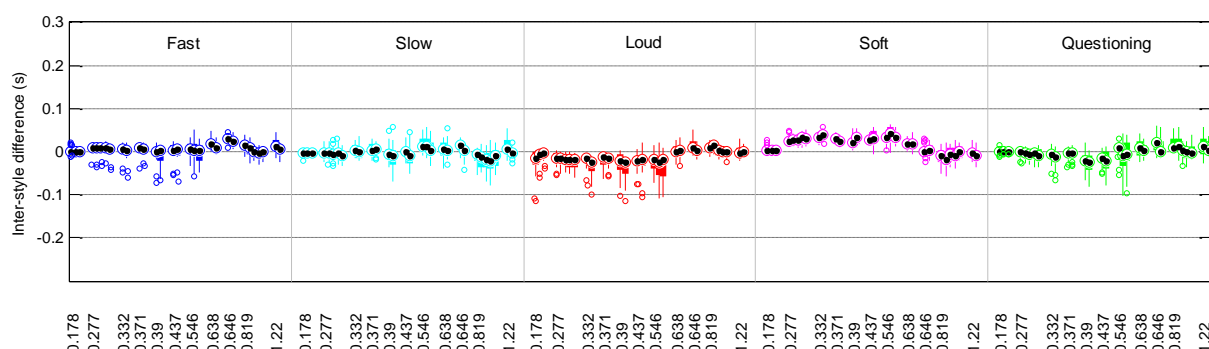

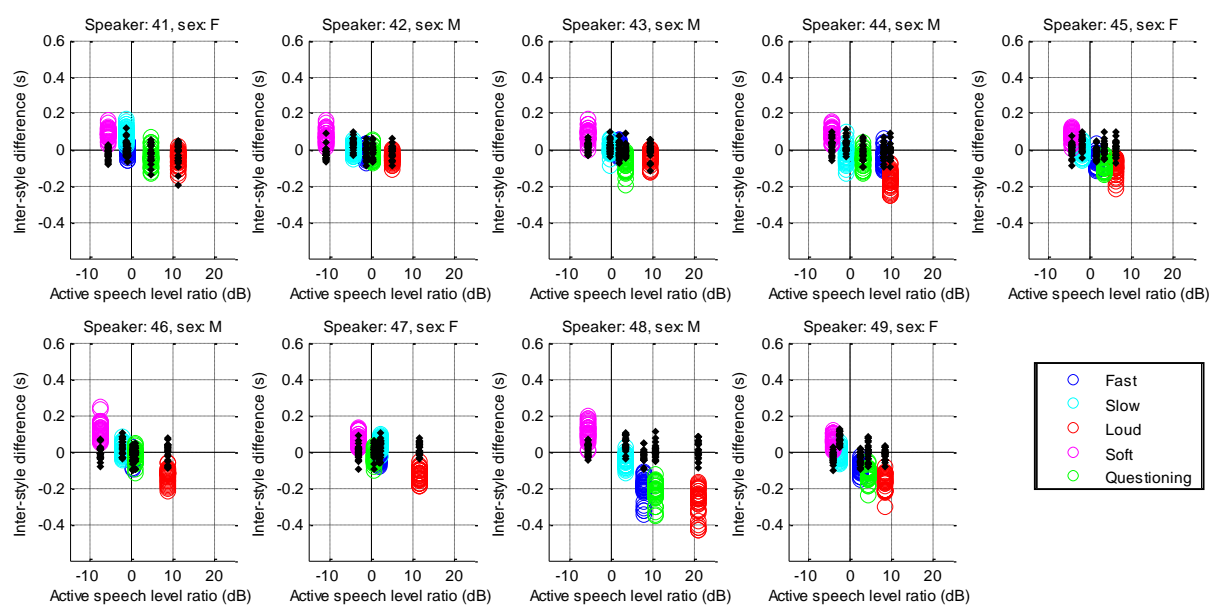**Fig. 6.** Inter-style differences for Eaton's algorithm. T_{GT} is shown on the x-axis

Fig. 7. Relationship between the ASL ratio and ISD for Prego's algorithm. Open circles: RIRs with $T_{GT} < 0.6$ s, Filled diamonds: RIRs with $T_{GT} > 0.6$ s
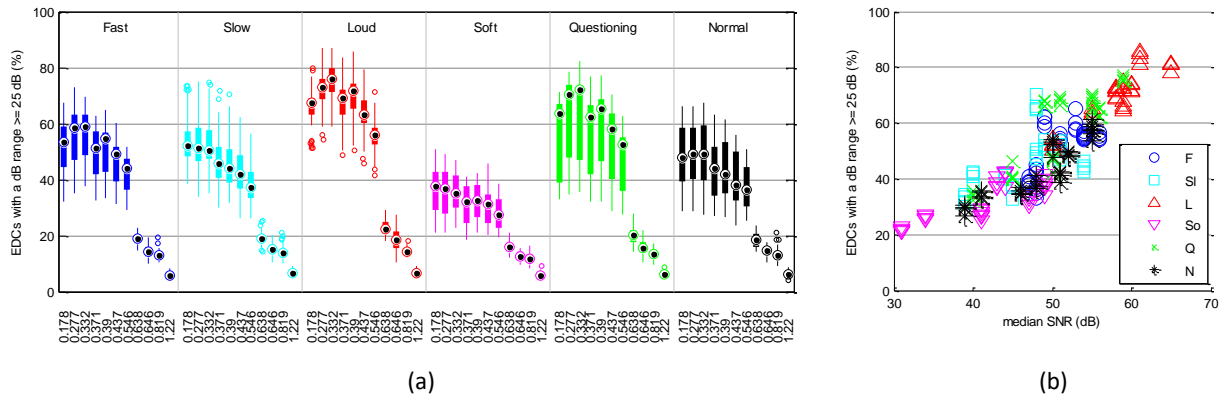
(a)

(b)

Fig. 8. a) Percentage of EDCs with a dynamic range equal to or greater than 25 dB. b) Relationship between the percentage of EDCs with a dynamic range equal to or greater than 25 dB for Office 2 RIRs and the SNR of clean speech recordings

6. ISO 3382-BASED MODIFICATIONS

The results presented in Section 5 clearly show that Prego's algorithm is primarily sensitive to the changes in the subglottal pressure – a well-known sensitivity that Schroeder's method exhibits to changes in the ratio of the room sound excitation to background noise level [15] reappeared, this time in the STFT domain.

In order to try to alleviate the observed influence of SGP on algorithm's performance, two different modifications based on two ISO 3382-2 measures of the quality of energy decay curves [15] are proposed. In both of the modified versions of the algorithm, the first part of it was left unchanged, i.e. the original number of frequency bands as well as the procedure for the detection of sub-band free-decay regions and subsequent T_{60} estimation were used, so that the same sub-band T_{60}s were obtained as with the original algorithm. These sub-band T_{60} estimates are then processed in one of the two following ways.

6.1. Degree of non-linearity

In the first ISO 3382-based modification, the degree of non-linearity (ξ), a measure obtained from the correlation coefficient of the linear least-squares fit to the energy decay curve [15], was calculated for each detected speech free-decay region. It was observed that a very large proportion of decay curves had ξ higher than the maximum of 10 ‰ allowed for Schroeder's method by the Standard. For instance, when speech files were convolved

with the Office 2 RIRs, the percentage of the curves that satisfied the linearity criterion was 30 % for the loud, 25 % for the normal, and 23 % for the soft style.

Hence, in this modification, all the sub-band estimates of T_{60} obtained from an energy decay curve with ξ above 10 ‰ were discarded, upon which the standard procedure, i.e. calculation of the final T_{60} estimate as the median of sub-band median T_{60}s, was performed. Unfortunately, no improvement could be observed – the ISDs were similar to the ones obtained with the original algorithm.

6.2. Dynamic range

In this modification, the dynamic range of each sub-band energy decay curve used for T_{60} estimation was calculated, and a criterion of 25 dB, a value half way between the two standard T_{60} estimation ranges [15], was set. Panel a) in Figure 8 shows the percentage of the energy decay curves of a reverberant speech file with a dynamic range equal to or greater than 25 dB that, not surprisingly, depends on the speaking style. To illustrate further how the percentage of EDCs with a dynamic range greater than or equal to 25 dB relates to the SNR of clean speech recordings, the results for the Office 2 RIRs are presented in Panel b).

Furthermore, in Panel a), for all speaking styles, the percentage of EDCs with a high dynamic range decreases as the T_{GT} increases due to temporal smearing of the speech signal that the room impulse response introduces – the higher the T_{GT}, the more of the fine structure of the speech signal envelope is lost. As a consequence of this

increasingly more severe loss of modulation depth, the differences in the percentages across the speaking styles are largest for the smallest values of T_{GT} and slowly disappear as the T_{GT} increases.

After all the sub-band T_{60} estimates obtained from EDCs of dynamic range lower than 25 dB were discarded, and the same standard procedure, i.e. calculation of the final T_{60} estimate as the median of sub-band median T_{60}s, was performed, an improvement in algorithm robustness was obtained for T_{GT} lower than 0.6 s. There was a significant increase in the percentage of ISDs within the [-50, 50] ms range – from 41 % for the original algorithm to almost 81 % for the modified version. Unfortunately, for T_{GT} above 0.6 s the percentage of ISDs within that range decreased from 75 % for the original algorithm to 48 % for the modified version.

Given this improvement in algorithm's robustness to changes in speaking style for T_{GT} lower than 0.6 s, the performance metrics for the normal style speech files were re-calculated. The following results were obtained – a decrease in the value of correlation coefficient to 0.76, a mean squared error of 0.034 s^2, and a bias of -0.048 s. The decrease in the correlation coefficient occurred due to estimates obtained from the room with the highest T_{GT} (Lecture room 2). After the data for that room were removed, a linear trend across the T_{GT}s and a decrease in the estimation bias were revealed – a correlation coefficient of 0.94 for the modified versus 0.96 for the original algorithm, a mean squared error of 0.005 s^2 versus 0.099 s^2, and a bias of -0.004 s for the modified versus 0.273 s for the original algorithm.

Based on these results and the data presented in Figure 8, it seems that, even though the silent parts of the speech files between individual sentences were of sufficient duration for the estimation of T_{GT} larger than 0.6 s (they were about 1 second long), the value of 0.6 s can be considered a threshold above which a dynamic range criterion is not useful when trying to achieve robustness to changes in speaking style. Finally, given the increasingly smaller percentage of EDCs with a dynamic range above 25 dB as the T_{GT} increases, it also seems that, in practice, the estimation of T_{60} on connected speech in the STFT domain can be performed successfully only for a subset of T_{GT} values, above whose upper limit it would be more appropriate to estimate the early decay time (T_{10}).

6.3. Discussion

After exploring the results of two modifications of Prego's algorithm, where neither of them could reduce the ISDs to the level observed for Eaton's algorithm, it seems likely that the robustness that the latter exhibits comes from the use of wide mel-bands and processing of the whole reverberant signal. Due to its use of mel-bands, Eaton's algorithm places more emphasis to T_{60} estimation in the lower frequency region where most of vowel energy is contained, whereas Prego's algorithm distributes weight equally across the frequency bands in the 0 - 4 kHz range. In addition to that, in Eaton's algorithm each sub-band speech decay can potentially produce multiple negative gradients, whereas in Prego's algorithm one detected sub-band free-decay always equals one sub-band T_{60} estimate.

7. CONCLUSION

The artificially reverberated phonetically balanced speech material uttered in six different speaking styles proved to be a challenging test set for the task of T_{60} estimation. Specifically, it was shown that even in high SNR conditions a T_{60} estimator based on Schroeder's method remains sensitive to changes in the subglottal pressure. With an ISO 3382-based dynamic range criterion for sub-selection of free-decay regions, a reduction in its sensitivity was achieved for rooms with T_{60} lower than 0.6 s, yet it remained higher than for an approach of decay rate estimation in mel-frequency bands.

Finally, since robust estimation of T_{60} from emotional speech signals remains a challenge, we strongly encourage wider use the OLLO corpus in future performance evaluation studies alongside other, well-known speech corpora in which the speech material is uttered in only one speaking style.

8. REFERENCES

[1.] Naylor, P. A. and Gaubitch, N. D. **Speech Dereverberation**. Springer, 2010.

[2.] Tashev, I. J. **De-reverberation**. **In Sound Capture and Processing: Practical approaches.** Wiley, pp. 341-358, 2009.

[3.] Löllmann, H. W. and Vary, P. **Low delay noise reduction and dereverberation for hearing aids,** EURASIP Journal on Advances in Signal Processing, pp. 1-9, 2009.

[4.] Kinoshita, K., Delcroix, M., Gannot, S., Habets, E. A. P., Haeb-Umbach, R., Kellermann, W., Leutnant, V., Mass, R., Nakatani, T., Raj, B., Sehr, A. and Yoshioka, T. **A summary of the REVERB challenge: state-of-the-art and remaining challenges in reverberant speech processing research**, EURASIP Journal on Advances in Signal Processing, 2016(7), pp. 1-19, 2016.

[5.] Lee, C.-C., Sridhar, K., Li, J.-L., Lin, W.-C., Su, B.-H. and Busso, C. **Deep Representation Learning for Affective Speech Signal Analysis and Processing: Preventing unwanted signal disparities**, IEEE Signal Processing Magazine, 38(6), pp. 22-38, 2021.

[6.] Gaubitch, N. D., Löllmann, H. W., Jeub, M., Falk, T. H., Naylor, P. A., Vary, P. and Brookes, M. **Performance comparison of algorithms for blind reverberation time estimation from speech**, in Proc. Intl. Workshop on Acoustic Signal Enhancement (IWAENC), 2012.

[7.] Eaton, J., Gaubitch, N. D., Moore, A. H. and Naylor, P. A. **Estimation of room acoustic parameters: The ACE Challenge**, IEEE/ACM Trans. Audio, Speech, and Language Process., 24(10), pp. 1681-1693, 2016.

[8.] Andrijašević, A. **Effect of phoneme variations on blind reverberation time estimation**, Acta Acustica, 4(1), pp. 1-17, 2020.

[9.] **Emotion - Merriam-Webster dictionary.** Available at: https://www.merriam-webster.com/dictionary/emotion

[10.] Quinto, L., Thompson, W. F. and Keating, F. L. **Emotional communication in speech and music: the role of melodic and rhythmic contrasts**, Front. Psychol. 4(184), 2013.

[11.] Kuwabara, H. **Acoustic properties of phonemes in continuous speech for different speaking rate**, in Proc. 4th International Conference on Spoken Language, pp. 2435-2438, 1996.

[12.] Rossing, T. D. **The human voice in speech and singing**. **In Springer Handbook of Acoustics.** Springer, pp. 669-712, 2007.

[13.] Prego, T. M., Lima, A. A. and Netto, S. L. **A blind algorithm for reverberation-time estimation using subband decomposition of speech signals**, J. Acoust. Soc. Am., 131(4), pp. 2811–2816, 2012.

[14.] Prego, T. M., Lima, A. A., Zambrano-Lopez, R. and Netto, S. L. **Blind estimators for reverberation time**

and direct-to-reverberant energy ratio using subband speech decomposition, in Proc. IEEE Workshop on Applications of Signal Processing to Audio and Acoustics (WASPAA), 2015.

[15.] ISO 3382-2:2008. **Acoustics - Measurement of Room Acoustic Parameters - Part 2: Reverberation Time in Ordinary Rooms**, Intl. Org. for Standardization, 2009.

[16.] Schroeder, M. R. **New method of measuring reverberation time**, J. Acoust. Soc. Am., 37(3), pp. 409–412, 1965.

[17.] Eaton, J., Gaubitch, N. D. and Naylor, P. A. **Noise-robust reverberation time estimation using spectral decay distributions with reduced computational cost**, in Proc. IEEE Intl. Conf. on Acoustics, Speech and Signal Processing (ICASSP), pp. 161-165, 2013.

[18.] Eaton, J., Gaubitch, N. D., Moore, A. H. and Naylor, P. A. **ACE Challenge results technical report**, Imperial College London, 2016.

[19.] Wesker, T., Meyer, B., Wagener, K., Anemüller, J., Mertins, A. and Kollmeier, B. **Oldenburg Logatome Speech Corpus (OLLO) for Speech Recognition Experiments with Humans and Machines**, in Proceedings of Interspeech, pp. 1273-1276, 2005.

[20.] Gross, V., Dittmar, A., Penzel, T., Schüttler, F. and von Wichert, P. **The relationship between normal lung sounds, age and gender**, Am. J. Respir. Crit. Care Med., 162, pp. 905-909, 2000.

[21.] Niu, J., Cai, M., Shi, Y., Ren, S., Xu, W., Gao, W., Luo, Z. and Reinhardt, J. M. **A novel method for automatic identification of breathing state**, Nature Scientific Reports, pp. 1-13, 2019.

[22.] **Objective Measurement of Active Speech Level**, International Telecommunications Union (ITU-T), Recommendation P.56, 1993.

[23.] Brookes, D. M. **VOICEBOX: A speech processing toolbox for MATLAB**. Available at: http://www.ee.ic.ac.uk/hp/staff/dmb/voicebox/voicebox.html

[24.] Boersma, P. and Weenink, D. **Praat: doing phonetics by computer**, version 5.1.43. University of Amsterdam, 2010. Available at: https://www.fon.hum.uva.nl/praat/

[25.] Rose, P. **The human vocal tract and the production and description of speech sounds. In Forensic Speaker Identification**. Taylor & Francis, pp. 125-174, 2002.

[26.] Jeub, M., Schäfer, M. and Vary, P. **A binaural room impulse response database for the evaluation of dereverberation algorithms**, in Proc. Intl. Conf. on Digital Signal Processing, pp. 1-4, 2009.

[27.] Diaz, C. and Pedrero, A. **The reverberation time of furnished rooms in dwellings**, Applied Acoustics, 66, pp. 945-956, 2005.

AAAA – 2023 – IZOLA - Conference Proceedings

[28.] Vincent, E., Gannot, S. and Virtanen, T. **Acoustics – Spatial properties. In Audio Source Separation and Speech Enhancement**, Wiley, pp. 31-46, 2018.

[29.] Johnston, J. D. **Transform coding of audio signals using perceptual noise criteria**, IEEE Journal on Selected Areas in Communications, 6(2), pp. 314-323, 1988.

DETERMINATION OF THE POSITION OF EQUIPMENT NOISE SOURCES IN EDUCATIONAL INSTITUTIONS ACCORDING TO SUBJECTIVELY EVALUATED SPEECH INTELLIGIBILITY

Mateja Dovjak [1]*, Denis Pirnat [2], Rok Prislan [3]

[1,2] Univerza v Ljubljani, Fakulteta za Gradbeništvo in Geodezijo, Jamova 2, 1000 Ljubljana, Slovenija, mateja.dovjak@fgg.uni-lj.si

[3] InnoRenew CoE, Livade 6a, SI-6310 Izola, Slovenia, rok.prislan@innorenew.eu

Abstract:

Building-equipment noise is the primary source of background noise in buildings. It is a key factor influencing speech intelligibility, along with room acoustics, sound insulation of the building envelope and the noise level in the room. The impact of building-equipment noise on the acoustic environment in educational institutions is poorly addressed in current design practice; attention is focused only on the requirements for maximum background noise levels and not on the position of noise sources in the room. Our study focuses on a characteristic lecture hall of an educational institution where an artificial speaker was used to simulate the speaker, while the noise typically produced by an HVAC system was generated by an omnidirectional loudspeaker. The position and level of the generated noise were varied for two listening/microphone positions. Under these conditions, (i) the Speech Transmission Index (STI), which objectively determines speech intelligibility, was measured, (ii) listening tests were performed to assess intelligibility of digits, and (iii) subjective assessment of intelligibility was performed using questionnaires. On this basis, recommendations for speech intelligibility in lecture halls and classrooms were developed in terms of equipment position and background noise level. The results show that although the position of the noise source has no significant influence on the STI, it can influence the perceived intelligibility. As such, background noise is not a sufficient criterion for including noise sources in the built environment, and the position of noise sources can be optimised in the design phase. This research was approved by the Ethics Committee for Research Involving Human Subjects, University of Ljubljana (012-2021; Ljubljana, 18 February 2022).

Keywords: equipment noise, speech intelligibility, noise source position

1. INTRODUCTION

The impact of background noise, particularly building-equipment noise, is an important aspect to consider in the building construction process to achieve a high quality acoustic environment. Studies [1-3] show that poor room acoustics, insufficient sound insulation of the building envelope and elevated noise levels in the room due to numerous technical building systems installed for building operation, often negatively affect speech intelligibility. Speech intelligibility plays an essential role in the successful speech delivery. It depends on i) speaker speaking ability (level and intelligibility of speech, ability to adapt to background noise); ii) listening ability (hearing disabilities, native language); and iii) external factors related to the room (room acoustic properties, level of background noise). As this way of delivering information is the basis of today's educational system, it is crucial to minimise external influences on speech intelligibility when planning classrooms and lecture halls, as designers have no influence on speaking or listening abilities. To ensure optimal speech intelligibility in educational institutions, it is therefore necessary to focus on the acoustic properties of the room, such as optimal reverberation time and effective sound insulation of the external and internal structural assemblies, the reduction of noise levels in the

lecture hall and the appropriate positioning of noise sources [4].

The impact of noise from technical building systems on the acoustic environment in educational institutions was studied by Serpilli et al. [2]. They investigated the impact of mechanical ventilation systems on the noise level and speech transmission in a lecture hall, which is determined using the STI parameter. They found that the introduction of mechanical ventilation increases the ambient noise levels and decreases the STI values, which proves to be particularly problematic in rooms that are already acoustically inadequate (in the study, rooms with too long reverberation time). They additionally point out the poor installation of the mechanical ventilation system: inadequate sound insulation at the contact between the penetrations and the building envelope and inadequate pipe insulation, which does not prevent the transmission of external sound to the interior environment.

All these factors degrade the speech transmission. It has been shown that students often have problems with hearing and understanding lectures; Čudina and Prezelj [5] state that speech intelligibility in many classrooms and lecture halls is less than 75%. This means that listeners with normal hearing abilities understand less than 75% of randomly spoken words. The problem was exacerbated during the Covid-19 pandemics, when lecturers had to wear face masks during lectures, and acrylic glass panels often obstructed the sound transmission path from the lecturer to the audience. Brown et al. [6] found that face masks significantly affect speech transmission even at moderate background noise levels. Thus, even at a Speech to Noise Ratio (SNR) of -5 dB, which in simplified terms means that the noise level is 5 dB higher than the speech level, speech intelligibility drops by 30%, both when using a cloth mask with a filter and when using transparent covers [6].

Despite the above research findings, the impact of building and equipment noise on the acoustic environment in educational establishments is still poorly addressed in current design practice; the focus is only on the requirements for maximum background noise levels, not considering the importance of the position of noise sources in the room. For example, for classrooms and lecture halls in Slovenia, TSG-1-005:2012: Noise

protection in buildings [7] specifies the maximum acceptable sound pressure levels LAeq = 30 dB(A), and noise generate by equipment LAFmax = 40 dB(A).

This study aims to investigate the influence of background noise levels and the position of the ventilation system (HVAC) on the speech intelligibility in the lecture hall. Our research objectives are: i) to record speech produced by an artificial speaker at different listening/microphone position in the room, where an additional noise source (positioned at different locations in the room and reproducing noise at different levels) generates noise as would be produced by the HVAC, ii) to measure the Speech Transmission Index (STI), which objectively determines speech intelligibility, under the same conditions, iii) to perform listening tests (N=80) to quantify the intelligibility of digits and subjectively assess speech intelligibility using questionnaires (N=80), iv) to compare the acquired speech intelligibility results acquired with the different approaches and to determine the suitability of the STI parameter as an indicator of speech intelligibility; and v) to develop recommendation for speech intelligibility in lecture halls and classrooms regarding the position and level of background noise levels.

2. METHODOLOGY

The STI measurements and the acquisition of the acoustic recordings were carried out in a lecture hall of a higher education institution with a net volume of 280 m^3 [Fig. 1], and a capacity of 40 listeners. In addition to STI, we measured the reverberation time according to ISO 3382-2:2008 [8] and evaluated it in relation to the national technical guideline TSG-1-005:2012 [7].

The recordings were made after the teaching activities on April 15 2022 in the 14:00-19:00 time range. The following measurement equipment was used:
- Reproduction of speech and of the STIPA signal (hereafter referred to as artificial speaker): NTi Audio, TalkBox,
- Spatial audio recording: 4th order ambisonics microphone: mh acoustics, Eigenmike®,
- Class 1 audio analyser and level meter: NTI Audio, XL2,

- Dodecahedron loudspeaker for reproducing the HVAC noise and for reverberation time measurements: NTi Audio, DS3 Dodecahedron (with NTI Audio, PA3 Power Amplifier),
- Binaural reproduction: AKG, K702 (Reference Studio Headphones),
- Computer audio interfaces: RME, FireFace UFX+ soundcard and PreSonus, HP60 headphone preamplifier,
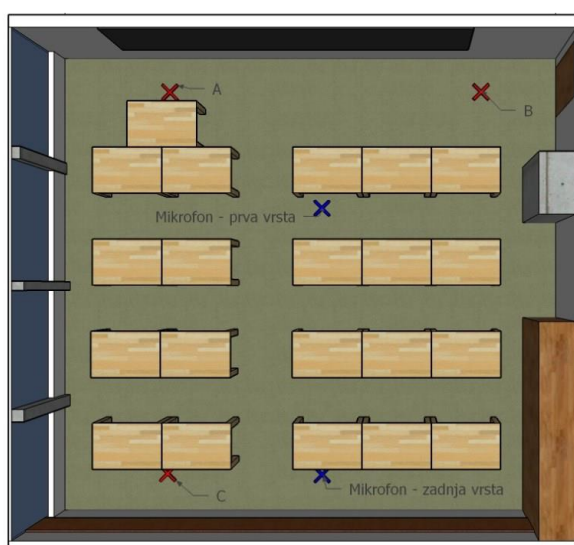- Diagnostic audiometer, Interacoustic, AD226.

Fig.1. The floor plan of the lecture hall used for the experiment (V=280 m³). The noise source position is indicated in red (A, B, C), the microphone positions are indicated in blue (first/last row), the artificial speaker was positioned at the location A.

2.1. The generated noise

A dodecahedron loudspeaker was used to generate the artificially added HVAC noise. The height of the dodecahedron was fixed to 183 cm, while the ground positions were in points A, B and C (see Fig. 1). The noise was generated at four levels of 40 dB(A), 50 dB(A), 60 dB(A) and 70 dB(A). The spectral characteristics of the generated noise followed the spectrum of the Noise Criteria Curves (NC), which are used to evaluate the background noise of unoccupied buildings and rooms [9]. Since the ANSI/ASA S12.2-2008 standard for schools suggests an NC value between 25 and 35, the NC-30 curve was used to generate the spectrum of the ventilation noise [10]. The lowest HVAC noise level also corresponds

to the nose level limits for more demanding intellectual work defined by the Slovenian Guideline for Ventilation of Classrooms.

2.1. Ambisonics recordings

An audio sample of random digits was recorded in advance by four different speakers under studio conditions. This audio sample was reproduced by the artificial speaker and recorded using an ambisonics microphone. The recordings were done under 26 conditions, differing in the level and position of the noise source. The recordings have been made with the microphone in two positions – in the first and last row (see Fig.1). In the next step, the digit recordings were processed to perform binaural listening tests.

2.2. STI measurements

The Speech Transmission Index (STI) was measured under the same conditions and microphone locations as the ambisonics recordings. The STIPA signal defined by EN 60268-16 [11] was reproduced by the artificial speaker. For each condition, three STI measurements were taken, and finally, the mean value was used for the analysis. We obtained STI values for each investigated condition, i.e., 26 in total.

2.3. Listening tests and subjective evaluation

Subjective assessment of speech intelligibility was performed using a standardised questionnaire (5-12 May 2022) [12, 13], which consists of three parts. In the first part, seven general questions related to noise in lecture halls were given; in the second part, two questions about the effects that the respondents experience due to noise were given; and in the third part, the participants listened to recorded audio samples of three random digits. For the third part, the order of listening to digits recorded at different conditions has been randomized. The participants were asked to write down the digits and to evaluate the perceived intelligibility corresponding to the digits on the 0-10 scale.

We recruited 80 volunteers to carry out the questionnaire after which we also evaluated their hearing threshold. From the obtained audiograms, we identified a hearing

impairment of one of the test subjects whose responses were excluded from the analysis. This research was approved by the Ethics Committee for Research Involving Human Subjects, University of Ljubljana (2012-2021; Ljubljana, 18 February 2022).

3. RESULTS AND DISCUSSION

The measured reverberation time was 1.5 s in the 1000 Hz 1/3 octave band. The value is almost twice exceeding the recommended values for the room to be used for lecturing and it has been estimated that reverberation time would be too long even when the room is fully occupied. In fact, the optimal reverberation time (T_{opt}) for the room would be 0.61 s with the upper tolerance range at 0.74 s [7].

3.1. Speech Transmission Index (STI)

The results of the STI measurements shown (see Fig. 2) that the highest speech intelligibility is achieved in the cases with no additional noise and in the cases with additional noise at a level of 40 dB. Under these conditions, the STI values are around 0.5, which, according to BS EN 60268-16 [11], is considered as *sufficient* for rooms such as lecture halls (classes H and G). At the 50 dB noise level, the STI values range from 0.40 to 0.44 corresponding to the *poor* intelligibility (class I), while at the 60 dB noise level the STI values range from 0.24 to 0.28 corresponding to *very poor* intelligibility (class U), which is also the achieved class for the 70 dB noise case, where the STI values range from 0.11 to 0.13.

The 40 dB level coincides with the recommendation of the current Guideline for the Ventilation of Classrooms (IZS MSS-01/2021), which sets a limit of 40 dB(A) as the maximum noise level from air-conditioning systems for the most demanding intellectual work [14]. The same limitation is also in the national Technical Guideline TSG-1-005 [7].

The effect of the noise source position on the STI is relatively small, but there is a clear trend towards position C being the most unfavourable. Similarly, we generally observe higher STI values for the position of the microphone in the last row. This is effect is most likely due to the directional properties of the speaker, which is

oriented more toward the recording position in the last row. This results in a higher proportion of higher frequencies in the acquired STIPA signal and, consequently, a higher STI, although the distance to the artificial speaker is larger for the last row recording. It is expected that in larger lecture halls the STI would behave differently and show the trend of decrease with distance from the source, due to the SNR distance decrease. This claim is supported by the results of Čudina and Prezelj [5], showing that both the A-weighted speech level [dB(A)] and the speech intelligibility index value decrease as one moves towards the last row.
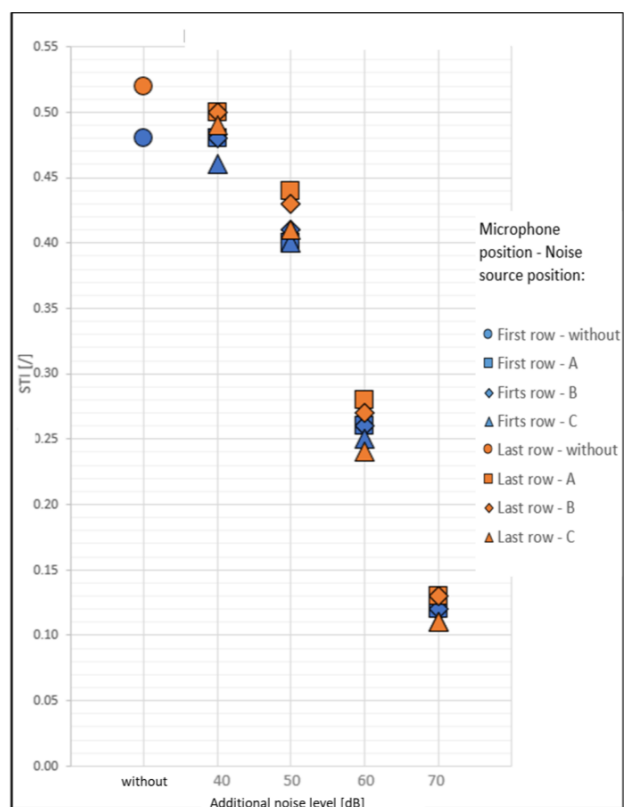

Fig.2. Measured STI for different positions and levels of HVAC noise and for the listening position in the first and last row.

3.2. Survey results

Fig. 3 shows the distribution of responses on the five-level Likert scale acquired with the questionary. Part 1 included 7 questions:

- *How likely is the specific noise experienced to influence the hearing capability of lectures?* (a-g)

Part 2 included 2 questions:

- *How often do you change the seat in the lecture hall due to noise?* (h) and
- *How often noise influences your concentration?* (i).

The participants confirm that it is likely (mean 3.56) for their concentration to be influenced by noise sources (question i). Nevertheless, they rarely take action, i.e., change seat due to noise in the room (question h, mean 1.80). Among the listed noise sources none of them significantly stands out. Noise of the devices (option c) and building equipment (option d) are the least reported with the mean of 1.62 and 1.67, respectively. The remaining options are relatively with the mean values around 2.5.

3.3. Number of errors

The total (cumulative) number of errors of the digit intelligibility is shown in in Fig. 4. As expected, the number of errors increases with the noise level. At noise levels of 50 dB or less an insignificant number of errors has been made by listeners, while at the high noise levels (70 dB) in most conditions all the 80 digits were unintelligible. In the investigate noise levels range, the intelligibility was very discreetly transitioning from the full intelligibility to the full unintelligibility. To observe a smoother transition, it would be interesting to additionally investigate the subjective intelligibility at intermediate noise levels.
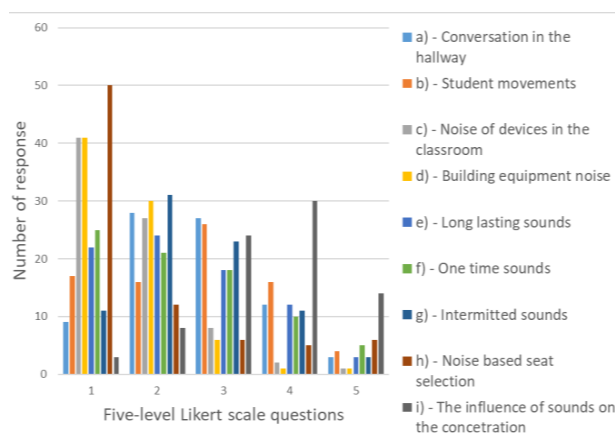

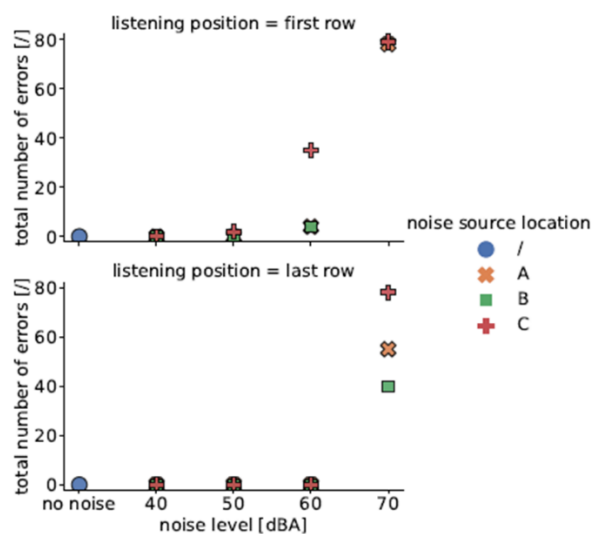**Fig.3. Number of responses on part 1 and 2 of the questionary on the five-level Likert scale.**

Fig.4. Total number of errors performed when listening to recorded digits at different microphone position, noise source position and generated noise levels.

Comparing the number of errors at the noise levels of 60 and 70 dB in relation to the microphone position, we can see that a lower number of errors occurred in the last row. In this row, is the number of errors also highest for the C noise source position. This indicates that the proximity to the noise source at high levels strongly affects the intelligibility.

The fact that more errors are present in the first row agrees with the trend observed for STI, which is favouring the recording/listening position closer to the axis of the speaker, i.e., in the last row. Nevertheless, no plausible explanation can be provided for the C position of the noise source at the 60 dB performing the worst, since the distances between the listener and the A, B, and C points is approximately equivalent.

3.4. Subjective rating – speech intelligibility assessment

The acquired subjective ratings of speech intelligibility are presented in Fig. 5. Similarly to the STI and digits errors, the subjective speech intelligibility scores decrease most markedly as the level of additional noise increases. Alike, is also the overall intelligibility in the last row higher.

The noise source position also influences the subjective speech intelligibility ratings. For the first row, the difference between A, B, C positions is relatively small,

with the position C generally producing slightly lower score. More interesting results can be observed for the last row listening. In fact, in the cases with low additional noise levels of 40 and 50 dB, the loudspeaker position has an effect depending on the direction of the speech and noise sources relatively to the listener; the more the two directions differ, the higher the subjective intelligibility scores. The fact that such dependency is not observed in the first row is most probably related to the listening position being further from the acoustic axis of the speaker. This reduces the high frequency components of speech and lead to a lower capability to discriminate between sound sources.

For this reason, the best configuration for the last row listening was C, in which case the noise source was most differing in direction compared to the speaker. This behaviour is not in agreement with the STI results which showed A noise source position as the best performing. It follows, that the different direction of the speaker and noise source cannot not be detected by STI which is in this sense a limited parameter.

On the other hand, at the higher noise levels of 60 and 70 dB the position of loudspeaker C generates the lowest perceived intelligibility. This means that at higher noise levels, the effect of the distance from the noise source and the related SPL becomes more relevant than the direction of sound sources. In this range, the results agree with measured STI values, in which case loudspeaker position C is also the worst performing.

From the last row results it can be summarized that two different regimes can be observed: a low noise regime, in which the direction of the noise source is more important, and a high noise regime, where the distance to the noise source is more important to achieve high intelligibility. We would expect that the observed regimes would be more pronounced if the investigated lecture hall would have a shorter acoustic response and as such facilitate the localisation and discrimination of sound sources.

4. CONCLUSION

The intelligibility in a lecture hall has been investigated for HVAC noise sources at different locations and SPLs. The complex research approach included advanced sound recording and reproduction techniques, listening tests, and questionnaires with the goal of identifying factors that are relevant for speech intelligibility. On this basis design recommendations for introducing noise sources into the built environment could be developed.

The main conclusions of the research are:
1. All intelligibility rating are most affected by the additional SPL level of the noise source.
2. STI indicators are also affected by the position of the microphone, showing that in the investigated room the position of the listener on the acoustic axis of the speaker is slightly favourable, which, in our case, was the case in the last row.
4. Considering the subjective assessment of intelligibility, the noise source furthest to the listener produces the best listening conditions at higher noise levels. In contrast, at low noise levels, moving the noise source away from the speaker is favourable.
5. Overall, on the basis of the obtains results it is possible to formulate the recommendation that at lower noise levels positions away from the speaker should be chosen
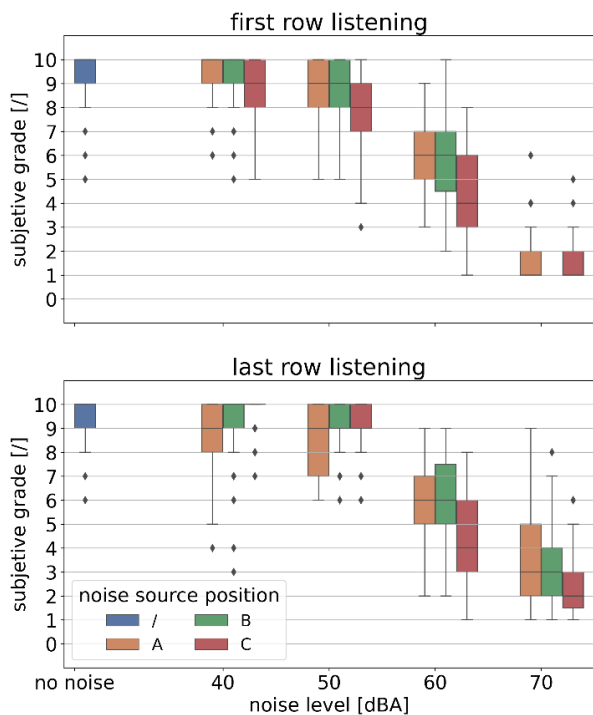

Fig. 5. Box plot of the subjectively rated speech intelligibility on the 0-10 scale for different noise levels and noise source position, when listening in the first (top) and last (bottom) row.

while at higher noise levels noise positions away from the listener should be used.

Generally, it can be concluded that the presented approach has produced valuable results. As part of future research, the digit test should be performed at more noise levels, to avoid the high quantisation of the obtained results. Furthermore, the research could be extended to include a broader variety of noise sources that is present in the built environment. In addition, it would be interesting to investigate, how different room acoustic conditions influence the obtained results.

Acknowledgement

5. REFERENCES

[1.] Madbouly, A. I., Noaman, A. Y., Ragab, A. H. M, Khedra, A. M. and Fayoumi, A. G. **Assessment model of classroom acoustics criteria for enhancing speech intelligibility and learning quality**, Applied Acoustics, 114, pp. 147 – 158, 2016. https://doi.org/10.1016/j.apacoust.2016.07.018.

[2.] Serpilli, F., Di Loreto, S., Lori, V. and Di Perna, C. **The impact of mechanical ventilation systems on acoustic quality in school environments** in 52nd AiCARR International Conference "HVAC and Health, Comfort, Environment - Equipments and Design for IEQ and Sustainability" E35 Web Conferences, Volume 343, 2022. https://doi.org/10.1051/e3sconf/202234305002.

[3.] Sieben, G. W., Gold, M. A, Sieben, G. W. and Ermann, M. G. **Ten Ways to Provide a High-Quality Acoustical Environment in Schools**, Language, Speech and Hearing Services in Schools, 31, pp. 376 – 384, 2000. https://doi.org/10.1044/0161-1461.3104.376.

[4.] ASHA. **Classroom acoustics**, American Speech-Language-Hearing Association, 2022. Available at: https://www.asha.org/public/hearing/classroom-acoustics/ (Accessed 8 July 2023).

[5.] Čudina, M. and Prezelj, J. **Intelligibility of speech in classrooms and lecture halls**, AR. Arhitektura, raziskave, 7(1), pp. 39 – 46, 2007.

[6.] Brown, V. A., Van Engen, K. J. and Peelle, J. E. **Face mask type affects audiovisual speech intelligibility and subjective listening effort in young and older adults**. Cognitive Research: Principles and Implications, 6: 492021. https://doi.org/10.1186/s41235-021-00314-0.

[7.] TSG-1-005:2012. **Noise protection in buildings**, 2022. Available at: https://www.gov.si/assets/ministrstva/MOP/Dokumenti/Graditev/tsg_005_zascita_pred_hrupom.pdf (Accessed 8 July 2023).

[8.] EN ISO 3382-2:2008. **Acoustics – Measurement of room acoustic parameters – Part 2: Reverberation time in ordinary rooms**, 2008.

[9.] Noise curves, 2022. Available at: https://web.archive.org/web/20180917215319/https://www.nti-audio.com/en/support/know-how/what-are-noise-curves (Accessed 8 July 2023).

[10.] ANSI/ASA S12.2-2008. **Criteria for Evaluating Room Noise**, 2008.

[11.] BS EN 60268-16:2011. **Sound system equipment – Part16: Objective rating of speech intelligibility by speech transmission index**, 2011.

[12.] Ricciardi, P. and Buratii, C. **Environmental quality of university classrooms: Subjective and objective evaluation of the thermal, acoustic, and lighting comfort conditions**, Buildings and Enviroment, 127: 23-36, 2018. https://doi.org/10.1016/j.buildenv.2017.10.030.

[13.] Jansen, S., Luts, H., Wagener, K. C., Frachet, B. and Wouters, J. **The French digit triplet test: Ahearing screening tool for speech intelligibility in noise**. International Journal of Audiology 49: 378-387. 2009. https://doi.org/10.3109/14992020903431272.

[14.] IZS MSS-01/2021. **Guidelines for classroom ventilation, recommendations for the implementation of effective mechanical ventilation**, 2021.

AAAA 2023 IZOLA 20. - 21. September
10th CONGRESS OF THE ALPS ADRIA ACOUSTICS ASSOCIATION

Contributed papers
Noise and vibrations

1. Integration of Psychoacoustic Perception for Enhanced Design of Axial Fans
   Nejc Cerkovnik (University of Ljubljana, Faculty of Mechanical Engineering)
2. Noise generating mechanisms analysis and its optimization on electronical commutated wet-dry vacuum cleaner suction unit
   Andrej Biček (Nela d.o.o)
3. Modeling and assessment wind turbine noise at different meteorological conditions
   Antonio Petošić (University of Zagreb, Faculty of electrical Engineering and Computing)
4. Evaluation of model based noise protection study based on in-situ vibro-acoustic railway track analy
   Krešimir Burnać (Faculty of Civil Engineering, University of Zagreb)
5. Steel reilway bridge noise, lack of reduction effect on airborne noise due to vibration dampers possibly acting a s noise sources.
   Rok Rudolf (ZAG)
6. Psychoaoustics of Pseudosound in Turbulent flow of Centrifugal Fan used in Household Appliance. Jurij Prezelj (University of Ljubljana, Faculty of Mechanical Engineering)
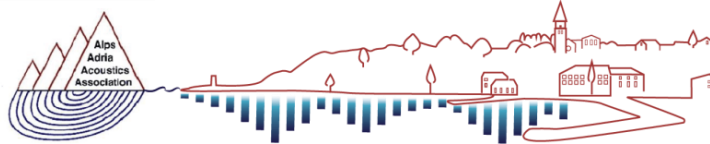
INTEGRATION OF PSYCHOACOUSTIC PERCEPTION FOR ENHANCED DESIGN OF AXIAL FANS

Nejc Cerkovnik, Anže Železnik, Luka Čurović, Jure Murovec, Niko Tivadar*, Jurij Prezelj

University of Ljubljana, Faculty of Mechanical Engineering
*Corsair, Slovenia

Abstract: *Axial fans are widely used in cooling systems but often contribute significantly to environmental noise. Although optimizing the fan geometry usually leads to a reduction in sound power, related noise annoyance is usually not considered. Therefore, the geometry design focus was shifted towards optimizing the geometry for psychoacoustic perception. A psychoacoustic model is developed to correlate measured noise characteristics with subjective noise evaluations, enabling the objective psychoacoustic evaluation of fan prototypes. Psychoacoustic tests were conducted with 100 respondents evaluating recorded signals of noise from nine different axial cooling fans operating at different conditions. Psychoacoustic features were extracted from the recorded signals and correlated to survey results using linear regression analysis. This approach provided a robust model for future evaluation of fan prototypes noise annoyance. The results show that high-frequency components have a major impact on the perception of fan noise. The use of aero-acoustic features on fan blades is suggested. This study highlights the importance of considering subjective noise evaluations in the design of axial fans. By integrating psychoacoustic perception into the optimization process, cooling systems can be engineered to minimize noise annoyance. The developed psychoacoustic model serves as a valuable tool for evaluating axial cooling fan noise of various prototypes, providing insights for future fan design improvements in terms of both acoustic performance and cooling efficiency.*

Keywords: axial fan, acoustics, psychoacoustics, noise

1. INTRODUCTION

In today's rapidly evolving world, which includes areas such as artificial intelligence, cloud computing, and advanced data processing, there is a growing global demand for efficient computer operations. Fast data processing causes the temperature of the processor to rise. Effective management of the accumulated heat is important to ensure processor reliability and performance. Within this thermal framework, the role of low-pressure axial fans as cooling components takes a prominent position. While the design of traditional fans has primarily focused on efficiency, the issue of noise reduction has become significantly more important, especially for fans used indoors where the user is directly exposed to the noise.

Noise pollution associated with computer cooling systems and axial fans can have a variety of effects that affect comfort, productivity and even health. The consequences of noise annoyance go beyond mere acoustic discomfort and can significantly affect various aspects of an individual's well-being.

Noise pollution affects people's comfort indoors. Quiet environments are sought out for relaxation, concentration, and overall well-being. Unwanted noise, especially from continuous sources such as cooling fans, can disrupt the desired atmosphere and hinder the creation of comfortable environments that invite work, rest, and social interactions.

Noise can also directly impact productivity and performance, especially in areas where concentration and cognitive tasks are critical. In workplaces where professionals are engaged in critical thinking and problem solving, disruptive noise can impede cognitive processes, reducing efficiency and task performance.

Prolonged exposure to noise can be detrimental to health. Chronic noise exposure, even at levels that do not cause

hearing damage, has been associated with sleep disturbance [1] the release of stress hormones [2], and consequently an increased risk of cardiovascular disease [3]. In the context of indoor spaces with cooling systems, individuals, particularly those who spend significant time in such spaces, may experience increased stress levels and impaired sleep quality due to persistent noise pollution.

While conventional approaches to fan design often focus on improving efficiency and reducing sound power levels, the psychoacoustic approach considers human perception of noise. By integrating psychoacoustic principles into fan geometry optimization, noise annoyance can be minimised, resulting in a more comfortable acoustic environment.

The main objective of our research is to establish a robust correlation between measured noise characteristics and subjective noise evaluations through the development of an objective psychoacoustic evaluation model that could be used to evaluate optimised prototype geometries of low-pressure axial fans. Prior to this, listening tests must be conducted with a representative number of participants to provide us with subjective ratings of existing axial fan noise.

The basic ideas of psychoacoustics metrics and the evaluation of the quality of a product based on its sound were developed by Fastl and Zwicker [4] in the 1960s and have become more widespread in the last two decades. Today, psychoacoustic metrics are used in the automotive industry [5,6], machinery fault diagnosis [7], in the household appliance industry [8-10], and in environmental noise monitoring [11].

Listening tests based on the subjective evaluation of sound by the listener have always been used to assess sound quality. In the subjective evaluation of sound quality, the use of semantic differentials is well known and has proven to be helpful.

However, because it depends heavily on the subjective responses of the listener, the human response to noise is inconsistent and unreliable [12]. As a result, numerous tests are required, leading to time-consuming and expensive methods for sound quality assessment. Psychoacoustic parameters that can be measured and standardized produce consistent results by streamlining processes and reducing costs. For any type of product, validation methods using listening tests and measured psychoacoustic parameters are the best way to demonstrate their value. To more accurately capture how people perceive technical sounds, noise annoyance

models derived from recorded microphone signals are constantly updated with new variables and features.

Standardised basic psychoacoustic parameters tonality T, percentile loudness N_5, roughness R, fluctuation strength F, and sharpness S exist for the evaluation of various technical sounds and are simply measured and calculated [4].

Zwicker proposed a model to estimate psychoacoustic annoyance from technical noise, such as household appliances, but the model ignores the influence of tonal noise and therefore underestimates it [4]. Tonality is mentioned as one of the main sources of annoying noise and usually occurs when the turbomachine operates under optimal operating conditions. Guoqing [13] (Eq. 1-4) extended the Fastl model [14] to include the tonality compensation term w_T and thus has been used in the evaluation of axial fan noise, which can be highly tonal due to the rotating nature of the machine.

$$PA_{Gouqing} = N_5 \left(1 + \sqrt{w_s^2 + w_{FR}^2 + w_T^2} \right) \quad (1)$$

$$w_s = \begin{cases} (S - 1.75)\, 0.25 \log(N_5 + 10) & S > 1.75 \\ 0 & S < 1.75 \end{cases} \quad (2)$$

$$w_{FR} = \frac{2.18}{N_5^{0.4}}\, (0.4F + 0.6R) \quad (3)$$

$$w_T = \frac{\beta}{N_5^\alpha}\, T \qquad \alpha = 0.52 \quad \beta = 6.41 \quad (4)$$

Lipar et al. [15] have used experiments and jury-based listening tests to develop an objective model for psychoacoustics for use with vacuum cleaners and suction units. They have found that higher roughness levels are preferable to achieve less disturbing sound and therefore this effect was included in the model (Eq.5).

$$PA_{Lipar} = 0.96 \left(\frac{100}{N} + \frac{100}{S} + \frac{1}{T} + F + R \right) \quad (5)$$

Since different authors have presented models for different technical sounds, the proposed metrics differ from each other. To obtain an objective psychoacoustic metric for low-pressure axial fans, subjective responses in the form of listening tests must also be included. Therefore, the aim of this work is to validate the presented models and compare them with subjective evaluations of cooling fans already performed and to develop appropriate metrics in case the existing ones are not sufficient

2. METHODOLOGY

Acoustic measurements were performed on 9 different types of axial computer cooling fans. They were installed in pairs directly on the water cooling radiator in the computer case. The fans drew air from inside the case and blew it out through the water cooling radiator. To avoid interference from ambient noise, measurements were performed in an anechoic chamber. Brüel & Kjaer and two Rode NT5 microphones were used in combination with a Brüel & Kjaer and Motu stage B-1 converter to record sound signals with such low sound pressure levels. All of the microphones were calibrated with a Brüel & Kjaer calibrator. Each pair of axial fans was recorded for 1 minute at various revolutions per minute (RPM) from a distance of 1 meter above the computer case. The experimental setup is shown in Figure 1. According to ISO 5801 [16], the airflow of each fan generated in the setup with the water cooling radiator mounted was measured. Listening test were conducted with 100 participants in the age group between 20 and 50 years. Stereo recordings from Rode microphones were replicated with headphones, and a special program was designed to guide participants through calibration, introduction with a series of examples of tonal-broadband, rough-soft, fluctuating-constant, and sharp-damped noise to prepare them for the test, and the final listening test, which consisted of 22 random order reproductions of axial fan recordings at two different rotational speeds. While listening to the recordings, subjects had to rate the sound they heard using semantic differentials on a scale of -5 to 5. They had to rate the quality of the sound subjectively in terms of the 4 differentials shown in the first column of Table 1. The second column in Table 1 contains 4 differentials that allowed participants to rate the subjective psychoacoustic metrics. After completion of the test, each individual's results were stored in a database. The semantic differentials used in the subjective listening tests and the objectively calculated metrics are summarized in Table 1. For the calculated metrics, the presented models (Eqs. 1 and 5) were used and compared with the subjective evaluation of the cooling fans using linear regression to determine the possible correlation between the two variables. The regression coefficient R^2 was calculated to indicate the strength of the correlation.

| Subjective attained semantic differentials	Calculated metrics from recordings
Week – Powerful	Sound pressure level L_p [dB]
Malfunctioning – well functioning	Loudness N_5 [sone]
Annoying – pleasant	Shapness S [acum]
Cheap – expensive	Roughness R [asper]
Rough noise – soft noise	Fluctuation strength F [vacil]
Sharp noise – damped noise	Tonality T [fone]
Tonal noise – broadband noise	A weighted sound pressure level L_{pA} in octave bands [dBA]
Fluctuating noise – constant noise	

Table 1: Measured variables
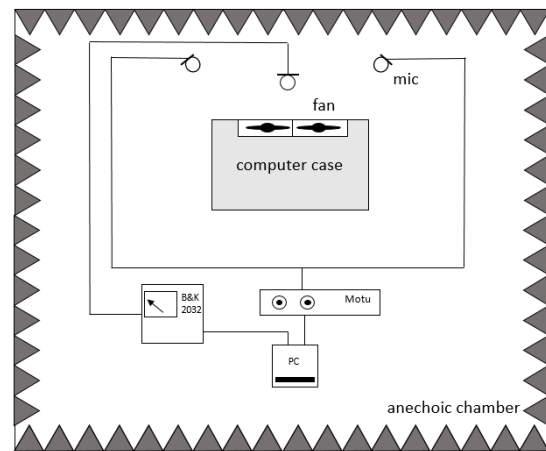
Figure 1: Measurement setup

3. RESULTS AND DISCOUSSION

The aim of the linear regression between two selected semantic differentials was to find the correlations between them and thus to emphasize the importance of the selected metric in order to take it into account in the design of new geometries of axial fans. The results in Figure 2 show us otherwise. The subjectively evaluated noise annoyance was compared with the calculated sound pressure level (SPL). We see that the correlation is low –

R^2 value of 0.24. This result clearly shows that the noise of quiet cooling fans is not necessarily pleasant and emphasizes the importance of including psychoacoustic perception in the design process of cooling fans.
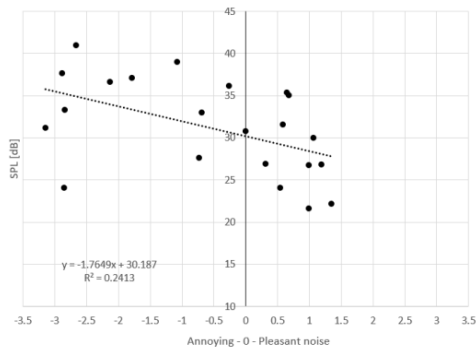

Figure 2: Correlation between measured SPL and subjectively evaluated perception of noise as annoying – pleasant.

Our results showed that the greatest effect on the sound pressure level and loudness of the axial fan is the amount of airflow delivered, an effect that is well known due to the intense vortex shading at the fan outlet [17]. Interestingly, the results showed that the subjective perception of a weak and strong noise is correlated with the amount of airflow conveyed. Figure 3A shows a correlation between airflow velocity, sound pressure level, and calculated loudness. When the linear regression function is positively sloped, it means that the loudness and SPL increase as the airflow velocity increases. Axial fans that produced higher airflow velocity were rated as more powerful by participants in the listening tests (Fig. 3C), and it was also found that the low-frequency component was related to both airflow velocity and the perception of the sound as weak or powerful (Fig. 3B). This implies that axial fans, which produce higher airflow for the same system resistance, produce more intense vortex shedding, increasing the overall sound pressure level, and are the source of the low-frequency components that contribute to the perception of the sound as more powerful. Unfortunately, no correlation was found between powerful sound and the semantic differentials of annoying-pleasant and cheap-expensive.
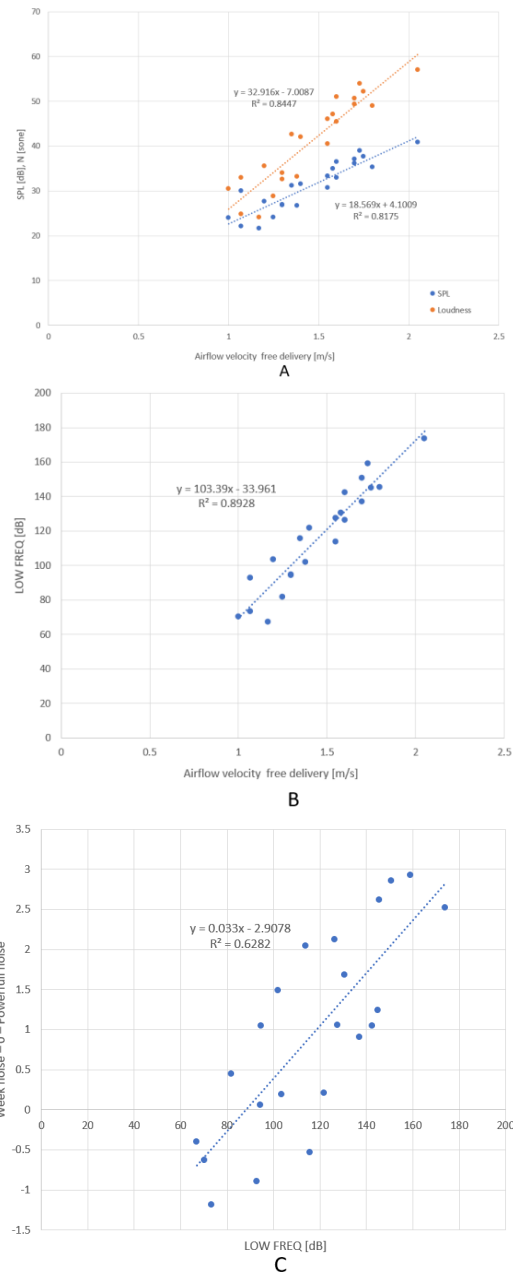

Figure 3: Correlation of delivered air flow of fans with low frequencies components in noise signal end its subjective perception.

The only strong dependencies found between the calculated standardised psychoacoustic metrics and the subjective evaluation of sound quality were the correlation of sharpness and the difference between annoying- pleasant noise. Sharp sound was found to be annoying, as shown in Figure 4. This finding needs to be

directly addressed in future axial fan geometries to avoid annoying noise components.
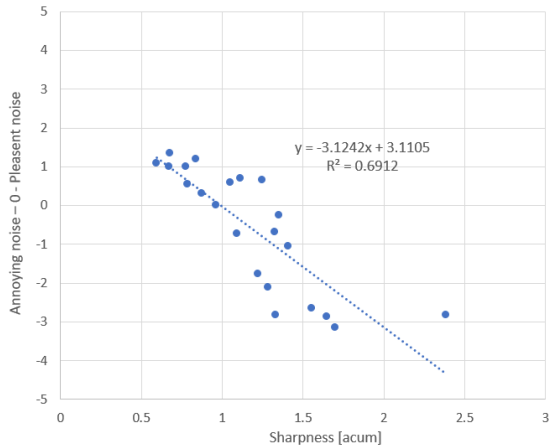

Figure 4: Correlation between sharpness and subjective assessment of noise quality in semantic differential of annoying noise – pleasant noise.

Further investigation into what these components might be revealed that the higher frequencies have a major impact on noise quality. Fig. 5 shows the correlation between the high-frequency component at SPL and various subjective differentials. The participants rated the noise with emphasised high frequencies as cheap (Fig. 5 B), also high frequencies in the fan noise could represent a possible malfunction of the machine (Fig. 5 A) and therefore the overall noise was perceived as annoying (Fig. 5 C).
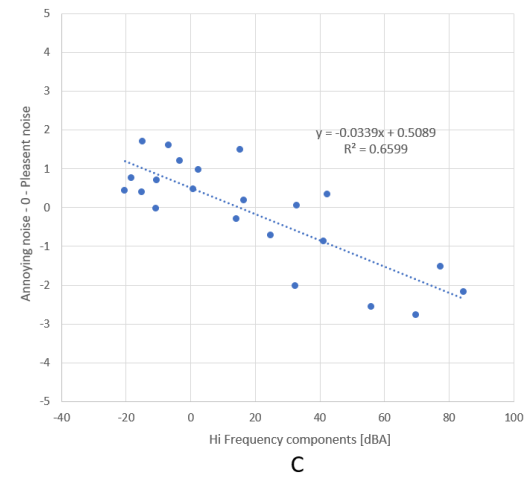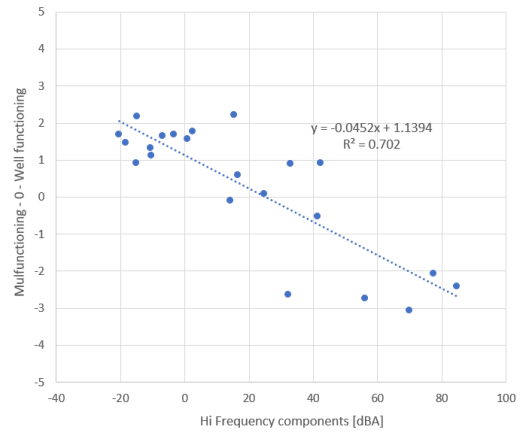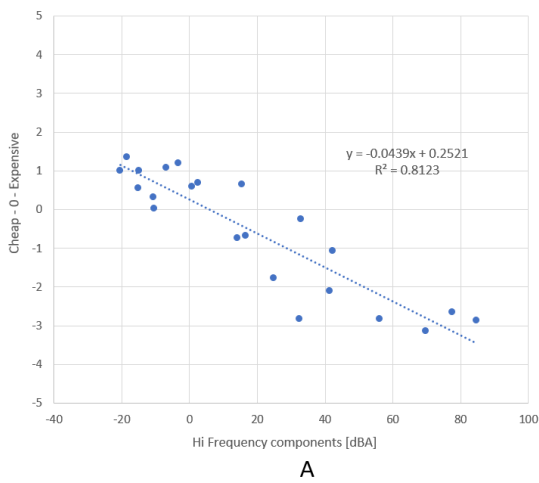

A

B

C

Figure 5: Influence of high frequency components to subjective assessment of noise quality.

Using psychoacoustic metrics from sound signals recorded with microphones, we calculated acoustic annoyance with Guaqing and Lipar models. Due to the large influence of the high-frequency components, we also developed a new objective psychoacoustic model. The acoustic annoyance was calculated using equation 6.

$$PA_{HFREQ} = 0.05 * T - 0.05 * HFREQ \qquad (5)$$

Where HFREQ is the sum of SPL at centre of the one third octave bands with frequencies 4000, 5000, 6300, 8000, 10000, 12500 and 16000 Hz and T is standardised tonality. The calculated values were plotted against the subjective evaluation of noise quality, more precisely against the semantic differential of annoying- pleasant noise. Linear regression showed us that Lipar´s and the newly proposed model provide results with strong agreement with subjective perception (Fig. 6B and 6C). The modified

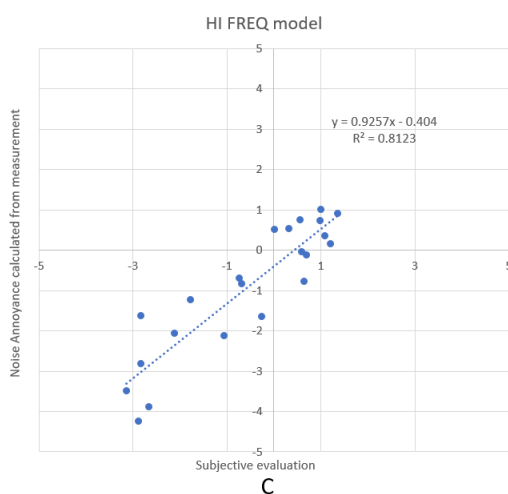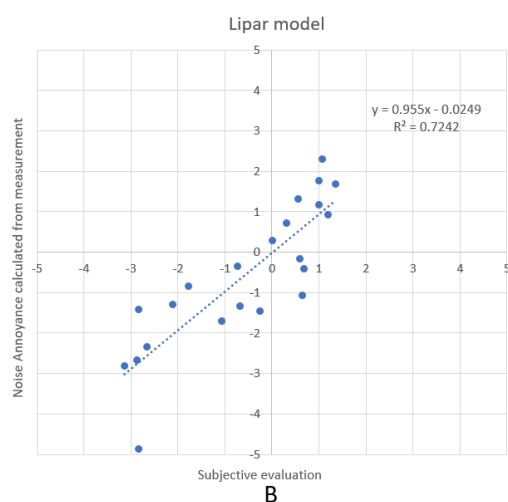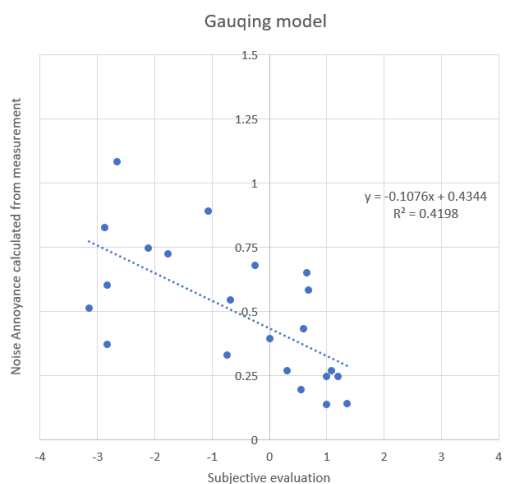Guaqing model does not provide useful results, as shown in Figure 6 A.

Gauqing model

$y = -0.1076x + 0.4344$
$R^2 = 0.4198$

A

Lipar model

$y = 0.955x - 0.0249$
$R^2 = 0.7242$

B

HI FREQ model

$y = 0.9257x - 0.404$
$R^2 = 0.8123$

C

Figure 6: Guaqing's (A), Lipar's (B) and newly proposed (C) model for objective psychoacoustic annoyance compared to subjective noise assessment.

4. CONCLUSION

The results of the conducted listening tests provide very interesting results. First of all, it was proved that the integration of psychoacoustic perception is important in the design of axial fans and that the single value of SPL is not enough to describe the sound as pleasant. It was found that axial fans producing higher airflow rates for the same system resistance of the water-cooled radiator had higher SPL levels measured and that the low frequency band (between 250 and 800 Hz) in the signal was more pronounced due to more intense vortex shedding. This is consistent with the subjective evaluation of the noise by the participants in the listening tests as being powerful. In addition, a large impact of high-frequency components (from 4 kHz to 16 kHz) was found on various subjective sound quality metrics. Sound signals containing the mentioned components were perceived as cheap and annoying. According to participants listening to the tests, such axial fans would be considered malfunctioning. In addition, sharp noises were considered annoying. All of the above issues must be carefully considered when designing axial fans. A simple solution to lower the overall level SPL and eliminate low frequencies would be to reduce the airflow generated, but with this change the axial fan loses its cooling capacity. Therefore, the focus must shift to eliminating higher frequencies from the noise. This could be accomplished by using aeroacoustics features such as serrated trailing edges [17], Gurney flaps [18], winglets [19], and swept blades [20]. Finally, the study has also shown that we can confidently use Lipar's and, in particular, the newly proposed model for a rapid assessment of objective noise annoyance in new axial fan designs without having to perform subjective listening tests with a large number of participants.

5. REFERENCES

[1.] Miedema H. M., Vos H. **Associations between self-reported sleep disturbance and environmental noise based on reanalyses of pooled data from 24 studies**, Behav. Sleep Med., 5(1), pp: 1-20, 2007, doi: 10.1207/s15402010bsm0501_1.

AAAA – 2023 – IZOLA - Conference Proceedings

[2.] Babisch W. **Stress hormones in the research on cardiovascular effects of noise**, Noise Health, 5(18), pp: 1-11, 2003, PMID: 12631430.

[3.] Sivakumaran K., Ritonja J. A., Waseem H., Al Shenaibar L., Morgan E., Ahmadi S., Denning E., Michaud D.S., Morgan R. L. **Impact of Noise Exposure on Risk of Developing Stress-Related Health Effects Related to the Cardiovascular System: A Systematic Review and Meta-Analysis**, Noise & Health, 114, pp: 107-129, 2022.

[4.] Fastl H, Zwicker E. **Psychoacoustics – Facts and Models**, 3rd ed. Heidelberg, Springer-Verlag, Berlin, 2007.

[5.] Arana M., San Martín R., Urroz J. C., Diéguez P. M., Gandía L. M. **Acoustic and psychoacoustic levels from an internal combustion engine fueled by hydrogen vs. gasoline**, Fuel, 317, 2022, https://doi.org/10.1016/j.fuel.2022.123505.

[6.] Leite R.P., Paul S, Gerges S. N. Y. **A sound quality-based investigation of the HVAC system noise of an automobile model**, Appl. Acoust., 70(4), 2009, https://doi.org/10.1016/j.apacoust.2008.06.010. Elsevier BV.

[7.] Kane P.V., Andhare A.B. **Critical evaluation and comparison of psychoacoustics, acoustics and vibration features for gear fault correlation and classification**, Measurement, 154, 2020, https://doi.org/10.1016/j.measurement.2020.107495.

[8.] Jeon Y.H., You J., Chang H.Y**. Sound radiation and sound quality characteristics of refrigerator noise in real living environments**, Appl. Acoust., 68 (10), 2007, https://doi.org/10.1016/j.apacoust.2006.06.005. Elsevier BV.

[9.] Novaković T. et al. **Psychoacoustic approach on centrifugal fan blade design**, Fourth International Acoustics and Audio Engineering Conference, 2017.

[10.] Novaković T., Ogris M., Prezelj J. **Validating impeller geometry optimization for sound quality based on psychoacoustics metrics**, Applied Acoustics, 157, 2020.

[11.] Kang J., Zhang M. **Semantic differential analysis of the soundscape in urban open public spaces**, Build. Environ., 45(1), pp: 150 – 157, 2010.

[12.] Fastl H**. The psychoacoustics of sound-quality evaluation**. Acustica-Acta, Acustica 1997.

[13.] Guoqing D. **An improved psychoacoustic annoyance model based on tonal noises**, Hamburg, Germany, 2016

[14.] Fastl H. **Hearing sensations and noise quality evaluation**, J. Acoust. Soc. Am., 87(S1), pp: 134-134, 1990.

[15.] Lipar P., Prezelj J., Rejec J., Čudina M. **Psychoacoustic approach used for developing the model of sound pleasantness of vacuum cleaners and suction units based on objective and subjective analysis**, 5th Congress of Alps-Adria Acoustics Association, 12–14 September (2012), Petrčane, Croatia.

[16.] ISO 5801: 1997**. Industrial fans – performance testing using standardised airways**

[17.] Qingyi S., Haodong X., Jian C., Jiangtao Z.**Experimental and numerical study on a new noise reduction design for a small axial fan**, Applied Acoustics, 211, 2023, https://doi.org/10.1016/j.apacoust.2023.109535.

[18.] Xuemin Y., Nan Z., Jiami H., Chunxi L., Zhanpu X. **Numerical investigation of the benefits of serrated Gurney flaps on an axial flow fan**, Energy, 252, 2022, https://doi.org/10.1016/j.energy.2022.124072.

[19.] Ye X., Zhang J., Li C. **Effect of blade tip pattern on performance of a twin-stage variable-pitch axial fan**, Energy, 126, pp: 535-563, 2017, https://doi.org/10.1016/j.energy.2017.03.057.

[20.] Park M., Lee D., Lee H. **Experimental and computational investigation of the effect of blade sweep on acoustic characteristics of axial fan**, Applied Acoustics, 189, 202, https://doi.org/10.1016/j.apacoust.2021.108613
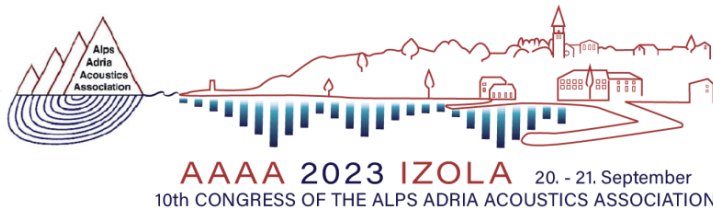
NOISE GENERATING MECHANISMS ANALYSIS AND ITS OPTIMIZATION ON ELECTRONICAL COMMUTATED WET-DRY VACUUM CLEANER SUCTION UNIT

Andrej Biček[1], Janez Luznar [2], Igor Markič[1]

[1] Nela d.o.o., Na plavžu 79, 4228 Železniki, Slovenia
[2] Domel d.o.o., Otoki 21, 4228 Železniki, Slovenia

[1] andrej.bicek@domel.com[1] , j.luznar@domel.com[2], igor.markic@domel.com[1]

Abstract: *Vacuum cleaner's market in EU has after cancelation of Energy labelling of vacuum cleaners nowadays face with the revised regulation which is expected to be started in autumn 2023. The Regulation will establish eco-design requirements for electric mains operated vacuum cleaners including hybrid vacuum cleaners. Domel as leading European producer of vacuum cleaner suction units today produce over 75% of those units in range of 600 to 900 watts of input electric power. Important share of production present electronical commutated motors and vacuum cleaner suction units for commercial and industrial applications. Demanding mounting conditions of those motors into devices and heavy operating duties requires introduction of new development methods and new technologies in production. Through this paper is presented systematic approach of detection of sound mechanisms and their optimization on electronical commutated wet-dry vacuum suction unit will be presented.*

Keywords: vacuum cleaner suction unit, electronical commutation, noise generation mechanism, sound power level, energy labelling, impeller geometry, rotor mass unbalance, vibrations, vacuum cleaner

1. INTRODUCTION

The worldwide vacuum cleaner market revenue in year 2023 is planned on €40,89 billion, but if we divide on individual markets €8,27 billion in the European market incomes are expected on and on China market €12,1billion [1].
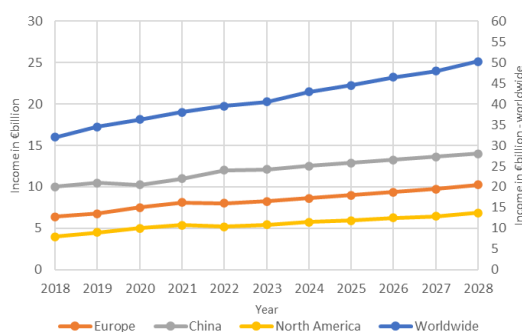
Fig. 1. Vacuum cleaner market revenue in period 2018-2028 for different markets [1]

The growing focus on promoting the use of energy-efficient home appliances in Europe has been driven the market for advanced household vacuum cleaners.

The Eco-design recommendations and Energy labelling regulations for vacuum cleaners were started in 2014 with electric power limitation to 1600W. At the beginning of 2017 the energy consumption of vacuum cleaners has been further limited to 900W, both regulation steps have been presented in paper by Biček et al. [2], [3] In November 2018 the Energy Labelling Regulation was annulled by General Court of the European Court of Justice (Case T-544/13 RENV). The regulation has been reviewed in 2019/2020 and is expected which is expected to be started in autumn 2023.[4]

Vacuum cleaners (in following the instead name Vacuum cleaner abbreviation VC will be used) in general can divided into the following types: upright VC, handheld VC, canister VC, stick VC, robot VC, wet/dry VC, central VC, backpack VC.

The topics that were reviewed are include:

- Tolerance set in the verification procedure for market surveillance purposes.
- Whether full-size battery-operated vacuum cleaners should be included in the scope
- whether it is feasible to use measurements methods based on a partly of loaded rather than empty canister [4].

Following types of vacuum cleaners or similar device will be out of scope of Energy labelling regulations: wet, wet &dry, battery-operated, robot, industrial and central VC, floor polishers and outdoor VC. [4]

Nevertheless, the buyers demand that product are developed according to Eco-design recommendations: energy efficient, high efficiency of dust management and emitted low noise. Important addition is now also use of ecological recycling materials and carbon footprint analysis. All these restrictions and recommendations are important also for vacuum cleaner unit producers and Domel is one of the biggest in Europe.

Fig. 2. Types of vacuum cleaners which will be subjected to energy labelling, left – canister vacuum cleaner with bag, right – upright cyclone cleaner [5]

Fig. 3. Types of vacuum cleaners which are excluded from energy labelling: left - battery hand cleaner, middle - floor polisher, right - ash and grass suction unit [2]

2. AN REVIEW OF PAST WORK

Emitted noise of vacuum cleaner suction unit (VCU) is consisting of aerodynamic and structural borne origins. Structural noise could be divided on mechanical, vibration and electromagnetic origins [6]

Čudina and Prezelj [7] are in 2006 described some noise origins of dry suction unit. The authors found that trend of vacuum cleaner development show speed increase from 50000 min-1 to 70000 min-1 or even higher, meanwhile lifetime of vacuum suction units is decreasing and level of emitted noise is opposite increasing. Further they describe origins of rotation and non-rotation noise and explain airflow and noise conditions in rotor depend of operating point.

Čudina and Prezelj further in article [8] systematic discuss effect of presence of blade and blades diffuser on aerodynamic performances and on noise level in closed acoustic field and its direction. They measured sound pressure on grid on vacuum suction surface. They found that sound pressure level is oriented and therefore is needed to consider that to use same positions at noise measurements. Further they measured sound pressure level of VCU at different speeds and loads.

Čudina and Prezelj in third article [9] performed analysis of structural excited noise on total noise level of VCU. They determined several positions on VCU surface and measured vibrations and sound pressure in the same. Through vibration velocity spectrum they determined noise origins regarding to frequency of rotation fR and blade passage frequency fRR. Additional they compared noise spectra of VCU with and without rotor of centrifugal blower (CB). They found that noise of electromotor alone is much lower compare of noise of centrifugal blower. At end authors concludes that dominant noise of VCU is aerodynamic origin, meanwhile electromagnetic origin depends on electromotor type, its geometry and load is main source of structure noise.

Prezelj and Čudina in next article [10] identify part of aerodynamic and structural excited noise. They setup experiment on way that fixed VCU on device (see figure *4*). Another VCU generated airflow through observed VCU, and they measured generated aerodynamic noise at blocked rotor. Structural noise they generated by mini shaker which excited housing of VCU. Result was transfer function of aerodynamic and structural noises depend on frequency.
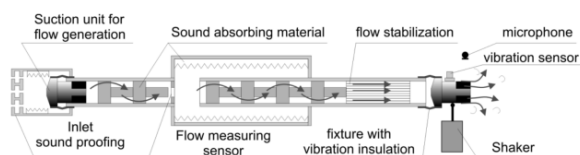
Fig. 4. Aerodynamic and structural noise experiment [11]

Ob structural noise could significantly influence rotor unbalance as rotational origin of VCU. Mass unbalance of rotor could be cause by design, material inhomogeneity, parts manufacture and assembly process [12]. Regarding to occurrence the rotor unbalance could be described as static, moment and dynamic unbalance.

Petrič et al. [13] describe problematic of unbalance rotor of alternator. They found that material cut out gaps on surface rotor due of balancing process collapse symmetry of geometry shape and consequently also magnetic symmetry of rotor because of local increased air gap between rotor and stator pole or magnet segments. By 2D finite element method (FEM) authors have been demonstrated that reduced density of magnetic field effect on reduced magnetic force. Experimental have authors confirmed that number and depth of gaps effect on vibrations. Measurements on motor bracket have shown that vibration levels before and after balancing remained at equal level, sometimes has been even increased.

3. SOUND GENERATING MECHANISM OF VACUUM CLEANER SUCTION UNIT

Sound generating process is complete system consist of 3 basic components like as sound origin, the path of propagation and noise detection (by listener or measurements). Starting point of noise generation are caused with several excitation forces through complex connections which are for vacuum cleaner suction unit in general listed in Fig. *5*. Elementary noise origins could divide on aerodynamics, mechanical and magnet sources, which effect through parts main function or parts geometry deviation generation forces on electromotor elementary lamination of structure (housing) of suction cleaner motor. Ratio of noise sources could be different regarding to type of electromotors like brush commutated electromotor or electronically commutated motor.
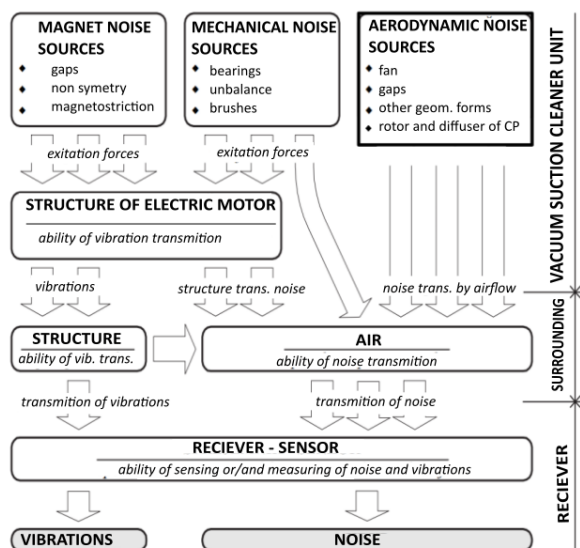
Fig. 5. Sound generating mechanisms of vacuum cleaner suction unit. [14]

3.1. Magnetic noise of electromotor

Magnetic noise is occurred due of periodic excitation of electromotor structure with magnetic forces and the phenomenon of magnetostriction. In the latter due variable magnetic field, the elastic deformation in material is occurred and this resulting in magnetostriction noise. This is typical for large lamination structures like the transformers, meanwhile for the medium or small electromotors this effect is usually neglected.

Fig. 6. Mechanism of noise and vibration generation in electromotors[15]

Electromagnetic forces can be shared on useful tangential forces that cause torque and radial forces that act on stator of electromotor and cause radial deformation and noise as shown Fig.*6* [15]

Last period has been on market increased ratio of electromotors controlled with electronical commutation, which is process of sequence control relative on rotor position. Electronical com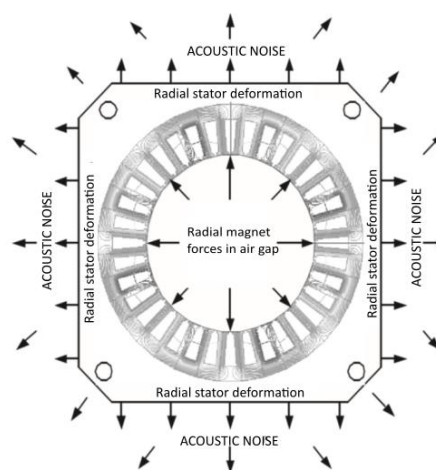mutation in this case fulfils traditional task of commutator and brushes with main difference that for commutation or switching of inductive windings control electronics is used. Complete scheme of electronically commutated electromotor from the input electric power supply to the mechanical output as torque is shown of Fig.*7*.
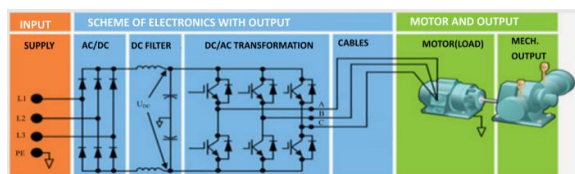

Fig. 7. Electronically commutated motor in 3 segments as input, electronics, motor [16]

Fig.*7* show electronics with 6 transistors care that electromotor is controlled with pulse – wide modulation (PWM). The PWM excitation harmonics cause electromagnetic forces, which interact with the structure. The PWM voltage excitation harmonics depend on the carrier type, the carrier frequency f_c, the fundamental frequency f_1 and the modulation index m_a ,generated frequency harmonics are shown on Fig.*8* .[17] The variable motor load results in different proportions of the switching harmonics in the in the PWM voltage excitation and therefore the structure-borne noise minimization is complex task
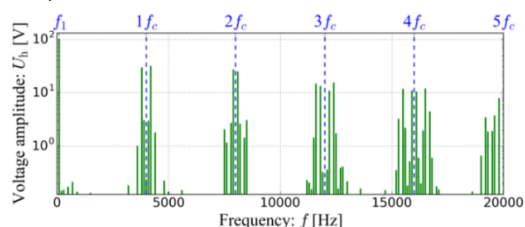
Fig. 8. Frequency contents of the voltage excitation harmonics for a sine-triangle PWM [17]

3.2. Structural dynamics
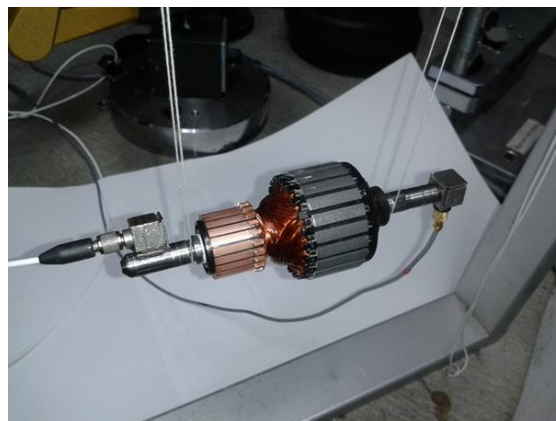
Fig. 9. Experimental rotor eigenfrequencies identification

Excitation forces effect on structure dynamics of electromotor parts and they should be tested to avoid later issues at electromotor operation. In development process are used mechanical simulations with Ansys software and results are subsequently confirmed with experimental modal test as it shown for rotor on Fig.*9*

3.3. Aerodynamic noise
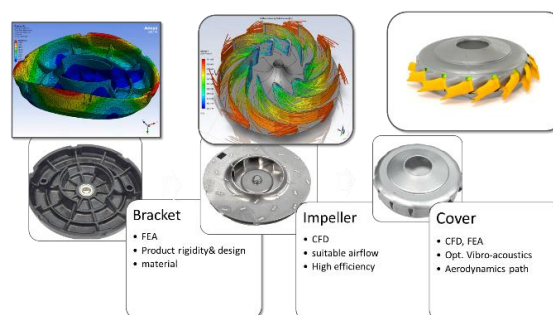
Fig. 10. Simulation tool for mechanical and aerodynamic optimization of parts of vacuum cleaner suction unit

Aerodynamic noise is occurred due high speed and nonstationary flow of air through aerodynamic part of vacuum cleaner suction unit and interaction of airflow with obstacles. Geometry of impeller (rotor) and diffuser (stator) ensure performance parameters on other side important effect also on acoustics behave. Therefore, beside experiences also simulation software like Ansys Fluent are used, simulation steps are presented on Fig.*10*

4. OBJECTIVES AND EXPERIMENT

4.1. Electronically commutated vacuum suction unit - (EC VCU)

Vacuum suction unit VCU 467 and its optimization has been presented in some previous papers. [18]
Eco design goals to developed energy efficient and less material weight products Domel used to developed new EC VCU 759 as it presented in Fig.*11*.

Fig. 11. Vacuum cleaner suction units (VCU) comparison: VCU467 and EC VCU759

4.2. Experiment design

At VCU optimization we designed experiment to analyse effect of input unbalance of rotors and impellers on vibrations on VCU. Test has been started with 2 groups of rotors and 2 groups of impellers (non-dimensional values of unbalance is presented in table 1) which has been separate prepared on balancing machine.

Table 1. Unbalance values of rotors and impellers for test

Group of EC VCU 759	Unbalance value [/]	
	Rotor unbalance	Impeller unbalance
1	0,45-0,75	>0,6
2	0,45-0,75	<0,45
3	< 0,3	>0,6
4	<0,3	<0,45

4.2. Balancing process

High requirements regarding low vibration levels of EC VCU require that rotors have low unbalance values. Domel developed new technology approach of precise balancing

rotors with laser material removal as is presented on Fig.*12*.
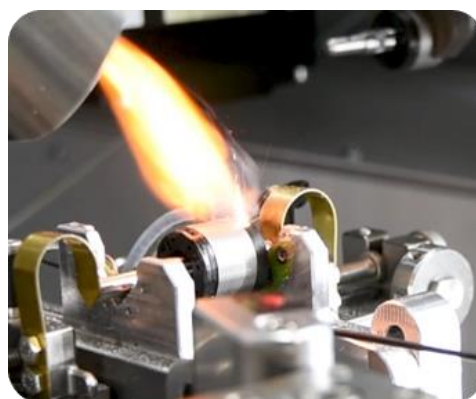

Fig. 12. Rotor balancing process with nonconventional technology.

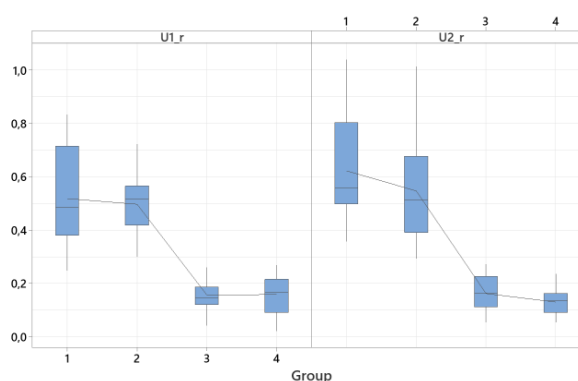Unbalance values of group of rotors and impellers prepared for test are presented on Fig.*13* and Fig.*14*.

Fig. 13. Unbalance values for rotors at balancing planes U1 and U2
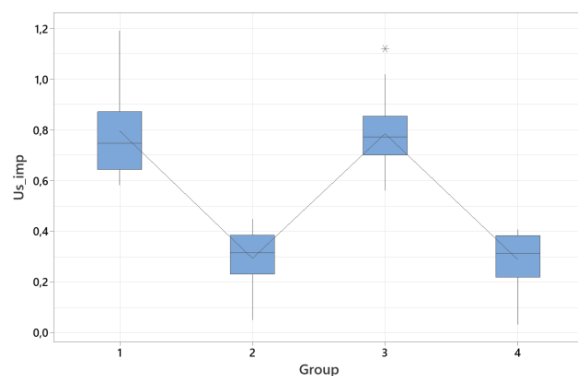

Fig. 14. Static unbalance values of impellers

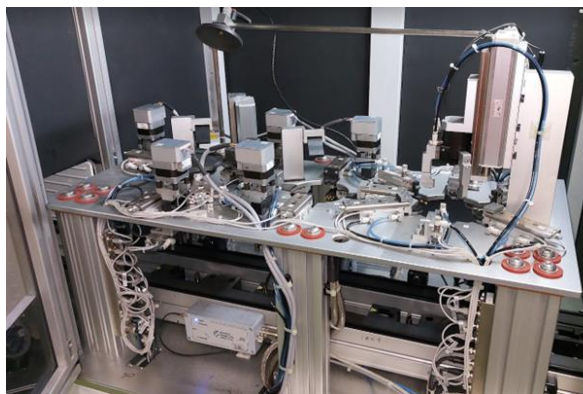### 4.3. Vibration measurements on assembly line

Fig. 15. Diagnostic device on assembly line for vibration control

EC VCU has been assembled on full automatized assembly line and inspected on 3 stage diagnostics control devices on end of assembly line. Vibrations on this device are measured with laser vibrometer Polytec IVS 500.

For each EC VCU vibrations has been measured on 3 positions on one section plane like axial on cover, radial on cover and radial on middle of stator lamination.
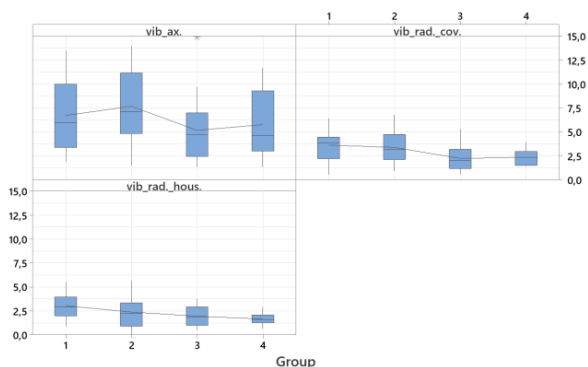
5. RESULTS

Fig. 16. Vibration velocity RMS values for vibration in axial, radial position on cover and radial position on housing (stator lamination)

Vibration levels on Fig.*16* show that there is present correlation between unbalance and vibration values.

According to input unbalance values on Table 1 we can see that radial vibration slightly in average slightly drop down.

At axial vibration there is no correlation which is logical due different vibration mechanism, like axial spring preload, axial magnetic forces, and impeller axial deviation.

6. CONCLUSION

Vibration RMS velocity scaled values were presented for 4 groups of EC VCU with 2 groups of balanced rotors and impeller. At development of new EC VCU generation new materials has been used therefore also new modelling approached has been needed. To achieve sharp requirements 2 new technologies in process like laser welding and balancing have been implemented. Issues will be used at new projects.

7. REFERENCES

[1] Vacuum Cleaners - Europe | Statista Market Forecast, https://www.statista.com/outlook/cmo/household-appliances/small-appliances/vacuum-cleaners/europe?currency=eur, (n.d.). https://www.statista.com/outlook/cmo/household-appliances/small-appliances/vacuum-cleaners/europe?currency=eur (accessed September 18, 2023).

[2] E. Commission, Guidelines accompanying : Commission Delegated Regulation (EU) No 665 / 2013 of 3 May 2013 supplementing Directive 2010 / 30 / EU with regard to energy labelling of vacuum cleaners and Commission Regulation (EU) No 666 / 2013 of 8 July 2013 implementi, (2014).

[3] Andrej. Bicek, Igor. Markic, Janez. Rihtarsic, Jozica. Rejec, Mirko. Cudina, Vacuum cleaner suction unit performance and noise characterization an overview, 6th Congress of the Alps Adria Acoustics Association, October 16th and 17th 2014, Graz. (2014).

[4] European Commission: Ecodesign and Energy Labelling Working Plan 2022-2024, commission_guidelines_ecodesign_requirements_for_vacuum_cleaners, (n.d.). commission_guidelines_ecodesign_requirements_for_vacuum_cleaners (accessed September 18, 2023).

[5] Electrolux Company website, https://www.electrolux.si/vacuums-home-comfort/vacuum-cleaners/, (n.d.).

[6] M. Čudina, Tehnična Akustika I, 2011.

[7] M. Čudina, J. Prezelj, Noise generation by vacuum cleaner suction units. Part I. Noise generating mechanisms - An overview, Applied Acoustics. 68 (2007). https://doi.org/10.1016/j.apacoust.2006.10.003.

[8] M. Čudina, J. Prezelj, Noise generation by vacuum cleaner suction units. Part II. Effect of vaned diffuser on noise characteristics, Applied Acoustics. 68 (2007). https://doi.org/10.1016/j.apacoust.2006.10.002.

[9] M. Čudina, J. Prezelj, Noise generation by vacuum cleaner suction units. Part III. Contribution of structure-borne noise to total sound pressure level, Applied Acoustics. 68 (2007). https://doi.org/10.1016/j.apacoust.2006.10.001.

[10] Jurij. Prezelj, Mirko. Čudina, Quantification of aerodynamically induced noise and vibration-induced noise in a suction unit, Proc Inst Mech Eng C J Mech Eng Sci. 225 (2011) 617–624.

[11] J. Prezelj, M. Čudina, Quantification of aerodynamically induced noise and vibration-induced noise in a suction unit, Proc Inst Mech Eng C J Mech Eng Sci. 225 (2011). https://doi.org/10.1243/09544062JMES2187.

[12] ISO 1925:, Mechanical vibration – Balancing – Vocabulary," Int. Organ. Stand., 2001.

[13] M. Petrič, M. Furlan, M. Boltežar, Primerjava masnega ter magnetnega neuravnoteženja rotorja glede na vibracije enosmernih elektromotorjev, Strojniski Vestnik/Journal of Mechanical Engineering. 49 (2003).

[14] M. Furlan, Karakterizacija magnetnega hrupa enosmernega elektromotorja = [Magnetic noise characterization in the DC electric motor] : doktorsko delo, 2003.

[15] J. Luznar, Vibroakustična karakterizacija elektronsko komutiranih motorjev: doktorsko delo, [J. Luznar], 2019. https://repozitorij.uni-lj.si/IzpisGradiva.php?id=113188.

[16] Fluke Inc., "How to measure output voltage from a VFD to a motor" , [Online]. Available: Http://En-Us.Fluke.Com/Community/Fluke-News-plus/Motors-Drives-Pumpscompressors/How-to-Measure-Output-Voltage-from-a-Vfd-to-a-Motor.Html. (2012).

[17] J. Luznar, J. Slavič, M. Boltežar, Experimental research on structure-borne noise at pulse-width-modulation excitation, Applied Acoustics. 137 (2018). https://doi.org/10.1016/j.apacoust.2018.03.005.

[18] A. Biček, I. Markič, J. Rihtaršič, J. Rejec, M. Čudina, Influence of cover outlet geometry on noise spectra of wet vacuum cleaner suction units, in: Hrvatsko akustičko društvo, 2012: p. NOI-03.
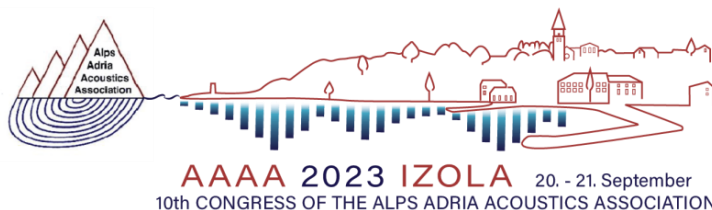
PAPER TITLE: MODELLING AND ASSESSMENT WIND TURBINE NOISE AT DIFFERENT METEOROLOGICAL CONDITIONS

Antonio Petošić, Domagoj Stošić, Mia Suhanek

University of Zagreb, Faculty of Electrical Engineering and Computing, Department of Electroacoustics, Unska 3, Zagreb

Abstract: *In this paper, a model for predicting wind turbine noise under different meteorological conditions (i.e., wind speed magnitudes and directions at 10 metres height) is shown, and residual noise is measured at several different locations around the wind turbine site. The CONCAWE meteorological model method is used for estimating the influence of meteorological parameters with different meteorological classes on noise propagation from the wind turbine as a noise source with different sound powers at different wind speed magnitudes. The modelling results and uncertainties are discussed in terms of acquired meteorological and residual noise levels at considered micro locations around the site. The limit rules for those types of sound sources are analysed for the day/evening/night period regarding the distance from the houses and residual noise at different wind speed magnitudes. Regarding the noise legislation, the measures for reducing wind turbine noise and its influence on energy production are discussed.*

Keywords: wind turbine noise, wind speed and direction, sound power, limit rules, measures for reducing wind turbine noise

1. INTRODUCTION

Noise levels estimation from array of wind turbines is a complex task due to their different sound power levels at different wind speeds and influence of meteorological conditions (favourable, neutral, unfavourable) on excess attenuation due to meteorological conditions (A_{met}) [1,2]. In Croatia there is a rigorous rule that the levels from new sound source(s) are not allowed to increase the residual noise levels more than +1 dBA or the level of new installed sources should be 5 dBA less than proposed limit value [2,3].

In the rural parts of the country (Croatia) the level of residual noise is usually between 20-30 dBA during the night depending on the wind speed at 10 metres and at hub height. The sound power of wind turbines installed at some height (100-200m) can be very high (>95 dBA) at lower wind speeds (3 m/s at 10m) and it is very difficult to obey this rule for increase the residual noise for +1 dBA when the wind turbine is installed at a small distance (>=500m) from the resident objects due to low sound attenuation of lower frequencies.

In this paper the measurement of residual noise at different wind speeds (due to aerodynamic noise around object) and wind directions during the representative period (together with assumed cloudiness for the most favourable propagation meteorological class) are done in duration of two months according to ISO 1996-2:2017 and ISO 1996-1:2016 [5,6]. The residual noise has been measured at critical locations in all wind directions (bins for wind direction in 30° and bins for wind speeds in 1 m/s intervals) around the planned wind turbine installation locations. After the measurements of initial state for residual noise from old wind turbine installed nearby the sound pressure level $L_{A,eq}$ from new sources have been calculated using appropriate modelling software while changing the input parameters which determine the propagation conditions to the resident objects around the old and new wind noise farm.

The modelling results for $L_{A,eq}$ have been compared with residual noise levels ($L_{A,eq,res}$) at each direction (mid of

the bin) and wind speed (mid of the bin). The limit rule for increasing the residual noise by not more than +1 dBA has been tested according to eq. 1.

$$L_{total} = 10 \cdot log_{10} \left(10^{\frac{Lresidual}{10}} + 10^{\frac{Lwindturbine}{10}} \right) \quad (1)$$

The sound power levels of wind turbines (testing different types, numbers, and locations) in one third octave bands are given for different wind speeds and modes of working. The sound pressure levels are calculated at different windspeeds directions (in bins 30 degrees) and the wind speeds when it starts working up to limit wind speed.

The modelling tool used in calculations was ISO 9613-2:1997 [7] with CONCAWE meteorological model [1,2] This calculation procedure is included in the estimation of sound pressure levels from old (calibration procedure for critical directions) and new noise sources installed for each wind speed, direction and meteorological classes (Pasquill) [1,2]. It is assumed in determination of appropriate Pasquill stability classes that in that area zero cloud octas were present during measurements- the worst meteorological class conditions for propagation. We have tried to use some other calculation models (Harmonoise, CNOSSOS-EU [8]). However, only in available programme support with ISO 9613-2:1997 calculation procedure the CONCAWE meteorological correction was available. According to the previous research the CONCAWE model is most suitable to assess A_{met} while estimating sound pressure levels.

1.1. Measurement and modelling situation

Measurement and modelling situation with installed wind turbine sources (old and new) is shown in Fig. 1.
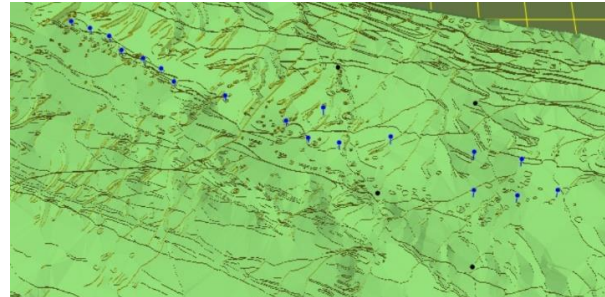
Fig.1. Measuring and modelling situation with critical measurement positions and old and new sound sources (8 wind turbines)

After analysing the residual noise levels at different wind directions and speed at different critical measurement positions the sound pressure levels from old wind turbine sources is calculated with known sound powers and the model parameters (reflection coefficient and wind speed at hub height-roughness has been calibrated). The residual noise level for the dominant propagation direction at 4 m/s speed (at 10 m height) has been compared with modelling result for old wind turbines at closest positions (MM1 and MM3) for the appropriate wind speed at hub (calculated by assuming logarithmic wind speed profile and measured one) and average difference was in the range of ±0,5 dB with ground reflection coefficient G=0.2. At higher speeds and further locations, the dominant part is aerodynamic noise around objects, so the results are not used in calibration of the model.

2. THEORETICAL PROPAGATION MODELL

The ISO 9613-2:1997 calculation model [7] assumes the that the sound power, directivity, reflection coefficient from ground (G=0.2), attenuation in air and meteorological correction in frequency range of interest (usually octave) is known to find sound pressure levels at different positions.

The calculation formula for sound pressure L_p is given by eq. 2,

$$L_p = L_w - 20 \cdot log_{10}(r) - 11 \, (dB) + D - \sum_{attenuation} A \, (dB) \quad (2)$$

where L_w is sound power of the source (usually in one third octave bands)
r (m)-distance from the source
D (dB)-directivity factor (D=0 at hub height, point source)

Attenuation factor depends on the many complicate factors for each propagation frequency as given in eq. 3.

$$A_{attenuation} = A_{atm} + A_{ground} + A_{obstacle} + A_{vegetation} + A_{meteorology} + A_{turbulence} + .. \quad (3)$$

The most critical factor in wind turbine noise is meteorology A_{met} which depends on the wind speed and direction (wind speed component in the source-receiver direction) and on the solar radiation. The detailed connection between Pasquill stability class and meteorological category which determine attenuation or amplification A_{met} is given in [1,2].

Usually in projects the worst-case scenario is assumed for propagation in all direction and limit value for the zone which is not in accordance with Croatian legislative (+1 dBA increase in residual noise or -5 dBA from limit value for the area).

3. MEASUREMENT AND MODELLING RESULTS

In this section the measured residual noise levels and modelled levels from wind turbines are considered.

3.1 Residual noise levels

The residual noise levels are shown in Table 1. for two different positions during day, evening and night periods and the model for old wind turbines (all working in maximum operating conditions).

The residual noise levels at different bins for different positions are shown in table 1. at different time periods (day, evening, night). The residual noise levels are mostly from old wind turbines installed before (without this type of calculation).

The purpose of this study was to see the influence of new wind turbines on the present residual noise levels at different wind speeds and directions.

Wind speed in bins at 10m (m/s)	0-29	30-59	60-89	90-119	120-149	150-179	180-209	210-239	240-269	270-299	300-329	330-359
3-4	24,2	26,9*	30,6	30,6	-	-	-	-	28,9*	33,4*	33,1	32,8
4-5	40,9*	37,1*	36,3	35,8	-	-	-	-		35,7*	38,4	38,5
5-6	47,1*		41,5	42,8	47,5*	-	-	-		42,9*	43,1	43,7
6-7	51,7*		44,8	46,2	-	-	-	-		44,7	45,6	47,5
7-8	51,6*		44,4*	48,6*	-	-	-	-			51,8*	53,7*
8-9	61,1*										58,2*	56,7*
9-10	64,8*										62,1*	58,7*
10-11	-										62,8*	63,2*
11-12	-											62,4*

*Only few samples averaged

Noise levels/ dB-nighr												
Wind speed in bins at 10m (m/s)	Wind direction in bins/°											
	0-29	30-59	60-89	90-119	120-149	150-179	180-209	210-239	240-269	270-299	300-329	330-359
0-1	19,2	20	19,8	19,5	19,5	19,7	19,9	19,8	20	20,3	19,8	19,9
1-2	22,4*	21,5*	20,7	21,1	20,5	20,4	21	22,7*	23,5*	20,4*	23,4*	22,7*
2-3	27,9*	28,0*	23,4	27,6	26,9	24,8	28,5*	34,3*	41,0*	28,4*	27,1*	27,5*
3-4	31,1*	-	-	30,4	30,4*	28,8*	-	-	-	42,2*	30,8*	30,8*
4-5	31,4*	-	-	35,6*	35	34,4*	-	-	-	-	36,6*	33,7*
5-6	-	-	-	37,2*	39,7*	37,5*	-	-	-	40,2*	-	-
6-7	-	-	-	-	43,0*	-	-	-	-	-	-	-
7-8	-	-	-	-	43,7*	-	-	-	-	-	-	-
8-9	-	-	-	-	-	-	-	-	-	-	-	-

*Small number of 10 min samples

Table 1. *Residual noise levels for MM1 and MM2 positions during the night period (most critical)*

A problem arises when trying to collect the samples at higher wind speeds, so they are estimated by using polynomial fitting curve.

The levels of residual noise are shown in Fig. 2. depending on wind speed at MM1 and MM2 (for all directions and range of windspeed magnitudes at different day periods) and approximation fitting curve with saturation at higher levels. The measurement place MM1 is under the influence of the old wind turbine noise so residual noise dependence on windspeed at 10m is more representative for MM2.

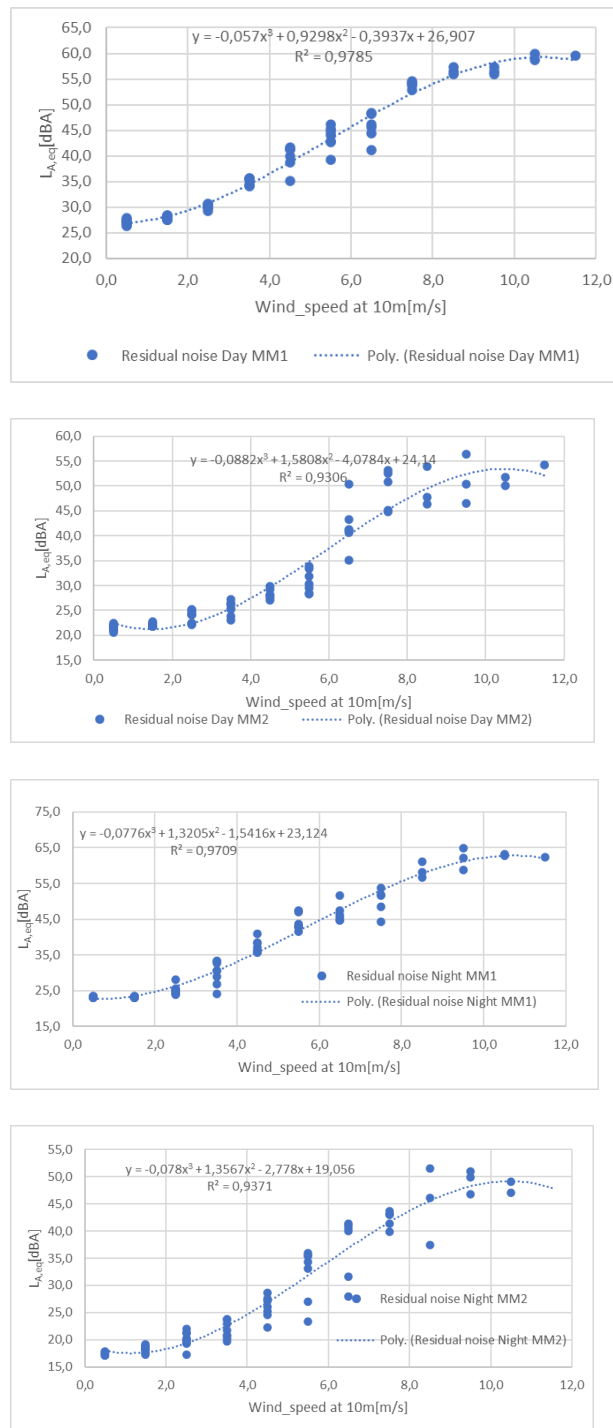| Noise levels (dBA)-night												
Wind speed in bins at 10m (m/s)	Wind direction in bins/°											
	0-29	30-59	60-89	90-119	120-149	150-179	180-209	210-239	240-269	270-299	300-329	330-359
0-1	23,2	23,1	23,1	23,2	23,2	23,3	23,3*	23,4*	23,0	23,1*	23,5*	23,0*
1-2	23,5	23,5	23,7	23,7	23,4	23,5*	23,8*	24,0*	23,9	23,3	23,7	23,7
2-3	23,9	24,2	25,1	25,1	28,1*	-	-	24,5*	25,5	24,4	25,4	25,2

Fig. 2. Residual noise levels at position MM1 and MM2 due to wind speed magnitude at 10m

It is visible that the residual noise increase versus wind speed at 10m according to saturation rule (averaged for all wind directions) is higher at position MM2 where there is no influence of old wind turbines.

The wind speed at hub height is estimated by using eq. 4. and it is used in calculation of sound pressure levels at different windspeeds (stability class and attenuation from wind speed direction in source receiver direction).

$$U(\text{h}) = U_0 \cdot \frac{log_e\left[\frac{\text{h}}{z_0}+1\right]}{log_e\left[\frac{\text{h}_0}{z_0}+1\right]} \qquad (4)$$

where z_0 is roughness parameter according HARMONOISE model (equation 5.90 in [2]) with roughness z_0=0.05 (comparison of measured velocities at different heights). The U_0 (m/s) is wind speed velocity at h_0=10m.

3.2 Modelling results for wind turbine noise

Different testing scenarios (different wind turbine types and heights and their numbers) are tested to see the available working modes which would not exceed the level of residual noise by more than +1 dBA (a very strict rule for the situation with the sound powers at lower speed velocities). At lower speed velocities there is no possibilities to change working modes because the difference between modes is negligible. At higher wind speed velocities at 10m (>6m/s) there is a possibility to reduce the sound power (and electrical energy production significantly) however, the residual noise levels are significantly higher. The wind speed at critical locations is measured at 10 metres height and noise levels are measure at 4 metres on the border in the free field (having no influence of reflection from nearby objects).

The ground factor has been tested for G=0 and G=0.2 and better agreement with some of the residual noise measurement results (downwind) was obtained with G=0.2 (old wind turbine results for samples where residual aerodynamic noise is estimated to be low).

According to the ISO 9613-2:1997 the ground reflection factor should be *G*=0 however, the soil around wind turbines is not fully hard so *G*=0.2 is used (the difference between results is 0.8 dBA with the same sound power with *G*=0 and *G*=0.2). In [1] it is written that the best solution is to put G=0 for the windfarm noise (the difference in the level is 0.8 dBA).

There is some grass in the vicinity close to the receiver so *G*=0.2 gives more realistic results rather than assuming a stricter value *G*=0. The sound power levels of wind turbines at different speeds and modes of working are shown in Fig. 3.
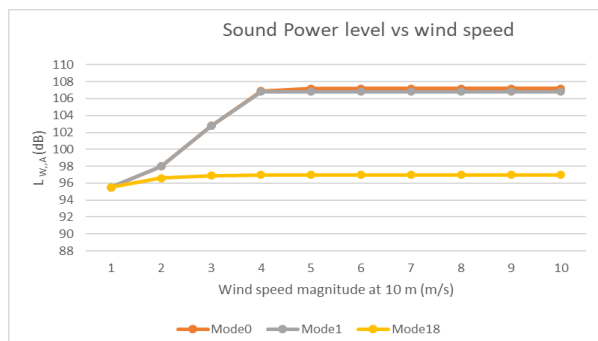
255°	29,1	16,7	30,3	23,7
285°	32,5	16,7	29,8	23,7
315°	**33,5**	16,7	28,6	23,7
345°	32,5	16,7	26,4	22,5

h=10m, v=3 m/s	Res1	Res2	Res3	Res4
Direction 15°	24,2	20,8	31,1	29,9
45°	26,9	19,7	30,4	30
75°	30,6	23,7	30,4	30
105°	30,6	23,7	30,4	30
135°	30,6	23,7	30,4	30,1
165°	30,6	23,7	**28,8**	29,5
195°	30,6	23,7	36	30
225°	30,6	23,7	38	31
255°	28,9	20,2	40	30
285°	33,4	20,8	42,2	33,1
315°	**33,1**	21,8	30,8	30,8
345°	32,8	23	30,8	29,4

*Results used for model calibration with measurement results

Fig.3. Typical sound power levels for wind turbine at different windspeeds at 10m height and different working modes

It can be observed that at lower speeds there is no possibility to reduce sound power which is not the case with higher wind speeds. In the case of increasing modes, the production of electrical energy is significantly lower.

The next step was to enter input parameters of sound sources in digital terrain model in mode 0 at different speeds (arithmetic average of bin velocity) and compare the results with measured residual noise at the same level.

If the residual noise level is increased more than +1 dBA for the same wind direction and velocity (assumed 0 octas) and most unfavourable stability class during different periods as obtained by measuring, the residual noise, the sound power od closest wind turbine is reduced if possible or turned off one by one until the limit condition (+1 dBA total level of noise) is satisfied.

The example for the results for wind speed at 10 m around measurement locations and comparison between old wind turbine levels with calibration point MM1 is shown in Table 2. Results for new sources (at height h= 138 m) is shown in Tables 3a).

Table 2. *Results for calibration of model with measured residual noise levels (old wind turbine)*

The results when all new wind turbines are working during night period (0 octas cloudiness) are shown in Table 3a) with increased values of residual noise in Table 3b).

Night, class E				
h=10m, v=4 m/s	Pos1-old	Pos2-old	Pos3-old	Pos4-old
Direction- 15°	29,1	16,7	23,8	19,1
45°	25,9	14,4	23,3	17,8
75°	22,8	11,7	23,4	16,6
105°	21,8	9,5	24,6	16,6
135°	21,8	9,5	28,2	17,6
165°	21,8	9,5	**29,3**	20,3
195°	22,8	11,7	30,2	23,5
225°	26,8	15	30,3	23,7

Night, class E				
h=10m, v=3 m/s	Pos1-new	Pos2-new	Pos3-new	Pos4-new
Direction- 15°	37,4	34,3	26,6	27,9
45°	37,4	34,2	27,4	27,8
75°	35,9	34,1	30,1	30,6
105°	34,9	32,2	32,3	33,7
135°	34,2	28,5	33,7	33,8
165°	33,2	27,3	33,7	34,7
195°	30,6	27	33,7	34,9
225°	30,5	27,4	33,5	34,9
255°	34,3	28,2	32,6	34,1
285°	35	32	29,5	31,5
315°	35,9	32,8	27	31,4
345°	36,5	34,3	26,4	28,8

Table 3a). *The level of noise from new wind turbines (all working in mode 0) and increase in residual noise.*

A significant influence on the results at each location depending on the wind speed component in source-receiver direction is obvious. The difference in levels is up to 7 dBA when all wind turbines are turned on and working in am mode 0.

h=10m, v=3 m/s	Difference1	Difference2	Diff3	Diff4
Direction- 15∘	13,4	13,7	1,3	2,1
45∘	10,9	14,7	1,8	2,0
75∘	6,4	10,8	2,9	3,3
105∘	5,7	9,1	4,1	5,2
135∘	5,2	6,0	5,0	5,2
165∘	4,5	5,2	6,1	6,3
195∘	3,0	5,0	2,0	6,1
225∘	3,0	5,2	1,3	5,4
255∘	6,5	8,6	0,7	5,5
285∘	3,9	11,5	0,2	2,3
315∘	4,6	11,3	1,5	3,3
345∘	5,2	11,6	1,3	2,7

Red-increased the residual noise level more than +2 dBA

Table 3b). *Increased values of residual noise at location MM1, MM2, MM3 and MM4 when new sources are turned-on*

It is visible that at lower speeds the increase of residual noise levels is significant and majority of wind turbines at these locations should be turned off which is not economic regarding the produced electrical energy.

The graphical representation of results with three different wind directions (0∘, 90∘ and 180∘) and wind speed magnitude at 10m v=6m/s are shown in figures 4a) ,b) c).
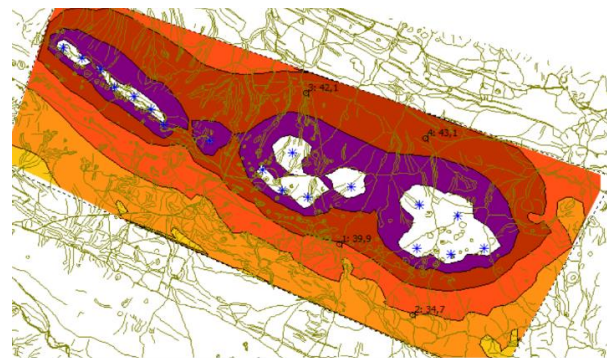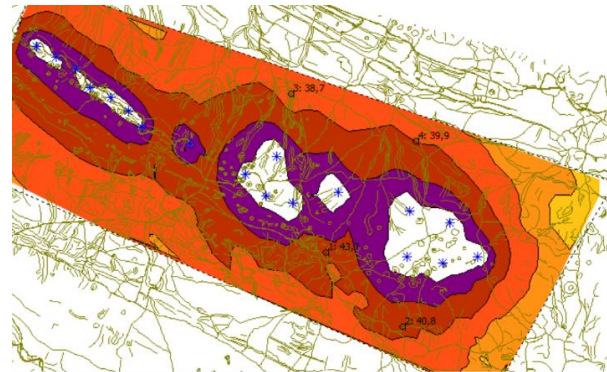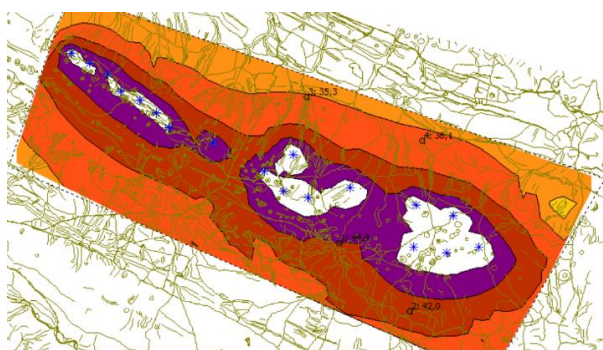

Fig 4. Graphical representation of wind direction influence (same meteorological class E) on noise levels around wind turbine sources at v=6m/s at 10m height for three wind directions a) 0∘, b) 90∘ and c) 180∘

The final results for working modes at different periods and at different wind speeds are shown in Table 4. for middle wind direction in bin (between 0∘ - 30∘)(mid 15∘).

Angle	(0-29)∘			
Day	Wind speed at 10m _3 m/s	4 m/s	5 m/s	6 m/s
VA-V-I	Mode0	Off	Mode18	Mode18
VA-V-II	Off	Off	Mode18	Off
VA-V-III	Off	Off	Off	Mode18
VA-7	Off	Off	Off	Off
VA-9	Off	Off	Off	Off
VA-12	Off	On(mode18)	Off	Off
VA-11	Off	Off	Off	Off
VA-13	Off	Off	Off	Off

Angle	(0-29)∘			
Evening	3	4	5	6
VA-V-I	Off	Off	Mode18	Off

VA-V-II	**Off**	**Off**	**Off**	**Off**
VA-V-III	**Off**	**Off**	**Off**	**Off**
VA-7	**Off**	**Off**	**Off**	**Off**
VA-9	**Off**	**Off**	**Off**	**Off**
VA-12	**Off**	**Off**	**Off**	**Off**
VA-11	**Off**	**Off**	**Off**	**Off**
VA-13	**Off**	**Off**	**Off**	**Mode18**

Night(23:00-7:00)				
Angle	**0-29**			
	3	**4**	**5**	**6**
VA-V-I	**Off**	**Off**	**Mode18**	**Mode18**
VA-V-II	**Off**	**Off**	**Off**	**Mode18**
VA-V-III	**Off**	**Off**	**Off**	**Mode18**
VA-7	**Off**	**Off**	**Off**	**Off**
VA-9	**Off**	**Off**	**Off**	**Off**
VA-12	**Off**	**Off**	**Off**	**Off**
VA-11	**Off**	**Off**	**Off**	**Off**
VA-13	**Off**	**Off**	**Off**	**Off**

Table 4. *Final results with working modes of wind turbines at different wind velocity magnitudes at 10m for different periods of day (stability classes) and wind directions*

It is evident that at lower wind speed in this configuration with proposed distances (i.e., min 800m) the wind turbines should stay turned off at lower wind velocity magnitudes during the night which is not profitable.

4. CONCLUSION

A lot of parameters (mainly meteorological and propertied of terrain) have an influence on determination of wind turbine modes, noise abatement and production of electrical energy if the wind turbines are installed very close to residential objects (>=800m). The critical parameters are ground reflection factor G, estimation of wind speed and velocity at critical locations and where the wind turbine hub is located (possible different wind directions near residential objects and hub).

In this paper the direction of wind is assumed to be the same at hub and at measured locations (where residual noise is measured). In simulations upper value of the windspeed magnitude bin was used to estimate sound pressure level and mid direction in bin to compare the simulation results from new sources to the residual noise levels with the same input parameters (wind direction, magnitude and cloudiness). In further steps more comparison between modelling and measurement results will be done in order to assess the modelling uncertainty.

5. REFERENCES

[1.] Hansen C.H, C.J. Doolan, K.Hansen. **Wind farm noise:Measurement assessment and control**, Wiley, 2017.

[2.] Bies A.D, C.C Hansen, C.Q., Howard, **Engineering Noise Control**, 5th Edition, CRC Press 2018.

[3.] Croatian Legislative regarded to noise, **https://zakon.hr/z/125/Zakon-o-za%C5%A1titi-od-buke**, 2020

[4.] Croatian legislative for limit noise values, **Pravilnik o najvišim dopuštenim razinama buke s obzirom na vrstu izvora buke, vrijeme i mjesto nas**tanka (nn.hr), 2021.

[5.] ISO 1996-2:2017, Acoustics - **Description, measurement and assessment of environmental noise -- Part 2: Determination of sound pressure levels**, International Organization for Standardization.

[6.] ISO 1996-1:2017, Acoustics - **Description, measurement and assessment of environmental noise --Part 1: Basic quantities and assessment procedures**, International Organization for Standardization.

[7.] ISO 9613-2:1996 Acoustics — **Attenuation of sound during propagation outdoors — Part 2: General method of calculation**, International Organization for Standardization.

[8.] Joint Research Centre, Institute for Health and Consumer Protection, Anfosso-Lédée, F., Paviotti, M., Kephalopoulos, S., **Common noise assessment methods in Europe (CNOSSOS-EU)** : to be used by the EU Member States for strategic noise mapping following adoption as specified in the Environmental Noise Directive 2002/49/EC, Publications Office, 2012, https://data.europa.eu/doi/10.2788/32029

Evaluation of model-based noise protection study based on in-situ vibroacoustic railway track analysis

Ivo Haladin, Krešimir Burnać

University of Zagreb, Faculty of Civil Engineering, Department for Transportation Engineering

Abstract: *In the design phase, newly built or reconstructed railway infrastructure requires a noise protection study to investigate noise sources and the need for noise protection around the railway line. Usually, such studies are based on modelling noise sources and their propagation through the environment, and they tend to overestimate actual noise levels. Therefore, in certain cases, before noise protection is built, investors want to re-evaluate the position, height, and length of noise protection walls foreseen by the noise study. This paper presents a novel approach to the evaluation of a noise protection study on a newly reconstructed railway line in Croatia. It involves vibroacoustic techniques for the characterization of vehicle pass-by noise and railway track properties such as rail roughness and track decay rate. Based on such properties and a series of in-situ measurements on a reference railway track and the observed newly built track, the noise protection study has been re-evaluated and need for noise protection walls reduced. Results of noise propagation models have further been tested and verified when the railway line has been completed.*

1. INTRODUCTION

A complex project of a railway infrastructure takes significant amount of time from the preliminary design phase, through numerous environmental studies, main design phase, tendering, building the railway infrastructure and finally getting a running permit and starting rail operations. In Croatian engineering practice this process can take from 5 up to 15 years.

It is therefore a challenging task to comply with all current standards and regulations and to keep up with other developments around the railway infrastructure which interconnected with it.

In this case, in 2022 a project of *Reconstruction and electrification of railway line Zaprešić – Zabok* has been near the end of construction phase. The noise protection study from 2013 has foreseen protection by means of 19 noise protection walls, total length of 1000 m. Noise levels have been estimated using a noise prediction model that is based on the German method "Schall 03". This method has shown some excellent results for railway noise calculation because it contains some parameters that have a considerable effect on noise levels (track curvature, vehicle length). However, they could be insufficient when assessing the noise levels from railway traffic in locations where traffic conditions are highly variable and have a higher influence on the noise levels (i.e. railway stations). In those situations, it is advised to conduct additional in-situ railway noise measurements to get more suitable results [1].

Moreover, input in this study (done 10 years prior to construction) anticipated use of mostly DMU passenger trainsets. It was later decided that all the passenger trains running on Zaprešić-Zabok section will in fact be new EMU trainsets (Končar HŽ-6112 series) which are, of course much quieter compared to old DMUs.

Project required control measurements of environmental noise prior to building foreseen noise protection walls to check if the walls are needed in the current in-situ conditions with new EMU trains running at design speed of up to 120 km/h. Since the section Zaprešić - Zabok had jet to go through final inspection and get a running permit, the speed was reduced to 40-80 km/h on the section and electrification has still not been in operation.

It was therefore impossible to perform in-situ environmental noise measurements with proposed operations (EMU trains running at up to 120 km/h).

This posed a challenge for the engineering team hence they turned to Faculty of Civil Engineering University of Zagreb for a solution proposal. The proposed method was to validate whether considerable noise protection from train traffic is required by reviewing the noise protection study and forecasting future noise levels. The method consisted set of noise measurements a reference railway section (M101 State border – Savski Marof – Zagreb main station), and a tested section (R201 Zaprešić – Zabok). It included measuring 24h environmental noise levels at 19 locations along the test track. Actual train pass-bys though had to be determined at a referent track where the trains could run at the speed of 120 km/h. To successfully transfer train pass by noise from the referent location to actual locations on test track, vibroacoustic parameters of the track had to be determine because at these speeds, the dominant source of railway noise is interaction between rail and wheel.

After the vibroacoustic parameters were determined and evaluated, it was possible to apply the measured noise levels from the reference track (120 km/h), as relevant on the tested track. Doing this, a necessary condition for both tracks to meet the vibroacoustic parameters according to the standard [2] is met, and they can be declared comparable in acoustic terms.

To determine the functional relationships of noise levels at different speeds of pass-by and distance from the track to apply the measured pass-by levels from the referent track to various speed/distance conditions at the tested railway track, three regression curves were created. This allowed a translation of pass-by noise levels of new EMU vehicles at speeds of up to 120 km/h from referent track to each of 19 locations on tested track.

To validate the results, a comparison based on pass-by speed, noise levels, and distance from the track was made both for reference and tested track, for different running conditions (acceleration and deceleration).

2. MEASUREMENTS

To get the 24-hour environmental noise levels in the 19 locations where noise barriers are planned to be constructed based on the noise study, several measurements and analysis steps needed to be conducted.

1) Vibro-acoustic measurements – to determine the acoustic similarity between referent and test track section.

2) Pass-by measurements - to determine the noise levels from the passing railway vehicles operating at different speeds and different distances from the rail track axis at referent track.

3) 24-hour environmental noise measurements – in-situ measurements that were done on the test section. In the total noise levels,

4) post processing - DMU trains operating on the tested section at speed of before the electrification were replaced with EMU trains from the referent section.

Only after the modernization and electrification were finished, under realistic circumstances, could actual noise levels be tested (design speed, number of trains, traction type - new, quieter EMUs).

EU regulation no.1304/2014 [3] prescribes the standard HRN EN ISO 3095:2013 [2] for the determination of the maximum noise levels from a train pass-by. Other standards that are used to determine track condition are HRN EN 15610:2019 [4] which is used for acoustic roughness measurements of the rail running surface, and HRN EN 15461:2011 [5] which gives guidelines for measurements of vibration damping of the track structure. Vibro-acoustic properties of the track (acoustic rail roughness and track decay rate (vibration damping of the track)), are an important part of the pass-by noise measurements because, with their determination and evaluation, two different railway lines can be defined as comparable [6]. With the determination of those two parameters, it is possible to determine the share of the track contribution to total noise levels during the train passage. If the results are similar for referent and test track, the pass by at a referent track can be regarded valid also for the test track.

2.1. VIBRO-ACOUSTIC MEASUREMENTS

The following measurements were carried out to inspect the acoustic resemblance of the test railway track R201 Zaprešić – Zabok and the referent railway section of the track M101: visual inspection of the track superstructure, determination of the track decay rate according to HRN EN 15461:2011 [5], and measurements of the acoustic railhead roughness according to HRN EN 15610:2009 [4]. Track decay rate is a vibroacoustic property of the railway track that describes how vibrations propagate along the rail, or what is the capacity of the track to absorb the vibrations [7]. The goal of this measurement was to establish the quality of the referent and tested rail track in terms of noise and vibration emission from the track-side. Several parameters can influence the track decay rate, such as rail cross-section, rail pad stiffness, rail inclination, and distance between two sleepers, and those parameters should be uniform for both railway sections according to the standard [4]. Measurements are conducted using a modal hammer with appropriate

stiffness (containing an accelerometer), and accelerometers installed on the head of the rail in vertical and horizontal directions.

Direct acoustic roughness measurement of the railhead running surface is a method for the determination of railhead roughness, which generates noise levels during a vehicle pass-by [8]. As a part of this research, acoustic railhead roughness was measured on one location on the referent track M101 and 3 locations on the tested track R201. It was measured using a RAILPROF 1000 device for direct rail roughness measurement, with a 1m effective measurement length.

The tested track on the railway section R201 is acoustically comparable to the referent track M101, according to the results of track decay rates and acoustic rail roughness. Furthermore, noise measurements on the referent track can be used to determine noise levels on the tested track. The abovementioned measurements are explained in more detail in the paper from the same authors [6].

2.2. PASS-BY NOISE MEASUREMENTS

To measure the noise levels emitted by passing EMU 6112 traveling at various speeds and distances from the rail track axis, pass-by measurements were made, both on referent and tested railway sections all according to standard EN ISO 3095 [2]. Pass-by measurements on the referent track were made at two locations, the first one in an open track section with maximum speed V_{max} = 120 km/h, and the second one

with reduced speed V= 80 km/h because of a nearby railway station.

Measurement devices that were used Brüel & Kjær - Hand-held Analyzers Type 2260, 2250, 2245, and 2270. Microphones were installed at distances 7.5m, 11.5 , 15 m, 19 m, 25 m and 29 m at each measuring location.

Pass-by measurements have been repeated on the tested track after the tested track got its usage permit (V_{max} = 120 km/h) to evaluate and confirm the method that was used using the same described procedure.

2.3 24 HOUR ENVIRONMENTAL NOISE MEASUREMENTS

To inspect if the number of locations and length of the barriers from the noise study (based on a calculation method with generic parameters) is in correspondence to the noise levels on the railway line, 24-hour in-situ environmental noise measurements were conducted in accordance with ISO 1996[9]. Measurements were conducted using Brüel & Kjær - Hand-held Analyzers Type 2260, 2250, 2245, and 2270, with measuring points at 4.0 m above the ground. Distance from the microphone to the track varied from 11 to 36 meters, dependent on field conditions and accessibility.

24-hour environmental noise levels that were recorded on the tested track section, were recorded while DMU – HŽ 7121 trains were in operation, which were operating at
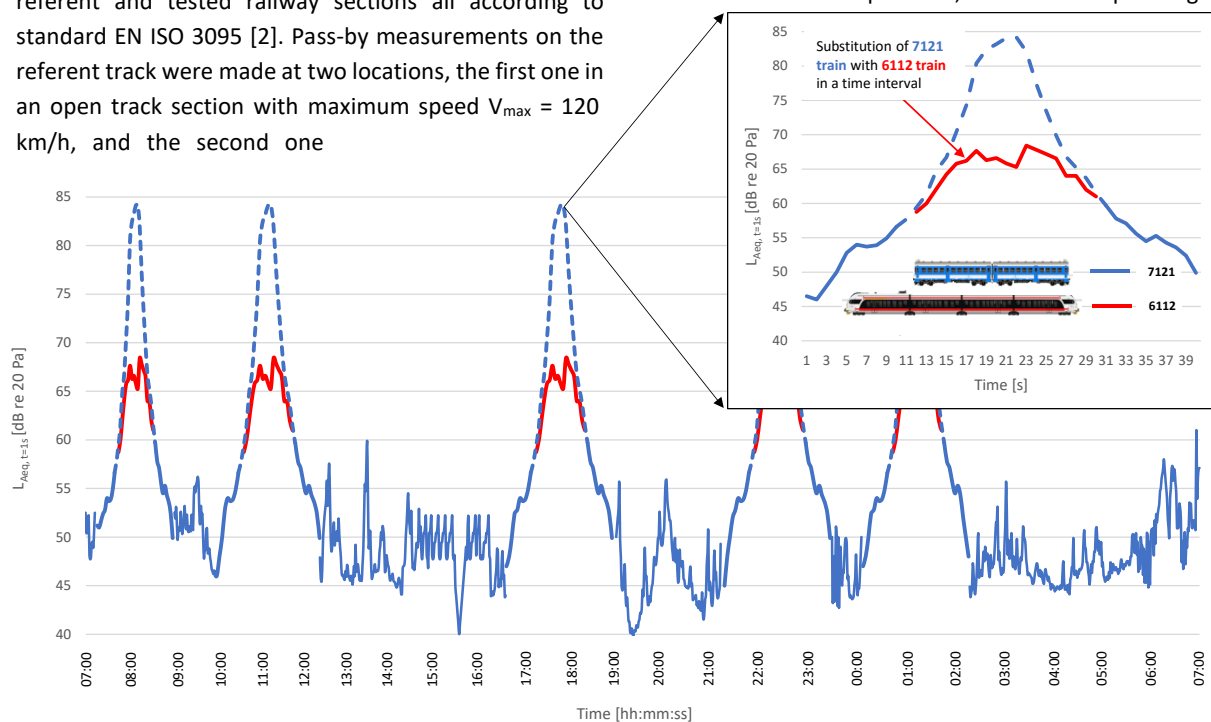

Fig. 1. Example of 24-hour environmental noise record with the pass-by noise levels from 7121 (DMU) train (blue), and 6112 (EMU) train (red), and an example of their substitution (detail)

lower speeds (Vmax=80 km/h). Those operating conditions would not fit the future situation after the modernization and electrification, and because of that, noise records of those DMUs had to be substituted with noise levels of new EMU-s that will be running after the reconstruction end (**Fig. 1**).

Pass-by noise levels for EMU trains were recorded on the referent railway section, where trains are operating at 120 km/h.

3. RESULTS ANALYSIS

Based on conducted measured quantities described in chapter 2 a methodology for calculating environmental noise levels on the tested track, based on the in-situ measurements of pass-by noise that were conducted on the referent track is explained in more detail. Furthermore, a comparison between pass-by noise levels, calculated based on a methodology explained in Chapter 3.1, and measured pass-by noise levels that were measured at the tested track (validation measurements) was made.

3.1 REGRESSION CURVES

After pass-by noise levels were recorded on the referent track, a general equation for calculating the equivalent noise levels (depending on the different speeds of the vehicle) was used [3] (with different n-coefficient for acceleration and deceleration) (1).

$$L_{p,V} = L_{p,V0} + n*\log(v/v_0) \; [dB] \; (1)$$

where:

$L_{p,V}$ noise level from train pass–by at speed V
V arbitrary speed for which noise level is determined
$L_{p,V0}$ noise level from train pass–by at reference speed (100 km/h)
V_0 reference train pass – by speed (100 km /h)
n coefficient (25 for acceleration, 20 for deceleration)

The n-coefficient from the formula (1) was determined empirically based on curve fitting to actual measured pass-bys. Regression curves were created for the variation of distances from the rail track axis, based on the equivalent noise levels normalized to a reference speed of 100 km/h ($L_{p,V0}$) (**Fig. 2**). Regression curves are based on results of pass-by noise on the referent section.
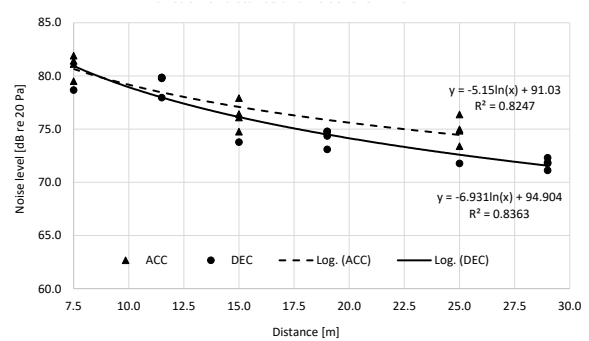

Fig. 2. Function of distance and noise level for EMU train 6112 on referent track (acceleration and deceleration)

Following that, two regression formulas were extracted based on the curves above (for acceleration and deceleration):

$$L_{p,V0,D} = -5.15*\ln(D) + 91.03 \; (R^2=0.82) \; (acceleration) \; (2)$$

$$L_{p,V0,D} = -6.931*\ln(D) + 94.904 \; (R^2=0.84)(deceleration) \; (3)$$

where:

$L_{p,V0,D}$ noise level from train pass–by (in dB) at the reference speed V0 and distance D
D chosen distance from the rail track axis [m]

3.2 VALIDATION OF THE METHOD

To validate the method described in 3.1, a comparison between **measured values ($L_{,meas}$)** of pass-by noise levels on the tested section after the modernization (V_{max} = 120 km/h), and **calculated values ($L_{,calc}$)** based on the measurements conducted on the referent section (V_{max} = 120 km/h), normalized at V = 100 km/h, and calculated according to the beforementioned method with regression curves.

Regression curves
The regression curves shown in **Error! Reference source not found.** and **Error! Reference source not found.**, were calculated for both acceleration and deceleration. They are based on the results gathered from the referent track as well as the validation results from measurements carried out on the tested track, after the opening of the electrified line. When the results of the referent and tested tracks are shown on a graph, they have an excellent match in the trendlines for both acceleration and deceleration.
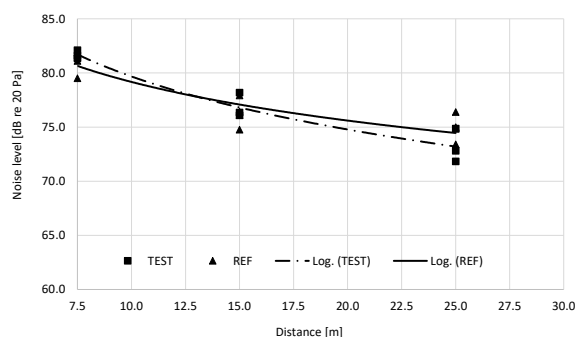
Fig. 3. Function of distance and noise level for EMU train 6112 on the referent track and tested track – acceleration
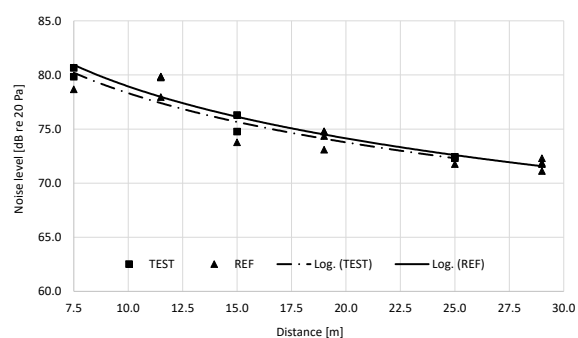

Fig. 4. Function of distance and noise level for EMU train 6112 on the referent track and tested track–deceleration

Pass-by noise levels
Calculated pass-by noise values from referent track are compared to measured noise levels for different actual pass-bys on the test track after opening of the line, for different operating speeds, type of operation (acceleration or deceleration), at three different distances from the axis along with the difference between L, meas, and L, calc noise levels, *Table 1*. For most of the situations, the difference between measured and calculated values is **below or around 1 dB**, with a few exceptions where calculated values are higher than the measured ones (Δ > 1 dB):

- first pass-by at 102 km/h (acc) and difference in noise levels Δ = -2.7 dB
- second pass-by at 65 km/h (acc) with Δ = -1.7 dB

at the distance D = 25m from the axis.
The cause for higher calculated values could be variations in environmental conditions such as wind, humidity, background noise, etc which are most evident at the furthest distance from the (25 m from the track) for the referent and tested section. The model overestimation of

these noise levels is on the safe side for further calculations on 24 noise levels based on modeled pass-by noise levels.

Table 1. *Comparison of noise levels (L, meas) from in-situ pass-by measurements on the test track and calculated noise levels based on the regression curves (L, calc)*

V (meas) [km/h]	Acc (<) Dec (>)	D [m]	L,meas [dB]	L, calc [dB]	Δ Lm - Lc [dB]
102	<	7.5 m	81.6	80.9	0.7
		15 m	76.3	77.3	-1.0
		25 m	72.0	74.7	-2.7
101	>	7.5 m	80.7	81.0	-0.3
		15 m	76.4	76.2	0.2
		25 m	72.5	72.7	-0.2
65	<	7.5 m	76.9	76.0	0.9
		15 m	71.7	72.4	-0.7
		25 m	68.1	69.8	-1.7
52	<	7.5 m	75.0	73.6	1.4
		15 m	71.1	70.0	1.1
		25 m	67.8	67.4	0.4
41	>	7.5 m	74.5	73.2	1.3
		15 m	68.4	68.4	0.0
		25 m	65.2	64.8	0.4
41	>	7.5 m	73.7	73.2	0.5
		15 m	68.3	68.4	-0.1
		25 m	64.8	64.8	0.0

4. FINAL RESULTS AND DISCUSSION
To calculate the 24 hour pass-by noise levels for operating condition with EMU trains and Vmax of 120 km/h, substitution of DMV trains in the 24hour signal has been conducted according to *Fig.1* for all of 19 positions where noise protection walls are foreseen by the noise protection study. With newly calculated noise levels, a final recommendation could be made on the need for noise protection walls . Based on pass-by measurements on the referent and tested track, a significant reduction in the number of locations and length of noise barriers was made. The noise study recommendation was to build a total number of 19 noise barriers (1000 meters in length), and the results from in-situ measurements have proven that only 5 noise barriers (240 meters in length) needed to be constructed (*Fig. 5*).
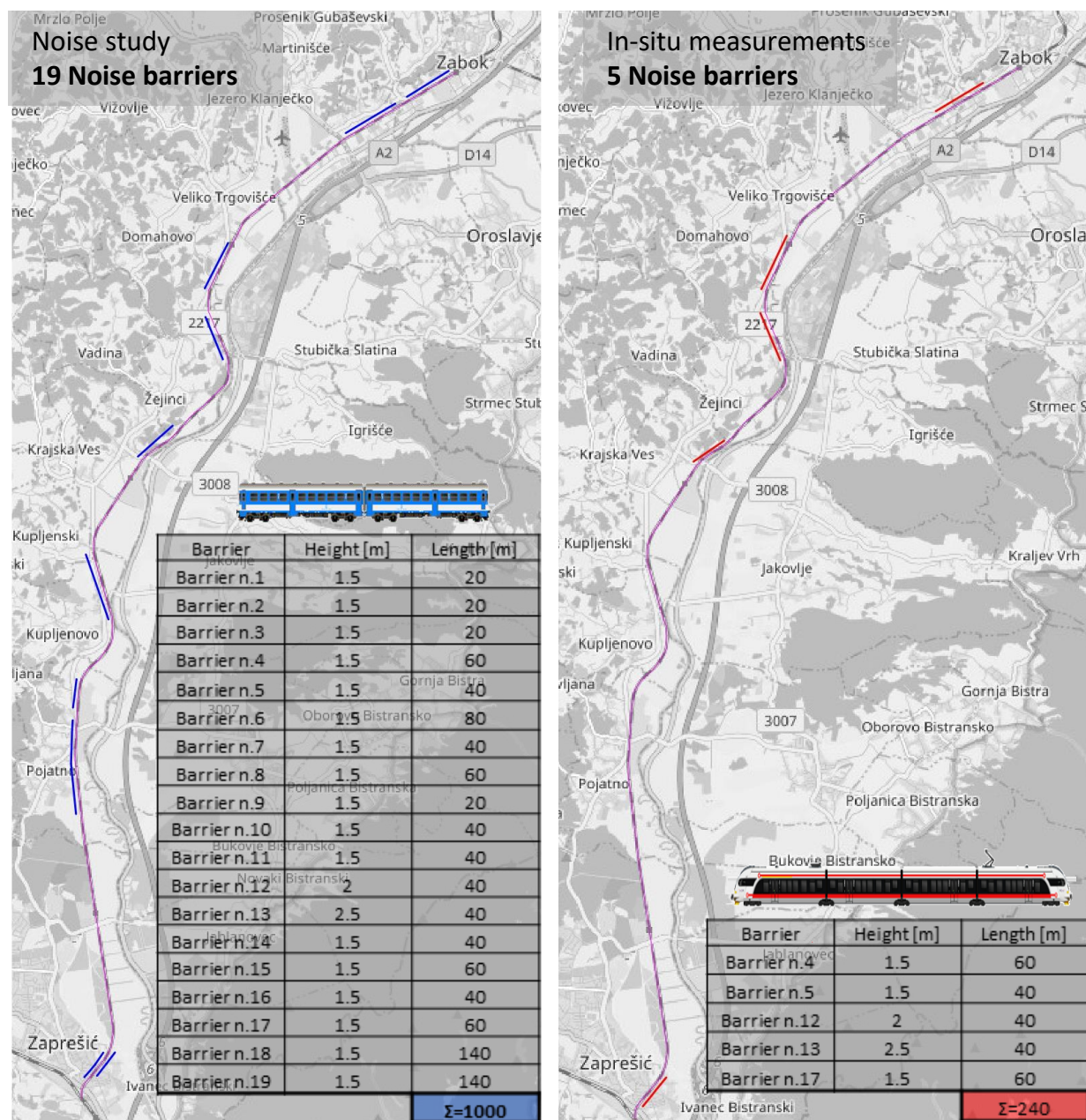
Fig. 5. Number of noise barriers that are required for railway noise protection, based on the noise study (left), and based on in-situ measurements (right)

5. CONCLUSION

Noise protection study results rely on a noise propagation model calculated to a certain accuracy for an area of interest. Accuracy of end results and relies heavily on noise source definition in the model, calculation method used and data validation at the end. Due to lengthy process of railway infrastructure project implementation, some of conditions and regulations related to noise levels can change and therefore challenge the conclusions of the noise protection study. Therefore, a correct decision, to verify the need for noise protection by means of in-situ 24-hour control measurements of environmental noise, has been made to validate the need for noise protection walls on a newly reconstructed and electrified railway line Zaprešić – Zabok.

Since the operating conditions could not be met prior to running permit for the track (electrification and Vmax of 120 km/h), to achieve representative 24h environmental noise levels, a substitution of train noise signals has been proposed, based on pass-by noise measurements on a

referent track with similar operating conditions. To verify the acoustic similarity of the tracks, vibroacoustic parameters of rail surface roughness and track decay rate have been determined and compared.

Regression curves have been established to calculate noise levels for any distance from track/train speed combination that is needed for the noise study.

Validation of the model based on actual measured values after track opening has been performed. < 1 dB difference between calculated noise levels on the referent track and recorded in-situ noise levels on the tested track (Table 1) can be observed, and it was concluded that the model is well built and could be further used.

Based on proposed procedure, a revaluation of noise protection resulted in reduction of needed noise protection from initial 1000 m to 240 m in length. This significant reduction greatly impacted the project budget and timeline resulting in timely issuing of running permit and start of operations.

ACKNOWLEGDMENTS

6. LITERATURE

[1] Džambas, T., Lakušić, S., Dragčević, V., **Traffic noise analysis in railway station zones**, Applied Acoustics;137:27–32., https://doi.org/10.1016/j.apacoust.2018.03.006, 2018.

[2] European Commission, **Commission Regulation (EU) No. 1304/2014** of 26 November 2014 on the technical specification of interoperability relating to the subsystem "rolling stock - noise.", Official Journal of the European Union, 2014 (17), 2014.

[3] CEN, **HRN EN ISO 3095:2013 Acoustics - Railway applications - Measurement of noise emitted by railbound vehicles**, 2013.

[4] CEN, **HRN EN 15610:2009 Railway applications -- Noise emission – Rail roughness measurement related to rolling noise generation**, 2019.

[5] CEN, **HRN EN 15461:2011 Railway applications - Noise emission - Characterisation of the dynamic properties of track sections for pass-by noise measurements**, 2011.

[6] Haladin, I., Burnać, K., Koščak, J. **Vibroacoustic track analysis and noise measurements on the R201 Zaprešić-Zabok railway line**, Road and Rail Infrastructure VII, Proceedings of CETRA 2022, 2022.

[7] Haladin I, Lakušić S, Košćak J. **Measuring vibration damping level on conventional rail track structures,** Gradjevinar 2016;68. https://doi.org/10.14256/JCE.1532.2015.

[8] Lakušić S, Haladin I, Jukić A, Andraši N, Piplica P. **Rail roughness measurement and analysis in frame of rail vehicle pass-by noise measurements**. Road and Rail Infrastructure II, Lakušić S, editor., Zagreb: Sveučilište u Zagrebu Građevinski fakultet; 2012.

[9] CEN, **ISO 1996-1:2016 Acoustics — Description, Measurement and Assessment of Environmental Noise — Part 1: Basic Quantities and Assessment Procedures**, 2016.

[10] CEN, **ISO 1996-2: 2017 Acoustics -- Description, measurement and assessment of environmental noise -- Part 2: Determination of sound pressure levels** , 2017.
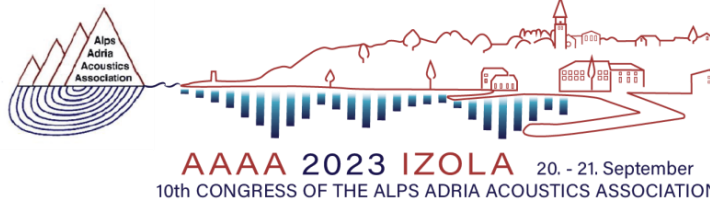
STEEL REILWAY BRIDGE NOISE, LACK OF REDUCTION EFFECT ON AIRBORNE NOISE DUE TO VIBRATION DAMPERS POSSIBLY ACTING AS NOISE SOURCES

Rok Rudolf

Slovenian National Building and Infrastructure and Civil Engineering Institute
Laboratory for Thermal Performance and Acoustics
Dimičeva ulica 12, SI-1000 Ljubljana

Abstract: *Steel railway bridges can be quite loud, especially in the low frequency range, and they typically last over 100 years- presenting a very persistent noise pollution problem. One way to tackle this problem is to use noise dampers on the bridge itself, damping vibrations and reducing the airborne noise emissions from the bridge. In one practical application case however, it became apparent that the noise dampers on a specific pilot bridge have substantially reduced the vibration of the bridge, but the airborne noise was barely affected. One possible explanation for this is that the noise dampers themselves act as sound sources. To research their contribution to total sound levels of the bridge, we have mounted one of the noise dampers on a vibration machine in a laboratory, and measured emitted sound during various excitation schemes. This way, we were able to assess the noise emitted by the damper at vibration levels typically encountered on a bridge during individual train pass-byes. This allowed us to add dampers as noise sources in a computer noise emission model of the bridge. Using this model, we assessed the effect that dampers as noise sources have on total noise, as measured on site*

Keywords: steel railway bridges, vibration dampers, noise sources, noise emission model

1. INTRODUCTION

Steel railway bridges represent a significant noise source, especially at low frequency ranges, producing a "thundering noise" sensation to nearby listeners. Steel bridges tend to vibrate at those ranges, producing large noise emissions that are difficult to reduce with conventional noise control measures like noise barriers[1]. Due to long life-span of steel railway bridges - typically over 100 years- this problem will not go away any time soon.

A noise and vibration monitoring system for steel railway bridges was developed as part of the EU Horizon 2020 project Assets4Rail (part of Shift2Rail) and tested on a pilot bridge with and without specifically designed vibration dampers used as noise control [2]. These dampers were installed on the main supporting element – bridge web-plates[3].

The system for monitoring showed a peculiar set of result on a pilot bridge however. Once vibration dampers were installed, vibration levels on the bridge web plates were substantially reduced in the 1/3rd octave frequency bands with middle frequencies of 50 Hz and 63 Hz, where dampers were designed to be most effective[4]. Simultaneously, noise emissions from the bridge were also measured, characterized by bridge correction factor (BCF) parameter: that is, a difference in Z-weighted sound pressure levels measured at the bridge, and at some distant reference site on the same track, where there is no influence of bridge noise emissions. This way, the noise emissions particular to the bridge itself can be shown separately from the noise emissions from the railway tracks away from the bridge. However, results showed that BCF before and after installation of vibration dampers has changed much less than expected in the 1/3rd octave frequency band at 63 Hz where BCF was highest[4].
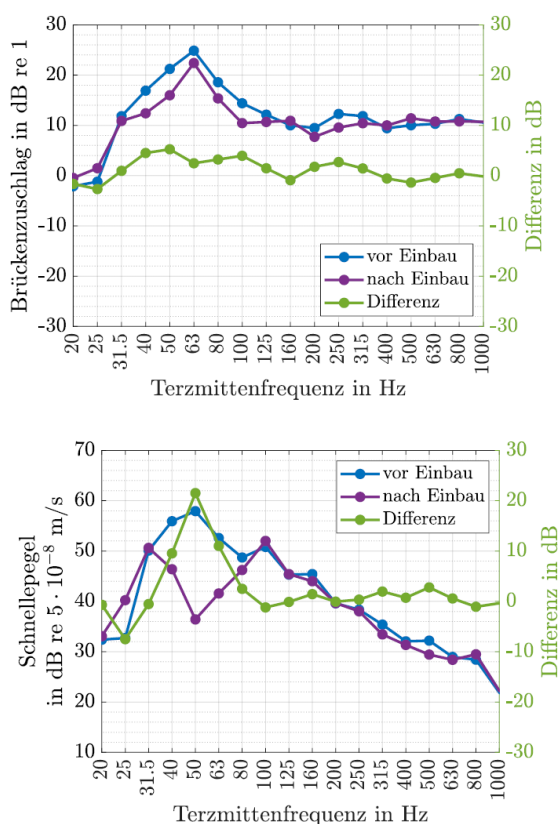
Fig.1. *substantial difference (>20 dB) in web plate vibration due to damper installation (top graph – German: „Schnellepegel") does not translate to reduction in noise emissions, characterized by BCF (bottom graph– German: „Brückenzschlag"). Both shown before ("von Einbau") and after installation ("nach Einbau"). Source: TUB [4]*

So, as can be seen from figure 1, despite substantial reduction in the vibration of the bridge, bridge noise characterized by the BCF parameter remained only minimally effected.

How could this be? First, it was speculated that another part of the bridge was also vibrating and emitting sound in the relevant frequency range around 63 Hz. However, no obvious bridge element could be found, that could act as this additional source. Vibrations and subsequent emissions at these frequencies would imply a large source, comparable to the main web plates of the bridge that were the main focus of the investigations. No such elements existed on the bridge in question (see also next point for bridge description). Any elements considered were either much too small (e.g., hand rails), or too light

and oriented in a way that would reduce noise emissions on a level plain (e.g., walking plates).

Since no explanation was found with existing bridge elements, I have turned to check if a new element could be the source of additional noise emissions, that could explain the lack of reduction in BCF of the pilot bridge. Namely could the vibration dampers themselves, that vibrate at this frequency range by design, radiate enough sound to reduce the effect on the BCF. Could dampers themselves be a relevant sound source?

To test this hypothesis, one noise vibration damper was mounted on an axial vibration table MTS Bionix 370, and shaken at various frequencies with varying force, including the settings that correspond to the vibration excitation of the actual bridge under traffic (averaged over all trains) at main resonance frequency 53 Hz. Next, the sound emission from this system was measured in the room where vibration table is located, in effect treating this room as an reverberation room, so sound power levels of each damper could be determined according to a standardized method ISO 3743-2 [5]; once other contributions like background noise due to machine operation were discounted. And finally, a computer model of noise emission of the bridge in question was prepared in Predictor-LIMA software, according to the EU noise assessment methods CNOSSOS-EU [6].Noise sources corresponding in power to noise dampers assessed in the previous step were added to the model to calculate their contribution with measured total noise levels at the bridge [4] acting as reference. The process explained in this article can then give us an answer of how much of the total bridge noise is in fact due to noise vibration dampers acting as noise emission sources at relevant low frequencies (around 53 Hz) [4].

2. MEASUREMENT SETUP

Vibration damper is a central metal frame with 24 metal sandwich rods sticking out on two sides, in two rows. Each rod is of a sandwich construction with a bitumen-based layer between two steel layers. This bitumen-based middle layer ensures inner damping of each rod, while the length and dimensions of steel layers determines the resonant frequency, allowing for damper "tunning" – by making the rods longer or shorter, the resonance frequency where the damper is most effective is lowered or raised. This particular damper was tunned to the

resonance frequency of 53 Hz, same as the dominant resonance frequency of the bridge web-plates, and weighted in at 33 kg. The damper was designed and produced by Assets4Rail partner Schrey & Veit GmbH, based on the noise and vibration measurements at the bridge [4].

The vibration damper was mounted on an axial vibration table MTS Bionix 370 in a concrete walled room of volume 121,4 m³ at Slovenian National Building and Civil Engineering Institute (from Slovene: ZAG). The mounting to the vibration piston was done by 4 screws in the same way the damper would be mounted on an actual bridge.
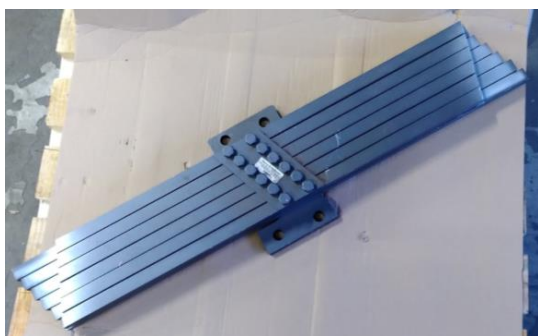
Fig.2. *vibration dampers from the measured bridge, as received*
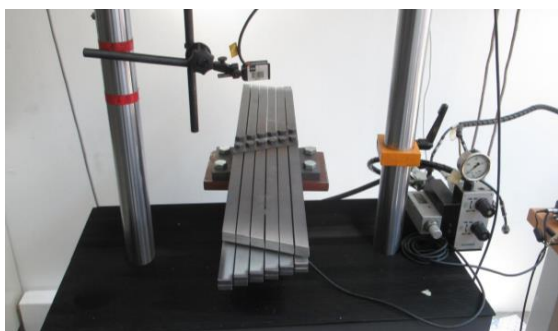
Fig.3. *dampers mounted on the vibration table by screws, note the 12 rods in two rows to one side in the picture foreground*

The vibration damper was then vibrated with forced oscillation at various frequencies ν [Hz] and various forces – characterized by the maximum displacement in a vibration cycle *A* [μm] setting to the vibration table. At the

same time, sound levels were recorded inside the room with a B&K sound level meter with a microphone mounted on a rotating boom, in accordance with standard ISO 3743-2[5]. Background noise levels in the room L_{bck} [dB] while machine was operating but not actively vibrating, as well as room's reverberation time RT_{60} [s] were also measured, to be used to complete the calculations according to the same standard.

3. VIBRATION DAMPERS AS SOUND SOURCES

The results are presented on the following figure, with parameters L_{Zeq} measured at various 1/3rd octave bands with a rotating boom. For comparison the excitation of the actual bridge at damper locations before vibration damper installation is included. This excitation, corresponding to an average regional train pass-by, was measured at future damper location[1] as maximum velocity of $v_{max} = 8{,}12\ mm/s$ with a peak at 53 Hz[7]. From this we can get to maximum displacement with:

$$|A| = \frac{v_{max}}{2\pi v} = 24{,}4\ \mu m \tag{1}$$

This displacement is marked as "BV" (Bridge Vibration) line on figures.
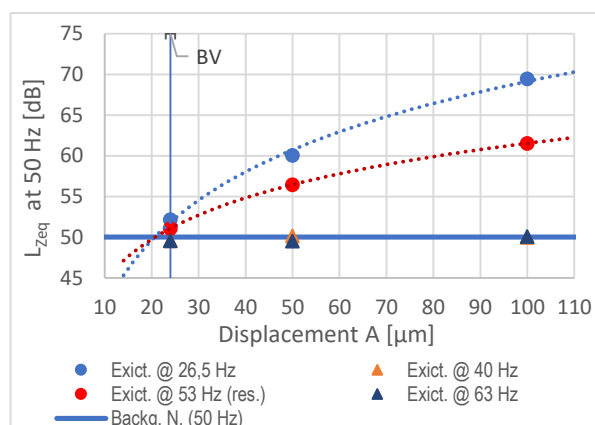

Fig.4. *graph of measured sound pressure levels at 1/3rd octave band with middle frequency 50 Hz, re. maximum displacement, at various frequencies of excitation. Logarithmic trend lines (dashed).*

---

[1] Dampers were located at two points on each web-plates, where vibration measurements confirmed the largest maximum velocity (displacement).

As can be seen from figure 3, excitation at frequencies other then expected damper resonance frequency yields low noise in 50 Hz 1/3rd octave band – at levels around background noise. This is not the case at resonance frequency at 53 Hz and at 26,5 Hz (half of resonance frequency), although at excitation levels encountered on the actual bridge (marked "Bridge Vibration") the noise levels are barely above background noise.

Another interesting aspect can be seen if we look at sound pressure levels in other 1/3rd octave bands that include excitation frequencies, as presented on the next graph.
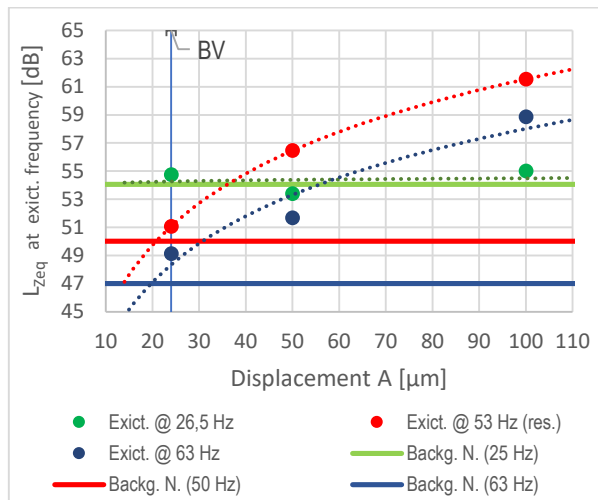
Fig.5. *graph of measured sound pressure levels in 1/3rd octave bands that include excitation frequency – relation to maximum displacement. Background noise in 3 relevant bands also presented.*

As can be seen from figure 4, the noise measured is highest near expected resonant frequency. Measuring in bands near 53 Hz still shows increased noise with respect to background – note that 1/3rd octave band with middle frequency 63 Hz includes frequencies from 56,2 to 70,8 Hz. At frequencies further away (e.g., 26,5 Hz), any increase is negligible compared to background noise.

Once sound pressure levels are determined, they can be used to determine band sound power according to ISO 3743-2 method [5], with the following equation:

$$L_W = \overline{L}_p - 10 \log \frac{T_{nom}}{T_0} + 10 \log \frac{V}{V_0} - 13 \, dB \qquad (2)$$

Where:

- $\overline{L}_p$ are mean band pressure levels measured with rotary boom around the reverberation room (L$_{Zeq}$ at middle frequency 50 Hz for our case),
- T_{nom} is the nominal reverberation time, determined by centering the measured reverberation time of the room, normalized to RT$_{60}$ at 1000 Hz acc. to standard [5], 1,1 s in our case,
- V is the room volume, 121,4 m^3 in our case,
- constants of $T_0 = 1 \, s$, $V_0 = 1 \, m^3$, and correction of - 13 dB.

To determine the sound power at measured bridge excitation levels ($|A| = 24{,}4 \, \mu m$ @ 53 Hz), we first determine the pressure levels. Our measurement is very close to the background sound levels at that excitation, as we measured a value 1,1 dB above background (see figure 3). Rather than try to deduct the background value, we extrapolate the expected pressure level from noise levels at higher excitation (larger displacement). With equation for trend line for excitation at 53 Hz from figure 3:

$$\overline{L}_p = L_{Zeq}@50 \, Hz = 7{,}3 \ln(A) + 27{,}912 \qquad (3)$$

, we get the mean pressure level and by putting this into equation (2), we get to the value of emitted sound power of each individual damper, when vibrated with measured bridge excitation levels: $L_w = 40 \, dB$, at 1/3rd octave band with middle frequency 50 Hz.

This sound power can then be used as an input parameter of the noise emission model of the bridge, to see the expected contribution of our sound source (vibration dampers) to total noise levels.

4. NOISE EMISSION MODEL

Noise emission model was prepared, using Predictor-Lima software (ver. 12.01) for environmental noise. The model included vibration dampers as point sound sources. It also included microphone measuring position as was used during the measurement campaign in the Assets4Rail project [4],[7]. This measurement position was chosen according to the measurement system [2] based on the ISO 3095 standard [8] – measuring was done 1/3rd from the north-east side of the bridge, at 7,5 m from the middle of the track and 1,2 m above top of the rail head (ToR).

AAAA – 2023 – IZOLA - Conference Proceedings

Fig.6. *photograph of the bridge Source: TUB [7]*

Fig.7. *photograph of the bridge between web-plates, with vibration dampers installed – 2 per each web-plate Source: TUB [7]*
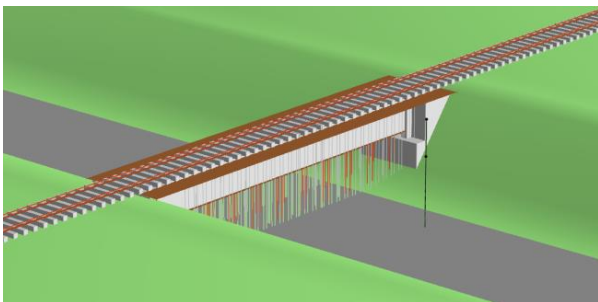

Fig.8. *Predictor-Lima noise emission model*

Measurement results at the bridge were used to calibrate the model – spectral emissions from sources were varied until model values were equal to values measured before vibration dampers were installed.

After, vibration dampers were included in the model with sound power as derived in chapter 3, it was calculated by

the model that extra noise emissions due to dampers acting as sound sources amount to $L_{calc,eq,50Hz} = 41\ dB$ in 1/3rd octave band at 50 Hz, calculated at position of measurement at the bridge. One can compare this calculated value to average total noise level measured at this position near bridge after noise damper installation ($L_{meas,eq,50Hz} = 88\ dB$) for regional trains [7]. With noise levels contribution calculated to 47 dB below measured total noise levels, it becomes quite clear that vibration dampers do not constitute any relevant contribution to total noise, even at noise bands where they are arguably the loudest.

5. CONCLUSION

As can be seen from our model results, we are no closer to finding the missing airborne noise source of a particular steel railway bridge, measured in Assets4Rail program. The vibration of web-plates was damped, but the noise persists. It might be possible that the result could be improved upon with some more advanced calculation model, that might for instance include resonance effects of the space below bridge itself. However, even if that were the case it seems impossible that this could amplify the noise of vibration dampers by nearly 50 dB. So, even with our simpler emission model, it can conclusively be said that vibration dampers are a negligible noise source compared to the noise of a steel railway bridge. The results of sound power of such dampers, as measured and calculated in chapter 3, might be more pertinent if such dampers were used in a less noisy environment.

6. REFERENCES

[1]   D. Thompson, **"Chapter 11 - Bridge Noise,"** in *Railway Noise and Vibration*, D. Thompson, Ed., Oxford: Elsevier, 2009, pp. 359–397. doi: https://doi.org/10.1016/B978-0-08-045147-3.00011-6.

[2]   J. Boehm, C. Gramowski, M. Ralbovsky, L. Rizzeto, and R. Rudolf, "**Assets4Rail Deliverable D1.2: Report on a noise emission monitoring solution for steel railway bridges**," 2021. Accessed: Aug. 23, 2023. [Online]. Available: http://www.assets4rail.eu/wp-content/uploads/2021/12/A4R-D1.2.pdf

[3] C. Gramowski, "**Assets4Rail Deliverable D4.2: Report on improved work approach for set up of bridge dampers**" (non public) Berlin, 2020.

[4] C. Gramowski, T. Hanisch, M. Ralbovsky, and R. Rudolf, "**Brückenakustik: Fortschritte bei Analyse, Theorie und Minderungsmaßnahmen im Rahmen des Shift2rail-projektes Assets4rail**," in *BAHNAKUSTIK 15. – 16. November 2021 Planegg München* , München, 2021.

[5] *SIST EN ISO 3743-2:2019 **Acoustics - Determination of sound power levels of noise sources using sound pressure - Engineering methods for small, movable sources in reverberant fields - Part 2: Methods for special reverberation test rooms***. 2019.

[6] Stylianos. Kephalopoulos, Marco. Paviotti, Fabienne. Anfosso-Lédée, and Institute for Health and Consumer Protection., ***Common noise assessment methods in Europe (CNOSSOS-EU) : to be used by the EU Member States for strategic noise mapping following adoption as specified in the Environmental Noise Directive 2002/49/EC*.** OPEU, 2012.

[7] T. Hanisch, M. Ralbovsky, C. Gramowski, and R. Rudolf, "**Assets4Rail Deliverable D1.2.1: Bridge Noise Measurements in Pressig, Germany, before and after the installation of bridge noise dampers**," (non public), 2022.

[8] *SIST EN ISO 3095:2013 **Acoustics - Railway applications - Measurement of noise emitted by railbound vehicles***. 2013.

Psychoaoustics of Pseudosound in Turbulent flow of Centrifugal Fan used in Household Appliance

Jurij Prezelj, Jurij Gostiša

University of Ljubljana, Faculty of mechanical engineering

Abstract: *As the performance metrics of household appliances from various manufacturers converge, acoustic performance is emerging as a pivotal differentiator for consumers. While strides have been made in noise control, further reductions in noise levels are challenging due to inherent physical constraints. Hence, the focus is shifting from merely reducing noise levels to reshaping noise to be less intrusive or even pleasant. While noise arising from vibrations has been largely manageable, aerodynamically generated noise, primarily due to the chaotic nature of turbulent flow, presents a significant challenge. The early turbulent flow studies introduced the term "pseudosound," highlighting the intricate connection between turbulence and acoustics. This research, with a focus on the centrifugal fan in a tumble dryer, employs a psychoacoustic approach to analyze turbulent flow. Our findings indicate a correlation between psychoacoustic features, namely roughness and fluctuation strength, and the turbulent properties of flow when analyzed through hot wire velocity signals. This leads to a compelling question: Why does human auditory perception possess the ability to discern the turbulent characteristics of flow?*

Keywords: Psychoacoustics, pseudo sound, aeroacoustics, turbulence, centrifugal fan

1. INTRODUCTION

Forward-curved-centrifugal (FCC) fans are distinct for two primary reasons: they possess a significant rotor outlet to inlet ratio (around 3:1) and are equipped with numerous short, chorded blades (typically around 40). Given their unique design, they've acquired various names worldwide: drum-rotor fan in Europe, squirrel-cage fan overseas, and also referred to as Sirocco fan or multivane impeller, a nomenclature credited to Eck [1].

Owing to their compact size and low noise emission, FCC fans have become a staple in both industrial and residential HVAC systems. They are particularly favored in applications demanding high airflow at moderate pressures, especially when efficiency is not the top priority. Frequently, the shape of the fan's inlet channel is dictated by spatial constraints, leading to suboptimal aerodynamics and, consequently, diminished efficiency. Yet, in spite of their limited efficiency, their utility in delivering high flow rates with a moderate pressure boost, coupled with their compactness, agreeable auditory

profile, and cost-effectiveness, ensures their widespread use in both domestic and industrial settings.

This ubiquity has piqued the interest of numerous research groups, prompting investigations to address and enhance the primary shortcoming of FCC fans: efficiency. Furthermore, noise control pertaining to these fans continues to be a focal point of scientific exploration, as evidenced by numerous studies [2], [3], [4], [5].

1.1 Motivation and problem formulation

Historically, the suboptimal efficiency of forward-curved fans has been largely attributed to flow separation within the interblade channel on the shroud side. This vortical flow spans approximately one-third of the rotor's width, leading to the choking of the interblade channel and, consequently, a reduction in efficiency. Many authors have delved deep into this phenomenon, yet studies addressing the effects of inlet flow channel design on fan performance have been sparse.

In his seminal work, Eck [1] dedicated an entire chapter to forward-curved fans, highlighting the flow

separation zone at the fan's inlet. While he proposed several design guidelines, he underscored the existing gaps in foundational knowledge for designing and computations. Since Eck's insights, numerous research groups have ventured into the realm of forward-curved fans. For instance, Kind [6], [7] elucidated the intricate flow patterns within the rotor, emphasizing the significant axial and circumferential nonuniformities, particularly evident at flow rates beneath the best efficiency point (BEP). Tsutomu's tripartite study [8], [9] on blade design and casing presented both numerical and experimental data, culminating in insights on optimal blade numbers, angles, and volute dimensions.

Subsequent research from the Oviedo University team in Spain [10], [11] focused on the aerodynamic and acoustic properties of forward-curved fans, especially the dual inlet variants utilized in automotive HVAC systems. Their work highlighted the pivotal role of volute tongue design in noise reduction and how the operating point profoundly impacts flow through the rotor. Parallel to this, Montazerin's group at Amirkabir University of Technology undertook comprehensive research, culminating in a 2016 publication [12] that covered key aspects such as inlet configuration and rotor/volute design, substantiated by both experimental and numerical data.

Echoing Montazerin's focus, Pham Ngoc Son [13] explored the influence of inlet geometry on performance metrics. Notably, their studies centered on fans with a free inlet configuration, where the inlet remains exposed to the ambient environment. As their results indicated, the relatively minor portion of the inlet channel doesn't considerably affect fan characteristics. Contrarily, Golamian [14] evaluated flow straighteners at the inlet, such as tubes and zig-zag plates, discovering their detrimental impact on pressure head and efficiency. Addressing spatial constraints, Xuanfeng Wen et al.'s work [15] explored the repercussions of a discontinuous volute profile, revealing its role in both decreasing efficiency and amplifying noise.

The intertwining of aero-acoustically generated noise with psychoacoustic features has garnered attention, especially in the automotive sector [16], [17]. Controlling flow-induced noise is paramount in product development, necessitating the consideration of near acoustic fields in the sound spectrum induced by flow [18].

1.2 Pressure oscillations in turbulent flow as pseudo-sound

Turbulent flows are characterized by changes in their pressure and velocity fields. Such alterations naturally lead to acoustic perturbations. In essence, hydrodynamic fluctuating velocity is responsible for these acoustic disturbances. Lighthill's analogy [19] casts light upon this concept by introducing an equivalent source term in the wave equation. Specifically, turbulence acts as a weakly radiating quadrupole source, the strength of which depends on the fluctuating hydrodynamic velocity. Notably, acoustic perturbations are substantially weaker in magnitude than their hydrodynamic counterparts.

It's pivotal to recognize that pressure fluctuations are not solely the offspring of acoustic modes. Vortical fluctuations also play a role in generating these fluctuations. There's a fundamental difference in propagation speeds between acoustic waves and hydrodynamic pressure fluctuations. The former travel at the speed of sound relative to the fluid, while the latter move with the local fluid velocity. As such, it's imperative to differentiate between the two. Acoustic fluctuations give rise to what we perceive as sound, whereas hydrodynamic fluctuations lead to pseudo-sound, which is also discernible to an observer [19].

In the realm of subsonic speeds, the pseudo-sound field holds dominance within and proximal to turbulence, constituting the acoustic near field. As one ventures further away, this field is overshadowed by the acoustic radiation field, which diminishes more leisurely with distance. Intriguingly, the pseudo-sound field closely mirrors the characteristics of the pressure field in incompressible flows. Dominated more by inertial forces than by compressional effects, it lacks wave propagation. This unique nature has earned it the moniker "pseudosound" [20].

To break it down mathematically, considering the turbulent flow's random nature, we can assume different segments of the flow act as uncorrelated or incoherent sources. This allows us to express the total pressure, p_{tot}, as:

$$p_{tot} = p_0 + p_{PS} + p_A \qquad (1)$$

Here, p_{PS} symbolizes the RMS value of hydrodynamic pressure oscillations due to turbulence, commonly termed pseudosound. On the other hand, p_A stands for the RMS value of pressure oscillations stemming from acoustic propagation. Though p_0 represents static pressure, it's typically excluded from considerations when focusing on dynamic phenomena in frequency ranges exceeding 1 Hz. It's essential to note that the RMS values of these oscillations are distance-dependent, with their origin being the source. The decay patterns are distinctive: while pseudosound's RMS decays following an inverse third-power law with distance, acoustic pressure's RMS adheres to an inverse law. This contrast is vividly depicted in Figure 1.
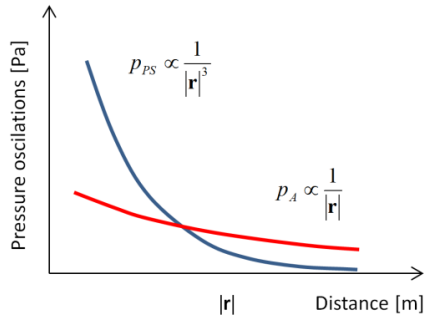
Figure 1: Sound pressure (red) and pseudosound pressure (blue) as function of the distance r

Within turbulent flows, pressure fluctuations are predominantly driven by the inertial effects linked to the vortices, such that $p_{tot} \approx p_{PS} \gg p_A$. Outside these flows, pressure fluctuations are largely due to propagating waves, signified by $p_{tot} \approx p_A$. Although turbulence-induced acoustic waves tend to have smaller amplitudes, they exhibit a more gradual decay [21].

An examination of the topology in the k_x–ω spectrum of each reconstructed pressure field highlighted the existence of three modal classes: hydrodynamic, acoustic, and a hybrid known as hydro-acoustic. The hydrodynamic and acoustic modes were defined by a spectral energy bump with phase velocities roughly equivalent to jet speed and at least equal to the ambient sound speed, respectively. Hybrid modes showcased multiple energy bumps, each having distinct phase velocities [22].

Interestingly, the potential energy of waves, represented by $E_{pp}(k)$ spectrum, can significantly surpass their kinetic energy, as described by $E_{dd}(k)$ spectrum. This disparity even leads to questions about the very notion of acoustic waves. Such observations prompted numerous scholars, including aeroacoustics pioneers like Lighthill, to refer to this phenomenon as the pseudosound regime, distinguishing it from genuine acoustics [19]. It's essential to highlight that pseudosound tends to dissipate in higher Mach number regimes, with its observations typically valid up to $M < 0.1M < 0.1$ [19].

Felli posited that intermittent pressure peaks, triggered by the transit of eddy structures, can be perceived as pseudosound. In contrast, consistent background fluctuations might be understood as sound [23]. A notable challenge with near-field pressure measurements is that only a fraction of the energy linked with pressure fluctuations radiates as sound. The remaining fluctuations, which don't align with the linear wave equation, can't be identified as sound. This non-

radiative contribution, often termed as pseudosound in literature [20], [24], relates to the traversal of eddy structures in the flow. Consequently, it travels at a pace considerably slower than sonic velocity, especially at lower Mach numbers. Much of the scholarly research has concentrated on deriving the pressure field from velocity measurements in turbulent flows using hot-wire techniques [25], [26], [27], [28].

Obi derived the pressure field from velocity measurements using Euler's equation of fluid motion (referenced as Eq.1) and opted to ignore the unsteady term [29]. Data secured via PIV underscored that the notable turbulence intensity observed between bodies originates from the oscillatory motion tied to vortex shedding. The impact of vortex motion is evident as a robust correlation between velocity and pressure gradient [29]. Here, nn and ss stand as orthogonal vectors, with nn being normal to the surface.

$$\frac{\partial p(t)}{\partial n} = -\frac{\partial \rho u_n(t)}{\partial t} - u_n(t)\frac{\partial \rho u_n(t)}{\partial n} + u_s(t)\frac{\partial \rho u_n(t)}{\partial s} \qquad (2)$$

Suzuki introduced a diagnostic method aimed at identifying instability waves in a subsonic round jet, employing a phased microphone array. This detection algorithm draws parallels with the beamforming technique, which is typically harnessed in conjunction with a far-field microphone array to pinpoint noise origins. Statistical evaluations of the results align with the concept that the pressure field corresponds to instability waves developing within the turbulent mean flow [21].

By utilizing the wavenumber-frequency spectrum method, one can assess levels of both acoustic and turbulent flow pressure fluctuations, in addition to estimating convective velocities present in the near acoustic field. Notably, acoustic pressure fluctuations have been found to dominate over those of turbulent flow at elevated frequencies within the near acoustic field [18].

When positioning a microphone within an airflow, it becomes susceptible to the turbulence present in said flow. Moreover, any turbulence generated due to the microphone's presence further interacts with its diaphragm. This interaction between turbulence and the diaphragm prompts the microphone to register noise levels attributable to this interference, rather than purely capturing the acoustic wave. For airflow velocities approaching 27m/s, foam windscreens seem ill-suited for acoustic measurements, given their inability to shield effectively against these turbulent disruptions [30].

1.3. Rotational sound of Aerodynamic Origin

The total noise level of a centrifugal fan is ussulay dominated by discrete frequency tones at the blade passage frequency and its higher harmonics. This is a result of the rotor blade interaction and the guide vanes [31, 32, 41]. Many of the noise sources are near the trailing edge of the rotor blades [33]. Fluctuating loads at the tips of the blades generate the dominant noise. Rotor blades are typical dipole sources [34].

Rotational noise of aerodynamic origin at the design point of operation (Q_{des}, Δp_{des}) is the result of pressure fluctuations caused by periodic fluid forces. Thrust and drag forces are induced on the blades as they move through the air. Rotational noise is also generated by impulsive interaction of the rotor blades with the inflow distortion and nearby stationary obstacles, such as the diffuser vanes and return passages. Aerodynamically generated noise from rotational origins at off-design operation and at constant rotational speed is theoretically equal to that at the design point of operation. But the rotational noise changes due to varying of both, the steady and unsteady loading effects, which characterize the off-design operation [35]. It was also observed that the number of blades does not significantly affect the noise level at the BPF [36].

1. 4 Non-rotational sound of Aerodynamic Origins

Non-rotational noise of aerodynamic origins is generated by random forces at the design and off-design point of operation. These forces are induced by the non-uniform flow fields, by turbulence and by interaction of the turbulent flow with the rigid structure along the air flow through the electric motor. Air flows through the suction unit to cool the electric motor. Heated air, exits the suction unit with high velocity, forming a turbulent air jet. There is a large disparity between the energy of the flow in the non–linear field and the acoustic energy in the far field. The hydrodynamic pressure p ranges from 10^4 Pa to 10^6 Pa, whereas the acoustic pressure p' ranges from 10^{-5} to 10 Pa. Therefore, the radiated acoustic energy of an unsteady flow is a very small fraction of the total energy in the flow. In general, the total radiated sound power of a turbulent jet scales with $\propto (v^8/c_0^5)$, and for a dipole source arising from pressure fluctuations on surfaces inside the flow scales with $\propto (v^6/c_0^3)$, where v denotes the characteristic flow velocity and c_0 the speed of sound [37].

The nature of the noise from jets cannot be accurately predicted, owing to the complex nature of the jet itself and the uncertainties associated with turbulence, nozzle configuration, temperature vacillations, and so on. However, first-order estimates can be derived from empirical data obtained for the most part from experimentation in the aviation industry. The earliest measurements of jet noise demonstrated that intensity and noise power varied very closely with the eight power of the jet exit (Lighthill's eight power law), and it is now generally agreed that the overall sound power can be expressed with quadrupoles as [38]:

$$P_q = K_q \frac{\rho_0 v^8 D^2}{c_0^5} \qquad (1)$$

Where K_q is a quadrupole radiation constant describing nozzle configuration, turbulence characteristics, temperature etc., D is the jet diameter, and ρ_0 is the density of ambient air, [38].

An interaction of the turbulent airflow with the solid surface also generates a broadband noise, which has no correlation with a rotation frequency. Curle [39] showed that the sound generated by turbulent flow in the region of a solid body is exactly analogous to the sound radiated by a 'free space' distribution of quadrupoles sources plus a surface distribution of dipoles. Sound power of acoustic radiation from an acoustically compact solid in turbulent flow can be expressed as [39]:

$$P_d = K_d \frac{\rho_0 v^6 L^2}{c_0^3} \qquad (2)$$

where K_d is a dipole radiation constant describing the shape of the solid body, turbulence characteristics, temperature, etc., and L is a typical length of the solid body of the solid object. Accordingly, these dipoles should be more efficient generators of sound than the quadrupoles of Lighthill's theory if the Mach number is small enough.

The non-rotational noise can also be generated by the rotating stall and by the surge [3]. Acoustic radiation can be attributed directly to the pressure oscillations due to unsteady operating conditions of the suction unit can be described as, [40, 41]:

$$P_m = K_m \frac{\rho_0 v^4 d^2}{c_0} \qquad (3)$$

where K_m is a monopole radiation constant describing suction unit geometry, and d is the diameter of the opening from the suction unit.

At higher flow rates, towards free delivery ($v \gg v_{des}$) aerodynamic non-rotational turbulent noise is generated due to higher jet flow velocities, i.e., boundary layer vortex shedding and incidence declination of the flow on the suction side of the rotor blade. At lower flow rates ($v \ll v_{des}$), the non-rotational aerodynamically generated noise is caused by vortices, flow declination, and especially due to the onset of the rotating stall and surge phenomena. Combined sound power generated by monopole, dipole and quadrupole sources can be written as:

$$P_c = K_q \frac{\rho_0 v^8 D^2}{c_0^5} + K_d \frac{\rho_0 v^6 L^2}{c_0^3} + K_m \frac{\rho_0 v^4 d^2}{c_0} \qquad (4)$$
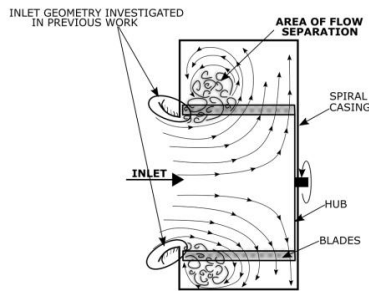
Figure 2: Typical flow pattern through a forward-Curved-Centrifugal fan.

1.4 Psychoacoustic features of audible sound

1.4.1 LOUDNESS

The loudness of a sound is a perceptual measure of the effect of the energy content of sound on the ear. It is related to the decibel (dB) which is a logarithmic scale used to quantify the power of a sound. Doubling the sound power of a sound does not lead to a doubling on the decibel scale but instead to an increase of 3dB. Perceived loudness, however, is also dependent on the frequency content of a sound so, for example a very low frequency sound such as a 20Hz tone at 40dB would be perceived to be quieter to a normal hearing person than a 1kHz tone at 40dB. This is explored in more detail below. Some examples of the use of loudness would include in examining sound quality in the car industry, measuring car interior noise, engine noise, exhaust noise etc. To examine earth-moving machinery noise emissions. It has also been used in research to quantify the sound quality of some domestic appliances, vacuum cleaners, or refrigerator

noise for example, and in the calculation of an unbiased annoyance metric.

A definition of the loudness of tones can be constructed from the results of experiments such as loudness 'magnitude estimation'. The 'loudness level' of a sound (introduced in the twenties by Barkhausen) is defined as 'the sound pressure level of a 1 kHz tone in a plane wave and frontal incident that is as loud as the sound; its unit is "phon".' (Zwicker & Fastl 1990). So a sound that is as loud as a 1kHz tone with a sound pressure level of 40dB (for example) is said to have a loudness level of 40 phon. This principle can be used to define the loudness of tones by comparing them with an equivalently loud 1kHz tone.

Reference: 1000 Hz tones. The loudness level of a tone of 1000 Hz in phones L is per definition its SPL (dB). According to the ISO definition, the loudness of this 1000-Hz tone in sones N' is found by:

$$N' = 2^{\frac{L_{SPL} - 40}{10}} \qquad (5)$$

This means that per definition the loudness of a 40-dB SPL, 1000-Hz tone is 1 (sone). Rule of thumb: From equation (1), it follows that a 10 dB increase in loudness level means a doubling in loudness. This holds quite well for 30<L<120 (phone).

However, this is not the end of the story, calculation of the loudness of more complex sounds requires further thought as the 'critical bandwidth' comes into play. Critical band width is a measure of the frequency resolution of the ear. For example, two tones less than one critical bandwidth apart will not be heard as two separate sounds instead the sounds will partially mask each other, making loudness summation a more complex process. Third octave bands can be used as an approximation to critical bands and BS 4198 (published 1967 as an equivalent to ISO 532/R) provides a graphical method (Method B) for the calculation of the loudness of complex sounds from third octave bands.

The sensation of sound volume of hearing is dpendent on frequency. Thus, sound events of equal level but different frequency do not always evoke the samo e sensation of sound volume in human beings. The volume level in the unit "phon" designetes the sound pressure level of a 1 kHz sine tone, which produces the same sensation of sonic volume as the tested sound event. Example: A sine tone at frequency 500 Hz, which is percieved to be as loud as 1 kHz sine of 50 dB is designeted a sound pressure level of 50 Phon. According to DIN 45631

the sound pressure level Ln of the loudness N can be calculated as follows:

$$L_N = 40 + 33,22 \log\left(\frac{N}{sone}\right) \quad \text{For } L_N > 1 \quad (6)$$

$$L_N = 40\left(\frac{N}{sone} + 0,0005\right)^{0,35} \quad \text{For } L_N < 1 \quad (7)$$

So, while it is more usual in acoustics to see the "loudness" of a signal expressed in dB(A), a better measure of the perceived loudness can be found by proper application of the critical bandwidths - A specific loudness can be calculated from the dB level for each third octave band using the assumption that' a relative change in loudness is proportional to a relative change in intensity.' (Zwicker and Fastl 1990)

So, values of specific loudness (N') in sone per Bark can be calculated using a power law. Masking curves can then be constructed around these levels representing the effect of critical bands. The final value for loudness (N) is then calculated as the integral (i.e., the area) under the curve and is presented in sones.

$$N = \int_0^{24bark} N' dz \quad (8)$$

$$N' = 0,08\left(\frac{Q_{TQ}}{E_D}\right)^{0,23}\left[\left(\frac{1}{2} + \frac{E}{2E_{TQ}}\right)^{0,23} - 1\right] \quad (9)$$

In which, QTQ is the excitation at threshold in quiet and ED is the excitation that corresponding to the reference intensity I0=10-12 W/m2.

1.4.2 SHARPNESS

Sharpness is the ratio of high frequency level to overall level. It is calculated as the integration of specific loudness which exhibits the distribution of loudness across the critical bands multiplied by a weighting function, divided by total loudness (hence, sharpness is level-independent). Here the zwicker's method is used for the sharpness S calculation:

$$S = 0,11 \frac{\int_0^{24bark} g(z) \cdot z \cdot N'(z) dz}{\int_0^{24bark} N'(z) dz} \quad (10)$$

where the denominator gives the total loudness (N). The upper integral is like the first moment of specific loudness over critical-band rate, but uses an additional factor, g(z), that is critical-band-rate dependent. This factor is expressed as:

$$g(z) = \begin{cases} 1 & ; z \leq 16 bark \\ 0,066 \cdot e^{0,171z} & ; z > 16 \text{ bark} \end{cases} \quad (11)$$

Where only for critical-band rates larger than 16 Bark does the factor increase from unity to a value of four at the end of the critical-band rate near 24 Bark. This considers that sharpness of narrow band noises increases unexpectedly strongly at high centre frequency.

The booming index can then be calculated by weighting these low frequency elements using the following weighting function and comparing them with the loudness in the rest of the spectrum:

1.4.3 FLUCTUATION STRENGTH

Owing to modulated sounds can elicit two different kinds of hearing sensations: at low modulation frequencies up to a modulation frequency about 20Hz, the hearing sensation of fluctuation strength (F) is produced. At higher modulation frequencies, the hearing of roughness (R) occurs. From modulation frequencies around 20Hz, there is a transition between the hearing sensation of fluctuation strength and that of roughness. A model of fluctuation strength based on the temporal variation of the masking pattern can be expressed as:

$$F = \frac{\Delta L}{\frac{f_{mod}}{4} + \frac{4}{f_{mod}}} \quad (12)$$

which shows the relationship between fluctuation strength (F) and the masking depth (ΔL) of the temporal masking pattern, as well as the modulation frequency (f$_{mod}$).

1.4.4 ROUGHNESS

To describe roughness quantitatively, three parameters are used. For amplitude modulation (AM), the important parameters are the degree of modulation and modulation frequency. For frequency modulation, it is the frequency modulation index and modulation frequency. Using the boundary condition that a 1-kHz tone at 60 dB and 100%, 70Hz AM, produces the roughness of 1 Asper, the roughness (R) of any sound can be calculated by:

$$R = 0,3 f \bmod \int_0^{24bark} \Delta L_E(z) dz \quad (13)$$

where fmod is modulation frequency, and ΔLE is the masking depth in critical band. The critical bands are auditory band pass filters, and its band number scale ("psychoacoustic" or "Bark" scale) is a frequency scale of the numbered critical bands 1 through 24, named Bark (named after von Barkhausen), and the width of a given critical band is approximately: 100 Hz, at center frequencies below 500 Hz; 0.2xfc, at center frequencies above 500 Hz. These bands derive from the frequency-to-place transform on the basilar membrane.

1.5 Conclusions based on literature survay and scientific contribution.

1. Flow Separation and Efficiency: A significant factor affecting the reduced efficiency of the forward-curved fan is flow separation. This phenomenon begins at the inlet, progresses through the blades, and extends into the volute. Such vortical flow accounts for approximately one-third of the rotor width, thereby leading to diminished flow rates and efficiency.

2. Psychoacoustic Metrics in Turbomachinery Noise Evaluation: In recent times, psychoacoustic metrics have emerged as a preferred method for assessing turbomachinery noise. Intriguingly, our survey did not yield examples where these metrics were applied to non-acoustic signal analysis. There's a tangible relationship between pressure and velocity fluctuations in fluid flows, which validates the application of psychoacoustic metrics to velocity signal analysis. Consequently, metrics such as loudness (DIN 45631/A1), sharpness (DIN 45692), fluctuation strength, and roughness have been employed to elucidate flow properties that impact efficiency and noise levels. Based on these insights, an innovative prototype of the inlet channel was designed, enhancing the fan's efficiency, and minimizing noise emissions.

3. Influence of Inlet Configuration on Performance: The focal point of the research presented in this paper centers on the impact of inlet configuration design on local inlet flow field attributes and, consequently, the performance dynamics of the FC fan. We undertook a series of experiments to gauge the fan's performance traits, assess the inlet flow field using HW anemometry, and measure emitted acoustic pressure fluctuations. Average velocities were computed for each data point and visualized on a contour graph relative to the given volume flow rate. Meanwhile, sound pressure signals were depicted on a spectrogram, contingent on volume flow rate. An avant-garde approach was introduced by integrating psychoacoustic metrics into velocity signal analysis.

4. Interrelation of Sound and Turbulent Flow: There exists a pronounced linkage between sound and turbulent flow. Drawing from this relationship, we have postulated that methodologies used in sound signal processing can also serve to analyze turbulent flow. More explicitly, strategies formulated for the psychoacoustical interpretation of sound can be repurposed as descriptors of turbulent flow characteristics.

2. EXSPERIMENT

Experiments were conducted on a measurement setup constructed in accordance with ISO 5801 standards, specifically the installation of category B, which entails a free inlet and a ducted outlet. A schematic representation is provided in Figure 3 and 4. The setup includes:

1. Test Section with a Spiral Casing (Figure 2-1): The fan, housed within a spiral casing, serves as the primary focus of the experiment. The design of this casing was influenced by guidelines put forth by Montazerin [12]. A differential pressure transducer, designated for capturing the pressure difference across the fan, was connected at point A (as shown in Figure 2-1), with its secondary port exposed to ambient conditions.

2. Fan Specifications: The runner used had a width of 60 mm, a diameter of 155 mm, and featured 40 blades. Powering the fan was a 400W servo motor, ensuring a consistent rotation frequency of 50 Hz irrespective of the operating conditions and facilitating shaft torque measurements.

3. Flow Rate Measurement (Figure 2-2): An ISO 5167-compliant orifice with flange tapings was integrated to measure the flow rate.

4. Operating Point Modulation (Figure 2-3): An auxiliary fan combined with a motorized throttle valve was used to create a diverse set of operating points.

6. Noise Measurement: Noise profiles were captured using a Norsonic Nor140 Sound Analyser placed 1 meter from the fan.

The initial segment of the experiment was devoted to gauging the performance and noise attributes associated with different inlet configurations: the free inlet, the pre-existing inlet channel (referred to as the TD inlet), and a newly devised inlet channel. For the subsequent phase:

7. 3-Axis Traversing System: To identify deterministic flow patterns within the inlet channel, a system utilizing three motorized linear rails driven by stepper motors was

crafted. A Dantec type 55P11 1D hot-wire anemometer, placed orthogonal to the flow direction, surveyed 144 distinct points as depicted in Figure 2 (right section). Prior to data collection, the probe underwent calibration. At every measurement location, a 10-second velocity signal snapshot was collected at a sampling frequency of 25 kHz. This data collection was facilitated by an NI9222 module, housed within an NI9147 cDAQ chassis. Automation was a key feature, with both measurement and probe positioning being controlled by a custom-built software developed in the NI Labview environment.

8.   Inlet Design Exploration: Alongside the existing inlet (shown in Figure 3, left), a novel inlet was conceptualized, derived from observed flow patterns within the inlet channel. The research process encompassed multiple design iterations. Initially, the team aimed to emulate the free inlet configuration. However, this design, when juxtaposed against the pre-existing inlet channel, exhibited reduced efficiency. Consequently, a secondary approach was undertaken. This new design, as presented in Figure 3 (right), was optimized to guide fluid streamlines towards the inlet opening, culminating in superior efficiency and diminished noise levels.
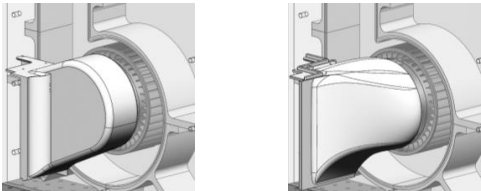
Figure 3: Progression of the inlet channel design - Original version (left) compared with the redesigned outline that follows fluid streamlines (right).
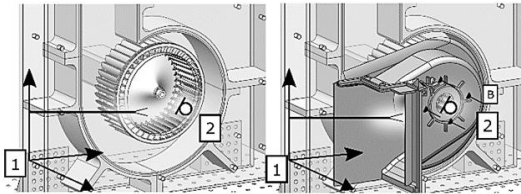
Figure 4: Depiction of the hot-wire anemometer probe, part of a 3-axis traversing system (marked as 1), and a microphone aligned with the fan's axis (denoted as 2).

4. RESULTS

The results present a comparative analysis of the free inlet, existing inlet, and the newly designed inlet configurations. The initial segment evaluates integral aerodynamic and acoustic parameters, specifically performance and noise characteristics. Meanwhile, the subsequent segment delves into the local properties of the inlet flow.

4.1 Integral aerodynamic and acoustic properties

Figure 5 depicts the performance characteristics for the free inlet and both ducted inlet configurations. Each configuration reveals a notable unstable operating region up to approximately 200 m3/h. Beyond these flowrates, fan operation stabilizes across all inlet configurations. The occurrence of partially filled interblade channels, which leads to an increase in pressure for FC fans compared to fans with backward-inclined blades at very low flow rates, is comprehensively discussed by Eck [1 - p.114]. A fitted second-order polynomial curve aptly describes the stable segment of these characteristics. The Best Efficiency Point (BEP) is found at 390 m3/h for the free inlet, 300 m3/h for the existing inlet, and 340 m3/h for the new inlet channel. The hydraulic efficiency at BEP is approximately 50% for the free inlet, 37.5% for the existing inlet, and 41.5% for the new inlet channel.

Regarding noise characteristics, as illustrated in Figure 6, all inlet configurations produce lower noise levels at reduced flow rates. However, the lowest noise levels do not align with the BEP as suggested by fan noise theory. For the free inlet, the Leq(A) levels tend to be higher compared to the two ducted configurations. This can be ascribed to the inlet channel's role in noise dampening. Thus, a direct comparison of these cases may not be appropriate. A comparison between the existing and new inlet channels reveals a 2 dB(A) noise reduction at higher flow rates with the new inlet design. In contrast, differences below 250 m3/h appear minimal. This noise disparity arises from the altered aerodynamics, as everything else, barring the inlet channel geometry, remained consistent. With the new inlet channel, the observed noise reduction and associated efficiency improvement are credited to decreased vorticity and enhanced flow conditions within the inlet channel.
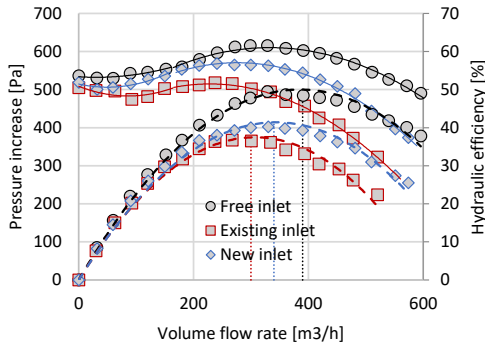
Figure 5: Performance and efficiency characteristics of the fan in free inlet configuration (black), with existing (red) and new inlet (right).
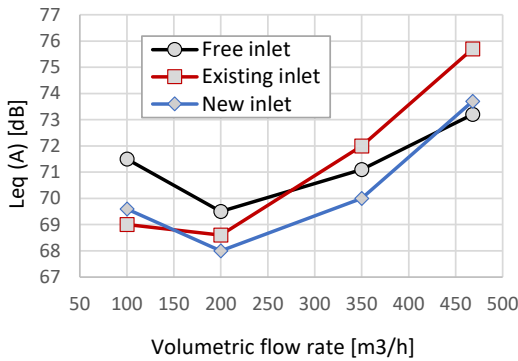

Figure 6: Noise characteristics of the fan in free inlet configuration (black), with existing (red) and new inlet (right).

While the maximal efficiency benchmark set by the free inlet remains about 10% superior, the new inlet channel design marks significant progress. To understand the underlying mechanisms that boost efficiency, further investigation was undertaken, the results of which are detailed in the subsequent subsection.

4.2 Local flow properties at the inlet plane

Local flow patterns at the fan inlet were identified through a combination of smoke visualization techniques and laser sheet illumination, supplemented later by hot wire anemometry. From the visualization, three distinct regions emerged: a well-populated region with minimal vorticity (Figure 7 lright A), a turbulent eddy zone with limited throughflow (Figure 7 right B), and an intermediate region marked by a pronounced continuous

vortex (Figure 7 right C). The vortex in region C is believed to be influenced by regions A and B, which themselves originate from the rotor's nature and the spiral casing. The photo depicted in Figure 7 left was taken with the existing inlet operating at 200 m3/h. Due to the inherent constraints of smoke visualization. The limitations of smoke visualization technique – dilution of smoke at high flow rates and view obstructed by the channel walls, make comparison of phenomena with respect to flow rate or inlet channel variation inconvenient. Hence the results of hot wire anemometry were used.
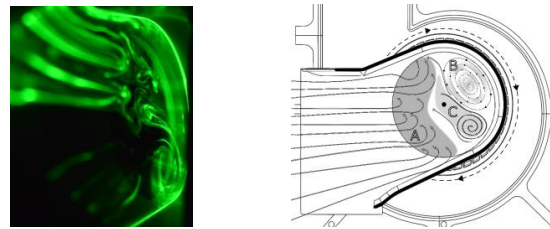
Figure 7: Visualization of the flow field in the existing inlet channel at 200 m^3/h (left) and a scheme of flow field as interpreted based on the visualization (right).
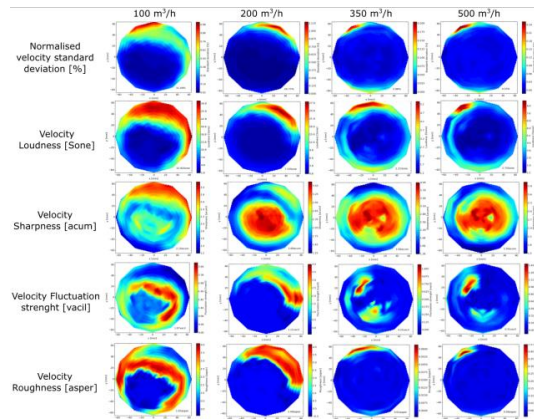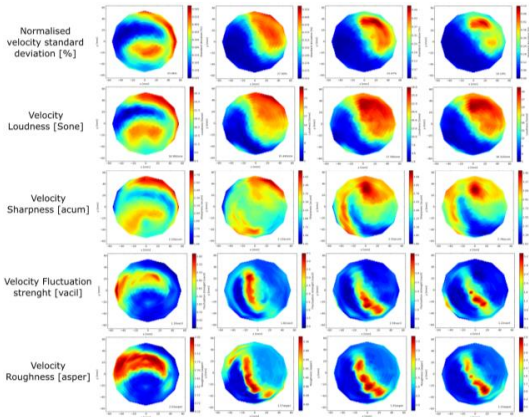

Figure 8: Normalised velocity standard deviation and psychoacoustic metric levels distribution over the inlet area as a function of flow rate in the case of free inlet

To reveal the flow dynamics in regions A, B, and C, we applied psychoacoustic metrics to the velocity fluctuation signals. Figure 8 displays the average velocity magnitude, turbulence intensity, and four psychoacoustic metrics—loudness, sharpness, fluctuation strength, and roughness—as functions of the flow rate. The results are

visualized as contour plots (with consistent scale ranges, barring the velocity distribution) illustrating each variable's distribution across the inlet area on fgures 8 to 10. The red-marked region represents the existing inlet, while the blue indicates the new inlet channel.

Reviewing the velocity distribution, two prominent zones can be identified: 1. a high-velocity zone on the inlet opening's left side and 2. a low-velocity pocket on the right, positioned behind the volute tongue. This observation aligns with earlier conclusions drawn from the visualization data. The high-velocity zone mirrors the well-populated area with minimal vorticity, while the low-velocity segment matches the turbulent eddy zone with sparse throughflow. Notably, the latter is also characterized by intense turbulence, confirming earlier assumptions. Using loudness as an analytical metric offers deeper insights into fluctuation behaviors within the turbulent zone, essentially reflecting the level of velocity fluctuation. An evident decrease in both loudness and sharpness is evident in the area labeled A in Figure 7. This change is attributed to the narrowing of the new channel at that specific location (as seen in Figure 3 and4). It seems this contraction positively directs the flow, diminishing vorticity within the turbulent eddy region (Figure 7).

Figure 9: Normalised velocity standard deviation and psychoacoustic metric levels distribution over the inlet area as a function of flow rate in the case of TD inlet.

While loudness does not provide specific information about the frequency band of the fluctuation, the addition of sharpness, roughness, and fluctuation strength offers a more comprehensive picture. Sharpness embodies a hiss-like quality of sound, dominated by high-frequency energy. Elevated sharpness levels, indicative of dominant high-frequency fluctuations, are typically observed in the turbulent eddy region. This pattern shares a similar spatial distribution to that of loudness. Consequently, it can be inferred that turbulent regions predominantly exhibit high-frequency fluctuations.
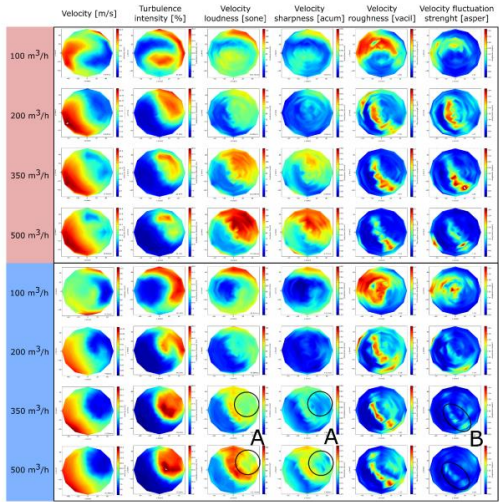

Figure 10: Local flow properties in the plane at the inlet of the fan for existing (red) and new inlet channel (blue) with respect to the volumetric flow rate.

The region situated between the well-filled area and the turbulent eddy region—where a distinct, continuous vortex is evident (as shown in Figure 7, right C)—displays heightened values across all psychoacoustic metrics, pointing to a broadband fluctuation characteristic. Uniquely, this is the sole region demonstrating elevated roughness and fluctuation strength. Meanwhile, the flow dynamics throughout the remainder of the inlet region are characterized by either high or low frequencies. The similar patterns exhibited by roughness and fluctuation strength suggest loudness modulations at frequencies both below and above 30 Hz. From an aerodynamics perspective, we associate the zones with increased fluctuation strength and roughness to the presence of extensive vortices. Such large-scale vorticity arises due to the pronounced velocity gradient in the transitional zone between the well-filled region with minimal vorticity (as seen in Figure 7, right A) and the turbulent eddy region (Figure 7, right B). Notably, at flow rates of 350 and 500 m3/h, a slight decrease in fluctuation strength is evident

with the new inlet (Figure 7, right B), potentially explaining the earlier mentioned efficiency improvements and noise reductions.

At 100 m3/h, heightened values of roughness and fluctuation strength manifest in the predominantly well-filled area with minimal vorticity—the left segment of the inlet opening. This suggests the presence of large-scale vorticity characteristic of low flow rates, which impedes the inlet channel, subsequently impacting efficiency.

On a broader note, the lowest noise levels correspond with a flow rate of 200 m3/h, a condition marked by diminished values across all psychoacoustic metrics. This relationship underscores the correlation between fluctuation intensity and noise emission. When considering volume flow rate, notable metric distribution changes were observed at 100, 200, and 350 m3/h. In contrast, the results between 350 and 500 m3/h displayed more consistency without significant shifts.

4. CONCLUSIONS

Forward curved fans are widely utilized across various industrial and domestic applications, and their operation has been thoroughly examined over the years. Despite this, the issue of efficiency reduction due to abrupt flow conditions in the inlet channel remained largely unexplored. This study primarily aimed to ascertain the impact of inlet channel geometry on the fan's integral aeroacoustic properties and to determine the nuances of local flow properties. This deeper understanding subsequently provided insights into variations in integral characteristics. The key insights and findings include:

1. Efficiency and Noise Improvements: Through modifications to the existing inlet channel, we achieved a 4% efficiency gain and a 2 dB(A) noise reduction.
2. Visualization Techniques: The integration of smoke visualization coupled with laser sheet illumination effectively revealed three distinct flow regions: a well-filled area with minimal vorticity, a turbulent eddy region with limited throughflow, and an intermediate zone with a pronounced continuous vortex.
3. Hot Wire Anemometry: Traversing the inlet plane with a hot wire anemometer provided essential data on velocity fluctuations. When processed, this data significantly elucidated the flow patterns in relation to channel geometry and flow rate.

4. Innovative Psychoacoustic Metrics: The study introduces a novel methodology by employing psychoacoustic metrics on velocity fluctuation signals. This method not only expanded our understanding of airflow dynamics but also proved invaluable for flow pattern interpretation, highlighting dominant fluctuation frequency bands relative to positions on the inlet plane.
5. Efficiency Factors: The redesigned inlet showcased a notable reduction in high-frequency fluctuation, specifically in the turbulent eddy region, as well as a decrease in vortex presence. These improvements directly contributed to the observed 4% efficiency spike and 2 dB(A) noise reduction.

In summary, the blend of traditional methodologies with innovative psychoacoustic signal processing has ushered in a transformative phase in the study of airflow dynamics within forward-curved fans. This research paves the way for future endeavors aiming to optimize aerodynamic efficiency and noise control in various applications.

4. REFERENCES

[1] B. Eck, Fans, Oxford: Pergamon Press, 1973.
[2] B. Jiang, J. Wang, X. Yang and W. D. Y. Wang, "Tonal noise reduction by unevenly spaced blades in a forward-curved-blades centrifugal fan," Applied Acoustics, vol. 146, pp. 172-183, 2019.
[3] C. Jian, H. Yuan, G. Li, W. Canxing, C. Liu and L. Yuanrui, "Aerodynamic noise prediction of a centrifugal fan considering the volute effect using IBEM," Applied Acoustics, vol. 132, pp. 182-190, 2018.
[4] J. Gonzalez and e. all, "Symmetrized dot pattern analysis for the unsteady vibration state in a Sirocco fan unit," Applied Acoustics, vol. 152, pp. 1-12, 2019.
[5] S. J. Kim, H. J. Sung, S. Wallin and A. V. Johansson, "Design of the centrifugal fan of a belt-driven starter generator with reduced flow noise," International Journal of Heat and Fluid Flow, vol. 76, pp. 72-84, 2019.
[6] Kind and R.J., "Prediction of flow behavior and performance of squirrel-cage centrifugal fans operating at medium and high flow rates," Journal of Fluids Engineering, vol. 119, 1997.
[7] R. Kind and M. Tobin, "Flow in a centrifugal fan of the squirrel-cage type," Journal of Fluids Engineering, vol. 112, 1990.
[8] T. S. N. Adachi and e. All, "Study on the performance of a sirocco fan (optimal blade design)," International Journal of Rotating Machinery, vol. 7(6), 2001.
[9] T. Adachi, N. Sugita and e. all, "Study on the performance of a sirocco fan (flow around the runner blade)," Journal Fluid Thermal Science, p. 13(3), 2003.

[10] R. Ballesteros-Tajaduraet and e. all, "Numerical model for the unsteady flow features of a squirrel cage fan," in Summer meeting, 2009.

[11] S. Velarde-Suarez and e. all, "Experimental study on the aeroacoustic behavior of a forward-curved blades centrifugal fan," Journal of Fluids Engineering, vol. 121, 1999.

[12] N. Montazerin, G. Akbari and M. Mahmoodi, Developments in turbomachinery flow: Forward curved centrifugal fans, Woodhead Publishing in Mechanical Engineering, 2015.

[13] S. Pham Ngoc and e. all, "effects of bell mouth geometries on the flow rate of centrifugal blowers.," Journal of Mechanical Science and Technology, vol. 25(9), 2011.

[14] M. Gholamian and e. all, "Effect of axial gap between diffuser inlet and impeller on efficiency and flow pattern of centrifugal fans," Applied Mechanics and Materials, pp. 446-447, 2013.

[15] Xuanfeng Wen, Datong Qi, Yijun Mao, Yijun Mao, Xin Yang. Experimental and numerical study on the inlet nozzle of a small squirrel-cage fan. June 2013. Proceedings of the Institution of Mechanical Engineers Part A Journal of Power and Energy 227(4):450-463. DOI: 10.1177/0957650913487530

[16] G. Lemaitre, C. Vartanian, C. Lambourg and P. Boussard, "A psychoacoustical study of wind buffeting noise," Applied Acoustics, vol. 95, pp. 1-12, 2015.

[17] R. Penna-Leite, S. Paul and S. Gerges, "A sound quality-based investigation of the HVAC system noise of an automobile model," Applied Acoustics, vol. 70, pp. 636-645, 2009.

[18] Y. Okutsu and N. Hamamoto, "Effects of Hydrodynamic and Acoustic Pressure Fluctuations on Transmitted Sound in Wavenumber-Frequency Domain," in Internoise,, Melbourne, 16-19 November 2014.

[19] P. Sagaut and C. Cambon, "Compressible Homogeneous Isotropic Turbulence," in Homogeneous Turbulence Dynamics, doi:10.1007/978-3-319-73162-9_13 , Springer International Publishing, 2018, pp. 621-689.

[20] H. Dryden and T. Karman, Advances in applied mechanics, New York: Academic press, 1964.

[21] T. Suzuki and T. Colonius, "Instability waves in a subsonic round jet detecteusing a near-field phased microphone array," J. Fluid Mech, vol. 565, pp. 197-226, 2006.

[22] M. Mancinelli, T. Pagliaroli, R. Camussi and T. Castelain, J. Fluid Mech., vol. 836, pp. 998-1008, 2018.

[23] S. G. M. F. Mario Felli, "A novel approach for the isolation of the sound and pseudo-sound contributions from near-field pressure fluctuation measurements: analysis of the hydroacoustic and hydrodynamic perturbation in a propeller-rudder system," Exp. Fluids, vol. 55, p. 1651, 2014.

[24] J. Ffowcs-Williams, "Noise source mechanisms," in Modern Methods in Analytical Acoustics Lecture Notes, Berlin, Springer, 1992, p. 313–354.

[25] F. Auteri and e. all, "A novel approach for reconstructing pressure from PIV velocity," Exp Fluids, vol. 45, pp. 56-45, 2015.

[26] O. Shinnosuke and T. Norihiko, "The pressure–velocity correlation in oscillatory turbulentflow between a pair of bluff bodies," Heat and fluid flow, vol. 27, pp. 768-776, 2006.

[27] C. Bogey and C. Bailly, "An analysis of the correlations between the turbulent flow andthe sound pressure fields of subsonic jets.," Journal of Fluid Mechanics, vol. 583, pp. 71-97, 2007.

[28] J. Charonko, V. Cameron, L. Barton and P. Vlachos, "Assessment of pressure field calculations from particle image velocimetry measurements," MEASUREMENT SCIENCE AND TECHNOLOGY, vol. 21, no. doi:10.1088/0957-0233/21/10/105401, pp. 1-16, 2010.

[29] S. Obi and N. Tokai, "The pressure–velocity correlation in oscillatory turbulent flow between a pair of bluff bodies," International Journal of Heat and Fluid Flow, vol. 27, pp. 768-776, 2006.

[30] J. Pearse and M. Kingam, "Measurements of sound in airflow," in The 13th International Congress on Sound and Vibrations, Vienna, Austria, 2. - 6. July 2006.

[31] Wan, H.J. and Duck, J.L. A numerical study on the flow and sound fields of centrifugal impeller located near a wedge, Journal of Sound and Vibration 266 (2003) 785–804

[32] Weidemann, J. Analysis of the Relation between Acoustic and Aerodynamic Parameters for a Series of Dimensionally Similar Centrifugal Fan Rotors, NASA TT F–13, 1971, p. 798.

[33] Wu, J.D. and Bai, M. R. Application of Feedforward Adaptive Active Noise Control for Reducing Blade Passing Noise in Centrifugal Fans, Journal of Sound and Vibration, 2001, 239 (5), 1051-1062,

[34] Hyosung, S., Hyungki, S., Soogab, L. Analysis and Optimization of Aerodynamic Noise in a Centrifugal Compressor, Journal of Sound and Vibration, 2006 289, 999–1018

[35] Čudina, M. and Prezelj, J. Noise Generation by Vacuum Cleaner Suction Units: Part I. Noise Generating Mechanisms – An Overview, Applied Acoustics, 2007, 68 (5), 491-502

[36] Wan, H.J. A Numerical Study on the Effects of Design Parameters on the Performance and Noise of a Centrifugal Fan Journal of Sound and Vibration 2003, 265, 221–230,

[37] Steffen Marburg, Bodo Nolte, Computational acoustics of noise propagation in fluids – finite and boundary element methods, Springer Verlag, March 2008

[38] Daniel R. Raichel, The Science and Applications of Acoustics, 14. Machinery Noise Control, pp. 357-408, Springer New York, 2006, ISBN: 978-0-387-26062-4

[39] N. Curle, The influence of solid boundaries upon aerodynamic sound, Proc. Roy. Soc. London, A 231, pp. 505-514, 1955,

[40] Fridolin P. Mechel, Formulas of acoustics, 2nd Edition, Springer Verlag, 2008

[41] J. Prezelj et.all, Quantification of aerodynamically induced noise and vibration-induced noise ina suction unit. Proceedings of the Institution of Mechanical Engineers. Part C, Journal of mechanical engineering science, 2011, vol. 225, no. 3, pp. 617-624
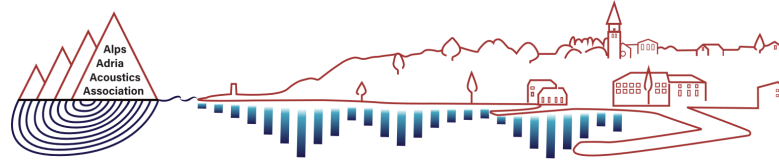
AAAA 2023 IZOLA 20. - 21. September
10th CONGRESS OF THE ALPS ADRIA ACOUSTICS ASSOCIATION

Keynote
Invited speech

Development of sound quality metrics using models based on human perception and their applications

Prof. Dr.-Ing. Roland Sottek

Chalmers Applied Acoustics, Department of Architecture and Civil Engineering

E-mail: roland.sottek@chalmers.se

Professor Dr.-Ing. Roland Sottek has a position as Adjunct Professor in Psychoacoustics at the Division of Applied Acoustics at Chalmers University of Technology since 2016. He received a diploma in Electrical Engineering / Communications Engineering from the Technical University of Aachen in 1987 and a doctor's degree in 1993 for his doctoral research study "Signal Processing Model of the Human Auditory System". From 1987 to 1988 he worked as a scientist at the Philips Research Laboratory Aachen. In 1989 he joined HEAD acoustics where he was first Principal Scientist, later Head of the HEAD Consult NVH department and since 2002 Head of the newly established HEAD Research NVH department. In June 2023 he received the new role of Chief Scientific Advisor, directly supporting the Managing Director with scientific expertise. During his work at HEAD acoustics, he was involved in numerous consulting projects mainly related to automotive applications, as well as in 18 publicly funded national and international research projects. He is author or co-author of more than 150 publications and supervisor of more than 30 theses. Current research work concerns models of human hearing, psychoacoustics, localization and characterization of sound sources, auralization of virtual environments, noise engineering and digital signal processing as well as experimental and numerical methods for sound-field calculation.

Sound quality metrics are often used to analyze complex sound scenarios, such as soundscape applications. Sound quality can also affect the health and well-being of people in a given environment. Therefore, it is of the utmost importance that the definition of good sound quality in a particular context is as precise as possible. In this aspect, psychoacoustic indicators are usually used to develop these metrics.

In his lecture, Roland Sottek will review the existing standardized time-varying loudness models: the Zwicker method (ISO 532-1) and the Moore-Glasberg-Schlittenlacher method (ISO 532-3), which he supported as project leader and as ISO working group member, respectively, as well as the Sottek Hearing Model Loudness (recently standardized in ECMA 418-2 2nd Edition), a new approach based on a nonlinear combination of partial tonal and noise loudness (introduced in ECMA-74 17th Edition as part of the Sottek Hearing Model Tonality, now moved to ECMA 418-2) to better account for the fact that the loudness of tonal components, i.e., tonal loudness, may have a stronger impact on the loudness perception than the loudness caused by the noise components, i.e., noise loudness. Additionally, he will give an overview of the psychoacoustic roughness based on the Sottek Hearing Model (standardized in ECMA-418-2 1st and 2nd Edition) for the evaluation of

fast modulated sounds and on another model for slow modulated sounds: the Sottek Hearing Model Fluctuation Strength, which will be standardized in the near future.

The talk will also provide insights into the complex mechanisms of forming overall noise assessments for some application examples with highly time-varying signals.

AAAA 2023 IZOLA 20. - 21. September
10th CONGRESS OF THE ALPS ADRIA ACOUSTICS ASSOCIATION

Contributed papers
Advanced measurement techniques in acoustics

1. Challenges in the introduction of timbre coordinates for violoncelli
   Daniel Svenšek (University of Ljubljana, Faculty of Mathematics and Physics)
2. Soundscape monitoring system for earthquake-affected urban spaces – Zagreb case study
   Karlo Filipan (Catholic University of Croatia)
3. Immission Directivity as a tool for generation of Noise Maps
   Jurij Prezelj (University of Ljubljana, Faculty of Mechanical Engineering)
4. Data Selection for Reduced Training Effort in Vandalism Sound Event Detection
   Stefan Grebien (Joanneum Research)
5. Experimental sound field characterization with automated high-resolution impulse response measurements
   Rok Prislan (InnoRenew CoE)
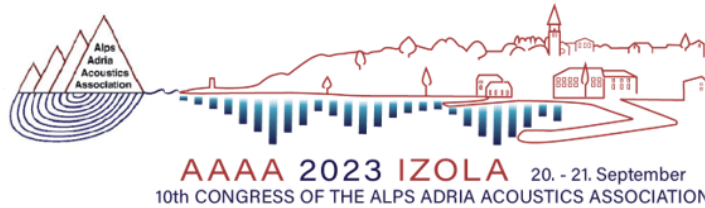
CHALLENGES IN THE INTRODUCTION OF TIMBRE COORDINATES FOR VIOLONCELLI

Daniel Svenšek[1,2]**, Urša Kržič**[3]**, Rok Prislan**[4]

[1] **Department of Physics, Faculty of Mathematics and Physics, University of Ljubljana, Slovenia**
[2] **Laboratory for Molecular Modeling, National Institute of Chemistry, Slovenia**
[3] **Music School Vrhnika, Vrhnika, Slovenia**
[4] **Acoustic Laboratory, InnoRenew CoE, Izola, Slovenia**

Abstract:

Musical instruments are known for their subtle nuances of sound, and as bodies of considerable size, they have complex radiation patterns. It is therefore a challenge to capture their sound in a robust and reproducible manner while preserving the finest structures required for timbre analysis. In fact, timbre has never been successfully used in practice as a measurable parameter of an instrument, although the ability of humans, especially musicians, to perceive subtle differences in sound colour between instruments of the same type has never been questioned. In recording cellos, we have succeeded in capturing their spectra in such a way that we can introduce harmonic timbre coordinates. These are quantifiers that represent the harmonic spectral aspect of an instrument's sound in a musically relevant way. The basic challenges of introducing timbre coordinates are presented using the cello as a case study, along with data processing steps required to generate timbre coordinates. The study is important because the introduced coordinates have the potential to change the world of musical instruments by providing an objective label for the harmonic sound color of each instrument.

Keywords: *musical instruments, harmonic timbre coordinates, linear timbre vector space*

1. INTRODUCTION

The differences between the sound of musical instruments of the same type, although certainly perceivable to sensitive ears, are extremely small. Small compared to the sensitivity of recording an instrument, related for example to the position of the microphone, the room and its acoustics, the instrumentalist's playing etc. Our quest began with the question of whether a robust, reproducible, and meaningful quantification of the timbre of identical instruments is possible, in an intentionally reduced framework as would be required. Our goal now is to show that this is indeed possible, at least for harmonic timbre. A particular and central challenge is to obtain a universal, robust, yet sensitive recording of a musical instrument that allows the analysis of even the smallest differences between instruments required for this task.

It is fair to admit that a scientific method, particularly in fields involving humanistic aspects like the one at hand, is inherently limited. It cannot substitute for the actual act of listening to and even more so, physically testing an instrument. Nevertheless, it can be a valuable initial step and a preliminary reference point when it comes to personal preferences, rather than un ultimate objective truth. Consider the significance that assigning concrete numerical values to describe the relevant sound properties of musical instruments might have for their production and the market as a whole. The harmonic timbre coordinates we introduced have the potential to serve precisely as such numerical indicators, though certainly only partial.

The pilot study is conducted with violoncelli. We stay almost entirely away from psychoacoustics [1, 2], apart from the basic connection between harmonic timbre and harmonic content of the power spectrum. Moreover, we adopt a front-end approach, concentrating solely on the instrument's audible output during normal play, which includes the complete sound radiation process. We intentionally avoid detailed mechanical analysis like the examination of sound or vibration modes or complex nonlinear models of tone generation etc., addressed in numerous rigorous physical treatments [3–8] on the one hand and arising in the practice of instrument making [6, 9] on the other.

2. CHALLENGES OF THE WAVE FIELD

The wave nature of the sound field entails hard physical facts that cannot be avoided. On the one hand, we are dealing with direct sound, i.e. with sound radiation with its complex radiation patterns [10–15]. On the other hand, we encounter the laws of the diffusive wave field [16–18], where care must and can be taken to ensure that the recording space is large enough to exclude modal effects.

Fig. 1. *The typical recording configuration for violoncello measurements. A microphone array of 33 microphones designed and built for this purpose was used. The positioning of the musician and the microphones was maintained between recordings.*

2.1 Understanding the radiation field

We are interested in the physical picture of the radiation process, not the details of the radiation patterns, which vary greatly from one instrument to another. The key factor is the size of the radiating instrument, i.e., the characteristic size of the space enclosed by its radiating surfaces, relative to the considered wavelength of the radiated sound. The larger the instrument in comparison to the wavelength, the greater the efficiency of radiation and the more intricate the angular dependence of the radiation pattern.

Let us inspect this in more detail. The radiated sound wave $p(\mathbf{r}, t) = p(\mathbf{r})e^{-i\omega t}$ with angular frequency ω and pressure amplitude p is described like every sound/scalar wave by the amplitude equation

$$\nabla^2 p + k^2 p = 0, \tag{1}$$

where $k = \omega/c$ and c is the speed of sound. The general solution is

$$p(\mathbf{r}) = \sum_{l=0}^{\infty} \sum_{m=-l}^{l} c_{lm} h_l^{(1)}(kr) Y_{lm}(\theta, \phi), \tag{2}$$

where $Y_{lm}(\theta, \phi)$ are spherical harmonics, θ and ϕ are polar and azimuthal angles, c_{lm} are general coefficients, and

$$h_l^{(1)} = j_l + in_l \tag{3}$$

are the spherical Hankel functions of the first kind (describing outgoing waves); j_l and n_l are the spherical Bessel functions of the first and second kinds (also known as the spherical Bessel and Neumann functions). Eq. (2) represents the multipole expansion of the pressure field of outward propagating waves, where l is the order of the multipole (monopole, dipole, quadrupole, octupole ... for $l = 0, 1, 2, 3 ...$)

Assuming the radiating surface is a sphere (we pursue the general picture, not the details) with radius a, the radial component of the acoustic velocity $\mathbf{v}$, which satisfies the equation of motion

$$-i\omega\rho\mathbf{v} = -\nabla p, \tag{4}$$

must match the radial velocity of the vibrating sphere at $r = a$. Let $v_r(\theta, \phi) = v_{lm} Y_{lm}(\theta, \phi)$ be a term in the expansion of the latter over spherical harmonics (the value of the coefficient v_{lm} depends on the angular shape of the oscillation). The boundary condition for the pressure is then

$$c_{lm} \left. \frac{\partial h_l^{(1)}(kr)}{\partial r} \right|_{r=a} = i\omega\rho v_{lm} \tag{5}$$

and determines the coefficient c_{lm} of the solution Eq. (2).

Let us determine these coefficients in the limit $ka \ll 1$, i.e., when the radius of the radiating sphere is small compared to the wavelength of the sound at a given frequency. In leading order, the Hankel function Eq. (3) is

$$h_l^{(1)}(kr \ll 1) \approx in_l^{(1)}(kr) \approx -i\frac{(2l-1)!!}{(kr)^{l+1}}, \tag{6}$$

where $(2l-1)!! = 1 \times 3 \times 5 \times \cdots \times (2l-1)$ and $(-1)!! \equiv 1$. It then follows from Eq. (5)

$$c_{lm} i(l+1)k \left. \frac{(2l-1)!!}{(kr)^{l+2}} \right|_{r=a} = i\omega\rho v_{lm} \tag{7}$$

and finally

$$c_{lm} = \frac{c\rho v_{lm}}{(2l-1)!!} \frac{(ka)^{l+2}}{l+1}. \tag{8}$$

In this small sound source limit, the amplitudes of all multipoles decrease strongly with decreasing ka. Their ratios to the amplitude c_{00} of the monopole are

$$\frac{c_{lm}}{c_{00}} = \frac{v_{lm}}{v_{00}} \frac{1}{l!!} \frac{(ka)^l}{l+1}, \tag{9}$$

again decreasing strongly with decreasing ka and for $ka < 1$ also with increasing l.

Note that the acoustic pressure field in the immediate vicinity of the sound source surface is that dictated by the velocity boundary condition via Eq. (4), i.e. with full angular dependence

of the source oscillation. When we move away, the contributions of higher multipoles rapidly decrease due to the leading dependence Eq. (6). However, if this decreasing dependence no longer holds at the surface, there is also no longer a decline of the higher multipoles.

In the vicinity of a small source ($kr \ll 1$, near field), the contribution of a multipole l to the total acoustic pressure Eq. (2) is thus

$$p_l(\mathbf{r}) = -\sum_m \frac{c\rho v_{lm}}{\cdots} \frac{(ka)^{l+2}}{l+1} \frac{\cdots}{(kr)^{l+1}} Y_{lm}(\theta, \phi)$$

$$= -\rho c v_{lm} \frac{ka}{l+1} \left(\frac{a}{r}\right)^{l+1} Y_{lm}(\theta, \phi). \qquad (10)$$

At $r = a$ it is as dictated by the oscillation of the source surface, and falls away from it as a power of a/r. Multipoles of higher order fall off faster with the distance from a small source.

Far away from the source ($kr \gg 1$, far field), the Hankel functions Eq. (3) take the asymptotic form

$$h_l^{(1)}(kr) \asymp \mathrm{i}^{-(l+1)} \frac{\mathrm{e}^{\mathrm{i}kr}}{kr} \qquad (11)$$

and the contribution of a multipole l to the total acoustic pressure Eq. (2) is

$$p_l(\mathbf{r}) = \sum_m c_{lm} \, \mathrm{i}^{-(l+1)} \frac{\mathrm{e}^{\mathrm{i}kr}}{kr} Y_{lm}(\theta, \phi). \qquad (12)$$

Note that the contributions of all multipoles, regardless of their order, fall off only as $1/r$ (as with any radiation field). This should not be confused with the rapid decay $1/r^{l+1}$ of static multipole fields. Thus, assuming that the coefficients v_{lm} are not small, the contributions of higher-order radiation multipoles are small only if their amplitudes c_{lm} are small – they do not become relatively weaker with distance!

For a small sound source ($ka \ll 1$), the coefficients Eq. (8) are small and so are their ratios Eq. (9) relative to the amplitude of the monopole. Only in this case the $l > 0$ multipoles are negligible and sound radiation has no substantial angular dependence, except in the immediate vicinity of the source. When the size of the sound source increases to $ka \sim 1$ and beyond, this is no longer true, as we already understand from the physical picture discussed after Eq. (9) and as also indicated by Eq. (9). Note that Eqs. (6)-(10) were derived for $ka \ll 1$. It turns out, however, that they are nevertheless acceptable over a much larger range, e.g., up to $ka \sim 4$ for $l = 4$ and $ka \sim 10$ for $l = 32$, so that Eq. (9) serves as a reasonable estimate of the relative strength of the multipoles. For example, c_{4m}/c_{00} becomes larger than 0.1 for $ka >\sim 2$.

In general, for each radiation multipole l there is a critical frequency above which that multipole is important and of undiminished relative amplitude even in the far field. Conversely, for each frequency there are significant multipoles with orders below a critical l. The angular dependence of these multipoles cannot be avoided. Therefore, the radiation pattern they form is inherently complex for sufficiently large ka. Assuming $a \sim 0.4\,\mathrm{m}$

for a cello, in the above example c_{4m}/c_{00} becomes greater than 0.1 for frequencies greater than about $275\,\mathrm{Hz}$.

When choosing the distance between the instrument and the microphones, it is useful to make sure that the multipoles, which are strong only in the near field, decrease sufficiently. The near-field solution Eq. (10) shows that simply a/r must be sufficiently small. However, we cannot do more – the angular dependences of the multipoles remaining in the far field cannot be eliminated and must be averaged by some strategy.

2.2 Understanding the diffuse field

First, we assume that the recording space is large enough to exclude modal effects – the choice of recording space is a controllable factor. Similarly, the most prominent early reflections can be mitigated by a sufficiently large recording space and, in addition, by the use of absorbing materials on critical sections of the surfaces. What ideally remains, is the diffuse sound field.

A diffuse field is stochastically irregular and homogeneous *on average*, but one must be cautious about the true meaning of the average. At a given frequency, the diffuse field is by definition not homogeneous as it knows about a characteristic length – its wavelength. Indeed, it is spatially correlated on the wavelength scale, with spatial pressure correlation function [16,17,19]

$$\chi(r) = \frac{\langle p(\mathbf{r}', t)\, p(\mathbf{r}' + \mathbf{r}, t)\rangle}{\langle p^2(\mathbf{r}', t)\rangle} = \frac{\sin kr}{kr}, \qquad (13)$$

where $\langle \rangle$ denotes averaging over space $\mathbf{r}'$ and time t.

That is, a monochromatic sound field is not actually diffuse and requires spatial averaging, which is essentially statistical in nature. When such field is stationary (a standing wave), its amplitude is a fixed and more or less regular function in space with modulations on the wavelength scale, and there is little randomness left. However, if the frequency or the configuration of the modal amplitudes change (e.g., due to a displacement or rotation of the sound source, reconfiguration of the room etc.), the shape of the stationary field changes abruptly when the conditions for a diffuse field are met.

It is thus common to smooth the signal obtained from a diffuse sound field by averaging its spectrum over frequency bands. However, in the case of musical instruments, whose tones consist of narrow and stable frequency peaks, this is not possible – we cannot avoid the peculiarity of the superimposed monochromatic sound fields corresponding to harmonic partials. Even in a large concert hall, where modal effects are completely absent, one can hear how individual harmonics of a distant instrument playing a steady note become fainter and louder when the listening position (or the position of the instrument) is slightly changed. Only spatial averaging can help here.

3. REQUIREMENTS FOR THE TIMBRE COORDINATES

If timbre coordinates are to be truly useful and have real value in the musical sense, they must meet crucial requirements of

relevance, robustness, and reproducibility. **i)** They should correspond to the situation of normal playing by a musician. No artificial excitation by devices is allowed. **ii)** It is essential that they remain robust and exhibit minimal variation when the same tone is played repeatedly in the same way. This inherent variation in natural excitation defines a *base tolerance*, which represents the upper limit of precision against which all other sources of errors should be judged and which must be sufficiently smaller than the timbre variations between instruments. **iii)** The variations arising from different performers should be minor in comparison to the variations between the instruments. Ideally, they should fall within the base tolerance margin, effectively rendering the performer as an irrelevant factor. **iv)** The coordinates should be largely unaffected by natural variations that occur during normal playing. These variations primarily stem from shifts in the position and orientation of the instrument during play, which influence the sound radiation pattern. **v)** The determination of the coordinates must be reproducible, even in different measuring spaces that comply with the standards.

4. MEASUREMENT AND ANALYSIS

Both the averaging of the sound radiation pattern and of the diffuse field, discussed in Section 2, is achieved by recording with a sufficiently large number of microphones distributed across a characteristic listening solid angle in front of the instrument and spanning a sufficiently large contour. A cross-shaped microphone stand was developed for the purpose, carrying 33 equidistant microphones in a horizontal and vertical line. We use phase-matched 1/4-inch microphones (B&K type 4958), declared with a frequency response in the range of $\pm 2\,\mathrm{dB}$ from 50 to $10\,000\,\mathrm{Hz}$. Data acquisition was performed with 24 bits and a sampling frequency of $65\,536\,\mathrm{Hz}$ (B&K Lan-XI data acquisition system).

The recording of the violoncelli was performed in a controlled environment using the recording setup shown in the photo in Fig.1. The cellist bows a selected tone several times in succession at a comfortable (mezzo) forte, where the responsiveness of the instrument is best and the tone production is most stable. The repetitions are used both for statistical averaging and to determine the base tolerance, which is the inherent measure of uncertainty in the resulting harmonic timbre coordinates.

The analysis starts with the selection of the most stable segments from the multichannel recordings of the sustained notes. For each channel, the power spectra of these segments are computed with optional windowing. The powers within the harmonic peaks are then integrated across their widths, averaged across all channels, and optionally weighted to obtain multicomponent vectors of the strengths of the harmonic partials, ty about 20.

So many harmonics are usually not so stable and reproducible that they would lead to well-defined timbre coordinates.
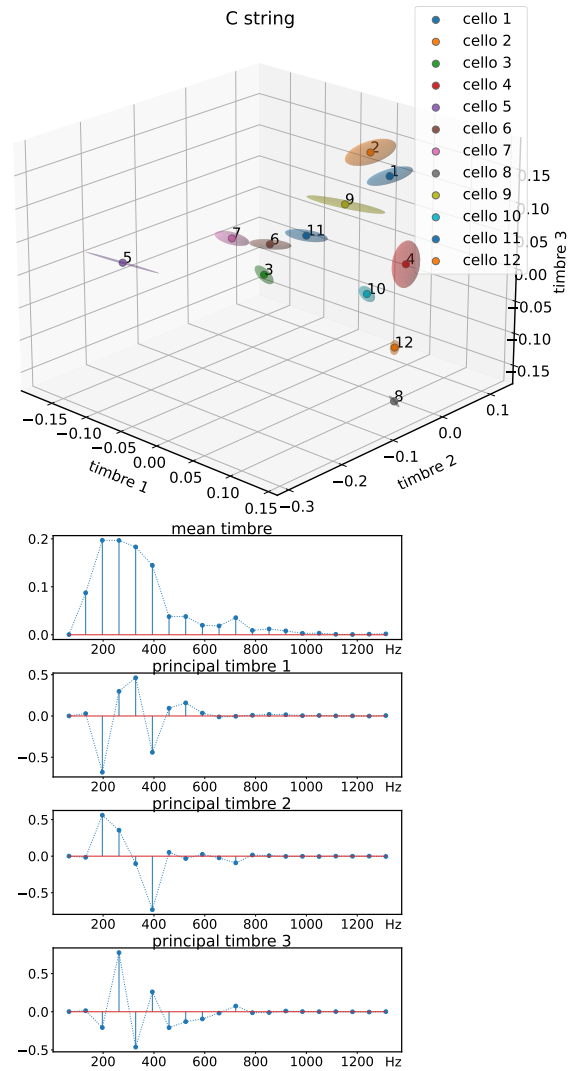
Fig. 2. *Top: The first three dimensions of the harmonic timbre space of the violoncelli C strings. Bottom: harmonic vectors of the corresponding mean timbre and the principal timbres – basis vectors of the above timbre subspace.*
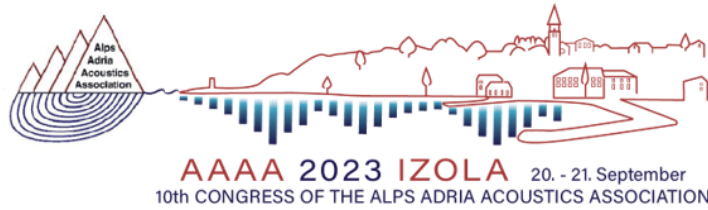
Therefore, by stacking all harmonic vectors of the analyzed collection of instruments, properly normalized, into a matrix and performing the singular value decomposition (SVD) of this matrix (which we do not discuss in detail here), we can determine a smaller number of relevant combinations of harmonics – the so-called principal timbres [20, 21]. They define a statistically optimum basis of the harmonic timbre vector space. The principal timbres are not known in advance and depend on the type of instrument, the register, the string, the dynamics of the playing and other possible variations, which then define specific principal timbre bases and specific sets of coordinates.

After "mining" these principal timbres solely from the front-end acoustic data, one can also listen to them and form his own psychoacoustic interpretations. Furthermore, one can envision an instrument in which the principal timbres are added with different weights (positive and negative). One can then explore instruments whose coordinates align with these specifications.

5. EXAMPLES OF RESULTS

We will present selected results based on a collection of 12 instruments recorded in the main concert hall of the Conservatory of Music and Ballet Ljubljana in May 2023 (many thanks to the Conservatory, Prof Karmen Pečar and her students). We analyzed the timbres of the four open strings of the violoncelli, thus characterizing each instrument by four timbres, one for each string. Above in the Figs. 2 and 3 are shown the resulting harmonic timbre spaces for the lowest (C) and highest (A) strings of the cello, more precisely, their dominant three-dimensional subspaces. The individual instruments form well-defined clusters in this subspace. The centre of the ellipsoid represents the mean of 10 repeated strokes of the open string of the corresponding cello, while the ellipsoids indicate the statistical uncertainty in each timbre direction, i.e., the base tolerance of playing.

For some instruments the tolerances are very small, for others much larger, especially for the A string in Fig. 3 (top). These are not only uncertainties of the determined timbre coordinates, but also suggest differences in the responsiveness (playability) of the instruments. Some of the ellipsoids are highly elongated (prolate), usually indicating pronounced variations of a particular single harmonic partial with each repetition of the tone. In principle, though less likely, it is also possible that two or more partials vary that happen to lie in similar directions of the represented subspace (but the directions of the individual partials are always orthogonal in the complete timbre space).

The decisive importance of spatial averaging of the sound of an instrument is demonstrated in Fig. 4. Here, the harmonic vectors of the individual channels are projected onto the timbre subspaces of Figs. 2 and 3, respectively, without changing the spaces themselves. It is obvious that the variations between the channels, even if they have a hint of regularity and are not completely stochastic, are extremely large and completely blur the well-defined clusters formed by the averages of the channels
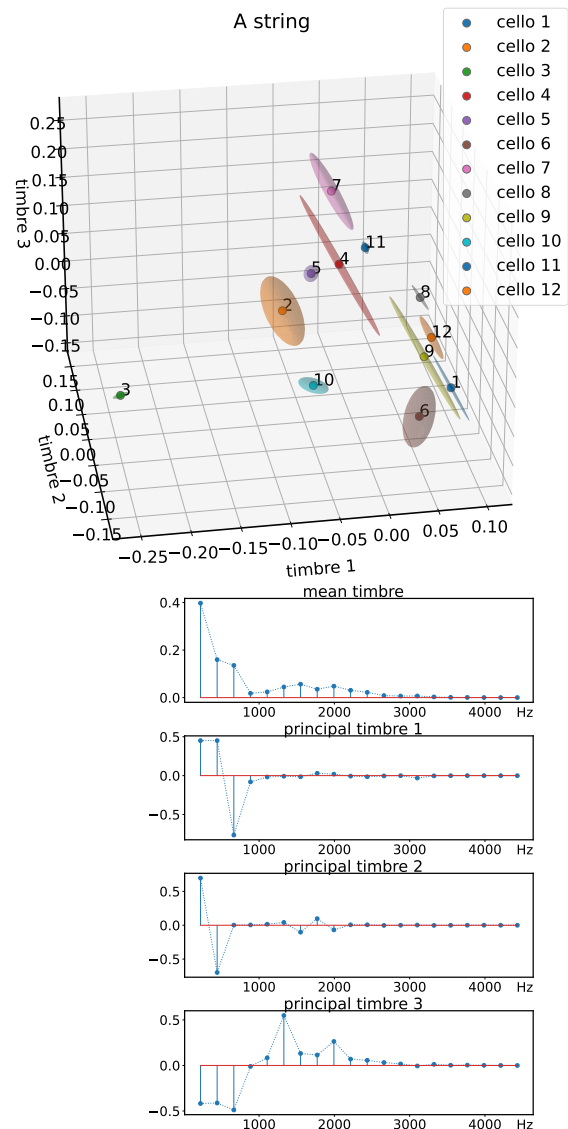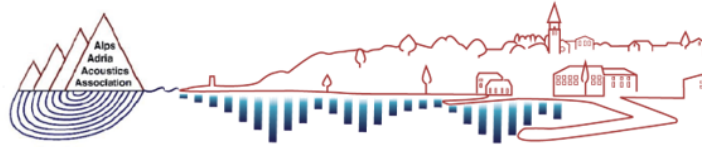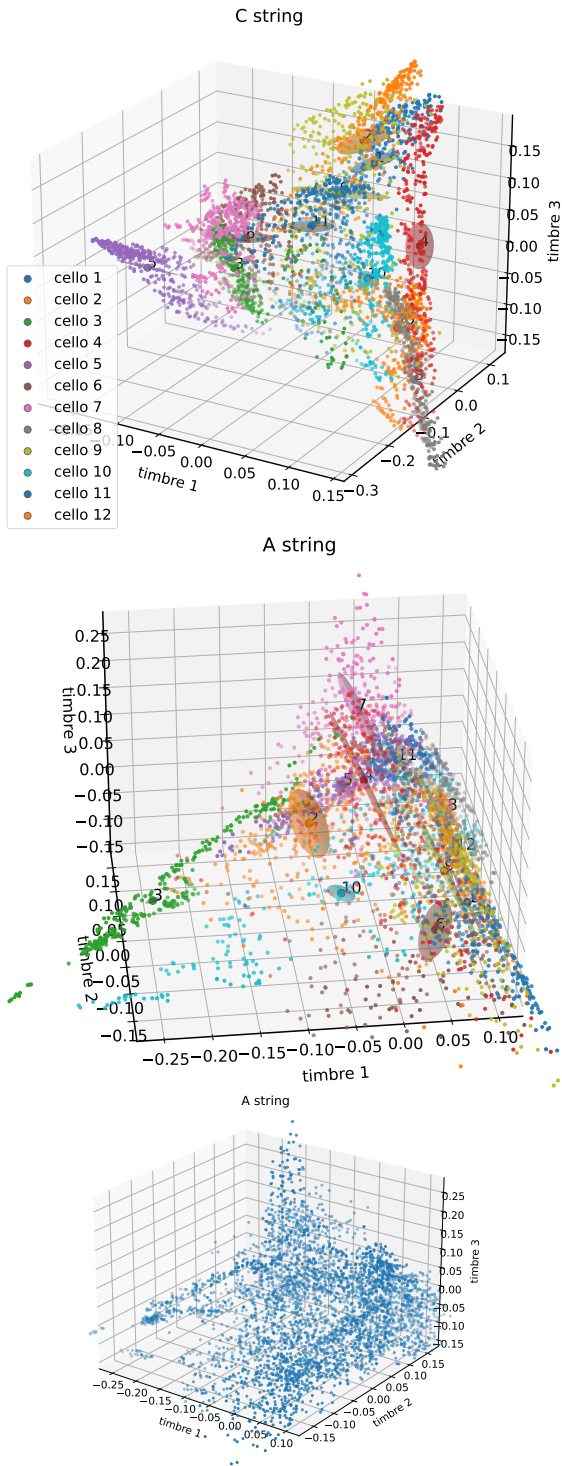

Fig. 3. *The same diagrams as in Fig. 2, but for the A strings of the celli. Note the considerable differences between the sizes and shapes of the uncertainty ellipsoids, discussed in the text.*

C string

A string

A string

Fig. 4. *Harmonic vectors of the individual microphone channels of the measuring array, projected onto the corresponding timbre subspaces of Figs. 2 and 3. Bottom: the*

– see below in Fig.4 what is left without the aid of supervised colour coding. Without spatial averaging there are no timbre coordinates!

6. CONCLUSION

We have highlighted some of the challenges associated with the pioneering attempts to quantify minute differences in the harmonic timbre of identical instruments. We presented some of the solutions to these challenges. For the measurement part of the process, this is primarily the issue of adequate spatial averaging of an instrument's sound field. When properly averaged, the introduced harmonic timbre coordinates are robust – their determination is reproducible almost entirely within the inherent tolerance of human playing. Ongoing experiments have shown that they are also largely independent of the measurement space, with a somewhat extended tolerance, provided the space is not too small – a chamber hall already proves to be large enough. Systematic studies to refine the definition of the tolerances are underway.

7. REFERENCES

[1] S. Town and J. Bizley, "Neural and behavioral investigations into timbre perception," *Frontiers in Systems Neuroscience*, vol. 7, 2013.

[2] S. McAdams and K. Siedenburg, "Perception and cognition of musical timbre," in *Foundations of Music Psychology: Theory and Research* (P. J. Rentfrow and D. J. Levitin, eds.), pp. 71–120, Cambridge: MIT Press, 2019.

[3] M. E. McIntyre and J. Woodhouse, "On the fundamentals of bowed string dynamics," *Acustica*, vol. 43, no. 2, pp. 93–108, 1979.

[4] M. E. McIntyre, , R. T. Schumacher, and J. Woodhouse, "On the oscillations of musical instruments," *J. Acoust. Soc. Am.*, vol. 74, no. 5, p. 1325, 1983.

[5] L. Cremer, *The physics of the violin*. Cambridge, Mass: MIT Press, 1984.

[6] C. M. Hutchins and V. Benade, eds., *Research Papers in Violin Acoustics, 1975-1993*. Acoustical Society of America, 1996.

[7] N. H. Fletcher and T. D. Rossing, *The Physics of Musical Instruments, 2nd Edition*. New York: Springer, 2010.

[8] A. Chaigne and J. Kergomard, *Acoustics of musical instruments*. Springer, 2016.

[9] CAS — Catgut Acoustical Society, https://www.catgutacoustical.org.

[10] G. Weinreich and E. B. Arnold, "Method for measuring acoustic radiation fields," *The Journal of the Acoustical Society of America*, vol. 68, no. 2, pp. 404–411, 1980.

[11] L. M. Wang and C. B. Burroughs, "Directivity patterns of acoustic radiation from bowed violins," *Catgut Acoust. Soc. J.*, vol. 3, no. 7, pp. 7–15, 1999.

[12] G. Bissinger, "Parametric plate-bridge dynamic filter model of violin radiativity," *The Journal of the Acoustical Society of America*, vol. 132, no. 1, pp. 465–476, 2012.

[13] N. R. Shabtai, G. Behler, M. Vorländer, and S. Weinzierl, "Generation and analysis of an acoustic radiation pattern database for forty-one musical instruments," *The Journal of the Acoustical Society of America*, vol. 141, no. 2, pp. 1246–1256, 2017.

[14] J. Meyer, *Acoustics and the Performance of Music*. Springer New York, NY, 2009.

[15] J. Pätynen and T. Lokki, "Directivities of symphony orchestra instruments," *Acta Acustica united with Acustica*, vol. 96, no. 1, pp. 138–167, 2010.

[16] R. K. Cook, R. V. Waterhouse, R. D. Berendt, S. Edelman, and M. C. Thompson, "Measurement of correlation coefficients in reverberant sound fields," *The Journal of the Acoustical Society of America*, vol. 27, no. 6, pp. 1072–1077, 1955.

[17] F. Jacobsen, *The diffuse sound field - Report No. 27*. The Acoustic Laboratory, Technical University of Denmark, 1979.

[18] B. Rafaely, "Spatial-temporal correlation of a diffuse sound field," *The Journal of the Acoustical Society of America*, vol. 107, no. 6, pp. 3254–3258, 2000.

[19] F. Jacobsen and T. Roisin, "The coherence of reverberant sound fields," *The Journal of the Acoustical Society of America*, vol. 108, no. 1, pp. 204–210, 2000.

[20] G. J. Sandell and W. L. Martens, "Perceptual evaluation of principal-component-based synthesis of musical timbres," *J. Audio Eng. Soc.*, vol. 43, pp. 1013–1028, december 1995.

[21] M. A. Loureiro, H. B. Paula, and H. C. Yehia, "Timbre classification of a single musical instrument," in *In Proc. Intl. Conf. on Music Information Retrieval (ISMIR*, 2004.

SOUNDSCAPE MONITORING SYSTEM FOR EARTHQUAKE-AFFECTED URBAN SPACES – ZAGREB CASE STUDY

Karlo Filipan[1], **Mia Šetić Beg**[2], **Dominik-Borna Ćepulić**[2], **Hrvoje Štefančić**[2]

[1] **Acoustics Lab, Catholic University of Croatia, Zagreb, Croatia**
[2] **Department of Psychology, Catholic University of Croatia, Zagreb, Croatia**

Abstract:
The experience of a sound stimulus is closely related to the meaning that people attach to it. In Zagreb area, after the series of earthquakes which struck in 2020, people have started reporting the increased noticing and reaction to the sounds similar to the ones produced by earthquakes. During the last year, project In-SPE(S) was started with the goals: a) to establish the infrastructure for measuring sound and vibrations in earthquake-affected urban areas, and b) to examine the connection between objective characteristics of sound and vibrations with people's perception, personality traits and previous experiences of earthquakes. Monitoring methodology is structured in two ways: sound and vibration measurements are performed using a network of sensor nodes, while respondents who live near the sensors provide their experience of the salient events captured by the sensors through a mobile application. This contribution will present the soundscape monitoring system and research methodology utilized in the project as well as discuss some preliminary results of the measurements campaign.

Keywords: *soundscape, sensor network, mobile application, physical measurements, perception evaluation*

1. INTRODUCTION

It is well-understood that people living in highly urbanized areas mention noise as one of the biggest nuisance factors of their lives. Since the second half of the 20th century, the negative effects of noise on health and human behavior have been systematically investigated [1]. However, in addition to the research on noise, the concept of soundscape has also been developed during the last 50 years [2]. In the more recent ISO standard [3], soundscape is defined as the: "acoustic environment as perceived or experienced and/or understood by a person or people, in context". Thus, soundscape analyzes detailed interaction of sound, environment and people, including both positive and negative effects [4]. Research has shown that the perception of the sound environment and consequent soundscape appraisal depends on the experience of prominent (salient) sound sources [5]. Therefore, the sounds that people hear, i.e. pay attention to and assign the meaning to, affect their experience of the place [6].

In 2020, Croatia was hit by two major earthquakes in the city of Zagreb and Banovina county. In addition to material damage, people have also experienced increased stress and anxiety levels induced by these earthquakes [7]. The earthquake events were felt by the strong vibrations of the built environment as well as by the sound that accompanied the earthquake [8]. Due to this traumatic experience, people started reacting even to the lower level stimuli such as the passing of a heavy vehicle, the slamming of doors and windows, the passing of an elevator, and the like.

In order to quantify such experiences, a long-term monitoring system for sound and vibration measurements and instantaneous soundscape appraisal is being established during project In-SPE(S) - **In**vestigation and Measurement of **S**oundscape **P**erception in **E**arthquake-affected Urban **S**paces. The data obtained by the system will be used to examine the connections between physical characteristics of sound and vibrations with people's perception, personality traits and previous experiences of earthquakes. In this contribution, we will give an overview of the established soundscape monitoring system as well as discuss some preliminary results and ongoing work.

2. SOUND AND VIBRATION MEASUREMENTS

In the proposed soundscape monitoring system (Fig. 1) sound and vibrations are measured by a network of sensor nodes placed on the residential buildings. The sensor node (Fig. 2) consists of a Raspberry Pi 3 Model B+ single-board computer to which various sensors and electronic components are connected to. The sensors are: integrated chip designed by the ASAsense company [9] with Knowles FG-23329-P07 microphone and ADXL345 accelerometer; and a DHT22 sensor used for measurements of temperature and humidity. All electronics are secured in a waterproof housing. The node is connected to electricity via power supply cable and to the Internet via WiFi. To obtain comparable sound measurements, a class 1 acoustic calibrator SVANTEK SV 36 is used to calibrate the microphone.

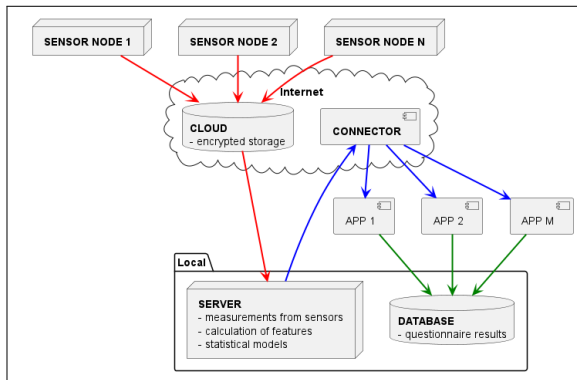The recorded sound and vibration measurements are stored

Fig. 1. *Soundscape monitoring system established during Project In-SPE(S): physical environment is measured by the sensor nodes and data is analyzed on the server (red); people are asked for their appraisal of salient events through mobile application (blue) and their answers are stored for further analysis and use (green).*

using a time-stamped data structure in the memory of the sensor node. The stored data is compressed and encrypted. This ensures that, in accordance with the GDPR directive, the data sent to the cloud cannot be read by third parties. Rclone software tool [10] is responsible for continuously encrypting and sending the measurements to the cloud as well as storing them into a directory structure according to the sensor's tag (location) and the time of recording.

Measurements from the sensors are analyzed on the Linux server. The rclone tool is again used to download and decrypt the data from the cloud. Some examples of the parameters continuously measured by the system can be seen in Figs. 3-6. Firstly, temperature and relative humidity are parameters which need to be accounted for when making the statistical models that include sound and vibration [11]. As it can be seen in Figs. 3 and 4, placement of the sensor also plays a role on their variability. Hence, although somewhat influenced by the enclosure and the heat from the electronics, measuring these values is useful. Moreover, they could also indicate potential faults of the equipment. For example, for sensor 1 (Fig. 3, bottom), humidity raised up significantly at 15 o'clock on a particular date. Knowing the local situation (rain shower), the leak of the enclosure was detected and accounted for.

From the sound measurements, indicators such as L_{Aeq} and L_{Ceq} can be calculated. A-weighted equivalent continuous level represents the overall sound/noise level, while the difference between the C-weighted and A-weighted levels indicates the low-frequency content typically associated with the traffic noise. As shown in Figs. 5 and 6, there is a difference between the overall sound levels for sensor nodes 1 and 2. Node 1 is placed

Fig. 2. *Top: placement of sensor nodes on external building envelope. Bottom: operational setup of the sensors (microphone, temperature and humidity sensor, sound and vibration acquisition board) connected to a single-board computer (Raspberry Pi 3 Model B+).*

on the building close by but somewhat shielded from the major arterial road, while node 2 is placed on the building looking over a side road. Hence, daily L_{Aeq} levels are higher for node 2. On the other hand, levels during night period, 23h-7h, drop more in the case of node 2. Regarding the frequency content, $L_{Ceq} - L_{Aeq}$ levels measured by node 1 (Fig. 5, bottom), show rush hour peaks (visible only during weekdays) which are not present in the side road as measured by node 2 (Fig. 6, bottom). Moreover, low frequency content is present largely during night periods for both measurement locations, although for the arterial road this is not as prominent as for the side road.

This brief analysis shows that by using the sensor measurements and simple statistical indicators, sound environments can be differentiated and explained up to a point. Nevertheless, people living next to the sensor node placed by the arterial road
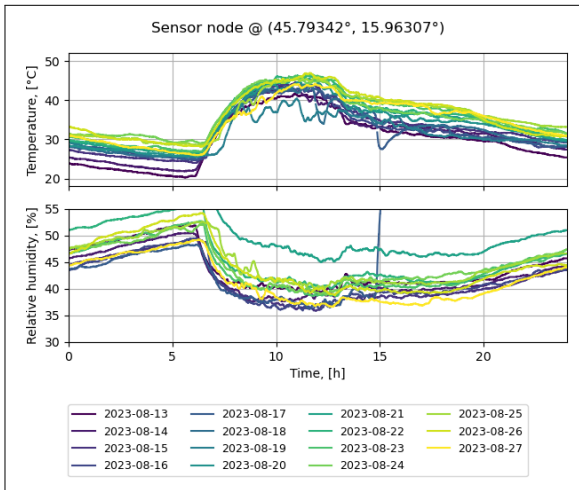
Fig. 3. *Daily variability of environmental parameters measured by the **sensor node 1** - placed on the window facing east: top) temperature; bottom) relative humidity.*
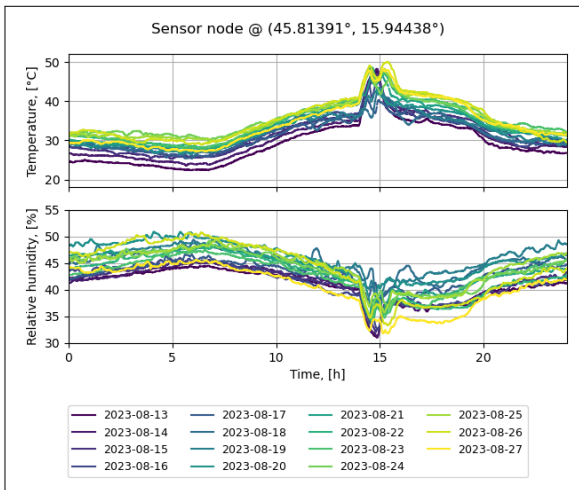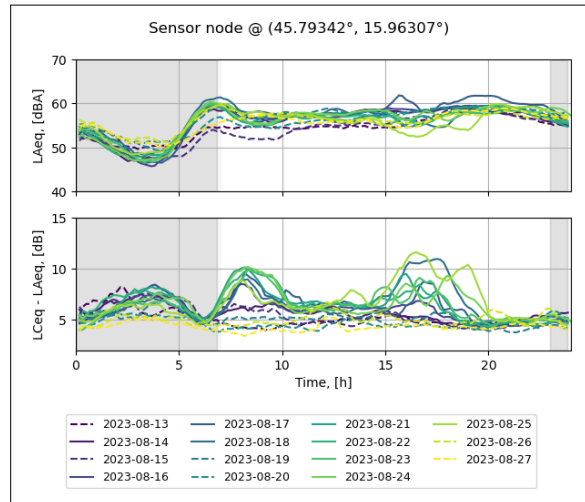

Fig. 5. *Daily variability of continuous sound levels measured by the **sensor node 1** - close by a major arterial road: top) A-weighted levels; bottom) difference between C-weighted and A-weighted levels. (Night times are shaded, and weekends and holidays are plotted with dashed lines.)*
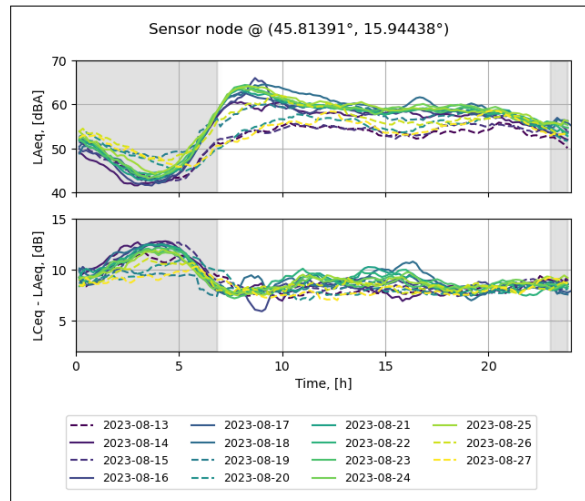

Fig. 4. *Daily variability of environmental parameters measured by the **sensor node 2** - placed on the window facing west: top) temperature; bottom) relative humidity.*

Fig. 6. *Daily variability of continuous sound levels measured by the **sensor node 2** - building in a side road: top) A-weighted levels; bottom) difference between C-weighted and A-weighted levels. (Night times are shaded, and weekends and holidays are plotted with dashed lines.)*

(Fig. 5), report disturbance from night pass-bys of fast and loud motorcycles and cars. What is more, the passing trucks also often produce tire whistling noise and, due to the exit from the underpass, loud rattling noise and vibrations coming from their bulk cargo.

Hence, in order to better evaluate the soundscape of the place and to relate it to people's perception, more detailed models need to be used. Thus, soundscape monitoring system was established for long-term monitoring which includes continuous recording of sound and vibration signals. Hence, in addition to the sensor nodes that gather the data, the server infrastructure was created to continuously acquire and evaluate the obtained measurements. Therefore, for the purpose of extracting information from the data, already published and available statistical, computational and machine learning models (e.g. [12–14]) for detection and labeling of the salient, i.e. noticeable events will be evaluated in the next phase of the project.

3. MEASURING PERCEPTION USING MOBILE APPLICATION

Another part of the soundscape monitoring system is the mobile application implemented for the Android operating system (Fig. 7). The mobile app is used to acquire the in-situ and (almost) immediate reactions to the sound and vibration events. The use of the app is twofold: the participants can label the sound and vibration events which they notice as well as assess the events which are measured by the sensor nodes.

The application will be used by the participants taking part in the case study. Each participant will give their informed consent prior to using the application. Participants will also be given unique registration keys for logging into the application. To protect their privacy, the keys will not be linked to their personal information but rather generated randomly and handled by the research team.

The app continuously monitors the signal from the server which sends the location and the time of the sound and vibration events detected by the sensors. In case the mobile phone (i.e. the participant) is inside the radius of the sensor node on which an event was detected, the application shows that something had happened (Fig. 7, left). The respondent is then taken to a short series of questions (Fig. 7, right) asking about their: noticing of the event, event characterization (intensity, pleasantness and source category) and evoked emotions (anxiety and disturbance from the event). The results of each questionnaire are then sent to a protected local database. Using the same procedure, the participants have the opportunity to initiate the questionnaire themselves thus reporting the event they had noticed.

To motivate the participants to provide their answers, the mobile application has been implemented with the gamification and social involvement processes in mind. Specifically, during the login process each user selects a non-profit association to which their answers are assigned to. Each time an answer is stored, a number of points is given to the selected association.
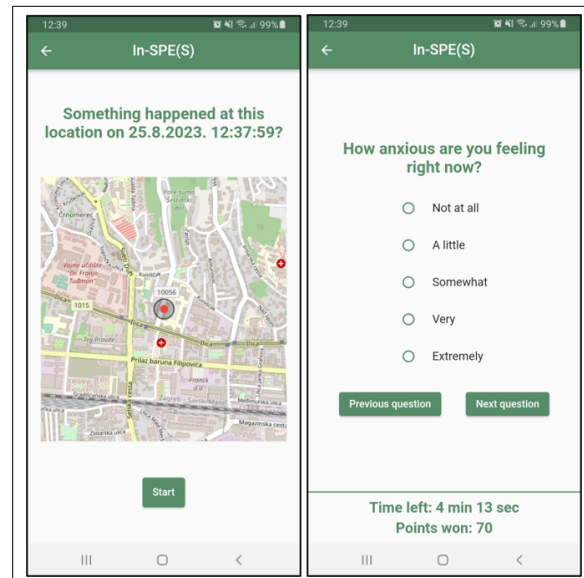

Fig. 7. Screenshots of the Android app: left) initial screen for starting up the questionnaire; right) question on self-reported anxiety level.

Participants will be notified that, at the end of the project, the assigned budget will be split proportionally between the associations based on the points collected by the participants. Another gamification characteristic of the app is the timer that counts down the time until the questionnaire for a particular event is active. This motivates the participant to answer and gather points relatively quickly and ensures that the information given is related to the event in question.

4. CONCLUSIONS

In this contribution, we have presented an overview of the soundscape monitoring system that is being established and used in project In-SPE(S). The system will enable long term monitoring and evaluation of soundscape in Zagreb area which was affected by the earthquakes.

Currently, the work on the statistical models for prediction of noticeable events is ongoing. The measurements and testing of the system are performed on the campus of the Catholic University of Croatia. In the short term, the participants who will use the mobile application will also be recruited from the student population. This would provide a somewhat controllable setting and enable tuning of the models as well as the whole soundscape monitoring system.

5. ACKNOWLEDGEMENT

6. REFERENCES

[1] Azrin, N. H. **Some effects of noise on human behavior,** Journal of the Experimental Analysis of Behavior, 1(2), 183, 1958.

[2] Schafer, R. M. **The soundscape: Our sonic environment and the tuning of the world.** Simon and Schuster, 1993.

[3] ISO 12913-1: 2014. **Acoustics – Soundscape – Part 1: definition and conceptual framework,** International Organization for Standardization, 2014.

[4] Aletta, F., Kang, J., and Axelsson, Ö. **Soundscape descriptors and a conceptual framework for developing predictive soundscape models,** Landscape and Urban Planning, 149, 65-74, 2016.

[5] Kang, J., Aletta, F., Gjestland, T. T., Brown, L. A., Botteldooren, D., Schulte-Fortkamp, B., Lercher, P., van Kamp, I., Genuit, K., Fiebig, A., Coelho, J. L. B., Maffei, L., and Lavia, L. **Ten questions on the soundscapes of the built environment,** Building and environment, 108, 284-294, 2016.

[6] Filipan, K., Boes, M., De Coensel, B., Lavandier, C., Delaitre, P., Domitrović, H., and Botteldooren, D. **The personal viewpoint on the meaning of tranquility affects the appraisal of the urban park soundscape,** Applied Sciences, 7(1), 91.

[7] Prizmić-Larsen, Z., Vujčić, M. T., and Lipovčan, L. K. **Fear of COVID-19 and Fear of Earthquake: Multiple Distressing Events and Well-Being in Croatia,** Psychological Reports, 00332941231156813, 2023.

[8] Tosi, P., Sbarra, P., and De Rubeis, V. **Earthquake sound perception,** Geophysical research letters, 39(24), 2012.

[9] Van Hauwermeiren, W., David, J., Dekoninck, L., Pessemier, T. D., Joseph, W., Botteldooren, D., Martens, L., Filipan, K., and Coensel, B. D. **Assessing road pavement quality based on opportunistic in-car sound and vibration monitoring,** In 26th International Congress on Sound and Vibration (ICSV 2019), 2019.

[10] Breitinger, F., Zhang, X., and Quick, D. **A forensic analysis of rclone and rclone's prospects for digital forensic investigations of cloud storage,** Forensic Science International: Digital Investigation, 43, 301443, 2022.

[11] Van Hauwermeiren, W., Filipan, K., Botteldooren, D., and De Coensel, B. **A scalable, self-supervised calibration and confounder removal model for opportunistic monitoring of road degradation,** Computer-Aided Civil and Infrastructure Engineering, 37(13), 1703-1720, 2022.

[12] ISO 532-1: 2017. **Acoustics – Methods for calculating loudness – Part 1: Zwicker method,** International Organization for Standardization, 2017.

[13] Sottek, R., and Lobato, T. H. G. **Tonal Component Separation of e-Vehicles Using the High-Resolution Spectral Analysis (HSA),** SAE Technical Paper No. 2023-01-1141, 2023.

[14] Bibbo, G., Singh, A., and Plumbley, M. D. **Audio Tagging on an Embedded Hardware Platform,** arXiv preprint arXiv:2306.09106, 2023.
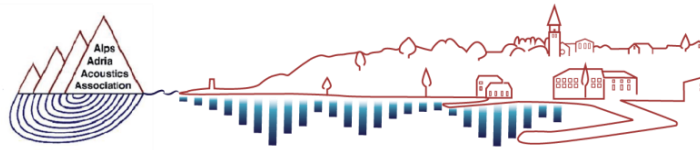
Immission Directivity as a tool for generation of Noise Maps

Jurij Prezelj, Jure Murovec, Anže Železnik, Luka Čurovič

University of Ljubljana, Faculty of mechanical engineering, Aškerčeva 6, 1000 Ljubljana, Slovenia

Abstract: *This research unveils a pioneering method for estimating the sound power level of elements on an emission plane, utilizing a network of immission directivity sensors on a parallel receiving plane, yielding toward measurement-based noise maps. Confronting the challenges of the ill-posed inverse problem in acoustics, we introduce an intuitive algorithm that draws from the statistical analysis of environmental noise source behaviour in the time domain and statistics of their spatial distribution. Assuming the monopole character of environmental noise sources, we employ the basic equation for correlation between sound pressure and sound power above partially absorptive surface. By statistical analysis of the set of the calculated sound powers for each element on the emission plane, we regularize the problem, rendering it well-posed. This heuristic approach, reminiscent of optimization techniques, requires further validation against more extensive experimental dataset.*

Our methodology, grounded in acoustics and signal processing principles, enables development of real-time visualization of the spatial distribution and intensity of industrial noise sources. Remarkably, only a few sensors are necessary to compute a noise source map, or sound power map, which can subsequently be converted into a traditional sound pressure map. This innovative solution addresses a typically unresolved inverse problem in acoustics. Although our preliminary results are limited, they serve as a proof of concept, indicating the potential of this technique in enhancing environmental noise management, bolstering noise control measures, and guiding the design of future industrial sites to mitigate noise impacts.

Keywords: Environmental noise, Noise mapping, Microphone differential array, Immission directivity

1. INTRODUCTION

In Europe, traffic noise pollution, costing over €2.7 billion annually, ranks as the second leading environmental cause of health problems [1-3]. To counteract this, the EU adopted the "Towards Zero Pollution for Air, Water, and Soil" Action Plan as part of the European Green Deal. A core goal of this plan is a 30% reduction in the population chronically disturbed by traffic noise [4]. The methodology we propose addresses this issue by integrating noise monitoring into noise mapping. Leveraging IoT microphone arrays to measure "immission directivity", we can generate advanced noise maps, pinpoint noise sources, and effectively manage noise pollution.

1.1. Problem identification

The current methodology for assessing the impact of noise on people primarily employs noise maps, which are derived from official yearly averages of road, air, and rail traffic data. This approach is designed to ascertain the number of individuals subjected to high levels of noise annoyance, sleep disturbances, and associated health risks. Regrettably, it overlooks the influence of other noise sources like industrial noise from ports, wind power plants, industrial premises, heat pumps, and air conditioners [5,6,7]. Additionally, the diversity of noise types within large ports necessitates their classification into five macro categories - road, railways, ship, port, and

industrial sources [5,6]. Despite their utility, noise maps present several limitations. The precision of these maps in predicting noise levels in shielded or quiet areas is relatively low, and they often fail to encapsulate less predictable sound sources [8]. Further, the propagation models utilized in commercial software packages are grounded in a number of approximations, such as disregarding diffusion through facades and fitting objects, and barely taking into account urban micro-meteorological conditions and vegetation [8]. Current methodologies do not consider the cumulative exposure to multiple noise sources [5,9] or interactions between distinct noise sources, such as the interplay between road traffic and industrial noise, or between natural sound sources and road traffic noise [5,10]. Most significantly, they do not account for fluctuations in noise levels [8,11,2,12,13,14], which can amplify the disturbing effects of noise and play a crucial role in the evaluation of high noise annoyance and sleep disturbances [9,11,12]. While strategic noise maps are an effective tool for identifying critical areas and proposing mitigation plans, they fall short when it comes to assessing spatiotemporal traffic conditions [15]. Thus, there is a compelling need for an innovative, robust methodology that can promptly differentiate among various noise sources and provide insight into their spatiotemporal distribution [12]. A deeper understanding of the primary factors influencing urban noise will guide the formulation of more effective noise control policies [16]. The development of a measurement system compatible with this novel methodology would furnish objective data on noise exposure in urban environments, thereby enabling more accurate assessments of smaller areas of interest over time.

1.2 State of the art in recent studies

Asdrubal et al. [17] provided a review of four promising and emerging research areas for assessing sound environments in urban settings: dynamic noise maps, smart sensors, and smartphones, and the soundscape approach. These areas are not yet fully matured from both a technological and legislative point of view. However, recent technical developments such as the miniaturization of electronic components, accessibility of low-cost computing processors, improved performance of electric batteries, innovations in communication networks, and acoustic signal processing have opened new prospects for the deployment of low-cost sensor networks [8,18]. Low-cost sound recorders are also available to draw a real picture of the sound environment over an extended area at a cost-effective solution [19]. Consequently, many researchers have focused on the development of low-cost sensors over the last fifteen years, ranging from proof-of-concept to the deployment of operational networks [8]. Several projects based on low-cost environmental noise sensor networks have been developed in recent years [20,18,21,22,23,24]. For instance, Alvares-Sanches et al. [25] see an integrated network of static sensors across a city to be the future, while Guillaumea et al. [7] merged noise modelling with measurements from fixed and mobile locations to extract the noise that is not generated by traffic. Benocci et al. [26,27,19] presented an automatic monitoring system based on customized low-cost sensors and a software tool implemented on a general-purpose GIS platform. This system performs the update of noise maps in real-time (dynamic noise maps) on a large urban area by scaling pre-calculated basic noise maps [27]. Balastegui et al. [28,29] demonstrated that mobile sampling could be an option to increase the spatiotemporal coverage of samples to produce a noise map with fewer resources. Furthermore, mounting a noise sensor in a bicycle showed good performance for the case of roads with high traffic [28]. Gajardo et al. [30] showed that a measurement duration of one week would provide sufficient data to estimate a yearly average and assess noise level fluctuations with an overall error of less than 2 dB. Benocci et al. [26] showed that measurements of SPL with low-cost measuring microphones provide a correlation $R2=0.9908$ with measurements of SPL with Class 1 Sound level meters, allowing for a large number of low-cost sensors to be used. Mahapatra et al. [31] showed that an absolute error for source localization of less than 3m can be achieved with six microphones in the network if distances between microphones are 35 m, and the source is also 35 m from the network axis. As a general rule, the lower the cost of the sensor, the more sensors must be used, and the more spatially accurate the data will be [20]. Quintero et al. [29] confirmed that with low-cost hardware, it is possible to generate reliable noise measurements with an equivalent accuracy to a Class 2 sound level meter for LAeq, and with a Type A standard uncertainty very similar to the one observed by the reference equipment. When measuring the sound pressure level (SPL) of a target noise source in an outdoor environment, a single microphone cannot efficiently select a target signal from a mixed sound source. Therefore, a microphone array can be used to enhance the target signal through beamforming, effectively restraining the interference of non-target signals [32]. Okatidiowo et al. [33] designed a beamforming antenna sensor for environmental noise detection to discriminate vehicle emission according to road conditions. Leiba et al. [34] proposed a monitoring system of urban areas based on the use of large

microphone arrays to extract the radiated sound field from each passing-by vehicle in typical urban scenes. They trained a machine learning algorithm to classify these extracted signals into clusters combining both the vehicle type and driving conditions. This system makes it possible to monitor the evolution of the noise levels for each cluster [34].

A review of the literature indicates a pressing need for time-dependent noise mapping derived from measurements. However, the sheer number of measurement locations required for this makes it impractical. Thus, we propose a novel concept for noise mapping that leverages measurements of immission directivity which significantly reduces the number of necessary measurement locations.

2. THEORETICAL BACKGROUND

The methodology we present is rooted in the concept of measuring the Immission Directivity at different locations. This is accomplished by using a network of differential microphone arrays. The idea of using a differential microphone array comes from its capacity to differentiate the direction of incoming sound, by measuring the arrival times of sound to microphones in the array. Thus, the primary function of individual array in the network is to pinpoint the direction of the temporal noise source and to quantify its intensity.

The proposed methodology, which is based on the network of differential microphone arrays, enables gathering measurements in real-time, which allows the system to adapt and react to changes in noise conditions rapidly. This real-time data capture, combined with efficient data management practices, enables us to assemble a comprehensive noise source map. These maps are capable of not only identifying and classifying different noise sources but also tracking their temporal variations. Hence, our methodology offers an effective means to identify, localize, and classify noise sources in real-time, providing a more accurate and comprehensive view of the noise environment in any given area. These noise source maps, updated in real time, are powerful tools that can contribute to more efficient control of noise pollution.

2.1 Immission directivity

Let us assume an emission plane with a finite number of noise sources W_i. These noise sources can be simplified and represented as monopole sources, each emitting an arbitrary wave function. The radiated noise from these sources propagates to a parallel immission plane. Each partial surface of this parallel plane can be regarded as an immission point, $p_{rms,j}$. All the noise sources collectively contribute to the sound level at each immission point, as shown in Fig. 1. Let us assume the distance between the planes h to be relatively small in comparison to the observation area dimensions and falls within the range of $0.5a < h < 2a$, where 'a' is the dimension of the discrete elements on both planes. For simplicity in this paper h, and a will be set to 1 m. Such a simplification is feasible because environmental noise sources (traffic, industrial sites, wind turbines, etc.) are typically distant from the measurement point. As a result, the direction of propagating waves can be considered parallel to the ground.
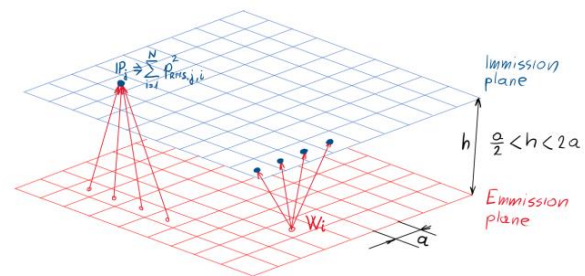
Fig. 1: Emission and Immission plane

Environmental noise sources are uncorrelated, and hence, the sound waves they generate are incoherent. The probability density function of a single monopole source is random and unique. It can be described in terms of the probability of its occurrence, including the conditions for its non-operation, [44]. In many practical cases, our interest lies in determining the location of the dominant noise source, its level, and its contribution to the total noise level. Due to the random statistical properties of environmental noise sources, long time intervals are required for such an assessment. After the equivalent level stabilizes within this time interval of duration τ_0, we can classify the entire acoustic system as stable within the length τ_0 of the measured time interval. Arguably, integrated samples describe the population of noise events and hence, of noise sources.

Let's observe waveforms during an arbitrary time window of duration τ_0. The contribution of all noise sources can be easily summed up at the arbitrary immission point IP_j. The contribution of each source W_i at the selected point is $p_{RMS,j,i}$ and the effective overall sound pressure at IP_j is $p_{RMS,j}$ can be calculated by a simple equation, Eq.1.

$$p_{RMS,j}^2 = \sum_{i=1}^{M} p_{RMS,j,i}^2 \qquad (1)$$

Here, the total effective sound pressure $p_{RMS,j}^2$ at the selected immission Point (IP) is the sum of all M sound waves propagating from all surrounding directions (noise sources on the parallel emission plane) towards the IP (elements on the immission plan). The discretization from the random arrangement of M sources around the immission point in the Cartesian plane (Fig.2, left) can be reconfigured into the radial coordinate system (Fig.2, right). This reconfiguration allows us to define the immission directivity.
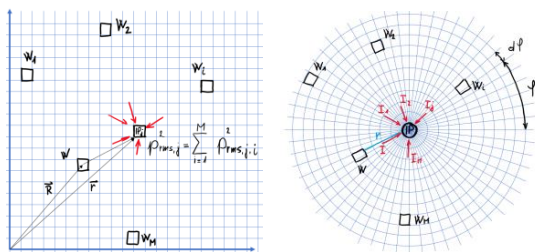
Fig. 2: Superimposed immission plane over the emission planes at height h in cartesian and in radial coordinates. Wi represents sources with sound power W>0 and IP represents selected Immission point.

The sound pressure level at the selected IP_j is a sum of all M sound waves arriving at the IP, as shown in Fig.2 left, and described in Eq.1. Therefore, we can rewrite the equation Eq. 1 for effective sound pressure at the IP for the radial coordinate system and rewrite it in a more general form as the integral of contributions of sound pressure from all directions in the plane. This form is used for the definition of sound immission directivity $p_{RMS}(\varphi)$.

$$p_{RMS}^2 = \sum_{\varphi=0}^{2\pi} p_{RMS,\varphi}^2 \Rightarrow p_{RMS}^2 = \int_0^{2\pi} p_{RMS}^2(\varphi)\, d\varphi \qquad (2)$$

In Figure 3, in the middle, the sound pressure immission plane is shown, parallel to the sound emission plane and uniformly distanced h above it. Two points i.e., the two sound sources can be clearly identified by bright orange colour for higher values of sound pressure, along with how the sound pressure decays with distancing from the source, where the sound level drops by 6 dB per doubling of the distance. The figure 3 also indicates the two immission points (white dots in a circle) and the immission directivity $p_{RMS}(\varphi)$ in these two points, Figure 3 left and right. The result clearly illustrates the ease of determining the location and sound power of two sources from

immission directivity measured on two locations, assuming that noise sources are monopole sources. The challenge arises as to whether it is possible to use the immission directivity in more complex sound fields with more noise sources than there are available immission points, as shown in Figure 4.
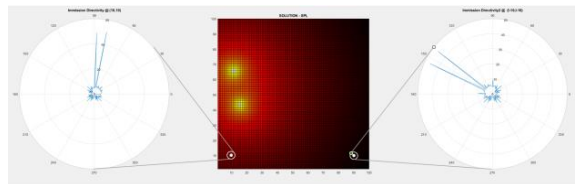
Fig. 3: Simulated Sound pressure on the immission plane and immission directivity at two selected immission points. Two sound sources are located on the emission plane.
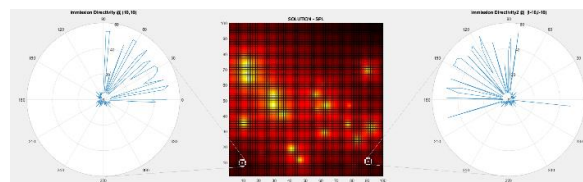
Fig. 4: Simulated sound pressure on the immission plane and immission directivity at two selected immission points. 32 sound sources with random power are randomly distributed on the emission plane.

2.2 Differential microphone array

The process of measuring immission directivity necessitates the use of a microphone array and a beamforming algorithm, tools that aid in localizing sound sources or determining the Direction Of Arrival (DOA) of sound. Differential microphone arrays (DMAs), a distinct subset in sound localization, have emerged as the most appropriate beamforming method for a variety of applications that require speech recognition over the past decade. These applications include hands-free systems, mobile phones, and hearing aids. Circular DMAs have undergone extensive examination for speech and audio applications, primarily due to their adaptability in control, the capacity to establish frequency-invariant directivity patterns, and superior directivity factor [35]. Their inherent benefits include significant beam alignment, frequency independence, and a compact geometrical configuration [36]. Several models have been constructed where all the first-order DMA computations are conducted in the time domain. This approach offers a crucial advantage - the computations exhibit minimal latency. This feature is particularly vital and advantageous

in real-time applications [37-39]. The principle of amalgamating microphone signals from a circular array [43] sparked the development of our unique algorithm [40-42]. This algorithm, designed to compute the DOA, utilizes a simplified method based on timed delay cascading pairs (as depicted in Figure 4 and given by Eq. (3)) to form a DMA. The differential beamforming algorithm based on sub-windowing (SubW-DBA), is developed for this application and is described in our previous work [44]. SubW-DBA has an advantage in that it is not limited to the low-frequency range, at least theoretically. In practice, the low-frequency limit is defined by the phase matching of the microphone pairs. The high-frequency limit depends on the nature of the sound. If the sound is random, there is no frequency limit. If the sound is harmonic, the boundary is at the distance between the microphone pairs, like the usage of sound intensity probes.

The algorithm defined in Eq. (3) was used to compute the instantaneous DOA to experimentally verify the hypothesis that the 2D immission directivity pattern can be obtained by associating the instantaneous total sound level (SPL) with the instantaneous dominant direction (DOA) during sub-windowing. The objective is to compile a collection of immission vectors from which an immission directivity pattern can be derived through consistent integration/averaging of the immission vectors.

$$argmin\, j = \left\| \sum_{i=0}^{D} \left[x_{\text{mic1}}(n) - x_{\text{mic2}}\left(n - \frac{D}{2} + i\right) \right]^2 \right\|_{j=1}^{N} \qquad (3)$$

$x_{\text{mic},1}(n)$ and $x_{\text{mic},2}(n)$ represent in Eq.3 the signals from microphone 1 and microphone 2 respectively. N denotes the number of directions. D_{min} is the number of samples in the observed window. The minimum value of D_{min} is defined by the speed of sound c, the sampling frequency f_s and the distance between two microphones X_{mic}, which determine the time resolution of direction detection. Index i represents the steering value, i.e., Δn, which is proportional to the time delay Δτ.

$$D_{min} = \frac{X_{mic}\, f_s}{c} \qquad (4)$$

For the fastest possible time response of detecting the direction we can set $M = N$.

$$\Delta t_{min} = \frac{D_{min}}{f_s} \qquad (5)$$

Using a differential array with four microphones and a diameter/side length of D_{array} = 0.04 m, it is possible to shorten the length of the direction detection sub-window to $2 \cdot D_{array}/c \approx 0.232$ ms. Shortening the subwindow to 0.232 ms provides 44 signal values for calculating DOA of the dominant sound source. If the signals from two microphones placed 40 mm apart are recorded at a sampling rate of 192 kHz, then 22 samples are needed to arrange the signals for the maximum delay for each direction, and thus the time resolution of detecting the dominant direction is 0.232 ms, [44].
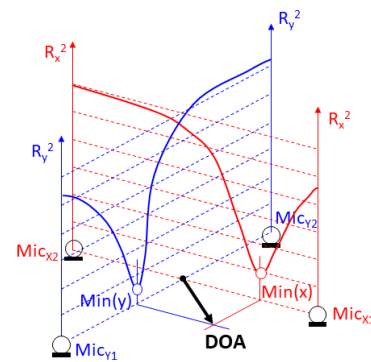
Fig.5: Differential microphone array of the first order, used during the experiment. Two pairs were used for the calculation of DOA on the immission plane, [44].

2.3 Noise source mapping

Noise source mapping or sound source localization, a key procedure in fields such as environmental sciences, telecommunications, and noise control, is defined by its ability to identify and quantify noise sources within a specific domain or structure. The propagation of sound from a noise source to a receiving plane, as well as the relationships between sound power, sound pressure, and distance from the sound source are fundamental to this process.

$$W = \oint pv dS = \oint \frac{p_{RMS}^2}{\rho c} dS \qquad (6)$$

Eq.(6) describes the relationship between sound power W, sound pressure p_{RMS}, and acoustic volume flow through the surface S in a free acoustic field and in the far field of a noise source. By integrating across the surface of a sphere S, we derive Eq.(7) for sound power, which highlights the link between sound power W and sound pressure p_{RMS} at a distance r.

$$W = p_{RMS}^2 \frac{2\pi r^2}{\rho\, c_0} \tag{7}$$

In the scenario where a monopole source is positioned on a plane with an absorption coefficient α, only a portion of the sound source energy radiates into a hemisphere. Eq.(8) describes how to calculate the amplitude of sound pressure p_{RMS} at a distance r from a sound source with power W on the emission plane with absorption coefficient α. This equation assumes that each element on the sound source plane is a monopole source on a partially absorbing surface.

$$p_{RMS}^2 = \left(\frac{\rho\, c_0}{2(1+\alpha)\pi r^2} \right) W \tag{8}$$

The receiving plane is of the same dimension as the transmitting plane, denoted as M x N. Every element on the immission plane is hit by a sound wave emitted from all the constituent elements on the emitting plane, each of which represent the noise source as monopoles. In this scenario, those elements on the sound emitting plane closer to an element on the receiving plane contribute more significantly than the distant elements. This relationship can be represented by Eq.9 in which $\vec{r}$ epresents the vector the receiving element and $\vec{R}$ signifies the vector to the sound source. The structure of this equation bears similarity to the Rayleigh integral used in vibroacoustics. Furthermore, the Eq.9 can be reformulated in discrete domain given by Eq.10, in which r_{ij} represents the radius to the point on the receiving plane and R_{mn} signifies the radius to the point on the transmitting plane, as depicted in Fig. 2.

$$p_{RMS}^2(r) = \frac{\rho\, c_0}{2(1+\alpha)\pi} \iint_{x,y} \frac{W}{|\vec{R}-\vec{r}|^2} dx dy \tag{9}$$

$$p_{RMS,ij}^2 = \sum_{m=1}^{M} \sum_{n=1}^{N} \frac{\rho\, c_0}{2(1+\alpha)\pi} \frac{W_{m,n}}{R_{m,n}^2 - r_{i,j}^2} \tag{10}$$

Equation can be rewritten in the matrix form:

$$\vec{p} = ATM \cdot \vec{W} \tag{11}$$

Where components of the vector $\vec{p}$ represent all elements $p_{RMS,j}^2$ on the receiving plane and $\vec{W}$ all sound sources elements W_i on the sound emitting plane. Both vectors have dimension M·N. **ATM** is an Acoustic Transfer Matrix with dimensions M·N x M·N and is defined in Eq. (12) by

where indices m and n run along the source plane and indices i,j along the receiving plane.

$$ATM = \frac{\rho\, c_0}{2(1+\alpha)\pi \left| R_{mn} - r_{ij} \right|^2} \tag{12}$$

If the sound pressure $\vec{p}$ on the receiving plane and the geometry of the source plane is well defined, then a vector $\vec{W}$ and hence the noise source maps can be calculated backward from Eq. (13) using the inverse of the Acoustic Transfer Matrix (ATM).

$$\vec{W} = ATM^{-1} \cdot \vec{p} \tag{13}$$

However, the practicality of this approach is limited as it demands a large number of measurements across the entire receiving plane. To circumvent this limitation, immission directivity measurements can be employed. The construction of a comprehensive sound source map necessitates the acquisition of an ample amount of data. Under ideal conditions, the measurement of sound pressure at a select few immission points can provide sufficient data for theoretical models, as depicted in Fig. 3. However, in real-world scenarios, as illustrated in Fig. 4, the construction of an accurate noise map requires the extraction of substantially more information from the measurements.

Immission directivity measurements provide sufficient information about the sound field in a specific location, thereby facilitating the creation of a sound source map. The formulation of immission directivity, as defined in Eq. 2, can be extended further. The contributions of all sound sources at various distances and at angle φ need to be integrated as per Eq. 14. Here, $W(\varphi,r)$ represents the spatial distribution of sound power along the radius r from the immission point at angle φ, demonstrated on the right of Fig. 6.

$$p_{RMS}^2(\varphi) = \frac{\rho\, c_0}{2(1+\alpha)\pi} \int_{r=r0}^{\infty} \frac{W(\varphi,r)}{r^2}\, dr \tag{14}$$

$$p_{RMS}^2(\varphi) = \frac{\rho\, c_0}{2(1+\alpha)\pi} \sum_{r=r0}^{Rmax} \frac{W(\varphi,r)}{r^2} \tag{15}$$

If the function $W(\varphi,r)$ was known, we could directly perform noise source mapping from it. However, in most instances, this function remains elusive. Nevertheless, we possess knowledge of its integral value, defined within Eq. 14 i.e., Eq.15 in terms of the contribution of sound pressure from the direction φ. Leveraging this

information, we can scrutinize a typical scenario of spatial distribution of environmental noise sources (denoted by red squares) and emission point, as shown on Fig. 6 above.
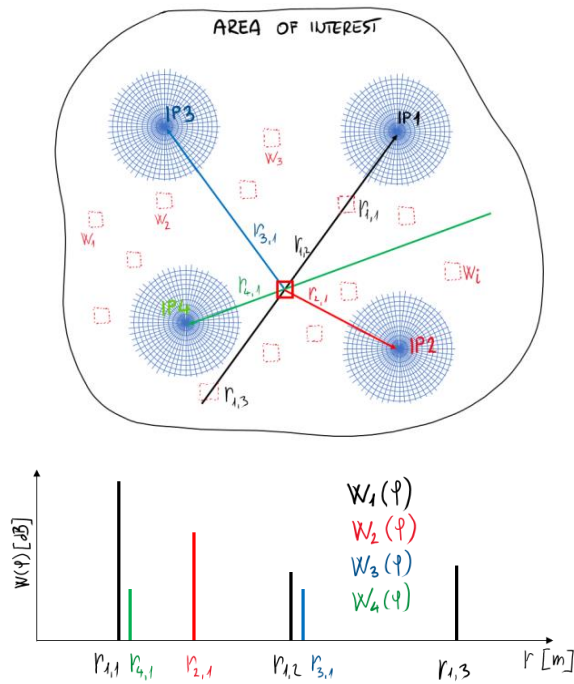

Fig.6: Typical Environmental Noise Source Configuration and Measurement Locations of Immission Directivity Depicted are the noise sources (represented by squares), along with the points IP of immission directivity measurements (above), and a plot of sound power along the radius at selected angles, extending from the (IP_j) (below).

Observing a single source W (represented by the black square), we perceive other sound sources (red squares) as parasitic. On the right of Fig. 6, the functions $W(\varphi,r)$ for four distinct immission locations are illustrated, through which we ascertain the sound power of the source W. Upon analysing these functions, it is evident that there is always a probability of encountering multiple parasitic sound sources for any chosen direction of immission, as illustrated in the function $W(\varphi_1, r)$ for IP1, denoted with black curve. However, the likelihood of encountering several parasitic sound sources across all functions; $W(\varphi_1, r)$, $W(\varphi_2, r)$, $W(\varphi_3, r)$, and $W(\varphi_4, r)$, aimed at determining the sound source W is exceedingly small. Because function is discrete, with only one peak, its integral value can be simply attributed to the elements on the emitting plane with the distance r, as given by Eq.16.

$$W(\varphi,r) = p_{RMS}^2(\varphi)\frac{2(1+\alpha)\pi}{\rho\,c_0}r^2 \qquad (16)$$

It follows that we can write a vector $\overrightarrow{W}$ with the dimension equal to the number of immission points with components $\overrightarrow{W}$= [W (φ_1, r), W (φ_2, r), …. W (φ_N, r)]. A simple statistical analysis can be performed on the components of the vector and the true sound power value for the observed sound source W can be extracted from it. During the measurement phase, we can also establish the lower limit of integration r_0 by estimating the distance to the nearest real noise source, allowing for further improvement of noise source mapping.

3. EXPERIMENTAL RESULTS

To conduct immission directivity measurements, we employed a differential microphone antenna (DMA) equipped with four measurement microphones. The digitization of each signal was performed at a sampling rate of 192 kHz with a 24-bit resolution. Prior to experimentation, the microphones underwent calibration and phase compensation. Signal acquisition was facilitated by LabView software, which enables the real-time determination of the Direction of Arrival (DOA) at 50-millisecond intervals. The immission directivity was derived through the process of energy averaging over a ten-minute duration at each immission point.
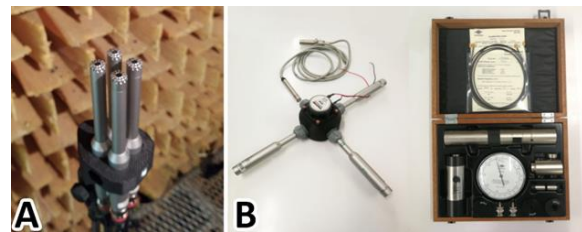
Fig. 7: A) Prototype system using DMA with square geometry and B) System for microphone calibration and phase matching.

The experiments were carried out under real-world conditions at four distinct locations:
- Industrial premises containing a carpentry.
- Surrounding of a busy traffic junction
- Industrial premises of oxygen plant in Kranj
- Industrial premises of Sandmilll Kresnice

These varied locations were selected to provide a diverse range of environmental conditions and sound sources.

3.1 Noise mapping of industrial premises - Carpentry

Our inaugural measurement set was conducted in the vicinity of Ovsenik Carpentry in Britof, henceforth referred to as 'the carpentry.' The primary noise contributors in this locale are the woodworking machinery in the yard and the workshop's ventilation system. We conducted immission directivity measurements at nine points (IP1-IP9) encircling the entire complex.

Several factors affected the clarity of the results at some locations, notably IP4 and IP5. The carpentry's surroundings comprise fields and forests, contributing ambient noise from tree felling and agricultural machinery operation. Furthermore, a nearby highway intermittently added to the ambient noise during relatively quiet periods. In the measurements at IP1, the primary noise source at 225° and 81 dB was evidently the ventilation system. Immission directionality measured at IP2 continued to show the ventilation system as the dominant noise source, although the peak was less distinct. Noise contributions from the neighbouring farm and the carpentry's machinery were also included. For IP3, the ventilation system noise again dominated at 162° and 77 dB. However, the workshop's yard machinery noise was not detected due to obstruction by a building. The measurement at IP4 differed significantly from previous readings. Here, the dominant noise source was not as noticeable, with the largest contribution coming from the carpentry yard at 108° and 75 dB. However, noise from forest sawing and nearby tractors was also perceptible. At IP5, multiple noise sources ranging from 45° to 200° were observed, originating from the carpentry yard's machinery. However, the dominant noise source was a stationary truck at 300° and 76 dB. Although we initially anticipated the machinery to be noisier than the truck, a yard fence interfered with the readings. The IP6 measurement introduced a new ventilation system, the dominant noise source at 108° and 81 dB. Other significant noise contributors were work in a nearby field (354°, 66 dB), a stationary truck (24°), and forest sawing (60°). At IP7, despite our initial expectation of prevailing noise from tractor work in nearby fields due to our increased distance from the carpentry, the yard work noise still dominated. The leading source was recorded at 84° with significant amplitude. For IP8, as expected, the workshop's ventilation system was the dominant noise source, discernible at 114° with an amplitude of 74 dB. The IP9 measurements were unclear, although the conditions were like the first measurement. Despite our expectations, the maximum amplitude measured was at 60° and 66 dB, which was less evident from the graph.

In summary, The ventilation system always emerged as the dominant noise source, with other contributors being a neighbouring workshop, a stationary truck, and agricultural activity. Although several measurements did not align with our initial expectations due to unforeseen noise sources, the collected data were adequate to identify and spatially determine the dominant noise sources at the carpentry.
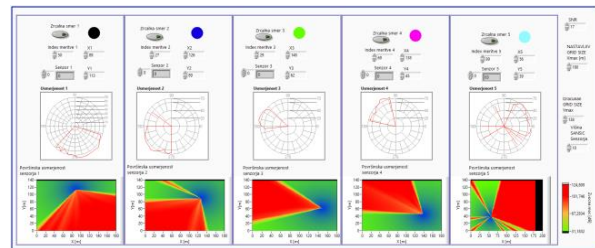
Fig. 8: Measurement results of immission directivity at locations IP1, IP3, IP4, IP 5 and IP9, around the carpentry with coordinates on the map and synthesized individual sound power maps predicted for each measurement location.
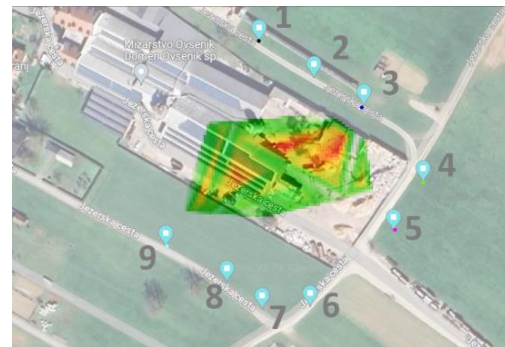

Fig.9: Combined Sound power map of the carpentry, synthesized from 5 sound power maps, for locations IP1, IP3, IP4, IP 5 and IP9

3.2 Noise mapping of traffic junction

Our objective was to assess noise pollution originating from traffic, one of the key noise producers in an urban environment. Unlike our previous location, where stationary sources like a ventilation system predominated, we anticipated fewer distinct peaks here due to the transient nature of vehicles. The junction, situated near the Brnik airport, facilitated a heavy flow of both cars and trucks, given the presence of several warehouses in the vicinity. We conducted nine measurements in parallel with the two main road encompassing the junction.

The results of the immission directivity measurement at IP 1, with an average amplitude of 71 dB, were directed towards the road, as predicted. There were no extraneous noise sources apart from vehicular traffic, providing an accurate representation of the noise immission. Similarly, IP2 measurements also pointed towards the road with a maximum amplitude of 81 dB. The primary noise source at IP 5 was the intersection, aligning with our expectations due to our proximity to the junction. There was some additional noise from the road diverging from the intersection, but the average noise level exceeded 70 dB, as expected. However, the measurements at IP 7 and IP 4 were affected by background noise from agricultural work, but if we disregard this, the maximum amplitudes facing the road were 75 dB and 74 dB respectively.

Comparing the maxima of the individual measurements illustrated that the noise originated predominantly from the traffic or the intersection. The loudest noises were detected before the intersection or road junctions, likely resulting from vehicular braking. Given the heavy traffic, vehicles were frequently stationary near our measurement sites. These stationary, constant noise sources often dominated our ambient noise measurements.
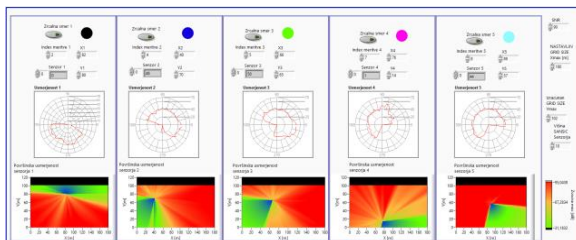
Fig. 10: Measurement results of immission directivity with coordinates on the map and synthesized individual sound power maps predicted for each measurement location.
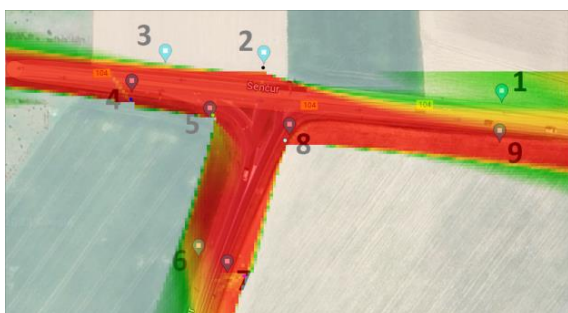
Fig.11: Combined Sound power map synthesized from 5 sound power maps, generated from measurements of immission directivity at IP2, IP4, IP5, IP7 and IP8

3.3 Noise mapping of industrial premises - oxygen plant

Our third test location featured two constant noise sources - the Škofja Loka oxygen plant and the adjacent Urbanscape factory. While our focus was primarily on the oxygen plant, measurements 1, 2, and 8 incidentally included noise from the nearby factory. It's worth noting that measurements 1, 2, and 3 recorded the sound of a passing train, though these results could be disregarded as irrelevant to our study. The auditory influence of the train was evident up to the 5th measurement.
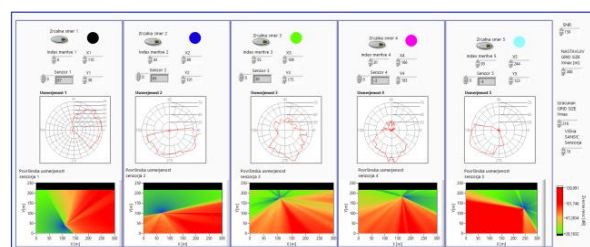
Fig. 12: Measured of immission directivity at IP 1, IP2, IP4, IP5, and IP7, with coresponding sound power maps predicted for each measurement location.
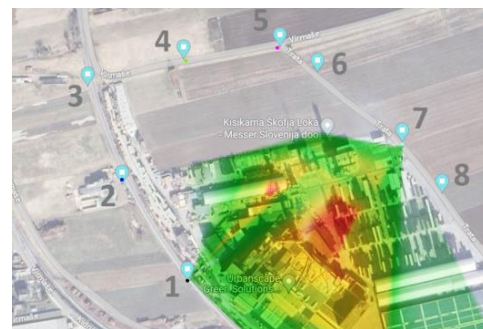
Fig.13: Combined Sound power map synthesized from 5 sound power maps IP1, IP2, IP4, IP5, and IP7

3.3 Noise mapping of industrial premises - Sand mill Kresnice

Our fourth site, situated at Kresnice, was characterized by the noise generated from a sand mill, with the objective of observing its noise propagation at various points. This location presented additional sources of noise which included a railway station with frequently passing trains, a bustling road across the river, and heavy machinery operating adjacent to the mill in the sand pit. As a result, apart from the main source (the sand mill), we also measured three ancillary noise sources. However, it should be noted that a calibration issue with the microphones affected the measurement of accurate

pressure level values. This calibration discrepancy did not impact the directivity measurements.
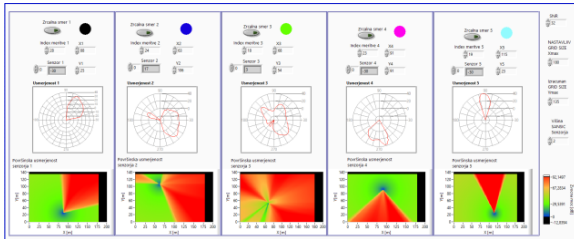

Fig. 14: Measurement results of immission directivity around sand mill Kresnice, at IP2, IP4, IP5, IP6 and IP 7, with coordinates on the map and synthesized individual sound power maps predicted for each IP location.
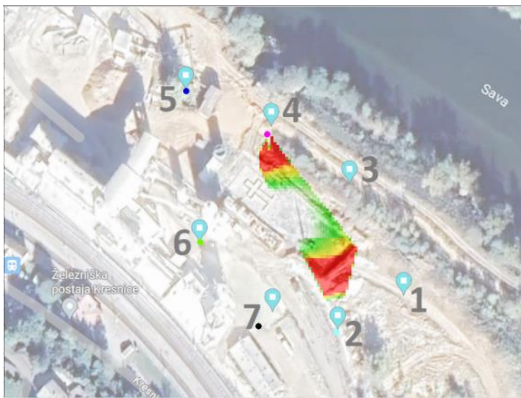

Fig.15: Combined Sound power map synthesized from 5 sound power maps, generated from immission directivities at IP2, IP4, IP5, IP6 and IP 7.

3. CONCLUSION

Through a series of systematic and varied measurements at four distinct locations, this study has validated the feasibility of calculating noise source maps from immission directivity measurements. By characterizing different noise sources, such as industrial machinery, traffic at busy junctions, and stationary equipment, we have been able to gather comprehensive data that allow us to understand noise propagation and develop a visual representation of these noise sources.

Each location presented unique noise sources, and despite certain challenges such as unexpected sources and calibration issues, we were able to effectively capture the necessary data and achieve our objectives. Through meticulous analysis of this data, we were able to interpret the immission directivity measurements and thereby generate accurate noise source maps.

This achievement has significant implications for the field of acoustical engineering and environmental noise management. It paves the way for more efficient noise monitoring and control, aiding urban planning, industrial site management, and other areas where noise impact is a critical factor. Further, it validates the effectiveness of utilizing immission directivity measurements as a method for noise source identification and mapping.

Presented proof of concept presents the next step in the modelling of noise maps, where it is no longer just an extrapolation of measurements with the help of models, but purely based on the measurement methods itself (DOA, immission directivity, etc.)

Going forward, the demonstrated concept could be further refined, and its accuracy improved with enhanced calibration of measuring equipment. Additional studies could explore different types of noise sources, expanding the breadth of applicability of this methodology. Ultimately, the success of this proof of concept lays a strong foundation for further research and application in the realm of noise mapping based on immission directivity measurements.

4. REFERENCES

[1] Environmental noise guidelines for the European region: WHO, Regional office Europe, 2018
[2] Assessment of potential health benefits of noise abatement measures in the EU, The Phenomena project, Contract number 07.0203/2019/ETU/815591/ENV.A.3, March 2021.
[3] Environmental noise in Europe — 2020, EEA Report No 22/2019
[4] Towards a Zero Pollution for Air, Water and Soil, the European Commission
[5] Luca Fredianelli, et.al, Source characterization guidelines for noise mapping of port areas, Heliyon, Vol. 8, (2022), pp. e09021
[6] Luca Fredianelli, et al., Classification of Noise Sources for Port Area Noise Mapping, Environments, Vol. 8(12), (2021), https://doi.org/10.3390/environments8020012
[7] Gwenaël Guillaumea, Pierre Aumond, Pierre Chobeau, Arnaud Can, Statistical study of the relationships between mobile and fixed stations measurements in urban environment, Building and Environment, Vol. 149, (2019), pp.404–414
[8] Judicaël Picaut, Arnaud Can, Nicolas Fortin, Jeremy Ardouin, Mathieu Lagrange. Low-Cost Sensors for Urban Noise Monitoring Networks-A Literature Review. Sensors, Vol.20 (8), (2020), pp. 10.3390

[9] Catherine Lavandier, et al., Influence of road traffic noise peaks on reading task performance and disturbance in a laboratory context, Acta Acustica (2022), Vol.6(3) Available online at: https://doi.org/10.1051/aacus/2021057

[10] Pierre Aumond, Léo Jacquesson, Arnaud Can, Probabilistic modeling framework for multisource sound mapping, Applied Acoustics, Vol. 139, (2018), pp.34–43

[11] Weigang Wei, Timothy Van Renterghem, Bert De Coensel, Dick Botteldooren, Dynamic noise mapping: A map-based interpolation between noise measurements with high temporal resolution, Applied Acoustics, Vol. 101, (2016), pp. 127–140

[12] Ziqin Lan, Canming He, Ming Cai, Urban Road traffic noise spatiotemporal distribution mapping using multisource data, Transportation Research Part D, Vol. 82, (2020), pp.102323

[13] Weijun Yang, Jinying He, Canming He, Ming Cai, Evaluation of urban traffic noise pollution based on noise maps, Transportation Research Part D, Vol. 87, (2020), pp.102516

[14] B. Doohan, et.al, The sound of management: Acoustic monitoring for agricultural industries, Ecological Indicators, Vol. 96, (2019), pp.739-746

[15] Sacha Baclet, et al., From strategic noise maps to receiver-centric noise exposure sensitivity mapping, Transportation Research Part D, Vol. 102, (2022), pp.103114

[16] Xueyi Xu, et al., Application of land use regression to map environmental noise in Shanghai, China, Environment International, Vol. 161, (2022), pp.107111

[17] Francesco Asdrubali, Francesco D'Alessandro, Innovative Approaches for Noise Management in Smart Cities: a Review, Current Pollution Reports, Vol. 4, (2018), pp.143–153

[18] Alías, F.; Alsina-Pagès, R.M. Review of Wireless Acoustic Sensor Networks for Environmental Noise Monitoring in Smart Cities, Journal of Sensors, Vol. 2019,(2019), pp.7634860

[19] Roberto Benocci, et al., Mapping of the Acoustic Environment at an Urban Park in the City Area of Milan, Italy, Using Very Low-Cost Sensors, Sensors, Vol. 22, (2022), pp. 3528

[20] Juan Manuel López, et al., A Digital Signal Processor Based Acoustic Sensor for Outdoor Noise Monitoring in Smart Cities, Sensors, Vol. 20, (2020), pp.605

[21] Mydlarz, C.; Salamon, J.; Bello, J.P. The implementation of low-cost urban acoustic monitoring devices, Applied Acoustics, Vol. 117, (2017), pp. 207–218. [CrossRef]

[22] Maijala, P.; Zhao, S.; Heittola, T.; Virtanen, T. Environmental noise monitoring using source classification in sensors, Applied Acoustics, Vol.129, (2018), pp.129, 258–267

[23] Sevillano, X, et al. DYNAMAP—Development of low cost sensors networks for real time noise mapping. Noise Mapping, Vol.3, (2016), pp. 172–189

[24] Peckens, C.; Porter, C.; Rink, T. Wireless sensor networks for Log-term Monitoring of Urban Noise., Sensors (2018), Vol.18, pp.3161

[25] Tatiana Alvares-Sanches, Patrick E. Osborne, Paul R. White, Mobile surveys and machine learning can improve urban noise mapping: Beyond A-weighted measurements of exposure, Science of the Total Environment, Vol. 775, (2021), pp.145600

[26] Roberto Benocci, et al., Accuracy of the Dynamic Acoustic Map in a Large City Generated by Fixed Monitoring Units, Sensors, Vol.20, (2020), pp. 412

[27] Roberto Benocci, et al., Optimized Sensors Network and Dynamical Maps for Monitoring Traffic Noise in a Large Urban Zone, Appl. Sci., Vol. 11, (2021), pp. 8363

[28] G. Quintero, Balastegui, J. Romeu, Traffic noise assessment based on mobile measurements, Environmental Impact Assessment Review, Vol. 86, (2021), pp.106488

[29] G. Quintero, Balastegui, J. Romeu, A low-cost noise measurement device for noise mapping based on mobile sampling, Measurement, Vol. 148, (2019), pp.106894

[30] Carlos Prieto Gajardo, Juan Miguel Barrigón Morillas, Guillermo Rey Gozalo, et al., Can weekly noise levels of urban road traffic, as predominant noise source, estimate annual ones?, The Journal of the Acoustical Society of America 140, 3702 (2016); doi: 10.1121/1.4966678

[31] Chinmayi Mahapatra, A.R. Mohanty, Optimization of number of microphones and microphone spacing using time delay based multilateration approach for explosive sound source localization, Applied Acoustics, Vol. 198, (2022), pp.108998

[32] Yong Chen, Ming Wua, Ling Lu, Xing Fang, Jun Yang, Sound pressure level real-time monitoring of outdoor directional noise, Applied Acoustics, Vol. 202, (2023), pp. 109141

[33] John P. Djungha Okitadiowo, A. Lay-Ekuakille, T. Isernia, A. Massaro, Design of a beamforming antenna sensor for environmental noise detection to discriminate vehicle emission according to road conditions, Measurement: Sensors, Vol. 23, (2022), pp.100389

[34] Raphaël Leiba, et al., Acoustical Classification of the Urban Road Traffic with Large Arrays of Microphones, Acta Acustica united with Acustica, Vol. 105. (2019), pp.1067 – 1077

[35] Gongping Huang, Jacob Benesty and Jingdong Chen, Design of robust concentric circular differential microphone arrays, The Journal of the Acoustical Society of America 141, 3236 (2017); https://doi.org/10.1121/1.4983122

[36] Buchris, Y., I. Cohen, and J. Benesty. Analysis and design of time-domain first-order circular differential microphone arrays. The 22nd International Congress on Acoustics (ICA). 2016.

[37] Benesty, Jacob, and Chen Jingdong. Study and design of differential microphone arrays. Vol. 6. Springer Science & Business Media, 2012.

[38] Buchris, Yaakov, Israel Cohen, and Jacob Benesty. First-order differential microphone arrays from a time-domain broadband perspective. 2016 IEEE international workshop on acoustic signal enhancement (IWAENC). IEEE, 2016.

[39] Buchris, Yaakov, Israel Cohen, and Jacob Benesty. On the design of time-domain differential microphone arrays. Applied Acoustics 148 (2019): 212–222.

[41] Salom Iva, Čelebič Vladimir, Todorović Dejan and Prezelj Jurij, An Implementation of Beamforming Algorithm on FPGA Platform with Digital Microphone Array, 138th AES Convention, 2015, Warsaw, Poland, Paper 9335.

[42] Todorović Dejan, Salom Iva, Čelebić Vladimir, and Prezelj Jurij, Implementation and Application of FPGA Platform with Digital MEMS Microphone Array, Proceedings of 4th International Conference on Electrical, Electronics and Computing Engineering, IcETRAN 2017, Kladovo, Serbia, June 05-08, ISBN 978-86-7466-692-0.

[40] Murovec, J., Curovic, L., Novakovic, T., & Prezelj, J., Environmental noise event classification based on self-organizing map using psychoacoustic features and spatial filtering. Universitätsbibliothek der RWTH Aachen, 2019.

[43] Huang, Gongping, Jacob Benesty, and Jingdong Chen. Design of robust concentric circular differential microphone arrays. The Journal of the Acoustical Society of America 141.5 (2017): 3236–3249.

[44] J Prezelj, L Čurovič, T Novakovič, J Murovec, A novel approach to localization of environmental noise sources: Sub-windowing for time domain beamforming, Applied Acoustics, Vol.195, (2022), pp.108836
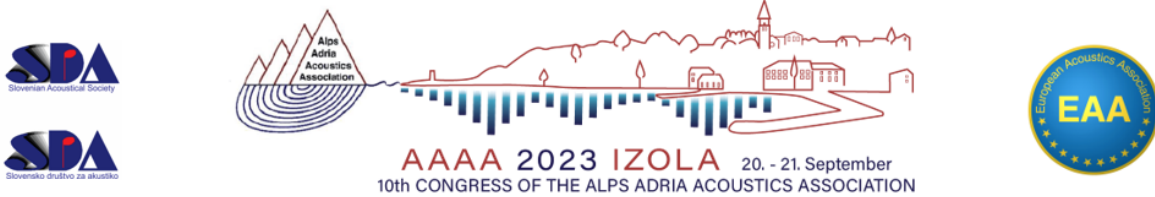
DATA SELECTION FOR REDUCED TRAINING EFFORT IN VANDALISM SOUND EVENT DETECTION

Stefan Grebien[1], Florian Krebs[1], Ferdinand Fuhrmann[1], Michael Hubner[2], Stephan Veigl[2], Franz Graf[1]

[1] **Joanneum Research, Intelligent Acoustic Solutions, Austria**
[2] **AIT Austrian Institute of Technology GmbH, Center for Digital Safety & Security, Austria**

Abstract:

Typical sound event detection (SED) applications, employed in real environments, generate huge amounts of unlabeled data each day. These data can potentially be used to re-train the underlying machine learning models. However, as the labeling budget is usually restricted, active learning plays a vital role in re-training. Especially for applications with sparse event occurrence, a data selection process is paramount. In this paper we (i) introduce a novel application for vandalism SED, and (ii) analyze an active learning scheme for reduced training and annotation effort.

In the presented system, the employed machine learning classifier shall recognize various acts of vandalism, i.e., glass breakage and graffiti spraying. To this end, we utilize embeddings generated with a pre-trained network and train a recurrent neural network for event detection. The applied data selection strategy is based on a mismatch-first, farthest-traversal approach and is compared to an upper bound by using all available data. Furthermore, results for the active learning scheme are evaluated with respect to different labeling budgets and compared to an active learning scheme with a random sampling scheme.

Keywords: *sound event detection, active learning, dataset selection, vandalism*

1. INTRODUCTION

Vandalism, the deliberate defacement or destruction of infrastructure, is a growing challenge to the public and causes economic damage due to the increased maintenance costs. Therefore, there is a growing demand for systems that are able to detect acts of vandalism in real time in order to facilitate immediate responses. Among these systems, acoustic monitoring emerges as a promising avenue, offering a non-intrusive means to detect and characterize acts of vandalism in various settings. Acoustic systems have therefore been proposed to detect events related to vandalism such as shouting [1], kicking-objects [2], screaming [2] and glass breaking [3].

At the core of these acoustic monitoring systems lie classifiers, typically trained on annotated datasets encompassing recordings of both target and background events. These datasets should, in the ideal case, contain a representative collection of acoustic events, that will occur within the environment of the deployed system. Nevertheless, in practical terms, the acoustic environment of the deployed system is often unknown during development and undergoes changes over time due to external factors like weather, seasons, temporal construction site noise, or other influences. Therefore, it is important to update datasets and classifiers regularly in order to react to these changes and adapt the system to local conditions. This can be implemented by periodically storing sound segments, selecting the most relevant ones, and annotating them in order to re-train the model. However, the selection and annotation process is tedious if performed manually. To this end, *active learning* offers ways to decrease the amount of human labelling effort.

While there exist several active learning approaches for image processing tasks [4–6], the literature is rather sparse for audio event detection. One of the few examples is an uncertainty-based selection strategy for a noise detection problem [7]. Another one is mismatch-first-farthest-traversal (MFFT) [8], a data selection method which iteratively samples new data from misclassified segments. At the same time, diversity between data items is enforced by maximizing the distance between currently and previously sampled data items. And most recently, Shishkin et al. [9] used pretrained embeddings and trained the last layer with Monte Carlo dropout to identify samples with high uncertainty. Again, samples with high uncertainty were selected first. However, as each approach was validated using a different dataset, it is still unclear which data selection strategy works best for a given application.

Therefore, this paper aims to provide the following contributions: (i) We propose a new system for acoustic vandalism detection which recognizes the sounds of glass-breaking, spraying, and shaking a graffiti can. (ii) We apply and analyze MFFT on both synthetic and real-world datasets in order to select the most relevant datapoints for training the vandalism detector. With these contributions, this work aims to take another step towards a practical applicability of active learning methods for SED systems.
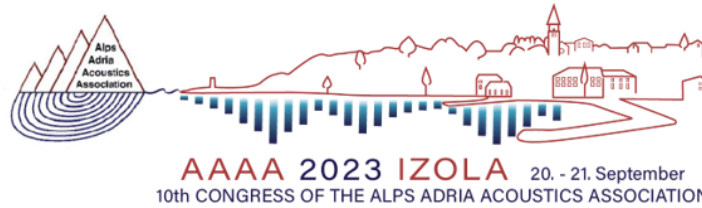
2. PROPOSED SYSTEM

The proposed system closely follows the active learning scheme presented in [8]. The input are unlabeled recordings and the output is a classifier for SED. At the beginning of the iterative active learning scheme, a subset of the data is selected to train an SED classifier. In the subsequent iterations, the trained SED classifier is utilized by the data selection process to generate the next training subset. In the following subsections we will present an overview of the system and highlight the differences to [8].

2.1 Data pre-processing

As suggested by Shuyang et al. [8], the system utilizes a pre-trained network to generate embeddings. This network follows the architecture in [10], the training material and validation criterion generally follows [11] and the trained embedding network is available online [12]. The input to the embedding network are log-mel spectrograms with 128 mel-bands, produced from raw audio recordings with a sampling frequency of $44.1\,\mathrm{kHz}$, a hop-size of 882 samples and a frame-size of 1764 samples. The embedding network produces an output of 256 embeddings at an output rate of $50\,\mathrm{Hz}$.

In order to split the files into shorter, homogeneous segments, each file is fed into a change point detection module, where change points are inferred from the peaks of a change function. This change function is computed for each time frame by the cosine distance of the mean over the K past embeddings and the mean over the K future embeddings, where K is set in such a way that $2K$ corresponds to $1\,\mathrm{sec}$. While [8] uses full recordings as input to the change point detection module, our system splits the raw audio recordings first in $10\,\mathrm{sec}$ long segments. [1] The change point module returns shorter segments with a minimum length of $1\,\mathrm{sec}$ which are used as input for the data-selection scheme in the active learning process.

2.2 Active learning scheme

The data selection process uses MFFT to choose a subset of the preprocessed segments, also called samples. MFFT utilizes two techniques for sample selection:

1. Mismatch first: After the first iteration, i.e., as soon as a trained classifier is available, the unlabeled samples are evaluated with the model to generate *model-predicted* labels. Furthermore, *model-propagated* labels are calculated using a nearest-neighbor classifier, i.e., the label of a unlabeled segment is predicted by finding the smallest cosine distance between the means of the embeddings of the labeled and unlabeled data. Then, the set of unlabeled samples is ordered according to the mismatch

---

[1] This is necessary, as we do not only use synthetic data, where all the recordings have the same length, e.g., data from the *TUT Rare Sound Events 2017* [13], but also real-world data with durations of up to $20\,\mathrm{min}$.

between model-predicted and model-propagated labels, with mismatching segments coming first.

2. Farthest traversal: This criterion aims at increasing the diversity within the selected data. It selects the sample farthest away from the already selected samples, using the ordering described above. To this end, the cosine distances between the mean of embeddings of the labeled and unlabeled data are computed. The data selection scheme adds one sample at a time, to ensure that the chosen sample is farthest away from the labeled data and the already selected samples in this iteration. Note that while mismatch-first can only be applied after the first iteration, farthest traversal is already used to select the first batch, except for the very first sample which needs to be chosen randomly.

The newly selected samples are then presented to an annotator who needs to assign weak labels to the chosen segments. By requiring weak labels only, the annotation effort can be reduced even more.

The samples selected for training are used to train to a bi-directional recurrent neural network (RNN) consisting of three layers of gated-recurrent units (GRUs) with 30 hidden units each. The model outputs $\boldsymbol{y}_t$ for each time-step. A fully connected sigmoid layer is used to generate *class probabilities* $\boldsymbol{p}_t$ for each time step. The weak label output used during training is computed in a similar fashion as in [8]. As we analyze binary classifiers only, we apply a sigmoid instead of a softmax function for generating the attention output.

3. EXPERIMENTS

We employ the proposed active learning scheme on three binary classifiers. The three different classes are glassbreaking (*glass-break*), spraying (*spray*), and shaking a graffiti can (*rattle*). As we aim at analysing the three classifiers independently, we train three individual classifiers in this work, instead of one mulilabel classifier.

3.1 Datasets

In order to evaluate the proposed vandalism detection system, two datasets are used. A summary is given in Tab. 1.

The first one, which is used for training the glassbreak classifier, is a subset of the *TUT Rare Sound Events 2017* set [13]. It was generated by mixing the target sound events from Freesound with background sounds from the TUT Acoustic Scenes 2016 dataset [14] in various event-to-background ratios. As we are interested in vandalism detection, we only use the glassbreak subset in this paper. In contrast to the setup in [8], we partition the dataset into non-overlapping 10-second chunks, in order to match the format of the second dataset. This yields 1500 segments of the *devtrain* split for training, and 1500 segments of
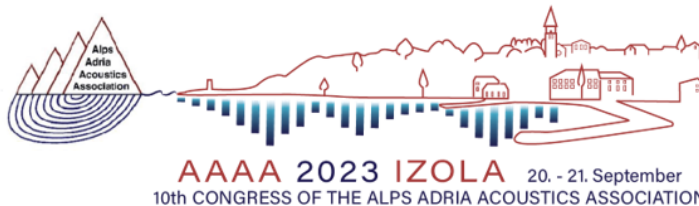
the *devtest* for testing. Approximately one sixth of the segments contain a target event.

The second dataset is an inhouse-dataset which consists of three parts of approximately equal size: (i) recordings of spray and can rattle sounds in various acoustic environments, (ii) false-positive detections recorded at various installations of the Graffiti Buster[TM 2] , and (iii) ambience recordings from various locations in the city center of Graz, Austria. The recordings are cut into non-overlapping segments of 10 seconds each, and were manually annotated.

	Total [minutes]	Ambient [minutes]	Target [minutes]
Glassbreak train	250	0	6
Glassbreak test	250	0	3
Spray train	1003	250	36
Spray test	217	0	17
Can rattle train	498	250	17
Can rattle test	235	0	11

Table 1. *Summary of the datasets used in this paper.*

Note that the *spray* and *rattle* datasets are already pre-selected data used for training and do not represent the real sparsity of the events.

3.2 Results

To be able to assess the performance of the data selection scheme, we apply the whole active learning scheme for each classifier three times (i.e., three *selection* iterations). The analyzed sizes of the subset used for training are $[1, 2, 3, 4, 5, 6, 7, 8, 9, 10, 12, 14, 16, 18, 20, 60, 100]$ %. In order to assess the influence of the (stochastic) training process on the performance, three networks are trained for each selected training subset, and the mean of the results among these three *training* iterations are presented. Note that for MFFT, we always used the third (of the three trained models) to select the data for the next selection iteration, using a threshold of 0.5. During training, 30 % of the selected training batch is randomly chosen as validation set.

In this study, the performance of the trained classifiers are evaluated with a segment-based F_1 score with segment-length chosen to be $1\mathrm{sec}$ [15]. For each individual result, the threshold leading to the best F_1 score is chosen.

The results for the three different event classes are presented in Fig. 1. The upper row depicts the percentage of positive samples within the current selection versus the dataset size, in percent of the total available data. The lower row shows the

---

² https://www.joanneum.at/en/digital/productssolutions/graffiti-buster accessed on 25.08.2023

average of the F_1 score as well as the minimum and maximum of the average F_1 score with respect to the training iterations.

Clearly, MFFT data selection (——) adds a disproportionately high number of positive samples to the training data during the first few iterations of the active learning scheme. The positive samples chosen by random data selection (- - -) are (as expected) directly proportional to the current percentage of the training dataset size.

For the *glassbreak* dataset, it is possible to achieve a F1 score of about 95% of the maximum F1 score already at a training dataset size of about 7 % with MFFT data selection. When using random sampling (- - -), about 20 % of the dataset is needed to achieve this performance.

For both the *rattle* and the *spray* dataset, MFFT (——) outperforms random sampling (- - -) for all dataset sizes except for 1 %. However, 95% of the maximum performance is only achieved when using at least 20 % of the data. We conjecture that these two datasets do not contain enough redundancy for the algorithm to choose a near optimal subset at lower percentages. This could be explained by the fact, that the datasets presented in Tab. 1 are already a selected subset of the sound scene at a sensor, containing mainly true positive and false positive examples of a previously trained classifier. Most of the redundant data at a specific installation is therefore already filtered out beforehand.

4. CONCLUSION

In this paper we introduced a novel application for sound event detection namely vandalism detection and analyzed an active learning scheme for reduced training and annotation effort. The presented active learning scheme selects data on the basis of a mismatch-first farthest-traversal criterion and clearly outperforms random sampling. Furthermore, we have shown that good performance can be achieved when using about 20 % of the datasets.

The next steps are to employ the active learning to the *complete* datasets for rattling and spraying a graffiti can. Additionally, we want to compare the effect of employing the algorithm to balanced and unbalanced multi-label datasets.

5. ACKNOWLEDGEMENT

6. REFERENCES

[1] P. W. van Hengel and T. C. Andringa, "Verbal aggression detection in complex social environments," in *IEEE Conference on Advanced Video and Signal Based Surveillance*, pp. 15–20, IEEE, 2007.
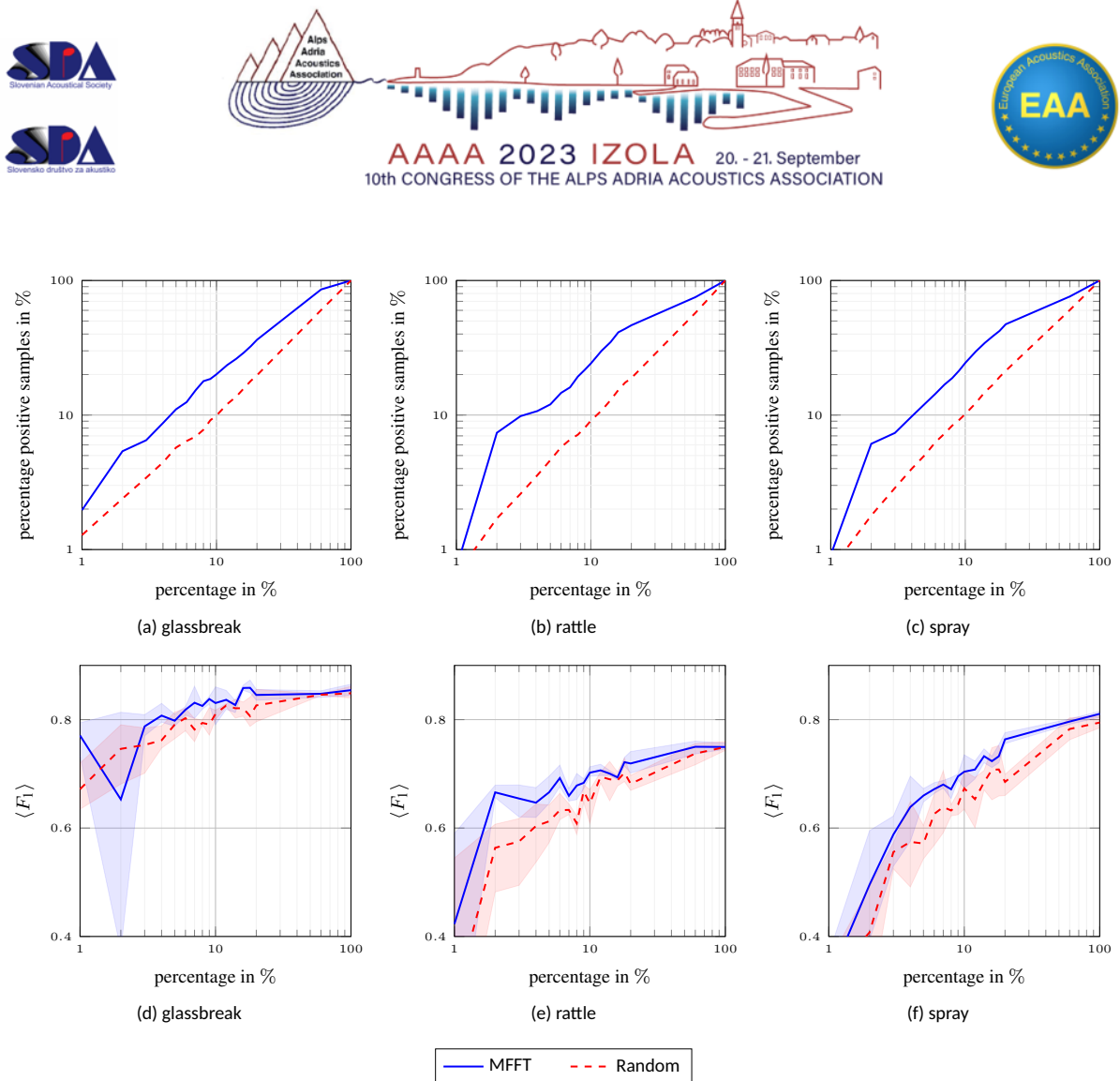
Fig. 1. *Results of the active learning scheme for MFFT-selection (——) and random-selection (- - -): The upper row shows the percentage of positive samples selected by the data selection scheme as a function of the overall percentage of the dataset. The lower row presents the average F_1-score including minimum and maximum. The three columns correspond to the different event classes: (a), (d) are for glassbreak, (b), (e) are for rattle, (c), (f) is for spraying.*

[2] J. F. Kooij, M. C. Liem, J. D. Krijnders, T. C. Andringa, and D. M. Gavrila, "Multi-modal human aggression detection," *Computer Vision and Image Understanding*, vol. 144, pp. 106–120, 2016.

[3] P. Foggia, N. Petkov, A. Saggese, N. Strisciuglio, and M. Vento, "Reliable detection of audio events in highly noisy environments," *Pattern Recognition Letters*, vol. 65, pp. 22–28, 2015.

[4] K. Wang, D. Zhang, Y. Li, R. Zhang, and L. Lin, "Cost-effective active learning for deep image classification," *IEEE Transactions on Circuits and Systems for Video Technology*, vol. 27, no. 12, pp. 2591–2600, 2016.

[5] D. Yoo and I. S. Kweon, "Learning loss for active learning," in *Proceedings of the IEEE/CVF conference on computer vision and pattern recognition*, pp. 93–102, 2019.

[6] P. Ren, Y. Xiao, X. Chang, P.-Y. Huang, Z. Li, B. B. Gupta, X. Chen, and X. Wang, "A survey of deep active learning," *ACM computing surveys (CSUR)*, vol. 54, no. 9, pp. 1–40, 2021.

[7] Y. Wang, A. E. M. Mendez, M. Cartwright, and J. P. Bello, "Active learning for efficient audio annotation and classification with a large amount of unlabeled data," in *IEEE International conference on acoustics, speech and signal processing (ICASSP)*, pp. 880–884, IEEE, 2019.

[8] Z. Shuyang, T. Heittola, and T. Virtanen, "Active learning for sound event detection," *IEEE/ACM Transactions on Audio,*

Speech, and Language Processing, vol. 28, pp. 2895–2905, 2020.

[9] S. Shishkin, D. Hollosi, S. Doclo, and S. Goetze, "Active learning for sound event classification using monte-carlo dropout and pann embeddings," in *Workshop on Detection and Classification of Acoustic Scenes and Events (DCASE)*, 2021.

[10] Y. Xu, Q. Kong, W. Wang, and M. D. Plumbley, "Large-scale weakly supervised audio classification using gated convolutional neural network," in *2018 IEEE International Conference on Acoustics, Speech and Signal Processing (ICASSP)*, pp. 121–125, 2018.

[11] A. Kumar, M. Khadkevich, and C. Fügen, "Knowledge transfer from weakly labeled audio using convolutional neural network for sound events and scenes," in *2018 IEEE International Conference on Acoustics, Speech and Signal Processing (ICASSP)*, pp. 326–330, 2018.

[12] Z. Shuyang, "Audio embedding segmentation." `https://github.com/zhao-shuyang/audio_embedding_segmentation`, 2020.

[13] A. Mesaros, T. Heittola, A. Diment, B. Elizalde, A. Shah, E. Vincent, B. Raj, and T. Virtanen, "DCASE 2017 challenge setup: Tasks, datasets and baseline system," in *Proceedings of the Detection and Classification of Acoustic Scenes and Events Workshop (DCASE)*, 2017.

[14] A. Mesaros, T. Heittola, and T. Virtanen, "Tut database for acoustic scene classification and sound event detection," in *European Signal Processing Conference (EUSIPCO)*, pp. 1128–1132, IEEE, 2016.

[15] A. Mesaros, T. Heittola, and T. Virtanen, "Metrics for polyphonic sound event detection," *Applied Sciences*, vol. 6, no. 6, 2016.

EXPERIMENTAL SOUND FIELD CHARACTERIZATION WITH AUTOMATED HIGH-RESOLUTION IMPULSE RESPONSE MEASUREMENTS

Rok Prislan[1], Alexis Dufour[2]

[1] **InnoRenew CoE, SI-6310, Izola**
[2] **CESI: École d'ingénieurs, Nanterre, France**

Abstract:

The technical development of the equipment used for acoustic measurements has allowed us to automate measurements and to use a large number of microphones simultaneously. This opens up the possibility of scanning the sound field, i.e., capturing room impulse responses with a high spatial resolution. In this paper, the development of such a measurement approach is presented. Several challenges and technical details are presented in connection with the approach, including the method for accurately determining the coordinates of the moving microphones. The developed experimental technique is used to study the characterization of the sound field. The study is therefore important to better understand concepts related to the diffuse and reverberant sound field, such as diffuseness and mixing, in the context of modal and statistical descriptions.

Keywords: *Acoustic scanning, measurement automatisation, microphone cable robot*

1. INTRODUCTION

The diffuse sound field is an important idealized field in acoustics for standardized acoustic measurements, simple predictions, and a wide range of theoretical derivations. Surprisingly, there is no general agreement on the definition of the diffuse sound field, its quantification and characterization; also, there is limited understanding on the required features of room boundaries that would lead to a diffuse sound field. Controversially, demands for its presence are given for a broad range of spaces and facilities.

Misconceptions about the diffuse sound field were exposed already by Schultz [1] in the 1970s and are still present, as pointed out by Jeong [2]. Several uncertainties exist with respect to various aspects, with the largest knowledge deficit arising from the absence of a predictable and measurable quantifier of the sound field diffuseness, i.e., the degree to which the sound field is diffuse. Such a quantifier would allow the evaluation of sound field environments that are currently only assumingly diffuse, such as reverberation chambers. These are

standardized test facilities in acoustics whose requirements are under revision [3] - partly because of the issues related to insufficient diffuseness.

To further investigate the diffuse sound field, new experimental approaches are being developed that will hopefully provide additional insight into the complexity of such sound field. This paper presents the development of a scanning measurement approach to study the reverberant sound field formed in the regular chamber that is part of the InnoRenew CoE Acoustics Laboratory. The paper is organized to present the theoretical background of the reverent sound fields in Section 2, the regular chamber facility in Section 3, the developed scanning microphone system in Section 4, and the conclusions in Section 5.

2. INVESTIGATING THE REVERENT SOUND FIELD

Several diffuseness quantifiers have been proposed in the literature, focusing on different sound field properties:

- spatial correlation [4–7]
- response decay fluctuations [8–11]
- intensity distribution [12, 13]
- directional characteristics [14–17]
- spatial uniformity of sound pressure [5]
- spatial uniformity of reverberation time [18]
- and higher order parameters [19–24]

These quantifiers are capable of evaluating certain sound field features, but none of them is complete enough to evaluate all aspects of the diffuse sound field.

An important branch of research focuses on the characterization of the sound field based on its spatial features. Experimental evaluation of these features involves various measurement methods, ranging from optical methods [25], to various sophisticated microphone scanning approaches. In this context, scanning is the process of systematically acquiring the room impulse response over a predefined grid of points in the volume of
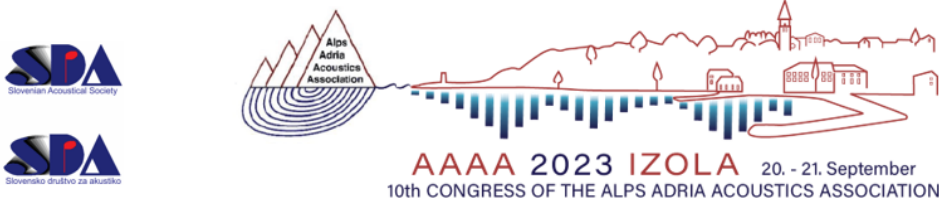
the room. Scanning is typically performed by robots [26, 27] that move one or more microphones across the scanned volume of the room.

To speed up the scanning process, multiple microphones arranged in a microphone array can be used simultaneously. The advantage of using multiple microphones is that the measurement process is faster by a factor equal to the number of microphones. The measurement time becomes relevant when the conditions in the room may vary, for example, when the air temperature or humidity in the room changes during the measurement. An important technical requirement for using multiple microphones is that the microphones are phase matched in the frequency range of interest. A disadvantage of using multiple microphones is that the microphone array generally presents a larger disturbance to the sound field, since such a structure can be relatively large. In addition to sophisticated robot-based methods, an accessible method for scanning the sound field was used by Prislan and Svešnek [28] to visualize modal shapes in the room. The acquisition was based on vertically stacked microphones that were manually moved across the floor plan of the room.

With post-processing of the large number of acquired impulse responses, it is possible to perform various sound field characterizations. The decomposition into plane or spherical waves is an important approach [29] because it allows us to extract sound field quantities, namely velocities and intensities, in addition to sound pressure. This also allows us to study the directional properties of the sound field, such as the isotropy of the reverberant field [26]. Another advantage of the large number of measurements generated by scanning is the possibility to apply statistics on various sound field characterization methods, such as the spatial uniformity methods [17] or the sound field sensitivity method proposed by Prislan at. el. [19].

3. THE TEST FACILITY

Experimental studies with the cable robot will be conducted in the regular chamber, a recently introduced test facility [30], that is part of the InnoRenew CoE Acoustic Laboratory. The facility represents a highly controlled acoustic environment whose geometry can be changed without drastically altering the volume, surface area, or other acoustically relevant properties of the chamber. Such geometric variability is rare in ordinary rooms, which are inherently static and whose geometry can be changed only by adding elements to the room.

The basic geometry of the regular chamber is a cuboid with volume $V = 37\text{m}^3$ and internal dimensions $l = 3\text{m}$ in length, $w = 2.5\text{m}$ in width and $h = 2\text{m}$ in height. The ratio of the regular chamber dimensions corresponds to the Bolt area [31]. The regular chamber consists of six plane surfaces, i.e. 4 walls, the floor and the ceiling. Two walls and the floor are perpendicular to each other and are fixed, while the remaining two walls and the ceiling can be tiled independently, as shown schematically in

Figure 1. The rotation of the non-fixed bounding surfaces is 10°, with the axis of rotation at the center of the surface to minimize changes in the volume of the room. A total of 6 different regular chamber configurations are possible, as shown schematically in Figure 2.
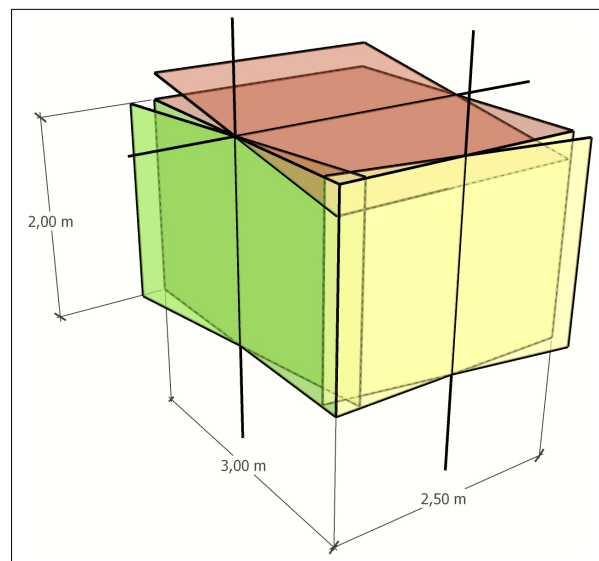
Fig. 1. *A graphical representation of the rotation of the ceiling (red) and two walls (green and yellow) of the regular chamber. The remaining walls and the floor are fixes and perpendicular to each other. The axis of rotation of the non-fixed surfaces is in the center of each surface and marked by a longer line.*

Another important aspect to mention is the expected influence of the changes in the geometry of the regular chamber on the sound field. For this purpose, the modal shapes and eigenfrequencies have been previously studied using FEM [30]. It has been shown that the distribution of the room resonances and the corresponding modal shapes do not differ significantly between the different chamber configurations.

4. THE DEVELOPMENT OF THE SCANNING MICROPHONE SYSTEM

4.1 The use of robots in room acoustic measurements

Sound field scanning, i.e., the acquisition of impulse responses with high spatial resolution, has previously been approached with various types of robots. Witew et. al. [27] installed a frame structure in the Eurogress hall in Aachen, Germany. The frame allowed a cart with 32 linearly arranged microphones to move in the horizontal plane of 5.30m by 8.00m.
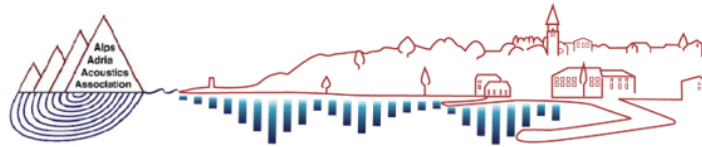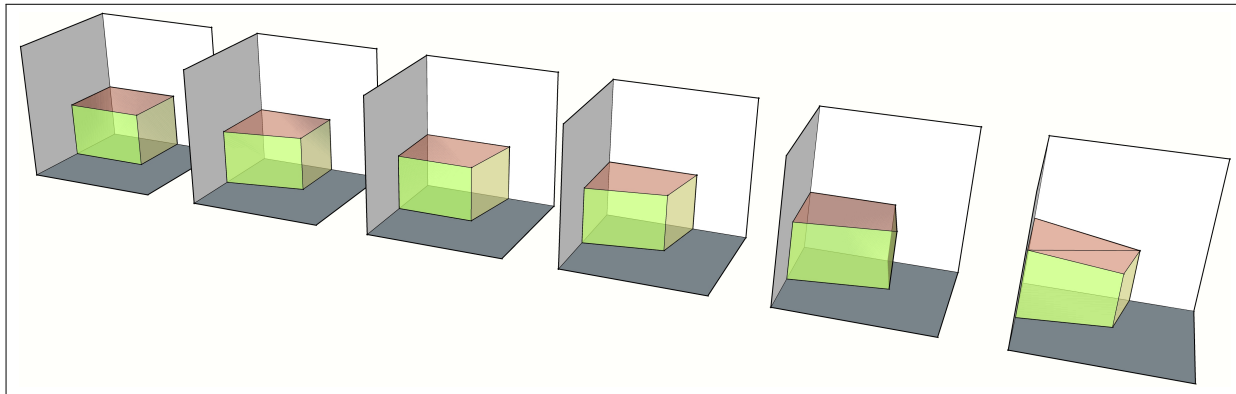
Fig. 2. *The 6 geometric configurations of the regular chamber (R1-R6).*

An arm robot moving a single microphone has been widely used for various investigations at the Technical University of Denmark [32], including measurements in a reverberation chamber, in an anechoic chamber, and in the field. When measuring with the robotic arm, the movement of the microphone is not limited to a vertical plane, but can follow any predefined spatial configuration. On the other hand, the movement of the robot arm is limited in range due to the limited size of the arm.

An important advantage of using robots for sound field scanning measurements is the high accuracy in positioning the microphone in the sound field. In contrast, manual methods [28], are, due to inaccurate microphone positioning, limited to low frequencies, where accuracy is always sufficient compared to the wavelength of interest.

4.2 Microphone positioning system

The accuracy with which microphone coordinates are known during scanning measurements is important because coordinates can be an input to post-processing analysis [28,29]. To mitigate positioning accuracy issues, a variety of microphone positioning systems have been used to date. One purely acoustic approach [33] is to use impulse response measurements to determine the distance between the microphone and a set of fixed loudspeakers at the known location in the room. From this, triangulation can be used to determine the coordinates of the microphone, as shown schematically in Figure 3. The accuracy of this method can be further improved by using multiple microphones in a fixed configuration.

An alternative method for microphone positioning that has already been investigated is the use of a laser scanner [34]. This involves placing colored markers on the microphone array (see Figure 4), the coordinates of which can be used to determine the coordinates of the individual microphones in the array.
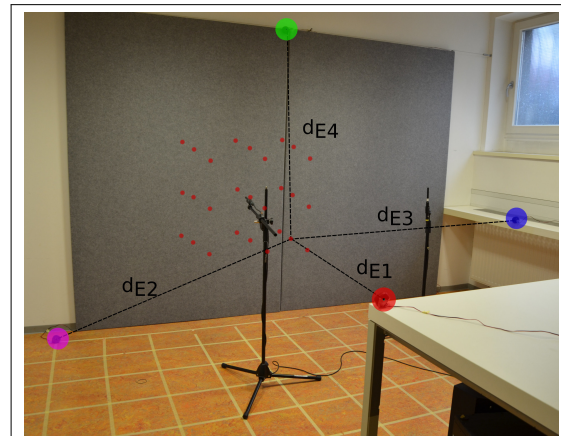
Fig. 3. *A graphical representation of the impulse response measurements principle used for microphone positioning [33] using four high frequency loudspeakers at known positions in the room.*

4.3 Cable robot

Cable-driven parallel robots are a type of parallel manipulator that uses flexible cables as actuators [35]. The advantages of cable robots are the relatively large span in which motion can be achieved. A less relevant advantage for the intended application is also the fast movement capability of cable robots. On the other hand, cable robots are less accurate in positioning compared to other types of robots due to the large spans over which the cables can considerably elastically extend at high tensions. It was therefore a design decision to combine the installation of the cable robot with the previously developed acoustic positioning system presented in Section 4.2.
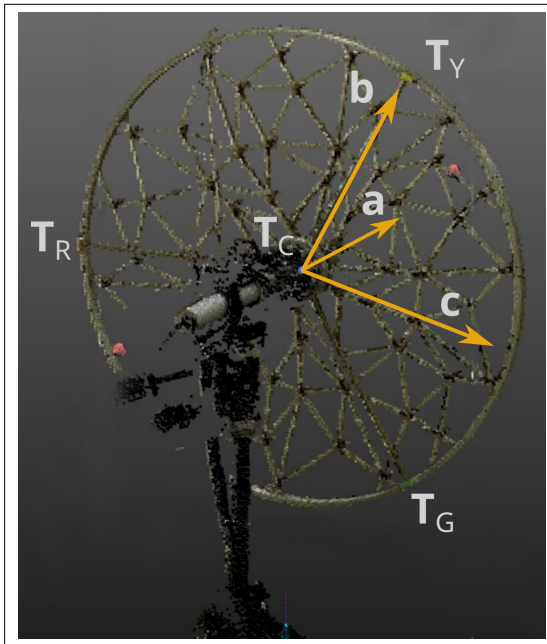
Fig. 4. *A laser scan of the back side of the microphone array with visible colored markers, from which microphone coordinates can be extracted using simple geometrical relations [34].*

Different cable robot configurations are possible, differing in the number of cables used and the distribution of fixation points at the room boundaries. In the case of the designed cable robot, 8 cables are used to control the microphone array, as shown graphically in Figure 5. This motion system is overdetermined, as the top 4 cables would be sufficient to fully control the position of the microphone array. The additional bottom cables were added to stabilize the position of the system, prevent axial rotation of the microphone array, and reduce the oscillatory motion that would likely occur with a pendulum-type design of the system. The developed model of the cable robot installation is shown graphically in Figure 5.

At the current state of the development, the microphone array to be used still needs to be determined. In fact, an important aspect is the integration of the cables, which should not interfere with the movement of the cable robot and at the same time allow a reliable connection of the microphones to the data acquisition system. At the same time, it is important to design the array as a miniature structure that minimally disturbs the sound field under investigation.

Including the geometrical considerations into the discussion, it is apparent that the desired coordinate of the center of the microphone array $\mathbf{T}$ is fully determined by the length of the 8 cables. In this context, the length of the cables is considered as the distance between the four attachment points of the cables on the array ($\mathbf{T}_1, \mathbf{T}_2, \mathbf{T}_3$ and $\mathbf{T}_4$) and the eight fixed attachment points at the room boundaries ($\mathbf{P}_1, \mathbf{P}_2, ...\mathbf{P}_8$). The lengths can be calculated as linear norms of the vector corresponding to the ends of each cable. A specific feature of the introduced design is that two cables are attached to the same fixation point on the microphone array.

Currently, the array is assumed to move in parallel to one of the fixed walls and the floor of the chamber. This is an added constrain to the motion of the cable robot, which enables that the position of each microphone in the array is fully determined from the coordinate of the center of the array $\mathbf{T}$. As such, an additional computation step is needed to determine $\mathbf{T}_1, \mathbf{T}_2, \mathbf{T}_3$ and $\mathbf{T}_4$ from $\mathbf{T}$ based on the dimensions of the array and its predetermined orientation in space.

Another aspect to consider is the positioning of the attachment points $\mathbf{P}_1, \mathbf{P}_2, ...\mathbf{P}_8$ on the boundaries, which represent the outer limit of the motion range of the microphone array. To enable an effectively scan a cuboidal volume, the eight attachment points have been put in the proximity of the corners of the chamber.

5. CONCLUSIONS

This paper presents the motivation for developing an automated sound field scanning system, i.e., a system for measuring the impulse response in a predefined volume with high spatial resolution. Previous approaches using robots for sound field scanning have been described in the context of the robotisation type and post-processing analysis, which is driving the development of such advanced acoustic instrumentation.

The limitations of accurate positioning of microphones with a cable robot were discussed and the acoustic positioning system was presented as an additional system to the cable robot. The aspect of accurate positioning was also considered in the design by the introduction of redundant cables, which are expected to stabilize the positioning of the microphones and also limit the unwanted rotations and oscillations of the microphone array.

In further steps, the developed cable robot will be installed in the regular chamber so that the sound field scanning can be performed in a highly controlled reverberant environment. In addition, the acoustic microphone positioning system will be integrated to autonomously determine the microphone coordinates with high accuracy. Furthermore, the microphone array will be further developed, paying special attention to the cable management system, which must flexibly support the required range of motion of the cable robot. With the developed measurement system, we intend to perform various investigations in the reverberant sound field, hoping to gain additional insight needed to better understand the concept of the diffuse sound field.
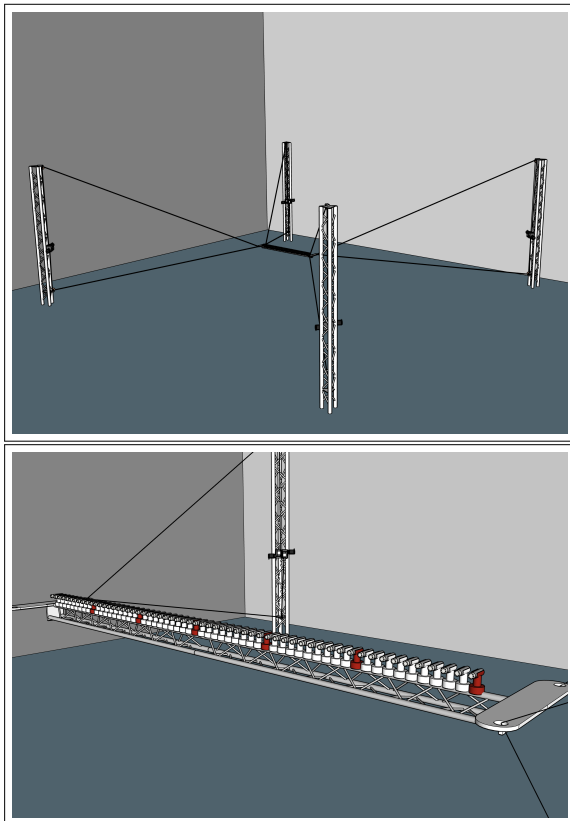
Fig. 5. *A 3D model of the developed cable robot consisting of 8 cables (top: distant view, bottom: zoomed view). The cables are attached in pairs to the four attachment points of the microphone array, forming a rectangular shape. The position of the microphone array is fully determined by the lengths of the 8 cables.*

6. ACKNOWLEDGMENTS

7. REFERENCES

[1] T. Schultz, "Diffusion in reverberation rooms," *Journal of Sound and Vibration*, vol. 16, pp. 17–28, 5 1971.

[2] C.-H. Jeong, "Diffuse sound field: challenges and misconceptions," pp. Pages 1015–1021, 2016.

[3] M. Vercammen, "On the revision of iso 354, measurement of the sound absorption in the reverberation room," Deutsche Gesellschaft für Akustik, 2019. Zweitveröffentlicht auf dem Publikationsserver der RWTH Aachen University. - Weitere Konferenz: 4th EAA Euroregio, 2019-09-09 - 2019-09-13, Aachen, Germany.

[4] F. Jacobsen and T. Roisin, "The coherence of reverberant sound fields," *The Journal of the Acoustical Society of America*, vol. 108, pp. 204–210, 2000.

[5] H. Nélisse and J. Nicolas, "Characterization of a diffuse field in a reverberant room," *The Journal of the Acoustical Society of America*, vol. 101, pp. 3517–3524, 6 1997.

[6] K. Bodlund, "A new quantity for comparative measurements concerning the diffusion of stationary sound fields," *Journal of Sound and Vibration*, vol. 44, pp. 191–207, 1976.

[7] R. K. Cook, R. V. Waterhouse, R. D. Berendt, S. Edelman, and M. C. Thompson, "Measurement of correlation coefficients in reverberant sound fields," *The Journal of the Acoustical Society of America*, vol. 27, pp. 1072–1077, 1955.

[8] C.-H. H. Jeong, J. Brunskog, and F. Jacobsen, "Room acoustic transition time based on reflection overlap," *The Journal of the Acoustical Society of America*, vol. 133, pp. 015002–015002, 5 2013.

[9] T. Hanyu, "Analysis method for estimating diffuseness of sound fields by using decay-cancelled impulse response," *Building Acoustics*, vol. 21, pp. 125–133, 2014.

[10] K. Eda and T. Sakuma, "A theoretical survey on temporal structure of reflections in decay-cancelled room impulse responses," *Acoustical Science and Technology*, vol. 36, p. 453, 2015.

[11] C.-H. Jeong, F. Jacobsen, and J. Brunskog, "Thresholds for the slope ratio in determining transition time and quantifying diffuser performance in situ," *The Journal of the Acoustical Society of America*, vol. 132, pp. 1427–1435, 9 2012.

[12] G. D. Galdo, M. Taseska, O. Thiergart, J. Ahonen, and V. Pulkki, "The diffuse sound field in energetic analysis.," *The Journal of the Acoustical Society of America*, vol. 131, pp. 2141–2151, 2012.

[13] M. Nolan, E. F. Grande, and C.-H. Jeong, "Characterization of diffusivity based on spherical array processing," 2015.

[14] B. N. Gover, J. G. Ryan, and M. R. Stinson, "Measurements of directional properties of reverberant sound fields in rooms using a spherical microphone array," *The Journal of the Acoustical Society of America*, vol. 116, pp. 2138–2148, 2004.

AAAA 2023 IZOLA 20. - 21. September
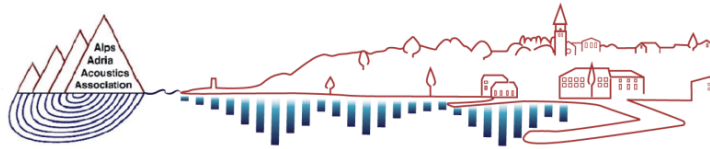10th CONGRESS OF THE ALPS ADRIA ACOUSTICS ASSOCIATION

[15] A. Politis, S. Delikaris-Manias, and V. Pulkki, "Direction-of-arrival and diffuseness estimation above spatial aliasing for symmetrical directional microphone arrays," pp. 6–10, 4 2015.

[16] N. Epain and C. T. Jin, "Spherical harmonic signal covariance and sound field diffuseness," 2016.

[17] M. Nolan, E. Fernandez-Grande, J. Brunskog, and C.-H. Jeong, "A wavenumber approach to quantifying the isotropy of the sound field in reverberant spaces a)," *The Journal of the Acoustical Society of America*, vol. 143, pp. 2514–2526, 2018.

[18] M. Lautenbach and M. Vercammen, "Can we use the standard deviation of the reverberation time to describe diffusion in a reverberation chamber?," *The Journal of the Acoustical Society of America*, vol. 133, p. 3348, 2013.

[19] R. Prislan, J. Brunskog, F. Jacobsen, and C.-H. Jeong, "An objective measure for the sensitivity of room impulse response and its link to a diffuse sound field," *The Journal of the Acoustical Society of America*, vol. 136, pp. 1654–1665, 2014.

[20] J.-D. Polack, "Modifying chambers to play billiards: the foundations of reverberation theory," *Acta Acustica united with Acustica*, vol. 76, 1992.

[21] A. Bidondo, N. Xiang, and J. Herder, "Experimental investigation on varied degrees of sound field diffuseness in enclosed spaces," *Proceedings of Meetings on Acoustics*, vol. 28, p. 15020, 9 2016. doi: 10.1121/2.0000436.

[22] G. Defrance and J.-D. Polack, "Estimating the mixing time of concert halls using the extensible fourier transform," *Applied Acoustics*, vol. 71, pp. 777–792, 9 2010.

[23] C.-H. Jeong, "Kurtosis of room impulse responses as a diffuseness measure for reverberation chambers.," *The Journal of the Acoustical Society of America*, vol. 139, p. 2833, 2016.

[24] H. Dujourdy and T. P. Jean-Dominique Pialot, Baptiste Toulemonde, "Modified wave equation for modelling diffuse sound field," 2016.

[25] S. A. Verburg and E. Fernandez-Grande, "Acousto-optical volumetric sensing of acoustic fields," *Physical Review Applied*, vol. 16, 2021.

[26] M. M. Nolan, S. A. Verburg, J. Brunskog, E. F. Grande, and E. Fernandez-Grande, "Experimental characterization of the sound field in a reverberation room," *Acoustical Society of America. Journal*, vol. 145, pp. 2237–2246, 4 2019.

[27] I. B. Witew, M. Vorländer, and N. Xiang, "Sampling the sound field in auditoria using large natural-scale array measurements," *The Journal of the Acoustical Society of America*, vol. 141, pp. EL300–EL306, 3 2017.

[28] R. Prislan and D. Svenšek, "Room mode shape visualization using a multi-microphone measurement technique," 2016.

[29] E. G. Williams and J. A. Mann, "Fourier acoustics: Sound radiation and nearfield acoustical holography," *The Journal of the Acoustical Society of America*, vol. 108, 2000.

[30] R. Prislan and J. Brunskog, "A regular chamber - design of a test facility for the investigation of the reverberant sound field," 2023.

[31] R. H. Bolt, "Note on normal frequency statistics for rectangular rooms," *The Journal of the Acoustical Society of America*, vol. 18, pp. 130–133, 7 1946.

[32] E. Fernandez-Grande, S. A. Verburg, and X. Karakonstantis, "Sound field reconstruction: Towards large-scale spatial sensing," 2023.

[33] R. Prislan, "Microphone positioning using acoustic location," 2020.

[34] R. Prislan and U. Kavka, "The potential of using a laser scanner to facilitate in-situ room acoustic measurements," pp. 510–515, 10 2022.

[35] A. Pott, *Cable-driven parallel robots: Theory and application*, vol. 120. 2018.

Contributed papers
Acoustic software and training

1. Audio exercises: quality, pitch statistics and long-term spectra of the sound files
   Andrea Andrijasevic (Polytechnic of Rijeka, Croatia)
2. Acoustics Knowledge Alliance project: the development of open-access interactive online educational materials in acoustics - strategy and results
   Marko Horvat (University of Zagreb, Faculty of electrical engineering and computing)

AUDIO EXERCISES: QUALITY, PITCH STATISTICS AND LONG-TERM SPECTRA OF THE SOUND FILES

Andrea Andrijašević[1], Mirta Čulina[2]

[1] Polytechnic of Rijeka, Vukovarska 58, 51 000 Rijeka, Croatia
[2] Clinical Hospital Center Rijeka, Krešimirova 42, 51 000 Rijeka, Croatia

Abstract: *Audio exercises is a free computer program created with the objective of supporting hearing therapy for adult persons with hearing impairments and tinnitus. It is intended for their home use and, as such, comprised of two parts: a set of twelve auditory exercises in the Croatian language to be used during the later stages of a person's adaptation to the prescribed hearing aid or cochlear implant, and a module for tinnitus perceived intensity reduction based on the Tailor-made notched music training (TMNMT) sound therapy approach. In addition to the program's main task of helping in patient's rehabilitation, it can also be used by the non-diagnosed individuals as a relatively straightforward monitoring tool that can inform them early of their hearing health deterioration. Given these manifold valuable potential applications of the program, in this paper we provide an analysis of the sound files quality as well as of the pitch statistics and long-term spectra of the speech and music examples provided in it. Since the auditory exercises are based on the verbotonal method that takes into account the optimal hearing frequencies of speech sounds, we also calculate the log-spectral distance between the long-term average spectra of the five classes of speech examples and, similarly, the distances between the spectra of the five music genres used for tinnitus therapy.*

Keywords: hearing loss, tinnitus, rehabilitation, music therapy, computer program

1. INTRODUCTION

According to the projections presented in the World Health Organisation's latest report on hearing, by 2025 nearly a quarter of the world population will have some degree of hearing loss [1]. Moreover, it is anticipated that one in fourteen people will require hearing care [1]. Hearing loss and tinnitus, the perception of a sound without an external source, besides the negative impact they have on speech intelligibility, commonly have a negative effect on both the psychological state and social life of affected individuals [2, 3].

Since for a part of the affected population the medical support, therapy and counselling can be expensive and time-consuming [4], a computer program titled "Audio exercises" was recently created with the intention of providing free and accessible support for the Croatian speaking adults [5]. It was written in C# and runs on Windows 7 and 10 operating systems. The program contains speech material for hearing exercises as well as pieces of instrumental music filtered according to the Tailor-Made Notched Music Training (TMNMT) tinnitus therapy principles [6]. As shown in Figure 1, the main program window contains three items:

- *Vježbe slušanja* (auditory exercises), which consists of a set of twelve auditory exercises (*Fraze - Veliki test 2*),
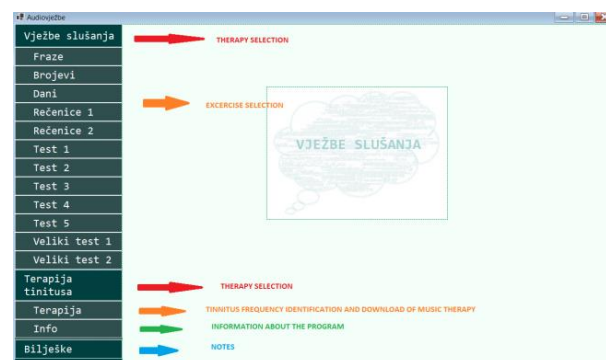- *Terapija tinitusa* (tinnitus therapy),
- *Bilješke* (notes).

Fig. 1. Main program window

In addition to the program's main task of helping in patients rehabilitation, it can also be used by the non-diagnosed individuals as a relatively straightforward monitoring tool that can inform them early of their hearing health deterioration. Given these valuable potential applications of the program, in this paper we provide an analysis of the phonetical and spectral characteristics of its sound files.

The remainder of the paper is organised as follows. In Section 2, we first present the phonetic content, sound quality, and spectral characteristics of the recorded speech material used in the program. We continue by analysing the spectral characteristics of the pieces of instrumental music used for tinnitus therapy in Section 3. Finally, with Section 4, we conclude our work.

2. SPEECH MATERIAL

The set of twelve auditory exercises is intended for patient use at home during the later stages of their adaptation to the prescribed hearing aid or cochlear implant. The exercises are based on the verbotonal hearing therapy method that takes into account the patient's optimal frequency range of hearing [7, 8]. Accordingly, the speech material used in them was carefully selected in order for it to contain an equal number of speech sounds from all frequency classes. It is in Croatian, and was read by a female person with an average sound pressure level of 71 dB in an anechoic chamber, recorded using the LingWaves system with a sampling rate of 22050 Hz.

For the analyses presented in Sections 2.3. - 2.5., the words and sentences used in exercises 6 - 12 needed to be separated into five classes based on the frequency range in which most of their energy is contained. This was performed in line with the classification of the Croatian language phonemes given in [9], an example of which is shown in Table 1.

2.1. Sound quality

The sound quality of speech files was evaluated using the estimates of their signal-to-noise ratio (SNR). To this end, noise power was estimated from both the first and last 50 ms of a file (i.e., from the parts with no voice activity), whereas speech signal power was estimated as the active speech level using the ITU-T P.56 Method B [10, 11] from which the previously estimated noise power was

subtracted. In this way, two SNRs were obtained for a speech file - one using the noise power estimate from the file beginning (SNR-B) and the second one using the file end noise power estimate (SNR-E). Figure 2 shows the SNRs and their exercise-level mean.

Phoneme class	Frequency range (Hz)	Croatian language phonemes
low (L)	150 - 300 200 - 400	/m/, /n/, /nj/ /b/, /p/, /u/
low-mid (LM)	300 - 600 400 - 800 600 - 1200	/v/ /g/, /o/ /h/, /l/, /lj/
mid (M)	800 - 1600 1200 - 2400	/a/, /k/, /r/ /d/, /dž/, /f/, /m/, /ž/
mid-high (MH)	1600 - 3200 2400 - 4800	/č/, /e/, /n/, /lj/, /š/, /t/ /đ/, /j/, /nj/
high (H)	3200 - 6400 4800 - 9600 6400 - 12800	/ć/, /i/ /c/, /z/ /s/

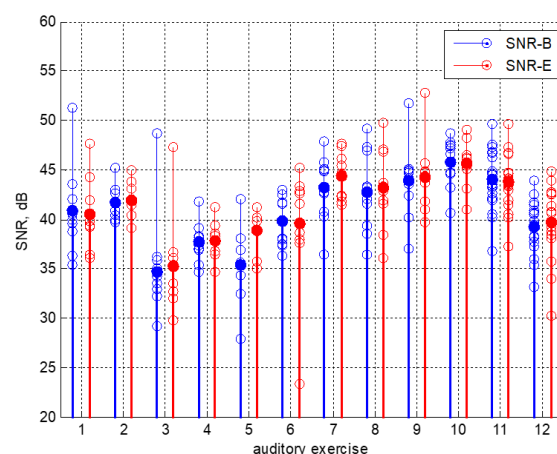**Table 1.** Frequency range-based phoneme classes

Fig. 2. SNR-B and SNR-E of the sound files. Filled symbol denotes the corresponding exercise-level mean

In the speech enhancement community, the general consensus is that speech signals with an SNR greater than 30 dB can be considered "clean", meaning they do not

require additional processing since above that value noise and reverberation do not reduce speech intelligibility or degrade the performance of systems for automatic speech recognition. This threshold was set even lower in two recent speech signal processing challenges [12, 13], where signals with an SNR of 20 dB were provided as the best case scenario. It can therefore be concluded that the recorded speech material is of excellent quality since 98 % of the files have SNR higher than 30 dB.

2.2. Pitch statistics

Pitch, i.e. the fundamental frequency (F0) curves of speech files were estimated using the Voicebox function *v_fxpefac* [11]. Figure 3 presents their mean, standard deviation and median F0, as well as the exercise-level mean. Overall, these pitch statistics indicate that there was no significant change in neither mean F0 nor its variation across the exercises. The grand mean F0 is slightly under 210 Hz with a standard deviation of 36 Hz.
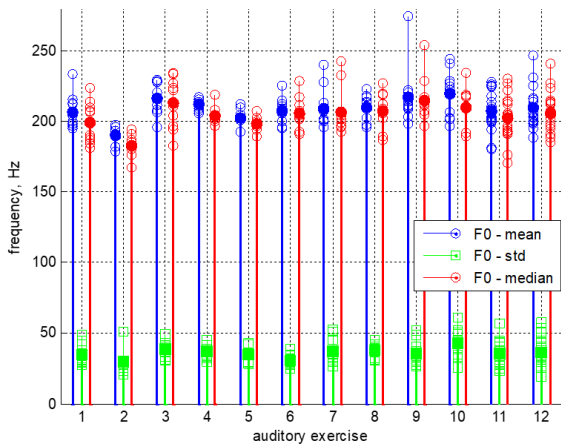
Fig. 3. Mean, standard deviation and median of the F0 curves. Filled symbol denotes the corresponding exercise-level mean

2.3. Phonetic content

Figures 4, 5, and 6 present the distributions of phonetic content of the speech files, based on the phoneme classes defined in Table 1. In the upper part of Figure 4, the distributions are quite similar across the files since all of them contain text "vidimo se u", whereas the other part of speech material consists mostly of mid and mid-high

phonemes. A higher level of similarity between the phonetic content distributions can be observed in Figure 5, where around 50 % of the phonemes belong to the class the sentence had previously been labelled with. Finally, for the recordings of words, the distributions presented in Figure 6 show larger variation due to a smaller total number of speech sounds present in the recordings, but, at the same time, it should be noted that the percentage of the phonemes that belong to the word label class is, on average, higher than in the former figure.
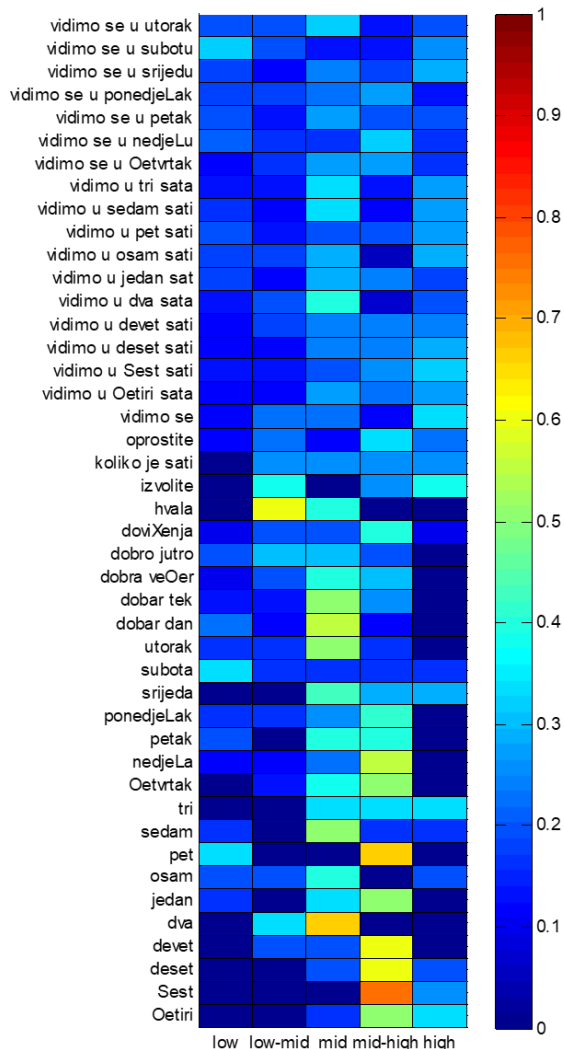
Fig. 4. Distributions of phonetic content of the speech files of the first five auditory exercises. Due to Matlab limitations, the following notation was used for a phoneme subset: /lj/ as /L/, /nj/ as /N/, /č/ as /O/, /ć/ as /C/, /ž/ as /Z/, /š/ as /S/, /dž/ as /D/, and /đ/ as /X/
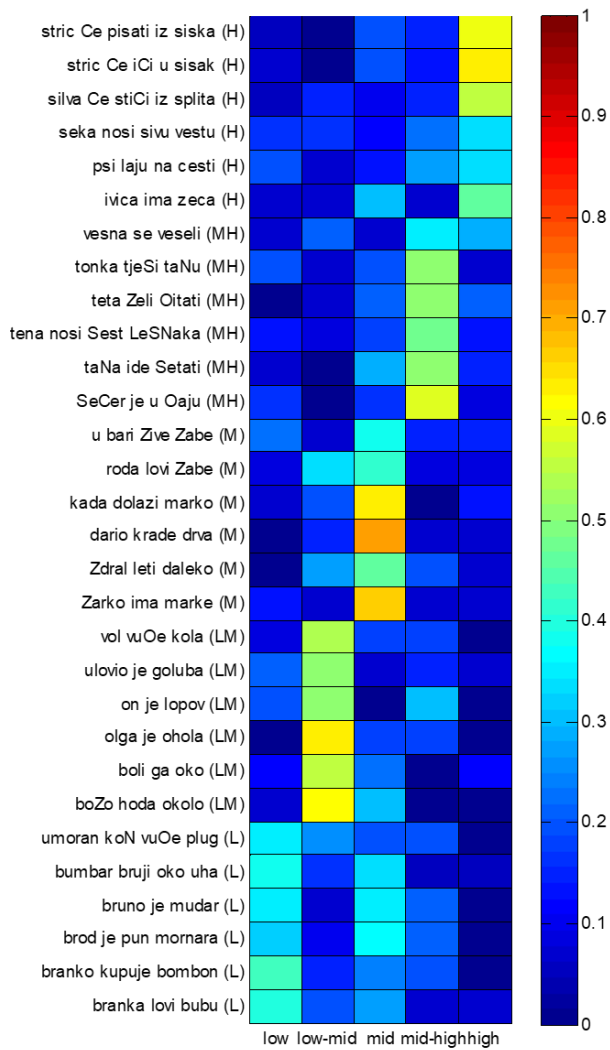
Fig. 5. Distributions of phonetic content of sentences saturated with phonemes of one class
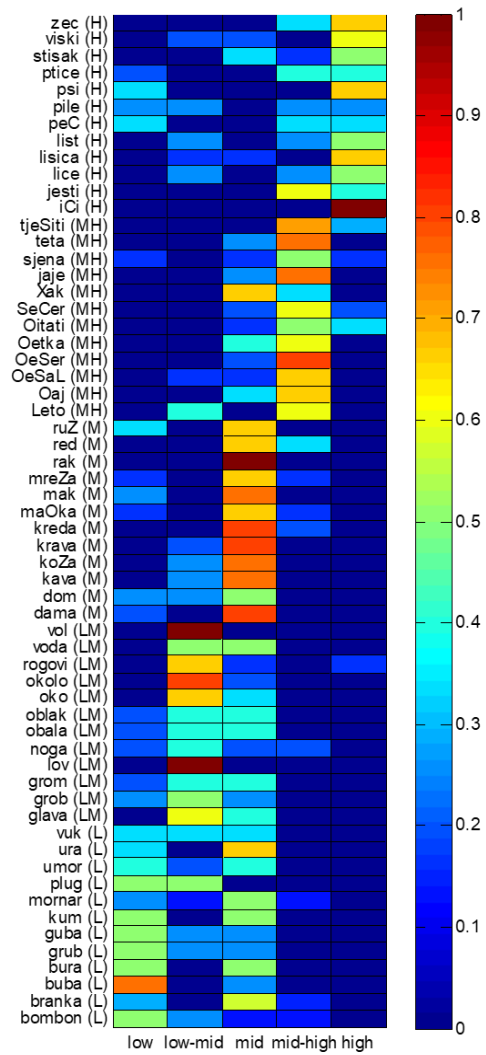
Fig. 6. Distributions of phonetic content of words saturated with phonemes of one class

Figures 7, 8, and 9 show the phonetic content dissimilarity (PCD) matrices for pairs of speech recordings, where the dissimilarity is calculated as the ratio of the number of phonemes that the longer utterance (i.e., the one with the higher speech sounds count) does not share with the shorter utterance and the total number of speech sounds present in the longer utterance. In case the utterances are of equal length, we calculate the PCD based on the second utterance's data.

To illustrate the suitability of this dissimilarity measure, we calculate its value for the pair of words "jedan" and "nedjelja" - the latter, longer word contains 7 speech sounds, of which one /e/ is not shared with the first word, as well as the phoneme /lj/, resulting in a PCD of 0.286, as shown in Figure 7. In the same Figure, the phonetic overlap that occurs for the recordings containing text "vidimo se u" is clearly visible (dissimilarity being low). Also interesting to notice are the results for the word "hvala", a utterance very dissimilar in its phonetic content to other utterances present in the first five auditory exercises, the only exception to this being the utterance "dva", as confirmed with the proposed measure.

The trends observed in Figures 5 and 6 can now be, even more easily, discerned in Figures 8 and 9. The phonetic content dissimilarity of the utterances labelled with the L class and other classes increases from left to right (and bottom to top) in both matrices. Even though these two matrices share a similar pattern, the overall PCD is higher for the latter matrix as words contain a smaller number of speech sounds than sentences, which consequently reduces the probability of phoneme overlap.

Fig. 8. Phonetic content dissimilarity matrix of sentences saturated with phonemes of one class
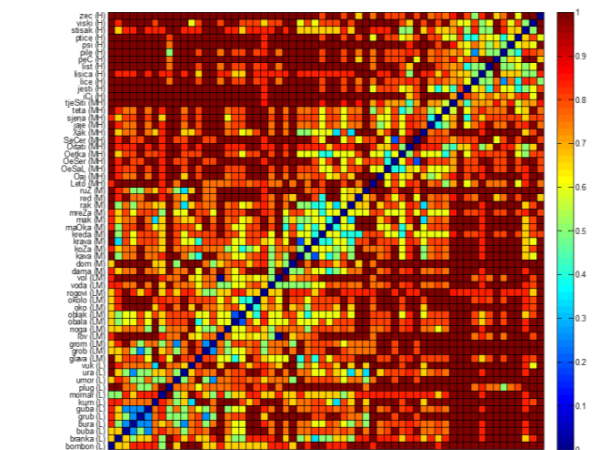
Fig. 9. Phonetic content dissimilarity matrix of words saturated with phonemes of one class

Fig. 7. Phonetic content dissimilarity matrix of the speech files of the first five auditory exercises

2.4. Long-term average spectrum

Figures 10, 11, and 12 show the long-term average spectrum (LTAS) [14] of the speech files obtained using a sliding 50 ms long Hamming window with 75 % overlap, and smoothed with a 1/20 octave Gaussian window [15]. It can be observed that the LTAS varies across the files depending on their phonetic content. To illustrate this, one can examine the LTAS of two utterances that differ in only one phoneme – "devet" (nine) and "deset" (ten) in Figure 10. The former utterance contains the voiced approximant /v/, whereas the latter one the voiceless fricative /s/ [16, 17, 18]. Due to the manner of its production, fricative /s/ is a sibilant speech sound of high energy [19], so that in the 5 - 10 kHz region the word "deset" contains considerably more energy than the word "devet".

The remaining Croatian sibilants /c/, /z/, /č/, /ž/, and /š/ [19] also generate large LTAS values in the region above 2 kHz, for example in the words "šest", "četiri", and "četvrtak". Similar LTAS shapes can also be observed in Figures 11 and 12, whenever a utterance contains one or more sibilant speech sounds.

Fig. 11. Long-term average spectrum of sentences saturated with phonemes of one class

Fig. 10. Long-term average spectrum of the speech files of the first five auditory exercises
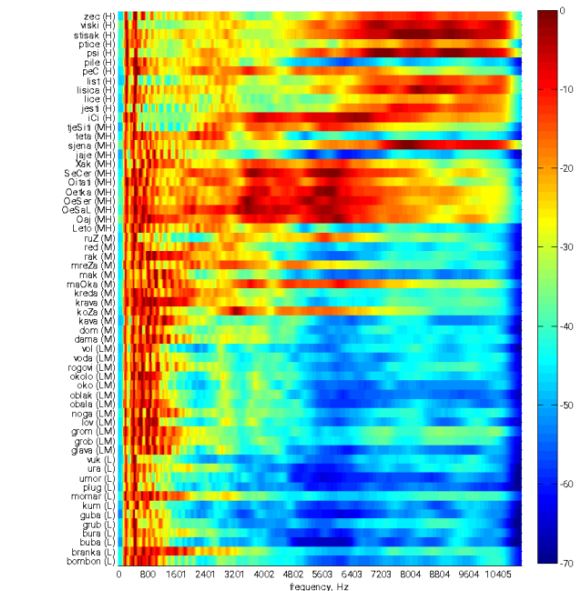
Fig. 12. Long-term average spectrum of words saturated with phonemes of one class

To describe the differences in LTAS observed in Figures 10, 11, and 12 with a single number, we calculate the log-spectral distance (LSD) between LTAS pairs using the following formula:

$$LSD = \sqrt{\frac{1}{2\pi} \cdot \int_{-\pi}^{\pi} [LTAS_1(\omega) - LTAS_2(\omega)]^2 \mathrm{d}\omega}$$

As can be seen in Figures 13, 14, and 15, this measure successfully captures the differences. Due to the presence of sibilants, the pairs of previously mentioned utterances from Figure 10 have small LSDs in Figure 13.

In Figure 14, smaller intra-class and larger inter-class LSD can be observed for the sentences. As expected, for the speech files of the first class (L), the LSD increases from left to right (and bottom to top). An interesting exception to this are the utterances "umoran konj vuče plug" and "božo hoda okolo" whose LTAS is closer to the LTAS of the M and MH class utterances due to presence of the sibilants /č/ and /ž/.

Finally, the LSD matrix for the auditory exercises containing words is presented in Figure 15. Again, inter-class LTAS similarity can be noticed, although now with a higher degree of similarity between the utterances labelled with L, and LM, and M classes than observed in Figure 14.

Fig. 14. Log-spectral distance matrix of sentences saturated with phonemes of one class
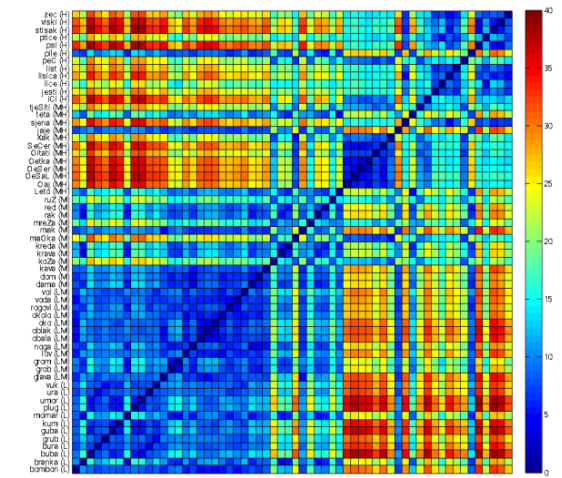
Fig. 15. Log-spectral distance matrix of words saturated with phonemes of one class

Fig. 13. Log-spectral distance matrix of the speech files of the first five auditory exercises

2.5. Relationship between PCD and LSD

In this section, we explore the relationship between the PCD and LSD. To this end, use only the PCD and LSD data obtained for the pairs of utterances that contain the same number of speech sounds. Figures 16 and 17 show the scatter diagrams in which the number of speech sounds is colour coded. Even though the relationship between PCD and LSD for utterances with five or less speech sounds is blurry, it becomes more clear as the number of speech sounds increases. Observed blurriness can be attributed primarily to a lack of manner of sound production class encoding in the PCD measure. For example, even though the phonemes /t/, /e/, and /š/ belong to the same class (MH), their spectral profiles differ due to the manner of their production [17]. The effect of this lack of encoding slowly decreases as the number of speech sounds in a utterance increases.

3. INSTRUMENTAL MUSIC

The tinnitus therapy part of the program contains instrumental music pieces of five genres - pop, rock, electronic, classical, and old time, downloaded from the *freemusicarchive.org* web page. In accordance with the TMNMT therapy principles, music files were filtered in Praat [20] using octave wide notch filters. In order to reduce the program complexity while retaining a perceptually appropriate resolution of tonal tinnitus frequencies [21, 22], the notch filter centre frequency corresponds to one of the ISO 266 standard one-third octave band centre frequencies in the 2 - 10 kHz range [23]. The user first identifies the frequency that most closely matches their tonal tinnitus frequency among the aforementioned centre frequencies, after which they can download the suitably filtered music files.

3.1. Long-term average spectrum

In Figure 18 we present the LTAS of the music files obtained using a sliding 50 ms long Hamming window with 50 % overlap. It can be noticed that the spectral profiles differ considerably. To quantify these differences, in Figure 19 we present the corresponding LSD matrix. Two clusters can be detected - the first one for the pop, rock and electronic music pieces, and the second one for the pieces of the remaining two genres. Interestingly, the

variation in LSD is quite small in the first cluster, whereas the more diverse spectral profiles observed for the classical and old time music pieces in Figure 18 are a direct result of a more diverse instrumentation utilised in these genres than in the former ones. Specifically, the files 29, 31, 34, 36, 39, 40, and 42 - 45, that differ most significantly from the files of the first three genres, are all either piano or guitar solo pieces, whereas the remaining pieces are performed by ensembles of different instruments, and therefore more similar to pieces of the first cluster.
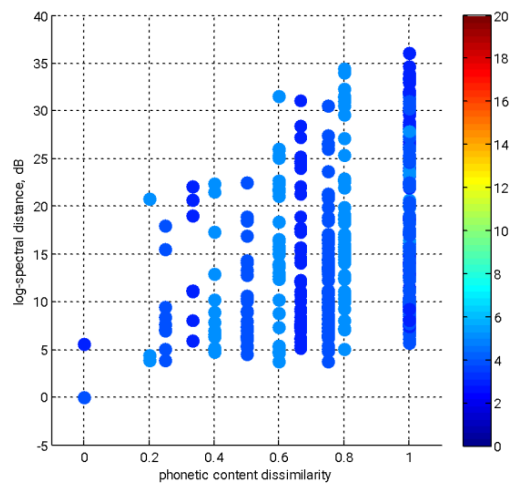

Fig. 16. Relationship between PCD and LSD for pairs of utterances consisting of five or less speech sounds. The number of speech sounds is colour coded
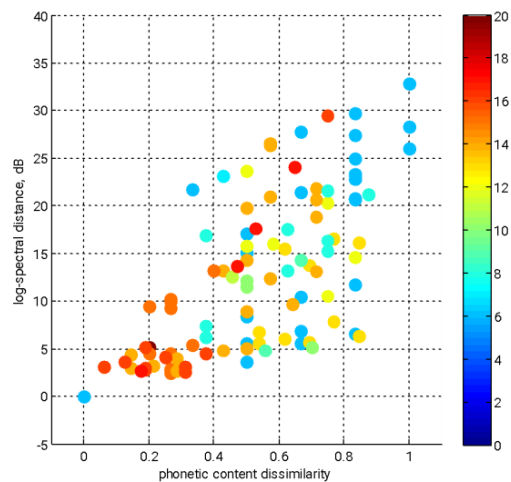

Fig. 17. Relationship between PCD and LSD for pairs of utterances consisting of six or more speech sounds. The number of speech sounds is colour coded
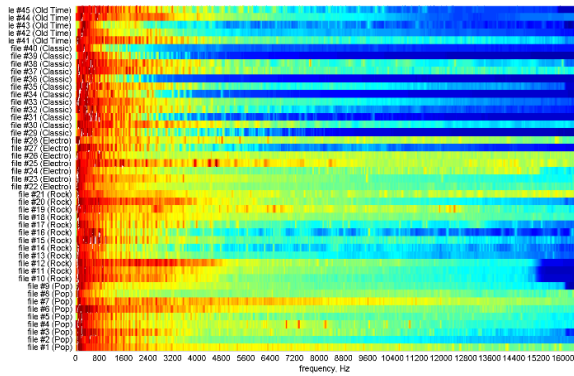
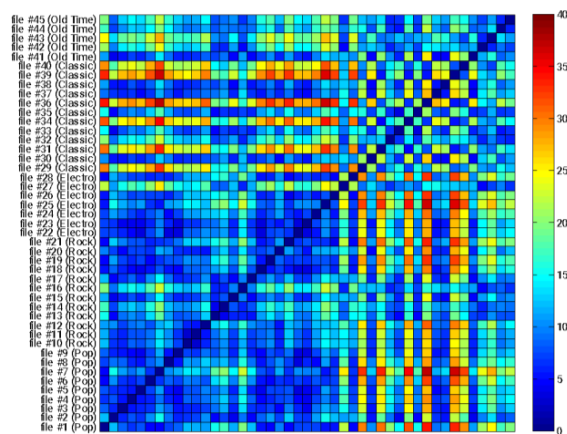**Fig. 18.** Long-term average spectrum of the music files

**Fig. 19.** Log-spectral distance matrix of the music files

4. CONCLUSION

In this paper we have presented a short overview of the "Audio exercises", a computer program for hearing and tinnitus therapy. We have shown that the speech recordings used for hearing therapy are of satisfactory quality, both SNR- and pitch statistics-wise. Furthermore, we also have highlighted the importance of assessing the (dis)similarity of recordings from multiple perspectives - one of them being phonetical, using the newly proposed measure of phonetic content dissimilarity, and the other one spectral, using the log-spectral distance of their long-term average spectra, as they provide complementary insights. Finally, even though music genre is not a deciding factor, the spectra of the instrumental music pieces do indicate that it should perhaps be advised to the tinnitus patients to listen to the music pieces performed by ensembles rather than solo pieces as the former provide richer spectral content.

5. REFERENCES

[1.] **The World Report on Hearing.** Available at: https://www.who.int/publications/i/item/97892400 20481 (Accessed 28 August 2023).

[2.] Reis, M., McMahon, C. M., Távora-Vieira, D., Humburg, P., Boisvert, I. **Effectiveness of Computer-Based Auditory Training for Adult Cochlear Implant Users: A Randomized Crossover Study**, Trends in Hearing, 25, 2021.

[3.] Bonetti, L., Ratkovski, I., Šimunjak, B. **Suvremena rehabilitacija odraslih osoba sa stečenim oštećenjem sluha**, Liječ Vjesn, 139, pp. 292-298, 2017.

[4.] Tuz, D., Isikhan, S. Y. and Yücel, E. **Developing the computer-based auditory training program for adults with hearing impairment**, Med Biol Eng Comput, 59, pp. 175–186, 2021.

[5.] Čulina, M. and Andrijašević, A. **Audiovježbe: računalni program za vježbe slušanja i terapiju tinitusa**, Zbornik Veleučilišta u Rijeci, 11 (1), pp. 331-351, 2023. Available at: https://doi.org/10.31784/zvr.11.1.18

[6.] Okamoto, H., Stracke H., Stoll W. and Pantev C. **Listening to tailor-made notched music reduces tinnitus loudness and tinnitus-related auditory cortex activity**, Proceedings of the National Academy of Sciences, 107(3), pp. 1207–1210, 2010.

[7.] Guberina, P. **Govor i čovjek: Verbotonalni sistem.** Poliklinika za rehabilitaciju slušanja i govora SUVAG, ArTresor naklada, 2010.

[8.] Guberina, P. **Verbo-tonalna metoda u audiologiji.** Zavod za fonetiku, 1965.

[9.] Rulenkova, L. I. **Kako malo gluho dijete naučiti slušati i govoriti primjenom verbotonalne metode**. Poliklinika SUVAG, 2015.

[10.] **Objective Measurement of Active Speech Level**, International Telecommunications Union (ITU-T), Recommendation P.56, 1993.

[11.] Brookes, D. M. **VOICEBOX: A speech processing toolbox for MATLAB**, Available at: http://www.ee.ic.ac.uk/hp/staff/dmb/voicebox/voic ebox.html

[12.] Eaton, J., Gaubitch, N. D., Moore, A. H. and Naylor, P. A. **Estimation of room acoustic parameters: The ACE Challenge**, IEEE/ACM Trans. Audio, Speech, and Language Process., 24(10), pp. 1681-1693, 2016.

[13.] Kinoshita, K., Delcroix, M., Gannot, S., Habets, E. A. P., Haeb-Umbach, R., Kellermann, W., Leutnant, V., Mass, R., Nakatani, T., Raj, B., Sehr, A. and Yoshioka, T. **A summary of the REVERB challenge: state-of-the-art and remaining challenges in reverberant speech processing research**, EURASIP Journal on Advances in Signal Processing, 7, pp. 1-19, 2016.

[14.] Rose, P. **Forensic Speaker Identification.** Taylor & Francis, 2002.

[15.] Institute of Sound Recording, University of Surrey. **IoSR Matlab Toolbox.** Available at: https://github.com/IoSR-Surrey/MatlabToolbox

[16.] Horga, D. **Hrvatsko i slovensko /v/ u akustičkoj usporedbi**, in Slovenski javni govor in jezikovno-kulturna (samo)zavest, Obdobja 38. Ljubljana: Znanstvena založba Filozofske fakultete, pp. 27-37, 2019.

[17.] Quatieri, T. F. **Production and classification of speech sounds. In Discrete-Time Speech Signal Processing: Principles and Practice**. Prentice Hall, pp. 55-110, 2001.

[18.] Andrijašević, A. **Effect of phoneme variations on blind reverberation time estimation**, Acta Acustica, 4(1), pp. 1-17, 2020. Available at: https://acta-acustica.edpsciences.org/articles/aacus/abs/2020/01/aacus200001s/aacus200001s.html

[19.] Jelaska, Z. **Fonološki opisi hrvatskoga jezika**. Hrvatska sveučilišna naklada, 2004.

[20.] Boersma, P. and Weenink, D. **Praat: doing phonetics by computer**, version 6.1.55. University of Amsterdam, 2021. Available at: https://www.fon.hum.uva.nl/praat/

[21.] Ueberfuhr, M. A., Wiegrebe, L., Krause, E., Gürkov, R. and Drexl, M. **Tinnitus in Normal-Hearing Participants after Exposure to Intense Low-Frequency Sound and in Ménière's Disease Patients**, Front Neurol., 7(239), pp. 1-11, 2017.

[22.] Pinel, J. P. J. **Biološka psihologija**. Naklada Slap, 2002.

[23.] ISO 266:1997. **Acoustics - Preferred frequencies**, International Organization for Standardization, 1997.
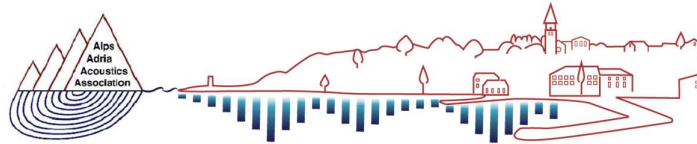
ACOUSTICS KNOWLEDGE ALLIANCE PROJECT: THE DEVELOPMENT OF OPEN-ACCESS INTERACTIVE ONLINE EDUCATIONAL MATERIALS IN ACOUSTICS - STRATEGY AND RESULTS

Marko Horvat[1], Lukas Aspöck[2], Andreas Herweg[3], Kristian Jambrošić[1], Karolina Jaruszewska[4], Manuel Melon[5], Antonio Petošić[1], Yannick Sluyts[6], Thomas Wulfrank[7], Seweryn Zeman[8]

[1]University of Zagreb Faculty of EE and Computing, Unska 3, 10000 Zagreb, Croatia
[2]Institute for Hearing Technology and Acoustics, RWTH Aachen, Kopernikusstraße 5, 52074 Aachen, Germany
[3]HEAD acoustics GmbH, Ebertstraße 30a, 52134 Herzogenrath, Germany
[4]KFB Acoustics Sp. z o.o., Mydlana 7, 51502 Wroclaw, Poland
[5]Laboratoire d'Acoustique de l'Université du Mans, UMR CNRS 6613, Avenue Olivier Messiaen, 72000 Le Mans, France
[6]KU Leuven, Department of Architecture, Campus Brussels and Ghent, Paleizenstraat 65/67, 1030 Brussels, Belgium
[7]Kahle Acoustics, Avenue Molière 188, 1050 Bruxelles, Belgium
[8]Jazzy Innovations Sp. z o.o., ul. Zygmunta Starego 22/42, 44100 Gliwice, Poland

Abstract: *In 2020, an interdisciplinary consortium made up of four universities and four companies started the Acoustics Knowledge Alliance (ASKNOW) project funded by the Erasmus+ Programme of the European Union, with the goal to develop freely accessible, online, interactive educational materials in five fields of acoustics, to be accessible and available on the already established Acoustic Courseware (ACOUCOU) online platform. The mission and the vision of the consortium was to bring this knowledge closer to educators, students, professionals in acoustics, but also specialists in other fields, as well as lay people. In particular, the materials were developed in the fields of acoustic fundamentals, psychoacoustics, acoustic simulations and auralization, electroacoustics, and room and building acoustics, to be grouped in five corresponding online courses. The building units that form the developed materials are lessons and practical cases with a theoretical part that gives the underlying theory, a principle part that illustrates the phenomenon being presented, and a task part that contains one or more tasks to be solved. The process of developing educational materials that will reach out to users and present the knowledge in an interesting and captivating way is complex and multidimensional, requiring an interdisciplinary approach. The intent of this paper is to present and discuss the key aspects of the development process. Moreover, as the project has reached its end, the paper will also present the overview of the content that has been developed, with selected examples of the developed materials in their final, ready-to-use form.*

Keywords: acoustics, online learning, open courseware, interactive material

1. INTRODUCTION

In modern times, technology and knowledge change and grow faster and faster, thus imposing the need of life-long and fast learning on professionals and specialists in their respective fields. Being fairly inert by nature, the educational institutions have considerable difficulties to keep up with these changes. They base their curricula on providing a knowledge basis to build on, but often neglect the problem-solving approach to gaining knowledge.

The COVID 19 pandemic has forced the educators to switch to online learning through different means: online

live lectures, pre-recorded material, online platforms, etc., and the high-speed data transfer enabled this transformation.

Fast changes in technology are a challenge to many people who struggle to follow these changes. For this reason, many avoid any kind of contact with the so-called STEM field (science, technology, engineering, and mathematics). As a part of STEM, acoustics seems to share the fate of other STEM disciplines.

A few years ago, a group of enthusiasts decided to tackle this situation by creating the Acoustic Courseware (ACOUCOU) platform [1], through which they would disseminate the knowledge in selected fields of acoustics to different target groups such as students and their teachers, professionals, but also to lay people who want to learn about acoustics. The knowledge is presented in form of freely accessible online materials developed over the course of several projects: the Architectural Acoustics Multibook (ArAc Multibook), the Acoustic Course for Engineers (ACE) and the Acoustic Course for Industry (ACI). More information on the platform itself and on the currently available materials is given in [1-4].

The Acoustics Knowledge Alliance (ASKNOW) project [5], funded by the European Union's Erasmus+ Knowledge Alliances programme, is the newest addition to the ACOUCOU platform. Eight partners take part in the project and form the project consortium, i.e. four higher education institutions and four small and medium enterprises. The project consortium is supported by outside partners. The outcome of this project are the freely accessible online teaching materials developed to provide fundamental knowledge in five fields of acoustics, namely Acoustic fundamentals, Psychoacoustics, Acoustic simulations and auralization, Electroacoustics, and Room and building acoustics.

As one of the project goals is to disseminate its existence and purpose to a wide range of audience, the status of the project and its progress and results have already been reported using different means of dissemination, which include the already published journal and conference papers [6-11].

In this paper, the aim of the authors is to present the working strategy that has been adopted and carried out over the course of the project to ensure a smooth and fruitful creative process. Since the project has already ended, the authors would also like to show representative examples of the developed online courseware for each of the five courses that cover the corresponding topics. The materials are in their final form and are ready to be tested and perfected before being presented to the public.

2. THE KEY ASPECTS OF THE DEVELOPMENT PROCESS

2.1. General aspects

As stated in the introduction, the work within the ASKNOW project was divided between eight partners, as detailed in the affiliation list. Four of them are universities, and the remining four belong to the business world and deal with acoustic consultancy and product development. In addition, the project employed a number of associated partners who collaborated with the project consortium in all aspects of the development process.

The work was divided into thirteen work packages with the tasks to: prepare guidelines for developing the educational materials, manage the project and ensure smooth execution, develop raw material in five different topics, compile all raw material and even it out with regard to form, to develop the courseware in its final form, to test the courseware and make appropriate adjustments, to deal with quality assurance and evaluation, and to disseminate the results of the project.

To ensure a smooth execution of the project, many forms of communication were established. Since the project was running almost entirely during the COVID-19 pandemic, the number of live meetings had to be reduced to a bare minimum. Instead, fruitful communication was achieved using electronic forms of communication, such as the Mattermost portal and numerous online meetings executed using available audio/video conferencing tools.

The progress of the project and its timely execution were monitored via an online progress chart in which the progress of each work package was recorded, with the emphasis on the ones that dealt with the development of courseware material in both raw and final form.

The workflow designed for the development of the educational materials is illustrated in Figure 1. In the preparation stage, the main task was to prepare guidelines and templates that will be used for the development of raw material. Once developed by experts from universities and companies, it was collected and analysed by teams of designers, who unified the appearance of the material and designed the appropriate

user interfaces to evoke the best user experience. The work was then taken on by programmers who implemented the proposed solutions and adjusted the material for successful use by end users. The material was repeatedly tested and adjusted based on the received feedback, to yield the final product.
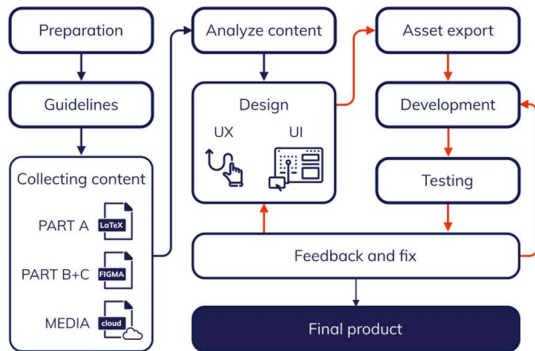

Fig.1. The workflow designed for the execution of the ASKNOW project

Special attention was paid to the quality of the developed material, which went through numerous stages of testing and reviewing, as illustrated in Figure 2.
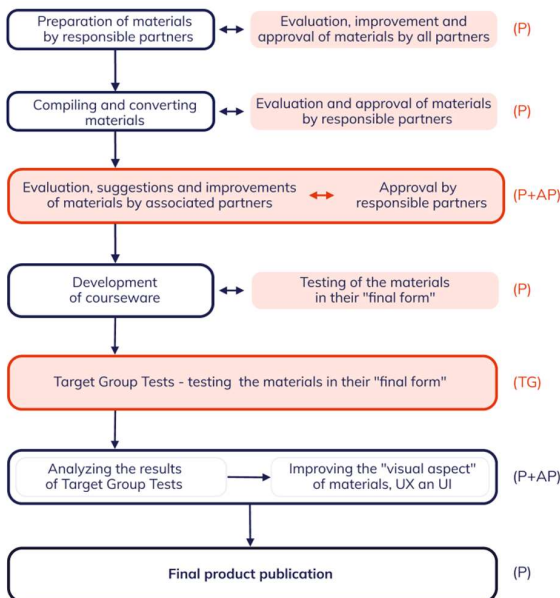
Fig.2. The flowchart of the testing and reviewing process implemented during the ASKNOW project

The partners involved in developing the educational materials had a crucial role in the reviewing process, in which they were involved from the very start to the final publication of the finished product. Internal reviews were intensively conducted during the preparation of raw material and its compilation and conversion to its final form, as well as during and after the testing had been done. Apart from internal reviewing, the material was reviewed by external reviewers and tested by members of target groups for which the product is primarily intended.

2.2. The structure of the educational materials

As stated above, the educational materials cover five different topics. Therefore, the logical development was to form as many self-sufficient online courses, each of which covers one topic. Due to their modular nature, these courses can be used as a whole, or selected modules / lessons can be utilized to enhance the teaching / learning process.

To achieve modularity, the educational materials are divided into lessons, each of which covers a single elementary particle of knowledge. Each of the five topics is covered with thirty such lessons. On top of this, each course contains two practical cases that show common issues, and present ways of solving these issues that stem from the knowledge covered by the lessons.

Each lesson consists of three parts. The theory part (part A) uses textual information complemented with equations, figures, and tables to explain the phenomenon covered by the lesson. The principle part (part B) presents the phenomenon through different kinds of audio-visual learning content such as charts, animations, interactive calculations, videos, sound samples one can listen to, etc., or a combination of them. The task part (part C) encourages the user to solve one or more short tasks, which can assume different forms, such as questions with multiple-choice answers, calculation tasks, grouping of images or other objects into appropriate categories, listening to sounds and deciding how they fit certain criteria, etc.

The layout of the lessons that has been devised and implemented in the online materials is shown in Figure 3. The main intent is to have the theory part displayed side by side with the principle part (and the task part), so that the user has access to both while studying the phenomenon covered by the lesson. The theory part consists of scrollable text the user can browse through. The principle part consists of one or more states that are

interlinked and can be called with navigation buttons or by changing the values of parameters in a way that is the most appropriate for the content being shown. For example, if a phenomenon is illustrated with four parameters, each of which can have two values, this yields a total of 16 different states. Each state is automatically called simply by changing the value of a single parameter.
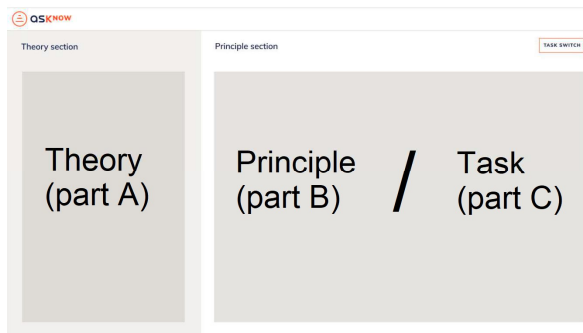

Fig.3. The layout of a lesson adopted for the developed educational materials

3. AN OVERVIEW OF THE DEVELOPED CONTENT

This section provides a short overview of the content that has been covered in the five selected topics and developed for the five corresponding courses. The courses are divided into logical subsections containing one or more lessons.

3.1. Acoustic fundamentals

This course presents the fundamental concepts in acoustics as the theoretical basis for other fields of acoustics.
The first section illustrates the fundamentals of sound and waves / 1D acoustics (tubes) via these lessons: 1 - Definition, what is a wave, speed of sound, physical quantities involved, order of magnitude; 2 - 1D equations of acoustics; 3 - Solutions of acoustic equations in the time domain; 4 - Equation of acoustics and their solutions in the frequency domain – stationary waves, SWR; 5 - Reflection; 6 - Transmission and reflection; 7 - Impedance; 8 - Proper frequencies and modes; 9 - Acoustic intensity and losses.
The second section deals with 3D waves and sources and consists of the following lessons: 10 - 3D equations of acoustics; 11 - Plane wave in 3D; 12 - Snell-Descartes laws;

13 - Spherical wave and pulsating sphere; 14 - Monopole, dipole, and quadrupoles; 15 - Solutions of wave equation in spherical coordinates; 16 - Radiation of a plane surface; 17 - Diffraction.
The third section presents the behaviour of waveguides and cavities through the following lessons: 18 - Boundary conditions and degrees of freedom; 19 – Waveguides; 20 - Modes in a cavity; 21 - Resonance in a cavity.
The final section collects miscellaneous topics that help the user grasp basic concepts of acoustics. For this, the following lessons were developed: 22 - The dB scale; 23 - Sources summation, 24 - Image sources, 25 - Dispersion, group and phase velocity; 26 – Dissipation; 27 - Surface impedance of materials; 28 - Transmission lines and analogies; 29 - Matricial formalism for waveguides; 30 - Horns.

3.2. Psychoacoustics

This course is focused on the underlying phenomena related to human perception of sound and tries to illustrate the applications derived from them.
The first section presents the human hearing system via these lessons: 1 - Anatomy of the ear; 2 - Signal processing of sound by humans; 3 - Bark bands (critical bands); 4 - Masking effects; 5 - Hearing threshold (How it is measured / age-related changes).
The second section deals with psychoacoustic parameters through the following lessons: 6 - Introduction to psychoacoustics; 7 - Loudness; 8 - Roughness and fluctuation strength; 9 - Tonality; 10 - Sharpness.
The third section is oriented on binaural hearing and measurements. It consists of these six lessons: 11 - Introduction to binaural hearing; 12 - Sound source localization; 13 - Head-related transfer function; 14 - Hearing models; 15 - Binaural recording and measurement; 16 - Equalization.
The fourth section illustrates the intricacies of speech production and speech intelligibility using these lessons: 17 - Speech production; 18 - Lombard speech; 19 - Speech in reverberation and noise; 20 - Binaural unmasking; 21 - Assessment of speech intelligibility (C50, D50, U50, STI).
The fifth section covers the field of psychoacoustic listening tests procedures via these five lessons: 22 - Introduction to listening experiments; 23 - Design of listening experiments; 24 - Common experimental methods (common listening test procedures); 25 -

Statistical evaluation of listening experiments; 26 - Sound system quality evaluation testing.

The final section strives to explain additional perception-related phenomena and contains the last four lessons: 27 - Perception of space, rooms, and distance; 28 - Introduction to the soundscape approach; 29 - Perceptual evaluation of noise; 30 - Auditory illusions.

The two practical cases give examples of how the presented concepts are used practical, real-life applications. The first case presents the process of producing aurally correct recordings to be used in listening tests designed for sound quality evaluation. The second case presents the design of a listening experiment that investigates the localization of sound sources.

3.3. Acoustic simulations and auralization

This course covers the field of acoustical simulations and auralization that stems from them and has proven to be an invaluable tool that helps us gain understanding about a range of phenomena by direct perception (listening).

The first section offers an introduction to this field via five lessons: 1 - Introduction and overview of acoustical simulation; 2 - Impulse responses; 3 - Convolution; 4 - Fourier transform; 5 - Discrete processing.

The second section focuses on the fundamentals of room acoustic simulations and consists of the following lessons: 6 - Geometrical acoustics; 7 - Prediction of reverberation time; 8 - Image source model; 9 - Ray tracing; 10 - Radiosity methods; 11 - Wave-based models.

The third section introduces the models used in noise control and sound design through the following lessons: 12 - Environmental sound propagation; 13 - Airborne sound in buildings; 14 - Impact sound in buildings; 15 - Binaural transfer path analysis.

The fourth section is oriented on auralization and introduces this technique via these lessons: 16 - Binaural synthesis; 17 - Synthesis of room impulse responses; 18 - FIR convolution; 19 - Real-time convolution.

The fifth section presents the techniques of sound reproduction and consists of these five lessons: 20 - Headphones; 21 - Binaural loudspeaker reproduction; 22 - Stereo and vector-base amplitude panning; 23 - Panning techniques and object-based audio; 24 - Ambisonics.

The last section discusses the applications and evaluation of simulations via these lessons: 25 - Architectural design; 26 - Noise mapping; 27 - Application of simulation and auralisation in research; 28 - Uncertainties of simulations; 29 - Interactive VR systems; 30 - Perceptual evaluation.

The first practical case displays a common topic in architectural acoustics, i.e. it investigates the degree to which the acoustic simulations of a closed space agree with actual measurements. The second practical case exhibits how the binaural transfer path synthesis technique can be applied to a car simulator.

3.4. Electroacoustics

Electroacoustics is a specific field as it involves both electrical engineering and acoustics. Moreover, it ties together the electrical, mechanical, and acoustical domain.

The course is divided into seven sections, and the first one is a refresher of sorts, as it covers the background knowledge required to successfully follow this course via these lessons: 1 - Introduction to electroacoustics; 2 - Basics of electricity; 3 - Mechanics: damped harmonic oscillator; 4 - Acoustical circuits; 5 - Mechanical-acoustical-electrical analogies; 6 - Radiation of simple acoustic sources.

The second section is focused on the characterization of audio systems through two lessons: 7 - Linear characteristics of transducers; 8 - Transducer limitations.

The third section introduces commonly used transduction principles and consists of three lessons: 9 - Electrodynamic transduction; 10 - Electrostatic transduction; 11 - Acoustical-mechanical transduction.

The fourth section deals with the modelling of transducers via the following lessons: 12 - Electromechanical source: the shaker; 13 - Electromechanical sensor: the geophone; 14 - Directive microphones; 15 - Electrodynamic microphone; 16 - Electrostatic microphone; 17 - Unidirectional electrodynamic microphone; 18 - Electrodynamic moving coil loudspeaker; 19 - Thiele & Small parameters: theory and measurement.

The fifth section illustrates the most common loudspeaker enclosures and systems and consists of the following lessons: 20 - Closed box system; 21 - Vented box system; 22 - Other types of enclosures; 23 - Multichannel speaker systems.

The sixth section explains advanced modelling techniques of loudspeaker systems and is composed of three lessons: 24 - T&S model limits; 25 - Advanced parameters estimation; 26 - Loudspeaker nonlinearities.

The final section deals with multi-transducer designs via these lessons: 27 - Microphone arrays; 28 - Loudspeaker arrays; 29 - Personal sound zones; 30 - Playback systems. The first practical case demonstrates the design of a two-way loudspeaker system. The second practical case shows the measurements that are made on a loudspeaker driver.

3.5. Room and building acoustics

This course deals with the overall acoustic comfort of closed spaces by addressing its three key components. The first one is room acoustics, which strives to provide acoustic conditions within a room that suit its size and purpose. The second one is building acoustics, which provides protection from sound coming from adjacent spaces, but also protects these spaces from sound generated in the room. The third one is internal noise emitted by noise sources within the room itself.

The course is divided into two large sections. The first one covers room acoustics, and the second one deals with building acoustics and noise. Since there is a commonly spread confusion and misconception about the difference between room acoustics and building acoustics, the course starts with an introductory lesson: 1 - What is the difference between room acoustics and building acoustics?

The section on room acoustics contains the following lessons: 2 - How a room responds to sound; 3 - Acoustic treatment - absorption, reflection, and diffusion; 4 - Volume and shape of the room and their influence on room acoustics; 5 - Reverberation time; 6 - How a sound source interacts with a room; 7 - How loudspeakers interact with rooms; 8 - Acoustic elements - absorbers; 9 - Acoustic elements - diffusers; 10 - General requirements for good acoustics; 11 - Objective and subjective parameters in room acoustics; 12 - Room and building acoustics design criteria; 13 - Single-speaker and multi-speaker environments; 14 - Acoustics of spaces for music; 15 - Room acoustic design elements at the disposal of architectural design.

The section on building acoustics (and noise) is composed of these lessons: 16 - Airborne and impact sound, direct and flanking transmission; 17 - Sound reduction index for simple and composite structures; 18 - Single-leaf and double-leaf walls; 19 - Floors and ceilings; 20 - Facades: curtain walls; 21 - Doors and windows; 22 - Measurement and evaluation of airborne and impact sound insulation;

23 - Acoustic classification of sound insulation; 24 - Examples of good and bad constructions and workmanship practice; 25 - Influence of absorption on sound insulation (or how room acoustics influences building acoustics); 26 - Materials in practice; 27 - Towards more sustainable and low-energy produced materials for buildings; 28 - Special construction types using vibration isolation; 29 - Background noise and the sources contributing to it; 30 - Practical approaches for innovative, sustainable, and cost-effective buildings.

As acoustic comfort depends on all three of its components, the two practical cases are joined into one that deals with acoustic comfort in a comprehensive manner, as illustrated with a number of practical examples embedded into the structure of the practical case. The intent is to display how the principles of room and building acoustics are used in real-life situations on different building designs.

4. SELECTED EXAMPLES OF DEVELOPED MATERIALS

This section displays some examples of the developed educational material. The material is presented in the ready-to-be-published form, after being redesigned by the graphic designers. As the interactive components cannot be displayed, the material is presented as images that depict only the layout and static content. The full interactivity of the courseware material can be explored on the ACOUCOU platform site [1,5]. The theory parts (part A) of the lessons are not shown here, as they are of classic design, i.e. based on text complemented with figures, tables and equations. Instead, examples of the principle (part B) and task (part C) parts have been chosen from lessons in all five courses, as they reflect the creativity displayed by their authors during the design process.

Examples of the principle parts of selected lessons are shown in Figures 4 to 8, while the task parts of the selected lessons are displayed in Figures 9 to 13.

The principle part shown in Figure 4 allows the user to choose between a shoebox, cylindrical, and spherical cavity of predefined dimensions. The pressure distribution of different modes can be observed both on the boundaries of the cavity and inside it by changing the number of nodes in appropriate axes. The frequency of the mode is displayed as well.
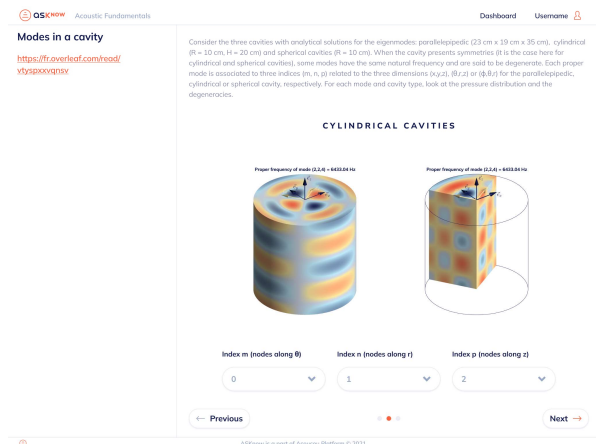
AAAA – 2023 – IZOLA - Conference Proceedings

Fig.4. The principle part of the lesson on modes in a cavity

Fig.6. The principle part of the lesson on convolution

The principle part shown in Figure 5 allows the user to perceive the width of Bark bands (critical bands) by listening. At low frequencies, a shift of 100 Hz is equal to 1 Bark, whereas the same shift at high frequencies (from 6400 to 6500 Hz) is equivalent to only 1/13 of a Bark.

The principle part shown in Figure 6 illustrates the technique of convolution. The user can change the reverberation time of an imaginary room, and a corresponding impulse response is generated through simulation. The impulse response of the room is convolved with a dry audio signal. The resulting audio signal sounds as if it was recorded in the simulated room, and the user can listen to both the original sound and the convolved sound and compare them, thus evaluating the effect of convolution.

The principle part shown in Figure 7 illustrates the modelling of the acoustic circuit that represents an open, empty wine bottle. The bottle is first modelled using a cavity (body of the bottle) with an elongated opening (bottleneck), and exact dimensions of the two parts are measured and input into the model. Using the appropriate formulae, one can calculate the theoretical resonance frequency of the bottle. The actual resonance frequency of the bottle is measured and recorded, and this sound can be listened to. At the same time, the spectrum of that sound can be checked, and it clearly shows the actual resonance frequency. Finally, length corrections are applied to the measured length of the bottleneck to account for the abrupt changes of the cross-section of the bottleneck at its ends, resulting in a considerably improved prediction of the resonance frequency.

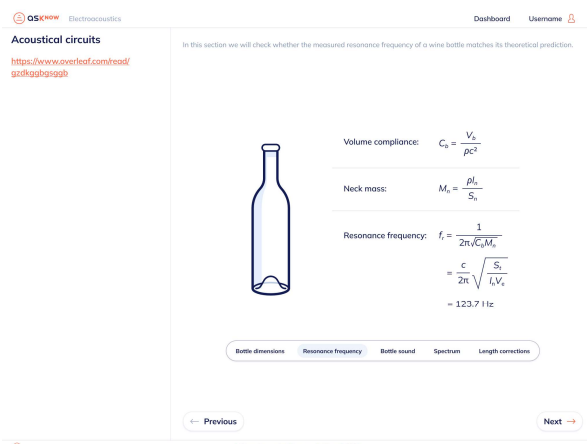**Fig.5.** The principle part of the lesson on bark bands

Fig.7. The principle part of the lesson on acoustical circuits

The principle part shown in Figure 8 allows the user to study the construction of porous and resonant absorbers by changing their configuration. The changes are illustrated by an image of the actual construction, and the calculated frequency-dependent sound absorption coefficient. In case of resonant absorbers shown here, the user can change the thickness and the percentage of perforation of the perforated panel, the thickness of the porous panel, the total width of the gap between the perforated panel and the base wall, and the flow resistivity of the porous material. Each of the five parameters has two distinct values, which enables the user to examine 32 different cases.

Fig.9. The task part of the lesson on resonance in a cavity

Fig.8. The principle part of the lesson on absorbers

Fig.10. The task part of the lesson on loudness

The task part shown in Figure 9 requires the user to figure out which modes in the illustrated cavity (two-dimensional for simplicity) will be excited by the source placed at the marked position (orange dot), and which will not be excited. Five different source placements are given for the same cavity.

The task part shown in Figure 10 requires the user to answer to a question regarding the dependence of loudness on different parameters and effects. This type of tasks is based on multiple-choice questions with one or more correct answers. In this case there are five correct answers.

The task part shown in Figure 11 requires the user to examine a simple mass-spring system that consists of a mass, a spring, and a damper, and is excited with Dirac excitation at $t = 0$. The user needs to determine the correct shape of the impulse response of that system.
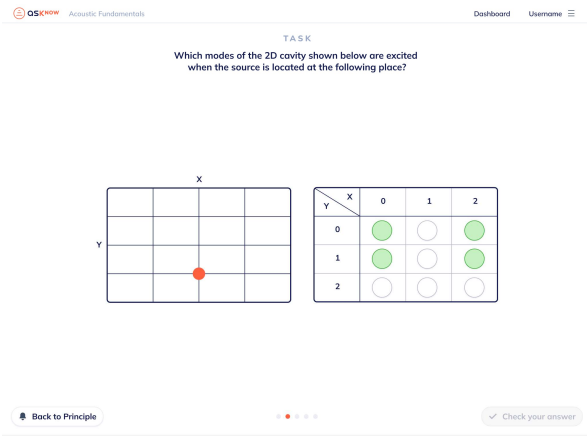

Fig.11. The task part of the lesson on (simulations)

The task part shown in Figure 12 challenges the user to determine the loudspeaker construction, among the four that are offered, which exhibits a bidirectional radiation pattern. The parameters to keep in mind are the physical layout of the loudspeakers, the polarity of the feed signals (for constructions with two loudspeakers), and the relative frequency range of operation determined with the relationship between the physical dimensions of the loudspeakers and the wavelength of the emitted sound wave.

In the task part shown in Figure 13, the user must identify architectural elements designed to modify the acoustics of a room and sort them into appropriate categories according to their dominant behaviour as absorbers, reflectors, diffusers, or sound-transparent elements.
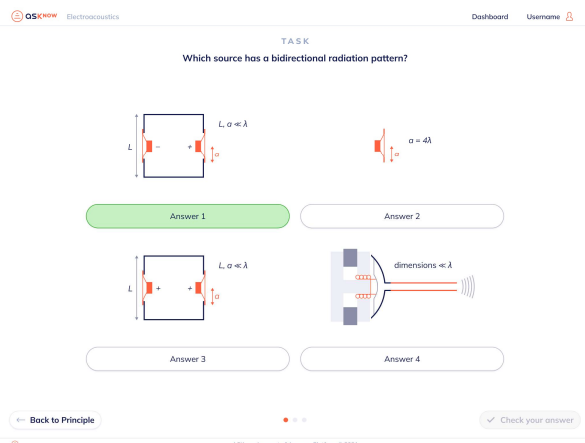
Fig.12. The task part of the lesson on the radiation of simple acoustic sources
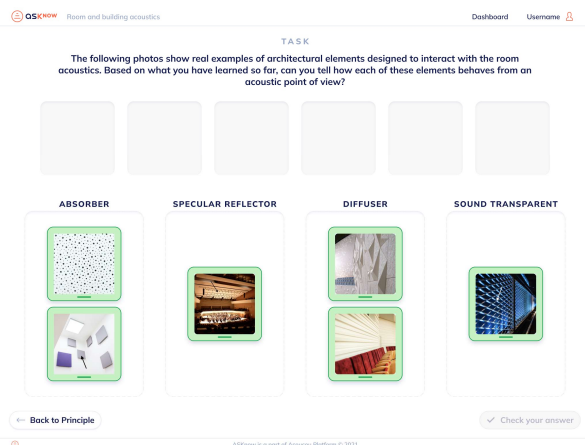
Fig.13. The task part of the lesson on acoustics of spaces for speech

5. CONCLUSIONS

At this moment, the Acoustics Knowledge Alliance (ASKNOW) project, funded by the Erasmus+ Knowledge Alliances programme of the EU, has officially ended. The results of the project reflect the tremendous effort put in by the project consortium over the past three and a half years. The consortium was composed as a symbiosis of the academic and the business world and aided by outside partners. Within the scope of the project, the consortium has successfully developed freely available online educational materials under the CC BY-NC-ND 4.0 license (Creative Commons license) that cover five different topics: acoustic fundamentals, psychoacoustics, acoustic simulations and auralization, and room and building acoustics in as many correspondingly named courses. The developed educational materials are infused with diverse forms of interactive content, thus enhancing the learning experience for the users, and making the process of knowledge transfer both engaging and effective. The primary target groups for which the materials have been developed are students and educators, as well as professionals in the field. As such, the content of the materials is not necessarily trivial, but it is the strong belief of the entire project consortium that they can be used by anyone who already has a basic understanding of acoustics and is interested in improving their knowledge.

6. ACKNOWLEDGMENTS

7. REFERENCES

[1.] **The homepage of the ACOUCOU platform**. Available at: https://acoucou.org (Accessed on 10 July 2023)

[2.] Jaruszewska, K., Barański, F., Piotrowska, M., Melon, M., Dazel, O., Vorländer, M., Aspöck, L., Horvat, M., Jambrošić, K., Rychtáriková, M., Kritly, L. and Herweg, A. **ACOUCOU Platform to Acquire Professional Skills and Knowledge in the Field of Acoustics.**, in Proceedings of the 23rd International Congress on Acoustics, pp. 4348-4355, 2019.

[3.] Jaruszewska, K., Melon, M., Dazel, O., Vorländer, M., Aspöck, L., Wulfrank, T., Jambrošić, K., Horvat, M., Rychtáriková, M., Sluyts, Y., Wojtyla, B., Herweg, A. and Barański, F. **ACOUCOU - online platform including interactive educational materials about acoustics**, in Proceedings of Forum Acusticum 2020, pp. 3023-3024, 2020.

[4.] Jaruszewska, K., Melon, M., Dazel, O., Vorländer, M., Rychtáriková, M., Horvat, M., Wulfrank, T., Herweg, A., Aspöck, L., Sluyts, Y., Jambrošić, K., Carayol, E., Wojtyla, B., Łuczak, M. and Chmelík, V. **The ACOUCOU platform: Online acoustic education developed by an interdisciplinary team**, The Journal of the Acoustical Society of America, 152(3), pp. 1922-1931, 2022.

[5.] **The homepage of the ASKNOW project.** Available at: https://asknow.acoucou.org (Accessed on 10 July 2023)

[6.] Horvat, M., Melon, M., Jaruszewska, K., Wulfrank, T., Sluyts, Y., Herweg, A., Aspöck, L. and Wojtyla, B. **Acoustics Knowledge Alliance (ASKnow) project as the latest addition to the Acoustic Courseware (ACOUCOU) learning platform**, in Proceedings of the 9th Congress of the Alps-Adria Acoustics Association, pp. 160-168, 2021.

[7.] Horvat, M., Jaruszewska, K., Raetz, S., Carayol, E., Sluyts, Y., Herweg, A., Aspöck, L. and Zeman, S. **The development of modern, interactive acoustic courseware material within the Acoustics Knowledge Alliance project**, in Proceedings of the Euroregio – BNAM 2022 Joint Acoustics Conference, pp. 225-234, 2022.

[8.] Melon, M., Sluyts, Y., Heimes, A., Horvat, M., Jaruszewska, K., Herweg, A., Wojtyła, B. and Dalmont, J.-P. **Open access online course in acoustics in the frame of AcouStics Knowledge alliance (ASKnow) project**" in Proceedings of the 16ème Congrès Français d'Acoustique, pp. 1-6, 2022.

[9.] Jambrošić, K., Aspöck, L., Carayol, E., Herweg, A., Horvat, M., Jaruszewska, K., Novak, A., Sluyts, Y. and Wojtyla, B. **The Acoustics Knowledge Alliance project: the most recent addition to the Acoustic Courseware online educational platform**, in Proceedings of Inter-Noise 2023, 2023.

[10.] Jaruszewska, K., Novak, A., Dazel. O., Melon, M., Sluyts, Y., Heimes, A., Jambrosic, K., Kruh-Elendt, A., Carayol, E. and Zeman, S. **Approach to developing online educational materials based on Acoustics Knowledge Alliance (ASKNOW) project**, in Proceedings of Forum Acusticum 2023, 2023.

[11.] Horvat, M., Raetz, S., Lotton, P., Sluyts, Y., Vorländer, M., Petošić, A., Jaruszewska, K., Ray, A., Wojtyla, B. and Wuflrank, T. **Open-access interactive online courseware in acoustics developed within the scope of the acoustics knowledge alliance (ASKNOW) project**, in Proceedings of Forum Acusticum 2023, 2023.
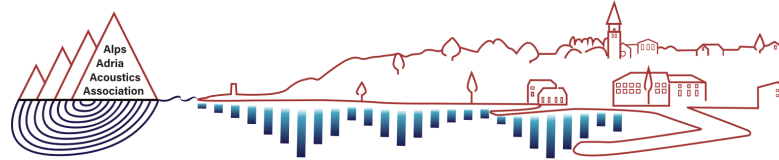
AAAA 2023 IZOLA 20. - 21. September
10th CONGRESS OF THE ALPS ADRIA ACOUSTICS ASSOCIATION

Keynote
Invited speech

Challenges in sound insulation of wooden buildings

Prof. Dr. Jonas Brunskog

Department of Electrical and Photonics Engineering, Technical University of Denmark (DTU)

E-mail: jbru@dtu.dk

Dr. Jonas Brunskog is Associate Professor at the Acoustic Technology group at the Department of Electrical and Photonics Engineering, at Technical University of Denmark (DTU). He is a co-author of 55 scientific journal articles, and more than 110 conference publications. His works have been cited 1960 times (Google Scholar). He has supervised 10 completed PhD theses as main supervisor, and 8 as co-supervisor. Scientific focus areas are: General acoustics, Vibro-acoustics, Building acoustics, Room acoustics, Numerical acoustics, Environmental acoustics, Signal processing, and Voice research.

Adequate sound insulation is important in buildings due to legal, comfort and health reasons, the latter emphasized by WHO. The sound insulation of a single homogenous wall is mainly given by the mass per unit area, the mass law, leaving not much room for improve-ment. Economic pressure as well as environmental demands of increased use of wood in buildings leads to reduced weight, which thus might resulting in poor sound insulation. However, there are also certain aspects that talk in favor for the use of wood constructions. In his lecture, Dr. Brunskog will review the acoustic challenges and possibilities when building with timber constructions. Timber constructions are used in both old traditional floor constructions in many countries, and in new innovative buildings with high sound insulation. Most traditional as well new timber floor constructions are spatially periodic, which will lead to periodic effects such as pass- and stop bands. In other areas of physics and engineering, such aspects are used as metamaterials. Another branch of constructions where innovative ideas are needed and are being used are CLT constructions.

AAAA 2023 IZOLA 20. - 21. September
10th CONGRESS OF THE ALPS ADRIA ACOUSTICS ASSOCIATION

Technical keynote
Invited speech

Design and construction of the InnoRenew CoE Acoustics Laboratory

Assist Prof. Dr. Rok Prislan

InnoRenew CoE

E-mail: rok.prislan@innorenew.eu

Dr. Rok Prislan is research group leader for Buildings and is leading research in the field of acoustics at InnoRenew CoE. Dr. Prislan is also holding the position of an assistant professor at the University of Primorska, where he teaches physics. His main research topics are advanced measurement techniques for sound field characterization and geometrical room acoustic modelling. As part of his career, dr. Prislan was working as an acoustic designer/consultant and has led over 60 projects in the field of acoustics and noise control. Dr. Prislan has two master's degrees, one in physics (mathematical physics) from the University of Ljubljana and one in engineering acoustics from the Technical University of Denmark (DTU).

InnoRenew CoE was established in 2017 as an international research institute with the goal of providing innovation and conducting cutting-edge research in the broad field of sustainable and healthy built environment. In just five years, the institute was built from the ground up by assembling an international team of researchers, investing in state-of-the-art laboratory equipment, and constructing the laboratories. The acoustics laboratory was the most technically challenging laboratory to design and build. In this talk, dr. Rok Prislan, who played a leading role in the design, will present this process. For the newly built reverberation and anechoic chambers, dr. Prislan will provide an overview of the given requirements, explain how the chambers were conceived, what the main design challenges were, and address the uncertainties that arise from the undefined guidelines for the design of such facilities. Dr. Prislan also explains the approaches used in this engineering adventure, including the acoustic modeling methods used to predict and the experimental methods used to evaluate the performance of the chambers. The presentation of the main construction steps is supported by rich photographic and video material.

AAAA 2023 IZOLA 20. - 21. September
10th CONGRESS OF THE ALPS ADRIA ACOUSTICS ASSOCIATION

Contributed papers
Building acoustics

1. Design and construction of a temporary test facility for sound insulation measurements of doors
   Nika Šubic (MK3 d.o.o.)
2. Acoustic performance of buildings, components and materials as a parameter for ecological and social sustainability assessments
   Franz Dolezal (IBO - Austrian Institute for Building and Ecology)
3. Improvement of impact sound insulation with tile underlay materials – impact sound insulation without floating floors
   Beáta Mesterházy (Department of Acoustics of OPAKFI, BME (Budapest University of Tecnology and Economics), Department of Building Constructions, Laboratory of Building Acoustics)
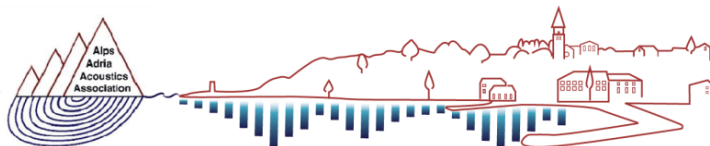
DESING AND CONSTRUCTION OF A TEMPORARY TEST FACILITY FOR SOUND INSULATION MEASUREMENTS OF DOORS

Nika Šubic[1], Andrej Šubic[1], Zdenka Šubic[1], Martin Klun[1], Rok Prislan[2]

[1]MK3 d.o.o., [2]InnoRenew CoE

Abstract: *To fulfill the sound insulation requirements for separating elements in buildings a common concern is reaching sufficient sound insulation of smaller construction elements, such as doors. Besides the construction of the door leaf, achieving quality sealing of the door leaf with the frame and floor is important as well as the on-site execution, which can greatly impact the final sound insulation of the whole separating element. To optimize the design of doors regarding sound insulation, repetitive testing is required which can be time consuming and expensive when performed on a different location by an external contractor. To facilitate the process for a Slovenian company, a temporary test facility was designed on their premises. The test facility was constructed in the existing building of the company using lightweight materials. The design and construction followed the requirements of the ISO 10140 standard, and the finished test facility can test door specimens with sound reduction index values of up to 56 dB.*

Keywords: sound insulation, test facility, measurement, doors

1. INTRODUCTION

Achieving sufficient sound insulation of doors in buildings is a in a common challenge, the main complication usually being inadequate sealing of the door leaf with the frame and the floor, as well as proper installation of the door frame in the separating wall. To improve the existing design of the doors and gain experience with the installation procedure a design of a temporary test facility for sound reduction index measurements was proposed. It was required that the new construction was lightweight since it was placed on the 1st floor of an existing building with structural limitations to sustain excessive loads such as of a concrete structure. Additionally, the lightweight construction can be more easily disassembled when it is not needed anymore. It is difficult to achieve good low-frequency sound insulation with lightweight construction however, it is equally uncommon to expect high values of sound reduction index at low-frequency for small construction elements. For this reason, it was foreseen that a lightweight test facility could be an appropriate solution for measurements of smaller construction elements such as doors and windows.

The paper presents the design and the acoustic characteristics of the completed test facility.

2. DESIGN OF THE TEST FACILITY

The design of the temporary test facility follows the guidelines of the ISO 10140-5 standard [1], with the distinction of a lightweight construction. The basic principle of the construction was to use a room-in-room design for the receiver room, while using the existing premises as the source room, for which minimal interventions are needed.

2.1. Existing structure, placement, and geometry of the test facility

The building in which the test facility is placed is mainly of massive construction. The walls are 18-20 cm thick and made of concrete, the floor is a prefabricated concrete slab with approximate thickness of 25 cm. The surface mass of all the separating walls and floor is at least 400 kg/m². The existing roof construction is a lightweight

metal sandwich construction with a suspended ceiling with a surface mass of approximately 45 kg/m². However the roof is not a part of the test facility structure as a secondary ceiling was designed and constructed.

The new test facility consists of two adjacent rooms situated at a far end of the existing premises, as shown in **Fig.1** and **Fig.2**. The source room has a net volume of 75,5 m³ and the receiver room a net volume of 65,5 m³ – both rooms fulfil the ISO 10140-5 standard [1] requirement of a minimal volume of 50 m³ and a difference in volumes of at least 10%.
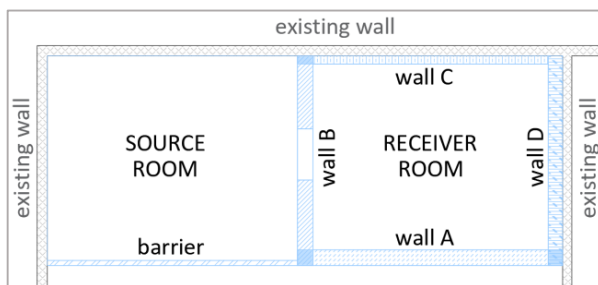
Fig.1. Floorplan of the test facility: The existing structure is shown in grey and the new walls in blue.
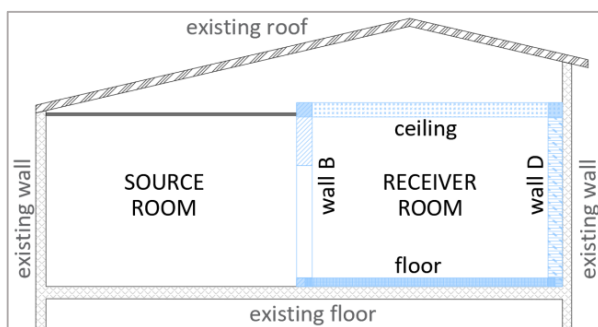
Fig.2. Cross section of the test facility: The existing structure is shown in grey and the new structure in blue.

2.2. New partition elements

The design of the test facility was mainly focused on achieving sufficient sound insulation towards the receiving room. That is why a room-in-room design was proposed taking full advantage of the existing massive construction. A separated double shell construction is designed for all separating elements of the receiving room.

For walls C, D (Fig.1.) and the floor (Fig.2.) the existing construction served as the outside shell, while the inside

shell was designed as an additional lightweight construction. Wals A, B and the ceiling were designed as a double shell lightweight partition.

The floating floor design had an 8 cm wooden structure with OSB board planking and sand as a filling material. The surface mass of the floating floor was at least 135 kg/m². The elastic layer was implemented in strips on the boarder of the floating floor – under the inside shell of the walls, and under the central part. The thickness of the material and size of the strips was selected according to the surface pressure of the floating floor, walls and ceiling weight in the specific area, with the goal of achieving a resonant frequency under 15 Hz. The finished floating floor hight was about 20 cm.

Walls A and B were designed as a double shell lightweight partition, with the inside shell placed on the floating floor and the outside shell placed on the existing concrete slab. The outside shell was designed with two layers of drywall and one layer of OSB planking with the surface mass of 29 kg/m² on a metal substructure. The inside shell had three layers of drywall and one layer of OSB planking with the surface mass of 38 kg/m² on a metal substructure. The 20 cm cavity was filled with mineral wool of density 45 kg/m³. The inside shell of walls C and D was designed in the same way as the inside shell of walls A and B, but with a smaller cavity thickness of 7,5 cm (metal structure filled with mineral wool) + 3 cm air gap towards the existing outer walls.

The ceiling construction also followed a double shell design, where the outside shell was supported by the outside shell of the walls and the inside shell was completely supported by the inside shell of the walls. Again, the outside shell had three layers of planking (two layers of drywall and one layer of OSB plates) and the inside shell four layers of planking (three layers of drywall and one layer of OSB plates). The cavity was 17,5 cm thick and filled with mineral wool of density 45 kg/m³.

The source room was mainly closed off by the existing construction. An additional barrier was designed towards the rest of the hall to limit the volume of the room.

Considering the mass law equation (ISO 12354-1 standard) [2] the minimal weighted sound reduction index (R_w) of the existing structure is R_w = 56 dB. With the proposed additional layers, the R_w of walls C and D is 70 dB. Regarding walls A, B and the ceiling partitions, a similar sound insulation rating of R_w = 68 dB is expected [3].

2.3. Opening for door specimens

The door opening was designed in a way that it can be adjusted in size; however, it is most commonly used for a door leaf of the dimension of 1 m x 2,1 m. Additional 5-10 cm are usually needed on each side of the opening for the door frame installation. The conjunction between the wall and the test element was designed in a way, to prevent flanking transmission and sound leakage in the greatest way possible. Two layers of OSB boards and one layer of drywall sheets was used, screwed together over a flexible sound insulation material. If the size of the opening is adjusted for a specific door element, the detail of the conjunction has to be replicated.

3. RESULTS AND DISSCUSION

All measurements were executed in accordance with ISO 10140-4 standard [4] in the frequency range 100 Hz – 5 kHz. The measurement methods used fixed microphone positions. Background noise level was more than 15 dB below the generated sound at all relevant frequencies. One person was present in the room during the measurements.

3.1. Reverberation time of the receiver room

The reverberation time was measured in accordance with ISO 10140-4 [4] and ISO 3382-2 [5] standards. Engineering method was applied with two source positions and four microphone positions. According to ISO 10140-5 standard [1] the reverberation time over the evaluated frequency range is limited with equation (1),

$$1 \leq T \leq 2(V/50)^{2/3} \text{ [s]} \tag{1}$$

where T represents the reverberation time and V the volume of the receiver room. In the specific case the reverberation time is in the range of $1 \text{ s} \leq T \leq 2,37 \text{ s}$. It is evident form the measurement results shown in **Fig.3.**, that the reverberation time of the receiver room is inside the required range at all relevant frequencies.
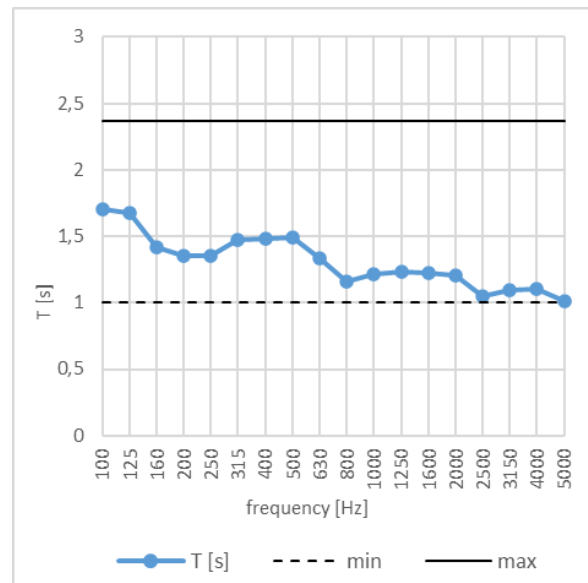

Fig.3. Measured values of reverberation time in the empty receiver room, which are inside the required range at all relevant frequencies.

3.2. Sound insulation of the test facility

To assess the maximal sound insulation of the test facility an additional multi-layer covering was applied over the door opening. The covering was of a similar composition as the wall to which it was tightly sealed. The airborne sound insulation was measured in accordance with ISO 10140-4 [4] and ISO 10140-5 [1] standards. The single value weighted sound reduction index (R_w) and the spectrum adaptation terms C and C_{tr} were calculated in accordance with ISO 717-1 standard [6] considering the whole wall as the separating structure. **Fig.4.** presents the measured values of sound reduction index of the test facility over the relevant frequency range, with the corresponding single number value at R_w (C, C_{tr}) = 62 (-2, -7) dB.

As expected for lightweight structure, the reduction index is below the reference curve at lower frequencies and above it at higher frequencies. No insulation drops usually associated with structural resonances can be observed.

In accordance with the limitations regarding flanking transmission (Annex A, ISO 10140-2 [7]) the sound reduction index of the measured element (door) must be at least 6 dB lower than the sound reduction index of the test facility at all frequencies. Therefore, the test facility permits testing of doors with R_w value up to 56 dB.
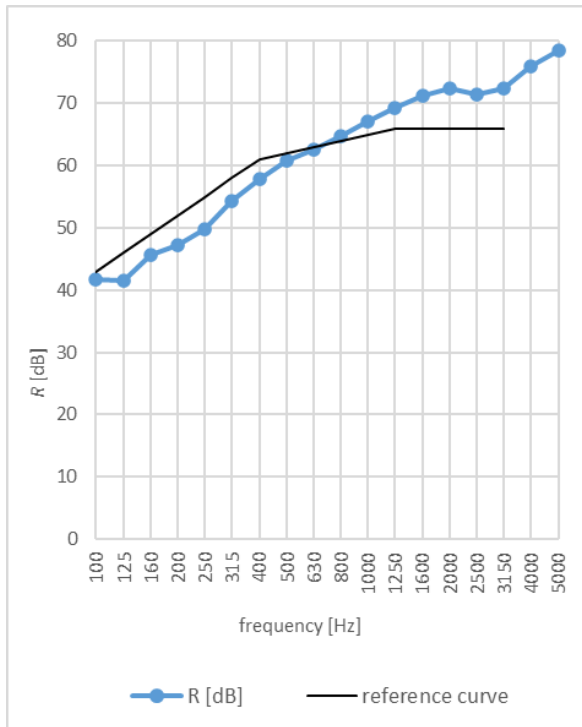
Fig.4. Measured values of maximal sound reduction index R of the test facility with the relevant reference curve (717-1).

3.3. Sound insulation of tested doors

More than 70 tests of doors were conducted until now in order to test different compositions, door elements and sealing options. The maximal measured sound insulation of the tested specimens reached R_w (C, C_{tr}) = 50 (-1, -4) dB. One of the specimens was also sent for official testing to a certified laboratory with intention of verifying the test result. The measured frequency dependent values (**Fig.5.**) are very comparable, with the official results ($R2$) showing a slightly higher sound reduction at high frequencies. Consequently, the R_w value is slightly higher for the $R2$ measurement (**Table.1.**). Excluding the frequency range above 1000 Hz, the standard deviation between measurements in each frequency band is less than 1,5 dB, while the maximal difference is 5 dB.

The lower sound reduction values at high frequencies, measured at our test facility could be a result of leakage at the installation of the door frame which is a common door installation failure. In addition, interlaboratory variations are expected to a certain degree, which is also the reason that standardized measurements procedures are constantly evolving and improving. Testing facilities commonly face challenges which have been systematically investigated since the 70's by Kihlman and Nilsson [8]. It has been also shown by Craik [9] that inter-laboratory deviation can originate from several design differences between facilities, which are not even specified by the standardized measurement procedures.
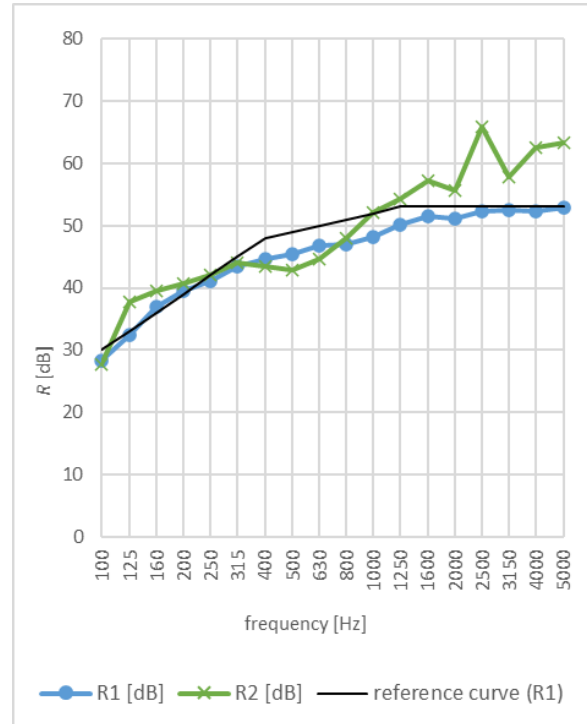

Fig.5. Measured values of sound reduction index of a specimen ($R1$) in comparison with the official results ($R2$) and the relevant reference curve for $R1$ values.

	$R1$	$R2$
R_w (C, C_{tr})	49 (-2, 5) dB	50 (-2, -6) dB

Table.1. Comparison of the measured ($R1$) and official ($R2$) R_w values.

4. CONCLUSION

A temporary test facility for sound insulation measurements was designed and built to support the development of high sound insulating doors. It enables testing of doors with sound insulation up to R_w = 56 dB, with R_w (C, C_{tr}) = 50 (-1, -4) dB being the highest measured value until now. The validity of test results was confirmed

with results of a certified laboratory, with the small single number rating deviation of 1 dB. Additional tests comparing the facility to certified laboratories would be beneficial to further investigate the reason behind the deviations observed at higher frequencies.

5. REFERENCES

[1.] ISO 10140-5:2010. **Acoustics – Laboratory measurement of sound insulation of building elements – Part 5: Requirements for test facilities and equipment**, International Organization for Standardization, 2010.

[2.] ISO 12354-1:2017. **Building acoustics – Estimation of acoustic performance of buildings from the performance of elements – Part 1: Airborne sound insulation between rooms,** International Organization for Standardization, 2017.

[3.] SIA, **Bauteildokumentation Schallschutz im Hochbau - Zusammenstellung gemessener Bauteile**, SIA Zurich, 2005.

[4.] ISO 10140-4:2010. **Acoustics – Laboratory measurement of sound insulation of building elements – Part 4: Measurement procedures and requirements,** International Organization for Standardization, 2010.

[5.] ISO 3382-2:2008. **Acoustics — Measurement of room acoustic parameters — Part 2: Reverberation time in ordinary rooms,** International Organization for Standardization, 2008.

[6.] ISO 717-1:2020. **Acoustics — Rating of sound insulation in buildings and of building elements — Part 1: Airborne sound insulation,** International Organization for Standardization, 2020.

[7.] ISO 10140-2:2010. **Acoustics – Laboratory measurement of sound insulation of building elements – Part 2: Measurement of airborne sound insulation,** International Organization for Standardization, 2010.

[8.] T. Kihlman, A.C. Nilsson, **The effects of some laboratory designs and mounting conditions on reduction index measurements**, Journal of Sound and Vibration, Volume 24, Issue 3, pp. 349-364, 1972.

[9.] Robert J.M. Craik**, The influence of the laboratory on measurements of wall performance**, Applied Acoustics, Volume 35, Issue 1, pp. 25-46, 1992.
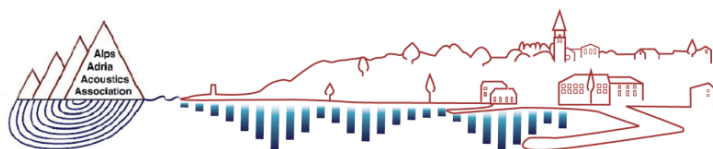
ACOUSTIC PERFORMANCE OF BUILDINGS, COMPONENTS AND MATERIALS AS A PARAMETER FOR ECOLOGICAL AND SOCIAL SUSTAINABILITY ASSESSMENTS

Franz Dolezal[1], Maria Fellner[1], Maximilian Neusser[2]

[1]IBO – Austrian Institute for Building and Ecology, 1090 Vienna, Austria
[2]Research Division for Building Physics, Technische Universität Wien, 1040 Vienna, Austria

Abstract: *Several initiatives have been launched to increase sustainability in the building industry. The consequence was a broader view of sustainability, not only based on the environmental, but on the economic and social performance of materials, components and buildings as well. A closer look on internationally acting Green Building Labels reveals that acoustic performance is, although a technical quality, handled as part of the social sustainability aspects of a building. Depending on the label, several credits are assigned for the fulfilment of requirements. Particularly for sustainable lightweight structures made of wood, sound insulation is to some extent defined by the properties of the insulation material, filled into the cavity of the timber joists. Especially the density and the dynamic stiffness, as well as the air flow resistivity, are important material parameters to achieve satisfying sound insulation properties. A comparison with different products and components has been carried out. It could be shown that the use of renewables leads to lower environmental impacts, though, the insulation material is not the most relevant parameter of the building components.*

Keywords: Sustainability, acoustics, sustainable building assessment, environmental performance, acoustic performance

1. INTRODUCTION

The building sector plays a major role when it comes to greenhouse gas (GHG) Emissions and tackling of climate change. According to [1], almost 40% of energy-related greenhouse gas emissions come from the building and construction sector. The importance of a more pronounced focus on sustainability in the building industry is proved by the fact that buildings and structures need 50 % of all natural resources utilized and create around 60 % of all wastes, as a consequence of their production, building, usage and maintenance [2]. Current holistic approaches in the construction sector include economic and social aspects as well. According to the general definition of sustainability, ecological, economic and social aspects and consequences – also called the "three columns of sustainability" – are taken into account to analyse and assess buildings and civil engineering works. This is already pictured in relevant voluntary, horizontal standards for the sustainable building

assessment, developed by CEN/TC 350 "Sustainability of construction works" since 2005 according the European Commission's mandate [3] with all aspects of sustainability included. Based on this strategy, building assessment and rating schemes offer solutions to achieving transformation to a more sustainable building sector, including the economic and social column of sustainability. Interestingly building physical aspects like acoustic properties of components and noise protection, according to EN 16309 [4], is assigned to the social aspects as shown in figure 1.

Considering climate crises and resulting UN Sustainable Development Goal number 13 [5] as well as the European Green Deal [6], environmental impact of building components becomes more and more important. Moreover, since the draft of the European Construction Product Regulation [7] indicates the assessment of the environmental impact as a basic requirement (sustainable use of natural resources of construction work) with a list of essential characteristics related to life cycle assessment

(LCA) to be covered, development is gaining traction and awareness of the industry regarding sustainability is rising.
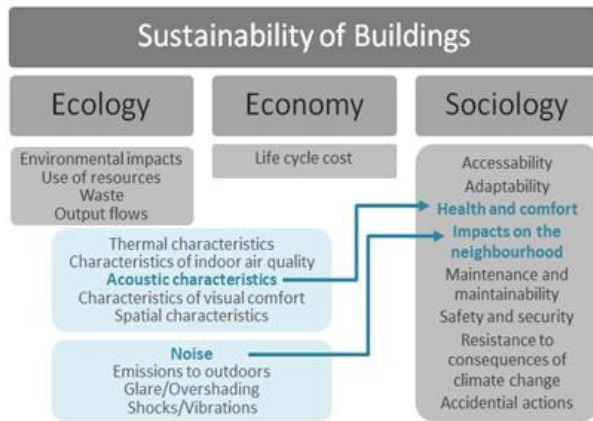

Fig.1. Three columns of sustainability with acoustic indicators shown as part of social sustainability aspects in EN 16309 (right column)

Though noise protection in buildings is seen as part of the social sustainability, sound insulation of components is mainly defined by their structure and the materials used. Selection of materials can have a significant impact on environmental sustainability and sound insulation properties as shown in [8] and with focus on the regional, renewable alternative straw as building material in [9].

2. SUSTAINABLE BUILDING ASSESSMENT SCHEMES

Social sustainability assessment of buildings is related to a variety of different issues. Concerning acoustics, according to EN 16309, acoustic characteristics are defined by airborne and impact sound insulation of separating walls and floors, sound insulation of the external envelope, noise level including service equipment noise, and reverberation time. Furthermore it is mentioned that different types of use shall be taken into account. A detailed overview of recommended aspects and standards for evaluation is given in table 1. Since EN 16309 serves as a methodological basis for Sustainable Building Assessment Schemes (SBAS) most of them try to consider all of these aspects.

Investigated were schemes from German speaking countries (DGNB, ÖGNI, IBO-Ökopass, BNB) as well as the ones with international importance (Level(s), BREAM). The objective was to figure out, if sound protection is seen

as an important issue of sustainability, which acoustic characteristics are considered and which methodological approaches are used for rating.

Acoustical aspect	Calculation	Measurement
Airborne sound	EN 12354-1	EN ISO 16283-1
Impact sound	EN 12354-2	EN ISO 16283-2
Sound from outside	EN 12354-3	EN ISO 16283-3
Service equipment	EN 12354-5	
Room acoustics	EN 12354-6	EN ISO 3382-2

Table 1. Recommended acoustical aspects and normative assessment methods acc. to EN 16309

Analysis is based on the web pages and publications on criteria, assessment and credits. To find out the impact of acoustic properties on SBAS`s rating results, the different assessment schemes had to be investigated.

Only the most important acoustic aspects concerning airborne and impact sound insulation have been considered. Moreover, focus was laid on schemes related to residential buildings have been taken into account.

2.1. Level(s)

Level(s) is a common framework for sustainable buildings which was launched by the European Commission in 2015 to improve the performance of buildings towards reduced carbon emissions, higher material and resource efficiency, health and well-being as wells as adaptations to climate change impacts, taking into account the whole life cycle of buildings. Level(s) offers open source manual and tools (beta-versions were relaunched and tested between 2015 and 2020). The assessment system corresponds with the goals of the EU Green Deal [6], new Circular Economy Action Plan [10] and the Paris Agreement to significantly reduce the carbon emissions in the construction industry by 2050 [11].

Acoustics and noise protection are defined as one of 16 core indicators, which have to be evaluated within three levels: level 1 the conceptual design phase, level 2 the detailed design stag, level 3 requires measurements to assess the as built performance classified by five subcategories: façade, airborne and impact sound insulation, service equipment and sound absorption where applicable. Core Indicators, categories or sub-categories have no weighting to each other within the Level(s) building assessment system. With regard to target

values, Level(s) does not define its own requirements, but refers to national building regulations or classification systems. Rating procedures are defined in accordance to ISO 717-1 [12] for airborne sound insulation and ISO 717-2 [13] for impact sound insulation. Besides the standard building acoustical frequency range from 100 Hz to 3150 Hz, low frequencies (below 100 Hz) can be taken into account "if the user wishes to take a more comprehensive and precautionary approach"[14].

2.2. BREEAM© GER/AT

BREEAM is a protected trademark of the BRE (British Research Establishment) Group. Developed in 1990 as one of the first environmental assessment systems, it has become the world's leading certification system for sustainable built environment. This is also due to the fact that documentation and evidence requirements have been broadly adapted to national standards via conformity lists or regional certification bodies have been established. For Germany and Austria, this task is fulfilled by TÜV SÜD Industrie Service GmbH.

For Germany, the following applies: Depending on the degree to which the requirements of DIN 4109-1 [15] are exceeded or undercut, 1 to 4 points are awarded: 1 point corresponds to 1 dB, 4 points to 5 dB exceeding (airborne sound insulation values $D_{nT,w} + C_{tr}$) or undercutting (impact sound insulation values $L'_{nT,w}$) of the requirements defined in the national standard [16]).

For Austria, the limit values to be achieved refer to globally defined target values as defined in the BREEAM International New Construction Scheme 2016 [17] and have not been adapted to higher requirements of the national building regulations. The highest rating level for airborne sound insulation of separating walls and floors including spectrum adaption term C_{tr} is defined as following: $D_{nT,w} + C_{tr} \geq 53$ dB (4 points), the entry level corresponds to $D_{nT,w} + C_{tr} \geq 48$ dB (1 point). For impact sound insulation, $L'_{nT,w}$ without spectrum adaption terms is used for evaluation: the following performance levels are defined for high performance $L'_{nT,w} \leq 54$ dB (4 points) and the entry level: $L'_{nT,w} \leq 59$ dB (1 point). Both values exceed the maximum permissible limits for $L'_{nT,w}$ for separating walls/floors with and without openings of the Austrian building code [18], which, conversely, means that all projects with Austrian building permission meet the requirements for the best BREEAM rating for impact sound insulation if validated via measurements.

Additionally, minimum requirements for project support have to be fulfilled: an appropriately qualified sound insulation / acoustic planner is appointed by the client at a suitable stage of the planning process to determine essential component properties according to building site conditions and tenants' needs.

The maximum significance factor for airborne and impact sound insulation values lies at 3.5 % for the overall result if the excellence level is achieved. In case of the entry values their influence is limited to 0.85 % for residential multi-storey buildings.

2.3. DGNB©/ÖGNI©

DGNB (Deutsches Gütesiegel für Nachhaltiges Bauen) was introduced to the market in 2007 as the sustainability building assessment system of the German Sustainable Building Council. Since founding, more than 10,000 projects in 27 countries have passed a successful DGNB certification. In more than 50 countries partnerships with local organisations exist. In the German-speaking area ÖGNI – Österreichische Gesellschaft für Nachhaltige Immobilien is responsible for the third party evaluation for Austrian projects.

For German projects: 90 points are reserved for airborne sound and impact sound insulation of separating building components, additional 20 points for room acoustics criteria. In total 110 points can be reached, what leads to a maximum of 4.2 % impact of the acoustic criteria in the total DGNB scheme [19].

For Austrian projects (ÖGNI), still the old scheme is in force, what leads to an impact of acoustics of 2.3 % in the overall result (only airborne and impact sound insulation max. 1.6 %) [20]. Details to the requirements are listed in table 2 (airborne sound) and table 3 (impact sound).

Components	Requirement	Credit points
Separating walls	$D_{nT,w} \geq 55$ dB	5
	$D_{nT,w} \geq 57$ dB	10
	$D_{nT,w} \geq 59$ dB	15
	$D_{nT,w} \geq 61$ dB	20
Separating floors	$D_{nT,w} \geq 55$ dB	7,5
	$D_{nT,w} \geq 58$ dB	15
	$D_{nT,w} \geq 61$ dB	20

Table 2. ÖGNI airborne sound insulation requirements and related credits

Additional criteria are exterior noise (max. 15 points) and insulation against noise from HVAC (max. 20 points).

Components	Requirement	Credit points
Separating floors	$L'_{nT,w} \leq 48$ dB	7,5
	$L'_{nT,w} \leq 43$ dB	15
	$L'_{nT,w} \leq 42$ dB	20

Table 3. ÖGNI impact sound insulation credits

2.4. IBO Ökopass

The IBO Ökopass is an Austrian sustainability assessment system of the first generation which was especially designed for residential buildings in urban context. Developed in 2001 by the Austrian Institute for Healthy and Ecological Buildings (IBO), it was applied mainly to subsidised multi-storey housing projects. The focus lies on health- and comfort-related criteria (60% weighting in four main categories), besides the environmental performance of the building [21].

Airborne and impact sound insulation as sub-criteria of the building acoustics section are weighted with a total of 8.6 % in the overall system which is the highest significance factor amongst the building assessment systems examined within this study. The IBO Ökopass does not only classify the overall building performance, but also the subcriteria in 4 levels: excellent, good, very good and satisfactory, whereby the minimum requirement level corresponds to the national building code.

To meet the Excellent level for airborne sound insulation, the following acoustical aspect must be fulfilled by separating walls and floors: $D_{nT,w} + C_{50-3150} \geq 63$ dB. The spectrum adaption term $C_{50-3150}$ according to EN 717-1 also includes low frequencies from 50 to 100 Hz.

For impact sound insulation, the IBO Ökopass requires an exceptionally high level for the best rating: the weighted standardised impact sound pressure level $L'_{nT,w}$ must be lower than or equal to 35 dB and the total value including spectrum adaption terms C_I and as well as for low frequencies $C_{I,50-2500}$ have to be fulfilled in the following way: $L'_{nT,w} + C_I \leq 40$ dB and $L'_{nT,w} + C_{I,50-2500} \leq 45$ dB.

2.5. BNB Assessment System for Sustainable Buildings

BNB system is used exclusively for German federal buildings and therefore does not include a residential building scheme. It is possible to evaluate buildings according to the following system variants: BNB-B (office buildings), BNB_U (educational buildings) and BNB_L (laboratory buildings). The BNB system comprises around 150 indicators which are grouped to 46 category profiles and 11 criteria groups. Therefore, the overall weighting of both indicators - airborne sound as well as impact sound insulation lies only at 2.7 % (in case of best rating) or 1.35 % (entry level). If only one indicator is considered, the mentioned significance factors are halved.

3. INTERRELATION BETWEEN SUSTAINABILITY AND ACOUSTIC PROPERTIES OF BUILDING COMPONENTS

Environmental impacts of acoustically investigated building components have been assessed according to the standardized, methodologies and results are compared.

3.1 Methodology

The methodology for Life Cycle Assessments (LCA) for building products and building components is roughly provided in EN 15804 [22] and EN 15978 [23] respectively. With regard to Global Warming Potential (GWP), EN 15804 prescribes the baseline model of 100 years of the IPCC based on IPCC 2013. Calculation has been carried out with software SimaPro, based on ecoinvent v3.8 database [24] for materials as well as for energy datasets.

In given research project, emphasis was placed on a selected set of indicators, including GWP divided into GWP_{fossil} and $GWP_{biogenic}$. All indicators, required according to EN 15804, are calculated, but the focal point of interpretation of results is put on GWP.

3.2 Measurement and calculation results for different insulation material in a lightweight wall

In an acoustic test facility in Vienna, airborne sound insulation property of a lightweight metal stud wall with the principal structure shown in figure 2 was measured.
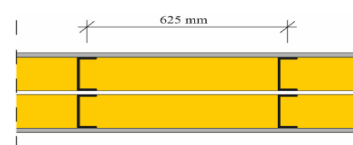

Fig.2. Structure of tested metal stud wall

The wall was made of 2 separated metal studs 75 mm, double planked with gypsum plaster board 12.5 mm and filled with different blow in insulation materials (mineral wool, cellulose fibre, straw and wood fibre). Results were compared acoustically (figure 3) and the influence on GWP has been assessed (figure 4) [8].
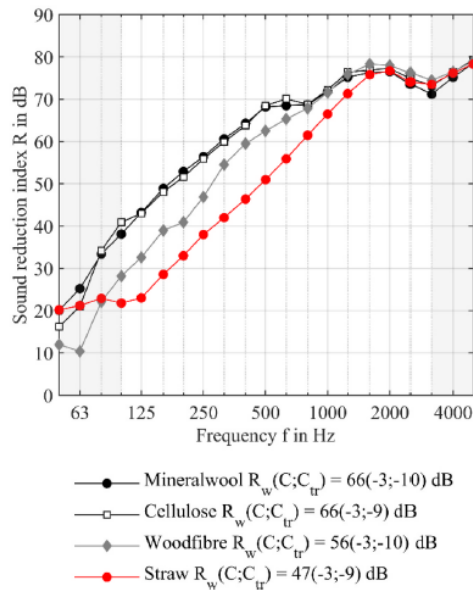

Fig.3. Sound reduction index of a metal stud wall with different blow in insulation material
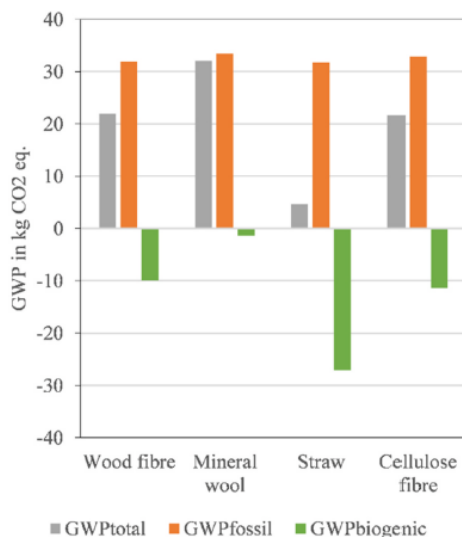

Fig.4. GWP for the metal stud wall with different insulation material - production phase

Sound measurement discovered a lower sound reduction index R for the straw filled wall, but a significantly lower GWP_{total} as well.

4. CONCLUSIONS

A critical review of some of the most important GBLs with focus on acoustic indicators leads to the conclusion that they influence results of GBLs quite differently. Usually indicators follow already standardised descriptors as pointed out above. As pointed out in figure 5, the average impact of the acoustic quality in Sustainable Building Assessment Schemes is around 5.9 %, which is quite a lot, considering the high quantity of different indicators, taken into account in the assessment procedure.
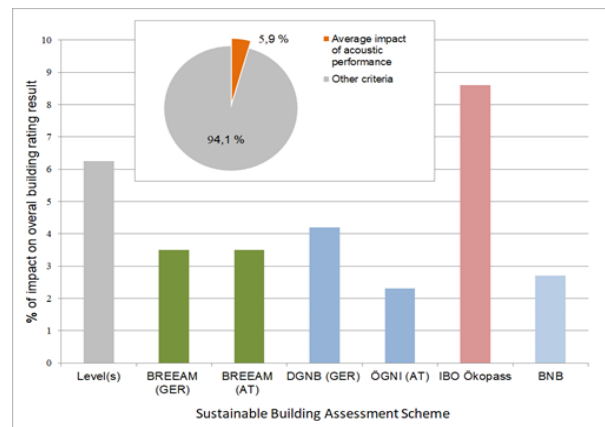
Fig.5. Average and maximum possible impact of acoustic aspects on results of SBAS for new buildings

The analysed metal stud wall showed lower sound reduction index for blow in insulations from renewable sources. In additional tests, a reduction of the (high) density of the blown in straw led to significantly improved results for the sound insulation. Regarding the environmental aspects of the wall, the carbon content of straw leads to the negative $GWP_{biogenic}$ and to good results for GWP_{total} for the production phase. GWP_{fossil} (GWP from fossil sources) is not significantly lower compared to the other insulation variants. This is a consequence of the little impact on GWP_{fossil} of the insulation material in general within this structure, since influence on this indicator of metal studs and gypsum plaster boards is significantly higher.

5. ACKNOWLEDGEMENTS

6. REFERENCES

[1.] IEA. **Global Status Report for Buildings and Construction: Towards a Zero-Emission, Efficient and Resilient Buildings and Construction Sector.**: Available at: https://www.iea.org/reports/global-status-report-for-buildings-and-construction-2019

[2.] Ebert, T., Eßig, N., Hauser, G. **Zertifizierungssysteme für Gebäude. Nachhaltigkeit bewerten. Internationaler Systemvergleich. Zertifizierung und Ökonomie.** Institut für internationale Architektur-Dokumentation GmbH und Co-KG. Redaktion DETAIL. München 2010

[3.] European Commission (DG ENTR) (ed.): **Standardization Mandate to CEN - M/350 EN, development of horizontal standardized methods for the assessment of the integrated environmental performance of buildings.** Brussels 2004.

[4.] EN 16309:2014. **Sustainability of construction works - Assessment of social performance of buildings - Calculation methodology.** European Committee for Standardization, 2014.

[5.] United Nations. **The Sustainable Development Goals Report 2022.** https://unstats.un.org/sdgs/report

[6.] European Commission. **The European Green Deal**. Brussels 2019. Available at: https://eurlex. europa.eu/legal- content/EN/TXT/PDF/?uri=CELEX: 52019DC0640&from=EN

[7.] European Commission. **Regulation of the European Parliament and of the Council laying down harmonized conditions for the market of construction products.** Draft 30.3.2022, Brussels.

[8.] Neusser, M., Dolezal, F., Wurm, M., Müllner, H., Bednar, T. **Evaluation of the acoustic and environmental performance of different wall structures with particular emphasis on straw.** Journal of Building Engineering 66. 2023. https://doi.org/10.1016/j.jobe.2023.105922

[9.] Teslík, J., Fabian, R., and Hrubá, B. **Determination of the Airborne Sound Insulation of a Straw Bale Partition Wall.** Civil and Environmental Engineering, vol.13, no.1, 3917, pp.20-29. 2017. https://doi.org/10.1515/cee-2017-0003

[10.] European Commission. **A new Circular Economy Action Plan for a cleaner and more competitive Europe.** Brussels, 2020. Available at: https://eur-lex.europa.eu/resource.html?uri=cellar:9903b325-6388-11ea-b735-01aa75ed71a1.0017.02/DOC_1&format=PDF

[11.] United Nations: **Paris Agreement.** 2015. http://unfccc.int/files/essential_background/convention/application/pdf/english_paris_agreement.pdf

[12.] ISO 717-1:2020. **Acoustics - Rating of sound insulation in buildings and of building elements – Part 1: Airborne sound insulation,** International Organization for Standardization, 2020.

[13.] ISO 717-2:2020. **Acoustics - Rating of sound insulation in buildings and of building elements – Part 2: Impact sound insulation,** International Organization for Standardization, 2020.

[14.] Nicholas, D., Shane, D. et al. **Level(s) indicator 4.4: Acoustics and protection against noise: User manual: introductory, briefing, instructions and guidance**, Publication version 1.1. JRC Technical Reports, ed. JRC, Unit B.5, 2021. Available at:

[15.] DIN 4109-1:2018. **Schallschutz im Hochbau – Teil 1: Mindestanforderungen,** Deutsches Institut für Normung, 2018.

[16.] BREEAM DE Neubau 2018, **Technisches Handbuch, SD BNBDE01**, Version 1.1., Stand 06/2022 (ed. TÜV SÜD Industrie Service GmbH – NSO BREEAM D-A-CH, BRE Global Ltd.) Available at: https://breeam.de/support/downloads/

[17.] BREEAM AT Neubau 2019, **Technisches Handbuch**, SD BNBAT01b, Version 1.1., Stand 11/2022 (ed. TÜV SÜD Industrie Service GmbH – NSO BREEAM D-A-CH, BRE Global Ltd.) Available at:

[18.] Österreichisches Institut für Bautechnik: **OIB-RL 5 Schallschutz**, Wien 2019.

[19.] DGNB System. **Kriterienkatalog Gebäude Neubau**, Deutsche Gesellschaft für Nachhaltiges Bauen. Stuttgart 2023.

[20.] DGNB System. **Kriterienkatalog Neubau**, ÖGNI TEC1.2 Schallschutz. Österreichische Gesellschaft für Nachhaltige Immobilienwirtschaft. 2020.

[21.] IBO. **ÖKOPASS Endbewertung**, v.2022. IBO - Austrian Institute for Healthy and Ecological Buildings.

[22.] EN 15804:2022. **Sustainability of Construction Works—Environmental Product Declarations—Core Rules for the Product Category of Construction Products**, European Committee for Standardisation Brussels, 2022.

[23.] EN 15978:2011. **Sustainability of Construction Works—Environmental Product Declarations—Assessment of Environmental Performance of Buildings**, European Committee for Standardisation Brussels, 2011.

[24.] Ecoinvent v2.2 and v3.8, **Ecoinvent Database**, Zurich 2017, 2021.
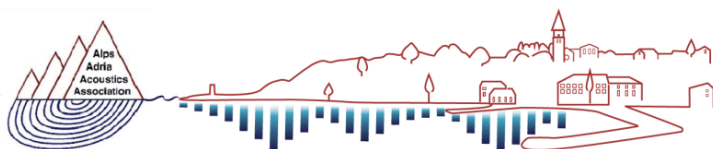
IMPROVEMENT OF IMPACT SOUND INSULATION WITH TILE UNDERLAY MATERIALS –
IMPACT SOUND INSULATION WITHOUT FLOATING FLOORS

Hanna Mária Csiszár[1], Gergely Dobszay[1], Alajos Miklós Hepke[1], Zoltán Hunyadi[1], Beáta Mesterházy[2], Zsófia Mária Wild[1]

[1] Faculty of Architecture, TU Budapest
[2] BME (Budapest University of Tecnology and Economics), Department of Building Constructions, Laboratory of Building Acoustics

Abstract: *Acoustical experts agree that the impact sound insulation of slabs can be improved with floating floors. The operation and planning methods of such mass-spring systems are well known and they are used widely today.*

On the basis of Hungarian Central Statistical Office (KSH) in 2021 1 million m^2 residential buildings were built in Hungary, wherein in our estimation min. 50.000 m^3 estrich screed was built in with the expense of 2 billions HUF (approx. 5,3 millions Euro) and with the CO_2 equivalent carbon footprint of approx. 142 290 tons. On the other hand the acoustical quality of existing buildings often can not be improved with floating floors considering the loadbearing capacity and interior height.

Building material producers provide different tile underlay materials which can be covered directly, but the use of these materials compared with other solutions is insignificant. The main goal of the research was to assess and quantify the performance and application field of solutions with special underlay materials and to develop possible layer orders without screed.

More than 50 measurements were carried out with 10 different underlay materials in the Laboratory of Building Acoustics of BME (Budapest University of Technology and Economics) and in-field. We found that the examined and developed structural solutions can be used to increase the acoustical quality of existing buildings without floating floors and can be applied cautiously in new buildings as well.

The base of this research was developed by the students of BME for a Students' Scientific Conference with the guidance of their professors. On the basis of this work we plan to carry out a research project in the future involving building material producers to develop specific solutions and layer orders.

Keywords: floating floors, impact sound insulation, resonance frequency, underlay materials, mass-spring system

1. INTRODUCTION

Floating floors have been known as a good solution for improvement of impact sound insulation for decades. Other floor coverings – e.g. flexible and soft floors – without floating estrich may have acceptable improvement, but there is often a demand for hard floor coverings. Floating floors can ensure the acoustical quality apart from the top layer of the floor.

Although the floating floor is a good solution from the acoustical point of view, it seems "wasteful" considering the environmental protection aspects by reason of high

cement need. In accordance with European climate policy it is necessary to develop alternative solutions that are more economical, eco-conscious whilst ensure nearly the same quality on the field of impact sound insulation. The question should be investigated from the point of view of existing buildings as well. Also in accordance with European climate policy it is necessary to increase considerably the rate of refurbishments however the acoustical quality should be provided or increased if possible. These facts justify to seek alternative solutions.

In many existing buildings – typically built with panel technology, prefabricated or thin reinforced concrete slabs – floating floors were not used. The slabs and floor coverings of these buildings do not fulfil today's acoustical requirements that is why they do not provide sufficient acoustical comfort. The original floor coverings – e.g. contact coverings (PVC, fitted carpet), or parquet on battens set on slag - are usually changed to hard (ceramic) or up to date flexible (laminated parquet) coverings, which usually results a worse acoustical quality.

The application of floating floor is not a possible solution in such buildings due to the limited interior height and loadbearing capacity. There is a need for a different solution. The topic is actual as between the 1960-80's approximately 500.000 panel flats were constructed in Hungary.

Besides floating floors underlay materials which can be covered directly are also available, but the use of them is not considerable in Hungary.

To show the acoustical effect and operation of floor coverings containing tile underlay materials we carried out a series of laboratory and in situ measurements. We investigated the available products and constructed alterative layer orders with the combination of existing products considering the questions of stability, rigidity and covering techniques, too.

We assumed that floor coverings with tile underlay materials may have a significant improvement of impact sound insulation. We did not assume that they are competitive with floating floors, but hoped that new layer orders may be used in existing and new buildings, fulfilling the acoustical requirements. We hoped that instead of the current "wasteful" solutions there are other more economical solutions.

In this research we focused on heavy slabs, thus we investigated the effect of developed layer orders with such constructions.

2. ACOSUTICAL BACKGROUND

The floor coverings may be classified into four groups from the acoustical point of view:

1. hard floor coverings (e.g. ceramic, stone) glued directly on the slab: these floor coverings can not improve the impact sound insulation.

2. soft floor coverings (e.g. PVC, fitted carpet) glued directly to the slab: these floor coverings can improve the impact sound insulation, usually $\Delta L_w \leq 30$ dB, but the improvement under 200 Hz is insignificant.

3. flexible floor coverings (e.g. parquet, laminated parquet): these floor coverings can improve the impact sound insulation, usually $10 \leq \Delta L_w \leq 20$ dB.

4. floating floors: these floor coverings can improve the impact sound insulation, usually $\Delta L_w \leq 35$ dB. The characteristics of screed and floating layer can be calculated and planned easily.

Floating floors can be considered as mass-spring system from the acoustical point of view. Its crucial elements are the mechanical "mass" which can be characterized with its specific mass (m', kg/m^2) and the "spring" which can be characterized with its dynamic stiffness (s', MN/m^3) and the resistance which may be neglected. The properties of the system can be defined with vibration methods. The mass-spring system's significant frequency is the resonance frequency (1) given in [1] and [2].

$$f_0 = \frac{1}{2\pi} \sqrt{\frac{s'}{m'}} \tag{1}$$

where

s' dynamic stiffness (MN/m^3)
m' specific mass (kg/m^2)

Floor constructions that operate as mass-spring system improve the impact sound insulation over the resonance frequency. The goal of the planning process is to decrease the value of resonance frequency which can be ensured with higher surface mass or softer spring.

We may assume that tile underlay materials with hard coverings operate the same way, where the tile underlay material is the "spring" and the hard covering with glue is the "mass", but it is necessary to investigate that question. We considered that the lack of mass will be shown especially at lower frequencies.

We examined the concerning previous studies about tile underlay materials. Hongisto et al. [3] investigated layer orders with 13 different resilient layers and used birch tree plate as floated layer, the thickness of the layer orders was 5-20 cm, which exceed the thickness that is generally used in residential buildings. Cobos et al. proposed tile underlay materials made of industrial waste and used them with floated estrich [4]. Kim K-W et al. investigated tile underlay materials having different dynamic stiffness in several layer orders with floated estrich, too [5]. R. Maderuelo et al. investigated thin (5-10 mm) sound insulation layers made of rubber waste, but the layers on the resilient layer is not detailed [6].

In conclusion the concerning previous studies investigated tile underlay materials and layer orders that differ from our concept in some aspects.

3. INVESTIGATED LAYER ORDERS

The examined layer orders were classified into four groups:

type "A" layer orders: The floor coverings (usually 8 mm ceramics, or 38 mm concrete paving element) were glued directly on one or more layers of tile underlay material (existing product) as recommended by the manufacturers. The total thickness of layer orders was approx. 20-30 mm.

type "B" ("hybrid") layer orders: The "hybrid" layer orders were prepared with multiplication and combination of existing products. The total thickness of layer orders was approx. 30-40 mm.

type "C" layer orders: The "hybrid" layer orders gave the idea to use ever softer layers from above to downward. In that combination the upper layer contained reinforcement (glass fibre mesh, polypropylene or galvanized steel mesh) to prevent cracks while the lower layers could be more softer, which is optimal for sound insulation. The total thickness of layer orders was approx. 30-60 mm.

type "D" layer orders: As up to date buildings are usually supplied with underfloor heating, we wanted to examine the acoustical effect of the special layers that are used for this purpose. Thus we made tests with so called insulated studded screed panels. To give a smooth surface for gluing the coverings the layers had to be filled in the whole depth and above them with equalizing mortar which gave an extra weight to the mass zone. These layer orders were measured in the same combinations as group "B" and "C". The total thickness of layer orders was approx. 30-90 mm. During the preparation and examination of layer orders we realised that there is a need to investigate the questions of stability, rigidity and covering techniques as well. Thus parallelly with the acoustical tests we carried out static tests related to above mentioned static problems. This examinations and their results exceed the frame of this paper, hence we do not present these results just refer to them if necessary.

4. LABORATORY MEASUREMENTS

In the laboratory we determined the improvement of impact sound insulation of the different layer orders and determined the dynamic stiffness of the resilient layers in addition. The measurements were carried out in the Laboratory of Building Acoustics at the Budapest University of Technology and Economics. The measurements were carried out according to ISO 10140 standard series and were evaluated according to ISO 717-2 standard, the dynamic stiffness measurements were carried out according to EN 29052-1 standard. The samples were prepared according to annex H of standard ISO 10140-1.

Generally, the acoustical performance of floor coverings may be characterized with improvement of impact sound insulation that can be described with formula (2) given in [7].

$$\Delta L = L_{n0} - L_n \qquad (2)$$

where

L_{n0} is the normalized impact sound pressure level of the reference floor without the floor covering;

L_n is the normalized impact sound pressure level of the reference floor with the floor covering.

The Hungarian national standard MSZ 15601-1:2007 gives the basic impact sound insulation requirement between flats with the quantity of L'_{nw} = 55 dB.

The impact sound pressure level is measured between 100-3150 Hz (optionally 50-5000 Hz), the single number quantity can be determined with a reference curve given in ISO 717-2 standard. The single number quantity is able to cover the frequency dependent behaviour of the structures.

The L_{n0} curve of the laboratory slab suits well to the $L_{n,r,0}$ curve of heavyweight reference floors that is given in ISO

717-2 standard. With the difference of the average of these curves and the curve of reference values for impact sounds shifted to position L_{500}=55 dB we defined the so called "goal curve". The "goal curve" shows the required frequency character of improvement of floor coverings, without taking into consideration the effect of flanking transmission which will be discussed later. The reference curves and the goal curve are shown in Figure 1.
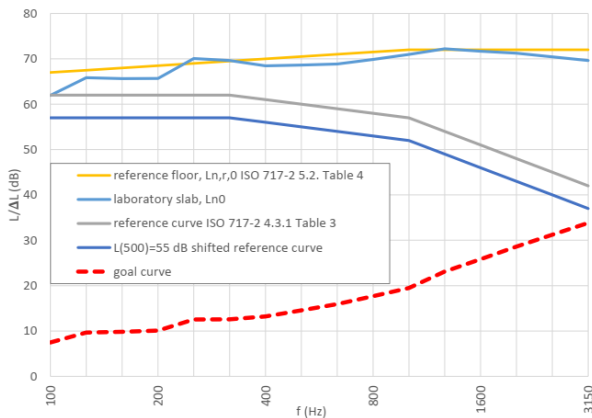

Fig.1. The "goal curve" showing the required improvement

The results of the measurements are discussed in groups.
Results of type "A" layer orders:
The improvement of impact sound insulation of layer orders type "A" are shown in Figure 2.
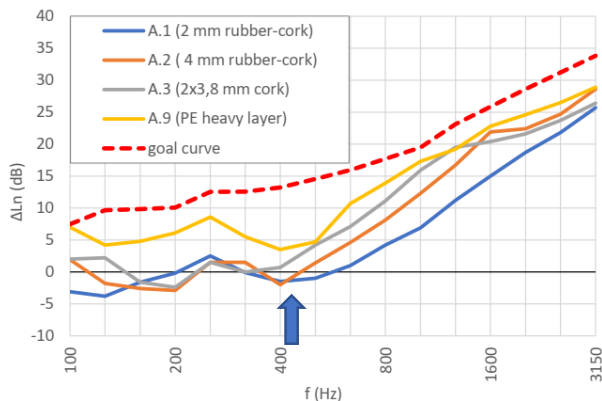
Fig.2. The improvement of impact sound insulation of layer orders type "A"

The improvement of these floor coverings is really slight, especially under 400 Hz, where the resonance frequency

is assumed. The calculated resonance frequency of sample A.1 (blue curve) was f_0=437 Hz (m'= 30 kg/m^2, s'= 226 MN/m^3) which confirms that assumption. The curves ascend over the resonance frequency with a slope of approximately 10 dB/octave. As the curves nowhere reach or exceed the "goal curve", it is clear that the 20-30 mm thin layer orders, which are recommended by the manufacturers have a weak improvement and slabs with them can not fulfil the requirements.
Results of type "B" layer orders:
The improvement of impact sound insulation of layer order B.3 is shown in Figure 3.
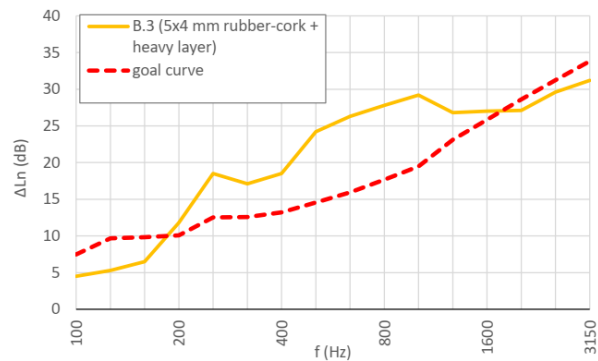
Fig.3. The improvement of impact sound insulation of layer order type "B"

In layer orders "B" one layer mounted heavy polyethylene layer and more layers of rubber-cork were used in combination. Due to this changes the curves reach and between 200-1600 Hz exceed the "goal curve" although there is a setback around 200 Hz probably due to the resonance frequency.
Results of type "C" layer orders:
The improvement of impact sound insulation of layer orders type "C" are shown in Figure 4.
The first examined layer orders contained just tile underlay materials. As the simultaneously performed failure tests proved the appropriateness of covering zone with reinforcement, we started to use traditional floating layers made of polystyrene, polyethylene or rockwool.
As it can be seen in Figure 4 the curves are mostly over the "goal curve". There is a strong setback at 800 and 1600 Hz in layer orders in which polypropylene mesh was used as reinforcement. The layer orders with rockwool has an outstanding performance. The lower performance of

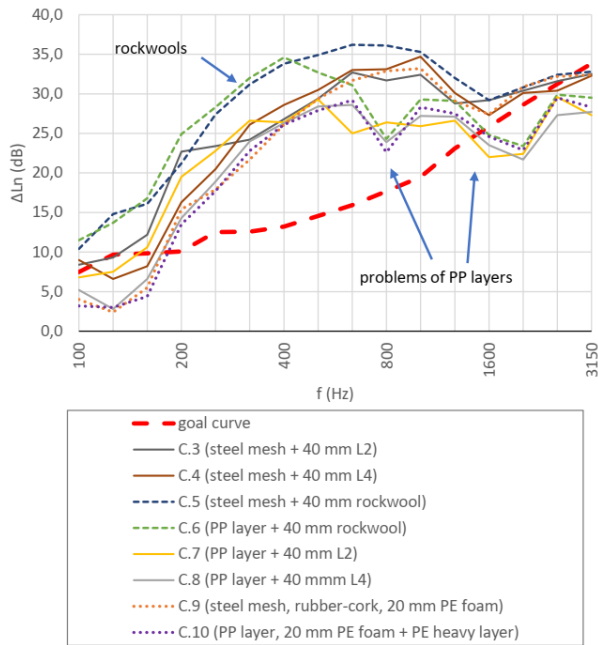polyethylene layers is probably related to the smaller thickness of these layer orders.

Fig.4. The improvement of impact sound insulation of layer orders type "C"

Results of type "D" layer orders:

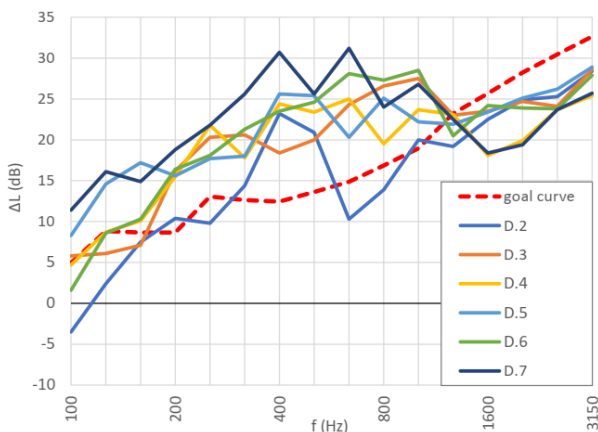The improvement of impact sound insulation of layer orders type "D" are shown in Figure 5.

Fig.5. The improvement of impact sound pressure level of layer orders type "D"

As it can be seen in Figure 5 the curves are mostly over the "goal curve", but there is a significant setback over 1250

Hz. The curve of sample D.5 shows a weaker performance which is probably due to the relatively thin layer order.

It is interesting to compare a layer order from group "D" with a layer order from group "A" which is shown in Figure 6. These layer orders differ in one aspect: A.2. does not contain the so called insulated studded screed panel. The beneficial effect of this panel is obvious.
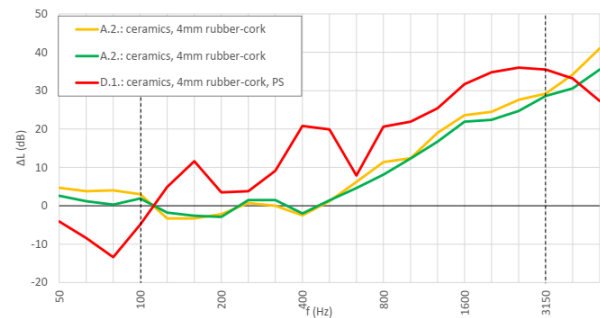
Fig.6. Comparison of the improvement of impact sound pressure level of layer orders A.2 and D.1

5. IN-SITU MEASUREMENTS

The in situ measurements were carried out in an existing building built with panel technology and in one of the buildings of the Budapest University of Technology and Economics.

The slabs of panel buildings were usually built with 15-18 cm reinforced concrete and typically soft floor coverings (PVC, fitted carpet) were applied on the top of them which gave a minimal improvement of impact sound insulation. The residents changed the floor coverings typically to ceramic tiles in wet rooms and to laminated parquet or fitted carpet in the rooms. The ceramic tiles and laminated parquet coverings usually result lower acoustical quality than the original coverings.

Figures 7 and 8 show the normalized impact sound pressure level of the existing slabs with ceramic tile (Figure 7) and laminated parquet (Figure 8) in the panel building. The single number quantities are L'_{nw}=67 dB and L'_{nw}=61 dB respectively, which exceed significantly the requirement.
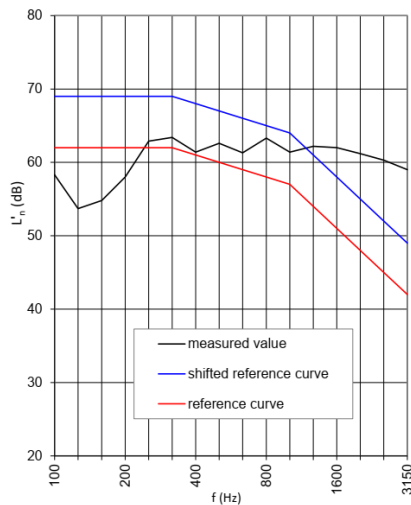
Fig.7. Normalized impact sound pressure level in panel building with ceramic tile floor covering, $L'_{n,w}$=67 dB
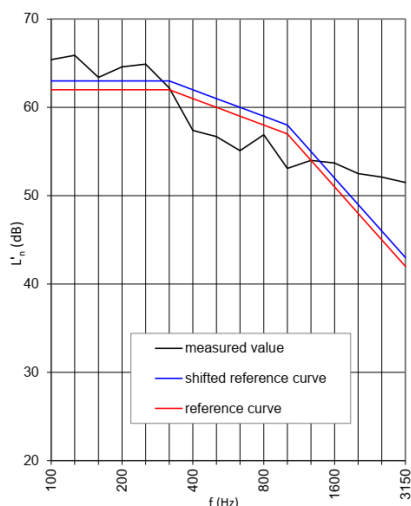

Fig.8. Normalized impact sound pressure level in panel building with laminated parquet floor covering, $L'_{n,w}$=61 dB

To demonstrate the possible improvement of the developed layer orders, we prepared small samples of the following layer orders: A3, B1, D1, D2 and determined the improvement of impact sound insulation compared to the original slab with ceramic tiles. Results are shown in Figure 9. It is obvious that the effect of layer orders which contained insulated studded screed panels (D.1 and D2.) is approximately the same than the effect of layer orders which contained multiple layers of tile underlay material (A.3 – it contained 3×4 mm rubber-cork). B1 layer order – which contained 2×4 mm rubber-cork - shows a weaker

improvement compared to other layer orders which is probably due to the smaller thickness.
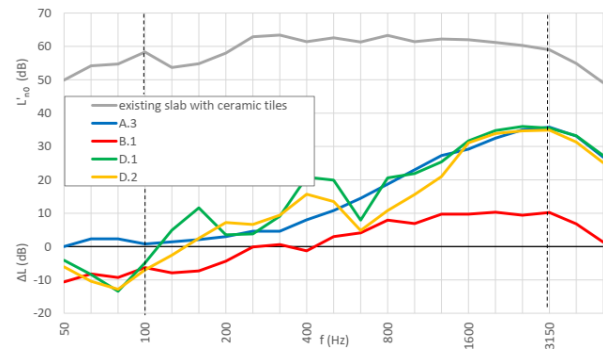
Fig.9. The improvement of impact sound pressure in panel building with layer orders A3, B1, D1, D2

Existing stairs may be an important application area of tile underlay materials. Today we build heavy stairs with resilient "springs" at the support of stair flights or landings and with isolation between the stair flights, landings and walls as it is described in [8].

Stairs have a monolithic contact in existing buildings thus the noise is transmitted to the rooms through the constructions. These stairs do not fulfil today's acoustical requirements but the required acoustical isolation can not be provided afterwards.

The application of underlay materials may give a solution to these problems. To illustrate the possible effect of layer orders made with underlay materials we carried out in situ measurements in staircases of existing buildings. We determined the difference of impact sound pressure level of existing structures with and without developed layer orders. In this measurements we examined layer orders of group "A", the results are shown in Figure 10.

As it was assumed all of the layer orders had an improvement compared with bare constructions, but the thicker layer orders with multiple resilient layers showed a much better performance.
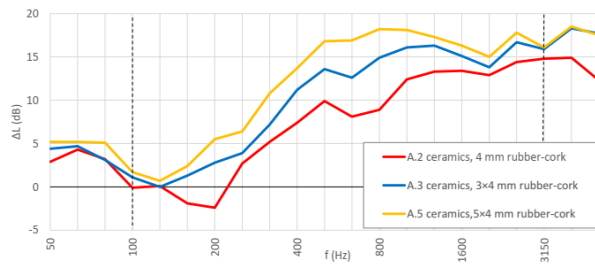
Fig.10. The improvement of impact sound insulation of stairs of existing buildings with layer orders A.2, A.3, A.5

6. CONCLUSIONS, FURTHER PLANS

In the end of the study we determined the single number quantities of the examined layer orders that are shown in Figure 11.
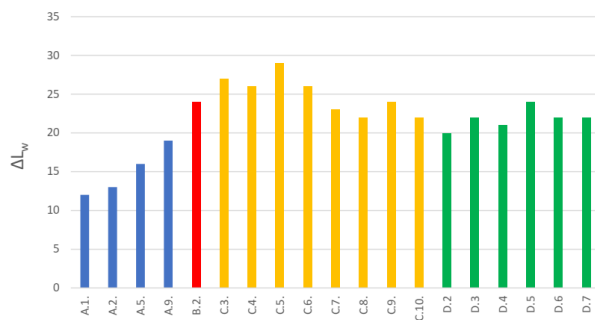

Fig.11. The weighted reduction of impact sound pressure level of layer orders

As we emphasized previously the compliance of a layer order should be examined together with the slab construction. The in situ performance may be determined according to ISO 12354-2.

We made calculations with the simplified model of ISO 12354-2 and determined that the examined layer orders may be applied with heavy slabs which weighted normalized impact sound pressure level is between $L_{n,w}$=64-79 dB. In this project we did not examine the different slab constructions, but it may be assumed that the typical weighted normalized impact sound pressure level of existing slabs is usually $L_{n,w}$=72-85 dB. That means that many of the examined layer order may give a suitable impact sound solution with most of the existing slab constructions, and may give a significant improvement to the rest. With the frequency dependent impact sound pressure levels the layer orders may be optimized.

It is interesting to investigate the thickness and the improvement of impact sound insulation of layer orders which can be seen in Figure 12.
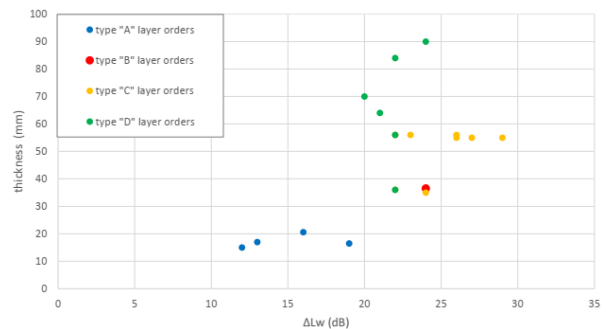

Fig.12. The thickness and improvement of impact sound insulation of layer orders

It is clear that the really thin layer orders (20-30 mm – group "A") do not give appropriate improvement. Thicker layer orders (min. 50-60 mm) may reach sufficient improvement. From that point of view group "C" seems a good compromise.

The most important results of the project are the following:

- 28 layer orders were prepared and measured altogether, more than 50 measurements were carried out which included 38 laboratory measurements and 12 in situ measurements, which contained 8 measurements related to stairs.

- During evaluation of data we made comparative analyses. Illustrating the frequency related improvement of coverings we defined a "goal curve" which shows the difference between the L_{n0} curve of reference floor and the average requirement. With this we could illustrate the frequency dependent character of certain solutions and identify the tendencies.

- We found that thin (20-30 mm) layer orders that were made on the basis of recommendation of manufacturers can not provide such improvement that would realize the application of these layer orders.

- We found that layer orders made with multiplication and combination of layers may provide significant improvement beside economical thickness (50-60 mm).

- We found that Insulated studded screed pane are not able to replace sound insulating layers, but may be combined with them for a better quality.

- We limited the slabs that can be able to fulfil requirements with the examined new layer orders.

- We declare that the examined layer orders are able to improve impact sound insulation, acoustical comfort and life quality of existing buildings.

In the future we plan to carry out a research project involving building material producers to develop specific solutions and layer orders.

Our goal is to specify the acoustical performance, the application area of existing materials and to develop layer orders without floated estrich as a possible alternative for floating floors, considering questions of stability, rigidity and covering techniques. We would like to extend the test to lightweight slab constructions as well.

The further goal is to create complex solutions that are suitable to improve the acoustical quality of existing buildings and can be appropriate in new buildings as well.

7. REFERENCES

[1.] Reis, F. **Az épületakusztika alapjai**, Terc, 2003, ISBN: 963 86303 6 1

[2.] P. Nagy J. **A hangszigetelés elmélete és gyakorlata**, Akadémiai Kiadó, 2004, ISBN: 963 05 8133 7

[3.] Hongisto, V., et al. **Acoustic Properties of Commercially Available Thermal Insulators - an Experimental Study,** Journal of Building Engineering, vol. 54, 2022.

[4.] Cobos, F.J.G and Maderuelo-Sanz, R. **Using different waste as resilient layers for impact sound insulation improvement: New alternative to commercial layers?,** Building Services Engineering Research and Technology, Volume 43, Issue 4.

[5.] Kim, K-W et al. **Correlation between dynamic stiffness of resilient materials and heavyweight impact sound reduction level**, Building and Environment, Volume 44, Issue 8, 2009.

[6.] Maderuelo-Sanz, R. et al. **The performance of resilient layers made from recycled rubber fluff for impact noise reduction**, Applied Acoustics, Volume 72, Issue 11, 2011.

[7.] ISO 140-1:2021 **Acoustics. Laboratory measurements of sound insulation of building elements. Part 1: Application rules for specific products.**

[8.] ISO 12354-2:2017 **Building acoustics. Estimation of acoustic performance of buildings from the performance of elements. Part 2: Impact sound insulation between rooms.**

Contributed papers
Soundscape and sound reproduction techniques

1. The soundscape of university campuses: sound essays on the Polytechnic University of València
Alberto Quintana-Gallardo (Centre for Physics Technologies (CTFAMA), Universitat Politècnica de València, Spain)
2. The Accuracy of Dynamic Sound Source Localization in Binaural Audio Systems with Head-Tracking Utilizing Generic and Individual HRTFs
Vedran Planinec (Faculty of Electrical Engineering and Computing, University of Zagreb)
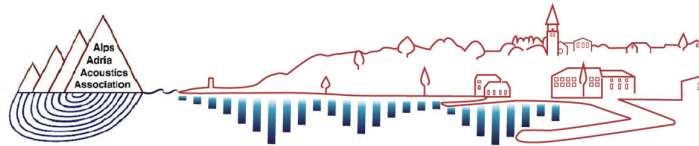
THE SOUNDSCAPE OF UNIVERSITY CAMPUSES: SOUND ESSAYS ON THE POLYTECHNIC UNIVERSITY OF VALÈNCIA

Alberto Quintana-Gallardo; Ignacio Guillén-Guillamón

Center for Physics Technologies, Universitat Politècnica de València, València, Spain

Abstract: *The Polytechnic University of València (UPV) is the biggest polytechnic university in Spain. This university, which was founded in 1971, started as a small Education Institute and now has more than 28000 students in a 620000 m2 university campus and has deep roots in the overall culture of the city of Valencia. This study reflects the acoustic heritage of UPV Campus de Vera and its value as an ever-changing cultural heritage. The objective is to produce sound essays that capture the ephemeral soundscape of the UPV campus and help the university community reflect on its influence on their day-to-day and even in the broader culture of the city. The methodology consists of three distinct phases. The first phase is a bibliographic study of the history of the UPV. This is done by analyzing the architectural projects that defined the university and the published books on the topic. This part is crucial to put the study into context. The second part is recording soundscapes on the campus using ambisonics microphones, sound walks with binaural microphones, and interviews with professors, students, and other university employees. The last part involves editing the audio using a Digital Audio Workstation (DAW). The study results are four sound essays distributed as podcasts on online platforms. After concluding the project, it can be stated that reflecting on the acoustic heritage of university campuses can help students, professors, and other employees create a sense of belonging and ultimately foster their formal and non-formal educational path.*

Keywords: Soundscapes; acoustic heritage; sound essays; university campuses

1. INTRODUCTION

Cultural heritage is often understood in visual terms. Preserving the heritage of a city involves maintaining the visual integrity, shape and colours, of the architectural landmarks. However, the acoustic heritage is commonly forgotten. The auditory experience is essential to the way we perceive spaces. The social context, nature and other kinds of sound sources that coexist at a particular time create soundscapes that, not only tell a story, but also configure the cultural identity of a place and time.

Contrary to other forms of heritage, the acoustic heritage does not leave a physical mark. The ephemeral nature soundscapes due to the physical nature of sound has not allowed humanity to know what ancient spaces sounded like. However, since the invention of modern-day recording techniques, it has been possible to capture and register soundscapes.

The idea of soundscapes was first introduduced in the 60s with a groundbreaking initiative called the World Soundscape Project. This project, led by the Canadian composer Murray Schafer, paved the way for a new generation of acousticians who started to focus on the uniqueness of sound in each space [1].

Soundscapes refer to the acoustic environment of the surroundings of a particular location [2]. They encompass all the sounds that shape the auditory perception of a specific place or space. This term goes beyond noise or music. It emphasizes the totality of sounds and their interaction with the surrounding environment. The World Soundscape project also introduced the idea of sound walks. Sound walks are experiential journeys that involve the listener moving, intentionally or unintentionally, through the location. They focus specifically on exploring and engaging with the soundscape of a particular location. Sound walks can be guided or self-guided, where

participants actively listen to sounds around them. This study focuses on how to use soundscape recordings to tell the story of university campuses in Spain and their interaction with the cities around them.

In the early 70s, during the last years of the dictatorial regime, several new university campuses were built in some of the major cities in Spain. These campuses tell an important chapter of the history of Spain during the second half of the 20st century. One of those universities is the Plytechnic University of Valencia (UPV) [3].

1.1. The story of the Polytechnic University of Valencia

The UPV started its activity in 1968 during the latter days of the Franco regime. This university was built in a context in which the need for qualified professionals was higher than the rate at which those professionals could be trained at the learning centers in the country [3].

The UPV was initially named Instituto Politécnico Superior. It was established in the northern part of the city in what was at the time cultivation fields. The first building to be built is marked in red on the lower left corner of Fig. 1. Designed by Carlos Prat Cambronera y Joaquín Hernández Martínez, this building hosted at the time the four degrees the Institute offered, Agricultural Engineering, Industrial Engineering, Civil Engineering and Architecture [4]. Despite the fact that it was initially planned to be used temporarily until a more permanent building was built, it is in use to this day. The building is structured using a modular grid system with three-meter intervals. It was designed as a one-story structure featuring generously proportioned areas for circulation and branches that serve as classrooms for the various university degree programs. The most distinctive feature of this design was the inclusion of three diagonally positioned interior courtyards, strategically placed to offer visual connectivity. The spacious corridors, larger than usual, reflect a prevailing European trend of the era. This trend emphasized the significance of informal education, recognizing that learning extends beyond the classroom when students engage in conversations and share experiences with each other. During that time, these spaces for social interaction were regarded as equally important as the classrooms themselves.

In 1971, a new set of buildings was constructed following the design of the architectural firm L35 Arquitectos and the institute was officially named Universidad Politècnica de Valencia. The project followed what at the time was an innovative architectural trend called Mat-buiding. Mat buildings are large-scale, high density structures organized in a modulated grid [4].

The design of the building was conceived as a functional system to meet the requirements of the architectural competition, accommodating the needs of all four degree programs. It was executed in the form of a departmental spatial organization, aligning with the prevailing European trend of the time, which contrasted with the American approach to campus organization, where each building represented a different school. The building was structured as a grid, with departments strategically positioned, enabling students to tailor their curriculum by moving between these departments.

The building had a three-level configuration. The ground floor housed parking and laboratories, while the first floor was dedicated to classrooms. The second floor was designated for offices. Notably, the buildings were arranged around an agora, with an east-west axis symbolizing power dynamics. On the west side, there was the dean's office, representing administrative power, and on the east side, the central library, symbolizing the power of knowledge [5]. Over the years, the university continued to expand and incorporate new facilities. In 2002, a significant change occurred when the concrete platform was dismantled, and car access was restricted in most parts of the campus. These decisions brought about a profound transformation in the campus's overall appearance. The removal of the platform resulted in increased isolation between the buildings and the various university departments, diluting the original concept of the Mat-building [5]. Conversely, these decisions also led to the creation of more green spaces and a stronger emphasis on integrating nature within the campus. This included the introduction of various bird species, which now dominate the acoustic environment in many areas.

Fig.1. Map of the Campus de Vera of the Polytechnic University of Valencia

1.1. Objectives

The present study has the following objectives:
- To register the most representative soundscapes of the present-day Campus de Vera of UPV.
- To find new ways of telling the story of the campus.
- To articulate the different clusters or groups of people that participate in the everyday life of the university.
- To answer the question, what does the UPV sound like?

2. MATERIALS AND METHODOLOGY

The work is articulated using sound walks, soundscapes, and narrative tools to convey the campus story. Besides that, the work also encompasses using audio-recorded interviews and narrative fiction. The audio pieces are used in the following way:
- Soundscapes: field recordings of the places relevant to each episode using ambisonics or binaural microphones, depending on the circumstances. The recordings are done following the guidelines of the international standard ISO/TS 12913-2:2018.
- Sound walks: These walks are carried out by tracing a route during which a binaural recording is made, giving the listener the sensation of walking through the sound.
- Interviews: designed to involve the university community and to incorporate their subjective impressions. The interviewees are related to the subject matter of each chapter.
- Narrations: recorded in the same way as the interviews or utilizing a condenser microphone connected to a sound card and processed with a Digital Audio Workstation (DAW).

To recreate sound environments, we will gather the impulsive reactions from selected locations. Impulse responses are used to mimic and simulate sounds in spaces that differ from their original settings through a convolution process. This is accomplished by treating each listening point as a time-invariant linear system. The various audio components are then blended and edited, organized into thematic chapters for proximity using the Adobe Audition Digital Audio Workstation (DAW). The final work will be uploaded to various digital platforms and made available free of charge. Key equipment details are outlined in Table 1.

Because of the dialogical nature inherent in sound essays, the creative process doesn't adhere to the conventional preproduction, production, and postproduction sequence. Instead, it adopts a recursive approach. The various interviews, typically a component of the production phase, have the effect of altering the script and sometimes even influencing the preproduction phase itself. The process initiates with the drafting of an initial script and the planning of interviews. As each interview is conducted, the script is continually revised and modified based on the interviewee's statements. Once all the interviews are completed, the script is then finalized, marking the commencement of the postproduction phase.

Description	Function	Model
Ambisonics microphone	Record the soundscapes at different locations	Zoom VRH-8
Binaural dummy head	Capture the audio of the sound walks	3DIO Free Space Binaural
Dynamic microphone	Record the interviews	Shure SM58
Audio recorder	Recorder with microphone inputs	Zoom H8 portable recorder
Digital Audio Workstation (DAW)	Edit the audio files	Adobe Audition

Table 1. Equipment employed to capture the acoustic environment.

3. RESULTS

Following the initial study, we've devised an interdisciplinary podcast framework to present a comprehensive portrayal of the location. This structure mirrors the concept of a dialogue, wherein the narrator cedes the floor to other participants, allowing them to contribute, challenge, and exchange their perspectives on the subject. You can find a detailed outline of this structure in Table 2.

Section	Content
Intro	Opening of the Podcast explaining the overarching idea of the sound essays and the project.
Hook	An explanation on the content of the episode that arises a question that the dialogue tries to answer
Narrator opening monologue	The narrator starts the dialogue with a on opening statement on the topic. This part will include facts, data and open questions to be answered along the episode
Interviews and speeches	After the narrator, several interviews will be concatenated and mixed with soundscapes.
Narrated soundwalks	Soundwalks will be recorded in chosen routes inside the campus. The soundwalk will include a narration describing some parts of the path.
Narrative fiction	Pieces of narrative fiction on the topic of the episode written and narrated by local writers. The objective is to approach the topic not only from facts but also from the collective imagination.
Conclusion	The narrator gives a closing monologue encompassing the most important takes from each intervention.

Table 2. Structure of the episodes

The planned division into chapters aligns with our goal of creating a comprehensive portrayal of the campus:

Chapter 1. Seeds and limits: This chapter embarks on an exploration of the university's origins and its boundaries. It delves into the quest to determine where the university's realm commences and where the city's boundaries lie. It ponders whether the university's enclosure shields it from the external world or if it isolates the outside from the university. The episode features interviews with individuals who were present during the early years of the university, accompanied by sound walks along the entrances and boundaries. The primary objective of this episode is to immerse listeners in the historical context of the university. By understanding this context, students, educators, and other university members can gain insights into the origins of many of the current customs and procedures.

Chapter 2. The sound of numbers: This chapter prompts reflection on what the UPV (University Polytechnic of Valencia) actually sounds like. It explores the acoustics of various campus spaces and the interplay between the natural and technological sounds that coexist within the university's precincts. Sound walks through different areas of the campus will be interwoven with interviews featuring experts in architectural acoustics, environmental specialists, and researchers in fields such as telecommunications and computer science, as well as other experts in digital signals. The primary aim of this chapter is to foster a closer connection between the university's community and their surroundings, facilitating a deeper understanding of both the built environment and the natural elements within the campus.

Chapter 3. Neverland: Generational tensions at the UPV. The university lives in continuous generational renewal, with an eternally young and changing student body that contrasts with the life of the workers. This chapter will deal with the generational tensions in the university and how its protagonists live it. This chapter aims to bridge the gap between the different generations that coexist in the university. Alleviating the generational tension is key to improve the relationship between students and educators. Understanding each other's background can improve the learning environment and their mental health.

Chapter 4. The end of the Polytechnic: This chapter seeks to imagine the future of the university and its possible end. When will the UPV end? There may come a day when universities are no longer necessary; perhaps it will end when it is no longer needed when technology kills technology itself. Futures in speculative fiction. The purpose of this chapter is to foster critical thinking on what the purpose universities have and what is the overall purpose of pursuing a university degree. Reflecting on this

can help in finding new ways of learning and teaching, as well as to create a more aware university community.

3. CONCLUSION

One of the key objectives of this study was to emphasize the necessity of reevaluating the approach to education and recognizing the significance of fostering engagement with the university campuses. Engagement holds paramount importance, not just for students but also for educators. This rationale guided our decision to dedicate a chapter to addressing the generational gap in the university. It is imperative to narrow this gap or, at the very least, find avenues for establishing common ground. With the advent of new tools, we have the capability to motivate both these groups effectively.

The accessibility of the tools required for producing educational content like this has never been greater, making initiatives such as this one feasible with relatively modest funding. An essential attribute that renders podcasts and sound-based content particularly suitable for non-formal educational projects is their ability to accommodate multitasking. While online educational platforms such as Coursera, EdX, or Khan Academy are invaluable resources, they demand undivided attention. In contrast, podcasts enable listeners to engage while simultaneously carrying out other activities. This characteristic can serve as a solution for individuals with time constraints and helps eliminate barriers to their initial engagement.

After this study, the following conclusions can be drawn:
- Experimental podcasts can be a viable tool for generating engagement in the university community.
- Leveraging audio formats to craft fresh narratives holds significant potential, particularly given the prevalent dominance of our sense of sight. This approach can tap into the power of sound to engage and captivate audiences.
- Initiatives like these can serve as valuable supplements to formal education and serve as wellsprings of inspiration for both students and educators. They have the potential to enrich the learning experience and stimulate creative thinking within the academic community.

4. REFERENCES

[1] H. Boucher and T. Moisey, "An Experiential Learning of a Philosophy of Music Education Inspired by the Work of Canadian Composer R. Murray Schafer," *Creat. Educ.*, vol. 10, no. 10, 2019.

[2] A. M. Botella Nicolás, "The soundscape as sound art," *Cuad. Music. Artes Vis. y Artes Escenicas*, vol. 15, no. 1, 2020.

[3] R. Castellanos Gómez and D. Domingo Calabiug, "1969: Las Universidades Españolas a Concurso. Bases, Resultados Y Polémicas," *Proy. Progreso, Arquit.*, no. 7, pp. 104–121, 2012.

[4] D. Domingo Calabuig, R. Castellanos Gómez, and A. Ábalos Ramos, "The strategies of mat-building," *Archit. Rev.*, no. 1398, pp. 83–91, 2013.

[5] R. C. Gómez and D. D. Calabuig, "Project and system: Instituto Politécnico Superior de Valencia," *arq Archit. Res. Q.*, vol. 20, no. 4, pp. 357–369, Dec. 2016.
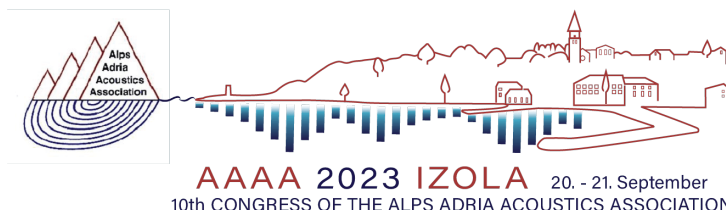
AAAA 2023 IZOLA 20. - 21. September
10th CONGRESS OF THE ALPS ADRIA ACOUSTICS ASSOCIATION

Accuracy of Dynamic Sound Source Localization in Binaural Audio Systems with Head-Tracking Utilizing Generic and Individual HRTFs

Vedran Planinec, Marko Horvat, Kristian Jambrošić, Petar Franček

Faculty of Electrical Engineering and Computing, University of Zagreb

Abstract: *The constant advances in spatial audio technology have the potential to revolutionize the overall audio experience through the integration of binaural systems with head-tracking devices. The hypothesis is that the use of individual Head-Related Transfer Functions (HRTFs) in binaural synthesis benefits the listeners by providing a deeper immersion into the sound scenarios created for virtual and/or augmented reality setups, and, ultimately, a more realistic listening experience. This paper presents the results of a listening experiment in which the listeners were asked to determine the position of a dynamic virtual sound source presented to them binaurally in the horizontal and the median planes, with the goal of assessing how accurately this determination can be done. The experiment was conducted in a controlled listening room environment using a wired head tracker in conjunction with headphones for binaural audio reproduction. The influential factor investigated in the experiment were the HRTFs, which have been varied between a generic HRTF set and the individual sets measured for each listener. The aim is to evaluate if there is any difference in localization accuracy between these two cases and to evaluate its significance through statistical analysis.*

Keywords: Individual HRTFs; Binaural audio; Head tracking; Listening experiment

1. INTRODUCTION

Binaural audio systems are used to create an immersive and realistic listening experience that gives the listener a sense of spatial presence and directionality. With the rise of virtual and augmented reality technologies (VR and AR), binaural audio systems have become even more important as they play a crucial role in creating a compelling sensory experience [1]. Binaural audio systems utilize Head-Related Transfer Functions (HRTF), which are essential for localizing sound in space and creating spatial awareness [2]. From gaming and entertainment [3] to medicine [4] to education and training [5], binaural audio systems and spatial audio are revolutionizing the way we interact with virtual and augmented environments.

While generic HRTFs are widely used in spatial audio to create a more accurate VR/AR experience [6], individualized or personal HRTFs can potentially personalize the experience even more.

The acquisition of the individual HRTF for a given person must be performed using one of the many available methods and measurement setups [7]. For this study, the methodology described in [8, 9] was used to determine individual HRTFs for the subjects who participated in the experimental measurements.

The purpose of this paper was to conduct experiments to test the hypothesis that the use of individual HRTF increases the accuracy of localization of virtual sound sources, providing a more realistic and natural experience for users, compared to the situation where generic HRTFs or another person's individual HRTF are used. A novel methodology for experiments was implemented that allows the hypothesis to be tested in highly dynamic virtual scenarios that replicate both real and virtual environments [10].

AAAA – 2023 – IZOLA - Conference Proceedings

2. MEASUREMENT METHOD

The process of obtaining individual HRTF was conducted in accordance with [8], with the exception that the measurements were taken in an acoustically isolated small anechoic chamber (as seen in **Fig. 1.**).

Fig.1. HRTF measurement in the anechoic chamber

The binaural sound system developed for the localization accuracy experiment was implemented using a high-quality open-type headphone set, a high-quality external sound card, a PC, a wired head tracker with a PC application to send tracking data via the OSC protocol [11], REAPER v6.75 as the software of choice for the Digital Audio Workstation (DAW) [12], and a Sparta Binauralizer VST plug-in [13, 14].

Prior to participating in the experiment, participants were provided with an informed consent form and written information and instructions about the research and experiment. Both the headphones and the head tracker were placed firmly on the participants' heads. To determine the direction in which the sound was arriving, participants sat on a swivel chair and were free to swivel their body and head. To localize the sound source and determine its azimuth and elevation directions, two paper bands were stretched symmetrically over a 180° arc around the listening position in the horizontal and vertical planes, with the azimuth and elevation angles marked at 1° resolution (as seen in **Fig. 2.**).

The radius of the paper arc was 1.5 m, and the precision of the markings was checked with the digital protractor.

Fig.2. Horizontal and vertical paper tapes used for determining the azimuth and the elevation of the sound source

To avoid negative values for azimuth and elevation, which would be more difficult for the participants to read, the frontal direction was assigned an azimuth and elevation of 90°, resulting in a range of 0° to 180° for both parameters. Participants were asked to determine the initial and final azimuth (or elevation) of a virtual sound source moving in the horizontal (or vertical) plane within the selected range of azimuth (elevation) angles.

The sound stimulus used in this experiment was a single knock on a piece of wood repeated at a rate of 3.53 knocks per second. The total duration of the stimulus was randomized and ranged from 8 to 12 seconds. The direction of arrival of the sound source changed continuously from an initial value to a final value with an inconsistent angular velocity (between 4° and 10° per second).

The angular velocity of the virtual sound source was randomized (by no more than 3° per second from the initial velocity) to avoid automatic rotation of the head after adaptation to the constant velocity of the sound source (in the case of a constant angular velocity). As an additional measure to avoid automatic rotation of the head, in some cases the sound stimulus was allowed to have a rotational azimuth in the horizontal plane, i.e., the position at which the virtual source changes its direction of motion, i.e., begins to move back toward the initial position. The vertical and horizontal planes were tested independently, and participants were informed which paper band to focus on before each individual

measurement. Participants were instructed to verbally indicate the initial direction of the virtual sound source immediately after its localization and the final direction from which they perceived the sound after the sound stimulus had ended (as shown in **Fig. 3.**).

Fig.3. A participant with head-mounted binaural system elements on a rotating chair, tracking the virtual sound stimulus

Prior to the start of the actual test, two test examples were played to each participant to verify the functionality of the binaural system and to ensure that participants understood the experimental protocol.

In total, each participant listened to 18 test cases and indirectly evaluated the effectiveness of three different HRTFs. The three HRTFs studied were the participant's own individual HRTF, a generic HRTF obtained from the Neumann KU100 dummy head [15], and another person's individual HRTF obtained from a single participant who had his individual HRTF measured but did not participate in the experiment. The SOFA file containing the generic HRTF was the only one with 2702 defined directions, whereas both individual HRTFs had 1460 defined directions (3° resolution). While a higher number of directions measured for the generic HRTF could imply a potential advantage of the generic HRTF over the individual HRTFs in terms of localization accuracy in the horizontal plane, it is unlikely to have an impact on localization accuracy in the vertical plane.

To minimize the possibility of developing a bias, measurements in the horizontal and vertical planes were systematically alternated every three measurements. In addition, the three HRTFs were randomly rearranged after each segment with three measurements to minimize potential confounding effects.

3. RESULTS

The following section presents the results of the statistical analyses of the raw data collected during the experiments and the adjusted raw data. In the statistical analysis, all statistical significance decisions were made at the 0.05 significance level. The statistical analyses were performed in R [16].

The statistical analysis used repeated measures of analysis of variance (ANOVA) [17]. It was performed according to [18]. There were 25 independent participants with multiple measured data. Their results with the same parameters (HRTF, vertical or horizontal plane, starting or ending angle) were averaged as independent data points. Each participant contributed 12 data points for the analysis.

For each of the three HRTFs, there existed perceived sound source directions represented by their azimuth or elevation angles, indicating horizontal or vertical starting and ending directions. The obtained data was statistically analyzed by computing the absolute (non-negative) values of the deviation from the correct azimuth (or elevation) starting and ending direction of the virtual sound source. In the event of missing data arising from participant uncertainty regarding the starting or ending angle of the virtual sound source, the average absolute deviation for the corresponding data point was computed without the missing value by utilizing other available deviation data from the same data point. It is noteworthy that there was always at least one selected angle for each data point for each participant, resulting in no missing data from the independent data points for all the participants, which was a crucial factor regarding the proper usage of repeated measures of ANOVA.

Given the small number of outliers (less than two outliers for every 25-point data set), the mean/median imputation technique was employed to adapt outlier values for ANOVA. Normality testing using Shapiro-Wilk's test was performed on all data sets, demonstrating that the data is normally distributed. Finally, Mauchly's test of sphericity was used to verify that the null hypothesis of equivalent variances of differences was fulfilled. Box and whisker plots were generated for the absolute deviation from true horizontal and vertical starting and ending points, as presented in **Fig. 4.**.
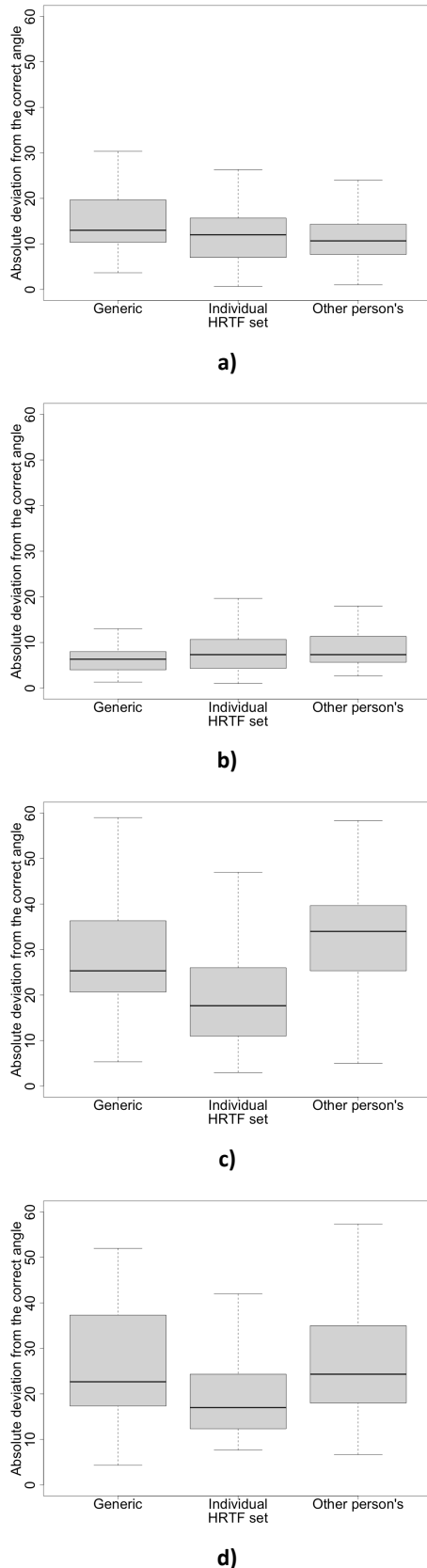
a)

b)

c)

d)

Fig.4. Box and whisker plots for the absolute deviation from a true angle as the measure of localization accuracy, depending on the used HRTF, for: (**a**) the horizontal starting angle, (**b**) the horizontal ending angle, (**c**) the vertical starting angle, and (**d**) the vertical ending angle of the virtual sound source.

ANOVA results were calculated as follows:

- For the horizontal starting angle: $F(48,2) = 7.052$, $p = 0.002$.
- For the horizontal ending angle: $F(48,2) = 3.223$, $p = 0.049$.
- For the vertical starting angle: $F(48,2) = 10.113$, $p = 0.000216$.
- For the vertical ending angle: $F(48,2) = 4.542$, $p = 0.016$.

The results derived from the experiment demonstrate the presence of statistically significant variances across all four parameters that were examined, with respect to the employed HRTF. In order to conduct a more comprehensive evaluation of the performance of each individual HRTF in comparison to other HRTFs, a pairwise comparison was executed.

The outcomes of the pairwise comparison concerning the horizontal starting angle indicate that there is no statistically significant difference in absolute deviation from the true angle between one's own individual HRTF and the individual HRTF of another person ($p > 0.05$). However, a statistically significant difference is observed between both of these cases and the case when generic HRTF is used ($p < 0.05$).

For the horizontal ending angle, there was no statistically significant difference between HRTFs.

The results obtained from the pairwise comparison indicate a significantly lower absolute deviation from true vertical starting and ending angles when one's own individual HRTF is used, compared to the remaining two HRTFs ($p = 0.007$ and $p = 0.016$).

Furthermore, the measurement results obtained from the participants were subjected to analysis to check the accuracy of determination of the direction of movement of the virtual sound source. In cases where the angular value of the sound source increased from the starting angle to the ending angle, it was assigned a value of "1". Conversely, if the angular value decreased, it was assigned a value of "0". This process was carried out for both the programmed values and the measurement results to

determine the correct direction of movement. The outcomes of this analysis are presented in Table 1.

	Generic HRTF	One's own individual HRTF	Individual HRTF of another person
Horizontal plane	98.67%	98.67%	100%
Vertical plane	44.12%	83.56%	55.07%

Table 1. Correct determination of the direction in which the sound source moves (in percent)

A Chi-Square (X^2) test was conducted to test whether the scores obtained for correct and incorrect determination of the direction of movement in the vertical plane carry any statistically significant difference from the values expected from purely guessing the direction by random chance. This was particularly important regarding the generic HRTF since the correct determination percentage was slightly below 50%. The results of the Chi-Square test imply that no statistically significant difference exists in this case, i.e. the determination of direction in the vertical plane using generic HRTFs is essentially based on guessing. A binomial test was also conducted, and it confirmed the results of the Chi-Square test (p=0.3961). The presented results demonstrate that using one's own individual HRTF leads to considerably higher accuracy when determining the direction in which the sound source moves in the vertical plane.

4. CONCLUSION

In summary, this study presents a novel methodology for evaluating the localization accuracy in binaural audio systems, with a particular emphasis on identifying potential enhancements through the use of an individual's own HRTF as opposed to a generic HRTF or that of another individual. While the findings indicate a statistically significant improvement in accuracy for an individual's own HRTF in the vertical plane, they also suggest the absence of universal statistically significant improvements in localization accuracy in the horizontal

plane when utilizing one's own HRTF in comparison to other HRTFs. Subsequent studies could concentrate on comparing the performance of the individual HRTF measurement method employed in this research with alternative approaches for measuring individual HRTF.

5. REFERENCES

[1.] Middlebrooks, J.C. Sound localization. In *Handbook of Clinical Neurology*; Elsevier: Amsterdam, The Netherlands, 2015; Volume 129, pp. 99–116.

[2.] Wightman, F.L.; Kistler, D.J. **Headphone simulation of free-field listening**. I: Stimulus synthesis. *J. Acoust. Soc. Am.* **1989**, *85*, 858–867.

[3.] Broderick, J.; Duggan, J.; Redfern, S. **The Importance of Spatial Audio in Modern Games and Virtual Environments**. In Proceedings of the 2018 IEEE Games, Entertainment, Media Conference (GEM), Galway, Ireland, 16–18 August 2018; pp. 1–9.

[4.] Johnston, D.; Egermann, H.; Kearney, G. **The Use of Binaural Based Spatial Audio in the Reduction of Auditory Hypersensitivity in Autistic Young People**. *Int. J. Environ. Res. Public Health* **2022**, *19*, 12474.

[5.] Dede, C.; Jacobson, J.; Richards, J. Introduction: Virtual, Augmented, and Mixed Realities in Education. In *Virtual, Augmented, and Mixed Realities in Education*; Liu, D., Dede, C., Huang, R., Richards, J., Eds.; Springer: Singapore, 2017; pp. 1–16.

[6.] Berger, C.C.; Gonzalez-Franco, M.; Tajadura-Jiménez, A.; Florencio, D.; Zhang, Z. **Generic HRTF May be Good Enough in Virtual Reality. Improving Source Localization through Cross-Modal Plasticity.** *Front. Neurosci.* **2018**, *12*, 21.

[7.] Li, S.; Peissig, J. **Measurement of Head-Related Transfer Functions: A Review**. *Appl. Sci.* **2020**, *10*, 5014.

[8.] Reijniers, J.; Partoens, B.; Peremans, H. **DIY Measurement of Your Personal HRTF at Home: Low-Cost, Fast and Validated.** Convention e-Brief 399. In Proceedings of the 143rd International AES Convention, New York, NY, USA, 18–21 October 2017.

[9.] Reijniers, J.; Partoens, B.; Steckel, J.; Peremans, H. **HRTF Measurement by Means of Unsupervised Head Movements with Respect to a Single Fixed Speaker**. *IEEE Access* **2020**, *8*, 92287–92300.

[10.] Planinec, V.; Reijniers, J.; Horvat, M.; Peremans, H.; Jambrošić, K. **The Accuracy of**

Dynamic Sound Source Localization and Recognition Ability of Individual Head-Related Transfer Functions in Binaural Audio Systems with Head Tracking. *Appl. Sci.* **2023**, *13*, 5254.

[11.] Wright, M.; Freed, A. **Open Sound Control: A New Protocol for Communicating with Sound Synthesizers.** In Proceedings of the International Computer Music Conference (ICMC), Thessaloniki, Greece, 25–30 September 1997; pp. 101–104.

[12.] COCKOS Inc. **Reaper: Digital Audio Workstation.** Rosendale, NY, USA, 2023. Available online: **https://www.reaper.fm** (accessed on 29 August 2023).

[13.] McCormack, L.; Politis, A. **SPARTA & COMPASS: Real-Time Implementations of Linear and Parametric Spatial Audio Reproduction and Processing Methods.** In Proceedings of the AES International Conference on Immersive and Interactive Audio, York, UK, 27–29 March 2019; p. 111

[14.] McCormack, L.; Politis, A. **Spatial Audio Real-Time Applications**. Available online: **http://research.spa.aalto.fi/projects/sparta_vsts/** (accessed on 29 August 2023).

[15.] **Neumann KU100 Operating Instructions**. Technical Report. Available online: **https://www.manualslib.com/manual/110720/Neumann-Berlin-Dummy-Head-Ku-100.html** (accessed on 29 August 2023).

[16.] R Core Team. *R: A Language and Environment for Statistical Computing*; R Foundation for Statistical Computing. Vienna, Austria, 2021; Available online: **https://www.R-project.org/** (accessed on 29 August 2023).

[17.] Park, E.; Cho, M.; Ki, C.S. **Correct use of repeated measures analysis of variance**. *Korean J. Lab. Med.* **2009**, *29*, 1–9.

[18.] Finnstats. **Repeated Measures of ANOVA in R Complete Tutorial**. Available online: **https://finnstats.com/index.php/2021/04/06/repeated-measures-of-anova-in-r/** (accessed on 29 August 2023).

AAAA 2023 IZOLA 20. - 21. September
10th CONGRESS OF THE ALPS ADRIA ACOUSTICS ASSOCIATION

Contributed papers
Noise and vibrations

1. Ilegal use of firecrackers and its consequences - case study of human rights violation at Slovenian courts – part i: legislation and court proceedings
    Ferdinand Deželak (Retired researcher)
2. Ilegal use of firecrackers and its consequences - case study of human rights violation at Slovenian courts – part ii: physical background
    Ferdinand Deželak (Retired researcher)
3. Low frequency noise measurement in the passenger cabin
    Samo Beguš (University of Ljubljana, Faculty of Electrical Engineering)
4. Measurement and Characterization of Control Valves Noise
    Egon Susič (Danfoss Trata d.o.o.)

Ilegal Use of Firecrackers and its Consequences - Case Study of Human Rights Violation at Slovenian Courts – Part I: Legislation and Court Proceedings

Ferdinand Deželak

Retired researcher

Abstract

In first part of this paper a human rights violation at some Slovenian courts is briefly highlighted. This violation has been firmly proved not just through a judicial proofs, but also by a full physical analysis. Apart of the court proceedings some important physical facts are described, which were quite misunderstood and even intentionally neglected at more Slovenian courts. The corresponding legislation which was misinterpreted or even ignored is shortly presented as well. Such ignorance resulted in quite contradictory and illegal judgments.

Some years ago, one attacker threw an explosive device at the victim, which consequently suffered a permanent hearing impairment. Although reporting this attack to the Police, further criminal and lawsuit proceedings at the different courts in Ljubljana against the attacker were corrupted, unprofessional and completely biased by some judges.

Lawsuit proceedings were started by one corrupted judge, who was later found guilty of corruption and dismissed from judicial service. The next judge then appointed one retired court expert witness in order to solve some audiometric and acoustic problems concerning a victim's hearing loss as a result of this explosion. However, he was not familiar with basic facts of acoustics and was not able to do that job correctly.

Keywords: audiometry, corruption, criminal proceeding, expert witness testimony, firecracker noise, hearing damage, high impulse noise, human rights violation, litigation, peak sound pressure level.

1. INTRODUCTION

The use of fireworks and firecrackers is strictly limited in most of the European countries. Unfortunately, some people still violate these legislative requirements. In many cases, police actions mitigate these problems by taking appropriate measures, especially of a preventive character. On the other hand, some problematic cases, where violence and personal injuries are involved for instance, are regularly entrusted to the courts, where it is expected a right and fair solution to be found. Often however, successful police actions are entirely revoked as a result of a corruption and erroneous court decisions. This paper describes one of such cases which was quite unprofessional and of a highly corruptive nature. It started in the District Court of Ljubljana (Slovenia). Even higher Slovenian courts were not able to solve and explain it till now.

In this article, a presentation of bad work practices at some courts is analyzed. Situations where some Slovenian courts select bad judges and experts witnesses without an appropriate knowledge and experience are not rare. Consequently, such expert testimonies can be quite wrong, including those in the field of acoustics and audiometry. In this paper one of such cases which is related to a set of other poorly guided procedures at these courts, violating law, human rights and dignity, is briefly highlighted.

It all started when one perpetrator (the attacker J.L.) threw a powerful firecracker, which exploded approximately 4 to 5 meters from the right ear of the plaintiff (victim F.D.). This loud explosion resulted in his hearing impairment, so the prosecution was submitted at the District Court against the attacker. However, the judges at this court were not interested in finding a fair and legal solution as they fully sympathized with the attacker. Therefore, the trial of this court was far from being fair and professional.

Apart of this, the first judge F.K., who started litigating process of this case, was generally not of high moral character and has been engaged in some activities which were quite incompatible with his position as an independent and impartial judge of a full-time office and with his general judicial function. Although he was suspended after four years of work on this case, another judge of this court, A.B., continued to apply this bad practice, especially in the field of acoustics and audiology, which were crucial elements of this case. So, the second judge appointed an expert witness A.G., (who was even not a member of the court experts society) in order to solve professional questions concerning this explosion and its consequences to the plaintiffs hearing impairment. However, this expert was not only in a biased position but

was also unfamiliar with fundamental acoustic and audiometric facts, so he has even not been able to provide the correct answers to the plaintiff questions and to the court. In this way the expert witness has given false and fraudulent testimony. Most of his methods were wrong or unreliable, so even the expert himself was unable to test and explain them properly. This affected the error rate, so it was quite impossible for someone else to reproduce the process. On the other hand, the new judge permanently intervened and discussed about the professional questions, although she did not understand them. In this way she proclaimed almost all important acoustic and medical questions as irrelevant. When such a situation does occur, it would certainly place the court and law firm in jeopardy. It comes as no surprise then that many Slovenian citizens do not trust to such a judicial system.

The author primarily focused on the incorrect position of this expert witness and the misleading aspects of his testimony, pointing further to bad practice in the District and other courts of higher instances, resulting in quite wrong conclusions and judgements.

2. EVENT DESCRIPTION AND COURT PROCESSING

On April 10th 2012, the perpetrator threw an explosive device (a stronger firecracker) at the victim without any warning. In this attack the plaintiff suffered a permanent hearing impairment, among other things. Such violation include both crimes and civil wrongs. The plaintiff, reported this attack immediately to the Police, which completed its job. Unfortunately further criminal proceedings at the District court in Ljubljana against the attacker were corrupted and completely biased, starting with the District judge at criminal department M.L.B. The former Minister of Justice M.K. namely intervened and protected the attacker with his undue influence and managed to reject the existing proofs and criminal proceedings against the attacker in this court.

2.1. Criminal Trial Dealing with the Attacker Criminal Act

Since the same beginning the District judge M.L.B., dealing with the attacker criminal liability, constantly tried to persuade a plaintiff to resign from further prosecution. When not successful she tried to divert attention and began harassing and intimidate the plaintiff with completely irrelevant questions, like whether he had written some insulting letters to one notary and which has nothing to do with the present case (except perhaps the judges connections with this notary). On the other hand, she deliberately ignored much more important facts, such as attacker obligations toward the victim. The Ljubljana District Court namely proposed itself and confirmed earlier another criminal trial IK 962/2004 [1], about the attacker obligations to avoid any conflict with the plaintiff. Despite the plaintiffs warnings about these

important things, the judge completely refused to consider these obligations of court, saying directly that she will decide what should be neglected and what not. Although the attacker caused permanent hearing damage to the plaintiff by its criminal action, he has been completely acquitted; even despite this obligation and the established judicial practice [2], which in such cases anticipates for high compensation and criminal liability. However, even the prosecutor herself was not interested about seriousness and consequences of the attacker infringements.

The aggressor who caused permanent health damage to a victim, by throwing an explosive device was thus completely released of any responsibility, and all costs of these criminal proceedings were covered from the budget, including the costs of his attorney employed by the former Minister of Justice M.K. On the other hand, the injured victim has been sentenced to cover all the costs by himself. Moreover, in contrast of the attacker the victim was even sentenced to fully pay the court taxes.

It is more than obvious that the District judge M.L.B. systematically and consciously violated the law and the human rights of the victim, just in order to fully protect the interests of the attacker J.L. In her judgment no. VI K 38124/2014 [3] she completely relieved the attacker of any obligations and responsibilities. She did this without any appropriate explanation, although it has been proved that the attacker intentionally threw an explosive device at the victim, causing him permanent injuries. It is not strange that such misconduct of judge, like a suppressing evidence from the victim, encouraging deceit from witnesses and prosecutorial bluffing (threats and intimidation) further encouraged the attacker, so his violent actions against the victim not only continued, but even escalated.

2.2. Start of Lawsuit Proceeding with a Corrupted Judge

There is no doubt that such trial of the attacker was quite unlawful and inadmissible. The plaintiff (victim) therefore also claimed for damages against the perpetrator J.L. at the District Court in Ljubljana for the fear suffered and permanent hearing impairment caused by his explosive device. Unfortunately, this civil procedure has been even more biased and taken over by another corrupted judge of the same court, F.K., who has later been found guilty of corruption and dismissed from judicial service. He has been sentenced due to acting in ways that are considered unethical and since he violated his judge's obligations of impartial conduct several times.

The explosion, which took place due to a perpetrator attack, has been unpredicted and unexpected, so the plaintiff's ears were totally unprotected and were exposed to a high-impulse sound pressure level exceeding 150 dBC. Independent audiometric tests showed that this resulted in hearing impairment of the plaintiff. However the first judge F.K., who started processing this civil case, ignored these audiometric tests completely together with the most valid evidence. After a five years his employment at the District Court was terminated due to several court scandals coming into publicity and which the court was unable to conceal any more, so the judge F.K. was consequently suspended.

2.3. Replacement of a Judge and Appointment of an Unreliable Expert Witness

The case was then handed over to a new judge, A.B., who was also immediately pressured by the former Minister of Justice. This new judge made it clear at the outset already, that the plaintiff has no chances of succeeding in this case, despite the indisputably proven guilt of the perpetrator (attacker). The former Minister of Justice and the attorney of the attacker even suggested that the plaintiff should be fined with a high penalty costs, which the new judge A.B. immediately took into consideration and in the end actually fined the plaintiff with 5.600 EUR[4, 34, 35, 36].

So, this replacement did not improve the situation in no way. A new judge A.B. adopted a similar corruptive practice. She decided to appoint an unreliable expert witness in order to resolve some professional questions on acoustics and audiology and to assess the seriousness of this explosion. Apart from her biased position, she selected the expert witness with an unprofessional knowledge and experience. It is imperative of course, that judge must choose their experts wisely, but she did not. This further resulted in a quite unprofessional work by this expert witness [5], including his poorly planned measurements, erroneous calculations and quite incorrect conclusions. Despite additional cross examination [6], he was unable to give correct and logical answers to the most important questions.

2.4. Wrong Expert Witness Working Methods and their Uncritical Confirmation by the Court

So this expert witness testimony was as expected, designed in advance, heavily biased and completely wrong. Expert witness testimony has not been based on a professional standard for the field of interest. Since the plaintiff, himself is an expert in this field as well, he has also been able to professionally observe and critically evaluate this expert's work. The plaintiff completed Ph.D. in the field of impulse noise [7] and also acted as a court expert witness himself in some similar tasks. As to the position regarding expertise of witness, there were no official trial for this to be examined, although such bad evidence is normally be ruled inadmissible. Instead, the judge A.B., a former minister M.K. and the expert A.G. simply took a position of their power and immunity, based apparently on the principle "la loi c/est moi". They simply understand their immunity as something quite absolute.

It is quite obvious that some judges of the District Court in Ljubljana, under the pressure of the former Minister of Justice, did not condemn the planned attack on the plaintiff, with a dangerous explosive device. Even more, they even approved this attack on the plaintiff's body, despite quite opposite international and slovenian law practice. A former Minister of Justice M.K. namely intervened again in the attacker's favor. In this way, the case completely deviated from the established practice of law and norms, just in order to protect the attacker interests for any price. All the plaintiff's appeals were in vain. The former Minister of Justice with his political influence further managed to convince the Higher Court in favor of the attacker as well. Indirectly, the Supreme and Constitutional Court were under his pressure as well. In this way the case acquired a completely new political and corruptive dimensions.

It is undisputed, and even the attacker himself did not deny the fact, that he deliberately threw an explosive device on the plaintiff, causing permanent health damages to him. It was thus proved beyond a reasonable doubt that the perpetrator committed the crimes charged, which consequently caused damage to the plaintiff. Additionally, this has been confirmed by the police investigations as well. In this way, the courts intentionally ignored all important evidences and proofs.

All court procedures were conducted quite in contrast to the proofs and established case law [2], which in such cases anticipates for high compensation and criminal liability. All previous court obligations of the attacker about settlement at the District Court in Ljubljana [1], where it was required that the attacker must make any effort to avoid conflicts with the plaintiff, were intentionaly neglected as well.

In its judgment [8], even the Higher Court uncritically

accepted the very similiar judgement as the District Court in Ljubljana did, confirming the unprofessional testimony of A.G. On the other hand, although the slovenian courts themselves do not have any knowledge in acoustical field they nevertheless interfere deeply into professional issues of acoustics, making new additional cardinal errors.

In a quite similar way the Supreme [9] and Constitutional Court of Slovenia [10, 11] confirmed that the plaintiff was not entitled to any compensation for the deliberately produced explosion, causing consequently a permanent health damage to him. Such activities of the four slovenian courts not only supported intentionally caused health impairments, humiliation, material damage to the plaintiff, his human rights and dignity violation. There is also the reputation of these courts in question, which, by uncritically confirming unprofessional claims and erroneous conclusions of expert witness A.G., were quite embarrassed. It is probably not necessary to emphasize that by confirming such a corrupted judgment, it has been fully accepted and transferred into established case law. The District Court even fined the plaintiff (a victim) additionally, with an unusually high penalty of over 5.600 EUR [4, 34, 35, 36]. The Higher Court confirmed this in order to compensate interventions of former minister M.K. [8]. This encouraged him, so after that he even raised that amount [34, 35, 36]. This can be interpreted of course, that since then the attack with the explosive devices should to be considered completely legal. Even more, in the case of criminal or lawsuit proceedings, the attacker can even be financially stimulated and rewarded, while the victim of the attack can expect to be punished.

In its answer, the Higher Court in Judgment [8] namely only routinely repeats the claims of the District Court, that the explosion of a firecracker presents no danger at all and that there is no possibility for any hearing damage, claiming further that this has been proved by objectively measurable data on blast intensity of the expert witness A.G. ?! First of all, the court nowhere explained what it understands by "objectively measurable data on blast intensity", since the expert witness had not perform any blast intensity measurements and analysis at all. Even more, the expert witness even refused to explain, what he understand under the term blast intensity. The court further reiterates the expert cardinal error that the intensity of the sound due to the firecracker explosion is 124.08 dB at a distance of 5 meters (no specification of decibels were stated). It did not explain which decibels it has in mind, repeating the same cardinal error as the

expert witness A.G. did before (see annex A). It further unfoundedly accused the plaintiff of not having knowledge about hearing, and then draws the final erroneous conclusion that the firecracker's explosion could not have caused any acoustic trauma at all, relying solely on the erroneous conclusion of the expert witness A.G. again, without any justification.

The plaintiff repeatedly emphasized the most important issue of the difference between 120 dB (A, imp), as considered by the European legislation on firecrackers and 130 dB to which the expert erroneously refers as limit value for hearing impairment (annex A). Due to the bad professional knowledge of expert witness A.G. and permanent influence of the former minister M.K., this most important issue remained unsolved by all courts; although the plaintiff had explained it several times. During the cross examination [6], the expert replied in confusion that we have a relative decibel and an absolute decibel and that he know these two kinds of decibels from an audiological point of view. Despite repeated trials, the expert avoided to explain to this most important question about decibel units, which he used incorrectly. To purely concrete questions, he merely replied in confusion that "he uses a level of 130 to 140 decibels, which can already lead to health damage." When asked again what decibels he was talking about, the expert becomes upset that he will not discuss about such questions and the judge A.B. fully supported him to refuse this the most important explanation. The use of such incorrect metrics by the expert resulted in a difference of 26 decibels, which means an error by factor of 400. In this way the expert got a completely wrong results and thus also the conclusion, which he was unable to explain. For the sake of transparency, the plaintiff made a comparison of EU Directive [12] and what the expert asserted. Namely, the requirement of this European Directive to which the expert actually refers, demands that the maximum noise level must not exceed 120 dB (A, imp) at the safety distance.

The difference between the two quotes is obvious. While the European directive [12] prescribes a limit of 120 dB (A, imp), the expert witness A.G. considered only the first part of this specification, that is 120 dB. He then compares this directly with the hearing protection directive [13], which uses dB (C, peak) as a metrics. Such processing of expert witness is quite wrong of course (see Annex A). Even more, he made some additional mistakes as described later. Interestingly, even the Higher and Supreme judges

stubbornly ignored this most important fact, although they were strictly and explicitly warned about it. Due to their missing knowledge the judges further confused the term "metrics" with "matrix," which of course denotes something quite different and with which these judges again merely ashamed themselves.

In addition, the expert witness also violated Regulation 679 EU 2016 on the protection of personal data and on the free movement of such data [14]. The expert witness A.G. namely disclosed many sensitive plaintiff's personal data, although they were not necessary for his testimony at all. Even the expert witness himself later admitted that he did not need nor used numerical data on the plaintiff's blood pressure, cholesterol, triglycerides and the like. Nevertheless he disclosed all these strictly confident numerical values to the opposite party without the plaintiff's consent. He did not need these data for expert testimony at all and, of course, he did not use them, as they have nothing to do with hearing impairment. If they had, the courts would have to take them into account, but of course, they didn't. The plaintiff also repeatedly pointed out these facts to the court. However, the judge A.B. merely responded vaguely to these warnings that she is not interested about the plaintiff's personal data. Interestingly, during the cross-examination, the District judge A.B. persistently blocked plaintiff's questions by emphasizing that expert was dealing with "audiological decibels". During the cross-examining expert witness the judge A.B. find herself wading into technical areas where she was far inferior. She was not prepared to such situation before stepping into the courtroom. Despite this, she interfered with most professional questions, although she has not been able to explain their definitions and meanings, or what she was actually talking about, till now. At the plaintiffs request she simply replied, that this is not her duty [15].

In the middle of cross examination she interrupted the plaintiff, not allowing him any further question and closed the process of hearing without finishing necessary investigation. Here the validity of an expert's testimony was also challenged due to the methodology used to form his testimony. However, the judge A.B. disabled no impeachment, neither allowed any further questions. Even more, she blocked any plaintiffs question requiring the clarification of such experts contradictions and encouraging him simultaneously not to answer to any further questions. Even higher courts in Ljubljana supported this behaviour so the plaintiffs right to fair trial

was heavily violated. He was not entitled to a fair and public hearing within a reasonable time by an independent and impartial tribunal established by law [16].

If a witness's testimony at hearing contradicts his earlier statements (as happened here as well), one or both parties might bring up these statement to impeach his testimony. The control and understanding of these processes is vital to producing verifiable and reproducible conclusions. However, no one of the factors that may be considered in determining whether the methodology used is valid, were used. No checks, like whether the theory or technique in question can be and has been tested nor its known or potential error rate were made, despite many plaintiffs objections in this direction.

The courts finally took a position that nothing was wrong with such processing. They even claimed that what happened during the hearing loss event due to firecracker explosion is quiet irrelevant. In this way, they completely and intentionally ignored the most important facts; namely that the plaintiff has been ambushed by the attacker with an explosive device. They further ignored that sound pressure level at his right ear exceeded 150 dB (C, peak), which is more than 15 dB (C, peak), or more than 30 times higher than allowed for the hearing conservation purposes by EU normatives [13]. On the other hand, it has been professionally proved that the plaintiff suffered hearing impairment as a result of the explosion caused by a deliberately thrown firecracker close to his right ear.

The Higher Court relied his decision on the short and erroneous arguments of the District Court as well as on a wrong expert witness testimony of A.G., which were completely erroneous [5]. At the same time, it clearly confirms that it did not consider the plaintiff's professionally substantiated remarks, making fun of his health, human rights and dignity.

The Supreme [9] and Constitutional courts [10, 11] also avoided to deal with these most important questions and just confirmed what the District and Higher court decided, without any further explanations.

Apart of criminal and lawsuit legislation many Directives, laws and standards were violated. Such infringement present a serious violation of human right and dignity of the plaintiff.

Even more, the executive department of the District Court [35] issued an order specifying a double amount of perpetrator costs to be paid for the same litigation and fined the plaintiff for the additional sum of EUR 1,600.00, i.e. a total of more than EUR 5,600.00. So far, the court did

not reveal what the background of this failure was: the deliberate attacker deception by the court help, or simply an extremely negligence of the court again [35], although their terrible mistakes were confirmed as well [36].

3. THE ROLE OF A EXPERT WITNESS

Generally, expert witness must have a reliable knowledge and be experienced in a entrusted court case. His duty is to interpret all important facts and to make a completely impartial and independent testimony relevant to the issues in the action. Expert witness, on the other hand, must prove the court the facts about his expertise in order to convince and to believe in the case at hand. Expert witness is called to have an objective testimony in court, completely relying on law and his experiences in the case under consideration. His presence is necessary in order to explain complicated scientific issues; on the other hand, he can not influence the jury or judge with fervor. If the expert witness violates such of his sworn duties, his testimony should not be considered as admissible [24].

When the expert witness lies, when he willfully fails to take into account all the circumstances involved in the case, or when his medical conclusions are outside the realm of accepted scientific method and practice, it can be considered as an unethical and unlawful testimony.

4. LEGISLATIVE REQUIREMENTS

4.1. Fireworks Act and EU Fireworks Directive

First of all, the use of fireworks and firecrackers is strictly limited in most of the European countries. According to Slovenian legislation, the use of certain categories of fireworks is permitted, but only between December 26th and January 2nd and even then only at appropriate locations [17]. Outside this time interval and these locations their use is strictly forbidden. The penalties for such offenses (even when no other accidents are involved) range from four hundred to 1.200 EUR. Despite this, the attacker has not been fined at all, even more, he was rewarded.

According to EU Directive 2013/29/ EU [12], fireworks are categorized according to their type of use, or their purpose and level of hazard, including their noise level, into four categories F1 to F4. They are intended only for outdoor use and minimum safety distance. In this Directive these distances and permitted noise levels are specified, which the expert witness used in a quite wrong

way.

4.2. Noise Protection and Health Directive

Directive 2003/10/EC [13] prescribes limit values of impulse noise, to which the human ears – usually at workplaces can be exposed.

4.3. International Convention for the Protection of Human Rights and Fundamental Freedoms

According to this Convention everyone has the right for fair trial. No one shall be subjected to inhuman or degrading treatment. Everyone is entitled to a fair and public hearing by an impartial tribunal. Everyone whose rights are violated shall have an effective remedy before a national authority not withstanding that the violation has been committed by persons acting in an official capacity. However, all these articles of this Convention were violated by different Slovenian courts.

4.4. Audiometric Standards

In order to obtain a reliable measure of hearing ability and its loss, many factors must be considered. For this purpose some tests are usually performed in specially designed audiometric test rooms. One of the most important requirements, in order to avoid masking the test signal by ambient noise in such a test room, is that the levels of the ambient noise shall not exceed certain values. The standards ISO 8253 [18,19] provide threshold levels, which indicate the maximum ambient sound pressure levels which are still permissible when other minimum hearing threshold levels are to be measured. It sets out procedures for determining hearing threshold levels by pure tone air conduction and bone conduction audiometry.

Ambient sound pressure levels in an audiometric test room shall not exceed the values specified in table 2 of the standard ISO 8253 – 2 [19]. The test subject and the tester shall be neither disturbed nor distracted by non-related events nor by people in the vicinity.

For this reason, permissible ambient noise for threshold determinations in an audiometric test room shall not exceed certain values in order to avoid masking the test tones. These values are specified as maximum permissible ambient sound pressure levels in one-third octave bands for the lowest hearing threshold level. So, to satisfy ambient noise requirements, it will be necessary in many

circumstances to use a sound-isolating booth. Furthermore, a calibration interval of not more than one year is recommended.

4.5. Personal Data Protection Directive

In EU personal information from individuals can be collected and processed in accordance with General Data Protection Regulation [14].

Expert witness can collect such sensitive personal data for specified, explicit and legitimate reasons. According to this Regulation, the health-related data is considered as sensitive personal data and is subject to specific processing conditions.

Personal data must therefore be adequate, relevant and limited to what is necessary in relation to the purposes for which they are collected and processed (data minimisation).

For this reason, the expert witness can use plaintiffs sensitive personal data, but only in a way that is adequate, relevant and not excessive. He is obliged to process personal data only where it is necessary to do so and for the purpose for which it was obtained. Such processing is thus limited to what is necessary to fulfil the purposes, for which he was appointed. If here a risk is identified, it needs to be eradicated or reduced. If he want to use personal data for other reasons, he must inform the plaintiff before doing so, and seek consent about this.

REFERENCES

[1] B.M.Krizaj, The decision of the District Court in Ljubljana, IK 962/2004 with the perpetrator's commitments, October 23th 2007.

[2] Judgment of the High Court in Koper, Cp 381/2012, Aug 8th 2012.

[3] M.L.Brecelj, Judgement of the District Court in Ljubljana, no. VI K 38124/2014, February 17th 2015.

[4] A. Bedene, Judgment of the District Court in Ljubljana II P 1669/2015, September 24th 2018.

[5] Anton Gros, Expert witness testimony n° II P 1669/2015, District Court of Ljubljana, pp. 1 – 10, August 14th 2017.

[6] The cross examination of the expert Gross at the District Court, II P 1669/2015; May 16th 2018.

[7] F. Dezelak, Influence of impulse noise transients on energy equivalent; Ph.D. thesis, University of Ljubljana, Faculty of Mechanical Engineering, Ljubljana 2005.

[8] K. Ceranja, B Javornik and A. Panjan, Judgment of the Higher Court in Ljubljana, I CP 2544/2018, June 12th 2019.

[9] R. Straus, N. Betetto and A.B. Penko, Decision of the Supreme Court in Ljubljana, II DoR 515/2019, November 21th 2019.

[10] M. Pavcnik, D. J. Pensa and R. Knez, Decision of the Constitutional Court in Ljubljana, II Up 96/20, March 9th 2020.

[11] Final decision of the Constitutional Court, II Up 96/20– April 21th 2020.

[12] Directive 2013/29/ EU of the European parliament and of the council of 12 June 2013 on the harmonisation of the laws of the Member States relating to the making available on the market of pyrotechnic articles.

[13] Directive 2003/10/EC on the minimum health and safety requirements regarding the exposure of workers to the risks arising from physical agents (noise).

[14] Regulation 679 EU 2016 on the protection of natural persons with regard to the processing of personal data and on the free movement of such data and repealing Directive 95/46/EC.

[15] A. Bedene, District Court in Ljubljana, II P 1669/2015, The refusal to explain false allegations during the expert cross-examination, March 6th 2020.

[16] European Convention on Human Rights, European Court of Human Rights Council of Europe F-67075 Strasbourg cedex.

[17] Explosives and Pyrotechnic Articles Act; Zakon o eksplozivih in pirotehničnih izdelkih, O.J. RS, 35/2008.

[18] EN ISO 8253 Acoustics- Audiometric test methods- Part 1: Basic pure tone air and bone conduction threshold audiometry.

[19] EN ISO 8253 Acoustics- Audiometric test methods- Part 2: Sound field audiometry with pure tone and narrow-band test signals.

[20] P. Teague, J. Conomos and V. Alexandrou »Overview of Developments in the Description and Assessment of High Intensity Impulse Noise Exposure«, Proceedings of Acoustics 2016, Brisbane, Australia, 9-11 November 2016.

[21] G.Richard Price: »Impulse noise hazard: From theoretical understanding to engineering solutions«, Noise Control Engineering Journal 60 (3), pp. 301-312, May - June 2012.

[22] G. R. Price: »Predicting Mechanical Damage to the Organ of Corti«, Hearing Research, Vol 226, pp. 5 – 13, April 2007.

[23] Non – binding guide to good practice for the application of directive 2003/10/EC Noise at Work; Chapter 7: Hearing damage and health surveillance, European Commission Directorate-General for Employment, Social Affairs and Equal Opportunities, pp. 112 – 119, December 2007.

[24] https://doi.org/10.1007/978-0-387-21818-2_7; Davis G.G. (2004) Unethical Expert Witness Testimony. Springer, New York, NY.

[25] IEC 61672 – 1, Electroacoustics – Sound level meters, Part 1: Specifications.

[26] P. Rasmussen, G. Flamme, M. Stewart, D. Meinke and J. Lankford, »Measuring recreational firearm noise«, Sound & Vibration, August 2009.

[27] Jeremy R. Gaston and Tomasz R. Letowsky, »Listener perception of single shot small arms fire«, Noise Control Engineering Journal 60(3), pp. 236-245, June 2012.

[28] M. Čudina, J. Prezelj and F. Deželak, »Noise immission from firecrackers«, Proceedings of the Eleventh International Congress of Sound and Vibration, St Petersburg, pp. 1291-1298, July 2004.

[29] F. Dezelak, J. Prezelj and M. Cudina, »Some Statistical Aspects of Firecracker Noise«, Journal of Mechanical Engineering, pp. 529-541, 55(2009)9.

[30] R. P. Hamernik and K. D. Hsueh, »Impulse noise: Some definitions, physical acoustics and other considerations«, JASA 90(1), pp. 189-196, July 1991.

[31] N. Kapoor and A. P. Singh: »Firecracker noise and its auditory implications«, Proceedings of the Tenth International Congress on Sound and Vibration, Stockholm, pp. 5063-5070, 2-6 July 2003.

[32] O. V. Mohanan and M. Singh: »Characterisation of sound pressure levels produced by crackers«, Applied acoustics, Vol. 58, pp. 443-449, December 1999.

[33] Military noise environment Hearing Protection – Needs, Technologies and Performance, NATO Technical report by Task Group HFM – 147, chapter 3, November 2010.

[34] M. Kozinc, Court correspondence with proposals of former minister to the District Court in Ljubljana, II P 1669/2015, July 16th 2019, August 23th 2019.

[35] P. Baša, Judgment of the High Court in Koper, I Ip 45/2023, Jun 15th 2023.

[36] E. Spetič, Explanation regarding the decision on enforcement of the District Court in Postojna, 0449 I 53/2022, July 7th 2023 and July 21th 2023.
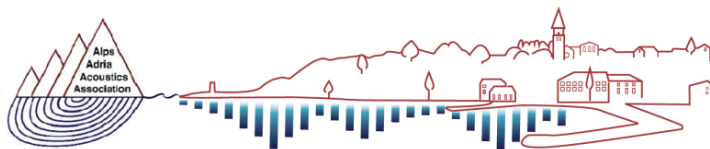
Ilegal use of Firecrackers and its Consequences - Case Study of Human Rights Violation at Slovenian Courts – Part II: Physical Background

Ferdinand Deželak

Retired researcher

Abstract

In second part of this paper a physical background of firecracker explosion and its influence on hearing damage is described. This explosion took place very close to the victim's right ear. The peak of its sound pressure was around 150 dBC. However, due to incorrect metrics used, the expert witness estimated intuitively this level to be much lower, with four hundred times to low energy value, received by the victim's ear. The expert completely misinterpreted several European directives concerning this field. Based on such erroneous assumptions, he concluded that no hearing damage could be possible as a result of this explosion. Apart from incorrect metrics, he also confused some important acoustic quantities and facts, resulting in additional cardinal errors. Due to a lack of fundamental knowledge regarding high impulse noise and its propagation, he was unable to recognize the importance of its amplitude and spectral characteristics for hearing damage. He further confused reflection, refraction, diffraction and other factors, resulting in misleading expert testimony and its wrong conclusions. Despite numerous warnings and evidence, the judges uncritically accepted these erroneous conclusions and made completely unacceptable and fraudulent judgments, resulting in the conscious violation of the victim's human rights by various Slovenian courts.

Keywordss: audiometry, corruption, criminal proceeding, expert witness testimony, firecracker noise, hearing damage, high impulse noise, human rights violation, litigation, peak sound pressure level.

1. SOME PHYSICAL CHARACTERISTICS OF FIRECRACKER NOISE

A firecracker usually consists of a cylinder-form tube, filled with an explosive, producing a loud noise when it explodes. In such explosions a definite amount of chemical energy is partially converted into electromagnetic energy (heat and light), and partly into mechanical energy as a shockwave. The physical characteristics of such explosions depend on the type of firecracker and its composition, primary on the size, weight and encapsulation of the explosive used which present the most important emission factors. Apart from emission, a considerable role in sound overpressure formation at the point of reception is played by the distance and presence of different objects that influence reflections, diffractions, etc (Annex B).

Firecracker explosions belong to a group of high impulsive noises which are particularly hazardous for hearing impairment. The firecracker explosion produces a transient sound signal which is manifested as an impulse noise with sharp rising time (more than some 100 dB/s) and of short duration.

It is true, that the noise from a gunshot, especially from some larger calibers, can be even noisier. However, it is important to note that shooters, bystanders and other personnel exposed to such noise usually tend strictly to apply hearing protection devices. On the other hand, when fireworks are used, such protection is almost never applied. This is especially true for persons not using firecrackers and during the time when their use is strictly prohibited.

2. THE INFLUENCE OF FIRECRACKER NOISE TO HEARING DAMAGE

When a firecracker explodes, it produces ear-splitting sounds which may be amusing to the user, but on the other hand, this is generally recognized as a source of danger noise pollution in the environment. This can further shift the hearing threshold or even produce deafness. Many impulse noises from firecrackers are so intense that a single unexpected impulse incident to unprotected ears can result in severe and permanent hearing loss, although the impulse is usually very short

and contains relative little energy.

Impulse noise from firecracker explosions creates several particular hazards to the human auditory system. First, the high peak levels associated with firecrackers may damage the cochlea by causing rapid mechanical failure and injury. A series of rapidly occurring impulses can be partially attenuated by the acoustic reflex, a reflexive contraction of the middle-ear muscles, while isolated impulses reach the cochlea unattenuated before activation of the acoustic reflex [20]. It is thus important that contraction of the middle ear muscles can occur prior to occurrence of the impulse noise if such a noise had been warned prior by another loud signal. Price refers to the human reaction to such an unexpected and expected sounds as the unwarned response and warned response [21, 22]. Thus, the expected occurrence of a noise impulse is much safer for the hearing organ (warned response) than the unexpected event (unwarned response - as was the case during the plaintiff's exposure to the firecracker explosion). This difference in human reaction may be caused not only by the anticipatory contraction of the middle ear muscles but also by lower general physiological stress within the auditory system. For example, an extreme unwarned response (the startle response) is characterized by vasoconstriction and can affect the biochemistry of the organ of Corti. Thus, single intense and unexpected explosions may result in large cochlear lesions and significant hearing loss. The most common symptom of such an acoustic trauma is tinnitus, manifesting as a ringing in the ears [20]. Although a certain amount of hearing recovery takes place after an acoustic trauma episode, the individual is often left with severe, permanent hearing loss. So at last 7% hearing loss of the plaintiff was undoubtedly the result of the firecracker explosion close to his right ear, which the expert was unable to explain and what was confirmed at auditory tests.

Exposure to noise levels greater than 140 dB can cause permanent hearing damage. Almost all firecrackers create noise with C peak level of over the 140-dB level at a distance of a few meters. In locations where the reverberation is present, sounds can bounce off walls and other reflecting surfaces, making noises louder and increasing the risk of hearing loss (see Annex B).

Exposure to the sound of a firecracker can result in permanent hearing loss, meaning the exposed person will have trouble discerning consonant sounds such as "t", "k", "s," "sh," or "p" and other high-pitched sounds. In such case it is also difficult to understand speech on social occasions, especially when many people are speaking simultaneously [23]. Such people may also suffer from ringing in their ears, i.e. tinnitus. This ringing, as accompanied with hearing loss, can be permanent.

It is true that exposed people can prevent hearing loss by using appropriate protective hearing devices, such as earmuffs or earplugs. Of course, this holds true only when such exposure is expected in advance. For this reason the additional importance of differences between expected and unexpected impulses must be taken into consideration.

High impulse noise, especially when a firecracker explosions are involved, has a different effect on the ear than usual continuous noise, as the protective mechanisms of the ear are less effective for a very short noise. A 1.5 ms lasting impulse noise at 150 dB can damage the ear permanently to some degree even though its equivalent energy level wouldn't be significant.

3. DESCRIPTION OF PROCEDURES UNDERTAKEN BY THE EXPERT WITNESS

3.1. Erroneous Medical Investigations

First the expert witness A.G., invited the plaintiff who has been exposed to this firecracker explosion, to undertake some audiometric tests. However, since the beginning of these tests, the plaintiff had many problems recognizing the audiometric signals. There was no significant sound absorption in the test room, and audiometric test signals were difficult to recognize due to the high level of background noise – see chapter *III.D*. A loud conversation between other clients and employees has been clearly heard from adjacent areas, so the plaintiff did not have the opportunity to recognize the audio signals clearly. He was disturbed and distracted by non-related events and by people in the vicinity. After the plaintiff pointed out this issue, the expert tried to mitigate this problem by simply sending her nurse to the adjacent rooms in order to quieten these loud and disturbing conversations. In this way the expert performed the audiometric tests under very unsatisfactory and unconventional conditions.

The expert did not describe the compliance with standards of the audiometric room in which he performed these auditory tests. He also failed to state whether the maximum permitted ambient sound pressure level, Lmax, was not exceeded in this test room. Also, he did not answer whether the ambient sound pressure levels were ever measured and compared with the maximum permitted levels of ambient sound pressure levels; for example Lmax according to ISO 8253-2 at a starting frequency of 125 Hz and a zero level of 10 dB [18]. Furthermore, he did not state what kind of walls the test room in which he carried out these audiometric investigations had, neither their sound insulation properties at individual frequency bands. Finally, he also failed to provide information on the sound absorption characteristics of this room.

The expert argued that the plaintiff would have sought medical help if he suffered hearing impairment due to a firecracker explosion. He did not explain, however, whether such a failure in his hearing, caused by a

firecracker, would even be curable. According to another independent expert, hearing impairment of between 7 and 12%, caused by a firecracker explosion, cannot be rectified.

3.2. Incorrect Procedures and Misuse ̂ of Plaintiff́s Sensitive Personal Data

The informations used by the expert were totally defective in order to draw any trustworthy conclusions. Instead of professional access, he operated with quite irrelevant data, like the description of the plaintiff's oral cavity colour, his tongue frenulum, his throat and the throat mucous [5]. Not only are such informations unnecessary for this kind of testimony from an expert witness but, by doing so, he also revealed sensitive personal data concerning the plaintiff's health unnecessary [14]. From the existing medical documentation he additionally fully revealed quantitative data about the plaintiff́s blood sugar, blood pressure, triglycerides and cholesterol levels. On the other hand, he completely omitted to correlate these values with eventual plaintiff́s hearing damage. These data were not required and were totally unnecessary as part of an expert's testimony, neither did the expert use them in any part of his testimony.

3.3. Wrong Metrics Used

According to [12], the safety distance for fireworks for category F2, is set to be at least 8m away. For category F3, fireworks must be ignited at least 15 m away and the maximum noise level at these distances must not exceed 120 dB (A, imp), or an equivalent noise level determined by another appropriate measuring method, at the safety distance.

It is obvious that there is not an arbitrary 120 dB limit (without any dynamics and weighting specification) as the expert used it, resulting in his quite wrong results and conclusions [5]. First, It is ridiculous what the expert did with this value! He used a point source model with reference 120 dB (A, imp) at a distance of 8m and calculated what the sound pressure level at 5m (the distance of the firecracker explosion to the plaintiff's ear, according to the expert's testimony) should be. He obtained 124.08 dB (without any specification?!). Secondly, neglecting the true limit of 120 dB (A, imp), he simply ignored dynamics and frequency weighting and compared this value with hearing damage limit directly. Then he drew the conclusion that this is even less than 130 dB (neglecting again any specification?!), so according to such reasoning, the plaintiff was not exposed to any risk to his hearing at all [5]. It is quite clear that decibels, measured with the dynamics impulse and weighted with filter A, are not identical with peak level decibels weighted with filter C or any other specification (see Annex A). Such

a difference is of crucial importance since the limits of a noise when assessing any risk to hearing is expressed as $L_{C\ peak}$, that is using the peak value and weighted with filter C [13]. Obviously, the expert does not distinguish between these basic acoustic descriptors, denoted by $L_{AI\ max}$ and $L_{C\ peak}$. The difference between these two indicators is enormous and in the vast majority of cases, including this one, affects the result decisively. During the cross examination the expert only insisted, that these are all "audiologic decibels", without any further explanation, convincing the judge which disabled any further questions after that.

The difference between the $L_{C,\ peak}$ and $L_{AI,\ max}$ indicators is about 26 dB in the actual case of the firecracker explosion. This means that a maximum noise level of 124.08 dB(A, Imp) corresponds to a much higher level of $L_{C,\ peak}$, which exceeded 150 dBC at the location of the plaintiff́s most exposed ear.

Here the expert made a cardinal mistake which was probably due to a lack of understanding the most important issues and fundamentals of acoustics. Misunderstanding these decibel units, he tried to calculate the sound pressure level at a distance of 5m for the F2 category firework and obtained 124.08 dB [5]. He did not explain which kind of decibels he had in mind. Based on this incorrect noise descriptor, he simply concluded that being 5 meters from such a firecracker explosion, the sound pressure level due to this firecracker explosion did not reach the limit value (130 dB) at which hearing loss could occur. He did not transform these metrics to the C-weighted level. Furthermore, he did not explain (and obviously even did not understand) which time dynamic he used for the limit value. In his confusion he simply denied any possibility of hearing loss or tinnitus, since, in his testimony, the plaintiff had not been exposed to a impulse noise of 130 dB or more. Of course, his conclusion was absolutely wrong, based on his incorrect calculation and the totally wrong use of the descriptors and their units. As already proved the $L_{C\ peak}$ level exceeded 150 dBC in this case.

According to Slovenian and European regulations, the cornerstone of hearing protection criteria against high impulse sounds is a peak permitted level, $L_{C\ peak}$. This stipulates that there is a risk of hearing loss above 135 dBC with respect to the reference pressure of 20 µPa. This corresponds to a sound pressure level of ppeak = 112 Pa. This means that at the time of the firecracker explosion, the plaintiff was exposed to at least 32x (over thirty times) greater sound energy level than it is permitted which, of course, resulted in acute hearing impairment. For impulse dynamics, the time constant, or the rise time is 35 ms during its increase [25]. The time constant is defined by the IEC standards. It also denotes the time needed to reduce the amplitude of an exponentially decreasing signal by a factor of $1 / e = 0.3679...$ (see Annex A).

The expert witness, A. G., was not familiar with these decisive facts and obviously confused the L_{Peak} with an alternative descriptor L_{Imax}, which led to enormous errors. The peak detector L_{Peak} on a sound level meter must have a response of less than 100 µs (100 microseconds). L_{Peak} is usually measured in combination with C or unweighted (flat) network. This is one of the most important reasons why the interpretations of the expert witness, A.G., are completely wrong.

Even using a rough comparison of the time constant for the impulse dynamics and the peak response time, an approximate ratio of 350: 1 is evident, which corresponds to the logarithmic ratio of about 25 dB. Additionally, the difference between the C weighted and A weighted filters also makes a little contribution to this difference. It is well known that C weighted levels are generally higher than A weighted ones, with the exception in one part of the high frequency audible region. However, since the spectrum of the firecracker explosions is shifted towards higher frequencies, this contribution is less than the contribution due to different time constants.

It is quite clear that the expert witness, A.G., confused peak level L_{peak} with the maximum level $L_{I, max}$. Peak is, by the IEC definition, the greatest absolute instantaneous sound pressure during a given time interval. On the other hand, $L_{AI,max}$ is the maximum level with A-weighted frequency response and Impulse time constant (see Annex A).

Additionally the expert here underestimated the risk impairment as well by using the firecracker of the F2 category, although most probably a type of firecracker of the F3 category was used in this case, whose peak levels greatly exceed 155 dBC at a distance of 5m.

3.4. Confusion about Sound Wave Phenomena

The expert witness considered the unevenness of the walls and the corners of the surrounding houses where, according to his testimony, the air waves were refracted [5]. There were obviously no air waves in question, but rather sound waves. Even worse, he completely confused the effects of reflection and refraction with diffraction and scattering. The expert witness obviously does not distinguish between these terms [5, 6].

3.5. Confusion about Low and High Frequency Content of an Explosion

According to his biased position, the expert was looking for some unrealistic facts in trying to explain the plaintiff's hearing loss. He namely declared that the plaintiff may have suffered hearing impairment during his military service in the artillery more than 35 years earlier. Without any evidence he guessed that he was certainly repeatedly exposed to strong impulse noise and hearing loss which consequently would, in his testimony, result in the

formation of a tinnitus [5]. These are again speculative and false statements, without any evidence, and also contrary to the theory of high-energy impulse noise.

The plaintiff here clearly explained and emphasized that he was actually in the artillery, but in the computing units far away from artillery fire operations. Additionally, during his service, only artillery firing simulations were performed, so he was never exposed to real artillery gunfire himself. Even if he were, his hearing damage would be different. Namely, the sound impulse bursts of the fireworks is quite different from that produced by artillery fire with a frequency spectrum that is markedly shifted towards higher frequencies, as proven in annex C. Also, a comparison of these physical facts and the plaintiff's hearing loss characteristics shows that his hearing impairment cannot be the result of artillery fire noise as the plaintiff had already explained that he had never been exposed to it. Also, medical evidence proved that the plaintiff's damage to hearing had increased by more than 7% between the two audiometric tests, in less than 2 years apart, soon after the firecracker explosion; on the other hand, this firecracker accident occurred more than 30 years after the plaintiff had completed his military service in the artillery computing units. Furthermore, the default assumption of the expert, A.G., that all soldiers and other personnel in artillery are exposed to artillery noise is ridiculous; this is similar to saying that all workers employed in court are judges or all workers employed in health care are doctors. Using such a set of incomplete and mainly erroneous information, the expert witness tried to speculate throughout his testimony. By ignoring most of such important data and lacking even the most fundamental theoretical knowledge he was unable to prove his claims of course.

3.6. Confusion and Misunderstanding of Occupational Noise Exposure

The expert witness further assumed that the plaintiff was occasionally exposed to high levels of noise at his workplace. He further speculated that the protective hearing devices were not sufficient as the noise was also transmitted through the cranial path to the inner ear [5]. However he did not provide any evidence about the propagation of the sound energy transferred to the inner ear through the bones of the skull against airborne transmission. Although he tried to explain hearing loss in this way, he was unable to give any estimate of how much of the sound energy was transferred to the inner ear through the bones of the skull against airborne transmission. These expert statements were thus again baseless. The use of earplugs and earmuffs (especially when combined) successfully protects or reduces the exposure of auditory organs to noise levels by up to 40 dB in the frequency region of interest. Only when even higher reductions are required it is necessary to reduce the

transmission to the inner ear by the cranial path as well. Neither the plaintiff nor the vast majority of workers have need to take any of such precautions so far. The plaintiff suggested the expert to describe one practical case where, according to his experience, such or a similar problem arose in his practice, but he was unable to give any answer at all again.

In the case of any excessive noise, or even on a suspicion of it, the plaintiff always used personal protective equipment to protect his hearing; if necessary even additional protection, by which the noise emission levels in the ears were reduced by up to 40 dB. This was also his duty, as he provided a professional service in this field, such as noise assessment and its control. So it is quite clear that different occupational and recreational types of noise to which the plaintiff was subjected to through his duties presented no risk of damage to his hearing. The emission levels of sound energy released during occasional bursts and similar noisy events which he received during his workshift, were consequently approximately ten thousand times lower than that which the plaintiff's inner ear received during the firecracker explosion. On the other hand, the plaintiff found himself in a quiet different situation on April 10, 2012, as he was been completely surprised by an unexpected firecracker explosion. So he did not have any chance to take the appropriate preventive measures or to use any other form of protection for his health.

The expert witness further insisted that during recreational shooting and, at some workplaces, strong vibrations are transferred through the bones to the inner ear. However, he was again unable to clarify what he meant by "strong vibrations", even not in which units these vibrations are expressed and what their amplitude should be.

3.7. Deficient Expert Witness Testimony Regarding Asymmetric Exposure during Sport Shooting

The expert witness further speculated about information of the plaintiff's involvement in some sport shooting activities without any professional background [5].

For this reason a few words about sport shooting activities should be mentioned first. Here, the expert witness fully misinterpreted the information about the plaintiff's involvement in sports shooting. The applicant was actually engaged in some occasional sports shooting activities. However, there are some facts in relation to shooting itself that must be elucidated. During sport shooting activities, there is namely a pronounced asymmetry in the exposure and the impairment risk of both ears [26]. During shooting, the right part of a shooter head rests slightly on the right shoulder and the left ear is directed against the barrel that is on the side of the explosion (Fig. 1). Consequently, the left ear is much more exposed to the resulting sound impulse burst than the right ear. On the

other hand, the right ear is located in the shadow of the head, which protects it, particularly at high frequencies. The ear that is tucked into the shoulder thus sustains lower dB levels than the ear that is exposed to the muzzle of the gun, so the left ear sustains higher levels of damage than the right ear in right handed shooters. When shooting right-handed (as in the case of the plaintiff) the shooter's left ear is facing forward and thus receives more of the muzzle blast energy than the right ear which is more backward facing. On the other hand, the plaintiff, as most shooters, used correctly fitting personal hearing devices for ear protection to both ears.

This fact is indisputably confirmed by a number of investigations and statistics regarding hearing damage of shooters, especially hunters who rarely use personal protective equipment. Such asymmetry in noise exposure applies practically to all shooters (except to left-handed ones, who mostly use customized firearms especially adapted for them). A similar phenomenon occurs with many professional musicians as well, especially violinists and string players. It was consequently proved that the left ear predominantly experienced more hearing loss during sport shooting activities than the right. For this reason hearing loss amongst rifle shooters tend to be asymmetrical, since the left ear is closer to the barrel and tends to be more impaired as it is closer to the explosion whereas the right ear is additionally protected by the head [26].

In table I there is an example presenting average C-weighted peak pressure levels in dB when using three kind of weapons at both shooters ears [27].

TABLE I
C-weighted peak pressure levels in dB at both shooters ears using three kind of weapons

Weapon	CZ-75	M4	M14
origin	Czech Republic	United States	United States
Cartridge	9x19 mm	5.56x45mm	7.62x51mm
Muzzle velocity	360 m/s	880 m/s	850 m/s
Barrel length	4.7//	14.5//	22//
Left ear	156 dBC	156 dBC	154 dBC
Right ear	151 dBC	150 dBC	149 dBC

It is clearly evident, that the greatest level was measured at the left ear. The shooters were namely right handed and thus the tucking of the head to the right shoulder is expected to provide a significant attenuation to the right ear.

A quite opposite asymmetry was postulated due to the explosion of the firecracker being close to the plaintiff's right ear during the absence of personal protective

devices, exposing his right ear to the noise of the firecracker.

Even the expert A. G. himself, confirmed that the plaintiff's right ear is significantly more damaged than the left one. This assertion additionally confirms the fact that the plaintiff was unable to obtain such hearing damage as a result of some sport shooting activities, but as a result of a powerful and unexpected firecracker explosion which occurred in the immediate vicinity of his unprotected right ear.

4. CONCLUSION

It is undisputed, and even the attacker himself did not deny the fact, that he deliberately threw an explosive device on the plaintiff, causing permanent health damages to him. It was thus proved beyond a reasonable doubt that the perpetrator committed the crimes charged, which consequently caused damage to the plaintiff. Additionally, this has been confirmed by the police investigations as well. In this way, the courts intentionally ignored all important evidences and proofs.

Almost all criminal proceedings were corrupted and completely biased at the District court in Ljubljana against the attacker. The former Minister of Justice with his political influence further managed to convince the Higher Court in favor of the attacker. Despite a proven attack with explosive devices the attacker has been fully acquitted in criminal trial.

Similar misconduct was processed during the lawsuit. The lawsuit proceedings were conducted in a biased manner, starting with a District Judge F.K.. He was known for some of his scandals, which are completely incompatible with his judicial function. Since he violated his judge's obligations of impartial conduct more times, he was fired. Before that however, this judge delayed the case for almost five years in favor of the perpetrator. Despite this punishment the District Court still persistently conceals from the plaintiff and other publicity the details about this judge and his corruption.

The case was then handed over to a new judge, A.B., who was also immediately pressured by the former Minister of Justice. She did not condemn the planned attack on the plaintiff, with a dangerous explosive device. Even more, she even approved this attack on the plaintiff's body, despite quite opposite international and slovenian law practice. A former Minister of Justice M.K. namely intervened many times in the attacker's favor. In this way, the case completely deviated from the established practice of law and norms, just in order to protect the attacker interests for any price. All the plaintiff's appeals were in vain. Indirectly, the Supreme and Constitutional Court were under his pressure as well. In this way the case acquired a completely new political and corruptive dimensions.

Here, a very important role played a wrong expert testimony as appointed by judge A.B.. This expert witness heavily strayed from the truth in his testimony. The expert's testimony fell deeply below the reasonable standard for his profession.

In the existing expert testimony, there are a number of significant errors, many of them of a fundamental nature, which have a decisive influence on the final results of this expert testimony and its conclusions. The expert performed audiometric tests under extremely unfavourable conditions; he paid no attention to the fundamentals of acoustics and audiology, nor to the human perception and reaction to sound. He confused the acoustic characteristics of firecracker explosions with artillery and sports firearms. The expert did not take into account the basic acoustic characteristics of such different groups of bursts. Furthermore, the expert witness disregarded many physical laws and facts, such as differences in the spectral characteristics of small (firecrackers) and large explosions (artillery shells). He neglected the sound exposure asymmetry characteristics of the left and right ear during sport shooting and the efficiency of personal protective equipment used during a workshift, etc.

The most fatal error he made, however, was the confusion between different metrics he employed in the evaluation of high-impulse noise. He simply confused the descriptor $L_{AI, max}$ and $L_{C, peak}$, which differs by approx. 26 dB for firecracker explosions. This additional confusion in metrics resulted in a fatal error of the peak level by 26 dBC. This difference was even a little higher, as the firecracker applied in his calculation was of a third, rather than of a second category (Megatron or Extreme of type 3 instead of Pirate of type 2, with which the expert based his calculations). In this way, the expert's conclusion regarding the exposure to 124 dB peak level instead of a much higher value of over 150 dB was totally wrong of course. It is ridiculous that all judges involved still have faith in such erroneous data and conclusions.

Almost all expert witness conclusions were consequently completely wrong due to the substantial errors in his calculations, his incorrect application and misunderstanding of the metrics used.

Apart of criminal and lawsuit legislation many Directives and standards were violated at different slovenian courts. Such infringement present a serious violation of human rights and dignity of the plaintiff.

It is clear that judges must be accountable to legal and ethical standards in making an admissibility decision on expert testimony and other lawsuit procedures. However, they were not.

ANNEX A– THE IMPORTANCE OF DIFFERENT TIME WEIGHTINGS

A maximum sound level is the highest exponential -time-average sound level, in decibels, that occurs during a stated period. For a given nonsteady sound pressure waveform, the maximum sound level depends on exponential-time-weighting, which is used (fast, slow or impulse).

The maximum A-weighted noise level measured with the impulse dynamics presents the maximum effective (RMS) value, evaluated by the A filter weighting and measured by the dynamics with a time constant of 35 ms.

The RMS level describes the effective value of the square of the sound pressure, denoted as p_{RMS}, and is expressed in pascals (Pa). The RMS value is thus calculated by squaring the value of the time-dependent sound pressure $p(t)$, its averaging (integration) over a certain time interval t_2-t_1, and finally its root square is taken, which is mathematically written as:

$$p_{RMS} = \sqrt{\frac{1}{t_2 - t_1} \int_{t_1}^{t_2} p(t)^2 dt} \qquad (1)$$

In (1) t_1 and t_2 are the time moments of the beginning and end of the evaluating interval of this average.

It is therefore obtained by an integration of the squared value of the sound pressure, its time averaging and finally taking the square root of this value. Simple averaging would not give a representative value (for example, in the case of a sine wave, this value would be practically zero), while the RMS value is proportional to the energy of the sound signal, which is important to describe its effect on hearing impairment.

On the other hand, the peak level is, according to the IEC definition, the highest absolute level of the current sound pressure during a given time interval. Figure 1 shows the difference between the maximum Lmax and the peak Lpeak level. It is clear that, contrary to the expert witness opinion, these quantities are not identical.
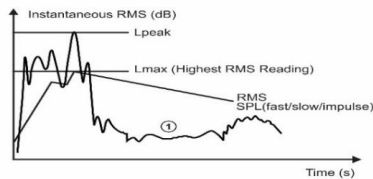
Fig. 1 Graphical representation of the difference between L_{max}

and L_{peak}. Contrary to the expert A.G. opinion, these are quite different quantities.

Noise levels can namely be measured or expressed with different dynamics, each with a specific time constant. In practice, three such dynamics are mostly used today, which are most often built into modern noise meters: Fast, Slow and Impulse [25].

When measuring the noise level, we actually detect changes in the sound pressure caused by the sound disturbance under investigation (in our case, a firecracker explosion). Such sound pressure levels change very quickly, so that their actual reading with a real-time measuring instrument would be very difficult. As a result, measuring instruments are fitted with certain dampers that dampen their response to such rapid time changes and allow for a smoother reading. Such a process is called time weighing.

The IEC 61672-1 standard [25] deals in more details with two different time weightings, Fast and Slow. Both are characterized by a certain damping, or a slow reaction of reading the screen of the noise meter. Dynamics Fast of course reacts faster, its damping is determined by the time constant τ = 125 ms; the dynamics slow is determined by an eight times larger time constant τ = 1 s. If, on the other hand, the sound stops suddenly, the signal on the display starts to decrease rapidly at 34.7 dB / s for dynamic fast. In the case of slow dynamics, this decrease is eight times slower, or 4.3 dB / s [7].

Figure 2 shows the response of the measuring instrument to a rectangular sound signal at both described dynamics.
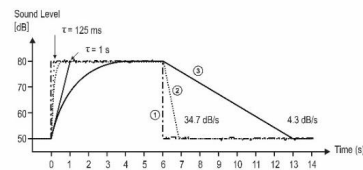
Fig. 2 Fast and slow dynamics properties:
1-real time sound level, 2-displayed Fast level, 3-displayed Slow level

For measurements of short impulse noise events (as in the case of a firecracker explosion), measuring instruments are usually equipped with a third type of dynamic - Impulse. However, in contrast to the described dynamics Fast and Slow this dynamic is asymmetric. Thus, the pulse dynamics adapts very quickly to the increase of the sound signal (τ = 35 ms), while its decrease after the termination of the sound signal is much slower, namely only 2.9 dB/s

with a tolerance of ± 0.8 to ± 1.3 dB/s, depending on the measuring class system. Figure 3 shows the response time to a sudden sound pulse at the slow, fast, impulse, and peak dynamics.

Indicators with time impulse evaluation are considered less appropriate today and are not recommended for assessing the risk of hearing impairment [25]. In any case, its use requires appropriate knowledge and experience.
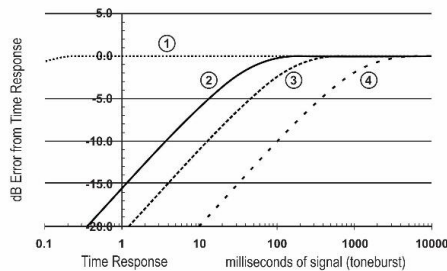
Fig. 3 Response time to a sudden sound pulse at different dynamics: slow, fast, pulse and peak: 1-Peak, 2-Impulse, 3-Fast, 4-Slow

Mathematically, time evaluation is usually expressed by an exponential function of time, or the corresponding time constant. This represents the weighting of the square of the current sound pressure. The time-weighted sound level, however, is defined in accordance with the IEC 61672 [25] standard as the twenty times of a common logarithm of the ratio between the square root of the square of the sound pressure and the reference sound pressure.

An A-weighted sound pressure level in decibels of an A-frequency weighted sound pressure signal and for exponential-time-weighting $e^{-(t-\xi)/\tau}$ is, at any observation time t, determined according to

$$L_{A\tau}(t) = 20 \log \sqrt[2]{\frac{\left(\frac{1}{\tau}\right) \int_{-\infty}^{t} p_A{}^2(\xi) e^{-\frac{t-\xi}{\tau}} d\xi}{p_0}} \qquad (2)$$

where

$p^2{}_A(\xi)$ is the square of the instantaneous A-frequency-weighted sound pressure in pascals

τ – a time constant, for a selected time weightings F, S or I

ξ – a dummy variable of integration in time interval between -∞ and t

$p_A(\xi)$ – the instantaneous A-frequency-weighted sound pressure in pascals

p_0 – the reference sound pressure of 20 μPa.

Running integration here occurs from some very distant start time (theoretically at -∞) to the present time t [7]. Dividing the result of the integration in above equation by

time constant τ yields a running time average of the frequency-weighted, squared sound presssure. The running time average indicates that an exponential-time-average sound level displayed by a conventional sound level meter is continuously updated as a function of observation time.

In the above equation, the numerator of the logarithmic argument is the exponentially weighted and frequency-evaluated rms value of the sound pressure at time t.

The standard design goals for fast and slow time constants are 0.125 second and 1.000 second, respectively. Time constant τ is equal to the time required for a quantity that varies exponentially with time to increase by the factor [1-(1/e)] or to decrease by the factor 1/e, where e is the base of the natural logarithm (e=2.71828).

The output of the sound pulse signal from the detector is thus most simply described by two functions, depending on whether it is increasing or decreasing. The increasing signal is illustrated by an increasing function with zero input according to the equation

$$L(t) = 10 \log (1 - e^{\frac{t}{\tau}}) \qquad (3)$$

This is an increasing transcendent function with a positive first and a negative second derivative, with no input signal at the initial moment.

The decaying signal after the termination of the pulse is illustrated by a uniformly decreasing function with zero output, [7]:

$$L(t) = 10 \log (e^{\frac{t}{\tau}}) \qquad (4)$$

which actually represents a linear function with a negative first derivative.

Figure 4 also shows a practical example of the responses of different noise dynamics to a pulse signal, which is relatively common in practice.
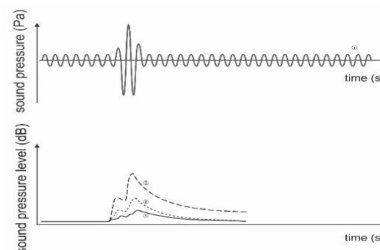
Fig. 4 A practical example of the responses of different time weightings to a impulse signal: 1- Impulse, 2-Fast and 3- Slow

ANNEX B. TYPES OF IMPULSE NOISE DUE TO FIRECRACKER EXPLOSIONS

A firecracker explosion outdoors, in an open space without any reflective obstacles, produces a non-reverberant A-type impulse noise with a single spike-form overpressure which can be approximated as a Friedlander impulse as shown in Fig. 5*a* and 6. On the other hand, a firecracker explosion indoors or in a semi-open space results in a reverberating effect and are usually described as a B- or C-type impulse, Fig. 5*b* and *c* [28].
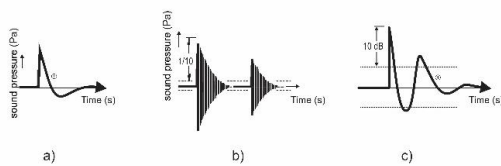
Fig. 5 Sound pressure levels of different types of impulse noise in time domain; *a*) A-duration, *b*) B-duration and *c*) C-duration

These types are characterized through rising time, impulse duration and peak overpressure as the main parameters describing impulse noise [29]. These parameters depend on the source, i.e., firecracker used.

The duration of A-type impulse (also called A-duration) is the time required for sound pressure to reach its unweighted peak value and then to fall for the first time to zero value, (t_2-t_o), Fig. 6. In the case of ideal waves, it is equal to the positive phase duration used in blast physics [29]. With B-duration, the total time required for the peak of a pulse level exceeding the criteria -20 dB, is depicted in Fig. 5b. C-duration is determined as the time required for the envelope of the unweighted peak sound pressure to decay by 10 dB (Fig. 5c). The corresponding level is therefore about two-thirds of the peak pressure value.

The A-type impulse can be described as a combination of linear function for the rising part and exponential function during its decay [30], (fig. 6):
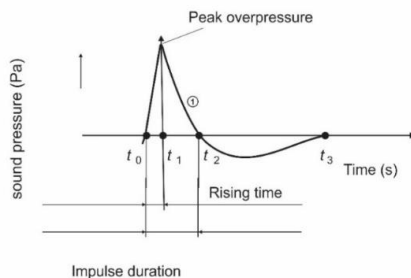
Fig. 6 The Friedlander wave as a firecracker explosion in time domain

$$p(t) = p_r(t) + p_p(t) \tag{5}$$

where

$$p_r(t) = p_{peak}\left(\frac{t - t_o}{t_1 - t_o}\right) \quad for \quad t_o \le t \le t_1 \tag{6a}$$

and

$$p_p(t) = p_{peak}\left(1 - \frac{t - t_1}{t_2 - t_1}\right) e^{-\frac{t - t_1}{t_2 - t_1}} \quad for \quad t \ge t_1 \tag{6b}$$

Here p_{peak} is the overpressure amplitude and t_2 is the time taken for the overpressure to fall to zero value for the first time.

In mathematical form the A-type of impulse is often described by the Friedlander pulse, starting with rapid rise from ambient pressure to a peak level, after which its more slowly decay follows back to the ambient pressure [29]. Usually, such kind of impulse appears as a result of explosion in an open environment with no reflecting surfaces.

The peak value of sound overpressure is the maximum absolute value of the instantaneous sound pressure in Pa. The rise time is the time interval between the start of an impulse and the time when the peak value is attained. Due to practical reasons, this is usually taken as the time required for the sound pressure to rise from 10% to 90% of its maximum absolute value [29]. Duration is the time interval between the start of an impulse and the time when an impulse decays to a zero value.

All of these parameters (peak level, rise time and duration) depend on the type of firecracker and its characteristics, such as its mass, charge, the type of explosive used, encapsulation, its geometry and design [29].

Typical firecracker explosions outdoors, at a distance of some meters, produces a peak sound pressure level highly exceeding levels as adopted for hearing protection. A typical firecracker exploding outdoors produces high sound pressure levels [31, 32], at distances of around 5m, peak overpressure levels is between 145 and 160 dBC. The spectral distribution of energy in such an impulse is controlled by the A-duration and the rise time.

Where there are reflective surfaces, such as the ground or walls, additional pulse components can appear (see Fig. 5*b* and *c*). Reflecting surfaces produce secondary reflected waves. These reflections can interefere with the original pulse, producing a complex temporal pattern. The time interval between the primary and secondary waves depends on the relative distances between the reflecting surfaces and the receiver. The peak and spectrum of the reflected components depend on the impedance characteristics of the reflecting surface.

ANNEX C – FREQUENCY CHARACTERISTICS OF DIFFERENT EXPLOSIVE SOURCES

When launching artillery missiles, one has to deal with

substantially larger masses of explosives, exceeding thousands of times the mass of firecracker explosives. For this reason, the duration of artillery explosions is considerably longer than that of firecrackers, resulting in lower frequency components.

In figure 7b and 8b the time dependence of sound overpressure is shown which is an approximation of sound impulses resulting from firecracker explosions and heavy weapon operations.

Here the rising time is very short, so only the exponential function during the decay (eq. 6b) of the Friedlander impulse is of practical importance. In the time domain, the sound pressure of the Friedlander pulse $p_F(t)$ can be written in the form

$$p_F(t) = p_{peak}\left(1 - \frac{t - t_1}{t_2 - t_1}\right)e^{-\frac{t-t_1}{t_2-t_1}} \tag{7}$$

where p_{peak} is the maximum peak sound pressure.

The time domain can be transformed into a frequency domain by using the Fourier transform $P_F(\omega)$ [7, 28]:

$$P_F(\omega) = \int_{-\infty}^{\infty} p_F(t)e^{-i\omega t}\,dt = \frac{i\omega t_p^2}{(1 + i\omega t_p)^2} \tag{8}$$

where $\omega = 2\pi f$ is the circular frequency.

Next, we find the effective value of $p_F(rms)$.

$$P_F(rms) = \sqrt{\frac{1}{T_P}\int_0^T p^2{}_F(t)\,dt} = \sqrt{\frac{1}{T_P}(e^{-2T/t_P}(-\frac{T_P^2}{2t_P} + \frac{T_P}{2} - \frac{t_p}{4}) + \frac{t_p}{4})} \tag{9}$$

whereby the T_P is selected as a point on the time axis in which the pressure $p_F(t)$ is asymptotically approximated to 1% of the baseline value, which is approximately $T_P = t_r + 6t_p$. Here T_P denotes the time required for such an approximation, where the time of rising is t_r and t_p is the time of the decreasing Friedlander pulse to zero.

In this way the frequency spectrum of the pulse or its energy distribution is obtained. The amplitude spectrum is given by the following equation [30]

$$|P_F(\omega)| = \frac{\omega t_p^2}{(1 + \omega^2 t_p^2)} \tag{10}$$

Looking for the extreme value of this function, yields

$$\frac{d|P_F(\omega)|}{d\omega} = \frac{t_p^2 - \omega^2 t_p^4}{(1 + \omega^2 t_p^2)^2} = 0 \tag{11}$$

from which it follows

$$\omega = 2\pi f_F = \frac{1}{t_p} \tag{12}$$

or $f_F = 1/2\pi t_p$ \hfill (13)

It is evident that the spectrum reaches the maximum amplitude at the frequency $f_F = 1/2\pi t_p$, and the maximum value of the amplitude spectrum is $|P(\omega)|_{max} = t_p/2$. Therefore, there is a significant difference between the duration of these two different explosions. For example, a firecracker produces an impulse with an A duration of about 1ms and a peak in the spectrum at about 2000 Hz. At launching an artillery shell, it has a duration of about ten times longer so the maximum spectrum level is shifted to lower frequencies by one decade, which is around 200 Hz (figure 7c and 8c)

(a)   (b)   (c)
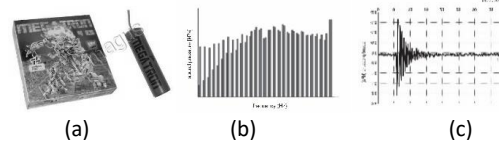
Fig. 7 Firecracker explosion characteristics a), time diagram of sound pressure b), shape of its spectrum shifted to high frequencies [33] c)

(a)   (b)   (c)
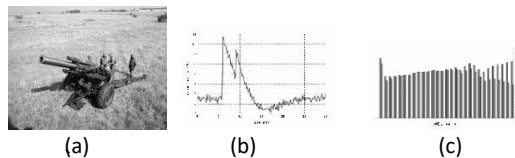
Fig. 8 Howitzer firing characteristics a), time diagram of sound pressure b), the spectrum is shifted to low frequencies [33] c)

Thus the sounds produced by large-caliber weapons have acoustic energy predominantly concentrated in the low frequency range (below 400 Hz), while the spectral content of sounds produced by firecrackers extends higher, around 1500 − 2500 Hz.
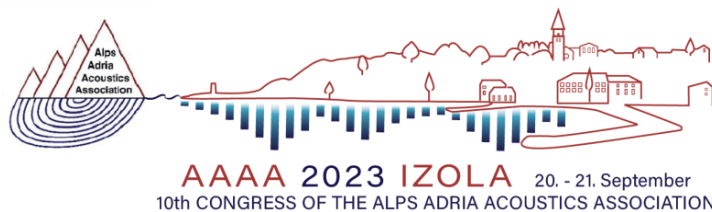
LOW FREQUENCEY NOISE MEASUREMENT IN THE PASSENGER CABIN

Domen Bartolj; Samo Beguš

University of Ljubljana, Faculty of Electrical Engineering, Tržaška cesta 25, SI-1000 Ljubljana, Slovenia

Abstract: *In recent years, the negative impact of sounds of infrasound and ultrasound frequencies on the health of people has been observed and documented. There are more and more sources of infrasound (e.g. traffic, wind farms) or ultrasound (e.g. electronic mole repellers, remote controls, sensors) in everyday life, but at the same time there are few recommendations and safety standards governing this area. Therefore, research on the impact of ultrasound and infrasound on humans is very important and necessary. A case study of the low frequency noise measurement in the passenger cabin is presented. A sound level meter with a separate microphone is used to assess the noise level in the passenger cabin when driving with closed or open window. Post processing is carried out later with different commercial and freely available software. The results show sound pressure levels of more than 100 dB and 110 dB in a car cabin with closed and open window respectively.*

Keywords: Infrasound, low frequency noise, sound pressure level measurement, passenger cabin, Room EQ Wizard, LabVIEW

1. IMPACT OF INFRASOUND ON HUMAN HEARING

People perceive the spectrum of frequencies with their auditory system in the frequency range from 20 Hz to 20,000 Hz. This range varies among individuals and can change with age, hearing disorders, and exposure to noise. Infrasound is generally not detectable by the naked ear but it can be perceived by increasing the sound pressure level (SPL) [1]–[5].

Exposure to low-frequency noise can lead to irritation and even damage to human hearing system. In this regard, numerous tests have been conducted. These tests include the threshold of audibility, which has been tested by many researchers, including frequencies below 20 Hz [1], [2].

Another test, known as the Temporary Threshold Shift (TTS), examines situations where prolonged exposure to intense low-frequency noise can temporarily cause reduced audibility or even permanent deafness [2], [6].

Ear pain and injuries are related to the mechanical movement of the middle ear beyond its normal operational limits. The pain threshold is not well defined and is different for each person. Furthermore, exposure to infrasound and low-frequency noise can lead to a sensation of pressure in the ear. Extensive research has shown that this effect of infrasound begins to occur at infrasound levels between 127 dB to 133 dB and does not necessarily increase proportionally with rising sound pressure[1], [2].

The impact of low-frequency noise on communication can be quite pronounced. At high intensity levels of low-frequency noise, effects have been reported such as voice modulation, feelings of muffled sound, and chest wall vibrations [2].

There is no clear evidence from experimental studies to support claims that infrasound has a negative impact on human performance, induces a "drunken" state in individuals, or directly triggers nystagmus. The effects observed at intensity levels ranging from 105 dB to 120 dB, if they can even be validated, are likely to have been exaggerated [7]. However, it is not precisely known at what level infrasound becomes dangerous to humans and how it affects their physical abilities.

Infrasound sources could be of natural or artificial origin. Natural sources of infrasound include earthquakes,

tsunamis, storms, and animals (mostly water animals). Artificial sources of infrasound include industry, traffic, various electrical devices, wind turbines, and human activities in construction works, among other things [1], [4].

Artificial noises have a more significant impact on people than natural ones, as people react to them more strongly, and in everyday life, we are exposed to them more. An example are wind turbines, as they indicate that the prevalence of low-frequency noise is a particular concern for communities living near these power plants. Today's low-frequency noise, primarily originating from machinery, can lead to perceiving it as a constant background noise but at night, when ambient noise decreases, low frequency noise dominates. Especially during the night, the low frequency noise could be perceived by humans [1].

Because we are constantly exposed to low-frequency noise and noise in general, environmental noise is measured. The measurements are conducted in accordance with the ISO 1996-2 standard. Additionally, legal regulations define the limits of permissible noise levels at different times of the day and in various environmental zones [8].

The largest source of noise pollution nowadays is traffic [9]. Noise, vibration, and harshness (NVH) is used to evaluate the noise and vibration characteristics in vehicles. The measurements conducted for noise and vibration are objective, whereas the harshness measurements are subjective, as they are evaluated by a group of evaluators or provided through analytical tools. They deal with the noise and vibrations experienced by passengers inside the cabin. External measurements focus on the noise emitted by the vehicle. Passengers are subjected to the noise, which depends on the environmental conditions (car type, driving speed, car resonances, open or closed windows, etc.) [10]–[12].

In the present article a measurement and analysis of a car cabin noise is performed to assess the conditions when driving. The SPL and spectrum of the cabin noise was measured.

1.2. Equipment used

The measurement were carried out in the Renault Clio Storia 1.2 car.

For noise measurement and data recording the Brüel & Kjær Type 2270 Sound Level Meter with Type 4189 prepolarized condenser microphone was used.

For a reference SPL calibration the Brüel & Kjær Type 4231 Class 1 Sound Level Calibrator was used.

Data processing was performed with LabView and a freely available software Room EQ Wizard (REW).

1.3. Procedure and setup

The process of conducting the measurement in the Clio Storia car involved installing a microphone, which was placed on the headrest of the passenger seat and connected to a sound level meter placed on the passenger seat.
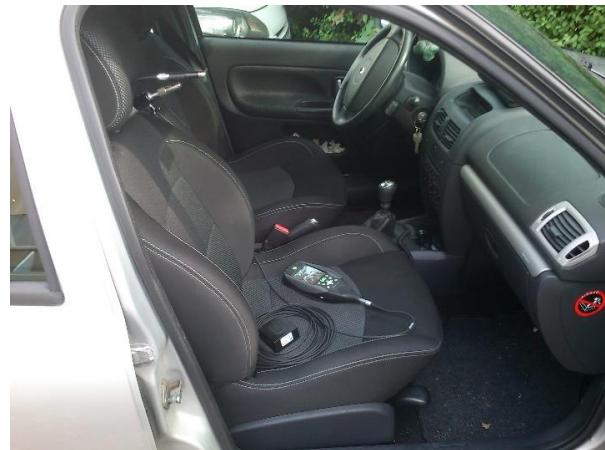
Fig.1. Measurement equipment set-up in the car.

The microphone was set up for measurement in the diffuse field environment. With this selection, the sound level meter also automatically sets correction filter for each microphone, optimizing its frequency response [13], see **Table 1**.

Microphone	Application	Optimized For	Dynamic Range*	Free-field ±1 dB Frequency Range	Free-field ±2 dB Frequency Range
4189	Standard Prepolarized	Free Field Diffuse Field	16.6 – 140 dB(A)	6.8 Hz – 22.4 kHz† 7.8 Hz – 22.4 kHz	4.2 Hz – 22.4 kHz† 6.3 Hz – 22.4 kHz

Table 1. Free-field frequency range for microphone type 4189 [13].

Before starting the measurement, we calibrated the sound level meter using a sound calibrator. Location logging and driving speed measurements were recorded by a telephone GPS receiver [14], [15].

After the calibration we drove the car along the streets of Ljubljana, including the highway. Our journey commenced in front of the Faculty of Electrical Engineering in Ljubljana, starting on Barjanska Road, then transitioning onto the highway until the Brdo exit, followed by driving along the road towards Brdo, see **Fig 2**.

During the measurements, the recordings were saved as WAV file for later analysis.
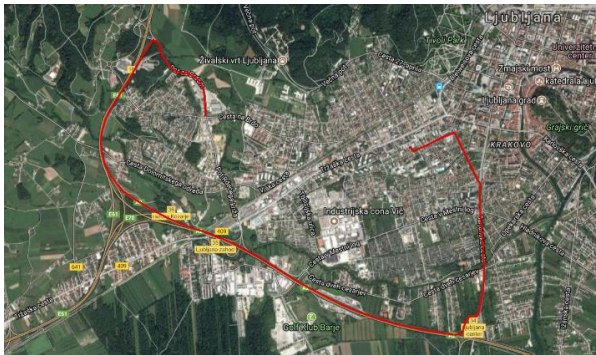
Fig.2. Presentation of the driving path

1.4. Data analysis

Post processing and visualization of the data was performed using a commercial program LabView [16] and with a freely available program REW [17]. For the playback, we employed the freely available program Audacity [18] and utilized the VB-Audio Virtual Cable [19] to avoid linear frequency distortion and reduction of signal to noise ratio to feed the signal from recorded wav file to the program REW.

Program REW can utilize a SPL logger to visualize the SPL change in time, display a signal spectrum and use frequency weightings.

To calibrate SPL levels in LabView and REW the reference SPL levels of 94 dB and 114 dB recorded at the beginning of the measurement session were used.
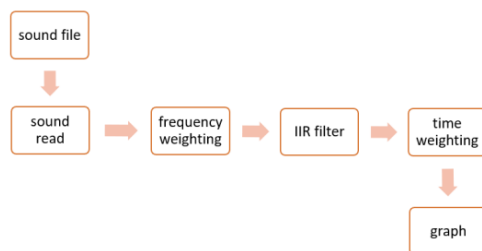
Fig.3. Data processing block diagram in LabView program.

Using LabView data processing and data flow is presented In **Fig 3**. LabView is able to read directly from a wav file. The signal read from the file is frequency weighted, band pass filtered (if we want to limit the frequency range of interest), time weighted and plotted. Car speed data is also read from the file and visualized in a plot.

2. MEASUREMENT RESULTS

Before starting the measurements, it was necessary to calibrate the sound level meter. We accomplished this by using the B&K sound calibrator type 4231. We performed calibrations at SPL levels of 94 dB and 114 dB. Spectrum at 114 dB is shown in **Fig. 4**. The reference SPL is also visible in **Fig. 5** and **Fig. 6** in the time interval from 1:00 minute to 1:20 minute.
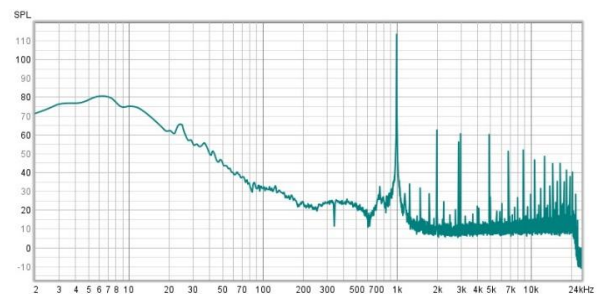
Fig.4. Reference 114dB frequency spectrum in REW.

During the measurement, the sound level meter stopped logging the data for approximately a minute and therefore there is a 1 minute long loss of data, which can be seen in the **Fig. 5** and **Fig. 6**. The average SPL at lower speeds was approximately 95 dB. When the car stopped, this level dropped to 80 dB. Peaks on the graph are due to the nearby traffic.

However, on the highway at higher speeds, the SPL without frequency weighting is more than 100 dB. The highest SPL can be observed with open windows, when the SPL exceeds 110 dB. A window at the passenger seat was fully opened. Same results can be observed with REW and LabView software. With the LabView software an additional filtering was performed, with two band-pass filters with frequency ranges from 1 Hz to 20 Hz and from 20 Hz to 40 Hz.
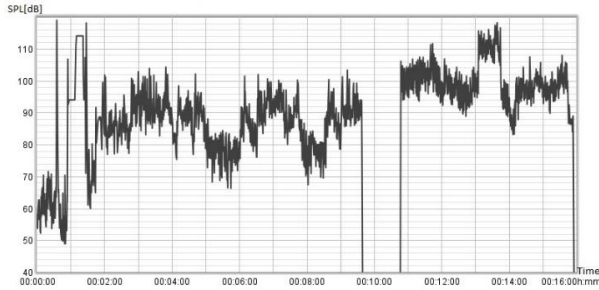
Fig.5. SPL level during the measurement, no frequency weighting applied. REW software.
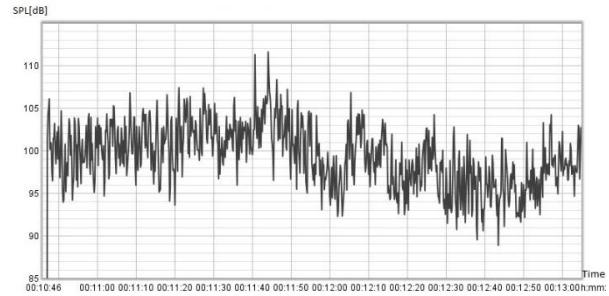
Fig.7. Closed window measurement without frequency weighting. REW software.

Comparing the measurements, SPL difference of 15 dB can be observed when driving with speeds higher than 70 km/h on a highway.

At an approximately equal speed of 110 km/h with the window open, the SPL increased to around 112 dB, and the duration of the open window was approximately 39 seconds, see **Fig. 9** and **Fig. 10**. With the window open, the SPL increased by approximately 9 dB due to changes in air circulation, consequently leading to an increase in low-frequency noise.
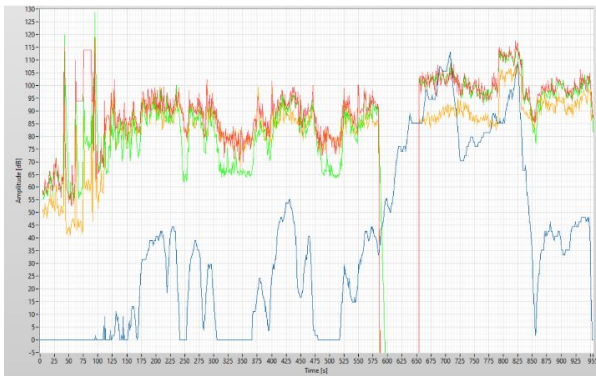
Fig.6. The SPL during the whole measurement session: no filtering (red), band-pass filtering 1 Hz to 20 Hz (green), band-pass filtering 20 Hz to 40 Hz (orange), and car speed in km/h (blue). LabVIEW software.

Fig.8. Closed window measurement: no filtering (red), band-pass filtering 1 Hz to 20 Hz (green), band-pass filtering 20 Hz to 40 Hz (orange), and car speed in km/h (blue). LabVIEW software.

When driving on the highway at approximately 110 km/h, the SPL with the window closed was around 103 dB, and the duration of the closed window was 2 minutes and 15 seconds. The cabin noise could be reduced with better sound insulation of the vehicle, improved window and door sealing materials, enhanced suspension since vibrations contribute to low-frequency noise, and a smoother driving style.

In the **Fig. 8** and **Fig. 10** it is evident that with the window closed, the SPL of the low pass filter up to 20 Hz is at the same level as the SPL without the filter, indicating that frequencies up to 20 Hz were dominant.

A similar study was conducted involving the observation of noise level in passenger car, but they used different car models a small opening of the window [20].

As evident from the **Fig. 8** and **Fig. 10**, the speed is changing, yet the noise remains approximately the same both with the window closed and open. It can be stated that the noise in the car cabin at speeds of 80 km/h and above changes less than at a low speed.
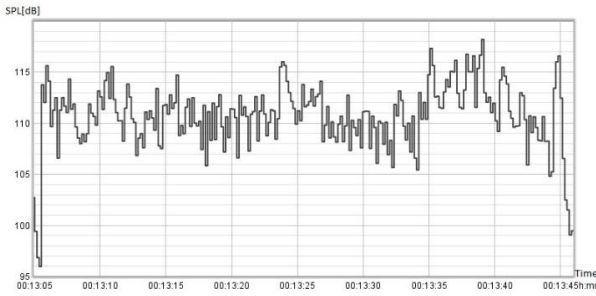
Fig.9. Open window measurement without frequency weighting. REW software.

When comparing the closed and open window spectrum measurements, see **Fig. 11**, it is evident that the difference in SPL at frequencies up to 20 Hz is approximately 15 dB. With the window closed, higher harmonic components appear at the fundamental frequency of 40 Hz, at around 80 Hz and around 160 Hz, likely due to resonances in the car's cabin.

Fig.10. Open window measurement: no filtering (red), band-pass filtering 1 Hz to 20 Hz (green), band-pass filtering 20 Hz to 40 Hz (orange), and car speed in km/h (blue). LabVIEW software.

With the window open, there is an increase in SPL around 700 Hz up to approximately 2 kHz. It could be due to the absence of a windscreen on the microphone.

SPL / dB	Window closed		Window open	
	average	max	average	max
Wideband	100	111	113	117

Table 2. SPL comparison with open and closed window. REW software.

A short summary of the findings is collected in the **Table 2** and the **Table 3** where SPL comparison with different frequency weightings and with open and closed window from LabView and REW programs are shown.

SPL / dB	Window closed		Window open	
	average	max	average	max
Wideband	101	110	113	117
1 Hz – 20 Hz	100	109	112	115
20 Hz – 40 Hz	88	95	105	110

Table 3. SPL comparison with different frequency weightings, open and closed window. LabView software.

The average and maximum SPL are recorded. As mentioned earlier the driving conditions with open and closed window are not exactly the same.
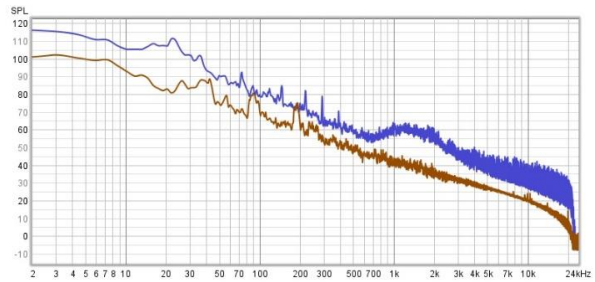
Fig.11. Comparison of open and closed window spectrum: open window (blue), closed window (brown). REW software.

Comparison of the measured values using LabView and REW software shows good agreement, see **Table 2** and **Table 3**.

3. CONCLUSION

We investigated the low-frequency noise in the car cabin with the window either closed or open. The results indicate that opening the window affects the level of low-frequency noise in the vehicle's interior, especially in the infrasound range, below 20 Hz. However, an open window also presents different challenges associated with wind, affecting passenger comfort and health. The sound pressure levels of more than 100 dB and 110 dB in a car cabin with closed and open window respectively were measured. The noise level could be lowered with a

different vehicle design, alternative materials, and better vehicle insulation. It is crucial to emphasize that our findings are not easily replicable, as results vary depending on weather conditions, traffic, and other factors. For quieter, more comfortable, and pleasant journeys, collaboration between the industry, researchers, and designers is necessary to achieve progress in this demanding goal.

4. REFERENCES

[1]	B. Berglund, P. Hassmén, and R. F. S. Job, **Sources and effects of low-frequency noise**, *The Journal of the Acoustical Society of America*, vol. 99, no. 5, pp. 2985–3002, May 1996, doi: 10.1121/1.414863.

[2]	N. Broner, **The effects of low frequency noise on people—A review**, *Journal of Sound and Vibration*, vol. 58, no. 4, pp. 483–500, Jun. 1978, doi: 10.1016/0022-460X(78)90354-1.

[3]	C. S. Pedersen, **Human hearing at low frequencies with focus on noise complaints**, National Wind Watch. Available: https://docs.wind-watch.org/Pedersen-human-hearing-low-frequencies.pdf

[4]	M. Weichenberger *et al.*, **Brief bursts of infrasound may improve cognitive function – An fMRI study**, *Hearing Research*, vol. 328, pp. 87–93, Oct. 2015, doi: 10.1016/j.heares.2015.08.001.

[5]	H. Moller and C. S. Pedersen, **Hearing at low and infrasonic frequencies**, *Noise and Health*, vol. 6, no. 23, p. 37, Jan. 2004.

[6]	D. L. Johnson, **The Effects of High Level Infrasound**, Defense Technical Information Center, Fort Belvoir, VA, Feb. 1980. doi: 10.21236/ADA081792.

[7]	C. S. Harris, H. C. Sommer, and D. L. Johnson, **Review of the effects of infrasound on man**, *Aviat Space Environ Med*, vol. 47, no. 4, pp. 430–434, Apr. 1976.

[8]	**Meritve hrupa – Epi Spektrum d.o.o.** Available: https://www.epi-spektrum.si/sl/varstvo-okolja/varstvo-okolja-pred-hrupom/splosno-o-ocenjevanju-hrupa-z-meritvami-2/

[9]	I. CORPORATIVA, **La contaminación acústica, cómo reducir el impacto de una amenaza invisible**, *Iberdrola*. Available: https://www.iberdrola.com/sustainability/what-is-noise-pollution-causes-effects-solutions

[10]	**NVH testing (noise, vibration, harshness)**, *ATESTEO*. Available: https://www.atesteo.com/en/testing/nvh-testing/

[11]	**NVH Testing – Noise, Vibration, and Harshness**, *Data Acquisition | Test and Measurement Solutions*. Available: https://dewesoft.com/applications/nvh-testing

[12]	**Noise, vibration, and harshness**, *Wikipedia*. Available: https://en.wikipedia.org/w/index.php?title=Noise,_vibration,_and_harshness&oldid=1162539682

[13]	Brüel & Kjær **Hand-held Analyzer Types 2250 and 2270 User Manual**, Available: https://www.bksv.com/downloads/2250/be1713.pdf

[14]	**GPS Visualizer**. https://www.gpsvisualizer.com/

[15]	Edit *et al.*, **New NMEA - GPS library**, Jul. 17, 2015. Available: https://forums.ni.com/t5/Example-Code/New-NMEA-GPS-library/ta-p/3518883

[16]	**What is LabVIEW? Graphical Programming for Test & Measurement**. Available: https://www.ni.com/sl-si/shop/labview.html

[17]	J. Mulcahy, **REW - Room EQ Wizard Room Acoustics Software**. Available: https://www.roomeqwizard.com

[18]	Home, *Audacity ®*, Apr. 25, 2023. Available: https://www.audacityteam.org

[19]	**VB-Audio Virtual Apps**. Available: https://vb-audio.com/Cable/

[20]	S. D. Haddad, **An Investigation into the Significance of Infrasound in some Passenger Cars**, SAE International, Warrendale, PA, SAE Technical Paper 891158, May 1989. doi: 10.4271/891158.
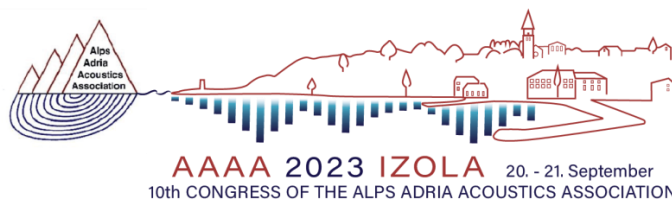
MEASUREMENT AND CHARACTERIZATION OF CONTROL VALVES NOISE

Egon Susič, Miha Pogačar

Danfoss Trata d.o.o. Jožeta Jame 16, 1210 Ljubljana, Slovenia

Abstract:
Valves that control water flow in heating/cooling systems are often source of annoying noise. At the same time emitted noise can carry valuable information about flow condition. In spite that design of globe valves utilizes similar principle for reducing flow, the resulting noise exhibits many different characters and levels regarding dimension and material used. To enable noise control a measuring system is designed and applied predominantly at development stage of new valves. Most of typical noises are characterized by power spectral density function. By analysing noise and correlations with respect to internal geometrical features and flow conditions we manage to produce quieter valves and push the boundaries of operating conditions.

Keywords: Control valve, noise measurement, flow induced noise

1. INTRODUCTION

Motorized Control Valve is a key element that delivers water flow through heating/cooling systems is the main subject of our research. Heating/cooling systems mostly utilize water to transfer heat energy from source to the user. Addressed systems can be regarded from different prospectives starting from district heating /cooling networks down to local single flat HVAC system [1]. Many of these applications are designed to be located close to or directly in living spaces. During the valve operation, where due to water flow through connecting pipes and valve internal cavities, audible noise might appear.

When valve noise, also known as flow noise [2], becomes significantly higher than ambient noise, it can be a nuisance factor that negatively affects people who live or work nearby. To tackle this issue, we built a measurement system enabling us to monitor and examine valve performance also with respect to emitted noise. Furthermore, the noise can be a carrier of valuable information reflecting typical and atypical flow behaviour. By analysis of this information and establishing correlations between noise character and valve internal geometrical features we can influence valve design and control noise level to certain extent.

During the development process of valves some crucial constrains should be addressed. EU ESG policy demands sustainable energy sources, low CO2 footprint to name only few of them among many other directives [3,4]. Industry must follow these trends and demands as for example a usage of low temperature heating systems. Consequently, lower temperatures mean smaller temperature differences and higher flow needed to transfer adequate energy demands. Higher flow produces higher flow speed, and also reduction of material usage and smaller dimensions additionally increase flow speed. High flow speed inevitable produce higher flow noise which in some cases is very unpredictable in can develop in tonal high frequency components that can be extra annoying and non-acceptable in living places. Upper limit is when cavitation takes place [5] and destructive abrasive process deteriorate valve internal components and might end by destroy valve with unpredictable consequences with high stakes.

Focusing on valve performance we should parametrize the process of delivering demanded flow. For this purpose, we must address all known and measurable parameters that are present. First of them is the differential pressure across the valve [6]. Next, high pressure is measured in front and static pressure behind

the valve as well as water temperature. Valve opening position is measured and driven by actuator which produces enough force for closing the valve. Noise is measured independently in real-time.

This paper is structured as follows. Section 2. represents measuring system and testing principle. In section 3. are obtained results and analysis. Section 4. is discussion and the last section is conclusion.

2. MEASUREMENT SETUP

Our measurement system is comprised of sensors that simultaneously measure all above mentioned parameters. All sensors are calibrated and compliant to EN17025 standard demands [6]. The setup consists of pipes of adequate diameter, water tank, pump and flowmeter. This represents basic closed hydraulic loop. The water flow through this loop is controlled by multistage high-pressure pump driven by frequency-controlled motor and the pressure differential across the valve is maintained by a custom controller with variable closed-loop PID algorithm. This loop resembles typical control valve application environment. According to the relevant standard [7] valve's characteristic is measured at constant pressure drop over the valve while the opening position is independent control variable starting from closed position to completely open. Valve opening position is measured by incremental device that is side mounted to actuator and actuated by cantilever on clutch attached to valve

stem. For the noise measurement there are three different positions on the piping system.

Microphone MIC A is located inside semi-anechoic room and measure structure borne emitted noise from radiator. The radiator resembles a standard piece of room equipment that is usually located in living spaces. Radiator pipe structure is connected to main hydraulic circle and represents a waveguide of emitted noise from the control valve indicated as valve sample on Fig 1.

MIC B is positioned in the insulated box. Through this box a steel pipe connected directly to outlet of valve (sample) is mounted. By this arrangement we can measure emitted noise presumably guided by the water and pipe itself. This is also regarded as structure noise.

MIC C is located in valve's proximity and measures valve emitted noise as airborne and by changing a distance between source and microphone we can determine noise source taking into consideration inverse-proportional law [8]. On another position far from the source the obtained signal is regarded as background noise.

Measurement protocol follows demand of control valve measurements defined in relevant standards while noise measurements comply with adequate acoustic standard [9].

Hydraulic System control and data acquisition is presented in Fig. 2. Hydraulic closed loop is controlled by standard PLC controller which is in feedback loop with control variable. Pressure drop over valve indicated as
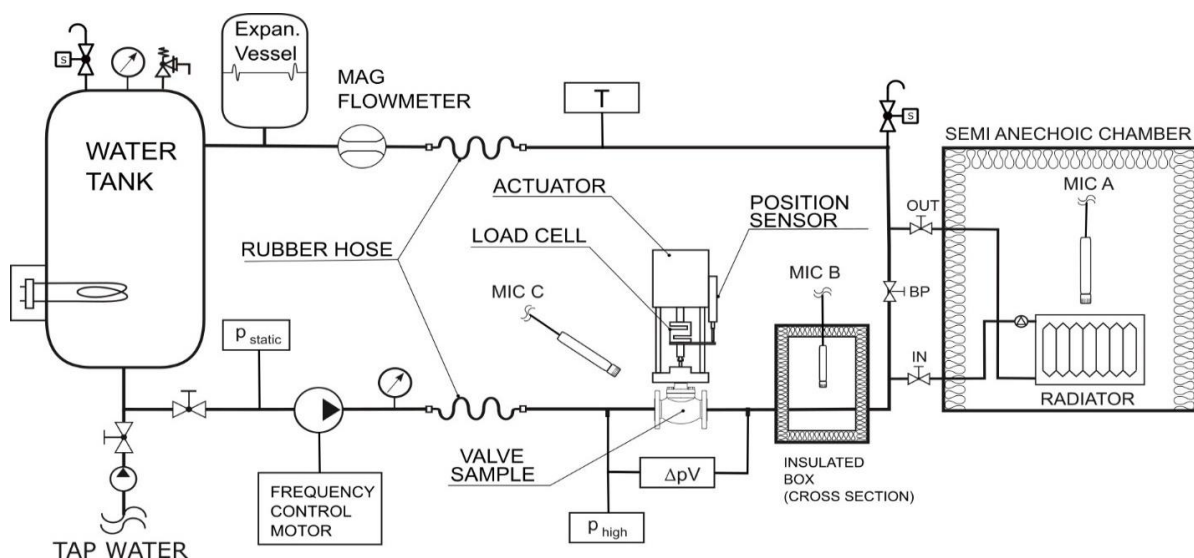
Fig.1. Measurement system with hydraulic closed loop control.
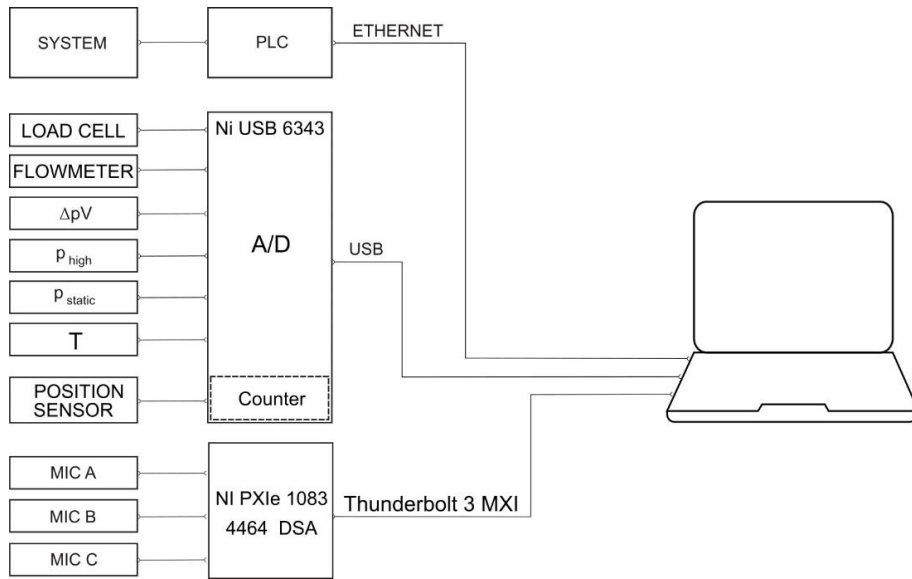
Fig.2. System control and data acquisition setup

ΔpV in Fig .1. is predominantly used as constant value or linear increasing-decreasing function. All physical parameters mentioned in introduction section of this paper are indicated in Fig,1 and Fig.2 respectively. Sensory signals are fed to A/D converter and processed [10], filtered and stored every 200 ms. Graphs can be seen in Fig.3. This gives us resolution for monitoring and recording important parameters approximately 5 times faster that significant change of values occurs. In parallel we measure noise via MIC A, MIC B or/and MIC C respectively. For this purpose, we utilize Dynamic Signal Analyzer (DSA in Fig. 2). Through software application based on LabView platform noise analysis is done. For each channel we use FFT procedure for obtaining power spectral, density shown on Fig .4, and 1/3 Octave analysis [10] that is compliant to standard ISO 3743. To have complete picture of power spectra we plot waterfall graph in respect to control parameter that is indicated in Fig.5.
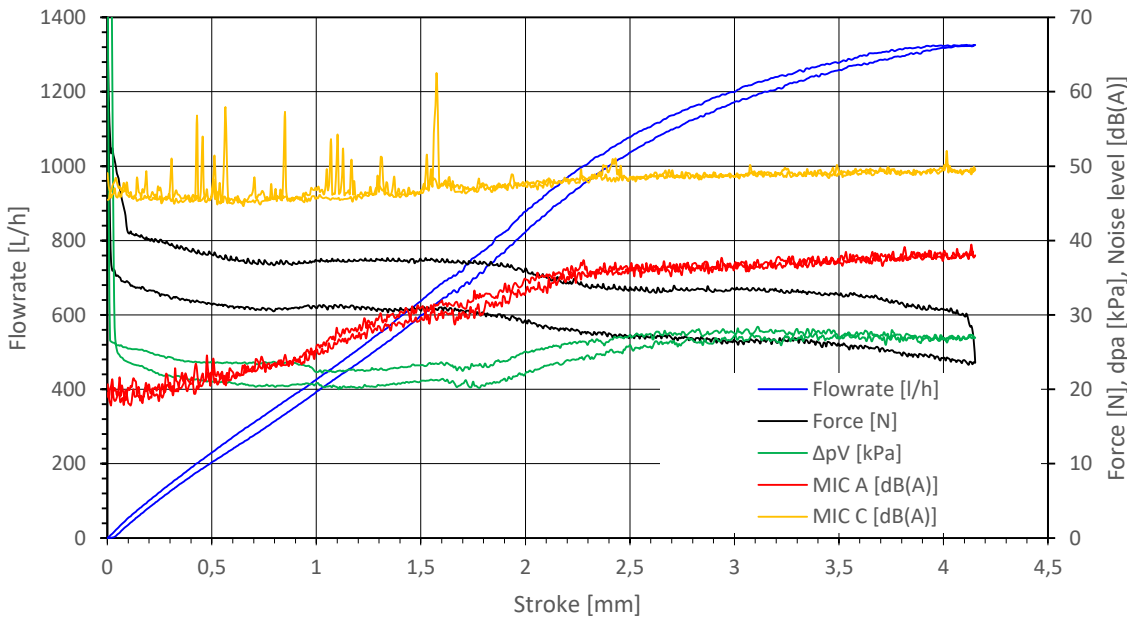
Fig.3. Measured quantities during functional testing of valves.

Power Spectral Dencity
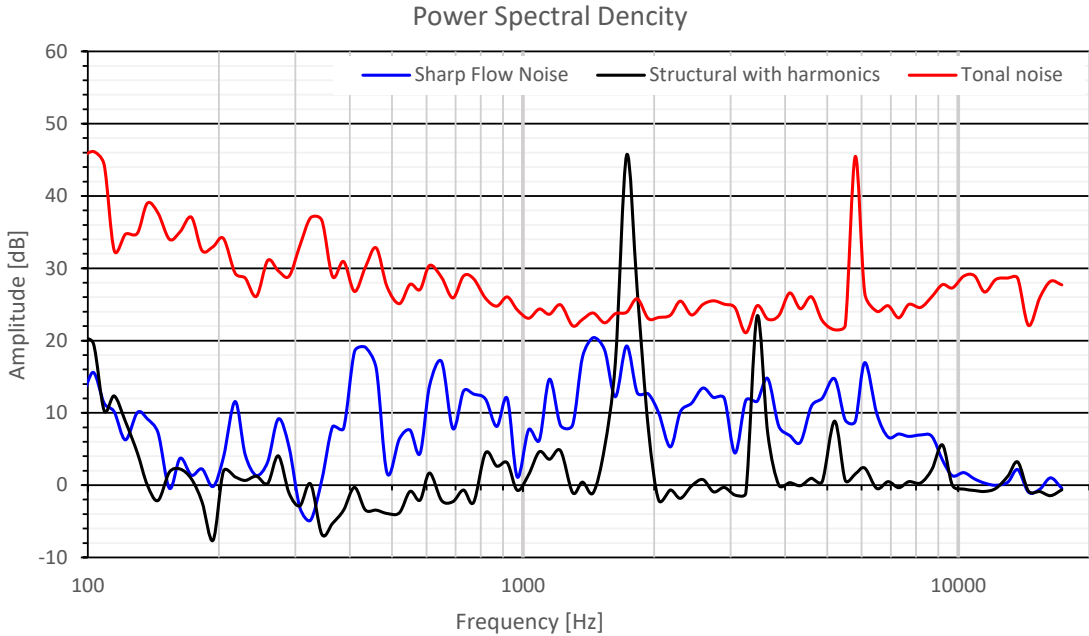
Fig.4. Power spectral density of Sharp, Structural with Harmonics and Tonal noise.

3. RESULTS

Measurement protocol for valve characteristic assumes that recording is triggered at valve closed position and applied nominal force by actuator. Then the force decreases as actuator drives the valve stem to fully open position and after in reverse direction towards closed position. Stem movement is indicated as stroke and represent independent control parameter.
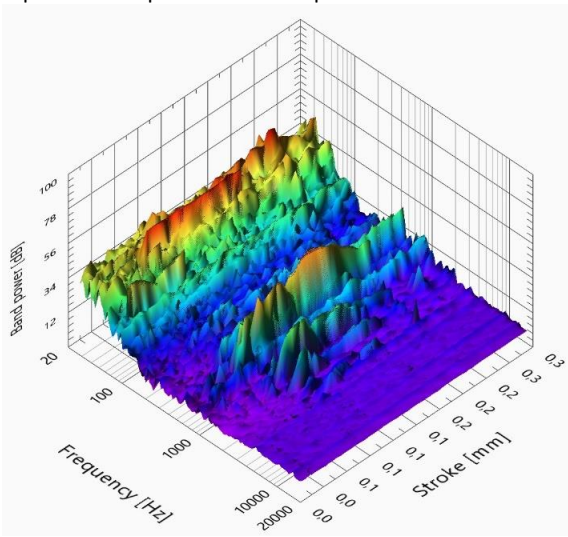
Fig. 5. Waterfall spectrogram of atypical valve noise with respect to stroke position.

The speed of actuator is small enough that we can consider this process as quasi-stationary. Every 0,006 mm of stem displacement one record of all parameters and noise pressure level are captured simultaneously. By doing so, obtained values can be regarded as continuous curves with linear interpolation between consecutive discrete data points in respect to stroke domain. In Fig 3. a typical measurement is shown. Additionally, to mentioned recording also power spectral density is calculated through FFT function and plotted into waterfall spectrogram shown on Fig. 5. Complete described measurement protocol runs in on-line mode with 200ms pace rate.

4. DISCUSSION

Results of analysed measurements show that noise pressure level values slowly increase with increasing water speed through valve. During one measurement cycle we can accurately observe evolution of noise level. If these levels are within acceptance criteria, then valve pass quality check. However, beside level also noise character is evolving and this gives us a huge increase in complexity of noise emissions. Namely, characterization is done by power spectral density function which can discriminate among different phenomena that can take

place in running water flow. Starting at very low flow at almost close position of the valve we can detect a transients followed by flow noise. This flow noise increases with increasing flow and might end in cavitation if extremes are reached with pressure conditions in the flow. However, in some cases additional phenomena can be observed. These occurrences can be classified as noise due to structural vibrations and flow induced tonal effects. Vibrations are usually a consequence of design features of internal parts and cavities [11]. A significant contribution can be from connecting pipes and other features in closed loop water circle. To minimize pumps and other disturbances a rubber hoses (Fig.1.) are used to acoustically decouple valve from other elements. Assuming that measured noise is prevalently from valve we consider noise due to structural vibrations when power spectral density shows natural frequency component and higher harmonics as well. These noises can be heard by human ear and recognised as kind of pattern. Many of different pattern might occur and we clustered them in some main groups and addressed them like rattling, fluttering, hammering, … On another hand tonal transients called whistling are represented by a single frequency component usually occurred at frequencies higher than 1 kHz as can be seen

in Fig.4. This is considered as fluid induced noise and a root cause is not well understood. Conditions are unpredictable and tonal noise appearance is within very narrow window of measured parameters.

5. CONCLUSIONS

Valve noise can be annoying in cases where people are exposed when appear in living spaces or their proximity. Valve producers must comply with legislation based on adequate environmental standards and directives. Noise level is also measured to determine key feature of products quality. To reduce noise emissions a better valve design is needed. It is well known that emitted noise contains valuable information about basic physical phenomena. For this reason, we utilize power spectral density function to characterize and differentiate among different noises.

Proposed measurement setup works as an on-line monitoring and diagnostic system. Most of flow induced noise phenomena can be related to valve geometrical features. By changing addressed features we can analyse valve noise and with the gathered information produce better performing and quieter valves while preserving all desired features and functions.

4. REFERENCES

[1.] Rezaie, B., Rosen, M.A. **District heating and cooling: Review of technology and potential enhancements**, Applied Energy, 93, pp.2–10, 2012

[2.] Ng, K. **Control Valve Noise**, in ISA Transactions, 33(3), pp.275-286, 1994

[3.] **EU Technical Expert Group (EU TEG). Overview of the TEG final report on EU climate benchmarks and benchmarks' ESG disclosures - 30 September 2019**. Available at: https://commission.europa.eu/system/files/2019-10/190930-sustainable-finance-teg-final-report-overview-climate-benchmarks-and-disclosures_en.pdf#:~:text=This%20assessment%20must%20gradually%20integrate%20Scope%203%20emissions,for%20EU%20CTBs%20and%2050%25%20for%20EU%20PABs. (Accessed 30 August 2023)

[4.] Connolly D., Lund H., Mathiesen B.V., Werner S., Möller B., Persson U., Boermans T., Trier D., Ostregaard P.A., Nielsen S. **Heat Roadmap Europe: Combining district heating with heat savings to decarbonize the EU energy system**, Energy Policy, 65, pp.475-489, 2014

[5.] EN 60534-2-1:2011. **Industrial-process control valves – Part 2-1: Flow capacity – Sizing equations for fluid flow under installed conditions**, International Electrotechnical Commission, 2011

[6.] EN ISO/IEC 17025:2017. **General requirements for the competence of testing and calibration laboratories**, International Electrotechnical Commission, 2017

[7.] **EN 60534-1:2005. Industrial-process control valves – Part 1: Control valve terminology and general considerations, International Electrotechnical Commission, 2005**

[8.] Kinsler, L.E., Frey, A.R. **Fundamentals of acoustics**, John Wiley & Sons, 1982

[9.] EN ISO 3745:2012 **Acoustics - Determination of sound power levels and sound energy levels of noise sources using sound pressure – Precision methods for anechoic rooms and hemi-anechoic rooms,** International Standards Organization, 2012

[10.] Oppenheim, A.W., Schafer R.W. **Discrete-time Signal Processing**. Pearson, 2010.

[11.] Frank Fahy, **Foundations of Engineering Acoustics,** Academic Press, 2001

Keynote
Invited speech

Modelling of sound and vibration using a virtual-source approach

Prof. Dr. Goran Pavić

Professor Emeritus at Institut National des Sciences Appliquées de Lyon, France

E-mail: goran.pavic@insa-lyon.fr

Goran Pavić holds BSC in Mechanical Engineering and PhD in Goran Pavić holds BSC in mechanical engineering and PhD in vibration and acoustics. After spending most of his career in industry research he joined in 1998 the National Institute of Science in Lyon as a full professor and, after the retirement, occupies the post of prof emeritus. His research covers sound and vibration energy flow, vibroacoustic modelling, characterization of sources and advanced experimental methods. He was actively involved in a large number of national and international research projects as well as in the organisation of numerous scientific events.

The virtual-source approach enables the use of known analytical solutions of either a vibration or a sound field of a simple surrogate space to construct the field of a more complex space of arbitrary shape and boundaries. The field of the targeted space driven by the original primary excitation is obtained by superposing two fields of the surrogate space: one produced by the same primary excitation, the other by a (large) number of virtual sources. The latter are tuned to the primary excitation in such a way as to reproduce the required boundary conditions of the target space. The tuning is normally obtained by an inverse procedure which leads to the discretisation of boundary conditions. It is shown how the error induced by discretisation is evaluated and controlled. Numerous examples of vibration and sound fields are shown to illustrate the approach.
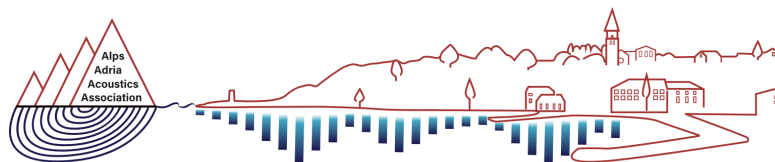
Contributed papers
Soundscape and sound reproduction techniques

APPLICATION OF AMBISONICS TO BUILDING ACOUSTICS – CHALLENGES AND OPPORTUNITIES

Armin Wilfling, Franz Dolezal

IBO – Austrian Institute for Building and Ecology, 1090 Vienna, Austria

Abstract: *Concentrating on existing, standardized methods with an insufficient relation to human perception is not a satisfactory approach to comprehensibly characterize the nuisance caused by impact noise sources. Perception can no longer be condensed to a single number (the so called weighted impact sound pressure level), which is based on a low structural diversity of building components. Thanks to novel recording technologies, their unique combination and mathematical modelling, together with advanced methods for the analysis and interpretation of human perception, a holistic understanding of the acoustic and vibrating interrelationship between building and occupant can be created. Recordings of impact noise caused by neighbours are carried out using different methodologies with the intention to capture a full sphere surround sound for reproduction to test persons in an anechoic chamber.*
Impact noise caused by walking on a ceiling, built according to the (Austrian) standards, usually is of very low level with a low frequency emphasis. That specific kind of signal turned out to be challenging for Ambisonics© recording; the eigennoise of the microphones used became a limiting factor in the recording and reproduction process. Single microphone techniques were compared to multichannel recording systems, focusing on their performance on low level, low frequency signals.

Keywords: Ambisonics, Impact Noise, Recording, Signal to Noise, IRIS Project, Eigenmike

1. INTRODUCTION

Almost 25 years ago Scholl and Maysenhölder rose the question "Is todays description of the impact sound behaviour of ceilings correct and adequate?", and pointed out, that a tapping machine does not represent the most common source of impact noise – a walking person [1].
They stated that wooden ceilings sound different from concrete ceilings. Moreover the transmission of the tapping machines' noise depends on the impedance of the ceiling. Nevertheless, the tapping machine still is the most widely used standardized source for impact sound measurements in Europe.
To compare the annoyance of different ceiling types it is desirable to record the noise signals and play the signals to a test person in rapid succession [2]. The widely used reproduction tests with headphones do not represent the actual sound field in a room, therefore multichannel loudspeaker systems may offer a better representation of the actual sound in the room. [3,4].
Having these findings in mind, the IRIS Project chose to record and reproduce different sound-samples of ceilings for listening tests in the surround sound format Ambisonics©.

2. PRELIMINARY CONSIDERATIONS

2.1. The Ambisonics Signal

Ambisonics© is a full-sphere surround sound format. Unlike most common surround sound formats, signals are not discrete (every signal goes to its dedicated speaker on a predefined position). Ambisonics signals carry encoded position information, representing the sound field in the so-called B-format.
This B-format signal is decoded individually at the listeners monitor setup, providing best possible representation of the recorded signal at that very own setup.
Therefore, on one hand side, Ambisonics© reproduction is perfectly scalable to diverse setups. On the other hand side, the exactly same representation at every setup cannot be guaranteed, which is the case in discrete surround sound formats. [5]

2.2. Impact Noise

2.2.1. Impact Noise Sources

Impact noise sources in residential areas normally include signals like walking – barefoot or with shoes -, jumping,

mechanical noises etc. All those sources reproduced by any ceiling construction do show a significant emphasis on low frequencies (below 100Hz) [6].

2.2.2. Normative Representation

In Austria an intermediate floor in a multi-storey dwelling, according to the Austrian building legislation OIB-RL5 [7], fulfils the requirement, if it transmits a weighted standardized impact sound pressure level $L'_{nT,w}$ of 48 dB or less. $L'_{nT,w}$ as a single number rating does not take the low-frequency parts of the signal into consideration. Requirements across Europe differ significantly between 48 and 65 dB $L'_{nT,w}$ [8].

Low-frequent signals – causing the majority of complaints about impact noise, particularly in timber buildings [9] – are rarely represented in the valid standards. However, also Hagberg states in [10] that in low frequencies, prevailing acoustic theories are doubtful and the design has to be adapted to a new methodology.

3. RECORDING REQUIREMENTS

3.1. The Input Signal

To recheck the assumptions above, that the signal to be represented in the Ambisonics© systems is going to be very soft and low-frequent, we recorded different signals at the test suite at Technical University of Vienna (TU Wien) to compare their input spectra.

Fig.1. Test suite at TU Vienna with tested floor and flanking path decoupling with flexible interlayers

The test suite has the dimensions 540 x 330 x 340 cm and consists of a mass timber structure with flexible shells on the inside of the walls with double planking of gypsum plaster board to avoid noise from flanking transmission as well as disturbing noise from the outside of the test suite. Additionally flanking transmission is damped with flexible interlayers (figure 1) which are adjusted to the weight of the floor test specimen for an optimized absorption effect.

We decided to use every-day impact noises and agreed on having a test person (70 kg) walking – barefoot and with shoes on. Recordings should be captured at a common listening height of 50 to 150 cm (lying to standing), not close to the ceiling. Jumping on the floor – which produced higher levels and therefore better signal-to-noise ratio (SNR) – was not considered, since we failed to keep the levels steady when repeating measurements. For better comparability and to get valid $L'_{nT,w}$ values for our ceilings under test, a tapping machine was added to the comparison and to all further measurements.

The tapping machine did, of course, generate far higher levels, but the spectrum produced is obviously very different from a person walking. Figure 2 shows the frequency responses of the tested signals, matched at 1 kHz. At 100 Hz (1/3 octave) the spectra differ by more than 10 dB, diverging even further below 100 Hz.
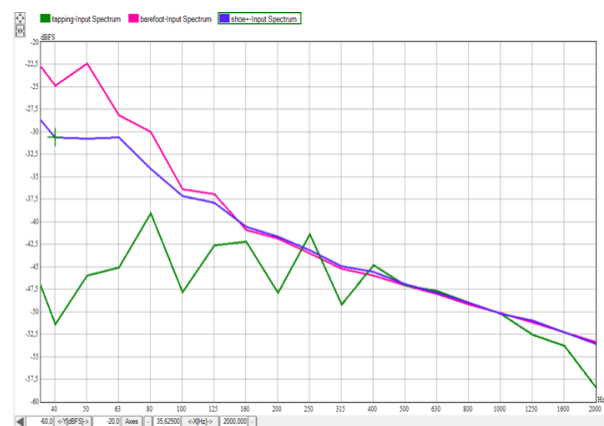
Fig.2. Comparison of input spectra produced on a wooden ceiling (levels matched at 1kHz) walking barefoot, with shoes and tapping machine

Still - in absolute levels the tapping machine produced far higher outputs, ranging more than 20 dB above the walking noise.

3.2. Recording Techniques

These specific low-frequent, very soft signals to be captured turned out to be a challenging task for the recording equipment.

There are two basic approaches to recording that demanding signal and representing it in Ambisonics©.

The first one is capturing the recording with an Ambisonics© microphone – instantly coding the captured sound field into B-format. The second approach is to capture with a single low-noise microphone and adding the sound field information in postproduction. Latter procedure is supposed to improve SNR.

A short overview about those approaches and its advantages and disadvantages is shown in Table 1.

	Ambisonics© 32 Microphone Array (4th Order)
+	Captures movement and sound field information
	Encodes B-Format signal using its proprietary software
	Convenient to use
–	Needs extra microphone for (calibrated) level information

	Class 1 Standard measurement microphone
+	Supposedly better SNR
	simple Calibration process
–	Massive postprocessing needed, virtually producing movement and sound field

Table 1. Advantages and disadvantages of the two possible approaches to Ambisonics© recording

3.3. Microphone Selection

In the anechoic chamber at TGM Vienna we compared SNR of a standard measurement microphone (Norsonic 1225 / 1209) to the Eigemike Ambisonics© microphone array (figure 3) by recording pink noise bursts at 28 dB(A) - representing a good ceiling - and 48 dB(A) for a mediocre one.

Fig.3. Comparison of the eigennoise of Eigenmike em32 Ambisonics microphone to a Norsonic 1225/1209

The SNR was captured and compared in those recordings, shown in figure 4.
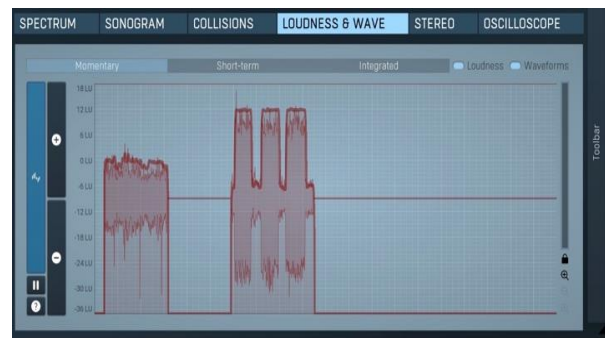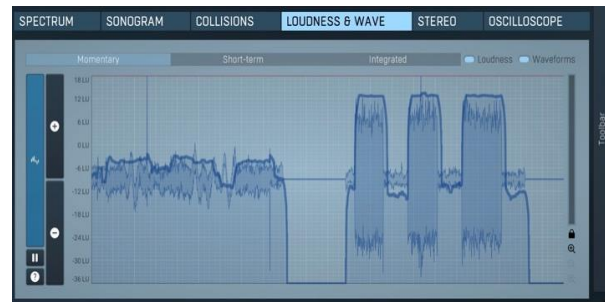
Fig.4. Comparison of the recordings of the pink noise bursts (left 28 dB(A), right 48 dB(A) standard microphone capsule (blue) and a single capsule of the Eigenmike em32 (red)

The first comparison met the expectation that the single microphone provided higher SNR. The difference of about 4 dB SNR was smaller than expected though.

It still seemed worthwhile to give the Ambisonics© microphone array another try, keeping in mind, it would capture the real and actual sound field in the room, rather than adding a virtual one. Furthermore 1st order Ambisonics – used in the lowest coding band – should improve the SNR for the crucial low frequencies.

In case the SNR would not be sufficient in the microphone array, we decided to also include a low-noise single microphone in the next step. That should improve the SNR for the single microphone technique by about 8 dB. Experiments to denoise the recordings or to introduce noise-shaping-algorithms in postproduction were turned down, since that editing produced artefacts clearly audible.

Trying a low-noise microphone and comparing it to the standard microphones we already tested, was the next step - back in the test suite of TU Wien. To turn its receiving room into a more living-room-like acoustic situation, we added absorption to the walls and floor, decreasing its reverberation time below 0.5 s. A Gras 26 HF / 40 EH low noise microphone was added to the test setup (figure 5).

Fig.5. Setup of the different recording approaches at the adapted test suite

By the time those tests were conducted, the Ambisonics[©] listening facility at InnoRenew was ready to start with the first listening tests (figure 6).

First listening tests indicated that the superior sound field information captured by the Ambisonics[©] microphone array outweighed the better SNR captured by the single microphone. However, the relatively low SNR of the Eigenmike em32 compromises measurements and reproduction – especially for ceilings that exceed normative demands. But to put that into the right perspective: walking on a floor which is far better than the Austrian standard or building legislation requirement, is hardly audible in typical living environments [11].

Fig.6. Listening test in the unechoic chamber at InnoRenewCoE

Adding more options, a Sennheiser Ambeo VR – a four capsule Ambisonics[©] microphone –was investigated as well. The SNR was in a comparable range to the Eigenmike em32, although the eigennoise did sound slightly different. The localisation of the sound sources seemed to suffer a bit from the decreased number of capsules, but was in a satisfactory range. In contrast to the Eigenmike em32 the Ambeo VR does not generate a B-format file, thus it can be easily generated by a software provided by the manufacturer. Advantages of the Ambeo VR are that it provides four XLR outputs, allowing the user to pick from a wide variety of audio interfaces and its very competitive pricing. Ambeo VRs SNR may also benefit from using higher quality preamplifiers. For this test decent quality preamplifier (microphone amplifiers in the Roland Octacapture and the MOTU 8pre interfaces) were used.

A few other microphones we tested, but unfortunately they did not meet our expectations.

4. RECORDING PROCEDURE

It was then decided to define a recording procedure for recording Ambisonics sound samples of ceilings for the IRIS project. Those demands had to be meetable in the test suite as well as in in-situ recordings at building sites. Signals were defined to be a person walking on the floor above at 80 and 100 steps per minute (using a metronome for comparability), each with shoes on and barefoot. Our test-walker weighs 70 kg. As a further signal a tapping machine was added. The signal is recorded in Ambisonics[©], but primarily the tapping machine is needed to measure $L'_{nT,w}$ of the specimen for documentation.

Microphones are level matched (the actual level is calibrated for the $L'_{nT,w}$ measurement) by playing pink noise at 70 dB(Z) on a Genelec 8020 loudspeaker. The same model used in the listening room.

At least 3 positions - recording the whole set of signals - were postulated to represent different acoustic shadings within a listening room. Each sample recorded shall be 1 minute. Since more than one recording devices is used (Ambisonics[©], standard measurement and vibration – which is not mentioned in this paper) some kind of slate was demanded to synchronize the recordings for postproduction and reproduction. We decided to jump at the start of each recording, giving a good impulse to easily synchronize.

5. CONCLUSIONS

It turned out, that using Ambisonics[©] systems for building acoustic purposes requires a lot of preparatory work and preliminary studies that have to be done. Comparison with standard and low noise microphones revealed a low SNR that might be too low for a reproduction with test persons simulating the real noise impression in the test suite at InnoRenewCoE in Izola. It could be shown that standard measurement microphones as well as

particularly low noise microphones do fulfil the necessary requirements but obviously cannot record the spatial impression required for the reproduction. At the present stage of the research project, the majority of the foreseen recordings have been carried out with all mentioned equipment. Recordings are provided for the use in the test suite, where they are verified if they are suitable for our purpose. If this is not the case, additional efforts of post processing will be necessary.

6. ACKNOWLEDGEMENTS

7. REFERENCES

[1.] Scholl, W., Maysenhölder, W. **Wird das Trittschallverhalten von Gebäudedecken derzeit richtig und ausreichend beschrieben?** in WKSB, 43/1999.

[2.] Bregman, A. **Auditory Scene Analysis: The Perceptual Organization of Sound**, MT Press, 1994.

[3.] Wiersdorf, H., Raake, A., Spors, S. **Psychoakustik der Wellenfeldsynthese: Vor- und Nachteile binauraler Simulation,** in Proceedings of DAGA, Darmstadt 2012.

[4.] Koehler, M., Weber, L., Späh, M. **Trittschallminderung von austauschbaren Bodenbelägen,** Fraunhofer IRB Verlag, 2014.

[5.] www.waves .com **Ambisonics Explained: A Guide for Sound Engineers**, 2017. Available at: https://www.waves.com/ambisonics-explained-guide-for-sound-engineers

[6.] Maack, J., Möck, T. **Trittschallschutz**, in Bauphysik-Kalender 2009, John Wiley & Sons, 2009.

[7.] OIB Richtlinie 5, Schallschutz. Österreichisches Institut für Bautechnik 2019.

[8.] Rasmussen, B. **Acoustic classification of buildings in Europe – Main characteristics of national schemes for housing, schools, hospitals and office buildings**, in Proceedings of the Baltic-Nordic Acoustics Meeting, 2018.

[9.] Dolezal, F., Neusser, M., Teibinger, M., Bednar, T. **Akustik Center Austria – neue Prüf- und Forschungskompetenz für Holzkonstruktionen in Österreich mit Fokus auf tiefen Frequenzen**, in Proceedings of DAGA, Aachen 2016.

[10.] Bard Hagberg, K. **Management of acoustics in lightweight structures**, Dissertation, Department of Construction, Lund University, 2018.

[11.] ÖNORM B8115-5:2021 **Schallschutz und Raumakustik im Hochbau - Teil 5: Klassifizierung**, Austrian Standards, 2021.

AAAA 2023 IZOLA 20. - 21. September
10th CONGRESS OF THE ALPS ADRIA ACOUSTICS ASSOCIATION

A COMPARISON BETWEEN REAL AND REPRODUCED SOUND FIELDS FOR IMPACT NOISE ANNOYANCE RATINGS

Martina Vrhovnik[1], **Dr. Rok Prislan**[1]

[1] **InnoRenew CoE, Acoustics Laboratory, Izola, Slovenia**

Abstract:

The most common way to evaluate subjectively perceived annoyance of impact noise is conducted with the help of listening tests. Impact noise recordings are played back through headphones or loudspeakers under controlled conditions in which the reproduced impact noise should be perceived and rated consistently to the impact noise in a real environment. According to the standard ISO/TS 12913-2 binaural reproduction are preferred over a multichannel loudspeaker approach. Arguing that multichannel playback lacks a standard technique and examples of best practice. On the other hand, studies in the built environment imply that playback through loudspeakers contributes to the ecological validity of the test environment. Participants are able to move their head or entire body and get a better impression of the sound field which leads to more valid test results. As such further investigations related to the optimal listening approach are needed. This paper presents preliminary results of a listening test in which the participants rated their annoyance when exposed to real impact sources and their acoustical reconstruction in a direct comparison. Participants were exposed to real impact noise, excited on the upper floor, and its reproduction through a higher order Ambisonics system. Annoyance ratings for different impact noises were evaluated regarding the distinguishability between real sound field and its reproduction through loudspeakers. Results expose differences in the perceived annoyance depending on the reproduction technique.

Keywords: *higher order ambisonics, plausibility, qualitative testing, impact sound*

1. INTRODUCTION

In simu applications are used as a substitute for acoustic reality in terms of comparative qualitative evaluation of a sound scene. The InnoRenew CoE's acoustics laboratory is equipped with a 64-channel Ambisonics loudspeaker system that serves as a playback environment for listening tests that we use to investigate acoustic comfort in the built environment. The loudspeakers are mounted on a spherically arranged support system installed in the anechoic chamber of the laboratory. It consists of seven horizontal levels, named alphabetically from top (A) to bottom (G). Two loudspeakers are mounted on the upper level A) and lower level G), while levels B) to F) are arranged in circular rings holding the loudspeakers. Their arrangement is horizontally symmetrical with ring D) defining the plane of symmetry.
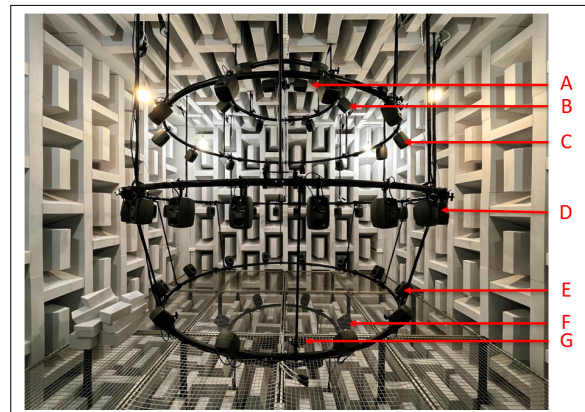
Fig. 1. *Symmetrical Ambisonics loudspeaker setup at the InnoRenew CoE. Number of loudspeakers per ring: Ring A & G: 2, B & F: 6, C & E: 12, D: 24*

The reproduction of auditory sound scenes using the Higher Order Ambisonics (HOA) method differs from a "standard" multichannel loudspeaker setup. Unlike other multichannel formats, the reproduction of the sound field is loudspeaker independent. The sound field is recorded with a spherical microphone and the recordings are encoded in the so-called B-format. Each signal in this format contains and reproduces specific sound field properties in the form of spherical harmonics and therefore takes into account the directional properties [1].

For a realistic reproduction with HOA, a so-called perceptual "sweet spot" at a central listening position is required [4]. In the loudspeaker system presented here, this central listening position is also the center of the sphere created by the loudspeaker

holding system itself. In the technical specifications of ISO 12913-2 it is argued that multichannel reproduction lacks of a standard technique, examples of best practice, and that there is still a need for research in realistic sound reproduction [2]. However, in addition to the commercial breakthrough in surround sound applications offered by Google[1] or Facebook[2], B-format playback has gained recognition in the scientific environment and is increasingly used as an audio framework for virtual reality [4]. One of the drawbacks of this method is its poor directionality, especially at first order [1]. In addition, high-frequency components reproduced in a high-density loudspeaker array can be degraded if decoded to a low- order of Ambisonics [3]. Impairment of localization is also possible if the number of loudspeakers exceeds the minimum requirement [3]. To assess a realistic reproduction, it is essential to diagnose and correct sensory deficiencies in the reproduction environment with HOA. Therefore, a direct comparison between a real sound scene and its reproduction was necessary. Due to the construction of the acoustics laboratory and the anechoic chamber, it is not possible to create "everyday" impact sound (e.g. walking, slamming doors etc...). We decided to set up the Ambisonics loudspeaker setup at a different location where the generated impact sounds could reflect everyday acoustic conditions of a living environment.

2. METHOD

2.1 Test Setup and Measurements

In one of the offices on the second floor of the InnoRenew CoE, we built a reduced version of the HOA consisting of 18 loudspeakers, also assembled in a spherical arrangement, and a subwoofer with a crossover frequency of 60 Hz.

The speaker setup consisted of four levels with 2 speakers on the top (plane A), 4 speakers on level B, 8 loudspeakers at listening height at 1.3 m on level C, and 4 loudspeakers on the floor (level D). The floor of the room was wooden parquet the ceiling was composed of an sound absorbing suspended ceiling. To further reduce room reflections, a wooden structure (3.5m x 3.5m) was built to support sound-absorbing curtains that surrounded the listening test area. Impact noise was generated on the third floor, directly above the listening test area (see Fig.3) .

A standardized tapping machine and real barefoot walking (pace: 90 bpm) were generated as impact sound. We recorded both source types using an omnidirectional microphone and a spherical microphone (mhacoustics' Eigenmike em32). Both were placed in the "sweet spot", at 1.3 m ear level. The reproduced impact sounds were played back in Reaper[3] . For decoding to the loudspeakers, we used the AllRAD decoder from the
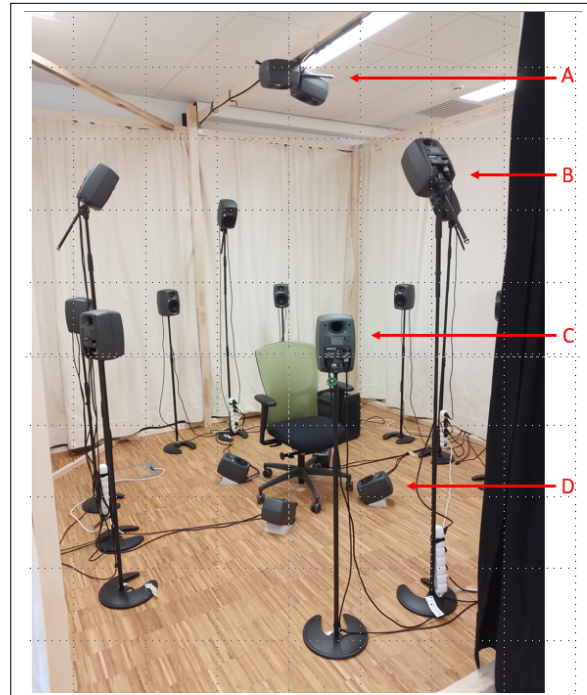
Fig. 2. *Listening test setup on the second floor of the InnoRenew CoE*

Ambisonics IEM plug-in suite developed at the University of Music and Performing Arts in Graz, Austria[4] .

The spherical recordings were then equalized and normalized. This was done by measuring the sound pressure level of the playback with the omnidirectional microphone and adjusting it within octave bands until it matched the level of the real impact sound.

2.2 Listening Tests

The focus of our investigation is on evaluating the perceived differences between real and reproduced impact sound. For this purpose a preliminary study has been performed from which the pilot listening tests results are presented. In a direct comparison, nine participants rated the differences between the real impact sound and its reproduced counterpart on nine qualities. First, they answered a closed question ("yes" or "no") whether they perceived any difference at all. The ratings of the following seven qualities,(*annoyance*, *plausibility*, *thumping noise*, *tone color*, *localizability*, *clarity*, and *artifacts*), included two questions. In the first question, participants rated the difference between two sounds with respect to a particular

Fig. 3. *Position of the tapping machine and walking path (pink) on the third floor of the InnoRenew CoE*

property using a nine-point scale. The second question was also a closed question, asking which of the two sounds presented ("*1st*" or "*2nd*") corresponded more to certain adjectives describing the qualities (see table 1). To query another perceived difference that was not mentioned, participants could describe it in the last open question using the label "*other*".

Quality	Property
Annoyance	more annoying
Plausibility	more plausible
Thumping noise	more thumping
Tone color	brighter
Localizability	easier to localize
Clarity	clearer
Noise artifacts	more noise-like artifacts

Table 1. Evaluated qualities and their descriptive properties

Since auditory memory is only a few seconds long, the participants needed to hear the impact sounds to be compared more often in order to answer all of the questions correctly. Therefore, the two impact sounds were played consecutively for the listeners to rate each of the assessed quality. After the playback, the participants had 30 seconds to answer each question.

3. RESULTS

The boxplots 4 (tapping machine) and 5 (walking) show the averaged results of nine participants for all 8 qualities. The odd columns show, in chronological order, the responses to the nom-

inal scaled questions for the quality overall difference ("*yes*" or "*no*") and which of the two sounds corresponded more to a particular adjective describing the quality (*1st* or *2nd*).
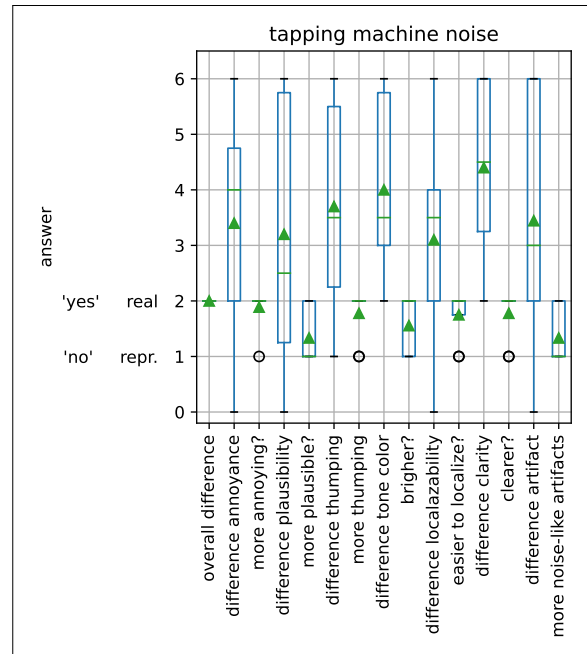
Fig. 4. *Listening test results for the impact sound source "tapping machine".*

For the *tapping machine* all participants were able to distinguish between the real tapping sound and its reproduced counterpart. The real sound was rated as more annoying but not as plausible as the reproduction. The real sound was also rated as more thumping, easier to localize, and clearer. The reproduction was rated as having more noise like artifacts. In regard to tone color the averaged results show the participants' indecision. On average, half of them said that the reproduction sounded brighter, while the other half found the real impact sound brighter.

In terms of individual scale scores for each quality, participants' average scores ranged from 3 to 4.5, with the highest scores given for differences in *thumping noise, tone color* and *clarity*.

The results for the impact sound type *walking* are quite different. On the one hand, for each quality, the standard deviation as well as the range of values given in terms of perceived difference are lower than for tapping machine. One participant perceived no difference (represented as a dot) between the reproduced and the real walking sound. Except for two participants, the difference in annoyance was rated as slightly different on average
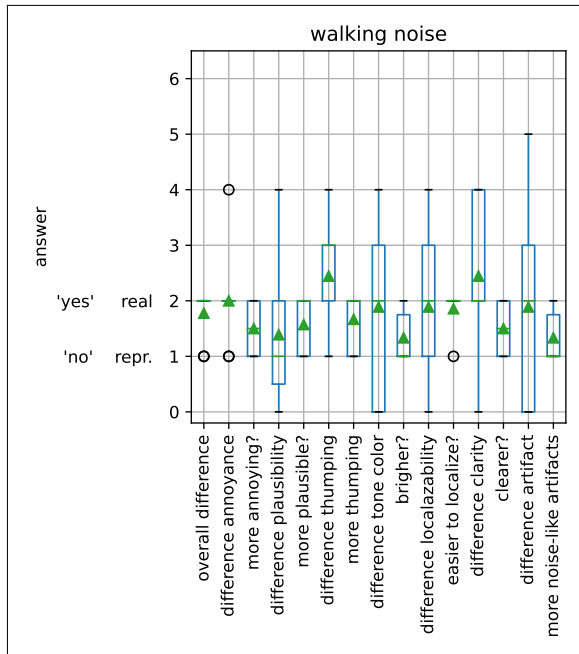
Fig. 5. *Listening test results for the impact sound source "walking"*.

by the other participants. However, they did not have the same impression of which of the two sounds was *"more annoying"*. On average, half of the participants chose one of the two sounds at a time.

Similar results are shown for *"more plausible"* and *"clearer"*. On average, the reproduction was rated as slightly *brighter*, but also as having *more noise-like artifacts*. The real walking sound was rated as *more thumping* and *easier to localize*.
The differences between the real and reproduced walking were with one exception (*artifacts*), not rated higher than with 4, which would be *moderately different*. On average, the ratings for all qualities did not exceed 2.5. For both impact sound types the qualities *thumping noise* and *clarity* had the highest difference ratings on average across all participants.

4. DISCUSSION & OUTLOOK

In terms of the results, it can be said that the reproduction of both impact sound types, tapping machine and walking, is distinguishable from their real counterpart. For each quality, the ratings of differences for the tapping machine sounds have a wider spread with maximum values up to 6 (*"very different"*).

One reason for this could be the insufficient reproduction of higher frequency content, which could lead to a lack of clarity [6]. Since the qualities *tone color* and *clarity* have the highest

difference scores, this could indicate that the tonal impression was not accurately reproduced. In this respect, for future listening tests we envision the application of additional loudspeakers into the ceiling area. It is as well interesting to point out that for the brightness, the listeners were highly confused/indecisive which of the stimuli is brighter, although they rated the difference in brightness relatively high. It will be interesting to investigate if this behavior will persist when a higher number of test subjects will be evaluated.

The reproduction of the barefoot walking sound was more difficult for the participants to distinguish. Barefoot walking sound is characterized by its dominant sound energies at low frequencies below 100 Hz. We used a subwoofer to reproduce frequencies below 60Hz. This could be a reason for a more plausible reproduction compared to the reproduced tapping machine sound. The quality *thumping noise* has the highest average rating among all participants. This is because apart from *clarity* with a similarly high rating, all other ratings are considerably lower. This suggests that the reproduction could be improved by including the reproduction of impact vibration [5].

However, one must also consider the composition of the two tapping sounds. While the tapping machine produces a continuous hammering, walking produces more hollow, thumping noise at greater intervals between the actual impacts. The author assumes that because of their composition, the auditory analysis to determine differences was inherently "easier" for the tapping machine.

5. CONCLUSION

In this paper we presented a listening test procedure to evaluate the distinguishability between real impact noise of a tapping machine and barefoot walking and its reproduced counterpart in B-Format, decoded to an 18-channel loudspeaker system. The presented preliminary results included the response obtained from the pilot listening tests. In a direct comparison, 9 participants rated the differences using 9 auditory qualities. The results suggest that differences in tapping machine sound were easier to detect due to the lack of high-frequency content in the reproduction. Differences in walking sound were more difficult to perceive, possibly due to the plausible reproduction of the dominant low-frequency content of this impact source. Because differences in *thumping noise* had the highest ratings for both impact sources, inclusion of impact vibration in the reproduction could result in a more plausible auditory simulation.

It should be noted that the results of a pilot study were presented. As such, they are based on an insufficient number of participants to draw statistically significant conclusions. Nevertheless, some interesting correlations between the observed stimuli were uncovered, which will lead to technical and questionnaire improvements in further listening tests that will include a much larger number of participants.
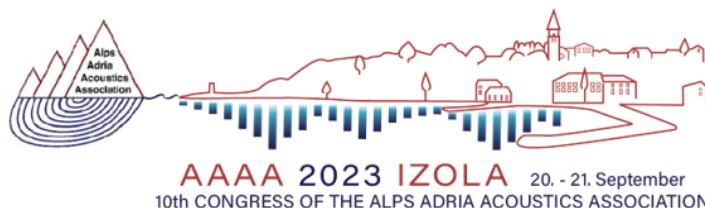
6. ACKNOWLEDGMENTS

7. REFERENCES

[1] Arteaga, Daniel **Introduction to Ambisonics,** 2015.

[2] International Organisation for Standardization **Acoustics - Soundscape - Part 2: Data collection and reporting requirements,** International Organisation for Standardization, 2018.

[3] Shu-Nung Yao and Tim Collins and Peter Jančovič **Timbral and spatial fidelity improvement in ambisonics,** Applied Acoustics, 93, pp.1-8, 2015.

[4] Zotter, Franz and Frank, Matthias **Ambisonics: A Practical 3D Audio Theory for Recording, Studio Production, Sound Reinforcement, and Virtual Reality,** Springer International Publishing, 2019.

[5] Prislan, Rok **The Design of an Impact Sound Vibration Exposure Device,** in Proc. of the 10th Convention of the European Acoustics Association, 2023.

[6] McKenzie, Thomas and Murphy, Damian T. and Kearney, Gavin **Diffuse-Field Equalisation of Binaural Ambisonic Rendering,** Applied Sciences, 2018.
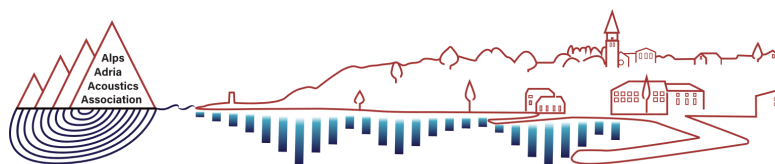
Contributed papers
Noise and vibrations

1. Proposing noise barriers along existing national roads through settlements - the case of Novo mesto and its surroundings
   Mihael Žiger (Nacionalni laboratorij za zdravje, okolje in hrano)
2. Measurement and modeling uncertainty in accredited acoustic procedures
   Antonio Petošić (University of Zagreb, Faculty of electrical Engineering and Computing)
3. Development of a special standard for outdoor music events in Slovenia based on measurements and calculations
   Luka Čurović (University of Ljubljana, Faculty of Mechanical Engineering)

PROPOSING NOISE BARRIERS ALONG EXISTING NATIONAL ROADS THROUGH SETTLEMENTS - THE CASE OF NOVO MESTO AND ITS SURROUNDINGS

Mihael Žiger

Nacionalni laboratorij za zdravje, okolje in hrano (NLZOH), Prvomajska ul. 1, SI – 2000 Maribor

Abstract: *Noise barriers are widely used in Slovenia along motorways and more recently along railway lines, to cope with exceedances of limit values, identified by noise monitoring and strategic noise mapping. Noise barriers along other national roads are mainly used for new developments (bypasses, reconstructions). As the use of passive measures along existing national roads through settlements was considered the only appropriate option, there has been virtually no systematic approach to noise barriers along the existing national roads.*
In 2021, the Directorate of the Republic of Slovenia for infrastructure (DRSI) commissioned noise studies along major roads under its management. Our institution has carried out a noise study for the area of the town Novo mesto and its surroundings, for three road sections with a total length of about 15 km, mostly within built-up areas. We have established baselines for the feasibility of noise barriers and found seven areas where noise barriers can be proposed.
The results show that along the existing national roads through settlements - in addition to the usual passive measures on buildings, and considering limited possibilities of using quieter asphalt and lower speed limits - it is reasonable to consider noise abatement also by noise barriers.

Keywords: noise, barrier, road, settlement, study, Novo mesto, Ribnica

1. INTRODUCTION

This article presents findings of the noise study for three road sections with a total length of about 15 km in the area of the town Novo mesto and its surroundings, commissioned by the Directorate of the Republic of Slovenia for infrastructure (DRSI) and carried out by NLZOH [1]. The road sections are:

R2-419/1203 Soteska - Novo mesto, km 12,253 - 14,513,

G2-105/0256 Novo mesto (Revoz) – Metlika, km 0 - 3,184 and

G2-106/0263 Žlebič – Kočevje, km 0 to km 9,505.

The road sections are in the area of the municipalities Ribnica and Novo mesto, mostly running through built-up areas. The main goal of the study was identifying areas to be protected by noise barriers and proposing them.

In this article, we focus on identifying areas, suitable for noise barriers, the criteria for their placement and the solutions for barriers at the study level, rather than on the model calculations and measurements that we carried out, which were of course necessary for such a task.

The paper is structured by first providing baselines for the feasibility of noise barriers, then roughly presenting model calculations including road, traffic and environmental data, and finally, after identifying suitable areas, moving on to the noise barrier proposal.

2. BASELINES FOR NOISE BARRIER PLACEMENT

The work began by establishing appropriate baselines for the placement of noise barriers, a result of joint work of noise companies proposing barriers at different areas, the engineer and the commissioner:

1. The noise barrier should protect at least a group of three overexposed (exposed to noise, which exceeds the limit values) residential buildings and should have no interruptions (pedestrian passageways are allowed with appropriate overlaps or doors).

2. When protecting unbuilt areas, only public areas such as the surroundings of educational establishments (kindergartens, schools), cemeteries and, conditionally, park areas and areas adjacent to multi-apartment buildings should be considered. All such areas should be subject to a detailed inspection to verify the justification and appropriateness of the protection.

3. Before proposing a noise barrier, it is also necessary to check the intended land use; barriers (for the protection of living space) should be mainly planned for residential areas or areas with predominantly residential use. Central (mixed) areas and areas with scattered buildings should usually not be protected by barriers.

4. The minimum height of the barriers shall be 2.0 m. The recommended height is between 2.0 m and 2.5 m, although higher barriers are possible in exceptional cases (which must be justified in the proposal).

5. The noise barrier shall reduce the noise by at least 5 dBA at the most exposed assessment point (at a height of 2 m) and provide a sufficient (best possible) economic eligibility index (index defined in [3]).

6. The proposal of noise barriers may also include a removal of a connection to a local road or driveway if access is provided otherwise.

Regarding the placement of shorter barriers by the owners themselves to protect their own buildings or areas from noise (such barriers were not the subject of the study), we have proposed that such barriers 1. shall not compromise traffic safety, 2. shall comply with the requirements of the municipal spatial plan, 3. shall be sufficiently absorbent at the road side (noise absorption panels that reduce noise by at least 8 dB on reflection, conditional gabions - exceptions to this condition being only possible if there are no existing or planned noise-sensitive buildings or areas on the opposite side of the road, and 4. shall be sufficiently insulating to reduce noise by at least 25 dB on transmission (noise barriers, gabions, solid walls, etc.) - gaps in the barrier (between the posts and the panels, or between the base and the panels) or other openings or breaks shall be avoided, as they significantly reduce the noise-abatement effect of the barrier.

3. CALCULATION OF ROAD NOISE

We set up a three-dimensional noise model. The modelling and noise calculations were carried out using the CadnaA software tool (DataKustik, Munich, Germany, version 2022). The calculation method for road noise was XPS 31-133, and we have introduced road, buildings, terrain, ground absorption, existing (noise barriers), all with the appropriate properties. We calculated noise maps at a height of 4 m and maximum noise levels at all noise-sensitive buildings up to a distance of at least 200 m from the road. Calculations were carried out for all the mandatory noise indicators (L_{day}, $L_{evening}$, L_{night}, and L_{dvn}). The noise maps were calculated at a 5 m x 5 m grid. In the areas where noise barriers were proposed (see next section), further calculations were carried out, such as a noise map at a height of 2 m, façade maps for every building floor, noise at the receivers on the most exposed façades per floor, all with and without the proposed noise barriers.

The horizontal and vertical alignment of the roads in the model were taken from the operational monitoring [2], with minor corrections only. Road data were also taken from operational monitoring – traffic speeds, asphalts, traffic flow, but with field verification. Traffic on most roads was also based on traffic from operational monitoring, increased by an annual growth rate of 1.5% (after analysis of traffic counter data) until 2045. On the section G2-105/0256 Novo mesto (Revoz) - Metlika, which is planned to be bypassed by a parallel road, such an increase in traffic is not realistic and we took into account the relevant traffic study of this bypass.

Buildings were taken into account according to the operational monitoring [2]. However, the buildings in the first line of houses along the road were inspected by field visits in autumn 2021 and modified, added or removed as necessary. The configuration of the terrain in the form of contour lines was taken from the operational monitoring, with minor corrections. The ground absorption in the operational monitoring had been set according to the actual use and was not presented in a way that would uniquely allow its reproduction, so in this study it was set according to the planned land use defined in the plans of the municipalities (Ribnica and Novo mesto). For example, transport infrastructure (road) and water areas were considered as reflective (G = 0.0), most of the natural and agricultural environment as absorptive (G = 1.0) and most of the built-up areas as partially absorptive (G = 0.7). For residential and other noise sensitive buildings, the national noise limit values (III. noise protection zone) L_{day} 65 dBA, $L_{evening}$ 60 dBA, L_{night} 55 dBA and L_{dvn} 65 dBA for the road as a noise source were used. Other noise sources

were not taken into account, as they were negligible compared to the roads under consideration.

4. IDENTIFYING AREAS SUITABLE FOR NOISE BARRIERS

The descriptions and tables start with the road section R2-419/1203 Soteska - Novo mesto from km 12,253 to km 14,513, then G2-105/0256 Novo mesto (Revoz) - Metlika from km 0,000 to km 3,184, and finally G2-106/0263 Žlebič - Kočevje from km 0,000 to km 9,505, all in the direction of stationing. "Overexposed" in this chapter means exposed to noise above the limit value L_{night} 55 dBA in 2045.

Areas suitable for noise barriers are presented in the following text and figures from 1 to 6. The road sections are shown in red, noise sensitive buildings in blue, other buildings in grey and the proposed noise barriers in black.

Area 1 (see figure 1), section 1203: Between km 12.3 and 12.4 there are three overexposed residential buildings and their functional land to the right (Novo mesto: Drska 2, Drska 1 and Drska 24), which are mostly slightly below the road in terms of elevation and do not have direct access from the national road. There are good possibilities for a noise barrier. The beginning of the barrier is limited by the intersection with Slavka Gruma Street, the end by the cycle path and driveway at Drska 24. The regional road is cut in immediately after the cycle track, so from the cycle track onwards we also have noise protection of the area due to the road cut. The planned use of the area of the buildings is SS - residential.

Area 2 (see figure 2), section 0256: Between km 0.6 and 0.9 to the left there is a residential area along Ulica Ivana Roba. The first two buildings are above a road cut (Nos 33 and 2), and then the road passes into the embankment, so that between km 0.7 and 0.85 the buildings are below the road in height. The entire area of houses is accessed from a junction at km 0.9, so there are no road accesses from the main road, the only pedestrian access being the staircase at No 33. There are more than 10 overexposed residential buildings. The planned land use of the area with the houses is SS - residential.

Area 3 (see figure 3), section 0256: In the area from km 1.5 to 1.95 to the right there is a larger built-up area along Pie in Pina Mlakarja Street. The initial (3) and final (5) few buildings (with the address Belokranjska road) have individual entrances or accesses from the main road, while the central part (10 houses with the address Ulica

Pie in Pina Mlakarja) has no entrances from the main road and thus a noise barrier is possible. The area is fenced even in its existing state, the house plots are mostly above the main road and therefore concrete retaining walls of 0 to 1.8 m height are present, on top of which are also fences of different heights and materials, some of them being even full, but without defined acoustical properties. A suitable noise barrier in area 3 should be somewhat higher than in other areas, due to existing height differences.

Area 4 (see figure 4), section 0263: The settlement of Grič has a compact built-up area to the left of the road and extends from km 1.2 to 1.8. The planned land use of the area with the houses is SS - residential. For the first two buildings (Road I 10, Road I 12, km 1.24 to the left), comprehensive noise abatement is not possible due to driveway and proximity. The first two buildings are followed by an area accessed by local roads (to Road IX at km 1.31, Road VIII at km 1.38, Road VII at km 1.46 and Road VI at km 1.52) up to the building Road VI 2 at km 1.55. In this area, the road reconstruction project foresees the removal of the connections of these four local roads to the main road, which allows the planning of a noise barrier in this area. From including the building Road VI 2 at km 1.55 (as well as in the whole area 4 to the right of the road), we again have individual entrances to the main road, which make noise barriers impossible.

Area 5, section 0263 (see figure 5): To the left of the road is the area of the primary school in Ribnica, extending from km 3.66 to the junction with Kolodvorska Street at km 3.74. There are two tall school buildings, named C and A, along the road, and it would not make sense to shield the buildings by a noise barrier. However, we consider this public area worth protecting by a noise barrier. In front of Building A, approx. km 3.71 to 3.73, there is a playground with play equipment for small children, and schoolchildren occasionally gather between buildings C and A (in front of the entrances to both school buildings). The school's land use is CD - central. Building A is under monument protection, and there are two wooden sculptures in front of the school. There is already a fence on the same line where the noise barrier would be located. The existing fence has already been demolished in its western part (probably for access to the parking spaces at the school) and we are not proposing a noise barrier in this part as it is not necessary to protect the play areas and entrances to the school buildings. The terrain, including the road, is predominantly flat.

Area 6 (see figure 5): To the right of the road in Ribnica, between the junction with Kolodvorska Street at km 3.74 and the block access at km 3.85, there is a diverse area of four overexposed buildings (the house Kolodvorska Street 8, two houses Prijateljev trg 7 and 8 and a 5-storey residential block Prijateljev trg 6). The planned land use of the area with houses is SS - residential, the same applies to the block. At km 3.775 there is a street, which (according to the usual curb on the pavement along the main road) is no longer accessed from the main road but can certainly be accessed from the other side (from the south). There is currently a pedestrian access at ca. km 3.81. The terrain, including the road, is predominantly flat. We propose the area for a noise barrier, although due to its central location in the settlement, the possible need for pedestrian passages and the very different heights of the buildings, we were somewhat hesitant to make this decision.

Area 7 (see figure 6): In Goriča vas, there are several overexposed residential buildings to the left between km 5.15 and 5.35. At km 5.22 there is a single junction to the left, otherwise there are no individual entrances from the main road. From the junction, the road continues on its left side over a bridge (river Bistrica). Buildings are at or slightly below road level. The buildings are zoned SK - rural settlement area, but in the part under consideration the buildings are mainly residential. Unfortunately, the junction will require an interruption of the barrier, but in spite of this only interruption, we have proposed a noise barrier, although the noise character (short higher levels at nearby houses when a vehicle crosses the interruption) might not be ideal.

The study describes in the same detail the areas suitable for noise barriers and the areas not suitable for noise barriers. In this article, we have described the areas suitable for noise barriers only. The reasons, why some areas were considered not suitable for noise barriers, are summarized here: too few overexposed buildings, buildings high above the road, extraordinary views (to the mansion, the old town, the river), houses directly on/near the road, houses with individual driveways directly from the road, most buildings not sensitive to noise, tall blocks with asphalted parking lots in the surroundings, scattered housing, old cemetery with stone wall under monument protection proposing (the settlement has a new cemetery), barriers are not possible for reasons of traffic safety (in a curve, at an intersection).

5. PROPOSAL OF NOISE BARRIERS

We proposed noise barriers in the seven areas described above. Before making a proposal for noise barriers, we detailed all the input data for the calculations in the area of the proposed barriers, calculated the economic eligibility index for the different barrier heights and decided on the appropriate barrier height based on the values. In total, seven sets of barriers were proposed in seven areas, respectively. One barrier is 3 m above the road, two barriers are 2.5 m high and the remaining barriers are 2.0 m high. The barriers have a total length of 1303 m and a surface area of 2928.5 m^2. The proposal of noise barriers is shown in table 1 and graphically on figures 1 to 6. The table gives information on the barrier number (equal to the number of the corresponding area), its length and height, its position in relation to the road (stationing from - to, side) and the need for absorption characteristics on the inside (towards the road) and outside of the barrier.

Noise barrier (PHO)	L (m)	H ** (m)	From (km)	To (km)	Side	Abs. In/Out
PHO 1	116	2,5	12,270	12,383	right	+/-*
PHO 2	258	2,0	0,637	0,891	left	-*/-
PHO 3	213	3,0	1,572	1,791	right	+/-
PHO 4***	295	2,0	1,245	1,537	left	+/-
PHO 5	79	2,0	3,664	3,737	left	+/+
PHO 6	103	2,5	3,743	3,842	right	+/-
PHO 7/1	68	2,0	5,155	5,220	left	+/-
PHO 7/2	171	2,0	5,228	5,395	left	+/-

* Absorption is not obligatory, but is recommended, at least on some parts of the barrier.
** All heights are relative to the national road, except for PHO 2 up to approx. km 0.7 (there above the ground - the upper edge of the cutting) and PHO 7/1 and PHO 7/2 near the junction (there above the local road).
*** The barrier PHO 4 can only be implemented at the same time as or after the reconstruction of the road, which removes the connections of the existing local roads to the main road.

Table 1. Proposed noise barriers

Each of the barriers is described in detail in the study (skipped in this article), in particular in terms of its route, the start and end points, the possibilities of breaks for (pedestrian) crossings, and other features that might be relevant for the design. The acoustical effect of noise barriers (L$_{night}$ with minus without barrier) is shown in the lower halves of figures 1 to 6.
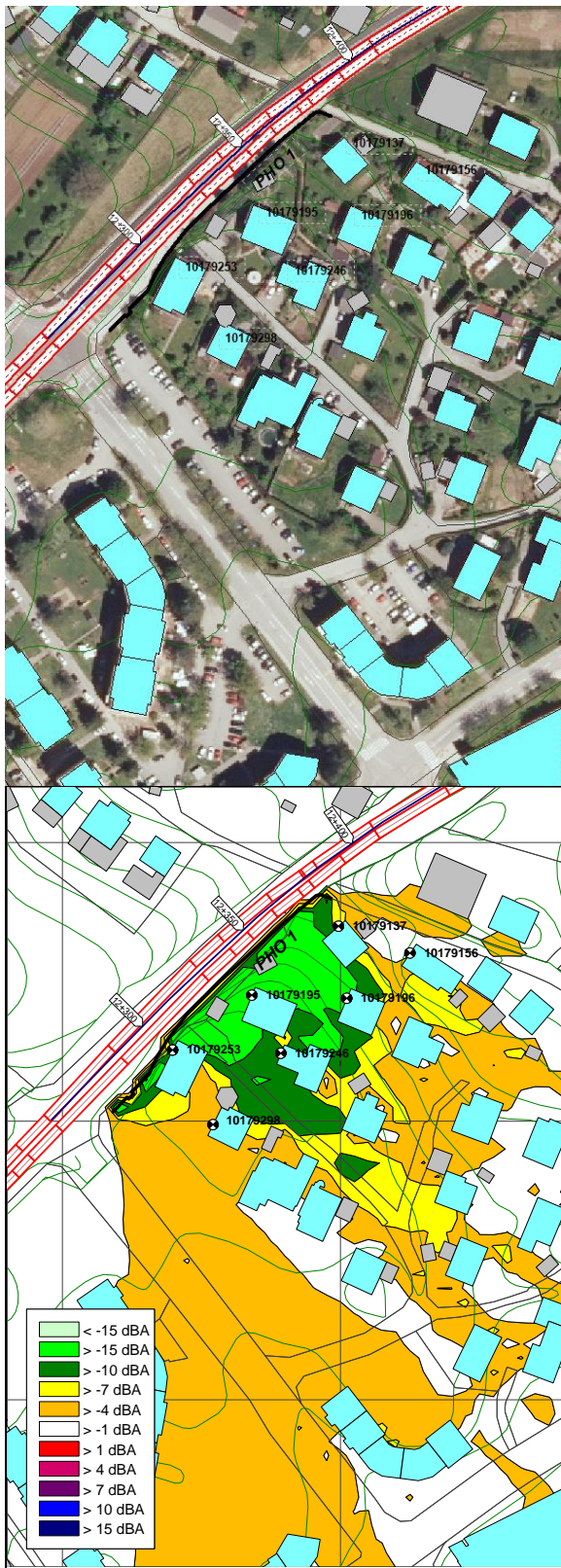
Fig.1. Area 1 and barrier PHO 1 (above) and effect of barrier PHO 1 at h = 2 m (below), M 1:2500
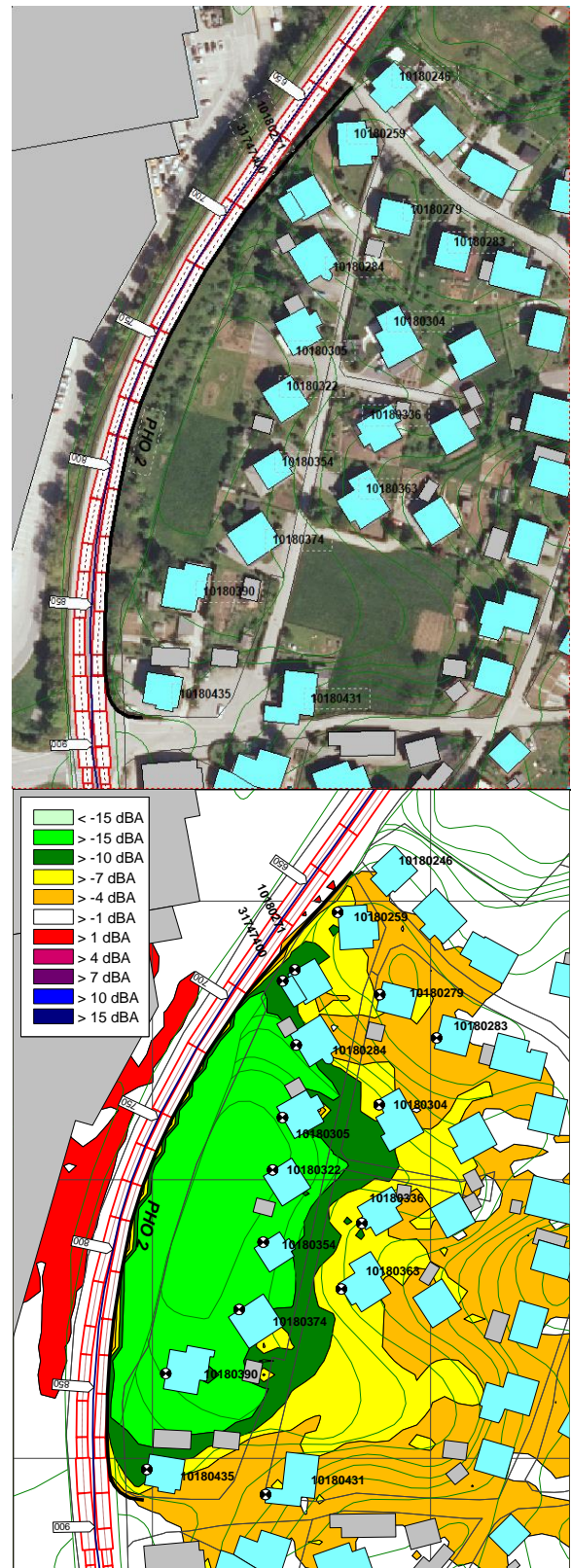
Fig.2. Area 2 and barrier PHO 2 (above) and effect of barrier PHO 2 at h = 2 m (below), M 1:2500
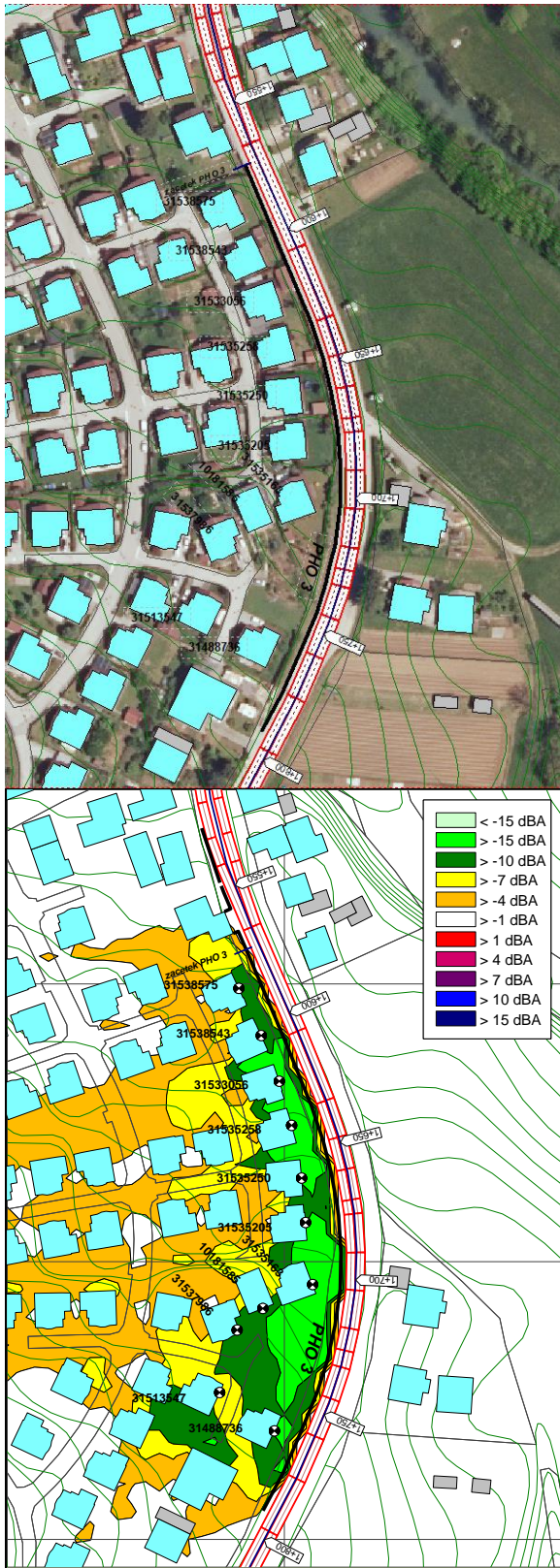
Fig.3. Area 3 and barrier PHO 3 (above) and effect of barrier PHO 3 at h = 2 m (below), M 1:2500
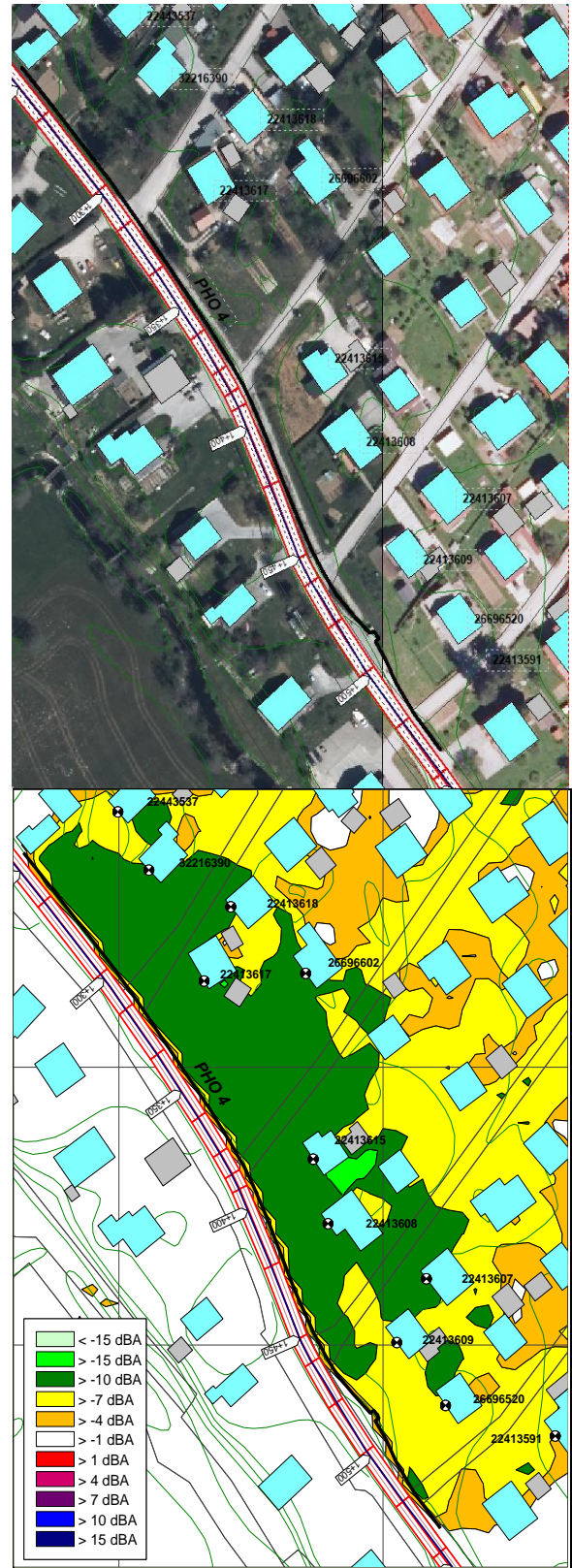
Fig.4. Area 4 and barrier PHO 4 (above) and effect of barrier PHO 4 at h = 2 m (below), M 1:2500 approx.
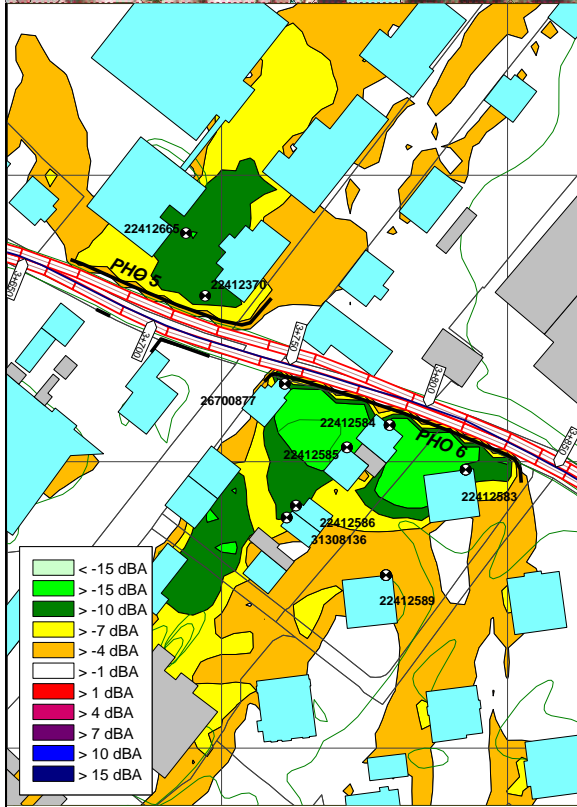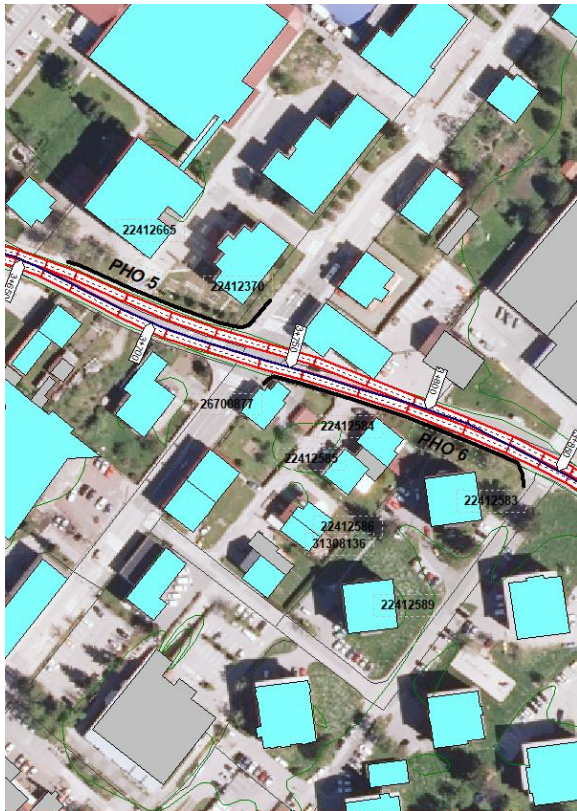
Fig.5. Areas 5 & 6 and barriers PHO 5 & 6 (above) and their effect at h = 2 m (below), M 1:2500
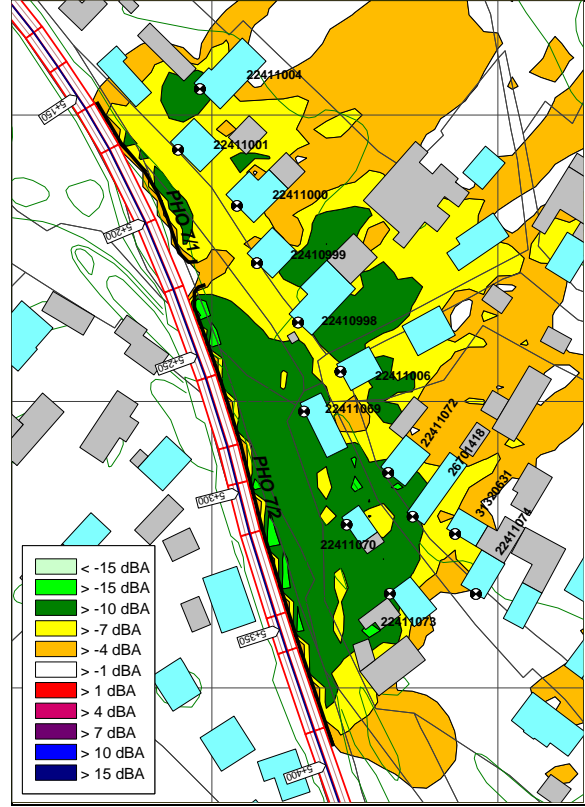
Fig.6. Area 7 and barrier PHO 7 (above) and effect of barrier PHO 7 at h = 2 m (below), M 1:2500

It was not possible and reasonable to protect all buildings in their entirety by noise barriers, so we also proposed passive protection in the noise barrier areas. Passive protection was proposed in areas 1, 2, 3 and 6 for 15 residential buildings, or rather for their upper floors. No passive protection was required in areas 4, 5 and 7.

We have not proposed quieter asphalt as it has a negligible acoustic effect compared to barriers at residential traffic speeds (50 km/h). We have also not proposed lower speed limits, as these are not effective from a noise point of view at 50 km/h. However, we have recommended that quieter asphalts should be used when resurfacing is necessary.

As part of the study, noise measurements were also carried out in some areas of the proposed noise barriers, in order to be able to assess the effect of each noise barrier after its implementation and to compare it with the expected results provided by this noise study.

6. CONCLUSION

We presented a noise study to identify the areas and extent of noise barriers along major roads managed by the Infrastructure Directorate of the Republic of Slovenia in the area of Novo mesto and its surroundings, which was carried out at NLZOH in 2021 and 2022.

The total length of the national roads concerned was around 15 km. As part of the study, road traffic noise emissions for 2045 were determined and an acoustic model developed. Based on the baselines presented, we identified seven areas where noise barriers make sense. We developed a proposal for noise barriers and associated passive protection. In total, seven sets of barriers (one 3 m above the road, two 2.5 m high and the remaining ones 2.0 m high) were proposed in seven areas, respectively.

They have a total length of 1303 m and a surface area of 2,928.5 m^2. The proposed noise barriers have a good or very good economic eligibility index and are going to reduce noise significantly. Passive protection was proposed for the upper floors of 15 buildings.

In this article, we have shown that there are viable options for noise barriers along existing main and regional roads through settlements. Although noise barriers proposals always are somewhat subjective, they should nevertheless be based on common baselines, e.g. such as we have outlined in this article.

7. REFERENCES

[1.] Žiger, M. (NLZOH) **Noise study for the identification of areas and dimensions of necessary noise barriers along important roads managed by the Infrastructure Directorate of the Republic of Slovenia in the area of Novo mesto and its surroundings**, No. 2920-21/97833-22, 2022 (in Slovene).

[2.] PNZ d.o.o., Epi Spektrum d.o.o. and A-projekt d.o.o. **Noise monitoring for roads with more than 3 million vehicle movements per year, managed by the Infrastructure Directorate of the Republic of Slovenia**, No. 17/650A, 2019 (in Slovene).

[3.] Epi Spektrum d.o.o. and PNZ d.o.o. **Expert basis for the operational program for noise abatement along motorways in the Republic of Slovenia**, No. 2018-015/IMS, 2019 (in Slovene).

[4.] Data on roads (DRSI), municipality plans and conditions (municipalities Ribnica and Novo mesto), general environmental and geographical data (internet), 2021 and 2022, and project documentation for reconstructions of individual road sections, all used for noise modelling.
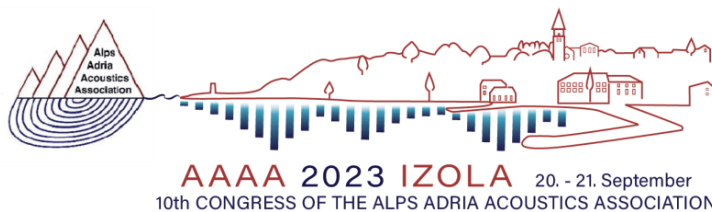
MEASUREMENT AND MODELLING UNCERTAINTY IN ACCREDITED ACOUSTIC PROCEDURES

Antonio Petošić, Domagoj Stošić, Toni Marinković, Mia Suhanek

University of Zagreb, Faculty of Electrical Engineering and Computing, Department of Electroacoustics, Unska 3, Zagreb

Abstract:. *The uncertainty in acoustic measurements and modelling is discussed in this article regarding the measurement method for determination of environmental noise parameters in accordance with ISO 1996-2:2017, the modelling methods in accordance with ISO 9613-2:1997, the NMPB-XPS 2007, and the EU CNOSSOS from the results of interlaboratory comparisons (ILC). Additionally, measurement uncertainties for airborne and impact building acoustic parameters measured in accordance with ISO 16283-1:2014, ISO 16283-2:2020, with determination of single number values in accordance with ISO 717-1:2020 and ISO 717-2:2020, from ILC are determined from each independent measurement and compared with tentative values from the ISO 12999-2020 standard and previous comparisons. The statistical analysis of the data shows that there is a significant difference in the proposed measurement uncertainty for equivalent sound pressure level at closer ranges. Modelling uncertainty from the findings is significantly less than the values provided by laboratories which use tentative value for u_{met}=2 dBA which is the most dominant component in uncertainty budged. When discussing building acoustic parameters, there is no discernible difference between the ILC findings obtained with one independent measurement and those recommended in standard ISO 12999-1:2020 and previous comparisons.*

Keywords: measurement and modelling uncertainty in acoustics, environmental noise parameters, building acoustic parameters, experimental measurement uncertainty standard deviations in repeatability and reproducibility conditions;

1. INTRODUCTION

Finding measurement uncertainties in acoustic measurements and modelling can be a very tedious task due to large number of parameters which have an influence on measurement results. In environmental measurement accredited procedure described in standards ISO 1996-2:2017 [1] there is a chapter about measurement uncertainty budget. The uncertainty for $L_{A,eq}$ and some other parameters can be calculated for each considered situation and different sources levels under the influence of residual noise levels. The measurement results are usually acquired in small time intervals (few hundred samples *in 10 minutes*) if longer term measurements are done or few minutes intervals if short term measurements are done. Most of laboratories do short term measurements at shorter distance where meteorological conditions do not play a significant role on the measurement results.

For some other procedures, e.g., in building acoustics, there is a separate standard ISO 12999-1:2020 [2] which considers the measurement uncertainty for airborne and impact and sound insulation parameters by using values for standard deviations in repeatability and reproducibility conditions.

In some other standard for determination of the sound power such as ISO 8297:1997 [3] the measurement uncertainty is predefined depending on the size of the measurement site (Table 1). The maximum value is up to U=+1,5 dBA (single side interval 95% confidence level).

In the standards ISO 3744:2010 [4] and ISO 3746:2010 [5] the measurement uncertainty is also provided, and usually a maximum value is given (U=4 dBA).

Measurement uncertainty for standard ISO 3382-1,2 [5,6] depends on the measurement results and number of measurements (source and receiver positions).

There are some additional procedures to estimate measurement uncertainty u (repeating the measurements and calculating standard deviations in repeatability conditions) and finding expanded measurement uncertainty u. Due to simplicity, the majority laboratories used the maximum predefined values for uncertainties from standard ISO 19962-2:2017. Usually, they did not use the uncertainties in assessment of conformity with limit values.

In this paper the main problems in measurement uncertainty determination for measurement procedures for environmental noise and building acoustics parameters is considered. Experimental measurement uncertainties obtained by different laboratories participating in several ILCs and overall experimental measurement uncertainty are compared.

1.1. Measurement uncertainty for environmental noise parameters by measurements and modelling

In the first step usually the background noise level is measured. The measurements should be done in most favourable meteorological conditions, if possible, from the dominant source of residual noise (highway, railway, road far away or industrial site). This can be a problem if the residual noise is measured in the state when it is not lowest during the day, evening, night period so sometimes $L_{A,90}$ is used as a parameter for estimating the residual noise level instead $L_{A,eq}$ [7].

The measurement procedure for determination of environmental noise parameters by measuring of residual noise, modelling the levels of new source, and checking modelling results by measurements of overall noise when new source should be installed near residential objects is shown in Fig. 1.
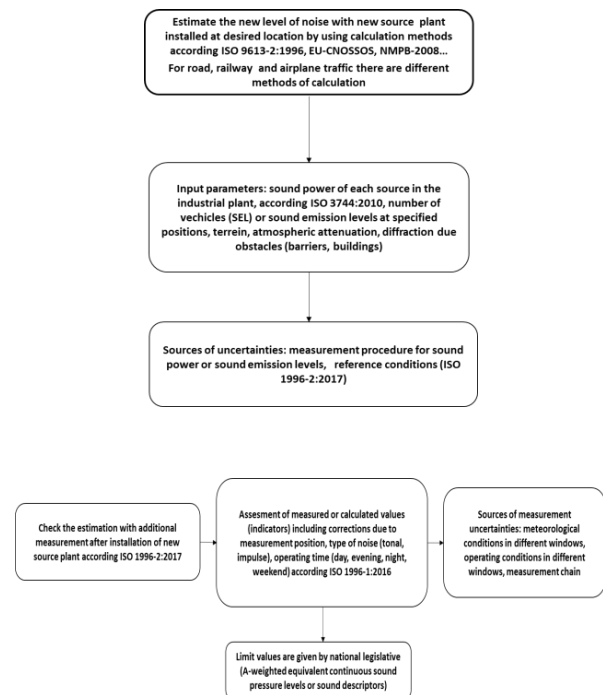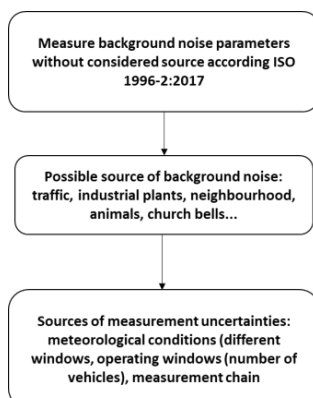
Fig.1. Procedure for determination of environmental noise parameters according to ISO 1996-2:2017 (measuring initial state, modelling new sources state, checking the results)

It is evident that the new edition from 2017 is more complex than previous version ISO 1996-2:2007 regarding the measurement uncertainty calculations. Each measurement situation and time of measurement can be subjected to different operating conditions from source and different meteorological conditions and therefore, measurement uncertainty cannot be fully controlled by the operator. The standard covers all types of sound sources (traffic, industry) and meteorological conditions (very favourable, favourable, neutral, and unfavourable). For some meteorological conditions (unfavourable) results should be omitted (problems with short term measurements on larger distance than eq. 11 in ISO 1996-2:2017) even this is very difficult to achieve during day period.

The possible strategies for measurements are shown in Figs. 2 upper and down. Majority of laboratories have done short term measurements with tracking meteorological conditions for both sources due to restriction of time for participation in ILC (several hours for environmental noise measurements and few hours for building acoustics parameters).
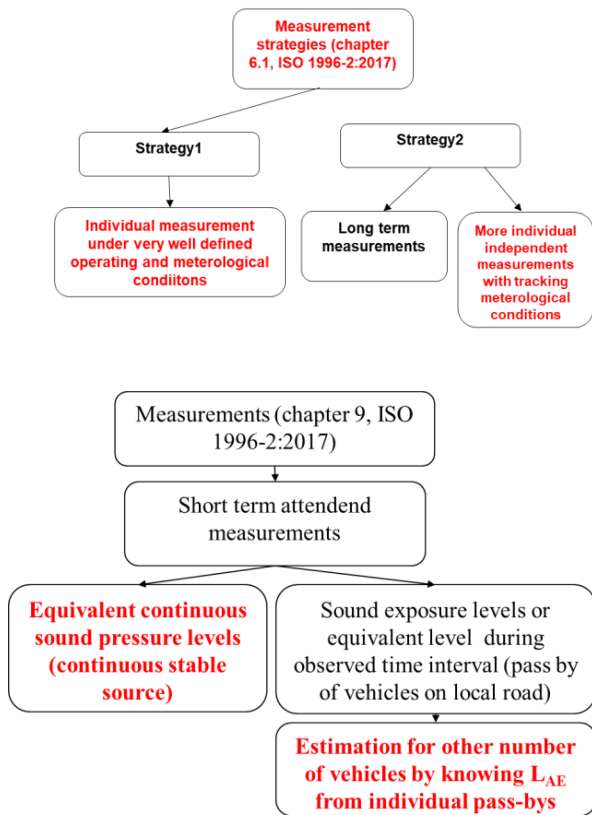
Fig 2. Possible strategies for measurements in ILC (upper) with some restrictions in (down) due to available time.

Q_{met}	0,0	2,0 (1,5)	1,00	2,00
Q_{loc}		0,0	0,00	0,00
Q_{res}		0,4	-0,01	-0,01
$L_{A,eq,res}$	39,1			
$u=\sqrt{u_1^2+u_2^2+..}$				2,08
$L_{A,eq}{}'$ corrected	58,2		Expanded k=2	U=4,2 (3,2)

*the largest component in uncertainty budget

Table 1. *Measurement uncertainty budget according to [1]*

In the ILC two different sources have been considered: stable industrial source with tonal component at 10 kHz and local road as a source of residual noise. The receivers' height for stable source was from 1.2 metres to 1.5 metres and for a local road (total length 4 metres).

The scheme of setup is shown in Fig. 3a). while Fig. 3b) shows the modelling site.

The process of measurement uncertainty estimation is much more complicated (influence of all parameters, equipment, repeatability conditions, different operating, and meteorological windows). The standard aims to cover all possible conditions however, it is a basis for developing more specific standards dedicated to the specific type of sound sources and goals.

A more complex way to calculate measurement uncertainty would be dividing the sound source work in different operating and meteorological conditions. The uncertainty budget is shown in Table 1. and it is slightly different from previous standard edition.

Quantity	Estimate	Standard Uncertainty	Senistivity Coefficient	Uncertainty Contribution
$L'_{A,eq}$	58,3	0,5	1,01	0,51
Q_{slm}	0,0			0,00
Q_{sou}	0,0	0,3	1,00	0,28

Fig 3. Measurement setup for ILC with noise sources and measurement positions a) and modelling site b)

Two measurement points for a stable sound source (located in the house with one window-surface source opened) are considered: free field (on the border 25m away) and in front of the facade (50m) and on the facade/near facade with corrections for all measured parameters (-3 dB).

All laboratories had to measure environmental parameters from the stable industrial source at two different positions (several short-term measurements i.e., several intervals to "cover" a 15-minute interval) to satisfy (or not) the conditions from eq. 11 in ISO 1996-2:2017 when meteorological windows have to be determined.

Laboratories which were measuring meteorological conditions, provided the measured meteorological data during measurements with determined meteorological windows (M1,M2,M3,M4) connected with noise samples and were compared with organizer meteorological data.

For the local road the sound exposure level (L_{AE}) [7] is measured during propagation of each individual type of vehicle (passenger, medium-heavy, heavy…) on one measurement position. If this was not possible, the laboratories measured the A-weighted equivalent sound pressure level in some period with given number of vehicles in order to find sound exposure level from individual pass-bys of different types of vehicles. The typical duration of measurement was 1 hour.

The levels of background noise from highway (500 m) were different at different measurements intervals due to increased traffic flow or favourable meteorological conditions from line source because highway as a source was main source of background noise.

The critical questions arise:
   a) Is the measurement uncertainty overestimated when $u_{met}=2$ dBA (for $L_{A,eq}$) and should we consider uncertainty when we are doing assessment?
   b) How to measure meteorological conditions during environmental noise parameters (resolution in time, which parameters to measure and use meterological windows or more detailed considerations at all wind directions)?
   c) Is it better to use results of interlaboratory comparisons results for uncertainty or to use GUM when expanded measurement uncertainty is calculated from each individual measurement results according Table 1.?

The results for measurement uncertainty from each laboratory and overall obtained in ILC have been compared.

Modelling the environmental noise parameters around the surface (radiating window) and local road as a "line source" is done by knowing the properties of terrain and objects. Modelling methods with all propagation effects are: ISO 9613-2:1997, CNOSSOS –EU for industrial source and EU-CNOSSOS and NMPB 2088 for local road. The points for providing results are given by the organizer.

The estimated sound source power (point source and line source) together with sound pressure levels at imission points of interest are calculated by the participants while using measurements in two different points.

2.3. Sound insulation setup

The measurement setup is shown in Fig. 4. with source and receiving rooms for airborne and impact sound insulation measurements according to ISO 16283-1:2016 [8] and ISO 16283-2:2020 [9] with single number values determination together with spectral adaptation terms described in ISO 717-1:2020 [10] and ISO 717-2:2020[11]. The laboratories determined measurement uncertainties according to ISO 12999-1:2020 [12].
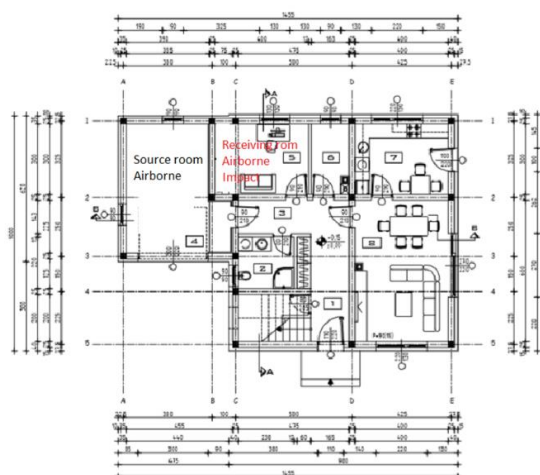
Fig 4. Measurement site for sound insulation parameters

The same receiving room was used for airborne and impact sound insulation measurements due to time restriction. Only one independent measurement is done with measuring all parameters which are used in sound insulation parameters calculations.

A new method for estimating measurement uncertainty considers standard deviations of measured SPL levels in the source and receiving room, reverberation times and influence of background noise and measurement equipment uncertainty. In addition, the results for R', L'_n, in a frequency range from 50Hz to 5kHz with all spectral adaptation terms and determined measurement uncertainties for each weighted parameter.

2. MEASUREMENT RESULTS

The measurement uncertainties for main measured parameters are shown (for each part of ILC-2019) in subsections.

2.1 Environmental noise parameters measurement results

The residual noise results are shown in Fig. 5. with experimental measurement uncertainty u_{res} and u_{sou}.
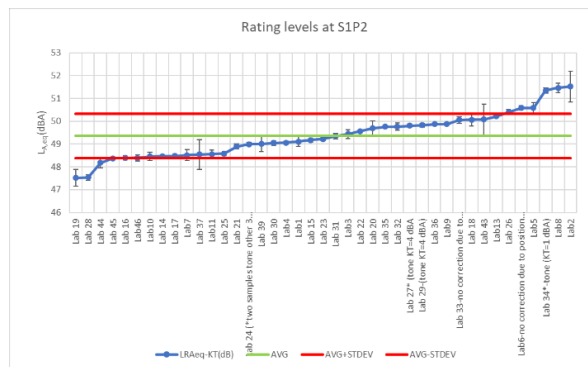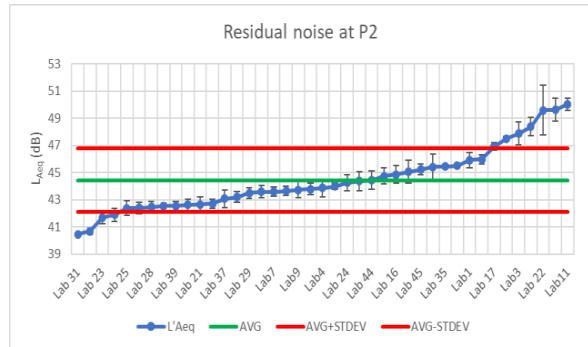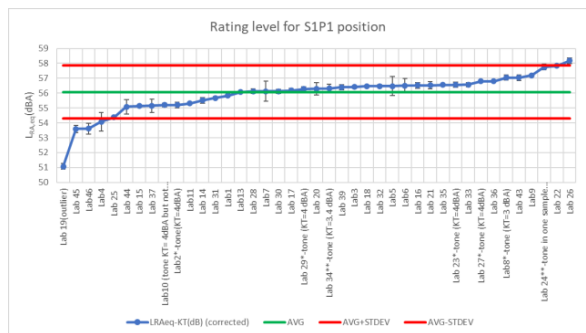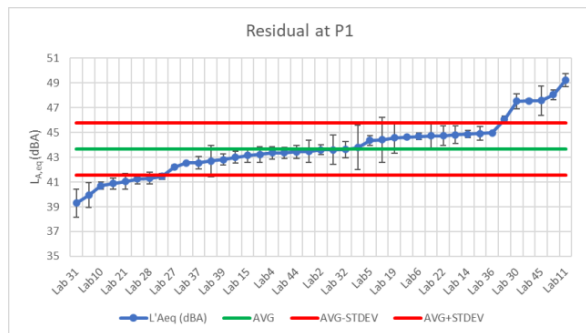
Fig. 5. Measurement results for $L_{A,eq}$ with u_{res} for residual noise and rating levels at two different positions (free field and close to the façade for stable industrial source).

The applied measurement uncertainties from each laboratory were slightly higher than u=2 dBA due to u_{met} and overall experimental measurement uncertainty for each position and parameter which is shown in Table 2.

Parameter	AVG (dB)	STDEV (dB)	Number of participants	u (dBA)
$L'_{A,eq}$-Residual noise -S1P1	43,6	2,1	41	0,3
$L'_{A,eq}$-Residual noise -S1P2	44,4	2,3	41	0,4
$L_{RA,eq}$- Source noise- S1P1	56,1	0,9	41	0,1
$L_{RA,eq}$-Source noise S1P2	49,4	1,1	41	0,2

Table 2. *Reported measurement uncertainty for measured parameters at two different locations (overall results)*

In addition, for local road measurement results are shown per parameter with experimental measurement uncertainty in Table 3. and logging procedure is shown in Fig. 6. The logging in 1 second interval has been done and furthermore, the vehicle

categories have been detected and L_{AE} parameter has been found for each vehicle category.
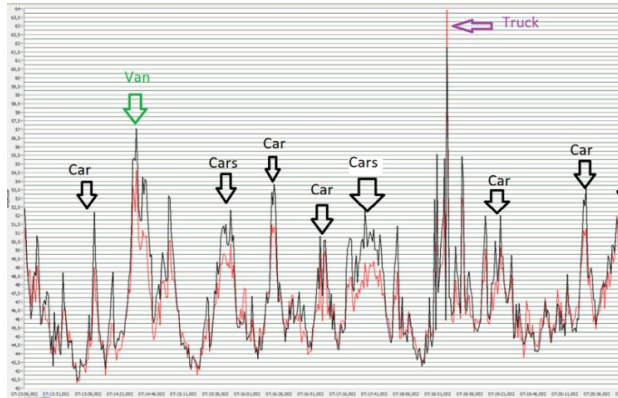
Fig 6. Example of logging the $L_{Aeq,1s}$ from each vehicle category

Parameter	AVG (dB)	STDEV (dB)	Number of participants	u (dBA)
$L_{RA,eq}$	45,6	2,3	20	0,5
$L'_{A,95}$	38,9	2,8	19	0,6
L_{AE} -L	50,7	3,1	15	0,8
L_{AE} -M	55,4	2,3	16	0,6
L_{AE} -H	60,8	3,2	16	0,8
$L_{A,max}$ -L	48,7	3,8	16	1,0
$L_{A,max}$ -M	50,5	3,6	16	0,9
$L_{A,max}$ -H	558	3,9	16	1,0

Table 3. *Experimental measurement uncertainty for local road parameters at 100m distance in free field measurement location*

The meteorological windows were calculated from each laboratory and compared to the organizer and during the day period only M1 and M2 meteorological windows are obtained.

There were a lot of problems with correction of the results due to positions (residual noise and source levels, corrections due to background noise, adding tonal penalty because a tone was added at 10 kHz).

2.2 Modelling noise parameters results

The laboratories used measurement results at closer position to calibrate the model (determine sound power of the source) and then that data was used to calculate the noise levels at other proposed locations.

2.2.1. Modelling results for the stable source

The results for stable source sound power with modelling uncertainty are shown in Table 4.

	AVG -ISO 9613-2:1997 (dB)	u(dB)- ISO 9613-2:1997	AVG-EU-CNOSSOS (dB)	u (dB)-EU CNOSSOS
S1-power	88,2	1,2	90,6	1,3
L_d-1	45,4	0,6	46,4	0,4
L_d-2	45,3	0,7	44,1	0,6
L_d-3	51,5	1,5	51,9	1,0
L_d-4	48,6	0,6	48,2	0,6

Table 4. *Overall results and experimental uncertainties for stable industrial source obtained by two modelling methods*

It is evident that approximately the same modelling uncertainties are obtained for two different methods ISO 9613-2:1997 [13], EU-CNOSSOS [14] and NMPB 2008 [15] and in addition, when compared with reported modelling uncertainties from laboratories they are much lower (u=3 dBA for sound power and approximately u=4 dBA for L_{day}).

2.2.2 Local road source

In this part of ILC, two different approaches have been tested. In the first approach, laboratories used measurement data at S2P3 position (source 2 position 3 in free field) to calculate noise levels at other positions with the number of vehicles during measurement from each lab (different time, different traffic density, different meteorological conditions) . In the second approach, only the model has been calibrated with the measurement results and the organizer provided the referent number of vehicles (day, evening night period) to calculate sound descriptors.

The results for number of vehicles during measurements, sound power is and descriptors L_d for two positions during the day period are shown and Table 5.

	AVG (dB)-NMPB	u(dB)-NMPB-XPS	AVG (dB)-CNOSSOS	u(dB)-CNOSSOS
S2-power	79,9	0,8	77,7	0,6
L_d-1	46,8	0,9	44,3	0,7
L_d-2	43,4	1,0	41,5	0,6
L_d-3	40,8	1,8	38,1	1,6
L_d-4	41,6	1,5	40,0	1,0

Table 5. *Modelling uncertainty for different methods of calculation (NMPB-XPS and CNOSSOS EU-8).*

The same procedure is repeated for defined number of vehicles during different periods and the results for modelling with different methods are shown in Table 6.

	AVG-NMPB	u(dB)-NMPB	AVG-CNOSSOS	u(dB)-CNOSSOS
S2-power	73,9	0,6	79,4	0,6
L_d-1	49,0	0,5	46,1	0,6
L_d-2	45,5	0,6	43,2	0,5
L_d-3	43,3	1,2	40,8	1,2
L_d-4	44,6	0,8	42,0	1,1

Table 6. *Modelling results and uncertainties with given number of vehicles during day (N_{light}=600 /hour , N_{medium}= 48 /hour, N_{heavy}=12 /hour).*

It can be observed that with the same data the sound descriptors obtained by CNOSSOS method are lower than compared to the NMPB-XPS method. The modelling uncertainty for all results is significantly lower than reported from the participants (for stable and local

road source sound power (u) from 2 dBA up to 2,5 dBA, and sound descriptors from 2 dBA to 3,5 dBA.

All laboratories measured noise levels in neutral on unfavourable conditions during day period and have not corrected the modelling results according to favourable or very favourable conditions.

The PDF distribution of the results is shown in Fig. 7. and it can be noted that the distribution is almost Gaussian for all measured parameters.
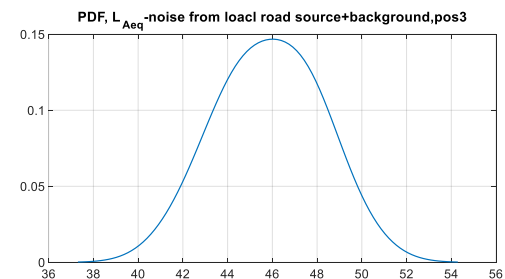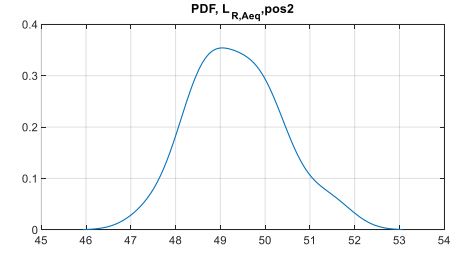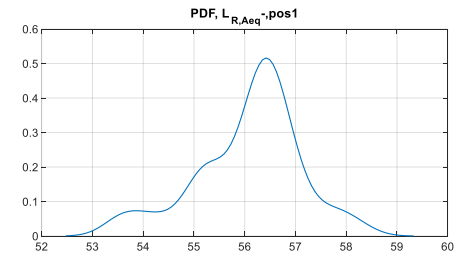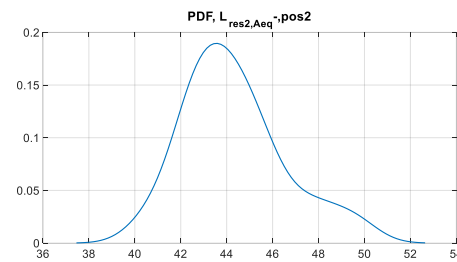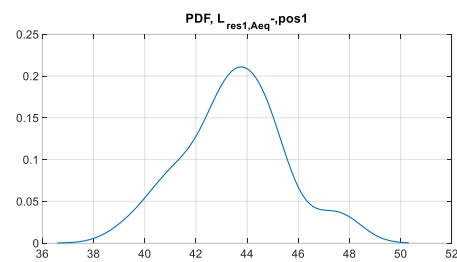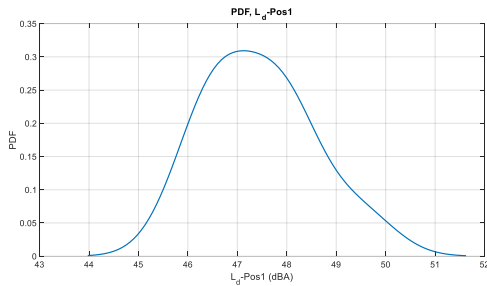
Fig 7. The PDF distribution of measurement and modelling results without outliers for stable and local road source

It is possible that the difference in shape has occurred due to the directivity of the source at closer position to the industrial source (main lobe width).

2.3. Sound insulation parameters measurement uncertainties

The obtained single number values with reported measurement uncertainties U (k=1, 95% confidence level) are shown in Fig. 8.
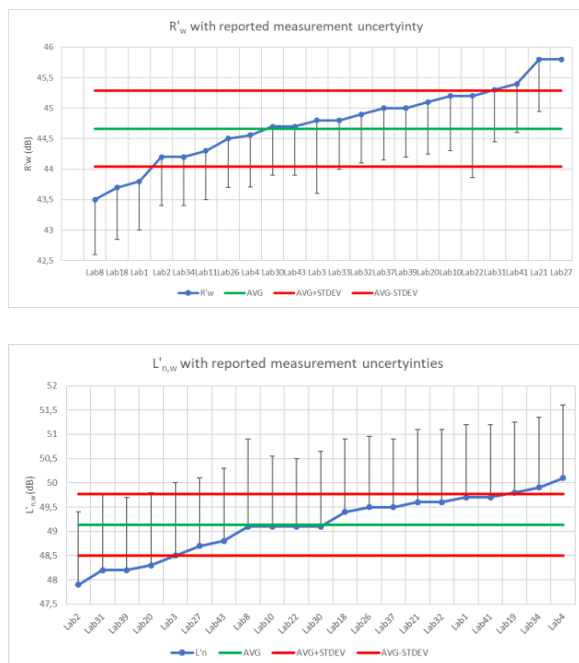
Fig 8. The obtained results for sound insulation parameters with reported measurement uncertainties (standard ISO 12999-1:2020)

It is evident that the reported measurement uncertainties (U=-0,9 dBA and U=+1,5 dB) are much higher than in cases of considering all measurement results (i.e., without outlier) assuming no correlation between the results ($u_{airborne}$=0,13 dB and u_{impact}=0,14 dB).

3. CONCLUSION

It can be concluded that the overall experimental uncertainty for measurement and modelling environmental noise parameters is significantly lower than those provided by laboratories (experimental measurement uncertainty u is slightly higher than 2 dBA according to ISO 1996-2:207 standard). It is very difficult to estimate if the residual noise will be increased more than +1 dBA if the residual noise levels are close to the overall levels (source+background) because according to new standard the conditions from standard ISO 1996-2:2017 are not satisfied in that case (3dBA difference).

The reported modelling uncertainty is much higher compared to the case of averaging all results and finding standard deviations and experimental measurement uncertainty from all results.

Regarding sound insulation, the single number uncertainty is at the highest point when values from ISO 12999-1:2020 standard are used to find upper and down curve for sound insulation compared to the situation when individual uncertainties are found from each independent measurement results for all parameters in one-third octave bands.

The main problem was to check and correct reported results from laboratories in order to obtain a real comparison because laboratories provided results with several mistakes (e.g., measuring point not in the middle of the main lobe, measuring samples from source far away in time from residual noise samples, using A-spectrum in building acoustics measurements, calibration of model not in meteorological conditions which appeared during measurements etc.)

Finally, the criterium for z-score is obtained assuming that there is no correlation between the results (ISO 5725-2:2019) [13] while the results between laboratories are obviously correlated.

4. REFERENCES

[1.] ISO 1996-2:2017, Acoustics - Description, measurement and assessment of environmental

noise -- **Part 2: Determination of sound pressure levels,** Geneva (Switzerland): International Organization for Standardization.

[2.] ISO 12999-1:2020 Determination and handling of uncertainties in building acoustics, **Part 1: Sound insulation**, Geneva (Switzerland): International Organization for Standardization.

[3.] ISO 8297:1994 :Acoustics — **Determination of sound power levels of multisource industrial plants for evaluation of sound pressure levels in the environment — Engineering method**, Geneva (Switzerland): International Organization for Standardization.

[4.] ISO 3744:2010, Acoustics — Determination of sound power levels and sound energy levels of noise sources using sound pressure **— Engineering methods for an essentially free field over a reflecting plane**, Geneva (Switzerland): International Organization for Standardization.

[5.] ISO 3382-1:2009, Acoustics — Measurement of room acoustic parameters — **Part 1: Performance spaces**, Geneva (Switzerland): International Organization for Standardization; 2010.

[6.] ISO 3382-2:2008-Acoustics — Measurement of room acoustic parameters — **Part 2: Reverberation time in ordinary rooms**, Geneva (Switzerland): International Organization for Standardization.

[7.] ISO 1996-1:2017, Acoustics - Description, measurement and assessment of environmental noise --**Part 1: Basic quantities and assessment procedures**, Geneva (Switzerland): International Organization for Standardization.

[8.] ISO 16283-1:2016: Acoustics -- Field measurement of sound insulation in buildings and of building elements -- **Part 1: Airborne sound insulation**, Geneva (Switzerland): International Organization for Standardization.

[9.] ISO 16283-2:2020: Acoustics -- Field measurement of sound insulation in buildings and of building elements -- **Part 2: Impact sound insulation**, Geneva (Switzerland): International Organization for Standardization.

[10.] ISO 717-1:2020 Acoustics, **Rating of sound insulation in buildings and of building elements – Part 1: Airborne sound insulation**, Geneva (Switzerland): International Organization for Standardization.

[11.] ISO 717-2:2020 Acoustics, **Rating of sound insulation in buildings and of building elements – Part 2: Impact sound insulation**, Geneva (Switzerland): International Organization for Standardization.

[12.] ISO 12999-1:2020, **Determination and handling of uncertainties in building acoustics. Part 1: Sound insulation**, International Organization for Standardization.

[13.] ISO 9613-2:1996 Acoustics **— Attenuation of sound during propagation outdoors — Part 2: General method of calculation**, International Organization for Standardization.

[14.] Joint Research Centre, Institute for Health and Consumer Protection, Anfosso-Lédée, F., Paviotti, M., Kephalopoulos, S., **Common noise assessment methods in Europe (CNOSSOS-EU)** : to be used by the EU Member States for strategic noise mapping following adoption as specified in the Environmental Noise Directive 2002/49/EC, Publications Office, 2012, https://data.europa.eu/doi/10.2788/32029

[15.] Dutilleux, G.; Defrance, J.; Ecotière, D.; Gauvreau, B.; Bérengier, M.; Besnard, F.; Duc, E.L. NMPB-routes-2008: **The revision of thefrench method for road traffic noise prediction,** Acta Acust. United Acust. 2010, 96, 452–462.

[16.] ISO 5725-2:2019 Accuracy (trueness and precision) of measurement methods and results – **Part 2: Basic method for the determination of repeatability and reproducibility of a standard measurement method**, International Organization for Standardization.

DEVELOPMENT OF A SPECIAL STANDARD FOR OUTDOOR MUSIC EVENTS IN SLOVENIA BASED ON MEASUREMENTS AND CALCULATIONS

Luka Čurović, Jure Murovec, Nejc Cerkovnik, Anže Železnik, Jurij Prezelj
University of Ljubljana, Faculty of Mechanical Engineering

Abstract: *In Slovenia, the standard ISO 1996-2 is used to conduct the environmental noise measurements. When planning and performing measurements, a large number of variables must be taken into account, including the sound-emitting characteristics of the noise source, meteorological conditions, and the specifics of local geography and noise-sensitive areas. In general, the standard attempts to cover all types of sources, so it is best used as a basis for developing more specific standards for particular sources such as modern loudspeakers and outdoor sound systems. The objective of this paper is to present the acoustic characteristics of sound systems used at outdoor music events and to identify the main influencing variables that should be considered in the design and evaluation of environmental noise based on measurements and calculations. Such a study could be a first step in developing specific practice guidelines and standards for outdoor music events.*

Keywords: Environmental noise, outdoor events, loudspeakers, standard

1. INTRODUCTION

The World Health Organisation (WHO) and the European Environment Agency (EEA) consider noise pollution, including recreational noise, to be a major environmental problem [1]. An important source of recreational noise is outdoor entertainment events using modern sound systems. Outdoor events are increasingly taking place in populated areas [2], and the number of complaints from the affected public has increased. The regulations in force in Slovenia on noise from musical events [3] and research in this field [1] have not been able to successfully address all the noise problems associated with modern sound reinforcement systems.

This paper discusses the existing regulations on environmental noise which is emitted from events with loudspeakers and presents specific problems related to modern music events. It highlights the main issues that need to be considered when evaluating the environmental noise of music events based on measurements and calculations.

2. CURRENT SITUATION IN SLOVENIA

In Slovenia, environmental noise caused by outdoor events is currently regulated by legislation that sets the permissible limits in front of buildings with residential premises, as well as the method of noise prediction and the monitoring procedure.

2.1. Prediction using modelling

Noise pollution or environmental noise pollution is calculated according to the simplified version of standard 9613-2 [4], taking into account only the geometric divergence (A) using the following equation:

$$L_{f,i} = L_W + D_c - A; \; A = 20 \times \log(d/d_0) + 11 \quad (1)$$

where $L_{f,i}$ is the sound pressure level at receiver location due to i-th loudspeaker at frequency f, L_W is sound power level of the source, D_c is the directivity factor, d is a distance between source and receiver and d_0 is a reference distance equal to 1 m. The total sound pressure level at receiver location is calculated using energetical summation.

$$L_f = 10 \times \log\left(\sum_{i=1}^{N} 10^{0.1L_{f,i}}\right) \quad (2)$$

The sound power level of a loudspeaker should be determined by measuring the sound pressure level at a distance of 1 m in front of the loudspeaker (in the axis of

the loudspeaker). The Slovenian regulation also introduces the term electrical working power, which is expressed as a percentage of the maximum electrical power of the loudspeaker.

The noise study should contain a description and determination of the permissible electrical working power, and the permissible electrical power should also be visible at the event.

The emission data of a loudspeaker can be expressed as sensitivity (E) in dB/W/m, which corresponds to the sound pressure level in dB at a distance of 1 m from the loudspeaker and an input power of 1 W. The actual sound pressure level is determined taking into account the power supplied by the amplifier P, according to:

$$L_p = E + 10 \times \log(P/P_0) \tag{3}$$

Where P_0 is the reference power, which is equal to 1 W. For example, the sound pressure level at 1 m in front of a loudspeaker with a sensitivity of 105 dB/W/m at an input power of 30 W is 105 dB + 10 log(30W/1W) = 120 dB. This equation is usually used to solve an inverse problem. Based on the location of the loudspeaker, the location of the noise-sensitive receiver, and the allowable sound pressure level, the sound pressure level at 1 m is determined using geometric divergence. The sound pressure level and sensitivity data are then used to determine the allowable electrical power for the selected loudspeaker.

For example, if the limit value at 20 m from the speaker with sensitivity of 105 dB/W/m is set at 70 dBA. The allowed electrical power is calculated by first determining the sound pressure level at 1 m:

$$L_p(d = 1m) = 70dB + 20 \times \log(20\,m/1\,m) = 96\,dBA$$

$$P = P_0 10^{0.1(L_p - E)} = 0.12\,W$$

The power supplied to such a loudspeaker would have to be less than 0.12 W, which is of course irrelevant for practical applications where amplifier power is much greater (over 500 W). Such a procedure is not common in other countries.

For this reason, in practice, loudspeaker systems are often characterized by their maximum sound power levels. The sound power levels are determined from environmental noise calculations according to 9613-2. Often the calculations are performed in a single 1/3-octave frequency band (usually 500 Hz) with directional characteristics that are not usually specified.

However, even if characterization of sound reinforcement systems by sound power level can be considered a standard practise in acoustics, its use for monitoring is very impractical because it cannot be easily determined

on the spot or monitored by sound engineers, listeners, affected neighbours, or local authorities. Labelling sound reinforcement systems by sound power level is also in direct conflict with the regulation.

2.2. Directivity

Legislation sets the requirements for directivity of loudspeakers. Currently, our legislation is based on a fundamental theoretical analysis carried out by Lord Rayleigh in the nineteenth century. The directivity of loudspeakers is based on the mathematical theory about the sound field in the far field generated by a circular piston (loudspeaker diaphragm) in an infinite baffle. According to the theory, the expression for far-field sound pressure at a given distance r, polar angle θ (angle between the direction of the receiver point and the main axis of the loudspeaker), frequency f, and piston diameter $2a$. The directivity factor D_c can be expressed as follows:

$$D_c = 20 \times \log\left(\frac{2 \times J_1(k \times a \times \sin\theta)}{k \times a \times \sin\theta}\right) = 20 \tag{4}$$
$$\times \log\left(\frac{2 \times J_1(z)}{z}\right)$$

where J_1 is first order Bessel function and the quotient $2J_1(z)/(z)$ shows the directivity function of the circular piston as a function of the wave number k at 800 Hz, loudspeaker radius a and an θ angle between the direction of the receiver point and the main axis of the loudspeaker.

2.3. Emission spectra

According to the current regulation, the directivity and sound propagation are calculated only at 800 Hz or at a frequency where the peak of the sound power level spectrum of the loudspeaker is specified by the manufacturer using equation 4. In this way, the frequency characteristics of the sound produced by modern sound reinforcement systems are not taken into account in the current regulation.

2.4. Measurements

Compliance is rarely verified by measurements. In fact, measurements are rarely commissioned by local authorities. Rather, measurements are commissioned by affected neighbours and performed by acoustic laboratories with or without the knowledge of the music promoters. The ordinance does not explicitly specify the measurement standard or who is authorized to perform the measurements. It specifies the measurement location,

AAAA – 2023 – IZOLA - Conference Proceedings

which must be chosen in front of affected buildings according to the standard ISO 1996-2 [5].

Noise limits, referred to as critical loads, are set according to the area where the measurement point is located and vary for daytime, evening, and nighttime hours, as well as for the duration of the event.

If the event is shorter than 8 hours, the integration time is equal to 8 hours. For longer events, the time duration is equal to the duration of the event. However, the integration time is often chosen by the acoustic experts performing the measurements.

Due to the long integration time and the measurement positions, which may be located at a great distance from the event, post-processing and quality assurance of the acquired acoustic data is a time-consuming process. In addition, the measurement report must be produced within 30 days of the event, which is often seen as an intentional delay by stakeholders that include the event organisers, neighbours, and local authorities.

3. STATE OF THE ART

The current assessment of environmental sound levels at outdoor events where amplified music is played does not address all relevant issues. The specific issues and state of the art related to modern music events were explored through a literature search, with a technical document published by AES as the primary source of information.

3.1. Directivity

Most modern- large-scale sound reinforcement systems consist of flown line arrays [99], in which identical arrays are placed symmetrically on the sides of a stage, and a subwoofer system designed to reproduce the lower end of the frequency spectrum (below 100 Hz). The subwoofer system is usually used as a horizontal array. Sound engineers spend a great deal of time configuring the sound reinforcement system to achieve uniform sound pressure distribution and frequency response throughout the audience area) This is achieved by placing the loudspeakers above the audience and optimizing their placement according to their characteristics such as directivity, filtering, time delay, etc. Optimization is performed using various tools such as EASE, EASE Focus, ArrayCalc, Sound Vision, Mapp Online, etc., based on the coherent addition of sound sources.

To investigate directivity, we performed simple directivity measurements. The measurements were performed in an anechoic chamber at the Faculty of Mechanical Engineering in Ljubljana. A Yamaha HS 5 loudspeaker was used. An E-sweep signal in the range from 20 Hz to 20000

Hz was used as the excitation signal. The distance between the microphone and the loudspeaker was kept constant at 1 m. The loudspeaker was rotated from 0 to 360 degrees with a resolution of 22.5 degrees. The measurement results were compared with theoretical calculations at 800 Hz using Equation 4. The results of the measurements and theoretical calculations are shown in Fig. 1. The directivity factor is shown in a polar diagram where the calculated and measured values were normalised to the major axis of the loudspeaker, which is determined by the polar angle of 0 degrees.
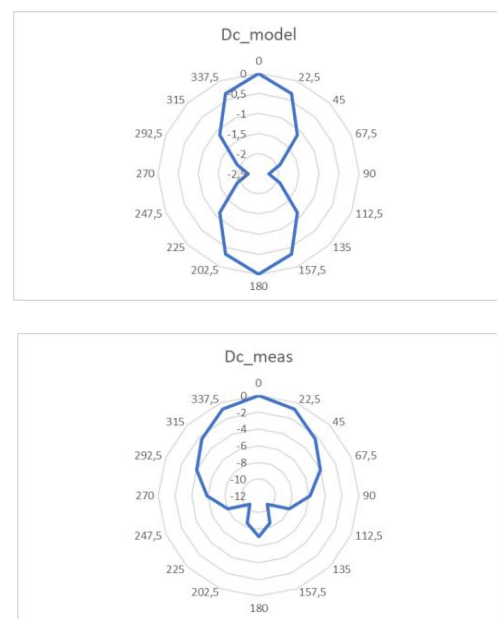
Fig. 1: modelled and measured directivity of a loudspeaker at 800 Hz.

The theoretical directivity cannot model the measured directivity and predicts smaller directivity pattern. The theoretical directivity predicts D_c = -2 dB in the 90^0 directions while the measurements show that the directivity D_c = -6 dB.

3.2. Influence of low frequency spectra

Several studies [284] show that annoyance is significantly greater when a sound contains strong low-frequency components. Live music can be characterized by the low-frequency content. Furthermore, when low-frequency sounds are cantered in the range that causes chest resonance (around 50 Hz), this has health implications (around 50 Hz); this can cause whole-body vibrations that can lead to annoyance and/or discomfort. In such cases, a reduction of the sound pressure level is required [76].

The frequency content of various music genres was studied. A Yamaha HS 5 loudspeaker was used, and the music was recorded in an anechoic chamber 1 m from the loudspeaker. The frequency spectra (third octave, normalized to 100 dB) between 31.5 Hz and 16000 Hz for different music clips are shown in Figure 2. Electronic music and heavy metal music are characterized by low frequency humps. Classical music and brass music are characterized by frequency spectra that follow the shape of A weighting filter.
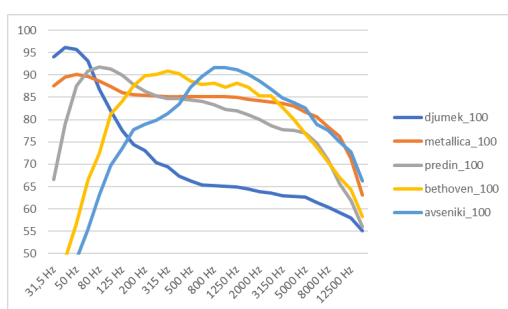
Fig. 2: frequency content of different music genres

3.3. Intermittent noise

Moreover, noise is more annoying when it is intermittent rather than continuous. The noise characteristics of musical events are obviously characterized by the duration of the songs, the phase of the event (e.g., the beginning, middle, and end of a musical event), and the time interval between successive events.

3.4. Integration time

The choice of integration time depends on the dynamics of the observed acoustic signal. It also has an important influence on the limits that can be set by regulatory authorities. Integration times for musical events range from 1 minute to 240 minutes in different countries. Limits based on short averaging times (1 – 5 minutes) could cause engineers to be overly sensitive to the measurement data, while long integration times of over 60 minutes do not follow the dynamics of the event and allow for greater variability between different parts of the event. Long integration constants are impractical and do not allow real-time adjustment of the sound reinforcement system. A compromise must be found. In most cases in Europe, a 15-minute integration time is used in practice along with real-time monitoring. A 15-minute integration time corresponds to about three songs.

3.5. Regulation

Most regulations at the national, regional, and local levels are based on LAeq with specified integration times. Regulations may also limit the duration of events, the number of events, and the time periods between successive events. In general, limits for regular music events in residential areas range from 50 to 75 dBA. In some cases, limits are set in relation to the background noise level (usually between 3 and 15 dB above the residual level). Noise limits for larger events can be 85 dBA or more in residential areas, but are generally limited to the hours up to 11 p.m.

Some countries (Denmark, Netherlands, United Kingdom, France, Ireland, Slovakia) set additional limits for LCeq or Leq in the octave range from 63 Hz to 125 Hz to account for low-frequency noise.

In general, noise in the lower frequency bands is limited to below 80 dB.

3.6. Measurements:

Noise monitoring is considered one of the most important tools for controlling sound emissions to the environment and has become ubiquitous at large outdoor (and indoor) entertainment events. One of the key challenges in noise measurements is that there is rarely only one noise source in an environment. Outdoor measurements taken in front of the façade of a building and at a height of 1.2 to 1.5 m above the ground, according to ISO 1996-2, are usually contaminated by residual noise.

To ensure accuracy and repeatability, measurements should be made under stable meteorological conditions, which is not always possible. The measurement campaign should include monitoring at the front-of-house mixing position (FOH) as well as at selected locations in the residential area, and the integration times should be synchronized [21].

Ideally, noise measurements should be continuous and conducted some time before, during, and after the event. The results should be available to sound engineers, event organizers, and local authorities in real time. Measurements should also be used in the preparation phase to calibrate prediction models and optimize sound system setup based on measured sound pressure levels. Measured data should include LAeq, Leq, and LCeq levels, as well as frequency spectra. Sound recordings could also be helpful in identifying unwanted noise.

3.7. Environmental noise prediction

Events using outdoor loudspeakers may be held if immission levels at selected receiver locations are below critical levels. Compliance can be demonstrated through a noise study that predicts environmental noise levels using a selected calculation model.

The most commonly used calculation model for environmental noise in Europe is described in Annex II of the Environmental Noise Directive.

Noise modelling is used to predict the propagation of sound from the source to the receiver.

The sound pressure level at the receiver is equal to the difference between the sound power level of the source and the summed attenuation factors, similar to equation 1, where the attenuation is the attenuation due to geometric divergence, atmospheric absorption, the ground, diffraction under favourable or homogeneous conditions.

The source is characterized by the source type and its acoustic properties. The model includes a topographic model with acoustically relevant objects such as buildings, barriers, ground and foliage.

The calculations are performed with computer software that uses ray-tracing algorithms with optimized search algorithms for relevant rays from all sources to each calculation point, including direct rays, reflections, and diffractions.

The model includes case specific:
1) emission
2) geo
3) building
4) barrier
5) ground
6) foliage data and
7) calculation parameters.

Sound emission or source data includes position, orientation, directivity, level, emission spectra, or frequency-dependent sound power level data (complex transfer function, delay in filter settings). Geospatial data includes elevation points characterized by a 3-dimensional array of longitudinal, horizontal, and elevation data or isoheight lines of various resolution. Buildings are characterized by their geometry data (position, area and height), but also by their sound reflection properties.

The barriers are characterized by their height, depth, position and shape as well as by their sound absorption or reflection properties. The ground area is determined by its geometry and its absorption properties, which are defined by a factor G. The foliage data is mainly determined by its area.

The calculation parameters include:
  1) calculation area,
  2) grid resolution,
  3) temperature,
  4) humidity,

5) meteo data as percent of favourable conditions,
6) number of reflections,
7) optimization parameters (such as search distance or fetching radius, dynamic error margin, terrain interpolation, etc.)

The calculation is standardized, but the results depend mainly on the selected geographical, acoustic and calculation parameters. The model is based on the specific parameters used in the calculation. This means that if the characteristics of sound sources change, the results may not be reliable.

Some examples of the influence of the choice of input parameters are shown in Figures 3-5. The choice of emission spectra with the same dBA level at the reference point (LAeq = 80 dBA) on dBA and dBC levels is shown in Figures 3 and 4.
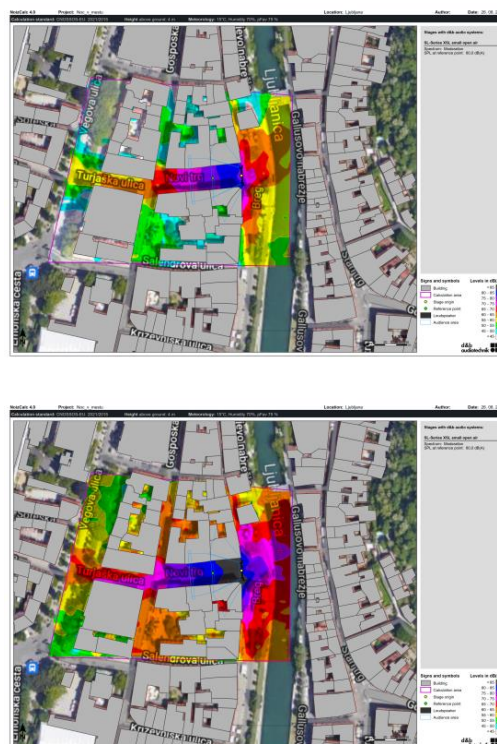
Fig 3.: dBA and dBC maps using spectrum of moderate music [7].

Fig 4.: dBA and dBC maps using spectrum of electronic music [7].
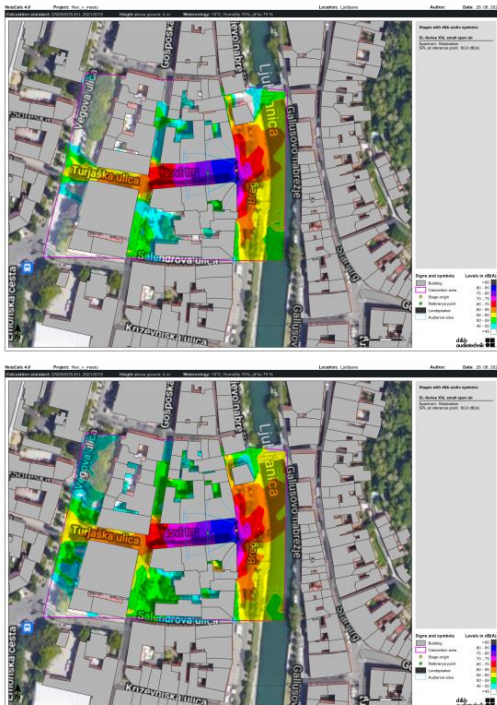
Fig 5.: dBA maps using different number of reflections in the calculations (1 vs 3) [7].

With respect to sound propagation modelling, source parameters should be carefully selected. The loudspeaker

arrays emit coherent sound waves, and complex summation should be used instead of simple energy summation (Equation 2). Complex summation is not currently part of commercial software, which means that modelling with available software should be subjected to a validation procedure.

4. CONCLUSION

In the first part of this work, the legislation in force in Slovenia was analysed and the following was established:
- The radiation characteristics of the loudspeaker are determined by the data of the electrical power of the amplifier, which are not applicable in practical (real) situations and cannot be monitored by the people concerned or even by experts in sound engineering and acoustics.
- The sound propagation model does not include all attenuation factors that are included in modern sound propagation models.
- The directivity of loudspeakers is based on the mathematical theory of Lord Rayleigh from the 19th century, which does not take into account the complexity of modern sound reinforcement systems.
- Prediction by calculation is done only for a single frequency, and the spectral characteristics of the radiated sound are not taken into account.
- Monitoring of the ambient sound pressure level can be done by measurements; however, the integration time and measurement locations do not take into account the dynamics of the musical event and the signal-to-noise ratio in the far field.
- The results of monitoring may not be known until after the event, and monitoring cannot be used to adjust the performance of the sound reinforcement system in real time.

In the second part, an overview of the state of the art was shown. It was noted that a specialized standard for outdoor music events should cover several complex topics, including low-frequency noise, integration time, on-site and far-field monitoring, loudspeaker directivity, and sound emission spectra.

An important step toward standardization of calculations would be a publication (a guide to good practice) of model parameters, including those for sound radiation, calculation, and propagation, which could then be used by acoustical experts in their studies, as is the practice in many acoustical standards.

Because of the large number of influencing parameters, such a task can only be undertaken by a group of professionals that includes environmental noise specialists, sound engineers, event organizers, and regulators. To carry out such a project, a communication

specialist could be brought in to avoid communication errors between the various parties involved.

4. REFERENCES

[1.] **Environmental Noise Guidelines for the European Region**, World Health Organization. Regional Office for Europe, 2018.

[2.] Hill, AJ **Understanding and managing sound exposure and noise pollution at outdoor events**, AES, 2020.

[3.] ISO 1996-2:2017. **Acoustics – Description, measurement and assessment of environmental noise — Part 2: Determination of sound pressure levels**, International Organization for Standardization, 2017.

[4.] ISO 9613-2:1996. **Acoustics – Attenuation of sound during propagation outdoors — Part 2: General method of calculation**, International Organization for Standardization, 1996.

[5.] **Uredba o načinu uporabe zvočnih naprav, ki na shodih in prireditvah povzročajo hrup (Uradni list RS, št. 118/05 in 44/22 – ZVO-2).** Available at: http://www.pisrs.si/Pis.web/pregledPredpisa?id=UR ED3652 (Accessed 01 September 2023)

[6.] **Directive 2002/49/EC of the European Parliament and of the Council of 25 June 2002 Relating to the Assessment and Management of Environmental Noise - Declaration by the Commission in the Conciliation Committee on the Directive Relating to the Assessment and Management of Environmental Noise.** Available at: https://eur-lex.europa.eu/legal-content/EN/TXT/?uri=celex%3A32002L0049 (Accessed 20 January 2022)

[7.] **d&b NoizCalc: Assessing and modelling noise immissions in the far field.** Available at: https://www.dbaudio.com/global/en/products/soft ware/noizcalc/?pk_source=Newsletter&pk_medium =Dotmailer&dm_i=3WB1%2CGVZR%2C48ASA8%2C1 T3IG%2C1 (Accessed 22 August 2023)
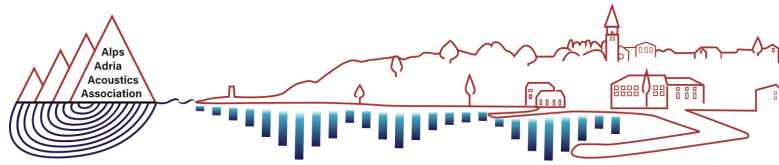
Contributed papers
Advanced meausrement techniques in acoustics

1. Estimating Speed of Sound in Granular Materials: Impulse Response Extraction and Wave Decomposition in an Extended Impedance Tube
Anže Železnik (University of Ljubljana, Faculty of Mechanical Engineering, LDSTA)
2. A smart method to calibrate universal testing machines by incorporating acoustic methods Sharath Peethambaran Subadra (Hochschule für Angewandte Wissenschaften Hamburg)
3. Unsupervised Classification of Welding processes based on Psychoacoustic Sound Features
Jurij Prezelj (University of Ljubljana, Faculty of Mechanical Engineering)
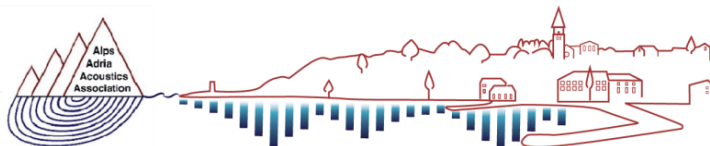
Estimating Speed of Sound in Granular Materials: Impulse Response Extraction and Wave Decomposition in an Extended Impedance Tube

Anže Železnik, Luka Čurović, Jure Murovec, Nejc Cerkovnik, Jurij Prezelj

University of Ljubljana, Faculty of Mechanical Engineering

Abstract: *The speed of sound in materials greatly affects their acoustic properties and is a key factor in determining the acoustic impedance of a surface, which governs the reflection, absorption, and transmission of acoustic energy. Granular materials offer an intriguing alternative to custom-made acoustic materials, as they can achieve high sound absorption or insulation through the use of different size fractions. By investigating the speed of sound within the pores of granular materials, one can estimate their acoustic properties. In this paper, a method for measuring the speed of sound in porous materials using an impedance tube and time-domain wave decomposition of the tube's impulse response is proposed, employing a single downstream microphone to assess various size fractions of recycled sand. The measurements encompassed granular fractions ranging from 0.1 to 4 mm. Notably, decrease in the speed of sound within granular materials as the granules became smaller can be observed, with the speed dropping below 100 m/s for the smallest fraction.*

Keywords: impedance tube, time-domain wave decomposition, speed of sound, granular materials

1. INTRODUCTION

Granular materials have emerged as a promising avenue in the field of sound absorption materials due to their favourable acoustic properties and relatively low cost compared to traditional acoustic foams. Extensive research has been conducted on the absorption coefficient of various granular materials, including glass spheres [1], rubber crumb [2], and natural and recycled materials [3-11]. However, the investigation of sound insulation properties in granular materials remains relatively limited [12-14]. Nevertheless, existing findings suggest that utilizing very small granules can yield high transmission loss values.

Impedance tubes have been widely employed to study the acoustic properties of granular materials. However, the standard transfer matrix method faces challenges when measuring the transmission loss of highly reflective samples like granular materials [13,15]. To overcome these limitations, we constructed an extended impedance tube specifically designed to examine the sound insulation

properties of granular materials using a simple deconvolution-based method to separate sound waves in the time domain. Our approach is reminiscent of the "Adrienne" reflection method introduced by Garai [16-18], but adapted for measurements within a closed tube. Similar methodologies have been utilized by Sun et al. [19,20] and Lefebvre [21] for sound absorption measurements, and subsequently modified by Sun et al. [22] for transmission loss measurements. The impedance tube employed in our study is akin to the method proposed by Sun et al., albeit with sound pulses obtained through deconvolution rather than direct measurements using a pulse generator.

When examining the transmitted sound pulse in the impedance tube, a delay can be observed when comparing the transmitted sound with and without a sample inserted into the tube. This delay, previously observed and employed by Oblak et al. [23] for speed of sound measurements in porous materials submerged in a liquid using the transfer matrix method [24], provides valuable insights into the influence of pore size on the

speed of sound within porous media. Because the speed of sound in a porous material influences the surface impedance, it is an important factor in determining acoustic properties of materials. Granular materials, due to their adjustable particle and pore sizes achievable through different size fractions, offer an intriguing avenue for investigating this phenomenon. For this study, recycled silica sand was separated into size fractions ranging from 0.1 mm to 3 mm using laboratory test sieves and a shaker. Two methods were evaluated to measure the delay in the impulse response of the transmitted sound wave caused by the granular material sample. The first method involved direct calculation of the delay in the impulse response, while the second method utilized phase differences in the phase of the measured impulse responses to derive a frequency-dependent speed of sound characteristic. To ensure accurate measurements of the speed of sound, multiple thicknesses of granular material samples were used to achieve a high signal-to-noise ratio.

2. METHODS

The impedance tube used for the measurements in this paper consisted of two long tube sections (4 m and 2 m) with a sample holder between them. The use of a long impedance tube enables the separation of sound waves coming from different directions in the time domain. A single microphone placed behind the sample was used to obtain impulse responses of the impedance tube with and without samples inserted. Samples were sealed in the sample holder using a dense sealing paste to reduce flanking sound transmission. Signals from a signal generator and a measurement microphone were used to deconvolve the impulse response of the impedance tube using spectral division and a 6-th order Butterworth filter was used to eliminate all frequencies outside the frequency range of interest. A sampling frequency of 192 kHz was used for the recordings to eliminate aliasing in the frequency range of interest and custom python software was used to calculate the speed of sound within samples. Because spectral division was used for deconvolution, sound recordings with the duration of 60 seconds were used and no time averaging was employed. The speaker and microphone were mounted according to the recommendations found in *EN ISO 10534-2:2001*. The

frequency range of the impedance tube is limited by the tube diameter that determines the highest frequency that can be measured due to cross-modes and by the signal-to-noise ratio and frequency resolution at lower frequencies. The valid frequency range of the impedance tube used in this paper is between 100 and 4000 Hz. A schematic of the measurement setup is shown in Fig. 1.
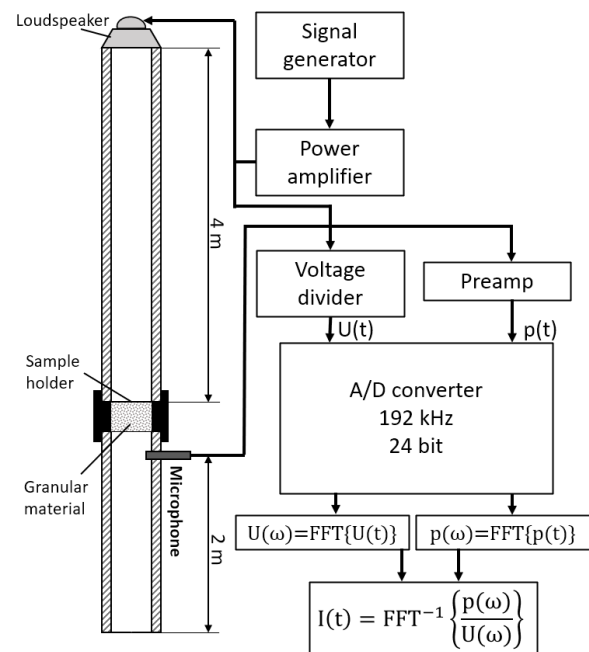
Fig.1. Schematic of the measurement setup.

The equipment used for the impedance tube:

- Brüel & Kjær Sine Random Generator Type 1027 signal generator
- Brüel & Kjær Power Amplifier Type 2706 power amplifier
- Visaton R 10 S loudspeaker
- PCB Piezotronics 130F20 microphone
- Data Translation DT9847-3-1 A/D converter

The microphone behind the sample can be used to measure the transmitted sound before and after a sample is inserted into the tube. The impulse response with and without a sample inserted is shown in Fig. 2. Multiple reflections can be observed in the impulse response, including the reflection off the tube termination. Because of that, the impulse response needs to be time-windowed to include only the directly transmitted sound. This enables the measurement of transmission loss using this

type of time-domain wave separation as a reduction of amplitude is evident when a sample is inserted (Fig. 2 b)).
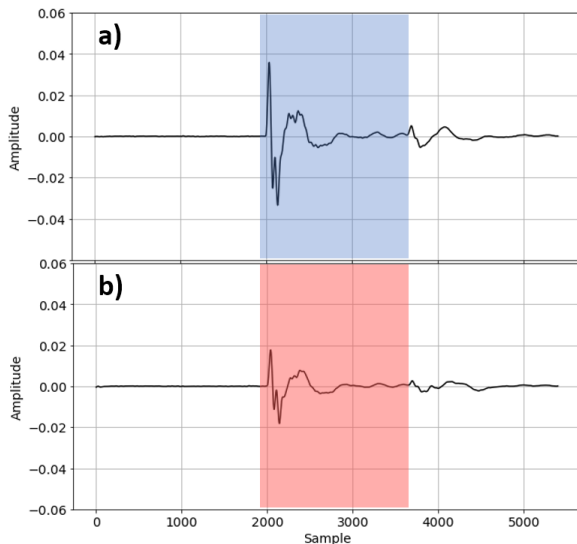
Fig.2. The impulse response without a sample inserted (a) and with a sample inserted into the tube (b).

The speed of sound inside a porous material can be measured inside an impedance tube because a change in the speed of sound inside a sample causes a delay in the transmitted sound wave. If the impulse responses without and with a sample are compared, this delay can be observed. The comparison between the reference impulse response and an impulse response obtained with a granular material sample is shown in Fig. 3.
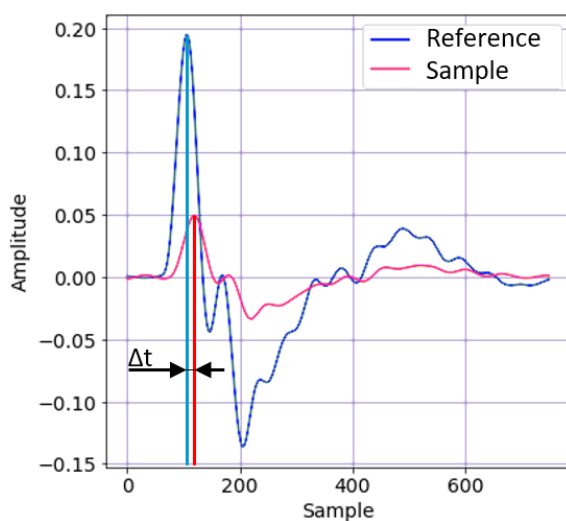
Fig.3. The delay caused by the sample.

In this paper, two methods are compared for determining the speed of sound in porous samples: using only the delay in the maximum value of the impulse response (as shown in Fig. 3) and using the phase difference in the impulse responses to determine the speed of sound for the entire valid frequency range of the impedance tube. For both methods, the speed of sound c_s is calculated using the measured delay caused by the sample (Δt), the thickness of the sample (d_s) and the reference speed of sound in air (c_0).

$$c_s = \frac{d_s}{\frac{d_s}{c_0} + \Delta t} \tag{1}$$

For the method using the phase of the impulse responses, c_s is obtained by calculating the phase of both impulse responses from their Fourier transform, unwrapping the phase and calculating the time delay between the phase characteristics for each frequency. This method allows for the evaluation of the calculated values and proved effective for eliminating measurements where the signal-to-noise ratio was not sufficient because of the high transmission loss values of samples and the method using only the delay between the two impulse responses was not sufficient.

The two main sources of measurement errors for speed of sound measurements are the sampling frequency and the signal-to-noise ratio. The limited sampling frequency causes errors for measurements where the speed of sound is not much different compared to the reference speed of sound and the impulse response is only shifted for a few samples. This is evident for granular fractions that do not change the speed of sound drastically, especially for thin samples. Because of this, thicker samples need to be used for measurements where the speed of sound within samples is similar to the speed of sound in air. Signal-to-noise ratio causes measurement errors where the transmission loss values of samples are high. This means that thinner samples yield more reliable results for samples where the speed of sound is very low (and transmission loss values are high).

The samples for the speed of sound measurements were prepared with a set of laboratory test sieves and a shaker. Ten different size fractions were measured: 0-150 µm, 150-180 µm, 180-210 µm, 210-250 µm, 250-300 µm, 300-425 µm, 425-600 µm, 600-1000 µm and 3-4 mm. To ensure a sufficient signal-to-noise ratio for the

measurements, 7 different thicknesses were measured for all the fractions: 5 mm, 10 mm, 20 mm, 30 mm, 40 mm, 60 mm and 80 mm.

3. RESULTS AND DISCUSSION

The average measured speed of sound using only the delay in the maximum value of the deconvolved impulse response for all sample thicknesses is shown in Fig. 4. The error bars indicate the standard deviation for measurements of the same granule size fraction. It is evident that the standard deviation using this method is too high to reliably estimate the speed of sound in granular samples. Because there is no way to estimate which measurements are valid in terms of signal-to-noise ratio with this method, using only the delay in the impulse response is deemed insufficient for reliable speed of sound measurements in porous samples.
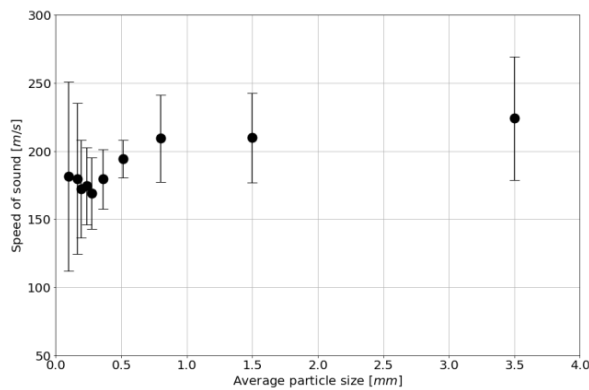
Fig.4. Measured speed of sound using the delay in deconvolved impulse responses.

Using the method comparing the phase delay in the impulse responses gives a frequency dependent speed of sound characteristic that can be used to estimate the separate measurements and the frequency ranges in which the speed of sound measurements are valid. For this study, the criteria for the speed of sound measurements to be considered valid are: a) the speed of sound characteristic is relatively flat across the frequency range of interest (eliminating resonances and measurements where the signal-to-noise ratio is insufficient) and b) speed of sound measurements of multiple sample thicknesses have similar values (eliminating measurements where phase delay is

insufficient). Examples for three granule size fractions are shown in Fig. 5. Frequency ranges and sample thicknesses where speed of sound measurements are deemed valid are shown in green. The three size fractions shown are 3-4 mm (a), 425-600 µm (b) and 150-180 µm (c). While the thicker samples are used for larger size fractions (a) and most sample thicknesses are appropriate for some granular size fractions (b), only the thinnest samples are appropriate for measuring the speed of sound of the smallest granules (c) as the transmission loss of these samples is very high and the signal-to-noise ratio is insufficient.
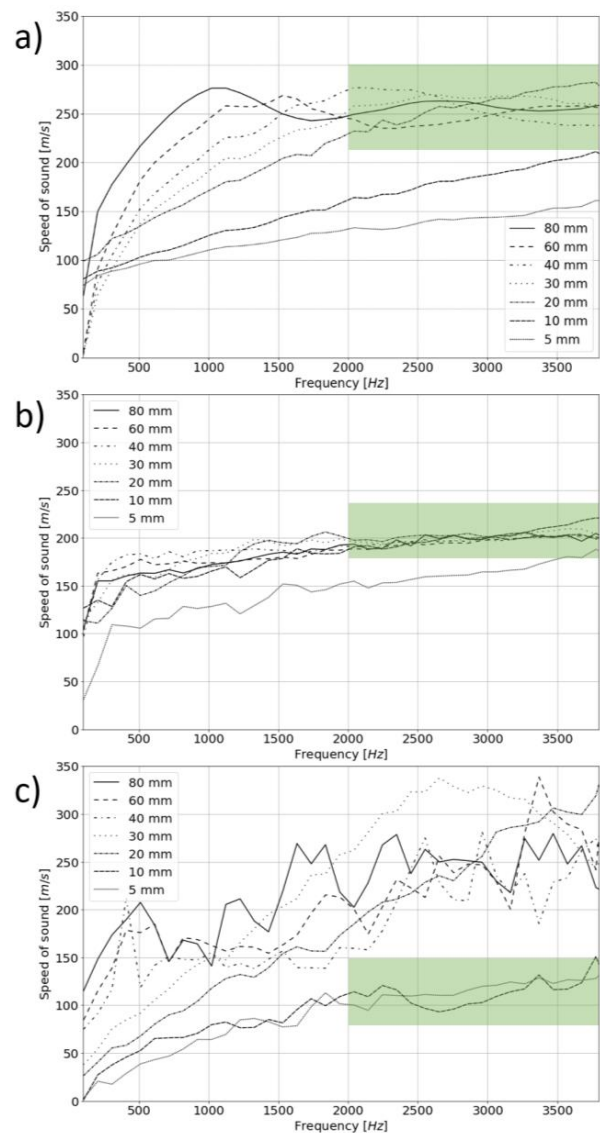
Fig.5. Valid frequency ranges and sample thicknesses: a) 3-4 mm, b) 425-600 µm and c) 150-180 µm granules.

The averaged speed of sound values meeting the predefined criteria were computed. These mean values, along with their corresponding standard deviations, are depicted in Fig. 6. Evidently, the speed of sound within granular material pores is notably lower as the granule size decreases. This phenomenon contributes to the high transmission loss values observed in granular materials [14]. This occurrence can be attributed to the substantial surface impedance mismatch arising from the considerably lower speed of sound within air-saturated granular materials compared to that in air. Consequently, a significant portion of sound is reflected from the granular material surface. The lower speed of sound in smaller granules could be attributed to increased sound scattering across numerous surfaces within the porous material, coupled with the longer trajectory traversed by the transmitted sound within smaller granular fractions.
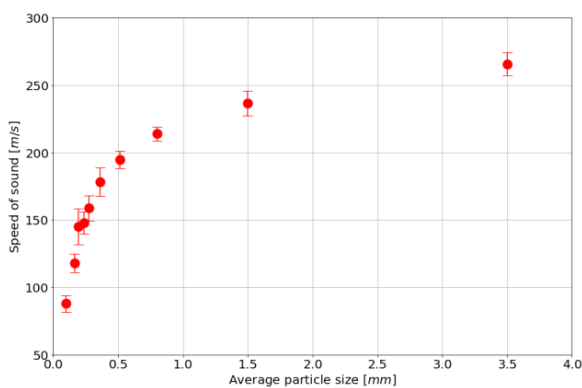
Fig.6. Measured speed of sound using the phase difference in deconvolved impulse responses.

While the speed of sound in granular materials decreases for smaller granules, the flow resistivity of smaller granular fractions increases significantly. Static flow resistivity values for 40 mm thick samples were measured using the direct flow method (*ISO 9053-1:2018*). Steady airflow was generated using a diaphragm pump and a 20 l pressure reservoir. A volumetric air flow meter and a pressure gage were used for measuring air flow and the pressure difference. Samples were mounted in the apparatus inside the same containers used for impedance tube measurements and were sealed with a dense sealing paste. The comparison between the trends for speed of sound and flow resistivity values dependent on particle size is shown in Fig. 7 a) and the relation between the measured speed of sound and flow resistivity is shown in

Fig. 7 b). The flow resistivity measured without granular material samples was 300 Pa s m^{-2}, and the fitted curve intersected this value at around 380 m/s. This intersection provides a relatively accurate estimation of the speed of sound in air, given the multitude of parameters influencing measurement outcomes.
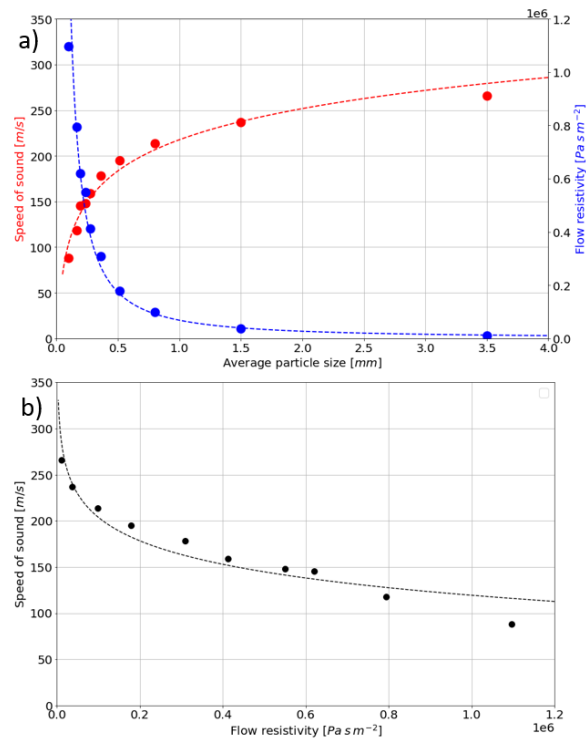
Fig.7. The relation between speed of sound and measured flow resistivity.

4. CONCLUSION

In this paper, a new approach for measuring the speed of sound in porous media using phase differences in deconvolved impulse responses using a long impedance tube is presented. The objective of this study was to develop a simple method that can be used for fast and reliable measurements of speed of sound while also measuring transmission loss values. The measurement results confirmed that the new method using phase differences is more reliable compared to the method using the delays in impulse responses. The results of measurements of different granule sizes show that the speed of sound is much lower for smaller granules, under 100 m/s for particles with diameters around 100 µm.

5. REFERENCES

[1.] S. Sakamoto, Y. Sakuma, K. Yanagimoto, S. Watanabe, Basic study for the acoustic characteristics of granular material (Normal incidence absorption coefficient for multilayer with different grain diameters), Journal of Environment and Engineering 7 (1) (2012) 12-22.

[2.] M.J. Swift, P. Bris, K.V. Horoshenkov, Acoustic absorption in re-cycled rubber granulate, Applied Acoustics 57 (3) (1999) 203-212.

[3.] F. Asdrubali, K.V. Horoshenkov, The acoustic properties of expanded clay granulates, Building Acoustics 9 (2) (2002) 85-98.

[4.] J. Sikora, J. Turkiewicz, Sound absorption coefficients of granular materials, Mechanics and control 29 (3) (2010) 149-157.

[5.] H. Zhou, B. Li, G. Huang, Sound absorption characteristics of polymer microparticles, Journal of Applied Polymer Science 101 (4) (2006) 2675-2679.

[6.] S.H. Zolanvari, C. Karlstetter, Development of Consolidated Granular Materials as Sound Absorbers: Acoustical and Mechanical Characteristics, in: Proc. AIA-DAGA, 2013.

[7.] S. Sakamoto, M. Sasaki, I. Kourakata, K. Yanagimoto, S. Watanabe, Basic study for acoustic absorption characteristics of soft and light granular material (basic characteristics for expanded polystyrene beads), Journal of Advanced Mechanical Design, Systems, and Manufacturing 7 (4) (2013) 677-689.

[8.] A. Biskupičová, M. Ledererová, S. Unčík, C. Glorieux, M. Rychtáriková, Sound absorption properties of materials based on recycled plastic granule mixtures, Slovak Journal of Civil Engineering, 29 (1) (2021) 15-19.

[9.] C. Bujoreanu, F. Nedeff, M. Benchea, M. Agop, Experimental and theoretical considerations on sound absorption performance of waste materials including the effect of backing plates, Applied Acoustics 119 (2017) 88-93.

[10.] A. Boubel, M. Garoum, A. Bybi, N. Laaroussi, Sound absorption measurements of some porous loose granular materials, in: INTER-NOISE and NOISE-CON Congress and Conference Proceedings, 2016.

[11.] S. Sakamoto, K. Yamaguchi, K. Ii, R. Takakura, Y. Nakamura, R. Suzuki, Theoretical and experiment analysis on the sound absorption characteristics of a layer of fine lightweight powder, The Journal of the Acoustical Society of America 146 (4) (2019) 2253-2262.

[12.] E. Levi, S. Sgarbi, E. A. Piana, Acoustic Characterization of Some Steel Industry Waste Materials, Appl. Sci. 11 (2021) 5924–5924.

[13.] G. Pispola, K. V. Horoshenkov, F. Asdrubali, Transmission loss measurement of consolidated granular media (L), The Journal of the Acoustical Society of America 117 (5) (2005) 2716-2719.

[14.] A. Železnik, J. Murovec, L. Čurović, N. Cerkovnik, J. Prezelj, Transmission loss measurement of recycled granular material using wave decomposition by impulse response extraction based on deconvolution, Applied Acoustics 211 (2023) 109498.

[15.] D. Caballol, Á.P. Raposo, Analysis of the measurement of transmission loss in rigid building materials with a standing wave tube, Construction and Building Materials 182 (2018) 242-248.

[16.] M. Garai, Measurement of the sound-absorption coefficient in situ: the reflection method using periodic pseudo-random sequences of maximum length, Applied acoustics 39 (1-2) (1993) 119-139.

[17.] P. Guidorzi, M. Garai, Advancements in sound reflection and airborne sound insulation measurement on noise barriers, Open Journal of Acoustics 3 (2013) 25-38.

[18.] M. Garai, P. Guidorzi, European methodology for testing the airborne sound insulation characteristics of noise barriers in situ: Experimental verification and comparison with laboratory data, The Journal of the Acoustical Society of America 108 (3) (2000) 1054-1067.

[19.] L. Sun, H. Hou, L.Y. Dong, F.R. Wan, Sound absorption measurement in a circular tube using the echo-pulse method, Acta Acustica united with Acustica 96 (5) (2010) 973-976.

[20.] L. Sun, H. Hou, Measurement of sound absorption by underwater acoustic material using pulse-separation method, Applied Acoustics 85 (2014) 106-110.

[21.] A. Lefebvre, G.P. Scavone, J. Abel, A. Buckiewicz-Smith, A comparison of impedance measurements using one and two microphones, in: Proceedings of ISMA, 2007.

[22.] L. Sun, H. Hou, Transmission loss measurement of acoustic material using time-domain pulse-separation method (L), The Journal of the Acoustical Society of America 129 (4) (2011) 1681-1684.

[23.] M. Oblak, M. Pirnat, M. Boltežar, An impedance tube submerged in a liquid for the low-frequency transmission-loss measurement of a porous material, Applied Acoustics 139 (2018) 203-212.

[24.] B. H. Song, J. S. Bolton, A transfer-matrix approach for estimating the characteristic impedance and wave numbers of limp and rigid porous materials, The Journal of the Acoustical Society of America 107 (3) (2000) 1131-1152.

A SMART METHOD TO CALIBRATE UNIVERSAL TESTING MACHINES BY INCORPORATING ACOUSTIC METHODS

Sharath P. Subadra[*], Shahram Sheikhi[*]

[*]Institute of Materials Science and Joining Technology, Research and Transfer Centre 3i; Hamburg University of Applied Science, Berliner Tor 13, 20099 Hamburg, Germany

Abstract: *The aim of this research is the development of a non-destructive testing methodology for tensile, compression and bending tests to ascertain the calibration status of universal testing machines. An algorithm which would be eventually included in the machine-bound control system keeps track of the calibration status by assessing errors which would be dependent on the acoustically determined material properties like elastic, shear and compression moduli. An "Acoustic Reference Sample" serving as a non-destructive reference material would be used to determine these properties. The reference sample material would have a large elastic range and hence can be loaded within this range several times to obtain the elastic properties, which would be subsequently cross-referenced with the acoustically determined material properties in the calibration stage. The machine-bound control system would make use of an in-built algorithm to keep track of this change in material properties and hence the calibration status. The development of this strategy would bring down costs associated with quality assessments and subsequently improve reliability of testing procedures considerably when there are long intervals in calibration of the testing equipment.*

1. INTRODUCTION

Elastic properties of materials especially the Young´s modulus (E-modulus or simply E) is an important material property, and it plays crucial role in design considerations and material quality control. These properties are certified according to DIN EN 10204 material test certificates. The material tests to determine the E-modulus can be either a direct or an indirect method, where the former involves the application of longitudinal and transverse deformations, whereas the latter involve deducing the E from other elastic constants such as shear and bulk moduli respectively [1,2]. Direct methods typically involve measuring the E from the slope of a stress-strain curve in the linear region obtained after a tension test, but the tests though widely used is expensive [3]. The material properties obtained via direct test methods are subject to calibration errors in the equipment and the inherent methods adopted while testing. Indirect methods are much more adaptable to industrial use and are easier, less expensive, and less time-consuming [4]. Dynamic measurements to determine E is much more accurate and the error is in the order of $\pm$ 1%

[2]. Dynamic mechanical analysis is a powerful technique where the sample is forced to vibrate in its natural frequency [5]. These frequencies can then be plugged into relevant equations to obtain the elastic properties such as Youngs and shear modulus [6,7]. Impulse excitation technique (IET) is a widely used technique to identify the natural frequencies. The method involves measuring the oscillations introduced by the impulse which can be measured by microphone, contactless vibrometer or a piezo crystal [8].

However, there exists differences in the E measured from static and dynamic tests respectively. Trubitz et al. [9] compared the estimated E from static and dynamic tests for various grey cast iron materials, and it was observed that ultrasonics tests gave 5% higher E values vis-à-vis a statically determined test such as a uni-axial tensile test. Similarly, Peixoto et al. saw 2% higher values when comparing a dynamic method with that of static methods, here the comparison was between one dynamic and two static methods respectively.

As opposed to the dynamic methods elaborated in the previous paragraphs, the elastic modulus obtained

through tensile testing methods as per relevant standards (EN 10002-1, ASTM E8 / E8M-09 and EN ISO 6892-2) exhibits scatter and variations. But these methods are advantageous owing to their wide usage and the possibilities of determining all the subsequent material properties, e.g. the beginning of yield, ultimate strength etc [10]. Therefore, these two methods (dynamic and static) can complement each other in calibration efforts especially when universal testing machines (UTMs) are considered. Since, UTMs are still the norm in extracting material properties, the reliability of the results depends on the calibration status of the UTM. Normally, the calibration is carried out once a year and in many areas of application this is not sufficient, since a significant variation in the calibration leads to faulty batches. This is true especially in the automotive, aviation and railway sectors where non-conformity after shipment can lead to costly claims of damages. The calibration errors in UTMs can occur on account of faulty software, an inclined position of the crosshead, faulty grips etc[1-10,13].

A method that is in practise in the context of calibration of UTMs and impact testing machines is the use of reference samples that are certified and conforming to the respective standards. The material parameters of these reference samples are known which can be used to calibrate the equipment. Therefore, the certified reference samples can provide indirect proof of stability, accuracy and precision of the test equipment. By referring the reference sample parameters, the suitability of the setting parameters in the testing software can be checked as well. Reference samples also form a tool for standard-compliant determination of the measurement un-certainty which is of interests to the customers. Large intervals associated with this calibration procedure means that the equipment is not monitored continuously, and hence significant deviations are often not taken into the account. Using reference samples which are irreversibly destroyed during calibration process adds to the expenses associated with this calibration procedure[1-10, 13].

This paper is part of a research project titled "ReuseDetect" carried out at Hochschule für Angewandte Wissenschaften Hamburg in cooperation with Schütz+Licht Prüftechnik GmbH, wherein the aim is to develop a non-destructive measurement technique to continuously monitor the calibration status of a UTM. The project is funded by the Federal Ministry of Economic Affairs and Climate Action under the aegis of Central Innovation Program for SMEs known by its German acronym ZIM. A reference sample is being developed as part of this project which can be used in conjunction with a non-destructive method (acoustic method) on a continuous basis without destroying the sample. The reference sample is ideally loaded in the lower elastic region to measure the modulus of elasticity and shear modulus, and these properties are compared with acoustically determined (dynamic measurement) moduli. If there are deviations from the measured value, the machine has deviated from its ideal calibrated state, since the dynamically determined parameters are dependent on the geometry and boundary conditions of the reference sample when its natural frequencies are excited. In addition to the non-destructive reference sample, an algorithm is being developed which is intended to perform calibration in two stages which would later be incorporated into the machine interface along with relevant hardware such as sensors and pre-amplifiers.

1.1. EXPERIMENTAL SETUP AND CALIBRATION ALGORITHM

1.1.1 Theoretical considerations

Determination of E of a prismatic beam with an asymmetric cross-section around one axis is based on three vibration modes namely the out-of-plane and in-plane bending modes respectively along with longitudinal vibration modes. Out-of-plane modes are easy to excite and there is minimal risk of combined loads appearing [20]. Bending vibration of beams obeying the Eulers-Bernoulli theory is a better choice to ascertain the modes and the respective frequencies. Since, the derivations of the equations for various boundary conditions are widely available, hence the derivations are beyond the scope of this paper. The equation (below) stands true for a beam simply supported, fixed ends and a cantilever type (boundary conditions). The coefficient C_n takes into these boundary conditions and the mode shapes (table 1). The other terms in the equation are either geometric parameters or material properties of the structure and its material respectively. I is the moment of inertia of the cross-section, h is the thickness, ρ the density, L the length of the structure and f the natural frequency [11].

$$\omega_n = C_n \sqrt{\frac{EI}{\rho A L^4}} \approx C_n \sqrt{\frac{E h^2}{12 \rho L^4}} \qquad (1)$$

$$E = \frac{\rho L^4}{h^2} \left(\frac{48 \pi^2 f^2}{C_n^2} \right) \qquad (2)$$

Table. 1. C_n *for different boundary conditions and modes* [11]

Modes (n)	Boundary Conditions		
	Simply Supported	Fixed-Fixed	Fixed-Free
1	π^2	22,3733	3,5160
2	$4\pi^2$	61,6728	22,0345
3	$9\pi^2$	120,9034	61,6972
4	$16\pi^2$	199,8594	120,0902
5	$25\pi^2$	298,5555	199,8600

1.1.2 Materials, equipments and design of experiments

A non-destructive reference sample was developed for the purpose of calibration (fig 1-A) from a high strength low alloy steel commercially available as ALFORM700M® (termed as M700 in this paper), the chemical compositions are seen in table 2. The sample dimensions were machined as per DIN 52125. A typical micro-structure of this steel is shown in fig 1-B (cross-section of the sample), which is dominated by granular bainite ferrite and martensite [12].
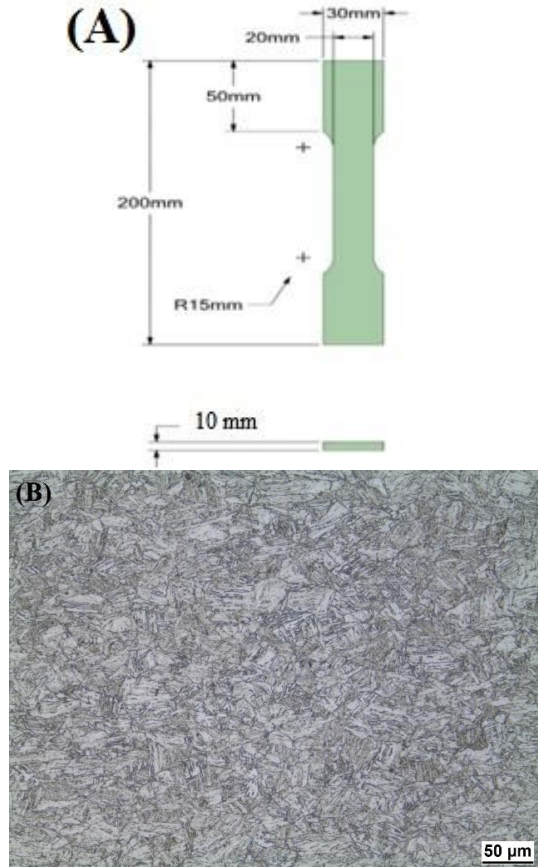
Fig.1. A) Reference sample (DIN 52125), B) Grain structure (cross section of the sample) of ALFORM700M®

Table. 2. *Chemical composition of the steel alloy*

Material	Chemical Composition [%]		
	Ti	Nb	V
Steel	0.18	0.10	0.08

Tensile tests were performed on a QASAR 200 tensile testing machine from Galdabini (Cardano al Campo, Italy). The machine was in a fully calibrated stage, and hence would serve as an equipment on which the algorithm developed would be put into test. The maximum load cell capacity of this machine is 200 kN, the grippings are hydraulic driven, while the loading is servo motor driven. Acoustic signals were collected from a QASS Optimizer 4D system from Qass GmbH (Wetter-Ruhr, Germany). The entire test setup can be seen in fig 2, were the Qass system is equipped with a 4 MHz sensor along with pre-amplifiers. The sampling rate was fixed at 400000 Hz for the purpose of signal conversion from time domain to frequency domain.
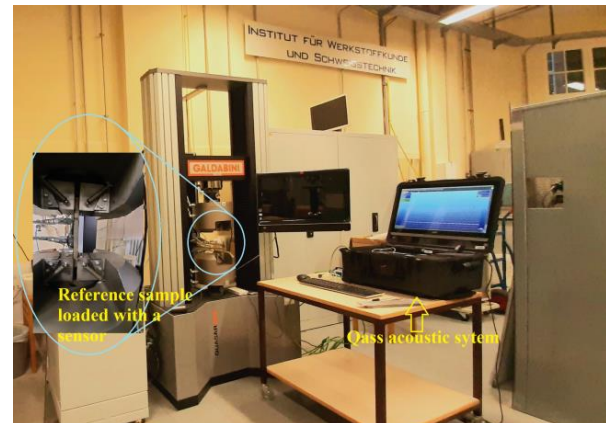
Fig.2. The test setup along with tensile testing machine and Qass acoustic system.

Two set of tests were performed at a strain rate of 0.00007/s and 0.00025/s respectively. The maximum yeild strenght of M700 was 781 MPa and hence all the tests were stopped at 550 MPa, this is to ensure that the same sample can be used several times for the purpose of calibration. Once, the stress-strain data has been obtained for these strain rates, a regression model was implemented on python to obtain the best fitting line from the stress-strain plot and hence the Young's modulus (E). 25 tests were perfromed at each of the strain rates and the E was tabulated for each of the tests to measure the standard deviation and hence to understand the reliability of the material as a universal non-destructive reference sample. For the sake of consistency 3 sample where considered for the study.

Acoustic signals are introduced into the sample, were the sample is constrained in a manner as seen in fig 3. Since, the project is in a stage of progression, different methods where tried, like introducing sound in the form of impulse directly into the sample by hitting it, introducing sound through the machine (by knicking at positions where singal is not lost in the form of damping etc), or by using a speaker and playing loud music. Signals were obtained before and after loading (after 25 loadings) to look into any form of deviations. The sampling rate was fixed at 400000 Hz. With the precise boundary conditions known and fixed, the Youngs modulu's is calculated using equation (2). The entire calibration process is elaborated in section 1.1.3
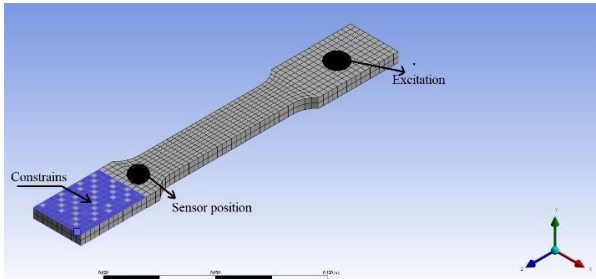
Fig.3. Typical reference sample contrained in a cantilever manner to excite the flexural modes.

Table. 3. Material properties of M700

Material properties	M700
Youngs Modulus, E [GPa]	206
Yield at 0,2% strain [MP]	781
Ultimate Strenght [MPa]	800

1.1.3 Algorithm for calibration of the universal testing machine

The algorithm is shown in the form of action taken by the user and corresponding execution to be carried out in the table below (Table 4).

Table. 4. Actions taken by the user and execution by the algorithm

Step	Action	Result
1	Importing the signal (time domain), and stress-strain date from Qasar 200	The signal is in CSV format and is imported by the algorithm, and the signal is shown in fig 4 (A).
2	Input specimen dimensions, uncertainty data	The specimens dimensions are used to determine the
	from calibration certificate (data for load cell and strain gauge)	Youngs modulus along with data from frequency spectrum, while uncertainty data is used to measure deviation of UTMs calibration
3	Perform FFT on the signal data	Generating the frequency spectrum to estimate the resonant frequency
4	Looking for the resonant frequency in the spectrum, by comparing the peaks in the spectrum with the frequencies estimated earlier in step 2.	The resonant frequencies are used to estimate the Young's modulus based on equations elaborated in eq (2)
5	Performing machine learning approach based on regression modelling to find Youngs modulus from stress-strain data.	As the machine loses its calibration the uncertainty differs, which the algorithm reads from the measured data and adds up to the Youngs modulus calculated and if this total (Emax) exceeds exceeds 3% [13] of the first measured E-modulus of the reference sample then the machine has partially lost its calibration.
6	Comparing the Youngs modulus measured from acoustic to that measured from tensions test.	The E-modulus measured from acoustic is given a max and min differing by 3%. If this range is still within the Emax from step 5, the machine is still in calibration. But if E-modulus from step 5 exceeds or is less than Emax and Emin in

		this step, the machine has lost its calibration.

2. RESULTS AND DISCUSSIONS

2.1 Frequency spectrum analysis

The algorithm reads the signal data generated and performs a fast fourier transforms to convert the time domain signal into a frequency domain singal also termed as a spectrum. The algorithm check the spectrum for domianant flexural modes, and latter untilises it for calcuting the E-modulus. The algorithm knows the frequencies based on a data-base it has access to having E-modulus of M700 steel from literatur. It calculates the frequenices based on the E-modulus and looks for similar frequencies within the spectrum. This is performed from step 1 to step 4 in table 4. A typical spectrum is seen in fig 4-B.
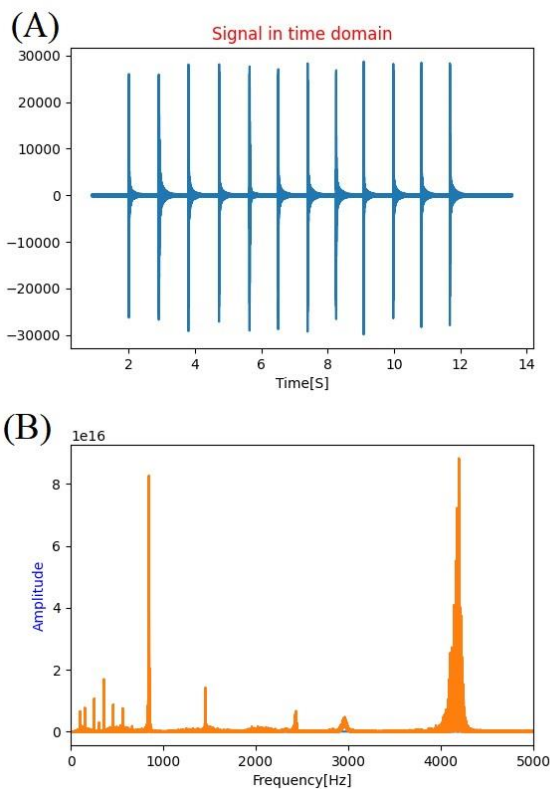
Fig. 4. A typical acoustic signal introduced by impulse excitation. A) Time-domain signal, B) Frequency domain signal.

2.2 E-modulus measurement from Qasar 200

Test were performed at two different strain rates to ascertain the correct rate which could be used to perform the calibration. Thus, regression modelling was performed on the data obtained from Qasar 200, to obtain the best fit for curve. The E-modulus was measured within a range of the elastic region of the stress-strain plot and the procedure elaborated in ISO 6892 was adopted. In keeping with the norm, an upper and lower stress values were identified where the upper limit corresponds to 40% of $R_{p0.2}$ while the lower limit was set at 10-20% of $R_{p0.2}$. Within this region a linear regression is performed via machine learning tools to obtain a curve fit. Coefficient of determination R^2 would serve as reminder of determining how good the curve fit is. In this case it was as close as 0.9992(this is close as recommended in per ISO 6892-1: 2019). Table 5(a) and table 5(b) shows the measurement from sample 1 at strain rates 0.00007/s and 0.00025/s respectively. It must be stated here that each of these samples were loaded 25 times each at the respective strain rates. The plots for the same sample can be seen in fig 4(a) and (b). A closer look into the plots reveals that at lower rates of loading, the plots seem to wither away towards the end of the test, while at a slightly higher rate of loading, the plots were coincident to a large extend and hence the standard deviation in E-modulus measurements were low. Thus, based on this non-destructive loading within the elastic region it was concluded that, for an effective calibration to be carried, the strain rate shall be fixed at 0.00025/s. The process elaborated in this section shall be performed from stage 5 until 6 in table 4.

Table. 5(a). E-modulus measurement at 0.00007/s

Test No	Strain [%]	E [GPa]
1	0.27	201.68
2	0.27	209.56
3	0.27	210.77
4	0.27	207.77
5	0.27	207.97
St.Dev		1.415

Table. 5(b). E-modulus measurement at 0.00025/s

Test No	Strain [%]	E [GPa]
1	0.27	207.36
2	0.27	207.88
3	0.27	207.32
4	0.27	206.38
5	0.27	207.25
St.Dev		0.539
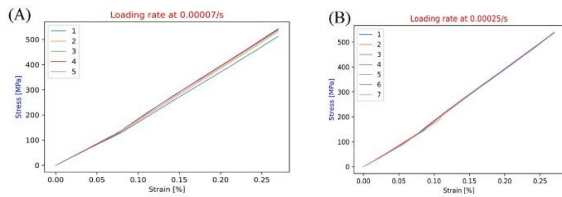
Fig. 4. Stress strain plot for single sample loaded at two different rates (A) 0.00007/s, (B)0.00025/s.

2.3 Calibration monitoring of Qasar 200

As mentioned in table 4, the algorithm read both the signal data from acoustics and the data from Qasar 200. Initially it generates a signal plot in time domain, the data is latter sliced if necessary, based on the amount of data. An FFT is performed on it and later the spectrum is generated, and from the spectrum natural frequencies in flexural modes are identified and its used to tabulate the E-modulus. A max and min is assigned to this calculated E-modulus termed as Emax and Emin, whereas the modulus calculated from dominant frequencies is termed as E-aco. And based on the E-modulus comparisons from the tension test, the calibration is monitored.
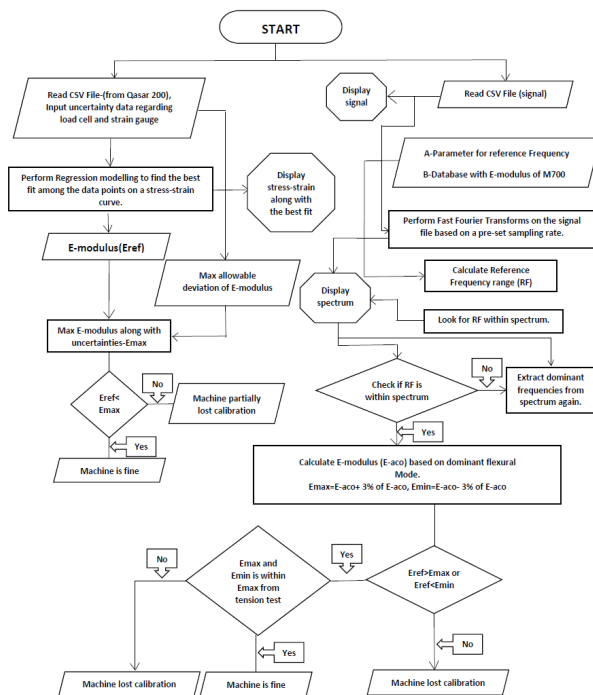
Fig. 5. A flow-chart of the algorithm for calibration

3. CONCLUSION

This paper was an attempt to use non-destructive testing techniques to ascertain the calibration and possible calibration of universal testing machine. Within this context a non-destructive test specimen machined from a

high strength low alloy steel commercially available as ALFORM700M® was used. Acoustic methods where initially implemented to obtain the Young's modulus, latter the sample was strained within the elastic region to obtain Young's modulus. Considering all the uncertainties stemming from the strain gauge, load cell etc, the E-modulus was tabulated. An algorithm was implemented to determine the modulus from these two methods and same was latter used to ascertain the calibration status of the universal testing machine. Several more rounds of testing would be implemented before, the algorithm would be integrated into the machine's interface so that a live monitoring of the equipment calibration status can be implemented.

4. REFERENCES

[1.] Sonja, K. et al. **Uncertainty in the determination of elastic modulus by tensile testing**, Engineering Science and Technology, an International Journal, 25, 100998, 2022.

[2.] Viala, R., Placet, V., and Cogan, S. **Identification of the anisotropic elastic and damping properties of complex shape composite parts using an inverse method based on finite element model updating and 3D velocity fields measurement (FEmu-3DFV): application to bio-based composite violin soundboards**, Compos. Part A Appl. Sci. Manuf., 106, pp. 91-103, 2018.

[3.] Sebastián, T., Walter, S., Alberto, S., and Angel, M. **Measurement of the Young´s modulus in particulate epoxy composites using the impulse excitation technique**, Materials Science and Engineering A, 527 pp. 4619 – 4623, 2010.

[4.] Lord, J.D., Morrell, R.M. **Elastic Modulus Measurement, Good Practice Guide No. 98,** National Laboratory, 2006.

[5.] Ho-Cheung Ho. et al. **Mechanical properties of high strength S690 steel welded sections through tensile tests on heat-treated coupons**, Journal of Constructional Steel Research, 166, 105922, 2020.

[6.] Advanced Technical Ceramics-Mechanical Properties of Monolithic Ceramics at Room Temperature-Part 2:Determination of Young´s Modulus, Shear Modulus and Poisson´s Ratio; German Version EN 843-2:2006; Beuth Publishing DIN: Berlin, Germany, 2007.

[7.] Philipp, L., Georg, F., Christoph, H., Florian, S., Florian, E., and Wolfram, V. **Acoustical and optical determination of mechanical properties of inorganically-bound foundry core materials,** Materials, 13(11), 2531.

[8.] Roebben, G., Bollen, B., Brebels, A., van Humbeeck, J., van der Biest, O. **Impulse excitation apparatus to measure resonant frequencies, elastic moduli, and**

internal friction at room and high temperature, Rev. Sci. Instrum, 68, pg. 4511-4515, 1997.

[9.] Trubitz, P., Rehmer, B., Pusch, G. In: Die Ermittlung elastischer konstanten von gusseisenwerkstoffen. Tagung wekstoffprüffung, Neu-Ulm, Germany, pp. 267-272.

[10.] Sebastian, S., and Marion, M. **A new approach for the determination of the linear elastic modulus from uniaxial tensile tests of sheet metals,** J. of Mat. Processing Tech., 241, pg. 64-72, 2017

[11.] Barboni, L., Gillich, G.R., Chioncel, C.P., Hamat, C.O., and Mituletu, I.C. **A method to precise determine the Youngs´s modulus from dynamic measurements**, In: Conf. Ser.: Mater. Sci. Eng, 416 012063.

[12.] Klein, M., Spindler, H., Luger, A., Rauch, R., Stiazny, P., Eigelsberger, M. **Thermomechanically hot rolled high and ultra high strength stell grades-processing, properties and application**, Material Science Forum. Trans Tech Publications, Ltd., November 2005.

[13.] Lord, J.D., Rides, M., Loveday, M.S. **TENSTAND WP3 final report: modulus measurements methods. NPL Report. DEPC-MPE 016.** URI: http://eprintspublications.npl.co.uk/id/eprint/3223

Unsupervised Classification of Welding processes based on Psychoacoustic Sound Features

Jurij Prezelj, Jaka Lavrih, Damjan Klobčar

Faculty of mechanical engineering, University of Ljubljana

Abstract: *Welding processes, to ensure the quality of the final products, often need to be controlled through external sensors. In MAG/MIG welding, the welder or welding operator also relies on hearing, i.e., audible sound emissions during the welding process. From the interpreted sound emissions during the welding process, the stability of the welding process can be determined. In the paper, we analysed short-circuit and pulsed MIG/MAG welding under different operating conditions. Signals of welding current, voltage and sound in the audible and ultrasonic range were recorded. During welding, we simulated poor welding conditions such as lack of protective gas atmosphere, distancing the welding torch from the welding surface, and improper preparation of the workpieces with greasy, coloured, and oxidized surfaces. Additionally, we applied unsupervised K-Means classification in combination with psychoacoustic features of audible sound to check the hypothesis that sound emission carries enough information about the process to classify it. By changing the number of classes, it was found out that sound can be used to monitor the welding process, identify the welding process type and further it revealed a specific mode of welding.*

Keywords: Welding sound, Audible noise of welding, Psychoacoustic features, Unsupervised classification, K-Means

1. INTRODUCTION

All areas of the industry are becoming increasingly optimized or refined, including welding. Real-time welding process optimization is already being used in modern welding processes. Adjusting the process in real-time allows for improved quality, reduced production times, and cost savings due to the elimination of defects, reworks, and inferior products. The outcome of the manufacturing process in the industry are often various products that must be made within appropriate tolerances and quality.

1.1 Motivation

In automated welding and joining processes, there is a desire to use various sensors to control the joining process in real-time and thus prevent the production of inferior products [1, 2]. In arc welding processes, welding current sources allow the setting of welding parameters, and the controller of the source adjusts welding parameters based on electrical quantities [3]. To ensure the quality of the welding process, it's also necessary to know other data about the environment, such as the local shape of the weld joint with potential irregularities, the temperature of the workpiece, the state of the workpiece clamping and its distortion, sound, etc. [4]. By knowing the appropriate values, we can adjust the joining process to ensure the appropriate changes to welding parameters and consequently achieve the desired quality of the welding process and product.

1.2 Goals

The purpose of the study was to experimentally check the influence of disturbances on the welding result and sound emissions during the weld surfacing, at which welding process disturbances occurred. A welding experimental plan was designed and executed to obtain information about the course of the process from various sensors. Based on the measured values of electrical quantities, sound quantities, and visual assessment, the aim was to determine the correlations between input and output quantities and induced errors during welding.

During experimental welding, we induced typical errors and disturbances that usually occur during the welding or weld surfacing process. We simulated these disturbances and errors with greasy stains, protective paint coatings, excessive surface oxidation (corrosion), and lack of a protective atmosphere, representing drafts. The goal of the task was to determine the correlation between process parameters and measured sound quantities in the ultrasonic range and whether the measured quantities could be used in real-time optimization.

2. THEORETHICAL BACKGROUND

In welding, we assume that the ignition of the welding arc is a monopole source of sound wave propagation with a changing volume of the medium. In the MIG/MAG process, when the welding wire contacts the workpiece, a short circuit occurs, leading to the formation of the arc.

2.1 Generation of sound during welding

The arc ignition heats the surrounding gases, which increase in volume. When the formed droplet at the end of the welding wire detaches, the arc extinguishes, the gases cool down, and their volume decreases. The volume's rate of change over time gives us the arc surface acceleration.
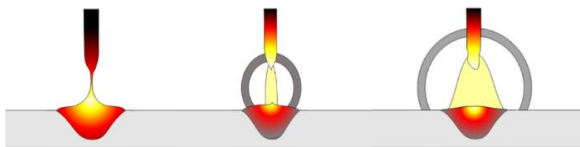
Fig. 1: Creation of air pressure disturbances during welding arc ignition

These changes result in air pressure variations or pressure disturbances, which we call the sound source. The formation of the arc and the creation of pressure wave disturbances are shown in Figure 1. The sound pressure is calculated according to Eq.1, related to Figure 2.

The connection between the electric current during welding and created sound pressure p disturbances is presented in equation Eq.3 and in Fig.3, which is graphical illustration of Eq.3.
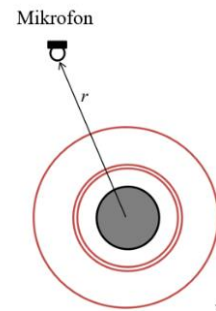
Fig. 2: Schematic representation of spherical disturbance propagation

Calculation of the pressure depending on the radius r as a function of volume flow, generated by the oscillations of the arc volume:

$$p(r,t) = \frac{\rho_0}{4\pi r} \frac{\partial Q\left(t - \frac{r}{c}\right)}{\partial t} \ [Pa] \tag{1}$$

where: r is the distance to the microphone and r/c is the time delay, Q(t) is the fluid volume flow generated by air displacement around the oscillating arc,

$$Q(t) = \oiint v(t,r,\phi)dS \tag{0}$$

Equation for calculating sound pressure change clarifies that sound pressure depends on power supplied to the electric arc, i.e., its volume:

$$p(t) = C_1 \frac{d}{dt}(UI) \tag{3}$$

where C_1 is the arc geometry constant and depends on r, U is arc voltage, and I is welding current intensity. Arc voltage is calculated using the equation [4, 5]:

$$U = RI + L\frac{dI}{dt} + \frac{RaI}{1 + i\omega CaRa} \tag{4}$$

where: I stands for electric current intensity, Ra is arc resistance, Rc is arc capacitance, and ω is angular frequency. Eq. 4 therefore indicates that there is a direct correlation between welding current and sound pressure.

Figure 3 represents the link on how welding current signals affect the generated sound signal. Each pulse of electric current can be linked to a change in sound pressure. The welding current increases during the electrode's short circuit with the workpiece, after which the welding arc ignites. After the arc ignition, with some

delay, the shock wave of the surrounding gases reaches our microphone, which we denote as time delay td.

Audible sound of welding has been studied and since the direct correlation to welding power has been proven, it was used for real time welding monitoring. So far, no studies have been done on application of psychoacoustic features for real time welding classification, although psychoacoustic features prooved to be very useful in combination with unsupervised classification algorithms, [8, 9, 10, 11]
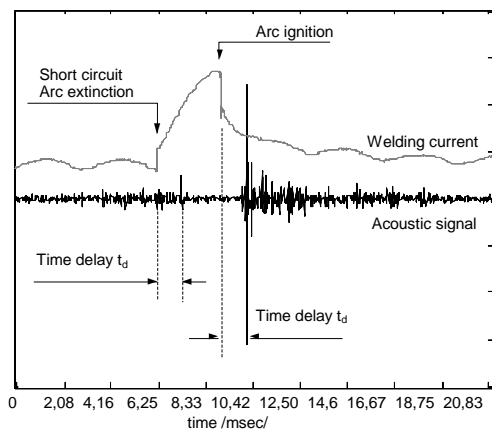
Fig. 3: Relationship between the generation of the welding arc and the change in air pressure

2.2 Psychoacoustic metrics and signal descriptors

Psychoacoustic metrics, like loudness, roughness, sharpness, and tonality were extracted, from the recorded sound signals, together with some other signal features like number of pulses, which represent number of short circuits events during welding. This feature also proved to be important during the classification process.

2.2.1 Loudness

Loudness is a term referring to the human perception of sound level [12]. The definition of loudness states that 1 sone corresponds to a 1 kHz tone at 40 dB. The loudness scale quantifies loudness to the human ear. Loudness represents the dominant feature for the evaluation of sound quality. To calculate it, specific loudness has to be determined, as given in Eq. (5).

$$N' = 0,08\left(\frac{E_{TQ}}{E_0}\right)^{0,23}\left[\left(0,5+0,5\frac{E}{E_{TQ}}\right)^{0,23}-1\right] \tag{5}$$

In this equation, E_{TQ} is the excitation at threshold in quiet and E_0 is the excitation that corresponds to the reference intensity $I_0 = 10^{12}$ W/m^2. The specific loudness reaches asymptotically the value $N_0 = 0$ for small values of E. Loudness N is then the integral of the specific loudness over the critical-band rate z in [Bark], or in the mathematical expression:

$$N = \int_0^{24\text{Bark}} N' \, dz \tag{6}$$

2.2.2 Roughness

Roughness correlates to how noticeable or annoying a sound is as heard by the human ear [12]. More specifically, roughness is a hearing sensation related to loudness modulations at frequencies too high to be discerned separately, such as modulation frequencies greater than 30 Hz. The roughness R in [asper] of any sound can be calculated using the following equations:

$$R = 0,3\frac{f_{mod}}{\text{kHz}}\int_0^{24\text{Bark}}\frac{\Delta L_E(z)}{\text{dBBark}}dz \ [\text{asper}] \tag{7}$$

$$\Delta L_E(z) = 20\log\left(\frac{N_{max}}{N_{min}}\right) \ [\text{dB}] \tag{8}$$

In Eq. (8), N_{max} and N_{min} are the maximum and minimum specific loudness in the current critical band, f_{mod} is the modulation frequency and $\Delta LE(z)$ is the amplitude of modulation.

2.2.3 Sharpness

Sharpness corresponds to the sensation of a sharp, painful, high-frequency sound and it represents the comparison of the amount of high frequency energy to the total energy [12]. It is calculated as a weighted area of loudness, like an area moment calculation, as shown in Eq. (9). In Eq. (9), g(z) is the weighting function that has a unitary value of 1 below 3 kHz and non-linearly increases from 3 kHz to 20 kHz, where it has a value of four. For high values of sharpness, significant spectral components at high frequencies are necessary.

$$S = 0,11\frac{\int_0^{24\text{Bark}} N' g(z) z \, dz}{\int_0^{24\text{Bark}} N' \, dz} \tag{9}$$

2.2.4 Tonality

Tonality represents the auditory perception character related to the pitch strength of sounds. There are many models for calculating tonality; in this paper, the Aures model is used [12]. where q_1 (Δz_i), q_2 (f_i) and q_3 (ΔL_i) represent weighting functions based on the bandwidth

(Eq. (11)), centre frequency (Eq. (12)) and prominence (Eq. (13)) of each tonal component and NGr is the loudness of the broadband noise component. Tonality is used to determine whether a sound consists mainly of tonal components or broadband noise [12].

$$T = c \left(\sum_{i=1}^{n} \left[q_1'(\Delta z_i) q_2'(f_i) q_3'(\Delta L_i) \right] \right)^{\frac{0.29}{2}} \left(1 - \frac{N_{Gr}}{N} \right)^{0.79} \quad (10)$$

$$q_1(\Delta z_i) = \frac{0,13}{\Delta z + 0,13} \quad (11)$$

$$q_2(f_i) = \left(\sqrt{1 + 0,2 \left(\frac{f}{700} + \frac{700}{f} \right)^2} \right)^{-0.29} \quad (12)$$

$$q_1(\Delta L_i) = \left(1 - e^{\frac{-\Delta L}{15}} \right)^{0.29} \quad (13)$$

2.3 Unsupervised k-means classification algorithm

The k-means algorithm is an iterative algorithm that attempts to classify the data set into K different, non-overlapping clusters, where each data point can only belong to one group. Data points are D-dimensional vectors, with each component representing a feature extracted from observations. The k-means algorithm attempts to arrange N observations in K clusters so that the data points within the clusters are adjacent, while keeping the clusters as far away from each other as possible. The evaluation is based on the Euclidean distance between the points, [8,10]. The distance between a centroid with the index c_m and the observed point x_n is defined by an equation,

$$\left| c_m x_n \right|^2 = \sum_{i=1}^{D} c_{m,i}^2 - x_{n,i}^2 \quad (14)$$

K-means algorithm assigns each data point to the nearest cluster defined with its centroid. The algorithm is based on minimizing the arithmetic mean of all data points that belong to the same cluster. The smaller the variation within clusters, the more homogeneous the data points are within the same cluster. K-means clustering therefore aims to classify the N observations into K (≤ N) clusters defined with the centroids $C = \{c_1, c_2, ..., c_k\}$ to minimize the sum of the squares within the cluster. Formally, the objective is to find:

$$\underset{C}{\arg\min} \sum_{i=1}^{K} \sum_{x \in c_i} \left\| x_i - \varepsilon_i \right\|^2 = \underset{C}{\arg\min} \sum_{i=1}^{k} \left| c_i \right| Var c_i \quad (15)$$

where e_i is the average of points attributed to c_i. This is equivalent to minimizing the pairwise squared deviations of points in the same cluster:

$$\underset{C}{\arg\min} \sum_{i=1}^{K} \frac{1}{\left| 2c_i \right|} \sum_{x,y \in c_i}^{k} \left\| x - y \right\|^2 \quad (16)$$

The equivalence can be deduced from identity:

$$\sum_{x \in c_i}^{k} \left\| x - \varepsilon \right\|^2 = \sum_{x \neq y \notin c_i} \left(x - \varepsilon_i \right) \left(\varepsilon_i - y \right) \quad (15)$$

Because the total variance is constant, this corresponds to maximizing the sum of the squared deviations between points in different clusters, which follows from the law of total variance. The k-means algorithm is usually initiated with a randomly filled matrix of centroids **C**. Euclidean distances are then calculated for each pair of data points to each centroid representing a class. Each data point is then assigned to a class, whose distance to the centroid is minimal. The new centroid is calculated from the new distribution of data points for each class. The new centroid of a given class is an averaged value of all data points assigned to this class. The Euclidean distances are calculated again and processed continuously until there are no more transitions of data points between the classes, [8,10].

3. EXPERIMNTAL SETUP

The set of devices for conducting experiments consisted of a welding current source for performing welding, a 3-axis CNC positioning system for moving the weldment, measuring instruments for capturing electrical quantities, and measuring instruments for capturing sound quantities. The entire system is shown in Figure 4. A 3-axis scissor type positioning system was used for movement, providing linear movements in three different axes. It was made in the Laboratory for Technical Cybernetics, Machining Systems and Computer Technology LAKOS, at the Faculty of Mechanical Engineering of the University of Ljubljana. It was later converted into a manipulator for 3D welding. A protective container was mounted on the movable table of the

positioning system, which protects the machine and the environment from UV radiation and molten metal splashes during the welding process. The clamping surface was air-cooled and electrically isolated from other parts of the machine. It is shown in Figure 4, [3].
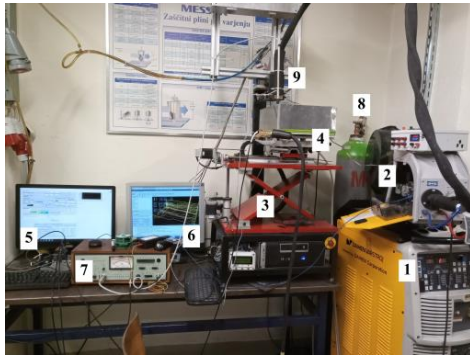
Fig. 4: Layout of the experimental system for welding

1 Welding current source Daihen Varstroj P500L
2 Feeder unit with additional material
3 Mechanism of the X positioning system
4 Protective container with weldment
5 Computer with LabView software
6 Computer for controlling the CNC system with G-code
7 Microphone pre-amplifier B&K 2636
8 Gas cylinder with protective gas Ferroline C18
9 Microphone for capturing sound waves B&K 4138

a) Measurement card NI 9222

All signals were aquired with a measuring card National Instruments NI 9222 with the corresponding NI cDAQ-9174 housing. It is shown in Figure 4. Through the measuring card, measurements of electric current, electrical voltage, and sound pressure were recorded. For measuring electrical current, we used additional output signal from the current clamps. For measuring electrical voltage, the measuring electrodes were connected in parallel to the welding process circuit.

b) Electric current

It was measured indirectly through the current clamps. The current clamps were from Voltcraft, type VC-511, placed on the negative pole of the welding source. Through their voltage output, they were connected in parallel to the measuring card. The output voltage factor against the measured electric current of the current clamp is 1 mV/A.

c) Electrical voltage

One electrode was connected to the positive pole inside the feeder unit of the welding source, and the other electrode was on the negative pole of the welding table. When measuring arc voltage, a voltage divider with a factor of 10 was additionally connected to the circuit. The measuring card allows us to measure voltage up to 10 V, which is beyond the operating level of the welding source.

d) Sound pressure

For measuring sound pressure, a system of a microphone, microphone amplifier, and measuring card was used. The microphone was of the Bruel & Kjaer 4138 type. It was connected to the Bruel & Kjaer 2636 type microphone pre-amplifier, from which the measured values were stored on the computer through the measuring card. Figure 4.9 shows the used microphone, and Figure 4.7 shows the used microphone pre-amplifier.

The measured data was displayed in the LabView software environment after the experiments were completed. For the calculations of sound quantities, a LabView program named 'Feature Extraction' was used, which was developed in the Laboratory for Technical Acoustics of the Faculty of Mechanical Engineering of the University of Ljubljana. The results were displayed and compared in certain frequency ranges of audible sound and ultrasound. The effective sound pressure value (RMS of sound), roughness, and fluctuation intensity were displayed in the frequency range between 80 kHz and 120 kHz for the entire length of the weld. Additionally, the recorded sound was processed with a low-pass and high-pass filter in the frequency range between 200 Hz and 80 kHz. Low-pass filtration was used due to disturbances from the controlled source and high-pass filtration due to environmental disturbances where the experiments were conducted.

4. EXPERIMENTAL PLAN

The aim of the experimental work was to demonstrate the influence of disturbances during the welding process on the quality of the weld and its effect on the measured results. Modern welding sources have the ability to overcome negative impacts during welding due to their advancement. Despite poor conditions, they can in some instances still provide a high-quality welding result. Before the execution of the experiments, a test plan was prepared. The plan was specified all the welding parameters, the type of disturbance to be executed during welding, and the required preparation of the base surface

to be welded on. The test plan was made for easier monitoring of the test execution, fewer chances of mistakes, and the most efficient use of time and work. It is presented in Table 1.

The chosen welding methods were Short Circuit (DC Low Spatter) and Pulsed (DC Pulse). The aim was to compare the two advanced modes of the MIG/MAG welding source operation. The Short Circuit with the Low Spatter function, as the name suggests, reduces spattering of the molten material during welding. Pulsed welding adds electrical current pulses of approximately 400 A to the welding current signal for better defined detachment of the material droplets. The welding parameters were set on the front control panel of the welding source. Table 1 displays the settings for each test. The welding torch's travel speed was the same for all tests, namely 300 mm/min. It was set during the trajectory programming of the Positioning System X. The initial distance of the welding torch, or the length of the free wire end, was 10 mm.

Table 1: Welding test execution plan, welding current 90A.

Weld No.	Welding type	Distortion	Gas flow [l/min]	Voltage [V]
1.1	(DC pulse)	Reference weld	13	21,8
1.2	(DC low spatter)	Reference weld	13	15,3
1.5	(DC pulse)	No protective atmosphere	0	21,8
1.6	(DC low spatter)	No protective atmosphere	0	15,3
1.7	(DC pulse)	Protective paint layer on the surface	13	21,8
1.8	(DC low spatter)	Protective paint layer on the surface	13	15,3
2.1	(DC low spatter)	Oily surface	13	15,3
2.2	(DC pulse)	Oily surface	13	21,8
2.6	(DC pulse)	Corroded welding surface	13	21,8
2.7	(DC low spatter)	Corroded welding surface	13	15,3

The chosen welding methods were Short Circuit (DC Low Spatter) and Pulsed (DC Pulse). The aim was to compare the two advanced modes of the MIG/MAG welding source operation. The Short Circuit with the Low Spatter function, as the name suggests, reduces spattering of the molten material during welding. Pulsed welding adds electrical current pulses of approximately 400 A to the welding current signal for better defined detachment of the material droplets. The welding parameters were set on the front control panel of the welding source. Table 1 displays the settings for each test. The welding torch's travel speed was the same for all tests, namely 300 mm/min. It was set during the trajectory programming of the Positioning System X. The initial distance of the welding torch, or the length of the free wire end, was 10 mm.

The welding trajectory was programmed in a program created in the LabView software environment. Other parameters related to the movements of the 3-axis CNC system X were also set in this program. The data was then transferred to the AXIS computer program, which controls the CNC manipulator. The trajectory of each weld is shown in Figure 5. The length of each weld was 145 mm, and the distance of the free electrode end increased along its entire length with seven equal increments of 2.5 mm. A transition can be seen between each increment. The purpose of increasing the torch distance was to capture the influence of different heights during a single test.
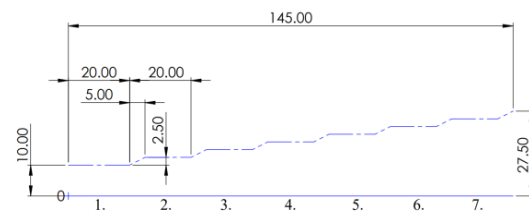
Figure 5: Welding torch trajectory for welding seams.
Used Materials
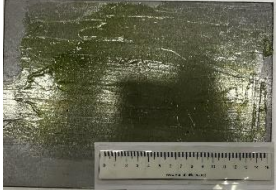
The base plate onto which the welding was done is made of structural steel labeled S235 J0. The dimensions of the plate were 140 × 200 × 5 mm. Structural steel is most used in construction. It has good weldability, formability, and mechanical properties. The material of the base plate was chosen due to its widespread use in the industry and availability. The physical properties of the material are: Density 7.85 [g/cm3]; Linear expansion coefficient

1.08·10-5 [K-1]; Thermal conductivity 56.3 [E/m·K]. Chemical composition of S235 J0 steel [5]: C =0.17%, Mn =1.40%, P=0.035%, N=0.012, Cu=0.55 and remaining is Fe. Mechanical properties of S235 J0 steel [21]: Yield strength Rp0.2 = 235 [MPa], Tensile strength Rm = 360-510 [MPa], Toughness KV > 27 [J] at 0°C.

The filler material was structural steel in the form of wire labeled VAC60, manufactured by SIJ Elektrode Jesenice, with a diameter of 1.2 mm. It was chosen due to its frequent use in industry and compatibility with the base plate material onto which the welding was done. Its chemical composition: C=0,06-0,1%, Si=0,9%, Mn=1,5%, S<0,025%, P<0,025% and Fe in remaining percentage. The mechanical properties of additive material: Yield strength Rp0.2 > 240 [MPa], Tensile strength Rm 500-640 [MPa], Toughness KV >47 [J] at -50°C. [6]

The shielding gas used in all tests was a gas mixture for MAG welding, specifically labeled Ferroline C18 produced by Messer. The gas composition was 18% CO_2, and 82% Ar. Gas flow rates were 13 l/min for optimal conditions and 0 l/min to demonstrate the case without a protective atmosphere. According to the manufacturer's data, the shielding gas is intended for welding plain, low-alloyed, and fine-grained structural steels by the MAG process. [10]

Table 2: Prepared base plates for welding

Unprepared base plate surface	
Surface prepared with a protective layer of paint	
Surface prepared with an application of machine grease	
Prepared corroded surface	

For each type of sample, an individual base plate was prepared for welding. For reference samples and those lacking a protective atmosphere, the surface of the base plate was only cleaned with a solvent. For samples welded on an oily surface, a thick layer of NLGI-2 type machine grease manufactured by Olma was applied to the welding area. The corroded surface was pre-treated with a solution of hydrogen peroxide and water. A cloth soaked in the hydrogen peroxide solution was placed on the cleaned, degreased surface for 24 hours. After halting the chemical reaction, the solution's remnants were washed off the plate. The plate with a protective paint layer was degreased and then given two passes with an hour interval of a thin layer of spray paint. Prepared welding plates are shown in Table 2.

5. RESULTS

For each weld signals were recorded, and signal features were extracted. Examples of extracted psychoacoustic features are presented in Figs. 6a and 6b.
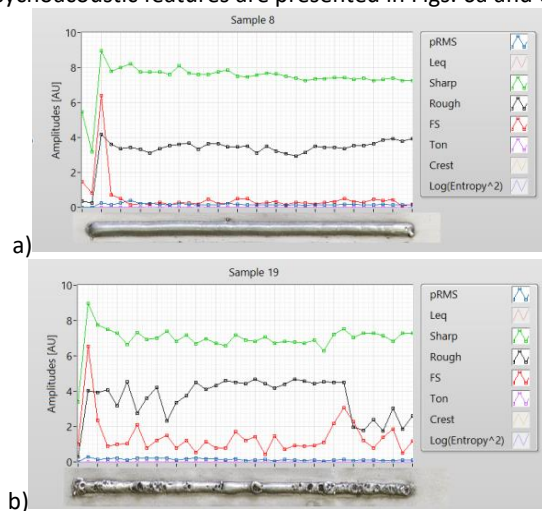
Figure 6: Psychoacoustic features and corresponding welds for done with DC low spatter a) referenced weld welded at 150 A and b) weld welded at 90 A without the shielding gas.

Each set of extracted values from the signal corresponds to the aligned location on the weld. Each weld was performed under different conditions, consequently different noise was emitted. Difference can be observed by different values of signal features and consequently in their feature vector combinations of the psychoacoustic features. From Fig. 6a and 6b can also be

clearly visible that any errors during welding can be easily detected. This means that sound can be easily analysed during the process and used for the classification of the welding process itself.

Statistical analysis of distribution of normalized feature values is presented in Fig. 7. From this figure different psychoacoustic features have different responses to defferent welding conditions. Only tonality is not relevant, becouse its value is for almost all samples always close to zero. Other psihoacoustic features Sharpness, Fluctuation strength and Roughness have faverable distribution.
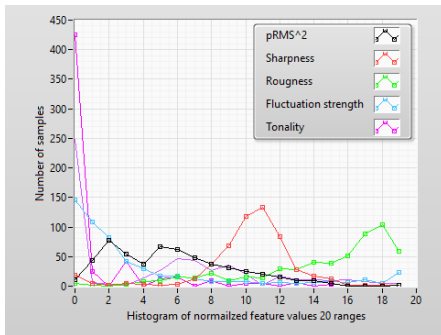
Figure 7: Statistical distribution of psihoacoustic features

Unsupervised classification is a statistical tool where an algorithm categorizes elements into classes. Each element has its own set of features, which mathematically can be represented by a vector. In our case, an element is a portion of the weld created over a duration of 1 second. From the measured signals within this 1-second period, we extract feature values. In our example, we used psychoacoustic features from the sound signal. The dimension of the vector is equal to the number of features. For the classification procedure, we utilized the K-means algorithm, often mentioned as a component of artificial intelligence. With unsupervised algorithms, we don't train the system; instead, we allow the algorithm to learn from the dataset on how to classify elements. The basic algorithm we used cannot determine the number of classes on its own, so we conducted the classification for three predetermined numbers of classes; 2, 3, and 4.

In classifying elements into two classes, the algorithm recognized the difference between elements belonging to the welding process and those related to idling, i.e., when the welding process is not operating, as depicted in Figure 8. From the image, it is clear that the algorithm can detect when a welding disturbance is so significant that the

process is interrupted, or in other words, when the arc goes out.
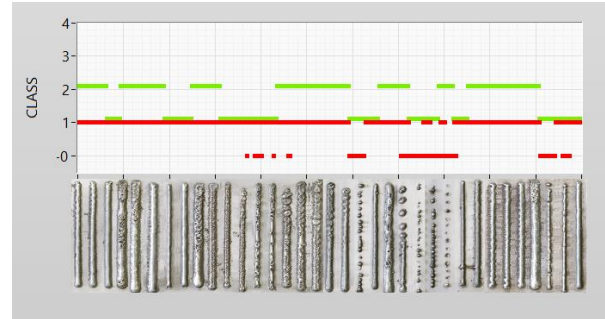
Fig.8: Classification of welding into two classes

In classifying into three categories, the algorithm distinguished elements into idle elements when the process is not operating, and onto elements it had previously identified as the welding process. Furthermore, it divided them into two additional categories. It turned out that the algorithm separated the process elements based on the basic welding mode, that is, elements belonging to the DC Pulsed welding mode and those pertaining to Short Circuit DC Spatter welding. Table 3 displays the Confusion matrix. We observe that for DC pulsed welding, the process is interrupted due to disturbances more frequently (64 times), whereas, in the DC Spatter welding, it only stops 19 times. The algorithm independently recognized that it could not classify the elements into either welding method but identified them as interruptions.
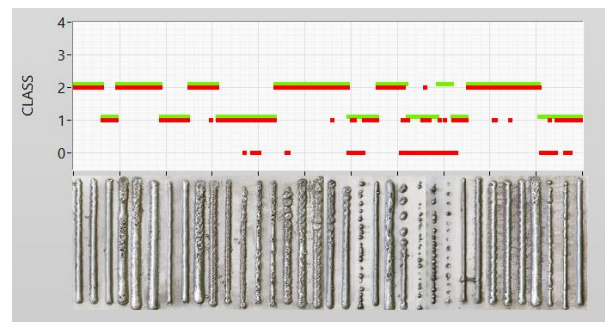
Fig.9: Classification of welding into three classes

From the confusion matrix in table 3, it can be inferred that the algorithm mistakenly identified DC pulsed welding as DC spatter welding only twice, and misidentified short circuit DC welding as DC pulsed welding just eight times. Such misidentifications occurred

only under extremely adverse conditions when the welding process was highly unstable. This indicates that the algorithm ensures more than a 95% accuracy rate.

Table 3: Confusion matrix for classification

	K-Means Class		
	(0) No welding	(1) DC Pulsed	(2) Spatter
DC Pulsed (1)	64	171	2
Short circuit DC Spatter(2)	19	8	289

Next, we increased the number of categories to four. The algorithm split category 2, which belongs to the DC spatter welding method. It classified 5 welds into an additional category, which are indicated in the image below, Figure 10, with arrows. From our analysis of unsupervised classification, it turned out that the algorithm automatically identified welds that were welded with an increased current of 150 A. The algorithm thus independently recognized welding with increased current as a new welding method.
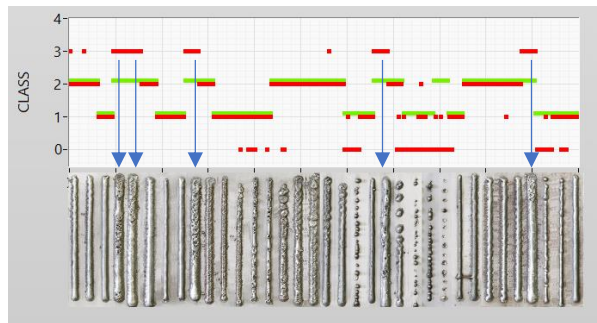
Fig.10: Classification of welding into four classes

When increasing the number of categories to five, the algorithm divided category 1, representing DC Pulsed, into two subcategories. In Figure 11, it's clear which welds from group 1 were newly categorized. However, as the number of categories increased, the clarity of classification became blurred. This is because the welding conditions within a single weld, due to the inclination of the weld piece and the consequent increasing distance between the weldment and the electrode, varied. As a result, the algorithm began to distinguish categories within a single weldment.
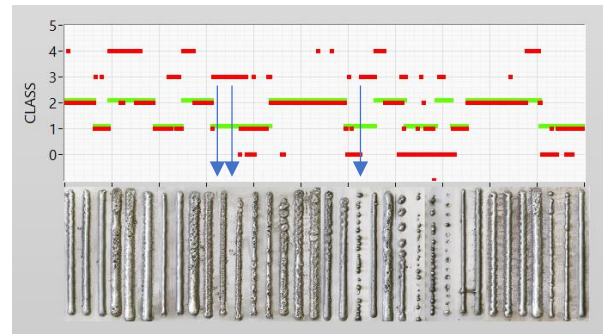
Fig.11: Classification of welding into five classes

3. CONCLUSION

Unsupervised classification of welding, based on psychoacoustic features of the sound generated by welding, has revealed that sound can be easily used to monitor the welding process. Furthermore, the experiment demonstrated that different welding methods can be differentiated based on classification with psychoacoustic sound features. The K-Means algorithm correctly distinguished between DC sputter and DC pulsed welding methods with a probability of more than 95%. Additionally, the use of unsupervised classification proved to be a useful tool for identifying processes that might otherwise be hidden in the noise of feature values. Through unsupervised classification, we identified that the activity during DC Spatter welding at very high currents over 150 A is intense, and the material transfer mechanism is changed, which can be easily identified by using classification algorithm based on psychoacoustic features.

4. REFERENCES

[1.] Zhang YM. **Real-Time Weld Process Monitoring**. Cambridge: Elsevier Science; 2008. http://qut.eblib.com.au/patron/FullRecord.aspx?p=1639763

[2.] Kah, P., Layus, P., Hiltunen, E., Martikainen, J., 2014. **Real-Time Weld Process Monitoring**. AMR 933, 117–124.https://doi.org/10.4028/www.scientific.net/amr.933.117

[3.] Ščetinec A., Klobčar D., Bračun D. **In-process path replanning and online layer height control through deposition arc current for gas metal arc based additive manufacturing,** Journal of

Manufacturing Processes, 64, pp. 1169-1179, 2021, https://doi.org/10.1016/j.jmapro.2021.02.038

[4.] Prezelj, J., et.al., Noise as a signal for on-line estimation and monitoring of welding process. Acta acustica united with Acustica. 2003, letn. 89, št. 2, str. 280-286.

[5.] Horvat, J., et.al., **Monitoring Gas Metal Arc Welding Process by Using Audible Sound Signal**, Strojniški vestnik - Journal of Mechanical Engineering, Vol. 57, (2011)3, pp. 267-278

[6.] Major, M., Nawrot, J., and Major, I. **Structural S235 and S355 Steels – Numerical Analysis of Selected Rods Connection,** IOP Conference Series: Materials Science and Engineering, Volume 585, 5th Annual International Workshop on Materials Science and Engineering 17–18 May 2019, Hunan, Changsha, China, pp. 2, 2019.

[7.] **Sij elektrode: welding consumables.** Available at: https://www.sij.si/assets/magazinefiles/Elektrod W eldinConsumables.compressed.pdf (Accessed 10 August 2023).

[8.] Murovec, J., et.al., **Automated identification and assessment of environmental noise sources**, Heliyon, Volume 9, Issue 1, January 2023, e12846

[9.] Murovec, J. et.al., **Psychoacoustic approach for cavitation detection in centrifugal pumps**, Applied Acoustics, Volume 165, August 2020, 107323

[10.] Prezelj, J., et.al., **Identification of different manifestations of nonlinear stick–slip phenomena during creep groan braking noise by using the unsupervised learning algorithms k-means and self-organizing map**, Mechanical Systems and Signal Processing, Volume 166, 1 March 2022, 108349

[11.] Lipar, P., et.al., **Psychoacoustic approach used for developing the model of sound pleasantness of vacuum cleaners and suction units based on objective and subjective analysis**, 5th Congress of Alps-Adria Acoustics Association, pp. 12-14

[12.] Hugo Fastl , Eberhard Zwicker, **Psychoacoustics Facts and Models**, Springer Berlin, Heidelberg, 2007

Index

AAAA 2023 IZOLA 20. - 21. September
10th CONGRESS OF THE ALPS ADRIA ACOUSTICS ASSOCIATION

Gold sponsors

IMS MERILNI SISTEMI D.O.O.

rothoblaas
Solutions for Building Technology

DEWESoft®
measurement innovation

KNAUFINSULATION

Silver sponsors

HEAD acoustics

getzner
engineering a quiet future

LESPATEX

Bronze sponsors

DOMEL®

FRAGMAT

URSA